Introduction to integrable probability

Vadim Gorin[1] Patrik Ferrari[2] Alexei Borodin[3]

November 3, 2026

[1]Departments of Statistics and Mathematics, University of California, Berkeley, USA. Email: vadicgor@gmail.com.

[2]Institute for Applied Mathematics, University of Bonn, Germany. Email: ferrari@uni-bonn.de.

[3]Department of Mathematics, Massachusetts Institute of Technology, USA. Email: borodin@math.mit.edu.

Abstract

This book introduces integrable probability through a selection of models whose asymptotic behavior can be analyzed using exact formulas for expectations of observables. The main examples come from interacting particle systems, interface growth, last passage percolation, random tilings, random matrices, and the six-vertex model. We prove limit theorems in which universal objects such as the Tracy–Widom distributions and the Gaussian free field arise. The methods draw on symmetric functions, determinantal point processes, steepest descent, and the Yang–Baxter equation.

Integrable probability is a large and growing field. Our aim is a rigorous, self-contained introduction to selected foundational results. The prerequisites are linear and abstract algebra, probability theory, and complex analysis at the advanced undergraduate level.

Contents

1 What is integrable probability? 4
- 1.1 Gaussian universality class . . . 4
- 1.2 Random deposition . . . 5
- 1.3 Ballistic deposition and KPZ universality class . . . 6
- 1.4 Last passage percolation: an integrable member of the KPZ class . . . 7
- 1.5 Domino tilings . . . 11
- 1.6 Alternating sign matrices and the six-vertex model . . . 13
- 1.7 Stochastic six-vertex model in the quadrant . . . 16
- 1.8 Simpler models obtained by degenerations . . . 18

2 Symmetric functions 19
- 2.1 Algebra of symmetric functions and its generators . . . 19
- 2.2 Schur functions . . . 22
- 2.3 Skew Schur functions . . . 26
- 2.4 Specializations . . . 30
- 2.5 Exercises . . . 35

3 Schur measures, PNG, and increasing subsequences 39
- 3.1 The discrete PNG . . . 39
- 3.2 The multilayer PNG . . . 41
- 3.3 From PNG to skew Schur functions . . . 44
- 3.4 Schur measures and Schur processes . . . 45
- 3.5 Continuous PNG . . . 48
  - 3.5.1 Poisson limit . . . 48
  - 3.5.2 Continuous PNG: singlelayer and multilayer versions . . . 49
  - 3.5.3 From PNG to LPP . . . 50
- 3.6 Longest increasing subsequences in a random permutation . . . 51
- 3.7 Exercises . . . 53

4 Determinantal point processes 56
- 4.1 Point processes and correlation functions . . . 56
- 4.2 Determinantal point processes . . . 61
- 4.3 Correlation functions of the Schur measure . . . 66
- 4.4 Gap probabilities and Fredholm determinants . . . 70
- 4.5 Rescaling a determinantal point process . . . 74
- 4.6 Exercises . . . 75

5 Steepest descent and its applications to local limits 82
5.1 Real integral: Stirling's formula . . . 82
5.2 Contour integral: local CLT for binomial random variables . . . 84
5.3 Edges of the Plancherel measure . . . 86
5.4 Bulk limit for the Poissonized Plancherel measure . . . 92
5.5 Decay of the Poissonized Plancherel measure outside the support . . . 96
5.6 Solution to the Ulam problem . . . 99
5.7 Shape and fluctuations of the continuous PNG droplet . . . 102
5.8 Edge limits for GUE . . . 103
5.9 Properties of the Tracy-Widom distribution . . . 110
5.10 Edge limits for discrete PNG and geometric LPP . . . 112
5.11 Exercises . . . 117

6 Domino tilings of the Aztec diamond 121
6.1 Combinatorics of tilings . . . 121
6.2 Shuffling algorithm . . . 125
6.2.1 Growth of Schur processes . . . 125
6.2.2 Push-block dynamics . . . 128
6.2.3 Shuffling of dominos . . . 130
6.3 Observables through operators . . . 134
6.4 Law of large numbers and the Arctic ellipse . . . 138
6.5 Field of fluctuations for the height function . . . 145
6.6 Multilevel observables . . . 148
6.7 The Gaussian free field . . . 151
6.7.1 Definition of GFF . . . 151
6.7.2 Complex structure and pullback for GFF . . . 154
6.7.3 Matching the Aztec fluctuations with GFF . . . 156
6.8 Exercises . . . 159

7 Six-vertex model with domain wall boundary conditions 163
7.1 Definition of the six-vertex model in a planar domain . . . 163
7.2 Domain Wall Boundary Conditions . . . 166
7.3 The Yang-Baxter equation . . . 168
7.4 Izergin-Korepin determinant . . . 173
7.5 ASM count and 2-count . . . 177
7.6 Gaussian and GUE limits at the boundary . . . 183
7.7 Exercises . . . 187

8 Stochastic six-vertex model in the quadrant 190
8.1 Model in the quadrant and link to ASEP . . . 190
8.2 A generalization of the Izergin-Korepin determinant . . . 194
8.3 Match with Schur measures and limit regimes . . . 196
8.4 Tracy-Widom limit for the height function . . . 200
8.5 Weak asymmetry and KPZ limit . . . 202
8.6 Exercises . . . 205

Acknowledgements

This book is based on graduate classes given at Harvard University, MIT, UC Berkeley, and University of Bonn in various years. The material corresponds to a course consisting of 30 lectures, 75 minutes each. We are very grateful to all the participants of the classes for their questions, feedback, and the motivation they provided to us. We are also very grateful to all our friends and colleagues who taught us most of the things in this book.

We want to especially thank Alessandra Occelli for the feedback and for help with typing parts of the material. We thank Grigori Olshanski whose treatment of determinantal processes substantially influenced Chapter 4. We thank Leonid Petrov for help with Figures 1.8, 1.15, 8.5, 8.6, 8.7; see his website `https://lpetrov.cc/simulations/` for more simulations. We thank Jaideep Padhi for help with Figures 1.13 and 7.15; see his website `https://vertsix.com` for more simulations.

The work of A.B. was partially supported by the grant SFI-MPS-SIM-00017348 of the Simons Foundation and by the NSF grant DMS-2450323. The work of P.F. was partially supported by the DFG grants EXC 2047/1-390685813 and CRC 1720-539309657. The work of V.G. was partially supported by the NSF grant DMS-2553163.

Chapter 1

What is integrable probability?

In this chapter we make a journey, meeting along the way a number of stochastic systems analyzed in this book and two key players in integrable probability: Schur symmetric polynomials and Tracy-Widom distribution.

1.1 Gaussian universality class

The term "integrable probability" has two parts, and we start discussion from the second one. The *Central Limit Theorem* is, perhaps, the most celebrated result of classical probability theory.

Consider a sample (*i.e.*, a collection of data) obtained by a large number of observations that are randomly and independently generated, and compute the average of the observed values. Repeating the computation many times, one will notice that the computed averages are distributed according to a normal distribution: this is the content of the Central Limit Theorem.

Theorem 1.1. *Let $X_1, X_2, \ldots$ be a sequence of independent, identically distributed (i.i.d.) random variables with mean μ and variance $\sigma^2 < \infty$. Let $S_n := \sum_{k=1}^{n} X_k$. Then*

$$\lim_{n\to\infty} \mathbb{P}\left(\frac{S_n - \mu n}{\sigma\sqrt{n}} \leq s\right) = \int_{-\infty}^{s} \frac{e^{-x^2/2}}{\sqrt{2\pi}} dx. \tag{1.1}$$

This means that, despite the model dependent features such as the mean and the variance, any sum of i.i.d random variables with finite variance will show the same limiting behavior, described by the normal distribution, and fluctuations around the mean value of order $n^{1/2}$. Physical and mathematical systems accurately described in terms of Gaussian statistics are said to be in the *Gaussian universality class*.

Theorem 1.1 illustrates well the universal and the non-universal quantities. The model-dependent and thus non-universal quantities are μ and σ^2, while the $1/2$ exponent in the normalization as well as the normal distribution are universal, *i.e.*, they do not depend on other features of the distribution of X_i beyond the mean and variance.

Theorem 1.1 is also a good illustration of the setting, which distinguishes "integrable probability" from other parts of probability theory. The first proof of the theorem goes back to the famous work of de Moivre [dM67] in the 18th century who studied the case when X_i are Benoulli random variables: $\mathbb{P}(X_i = 1) = p$, $\mathbb{P}(X_i = 0) = 1 - p$ with $0 < p < 1$, so that $\mu = p$ and $\sigma^2 = p(1-p)$. In this situation the probability distribution of S_n is fully explicit:

$$\mathbb{P}(S_n = k) = p^k (1-p)^{n-k} \frac{n!}{k!(n-k)!}, \qquad 0 \leq k \leq n. \tag{1.2}$$

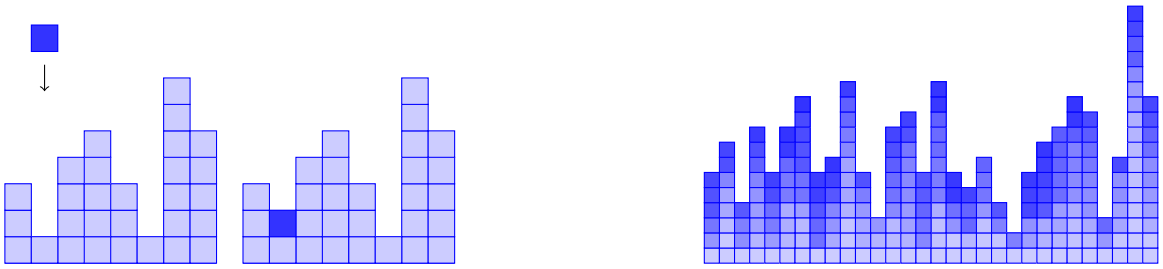


Figure 1.1: Illustration and simulation of the random deposition model.

The asymptotics of this formula can be directly analyzed[1] to yield (1.1): this amounts to using Stirling's formula $n! \sim \sqrt{2\pi n}\left(\frac{n}{e}\right)^n$ for approximating the factorials; the basic form of the latter was also first developed by de Moivre.

In the early 19th century Laplace [Lap20] extended the analysis of de Moivre and made the first steps towards universality by proving the convergence (1.1) for a class of random variables, going beyond the Bernoulli case. The method which Laplace used is reminiscent of the modern "steepest descent method", which will also play a role in our book, see Chapter 5. The next wave of discoveries in the early 20th century created the modern central limit theorems with essentially optimal conditions, through the developments by Chebyshev, Markov, Lindeberg and Lyapunov, see [Lya01, Lin22] and [Uly24]; this included both general distribution of X_i and relaxation of the i.i.d. condition in Theorem 1.1.

The original treatment of de Moivre is what we call the "exactly–solvable" or "integrable" case: here the exact formula (1.2) is available, but it does not extend to general X_i. Similarly, in this book we will be dealing with very special situations where interesting stochastic systems can be analyzed by the means of exact formulas. As in Theorem 1.1, one can expect that the results obtained in this way are universal, *i.e.*, they extend to much greater generality. However, for most of the systems we discuss there is no rigorous proof of it.

1.2 Random deposition

One of our main themes is models related to stochastically growing interfaces. Let us starts with two simple models, which, however, show very different limiting behaviors.

In the *random deposition model*, unit blocks fall down independently and in parallel onto $\mathbb{Z}$ after an exponentially distributed waiting time of parameter 1, see Figure 1.1. Due to the memoryless property of the exponential distribution, this model is a Markov process. Each column evolves independently and is a Poisson process. Denote by $h(x,t)$ the *height function* that gives the value of the height of the column on the site x at time t. By the Law of Large Numbers and the Central Limit Theorem, for any $x \in \mathbb{Z}$,

$$\begin{aligned} &\lim_{t\to\infty} \frac{h(x,t)}{t} = 1, \\ &\frac{h(x,t)-t}{\sqrt{t}} \overset{d}{\Rightarrow} \mathcal{N}(0,1). \end{aligned} \tag{1.3}$$

The model shows linear growth speed and lack of spatial correlations — the limits in (1.3) for different x are independent. The fluctuations belong to the Gaussian universality class.

[1] See Section 5.2 for precise asymptotics obtained using contour integrals and the method of steepest descent.



Figure 1.2: Illustration and simulation of the ballistic deposition model.

1.3 Ballistic deposition and KPZ universality class

It suffices to slightly modify the rules of the growth of the interface to lose the Gaussian behavior of the previous section. Consider the same model, but now, instead of landing on the ground or the interface, the blocks are sticky so that they also get stuck to the boxes of adjacent columns. Each falling block sticks to the first edge it meets as in Figure 1.2: this is known as the *ballistic deposition model*, introduced by Vold in 1959, see [Vol63]. This change in the evolution rules leads to large-time effects: the interface grows faster than in the random deposition model (the value of the velocity is still unknown), and simulations, as in Figure 1.2 and [BS95], show that the height function has smaller fluctuations, on the scale $t^{1/3}$, and nontrivial correlations on the transversal scale of $t^{2/3}$. Moreover, the rescaled height does not converge to the Gaussian distribution anymore.

The ballistic deposition model is believed to belong to the *Kardar-Parisi-Zhang* (KPZ) *universality class*. The key features of the models in this class are:

- **Random local** growth rules: the evolution of the height function depends only the local (in space and time) configuration of the interface and is being driven by random noise, which quickly decorrelates in space and time.
- **Smoothing**: there is a smoothing mechanism implying that deep holes are rapidly filled to smooth the interface. .
- **Non-linearity of the speed of growth**: the vertical effective growth rate should depend non-linearly on the local slope of the interface.

Simulations, such as the one in Figure 1.3, make one believe that the ballistic deposition model should indeed have these features. Mathematically rigorous results are limited, see introduction in [GRSZ25] for the most recent developments.

The KPZ universality class was introduced in the context of studying the motion of growing interfaces in 1986 in a paper of Kardar, Parisi and Zhang [KPZ86], where they studied a continuous stochastically growing height function $h(x,t)$ given in term of a stochastic PDE, known as the *KPZ equation*:

$$\frac{\partial h}{\partial t}(x,t) = \frac{1}{2}\frac{\partial^2 h}{\partial x^2}(x,t) - \frac{1}{2}\left(\frac{\partial h}{\partial x}(x,t)\right)^2 + \xi(x,t), \tag{1.4}$$

where $\xi(x,t)$ is Gaussian space-time white noise. Special efforts are required to make sense of this equation, since squaring white noise is an a priori ill-defined procedure; see *e.g.*, [BG97, ACQ11, Hai13, GP17] for different rigorous approaches. The equation contains the key features of random growth: local randomness (the noise ξ), the smoothing (from the Laplacian), the non-linearity (from the square of the gradient).

One of the major open questions is to produce an analogue of Theorem 1.1 and (1.3) which would cover generic models in the KPZ class, including ballistic deposition and many others.

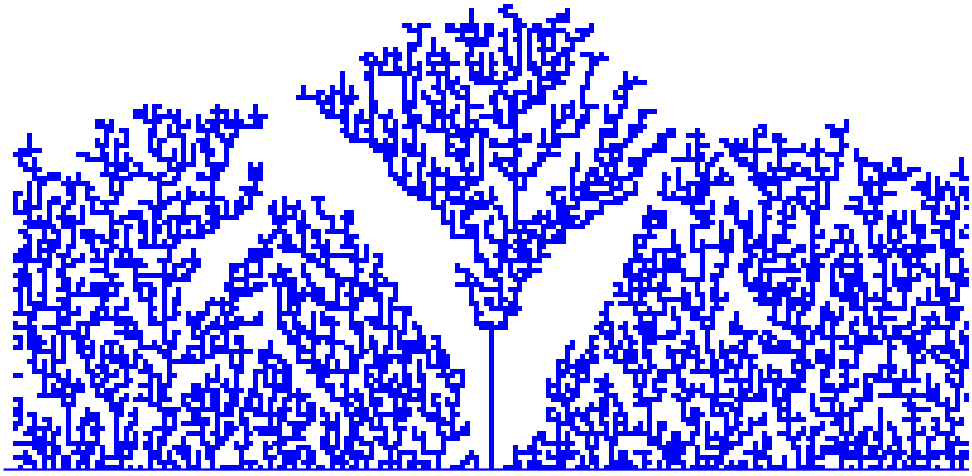


Figure 1.3: Ballistic deposition started from a stack of 30 boxes at the origin. The picture shows the configuration after ≈ 6666 depositions in the observation window.

1.4 Last passage percolation: an integrable member of the KPZ class

Let us now introduce an integrable growth, which plays a role for the KPZ class that is similar to the one played by de Moivre's Bernoulli case for Theorem 1.1.

Consider an interface modeled by a height function $h(x,t)$, $x \in \mathbb{Z}$, $t \in \mathbb{Z}_{\geq 0}$, with $h(x \pm 1, t) - h(x,t) \in \{-1, 1\}$. At time 0 the function is initialized as a *wedge* $h(x,0) = |x|$. The height function then evolves in discrete time according to the following dynamics: each local minimum turns into a local maximum after a geometrically distributed waiting time with parameter q, *i.e.*, of distribution $\mathbb{P}(\xi = k) = (1-q)q^k$, $k = 0, 1, 2, \ldots$, see Figure 1.4. Note that $\xi = 0$ with positive probability, and therefore many boxes can be added simultaneously.

An alternative description of the dynamics is obtained by starting with an array $w_{i,j}$, $i, j = 1, 2, \ldots$, of i.i.d. geometrically distributed waiting times for the local valley at (i,j) to become a local maximum. We further define the absorbtion times $t_{i,j}$ through the recurrence

$$t_{i,j} = \max(t_{i-1,j}, t_{i,j-1}) + w_{i,j},$$

which is solved by iterating

$$t_{i,j} = \max_{\pi:(1,1)\to(i,j)} \sum_{(k,l)\in\pi} w_{k,l}, \tag{1.5}$$

where the summation is over paths π made out of consecutive elementary steps of $(1,0)$ or $(0,1)$. For each $t = 0, 1, 2, \ldots$, we can further define the set of all boxes absorbed by this time as $\{(i,j) \mid t_{i,j} \leq t\}$. Rotating this set by $\pi/4$, rescaling by $\sqrt{2}$, and reading the top border, we arrive at the graph of $h(x,t)$ as a function of x, see the right panel of Figure 1.4 and a simulation in Figure 1.5. The evolution of $h(x,t)$ can be also viewed as a discrete time version of the Totally Asymmetric Simple Exclusion process (TASEP) — in the latter the waiting times $w_{i,j}$ are exponential rather than geometric random variables.

The representation (1.5) identifies $t_{i,j}$ with the *last passage time* and the model in this form is called the *last passage percolation* (LPP) with geometric weights. The name originates from the following interpretation: a group of people enters into the site $(1,1)$ and then travels from $(1,1)$ to (i,j) by all possible monotone paths. It takes time $w_{i,j}$ in order to enter the site (i,j) from one of its neighbors. Then $t_{i,j}$ is the time when the last person arrives at (i,j) (where we agree to include the waiting time $w_{1,1}$ in the total time).

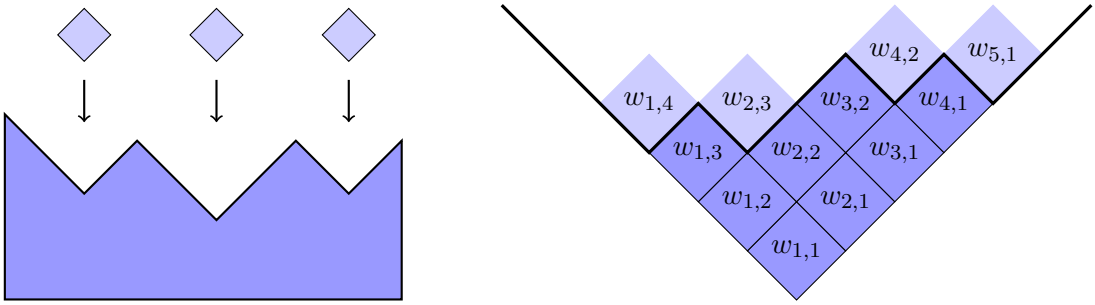


Figure 1.4: Integrable evolution of the height function.

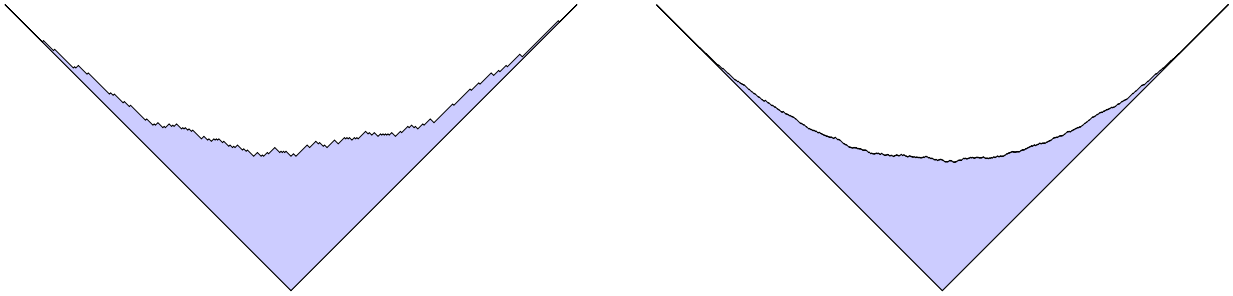


Figure 1.5: Simulation of $h(x,t)$ for geometric LPP model with $q = 0.8$, $t = 1000$ and $t = 5000$.

The geometric LPP model is believed to belong to the same KPZ class as the ballistic deposition of the previous section. Former, in contrast to the latter, is very well understood by now with plenty of asymptotic results available. The solvability of the model is based on *Schur symmetric polynomials* which we now introduce.

Definition 1.2. *The* Schur polynomial $s_\lambda(x_1,\dots,x_N)$ *is a symmetric Laurent polynomial in* N *variables* $x_1,\dots,x_N$ *parametrized by* N*–tuple of integers* $\lambda_1 \geq \lambda_2 \geq \dots \geq \lambda_N$ *(called* signatures*) and defined by*

$$s_\lambda(x_1,\dots,x_N) = \frac{\det\left[x_i^{\lambda_j+N-j}\right]_{1\leq i,j\leq N}}{\prod_{1\leq i<j\leq N}(x_i-x_j)}. \tag{1.6}$$

The first appearance of the ratio in the right-hand side of (1.6) dates more than 200 years back to the work of Cauchy [Cau15], see [Sta99, Notes at the end of Chapter 7] for the historic overview. A century later Schur realized the relevance of s_λ to the representation theory of symmetric, general linear, and unitary groups. In particular, [Sch01] matched the Schur polynomials with the characters of irreducible representations[2] of the unitary group $U(N)$ (or general linear group $GL(N;\mathbb{C})$). In other words, each s_λ corresponds to an irreducible representation T_λ over $\mathbb{C}$, *i.e.*, to a homomorphism to the group of linear automorphisms of a linear space V

$$T_\lambda : U(N) \mapsto GL(V;\mathbb{C}).$$

[2]Although representation theory sits in the background and underlies integrability of many of the stochastic systems of our interest, we will not use it directly for the asymptotic analysis, and the representation-theoretic paragraphs can be skipped without loss of understanding.

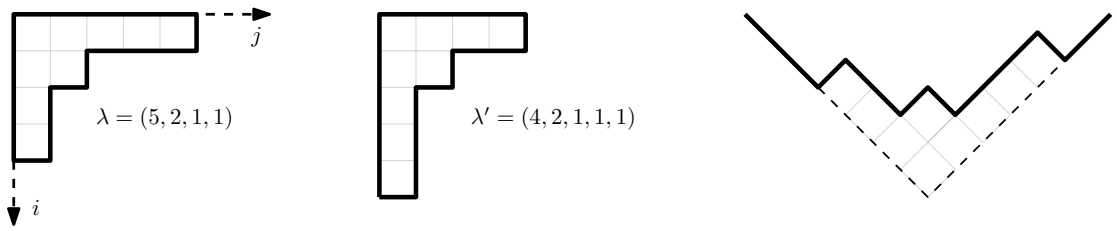


Figure 1.6: The Young diagram $\lambda = (5, 2, 1, 1)$ in English notation, its transpose, and its Russian notation.

The Weyl's character formula identifies

$$s_\lambda(x_1, \dots, x_N) = \mathrm{Trace}\left(T_\lambda \left[\begin{pmatrix} x_1 & 0 & \\ 0 & \ddots & \\ 0 & & x_N \end{pmatrix} \right] \right).$$

Throughout the book we will only use non-negative signatures, *i.e.*, such that $\lambda_N \geq 0$. In this situation, they are also called *partitions*.

Definition 1.3. *A* partition *of n is a sequence of non-negative integers $\lambda = (\lambda_1 \geq \lambda_2 \geq \cdots \geq 0)$ such that $\sum_{i=1}^{\infty} \lambda_i = n$. The numbers λ_i are called* parts *of λ, the number n is the* size *of λ denoted as $|\lambda|$, and the number of non-zero parts in λ is called the* length *of λ and is denoted as $\ell(\lambda)$.*

The difference between partitions and non-negative signatures is that the latter have prescribed number of parts, N, while the former do not keep track of this parameter. Partitions that differ by zero parts only are usually considered the same.

We identify each partition of n with a corresponding *Young diagram* of size n, which is a collection of n unit boxes in the plane with ith row having λ_i boxes. For this reason the λ_i's are sometimes called the *row lengths* of λ. There are different ways to draw Young diagrams; we adopt two of them known as the traditional "English notation" and the "Russian notation" (after the works of Vershik and Kerov). The former is shown in the left panel of Figure 1.6: in that drawing the index i grows from top to bottom and the Young diagram has λ_i boxes in the ith row counting from the top. If we flip the Young diagram λ drawn in English notation with respect to the main diagonal $i = j$, then we obtain a *transposed diagram* λ', as shown in the center panel of Figure 1.6. The row lengths of λ' are the column lengths of λ. In other words, for each i, λ'_i is equal to the number of j such that $\lambda_j \geq i$. Rotating the drawing of λ' by 135° counter–clockwise we obtain the *Russian notation* for the Young diagram, which is shown in the right panel of Figure 1.6; the set $\{(i, j) \mid t_{i,j} \leq t\}$ for LPP also forms a Young diagram in the Russian notation in the right panel of Figure 1.4. As is common, we will use partitions and Young diagrams interchangeably.

An important result for the Schur polynomials is the Cauchy summation identity:

$$\sum_{\lambda_1 \geq \lambda_2 \geq \cdots \geq \lambda_N \geq 0} s_\lambda(x_1, \dots, x_N) s_\lambda(y_1, \dots, y_N) = \prod_{i,j=1}^{N} \frac{1}{1 - x_i y_j}, \qquad |x_i y_j| < 1 \text{ for all } i, j. \tag{1.7}$$

In representation-theoretic language, (1.7) can be interpreted as decomposition of the linear space of polynomials in N^2 variables $(v_{i,j})_{i,j=1}^N$, treated as a representation of $U(N) \otimes U(N)$, with two copies of the unitary group acting on the left and on the right on the matrix $N \times N$ matrix $(v_{i,j})_{i,j=1}^N$. A direct

computation shows that the right-hand side of (1.7) is the character of this representation and (1.7) is a manifestation of its multiplicity-free decomposition into $\bigoplus_\lambda (T_\lambda \otimes T_\lambda)$. In Chapter 2 we present a direct elementary verification of (1.7) not using any representation theory.

The Cauchy identity motivated Okounkov [Oko01a] to define a *Schur measure* as the probability distribution on N–tuples $\lambda_1 \geq \lambda_2 \geq \cdots \geq \lambda_N \geq 0$ with weights:

$$\mathbb{P}(\lambda) = \prod_{i,j=1}^{N} (1 - x_i y_j) \cdot s_\lambda(x_1, \ldots, x_N) s_\lambda(y_1, \ldots, y_N). \tag{1.8}$$

The relevance of the Schur measures for the LPP problems was realized by Johansson[3] in [Joh00] by using the Robinson-Schensted-Knuth correspondence and eventually proving the following result:

Theorem 1.4. *Let $t_{i,j}$ be as in* (1.5) *with i.i.d. geometric $w_{i,j}$. Let $\lambda_1 \geq \cdots \geq \lambda_N$ be distributed as* (1.8) *with $x_1 = \cdots = x_N = y_1 = \cdots = y_N = \sqrt{q}$. Then[4], for constants $c_1, c_2 > 0$, we have:*

1. *In distribution, $t_{N,N} \stackrel{d}{=} \lambda_1$.*
2. *With F_2 denoting the distribution function of the GUE Tracy-Widom distribution,*

$$\lim_{N\to\infty} \mathbb{P}\left(\frac{t_{N,N} - c_1 N}{c_2 N^{1/3}} \leq s \right) = F_2(s). \tag{1.9}$$

It is instructive to compare (1.9) with (1.1): the first order linear growth cN is similar in both formulas; the size of fluctuations is much smaller in (1.9) — $N^{1/3}$ rather than $N^{1/2}$; the Tracy-Widom distribution F_2 replaces the Gaussian limit. It is believed that a similar result to (1.9) (with model-dependent constants) should exist universally, for any "good" choice of the distribution of i.i.d. random variables $w_{i,j}$. However, rigorous results at this moment are limited to very few particular cases.

We discuss the Tracy–Widom distribution in Section 5.9. It was originally discovered in the context of random matrix theory and the following result can be found in [TW94].

Theorem 1.5. *Let H_N denote a random $N \times N$ complex Hermitian matrix, whose diagonal matrix elements are i.i.d. $\mathcal{N}(0,1)$ and the elements above the diagonal are i.i.d. $\mathcal{N}(0, \frac{1}{2}) + \mathbf{i}\mathcal{N}(0, \frac{1}{2})$, and let λ_1^N denote the largest eigenvalue of H_N. Then*

$$\lim_{N\to\infty} \mathbb{P}\left(\frac{\lambda_1^N - 2N^{1/2}}{N^{-1/6}} \leq s \right) = F_2(s). \tag{1.10}$$

Two remarks are in order. First, the index 2 in the F_2 notation corresponds to our use of complex matrices; if we used real symmetric matrices instead, then an analogue of (1.10) would lead to *another*, GOE Tracy-Widom distribution F_1 instead[5]. Second, scaling exponents are different between (1.10) and (1.9) only because of our choice of the normalization of H_N, and they would be the same, if we multiplied H_N and λ_1^N by $N^{1/2}$. The latter rescaling is natural, because asymptotically it puts N eigenvalues into an interval of width proportional to N.

Similarly, just as Theorem 1.1 implied the asymptotics of random deposition model (1.3), Theorem 1.4 can be used to achieve the law of large numbers and scaling limit of fluctuations for the height function $h(0,t)$ as $t \to \infty$. The recentered and rescaled one-point limit will be given by the distribution F_2. In contrast to (1.3), the limits of $h(x,t)$ for varying values of x with shifts of order $N^{2/3}$ are now going to be highly dependent: the random curve governing the spatial limit is called the *Airy$_2$ process*. We will not study it in any detail, only introducing the proper rescalings in the exercises for Chapter 6.

[3]The work of Johhanson is independent from [Oko01a] and he uses different notational conventions.

[4]See Corollary 5.26 for the values of c_1 and c_2.

[5]One also finds F_1 in the study of LPP, when dealing with point-to-line, rather than point-to-point passage times, see [FS11].

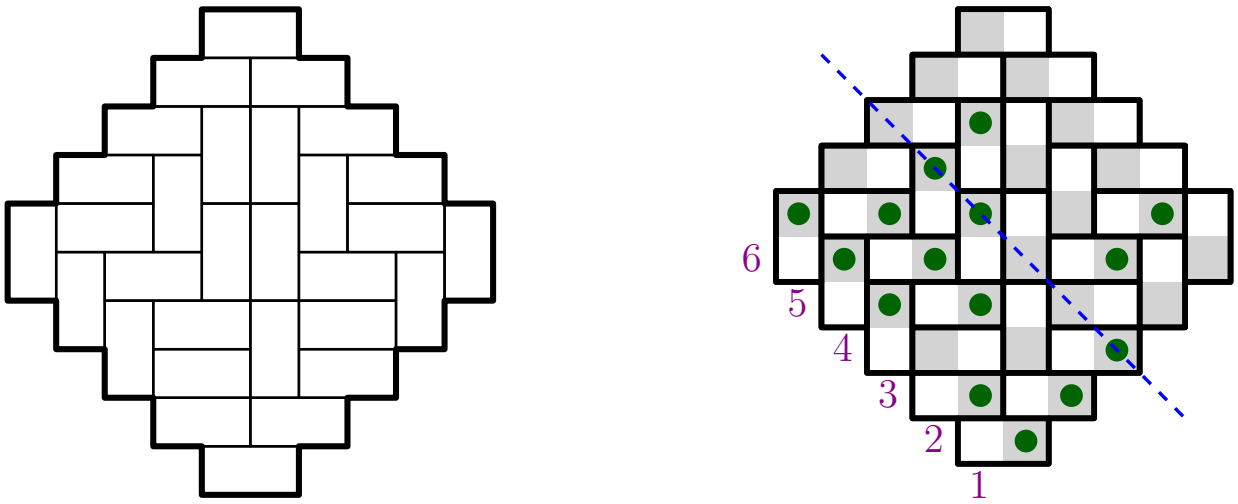


Figure 1.7: A domino tiling of the Aztec diamond of size $n = 5$ and corresponding particle system.

1.5 Domino tilings

The same algebraic structure of Schur polynomials and Schur measures underlies many other integrable stochastic systems.

We start the discussion of *domino tilings* on the square grid, where each domino is either a 2×1 or 1×2 rectangle. A general setup is to draw a large finite domain on the grid and study one of its tilings, chosen uniformly at random among all possibilities. One can tile various domains, but we concentrate on a particular one known as the *Aztec diamond*, mostly due to its fruitful combinatorics.

The Aztec diamond of size n is roughly a 45° rotated square with diagonal length $2n$ traced on the square grid, as shown in Figure 1.7. Interestingly, the total number of domino tilings of the diamond admits a very simple formula — it is $2^{n(n+1)/2}$, as we will prove in Chapter 6.[6]

It is convenient to distinguish not two (vertical and horizontal), but *four* types of dominos. For that we color the grid in a checkerboard pattern, in such a way that the bottom (*i.e.*, the Southernmost) left-right squares of the diamond are white-black, cf. the right panel of Figure 1.7. We call a horizontal domino *South* if its left square is white and it is called *North* otherwise. A vertical domino is *West* if its top square is black and it is called *East* otherwise. The origin of these names is readily seen on the sample of uniformly random tiling of a large Aztec diamond in Figure 1.8: in a typical tiling, the bottom part of the diamond is occupied by South dominos; the top, left and right parts are occupied by North, West and East dominos, respectively.

Once we distinguished the four types, a larger simulation in the right panel of Figure 1.8 reveals intriguing asymptotic phenomenology for the uniformly random domino tilings. We will study it in detail in Chapter 6 revealing the appearances of the Arctic circle, Tracy-Widom distributions, and the Gaussian free field.

The domino tilings also enjoy a connection to Schur polynomials. One combinatorial way to see it is through the interlacing particle configurations. Choose one out of two horizontal types of lozenges and one out of two vertical types. For the sake of concreteness, we choose South and West dominos. We put a particle at the black squares of such dominos and arrive at an interlacing particle configuration,

[6] This was first proved by Elkies, Kuperberg, Larsen, and Propp [EKLP92] in 1992.

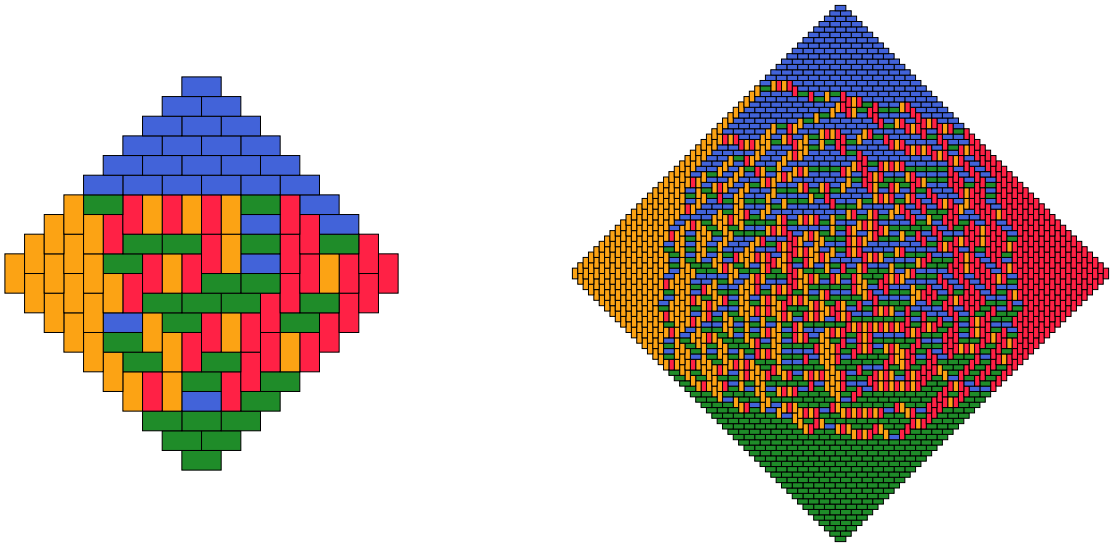


Figure 1.8: Left panel: a uniformly random tiling of an Aztec diamond of size $N = 10$. The North dominoes are blue, the South are green, the East are red, and finally the West dominoes are yellow. Right panel: $N = 50$.

as shown in the right panel of Figure 1.7. If we rotate the picture by 135° clockwise and encode each particle by 1 and the absence of a particle by 0, then we obtain a $n \times (n+1)$ matrix. It is also convenient to supplement the matrix by the row of all 1's at the top, thus arriving at a $(n+1) \times (n+1)$ matrix. In terms of the particle configuration, as in the right panel of Figure 1.7, we added six particles at positions 123456 (for $n = 5$) outside the diamond along its bottom–left border. The left panel of Figure 1.9 shows the matrix corresponding to the tiling of Figure 1.7.

We further encode the positions of all particles (or positions of 1's in the matrix) by an array of numbers. The k particles of row k are encoded by a k–tuple of decreasing integers; each integer is at least 1 and at most $n + 1$. Figure 1.9 (right panel) shows the coordinates of the particle configuration corresponding to the tiling of Figure 1.7. Note that the coordinates of the particles satisfy the constraints $\ell_i^{j+1} \geq \ell_i^j \geq \ell_{i+1}^{j+1}$:

$$\begin{array}{ccccccc} \ell_1^3 & & & \ell_2^3 & & & \ell_3^3 \\ & \searrow & \swarrow & & \searrow & \swarrow & \\ & \ell_1^2 & & & \ell_2^2 & & \\ & & \searrow & \swarrow & & & \\ & & & \ell_1^1 & & & \end{array} \tag{1.11}$$

In addition, the numbers in each row are distinct, *i.e.*, strictly ordered. Such arrays of numbers are sometimes called *strict Gelfand–Tsetlin patterns*, with other used name being *monotonone triangles*.

It turns out that the k particles in the kth row are again distributed by a variant of the Schur measure, given by:

$$\mathbb{P}(\lambda) = \prod_{i=1}^{A} \prod_{j=1}^{B} \frac{1}{1 + x_i y_j} \cdot s_\lambda(x_1, \ldots, x_A) s_{\lambda'}(y_1, \ldots, y_B), \tag{1.12}$$

where we emphasize the appearance of the transposed partition λ' in the formula.

$$\begin{pmatrix} 1 & 1 & 1 & 1 & 1 & 1 \\ 1 & 1 & 0 & 1 & 1 & 1 \\ 1 & 0 & 1 & 1 & 1 & 0 \\ 1 & 0 & 0 & 1 & 1 & 0 \\ 0 & 1 & 0 & 0 & 1 & 0 \\ 0 & 1 & 0 & 0 & 0 & 0 \end{pmatrix}$$

$$\begin{array}{ccccccccccc} 6 & & 5 & & 4 & & 3 & & 2 & & 1 \\ & 6 & & 5 & & 4 & & 2 & & 1 & \\ & & 5 & & 4 & & 3 & & 1 & & \\ & & & 5 & & 4 & & 1 & & & \\ & & & & 5 & & 2 & & & & \\ & & & & & 2 & & & & & \end{array}$$

Figure 1.9: Particle configuration encoded in a matrix (left panel) and the strict Gelfand–Tsetlin pattern corresponding to the tiling of Figure 1.7. The numbers in the pattern correspond to the coordinates of 1's in the matrix.

The exact connection is delivered by the following theorem, as well as the consequent asymptotic theorem proved by [Joh05].

Theorem 1.6. *Consider a uniformly random domino tiling of the $n \times n$ Aztec diamond and encode the kth row in the corresponding strict Gelfand-Tsetlin pattern via $(\ell_1^k > \ell_2^k > \cdots > \ell_k^k) = (\lambda_1 + k, \lambda_2 + k - 1, \ldots, \lambda_k + 1)$. Then:*

1. *λ_1 has the same distribution as (1.12) with $A = k$, $B = n - k$, and all x_i and y_j variables set to 1.*
2. *For each $0 < \kappa < 1$ with $\kappa \neq 1/2$, there exist two constants $c_1(\kappa)$ and $c_2(\kappa)$ such that*

$$\lim_{n\to\infty} \mathbb{P}\left(\frac{\ell_1^{\kappa n} - c_1(\kappa) n}{c_2(\kappa) n^{1/3}} \leq s \right) = F_2(s). \tag{1.13}$$

Explicit formulas for the centering and scaling constants $c_1(\kappa)$, $c_2(\kappa)$ can be extracted from the Johanasson's work on the Aztec diamond [Joh05].

1.6 Alternating sign matrices and the six-vertex model

The Aztec diamond with checkerboard coloring possesses two reflection symmetries, one of which was lost when we passed to the particles and Gelfand-Tsetlin patterns. It can be reconstructed by considering the *alternating sign matrices*, which are differences of consecutive rows of the matrix in Figure 1.9. Namely, we subtract the second row from the first, subtract the third row from the second, etc. The last row is kept unchanged. We arrive at a matrix filled with $\mathbf{0}$s, $\mathbf{1}$s and $-\mathbf{1}$s, cf. Figure 1.10. The sum of the matrix elements in each row or column of such matrix is 1, and $\mathbf{1}$s interlace with $-\mathbf{1}$s in each row and column, hence the name alternating sign matrix, or ASM, for short. It is important to note that the above constructed map from the domino tilings of the size n Aztec diamond to $(n+1)\times(n+1)$ alternating sign matrices is *not* bijective — each ASM corresponds to $2^{k_{-\mathbf{1}}}$ tilings, where $k_{-\mathbf{1}}$ is the total number of $-\mathbf{1}$'s in this ASM. One way to see that is by observing that each particle in the configuration (as in the right panel in Figure 1.7) corresponding to $-\mathbf{1}$ is a top corner of a 2×2 square covered with two dominos. These two dominos can either be oriented horizontally or vertically without changing the corresponding particle configuration. The total number of $(n + 1) \times (n + 1)$ alternating sign matrices is also much smaller than the total number of domino tilings of the Aztec Diamond of size n. The former is given by the following elegant formula, first conjectured in [MRR83], and proven in [Zei96, Kup96]; we give our

$$\begin{pmatrix} 0 & 0 & 1 & 0 & 0 & 0 \\ 0 & 1 & -1 & 0 & 0 & 1 \\ 0 & 0 & 1 & 0 & 0 & 0 \\ 1 & -1 & 0 & 1 & 0 & 0 \\ 0 & 0 & 0 & 0 & 1 & 0 \\ 0 & 1 & 0 & 0 & 0 & 0 \end{pmatrix}$$

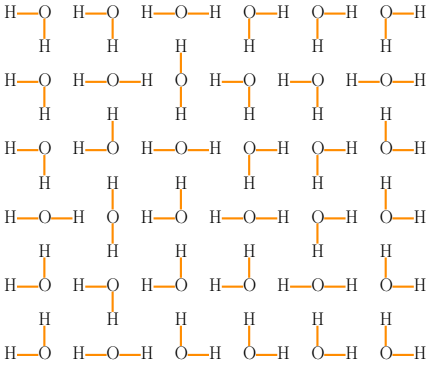


Figure 1.10: Left Panel: the alternating sign matrix corresponding to the tiling of Figure 1.7 and particle configuration of Figure 1.9. Right panel: the corresponding configuration of the square ice model with domain wall boundary conditions.

proof in Chapter 7:

$$\#\{(n+1)\times(n+1)\text{ ASMs}\} = \prod_{i=0}^{n} \frac{(3i+1)!}{(n+1+i)!}. \tag{1.14}$$

The alternating sign matrices sit at a crossroads where many well-studied $2d$ systems from combinatorics and statistical mechanics meet. The ASMs first appeared in the enumeration of terms in *Dodgson's condensation algorithm* for recursive evaluation of the determinant of a square matrix; they are also related to the notion of *λ–determinant*, see [RR86, DF13]. The right–hand side of (1.14) also counts the Totally Symmetric Self–Complementary Plane Partitions (TSSCPP), see [MRR83, MRR86]: this is an equicount without a bijective proof and combinatorialists have been trying to make sense of it for the last 30 years.

In another direction, the ASMs are in bijection with configurations of a *square ice* model (first introduced in [Lie67a] as a simplification of a 3d model of [Pau35]), which we now describe. Consider a square grid with atoms $\mathbf{O}$ of oxygen located at the vertices and atoms $\mathbf{H}$ of hydrogen positioned at midpoints of edges. A configuration of the model is a perfect matching of these atoms into molecules of water $\mathbf{H_2O}$, cf. the right panel of Figure 1.10. Another name for the square ice is the *six–vertex model* because there are precisely six ways to link an oxygen to two out of the surrounding four hydrogens, as in Figure 1.12.

For a precise mathematical definition, one typically considers a finite subdomain of the grid and matchings of the atoms inside this domain into molecules. The domain related to the $(n+1)\times(n+1)$ ASMs is the $(n+1)\times(n+1)$ square with hydrogens along the right and left boundaries and alternating hydrogens with oxygens along top and bottom boundaries, as in the right panel of Figure 1.10. Since 1980s this is known in the statistical mechanics literature as the *domain wall boundary conditions*. One readily sees that there are $(n+1)^2$ oxygens and $2(n+1)^2$ hydrogens, and there are plenty of perfect matchings into the molecules of water; one of such matchings is shown in Figure 1.10. The bijection between the configurations of the molecules in the $(n+1)\times(n+1)$ square and ASMs is very simple: one replaces each $\mathbf{O}$ with either $\mathbf{0}$, $\mathbf{1}$ or $-\mathbf{1}$ by the following rule. Every $\mathbf{O}$ in a horizontal $\mathbf{H_2O}$ molecule corresponds to $\mathbf{1}$, every $\mathbf{O}$ in a vertical $\mathbf{H_2O}$ corresponds to $-\mathbf{1}$, and the remaining $\mathbf{O}$'s turn into $\mathbf{0}$'s.

Although being clearly two–dimensional and flat, the square ice still mimics the structure of the real world ice; for instance, in the latter each oxygen is also surrounded by four hydrogens, cf. Figure 1.11. Similarities go further, as the computation of the leading order asymptotics for the partition function (*i.e.*,

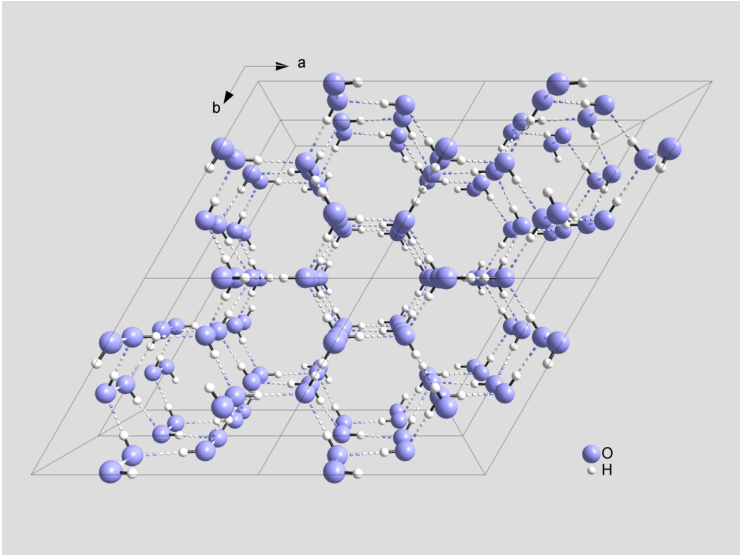


Figure 1.11: Structure of the real world ice [From Wikipedia]

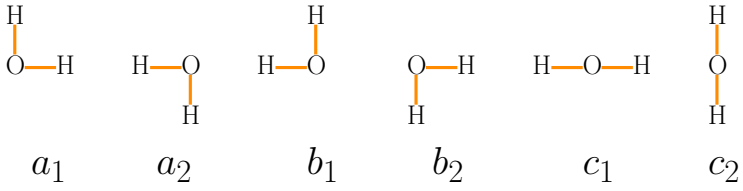


Figure 1.12: Weights of six types of vertices

the total number of the configurations) on the torus [Lie67a] closely matched the experimentally found *residual entropy of the ice*. Much more recent experimental work tried to force the real world ice to indeed form the square lattice in extreme conditions, such as when a very thin layer is squeezed between two sheets of the graphene; the results of these experiments were mixed, see [ASLW$^+$15] and [ZYW$^+$15].

When speaking about random configurations of the six-vertex model, one typically chooses six weights $a_1, a_2, b_1, b_2, c_1, c_2$ corresponding to the vertex types, for example, as in Figure 1.12. Then, probability of a configuration is defined in terms of the counts of vertex types as

$$\frac{a_1^{\#(a_1)} a_2^{\#(a_2)} b_1^{\#(b_1)} b_2^{\#(b_2)} c_1^{\#(c_1)} c_2^{\#(c_2)}}{Z(a_1, a_2, b_1, b_2, c_1, c_2)}, \tag{1.15}$$

where $\#(a_1)$ is the number of the vertices of the first type in the configuration, etc., and $Z(a_1, a_2, b_1, b_2, c_1, c_2)$ is the *partition function*, *i.e.*, the normalization constant ensuring that the weights sum up to 1. One can show (cf. [GN25, Section 2]) that the distribution (1.15) depends only on two rather than six parameters: multiplying all weights by the same constant clearly leaves the ratio unchanged, and there are three more similar conservation laws. Here are some special choices of the parameters:

- If $a_1 = a_2 = b_1 = b_2 = c_1 = 1$ and $c_2 = 2$, then the measure (1.15) is a projection of the uniform measure on domino tilings by the map described above.

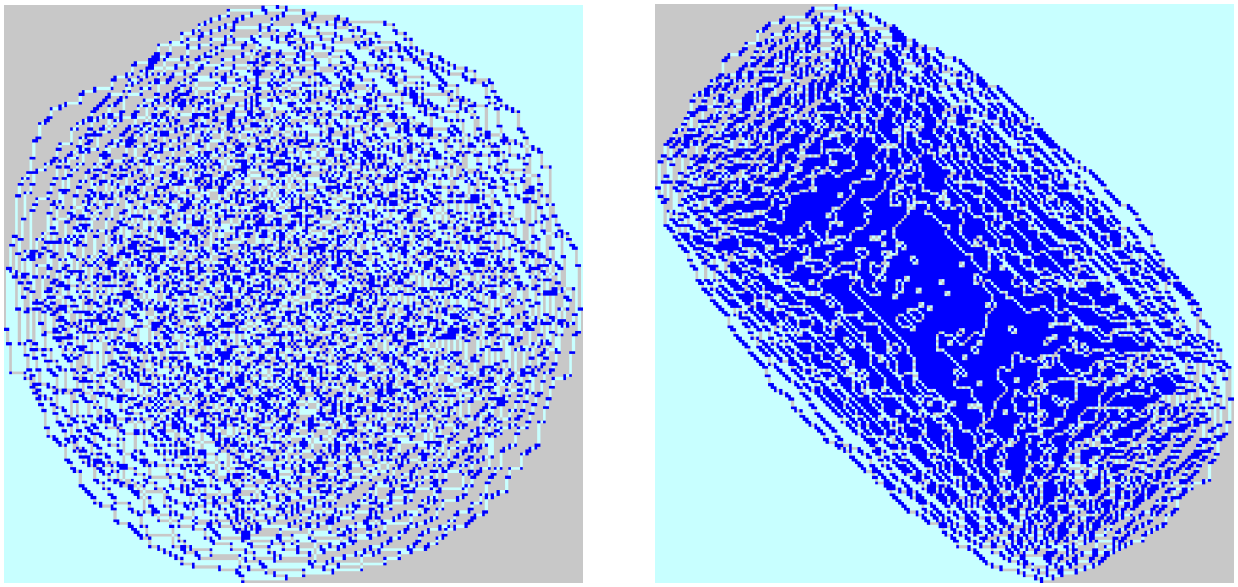


Figure 1.13: Simulations of the six-vertex model in 200×200 square with domain wall boundary conditions. The vertices of a, b, and c weights shown in light blue, light gray, dark blue, respectively. Left: $a_1 = a_1 = b_1 = b_2 = c_1 = c_2 = 1$. Right: $a_1 = a_2 = \frac{1}{2}$, $b_1 = b_2 = 1$, $c_1 = c_2 = 2$.

- More generally, $a_1a_2 + b_1b_2 = c_1c_2$ is called the *free fermion condition*, and in this situation the measure (1.15) can be obtained by projecting a biased measure on dominos, which favors horizontal over vertical dominos (or other way round). This situation is typically simpler than the most general case, because additional algebraic structures are available.

- If $a_1 = a_2 = b_1 = b_2 = c_1 = c_2$, then (1.15) turns into the uniform measure. This is known as "combinatorial" or "ice" point.

Figure 1.13 shows simulations of the model — many features of these pictures remain unexplained at the time of writing this book. For instance, an analogue of Theorems 1.4 and 1.6, including the appearance of F_2, is believed to be true, but has been proven only for the special values of the weights. The island clearly visible in the center of the right-panel of Figure 1.13 is also poorly understood. But a few things are known, as we discuss in Chapter 7.

1.7 Stochastic six-vertex model in the quadrant

Let us now turn to another variation of the square ice, known as the *stochastic six-vertex model*. For this version, it is convenient to use a different representation of the six-vertex model as a collection of lattice paths, which are allowed to touch each other in the corners, but never intersect or share an edge. This is achieved by a bijection of vertices, shown in Figure 1.14. In addition, we set the six weights to $1, 1, b_1, b_2, 1 - b_1, 1 - b_2$. The model is defined in the quadrant $\mathbb{Z}_{>0} \times \mathbb{Z}_{>0}$ with $n = \infty$ version of the domain wall boundary conditions: paths enter from every single position from the left and nothing enters from below.

The vertex types are sampled recursively: we first define the type of the vertex at $(1, 1)$, then types at $(1, 2)$ and $(2, 1)$, then types at $(1, 3)$, $(2, 2)$, and $(3, 1)$, etc. When we need to sample a vertex at (x, y),

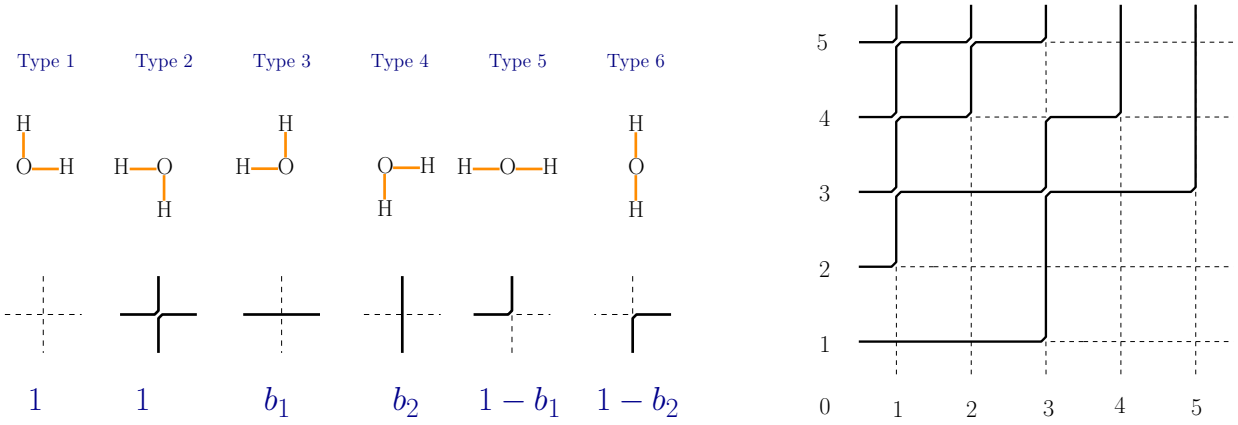


Figure 1.14: Stochastic six-vertex model in paths representation.

we already know whether a path is entering into it from below, and whether a path is entering from the left. Hence, there are four cases:

- If no paths are entering from either direction, then the vertex at (x, y) must have Type 1.
- If paths are entering from both directions, then the vertex at (x, y) must have Type 2.
- If a path is only entering from the left, then we flip an independent biased coin and set the vertex to be of Type 3 with probability b_1 and of Type 5 with probability $1 - b_1$.
- If a path is only entering from below, then we flip an independent biased coin and set the vertex to be of Type 4 with probability b_2 and of Type 6 with probability $1 - b_2$.

The stochastic six-vertex model on the torus first appeared in [GS92], and the version in the quadrant used here originates from [BCG16], see Figure 1.15. The latter paper proved the following asymptotics.

Theorem 1.7. *Assume that $0 < b_2 < b_1 < 1$ and let $H(x, y)$ be the number of paths below (x, y) in the stochastic six-vertex model in the quadrant. For any x, y such that $\frac{1-b_1}{1-b_2} < \frac{x}{y} < \frac{1-b_2}{1-b_1}$, we have*

$$\lim_{L\to\infty} \mathbb{P}\left(\frac{H(Lx, Ly) - Lc_1(x, y)}{-c_2(x, y)L^{1/3}} \le s\right) = F_2(s).$$

The exact values of $c_1(x, y)$ and $c_2(x, y)$ can be found in [BCG16, Theorems 1.1, 1.2], but note $x \leftrightarrow y$ flip between our notations here and that paper. Theorem 1.7 is a harder and more recent result than the previous theorems of this chapter. In Chapter 8 we will prove it by again exploiting a connection to the Schur measures, which becomes more delicate in this situation. The following statement is an example of this connection.

Theorem 1.8. *Let $H(N, N)$ be the number of paths below $(N + \frac{1}{2}, N + \frac{1}{2})$ in the stochastic six-vertex model in the quadrant with $b_1 = \frac{1-u}{1-tu}$ and $b_2 = t\frac{1-u}{1-tu}$, $0 < u < 1$. Let $\lambda_1 \ge \cdots \ge \lambda_N \ge 0$ be distributed as the Schur measure* (1.8) *with parameters chosen so that $x_1 = \cdots = x_N = y_1 = \cdots = y_N = \sqrt{u}$. Then, for each $N = 1, 2, \ldots$ and each $w \in \mathbb{C}$, we have*

$$\mathbb{E}_{6v}\Big(\big(1 - w\big)\big(1 - wt\big)\cdots\big(1 - wt^{H(N,N)-1}\big)\Big) = \mathbb{E}_{\mathit{Schur}}\prod_{i=1}^{N}\Big(1 - wt^{\lambda_i+N-i}\Big).$$

The notation means that in the left-hand side we take expectation with respect to the six-vertex model, while in the right-hand side it is over the Schur measure (1.8).

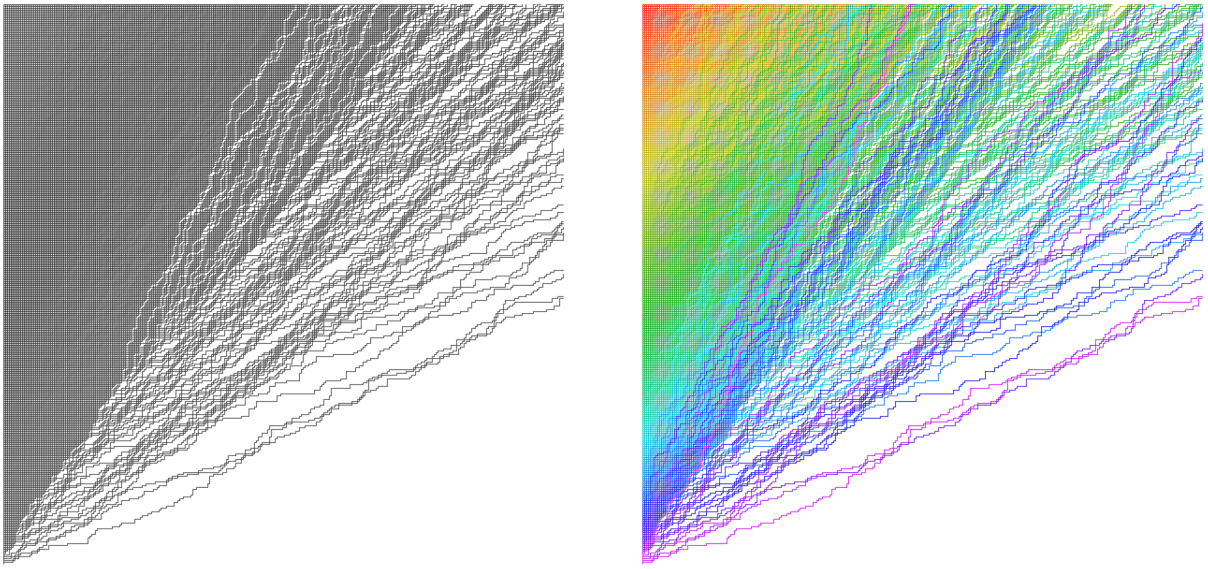


Figure 1.15: Simulation of the stochastic six-vertex model in 300×300 corner of the quadrant with $b_1 = \frac{2}{3}$, $b_2 = \frac{1}{3}$. Right panel is a colored version, as detailed in [BW22].

1.8 Simpler models obtained by degenerations

A number of other interesting and popular stochastic systems can be obtained through limit transitions from the settings of this chapter. We will discuss some of them in more detail later:

- Asymmetric Simple Exclusion Process (ASEP), Totally Asymmetric Simple Exclusion Process, and KPZ equation (1.4) can all be obtained as limits of the stochastic six-vertex model, see Chapter 8.
- Totally Asymmetric Simple Exclusion Process can be also reached from the geometric LPP model as $q \to 1$ and from (biased) domino tilings of the Aztec diamond, see Section 6.2.2.
- Another $q \to 1$ limit from the geometric LPP model leads to a continuum polynuclear growth (PNG) model, and marginals of the latter give rise to the Plancherel measure (on partitions) for the symmetric group and lengths of the longest increasing subsequences in the uniformly random permutations, see Chapter 3.

Chapter 2

Symmetric functions

In this chapter we introduce the algebras of symmetric polynomials and symmetric functions, their main bases and generators. They will be used in the next chapter for the key definitions of these book — the Schur measure and the Schur process, which are central to the asymptotic analysis of various stochastic systems from Chapter 1. More thorough treatments of the theory of symmetric functions are available in the classical textbooks [Mac95] and [Sta99, Chapter 7].

2.1 Algebra of symmetric functions and its generators

Let $\Lambda_N = \mathbb{C}[x_1, \dots, x_N]^{\mathcal{S}_N}$ be the space of polynomials with complex coefficients in variables $x_1, \dots, x_N$ which are symmetric with respect to permutations of the variables x_i's. Λ_N is a graded algebra: polynomials can be multiplied and Λ_N can be decomposed as

$$\Lambda_N = \bigoplus_{n \geq 0} \Lambda_N^n, \tag{2.1}$$

where Λ_N^n consists of homogeneous symmetric polynomials of degree n (together with the zero polynomial). In particular, the 0th graded component Λ_N^0 is the one-dimensional linear space of all constants.

For $\boldsymbol{\alpha} = (\alpha_1, \dots, \alpha_N) \in \mathbb{Z}_{\geq 0}^N$, we set

$$x^{\boldsymbol{\alpha}} = x_1^{\alpha_1} x_2^{\alpha_2} \cdots x_N^{\alpha_N}.$$

We recall Definition 1.3, and further denote

$$\mathbb{Y}_n = \{\text{partitions of } n\}, \quad \mathbb{Y} = \{\text{all partitions}\}, \quad \mathbb{Y} = \bigcup_{n=0}^{\infty} \mathbb{Y}_n, \tag{2.2}$$

where $\mathbb{Y}_0$ contains a single empty partition $0 \geq 0 \geq \dots$. For a partition λ with $\ell(\lambda) \leq N$, *i.e.*, with $\lambda_{N+1} = 0$, we define the *monomial* symmetric polynomials as

$$m_\lambda = m_\lambda(x_1, \dots, x_N) = \sum_{\boldsymbol{\alpha} \text{ are distinct permutations of } (\lambda_1, \dots, \lambda_N)} x^{\boldsymbol{\alpha}}.$$

In particular, omitting 0s from the notations, so that (1) is the same as $(1,0)$ and $(1,0,0)$, we have

$$m_{(1)} = x_1 + x_2 + \cdots + x_N, \quad m_{(2)} = x_1^2 + x_2^2 + \cdots + x_N^2, \quad m_{(1,1)} = \sum_{i<j} x_i x_j = x_1x_2 + x_1x_3 + \dots,$$

where the last sum has $N(N-1)/2$ terms. Clearly, polynomials m_λ with $\lambda \in \mathbb{Y}$ and $\ell(\lambda) \leq N$ form a linear basis in Λ_N. If we additionally fix $|\lambda| = \lambda_1 + \cdots + \lambda_N = n$, then m_λ form a basis of Λ_N^n.

Symmetric functions appear when we allow the number of variables to be infinite. Consider the homomorphism $\pi_{N+1} : \mathbb{C}[x_1, \dots, x_{N+1}] \to \mathbb{C}[x_1, \dots, x_N]$, which sends x_{N+1} to zero and other x_i's to themselves. Note that π_{N+1} maps elements of Λ_{N+1}^n to elements of Λ_N^n for each $n = 0, 1, \dots$, and acts on m_λ as:

$$\pi_{N+1} m_\lambda(x_1, \dots, x_{N+1}) = \begin{cases} m_\lambda(x_1, \dots, x_N), & \text{if } \lambda_{N+1} = 0, \\ 0, & \text{if } \lambda_{N+1} > 0. \end{cases} \tag{2.3}$$

The *graded* projective limit of Λ_N, $N \to \infty$, is called the algebra of symmetric functions and denoted by Λ. Formally,

$$\Lambda^n = \varprojlim_N \Lambda_N^n = \{(f_1, f_2, f_3, \dots) \mid f_j \in \Lambda_j^n,\ \pi_j f_j = f_{j-1}\},$$

$$\Lambda = \bigoplus_{n \geq 0} \Lambda^n.$$

The monomial symmetric function m_λ is the limit of $m_\lambda(x_1, \dots, x_N)$ as $N \to \infty$ or, more formally, a sequence

$$m_\lambda = \big(0, 0, \dots, 0, m_\lambda(x_1, \dots, x_N), m_\lambda(x_1, \dots, x_{N+1}), \dots\big),$$

where $N = \ell(\lambda)$. Equation (2.3) implies that $m_\lambda \in \Lambda$. In fact, $\{m_\lambda\}_{\lambda \in \mathbb{Y}}$ is a linear basis of Λ.

Equivalently, one can think of elements of Λ as formal power series in infinitely many variables $x_1, x_2, \dots$ of bounded degree which are invariant under permutations of the x_i's.

Example 2.1. *Here are a few examples.*

- $\sum_i x_i = x_1 + x_2 + \dots$ *belongs to* Λ*;*
- $\prod_i (1 + x_i) = (1 + x_1)(1 + x_2) \dots$ *does not belong to* Λ*, because it has infinite degree;*
- $\sum_{i<j} x_i x_j = x_1 x_2 + x_1 x_3 + \dots + x_2 x_3 + \dots$ *belongs to* Λ*;*
- 1 *belongs to* Λ*;*
- $x_1 + x_2^2 + x_3 + x_4^2 + \dots$ *does not belong to* Λ*, because it is not symmetric.*

Three simplest families of symmetric functions play an important role when working with Λ:

Definition 2.2. *For $n \geq 1$, the nth* elementary symmetric function e_n *is defined by*

$$e_n = \sum_{i_1 < i_2 < \cdots < i_n} x_{i_1} \cdots x_{i_n}. \tag{2.4}$$

We use the convention $e_0 = 1$.

For $n \geq 1$, the nth complete homogeneous function h_n *is defined by*

$$h_n = \sum_{i_1 \leq i_2 \leq \cdots \leq i_n} x_{i_1} \cdots x_{i_n}. \tag{2.5}$$

We use the convention $h_0 = 1$.

For $n \geq 1$, the nth power sum p_n *is defined by*

$$p_n = \sum_{i \geq 1} x_i^n. \tag{2.6}$$

Relations between these three families are best understood via their *generating functions*.

Definition 2.3. *We define the generating functions:*

$$H(z) = \sum_{k\geq 0} h_k z^k, \qquad E(z) = \sum_{k\geq 0} e_k z^k, \qquad P(z) = \sum_{k\geq 1} \frac{p_k z^k}{k}. \tag{2.7}$$

Lemma 2.4. *The following identities hold:*

$$H(z) = \prod_{i\geq 1} \frac{1}{1-x_i z}, \qquad E(z) = \prod_{i\geq 1}(1+x_i z), \qquad P(z) = -\sum_{i\geq 1} \ln\bigl(1-x_i z\bigr), \tag{2.8}$$

$$H(z)E(-z) = 1, \qquad H(z) = \exp\left(P(z)\right), \qquad P'(z) = \frac{H'(z)}{H(z)}, \qquad P'(-z) = \frac{E'(z)}{E(z)}. \tag{2.9}$$

Proof. We only prove (2.8), as (2.9) is an immediate corollary. For $E(z)$ we open the parentheses:

$$\prod_{i\geq 1}(1+x_i z) = (1+x_1 z)(1+x_2 z)\cdots = 1 + z\sum_{i\geq 1} x_i + z^2 \sum_{1\leq i\leq j} x_i x_j + \cdots = 1 + \sum_{k\geq 1} z^k e_k = E(z).$$

For $H(z)$ we use the geometric series formula and open the parentheses:

$$\prod_{i\geq 1} \frac{1}{1-x_i z} = \prod_{i\geq 1}(1 + x_1 z + x_1^2 z^2 + \dots)(1 + x_2 z + x_2^2 z + \dots)\cdots = 1 + z h_1 + z^2 h_2 + \cdots = H(z).$$

For $P(z)$ we use the Taylor expansion of the logarithm:

$$-\sum_{i\geq 1} \ln\bigl(1-x_i z\bigr) = \sum_{i\geq 1}\left(x_i z + \frac{(x_i z)^2}{2} + \frac{(x_i z)^3}{3} + \dots\right) = p_1 z + \frac{p_2 z^2}{2} + \frac{p_3 z^3}{3} + \cdots = P(z). \quad \square$$

Products of e_n, h_n, p_n also have a special notation. For a partition $\lambda \in \mathbb{Y}$, we set

$$e_\lambda = \prod_i e_{\lambda_i}, \qquad h_\lambda = \prod_i h_{\lambda_i}, \qquad p_\lambda = \prod_i p_{\lambda_i}. \tag{2.10}$$

For the empty partition of 0, we set $e_\emptyset = h_\emptyset = p_\emptyset = 1$.

Theorem 2.5. *Each system $\{e_n\}$, $\{h_n\}$, $\{p_n\}$ consists of algebraically independent generators of Λ,* i.e., *$\Lambda = \mathbb{C}[e_1, e_2, \dots] = \mathbb{C}[h_1, h_2, \dots] = \mathbb{C}[p_1, p_2, \dots]$. Equivalently, each of $\{e_\lambda\}_{\lambda\in\mathbb{Y}}$, $\{h_\lambda\}_{\lambda\in\mathbb{Y}}$, $\{p_\lambda\}_{\lambda\in\mathbb{Y}}$ is a linear basis of Λ.*

Proof. For e_λ Theorem 2.5 follows from triangularity of the $e_\lambda \leftrightarrow m_\mu$ transition:

$$e_{\lambda'} = m_\lambda + \sum_{\mu<\lambda} a_\lambda^\mu m_\mu, \tag{2.11}$$

where λ' is the transpose partition, a_λ^μ are certain real coefficients, and $<$ is the lexicographic ordering, so that

$$(1,1,1,1,1) < (2,1,1,1) < (2,2,1) < (3,1,1) < (3,2) < (4,1) < (5).$$

In order to see (2.11), notice that

$$e_{\lambda'} = e_1^{\lambda_1-\lambda_2} e_2^{\lambda_2-\lambda_3}\cdots = \left(x_1^{\lambda_1-\lambda_2} + \cdots\right)\cdot\left((x_1x_2)^{\lambda_2-\lambda_3} + \cdots\right)\cdot\left((x_1x_2x_3)^{\lambda_3-\lambda_4} + \cdots\right)\cdots,$$

where the product clearly has the leading term x^λ. Since $\{m_\lambda\}_{\lambda\in\mathbb{Y}}$ is a basis and transformation (2.11) is triangular, $\{e_\lambda\}_{\lambda\in\mathbb{Y}}$ is also a basis.

For h_λ we argue in a different fashion by introducing an algebra homomorphism of Λ:

$$\omega : \Lambda \to \Lambda, \qquad \omega(e_n) = h_n, \qquad n = 0, 1, 2, \dots. \tag{2.12}$$

The relationship (2.9) implies

$$\sum_{r=0}^{n} (-1)^r e_r h_{n-r} = 0, \quad n = 1, 2, \dots. \tag{2.13}$$

Since these relations express $\{e_0, \dots, e_n\} \leftrightarrow \{h_0, \dots, h_n\}$ and are symmetric with respect to e's and h's, we conclude that $\omega^2 = \mathrm{Id}$, *i.e.*, ω is an involution. This implies Theorem 2.5 for $\{h_\lambda\}$.

For p_λ, we rewrite (2.9) as *Newton formulas*:

$$n e_n = \sum_{r=1}^{n} (-1)^{r-1} p_r e_{n-r}.$$

This identity allows to express $\{e_n\}$ through $\{p_m\}$ in an invertible (and triangular) way, leading to Theorem 2.5 for $\{p_\lambda\}$. □

2.2 Schur functions

One more linear basis of Λ is the most important for our book — the *Schur symmetric functions*.

We first define the *alternant*, which is a skew-symmetric version of m_λ:

$$\mathrm{Alt}_{\boldsymbol{\alpha}}(x_1, \dots, x_N) = \sum_{\sigma\in\mathcal{S}_N} (-1)^\sigma x_{\sigma(1)}^{\alpha_1} x_{\sigma(2)}^{\alpha_2} \cdots x_{\sigma(N)}^{\alpha_N}, \qquad \boldsymbol{\alpha} = (\alpha_1, \dots, \alpha_N),$$

where $(-1)^\sigma$ is the sign of the permutation σ of N letters. We also denote $\delta_N = (N-1, N-2, \dots, 1, 0)$.

Theorem 2.6. *The Schur symmetric polynomial of* (1.6)*, defined for* $\lambda = (\lambda_1 \geq \cdots \geq \lambda_N \geq 0)$ *as*

$$s_\lambda(x_1, \dots, x_N) = \frac{\mathrm{Alt}_{\lambda+\delta_N}(x_1, \dots, x_N)}{\mathrm{Alt}_{\delta_N}(x_1, \dots, x_N)} = \frac{\det\left[x_i^{\lambda_j+N-j}\right]_{1\leq i,j\leq N}}{\det\left[x_i^{N-j}\right]_{1\leq i,j\leq N}}, \tag{2.14}$$

is a homogeneous symmetric polynomial in $(x_1, \dots, x_N)$ *of degree* $|\lambda|$*. As* λ *varies over* $\mathbb{Y}$ *with* $\ell(\lambda) \leq N$*, polynomials* s_λ *form a linear basis of* Λ_N*.*

Proof. In order to match (1.6) with (2.14), we use the Vandermonde determinant:

$$\prod_{1\leq i<j\leq N} (x_i - x_j) = \det\left[x_i^{N-j}\right]_{1\leq i,j\leq N}. \tag{2.15}$$

In order to prove (2.15), note that the right-hand side is skew-symmetric: it changes its sign under $x_i \leftrightarrow x_j$ and vanishes when $x_i = x_j$. Hence, the right-hand side is divisible by each $(x_i - x_j)$ and thus by the left-hand side. Both sides have degree $N(N-1)/2$, and therefore they have to agree up to a constant factor. Comparing the coefficient of the highest (or any other) monomial, we conclude that the constant is 1.

The same argument shows that (2.14) is a polynomial: $\mathrm{Alt}_{\lambda+\delta_N}$ is skew-symmetric and therefore divisible by the Vandermonde determinant. Since both numerator and denominator in (2.14) are skew-symmetric, their ratio s_λ is symmetric. Computing the degrees of numerator and denominator, we conclude that the degree of s_λ is $|\lambda|$.

Finally, s_λ form a basis in the space of symmetric polynomials, because alternants form a linear basis of the space of skew-symmetric polynomials, and multiplication by Vandermonde is an isomorphism between these two spaces. □

An important property of Schur polynomials is their stability under projections π_N.

Lemma 2.7. *For each $\lambda \in \mathbb{Y}$ with $\ell(\lambda) \le N+1$,*

$$\pi_{N+1} s_\lambda(x_1,\dots,x_{N+1}) = s_\lambda(x_1,\dots,x_N,0) = \begin{cases} s_\lambda(x_1,\dots,x_N), & \text{if } \lambda_{N+1}=0,\\ 0, & \text{if } \lambda_{N+1}>0. \end{cases} \tag{2.16}$$

Proof. If $\lambda_{N+1}=0$, then $s_\lambda(x_1,\dots,x_N,0)$ becomes

$$\frac{\det\begin{bmatrix} x_1^{\lambda_1+N} & \dots & x_1^{\lambda_N+1} & 1\\ \vdots & \ddots & \vdots & \vdots\\ x_N^{\lambda_1+N} & \dots & x_N^{\lambda_N+1} & 1\\ 0 & \dots & 0 & 1 \end{bmatrix}}{\det\begin{bmatrix} x_1^{N} & \dots & x_1^{1} & 1\\ \vdots & \ddots & \vdots & \vdots\\ x_N^{N} & \dots & x_N^{1} & 1\\ 0 & \dots & 0 & 1 \end{bmatrix}} = \frac{\det\begin{bmatrix} x_1^{\lambda_1+N-1} & \dots & x_1^{\lambda_N}\\ \vdots & \ddots & \vdots\\ x_N^{\lambda_1+N-1} & \dots & x_N^{\lambda_N} \end{bmatrix}\cdot x_1x_2\cdots x_N}{\det\begin{bmatrix} x_1^{N-1} & \dots & 1\\ \vdots & \ddots & \vdots\\ x_N^{N-1} & \dots & 1 \end{bmatrix}\cdot x_1x_2\cdots x_N} = s_\lambda(x_1,\dots,x_N).$$

If $\lambda_{N+1}>0$, then each term in $\mathrm{Alt}_{\lambda+\delta_{N+1}}$ vanishes at $x_{N+1}=0$ and so does s_λ. □

Definition 2.8. *For $\lambda\in\mathbb{Y}$, the* Schur symmetric function *s_λ is a sequence*

$$\big(0,\dots,0,s_\lambda(x_1,\dots,x_{\ell(\lambda)}),s_\lambda(x_1,\dots,x_{\ell(\lambda)+1}),\dots\big)\in\Lambda.$$

An important role in our exposition is played by the *Cauchy identity* for the Schur functions.

Theorem 2.9. *Taking two copies of Λ in two sets of variables $(x_1,\dots)$, $(y_1,\dots)$, the following identity of formal power series holds:*

$$H(x;y) := \sum_{\lambda\in\mathbb{Y}} s_\lambda(x_1,x_2,\dots)s_\lambda(y_1,y_2,\dots) = \prod_{i,j\ge1}\frac{1}{1-x_iy_j}$$
$$= \exp\left(\sum_{k\ge1}\frac{p_k(x_1,x_2,\dots)p_k(y_1,y_2,\dots)}{k}\right). \tag{2.17}$$

Each term in $\sum_\lambda$ of (2.17) is an element of the tensor product $\Lambda\otimes\Lambda$, and the sum is a series of homogeneous elements of the tensor product of growing degrees. Expanding the exponent in the right-hand side using $\exp(z)=1+z+\frac{z^2}{2!}+\dots$, we get the same series.

The last equality in (2.17) is obtained by taking $z=y_j$ in $H(z)=\exp\big(P(z)\big)$ of (2.9) and multiplying over j. In order to prove the middle equality we need two auxiliary determinant evaluations.

The first one is the Cauchy–Binet formula, which is a generalization of the well-known identity $\det(AB)=\det A\det B$.

Proposition 2.10. *Choose $K \geq N$ and let $A = \big[A(i,j)\big]$ and $B = \big[B(i,j)\big]$ be two matrices of $N \times K$ format. Then, with $^{\mathsf{T}}$ denoting matrix transposition, we have*

$$\det\left(AB^{\mathsf{T}}\right) = \frac{1}{N!}\sum_{\ell_1=1}^{K}\cdots\sum_{\ell_N=1}^{K}\det\big[A(i,\ell_j)\big]_{i,j=1}^{N}\det\big[B(i,\ell_j)\big]_{i,j=1}^{N}$$
$$= \sum_{K\geq\ell_1>\ell_2>\cdots>\ell_N\geq 1}\det\big[A(i,\ell_j)\big]_{i,j=1}^{N}\det\big[B(i,\ell_j)\big]_{i,j=1}^{N}. \tag{2.18}$$

Remark 2.11. One can take $K=\infty$ or assume the second index of A and B to be continuous, replacing the sums over ℓ_i with integrals. In all such settings, as long as all sides of (2.18) make sense and are absolutely convergent, an analogue of the identity would hold with a similar proof.

Proof of Proposition 2.10. First, note that if some ℓ_i coincide, then the corresponding term in $\sum_{\ell_1=1}^{K}\cdots\sum_{\ell_N=1}^{K}$ in (2.18) vanishes. Together with skew-symmetry of the determinants with respect to the swaps of columns, this implies the second equality in (2.18). For the first equality, we write

$$\sum_{\ell_1=1}^{K}\cdots\sum_{\ell_N=1}^{K}\det\big[A(i,\ell_j)\big]_{i,j=1}^{N}\det\big[B(i,\ell_j)\big]_{i,j=1}^{N}$$
$$= \sum_{\ell_1=1}^{K}\cdots\sum_{\ell_N=1}^{K}\left(\sum_{\sigma,\tau\in\mathcal{S}_N}(-1)^{\sigma\tau}\prod_{j=1}^{N}A(\sigma(j),\ell_j)B(\tau(j),\ell_j)\right)$$
$$= \sum_{\sigma,\tau\in\mathcal{S}_N}(-1)^{\sigma\tau}\prod_{j=1}^{N}\big[AB^{\mathsf{T}}\big](\sigma(j),\tau(j)) = N!\det[AB^{\mathsf{T}}]. \quad \square$$

The second ingredient is the Cauchy determinant evaluation.

Proposition 2.12. *For each $N=1,2,\ldots$ and $x_1,\ldots,x_N$, $y_1,\ldots,y_N$, we have*

$$\det\left[\frac{1}{1-x_iy_j}\right]_{i,j=1}^{N} = \frac{\prod_{1\leq i<j\leq N}(x_i-x_j)(y_i-y_j)}{\prod_{i,j=1}^{N}(1-x_iy_j)}. \tag{2.19}$$

Proof. Change the variables $y_j = 1/z_j$ and divide both sides by $(-1)^N z_1\cdots z_N$ to convert the desired identity into

$$\det\left[\frac{1}{x_i-z_j}\right]_{i,j=1}^{N} \stackrel{?}{=} \frac{\prod_{1\leq i<j\leq N}(x_i-x_j)(z_j-z_i)}{\prod_{i,j=1}^{N}(x_i-z_j)}, \tag{2.20}$$

which is equivalent to

$$\det\left[\frac{1}{x_i-z_j}\right]_{i,j=1}^{N}\prod_{i,j=1}^{N}(x_i-z_j) \stackrel{?}{=} \prod_{1\leq i<j\leq N}(x_i-x_j)(z_j-z_i). \tag{2.21}$$

The left-hand side is a homogenous polynomial of degree $N(N-1)$, which vanishes whenever $x_i=x_j$ or $z_i=z_j$ for some $i<j$. Hence, the left-hand side is divisible by the right-hand side and the ratio is a constant. Computing the coefficient of some monomial, we conclude that this constant is 1. $\square$

Proof of Theorem 2.9. As with most identities in Λ, it is sufficient to prove (2.17) for finite sets of variables $(x_1, \dots, x_N)$ and $(y_1, \dots, y_N)$, *i.e.*, we would like to show that

$$\sum_{\lambda=(\lambda_1\geq\dots\geq\lambda_N\geq 0)} s_\lambda(x_1, \dots, x_N) s_\lambda(y_1, \dots, y_N) \stackrel{?}{=} \prod_{i,j=1}^{N} \frac{1}{1-x_i y_j}. \tag{2.22}$$

By Proposition 2.12 and Definition 2.14, this is equivalent to

$$\sum_{\lambda=(\lambda_1\geq\dots\geq\lambda_N\geq 0)} \mathrm{Alt}_{\lambda+\delta_N}(x_1, \dots, x_N) \mathrm{Alt}_{\lambda+\delta_N}(y_1, \dots, y_N) \stackrel{?}{=} \det\left[\frac{1}{1-x_i y_j}\right]_{i,j=1}^{N}. \tag{2.23}$$

Expanding inside the determinant $\frac{1}{1-x_i y_j} = 1+(x_i y_j)+(x_i y_j)^2+(x_i y_j)^3+\dots$, treating this expression as the matrix element of AB^{T}, where A is $N \times \infty$ matrix $A[i,k] = (x_i)^k$, $k = 0, 1, 2, \dots$, and B is $N \times \infty$ matrix $B[j,k] = (y_j)^k$, $k = 0, 1, 2, \dots$, using Proposition 2.10, and identifying $(\ell_1 > \dots > \ell_N) = (\lambda_1 + N - 1, \lambda_2 + N - 2, \dots, \lambda_N)$, we arrive at (2.23). □

Theorem 2.13. *The Schur functions $\{s_\lambda\}_{\lambda\in\mathbb{Y}}$ form a linear basis of Λ. Their relations with the generators h_n and e_n are given by the Jacobi-Trudi and Nagelbach–Kostka formulas, respectively:*

$$s_\lambda = \det\left[h_{\lambda_i-i+j}\right]_{1\leq i,j\leq N} = \det\left[e_{\lambda'_i-i+j}\right]_{1\leq i,j\leq M}, \tag{2.24}$$

where by definition $h_k \equiv e_k \equiv 0$, for $k < 0$. Here N is an arbitrary integer satisfying $N \geq \ell(\lambda)$, and M is an arbitrary integer satisfying $M \geq \ell(\lambda') = \lambda_1$.

Proof. The Schur functions form a linear basis of Λ as a corollary of the same statement for finite N in Theorem 2.6.

Let us prove the first identity in (2.24). First notice that for $N \geq \ell(\lambda)$ the expression is stable, *i.e.*, remains unchanged under $N \to N+1$. If $\lambda_{N+1} = 0$, then the $(N+1)$st row of $[h_{\lambda_i-i+j}]_{1\leq i,j\leq N+1}$ has the form $(0, 0, \dots, 1)$ and the determinant of $(N+1)\times(N+1)$ matrix reduces to the determinant of its top-left $N \times N$ corner.

Hence, it is sufficient to prove the identity in N variables $(y_1, \dots, y_N)$. For this we claim that for any power series $f(y) = f_0 + f_1 y + f_2 y^2 + \dots$, we have

$$f(y_1)f(y_2)\cdots f(y_N) = \sum_{\lambda=(\lambda_1\geq\dots\geq\lambda_N\geq 0)} \det\left[f_{\lambda_i-i+j}\right]_{i,j=1}^{N} s_\lambda(y_1, \dots, y_N). \tag{2.25}$$

We multiply (2.25) by $\prod_{i<j}(y_i - y_j)$ to get an equivalent skew-symmetric identity:

$$f(y_1)f(y_2)\cdots f(y_N)\prod_{i<j}(y_i - y_j) = \sum_{\lambda=(\lambda_1\geq\dots\geq\lambda_N\geq 0)} \det\left[f_{\lambda_i-i+j}\right]_{i,j=1}^{N} \mathrm{Alt}_{\lambda+\delta_N}(y_1, \dots, y_N). \tag{2.26}$$

The latter identity is obtained by collecting the coefficient of $y_1^{\ell_1} y_2^{\ell_2} \cdots y_N^{\ell_N}$ for $\ell_1 > \dots > \ell_N$ in the left-hand side of (2.25), *i.e.*, in

$$\prod_{i=1}^{N}\left(\sum_{m\geq 0} f_m (y_i)^m\right) \sum_{\sigma\in\mathcal{S}_N} (-1)^\sigma y_1^{N-\sigma(1)} \cdots y_N^{\sigma(N)}.$$

This coefficient is $\det\left[f_{\ell_i-N+j}\right]_{i,j=1}^{N}$, which matches the coefficient of $y_1^{\ell_1}y_2^{\ell_2}\cdots y_N^{\ell_N}$ in the right-hand side of (2.26) under identification $(\ell_1,\dots,\ell_N)=(\lambda_1+N-1,\dots,\lambda_N)$.

The proof of the first identity in (2.24) is finished by applying (2.25) with

$$f(y)=\sum_{m\geq 0}h_m(x_1,\dots,x_N)y^m=\prod_{i=1}^{N}\frac{1}{1-x_iy},$$

where the second equality is (2.8), to the Cauchy summation identity in the form (2.22).

The proof of the second identity $\det\left[h_{\lambda_i-i+j}\right]_{1\leq i,j\leq N}=\det\left[e_{\lambda'_i-i+j}\right]_{1\leq i,j\leq M}$ can be found in [Mac95, Chapter 1, Section 2, (2.9')]. Here is a sketch. Define matrices $H=[h_{i-j}]_{0\leq i,j\leq K}$ and $E=[(-1)^{i-j}e_{i-j}]_{0\leq i,j\leq K}$, with $K=N+M-1$. Using (2.13), one obtains $HE=1$ and $\det[E]=\det[H]=1$. Then $\det\left[h_{\lambda_i-i+j}\right]_{1\leq i,j\leq N}$ is the determinant of a submatrix of H, which is equal to the determinant of the complementary cofactor of E^{T} (see *e.g.*, [Pra94, Section 2.5.2] for this generalization of the Cramer's rule). A straightforward computation identifies the latter with $\det\left[e_{\lambda'_i-i+j}\right]_{1\leq i,j\leq M}$. □

Comparing (2.24) with (2.12), we conclude that the involution ω acts nicely on Schur functions.

Corollary 2.14. *For each $\lambda\in\mathbb{Y}$, we have $\omega(s_\lambda)=s_{\lambda'}$.*

2.3 Skew Schur functions

Schur functions give rise to Schur measures, which we saw being relevant to the integrable probability models in the previous chapter. In order to encode the full two-dimensional systems (*e.g.*, particle configurations in the Aztec diamond in the right panel of Figure 1.7), we need an extension of Schur functions parameterized by two rather than one Young diagrams. These are called skew Schur functions, and they naturally connect to transitions between different sections of the Aztec diamond.

Consider two sets of variables $x=(x_1,x_2,\dots)$, $y=(y_1,y_2,\dots)$ and let (x,y) be the union of these sets. Consider a function $f(x,y)$ symmetric with respect to all permutations of the combined set of all variables x_i and y_j. Since $f(x,y)$ is also symmetric separately and finie degree in the x_i's and separately in the y_j's, it is always possible to express it in the form of a finite sum $f(x,y)=\sum_n f_n(x)g_n(y)$, for some symmetric functions f_n, g_n. For instance, if one takes for $f(x,y)$ the power sum (2.6), then

$$p_k(x,y)=\sum_{i\geq 1}x_i^k+\sum_{i\geq 1}y_i^k=p_k(x)+p_k(y). \tag{2.27}$$

We want to understand how the Schur function $s_\lambda(x,y)$ decomposes.

Definition 2.15. *Take $\lambda\in\mathbb{Y}$ and decompose $s_\lambda(x,y)$ into a linear combination of $s_\mu(y)$, $\mu\in\mathbb{Y}$:*

$$s_\lambda(x,y)=\sum_{\mu\in\mathbb{Y}}s_{\lambda/\mu}(x)s_\mu(y). \tag{2.28}$$

The cofficients of the decomposition are symmetric functions in x, called skew Schur functions $s_{\lambda/\mu}(x)$.

Let us consider some properties of the skew Schur functions.

Proposition 2.16 (Branching or consistency relation)**.** *Let x,y be two sets of variables. Then for any $\lambda,\mu\in\mathbb{Y}$*

$$s_{\lambda/\mu}(x,y)=\sum_{\nu\in\mathbb{Y}}s_{\lambda/\nu}(x)s_{\nu/\mu}(y). \tag{2.29}$$

Proof. Consider three sets of variables x, y, z. Then, by definition

$$s_\lambda(x,y,z) = \sum_{\mu\in\mathbb{Y}} s_{\lambda/\mu}(x,y)s_\mu(z),$$

but also

$$s_\lambda(x,y,z) = \sum_{\nu\in\mathbb{Y}} s_{\lambda/\nu}(x)s_\nu(y,z) = \sum_{\mu\in\mathbb{Y}}\sum_{\nu\in\mathbb{Y}} s_{\lambda/\nu}(x)s_{\nu/\mu}(y)s_\mu(z).$$

Comparison of the coefficient of $s_\mu(z)$ yields (2.29). □

The skew Schur functions can be expressed in terms of the complete homogeneous functions (2.5):

Proposition 2.17. *Set $h_k = 0$ for $k < 0$. Then for any $N \geq \max\{\ell(\lambda), \ell(\mu)\}$*

$$s_{\lambda/\mu} = \det\big[h_{\lambda_i-\mu_j-i+j}\big]_{i,j=1}^{N}. \tag{2.30}$$

This is an extenstion of the Jacobi-Trudi formula of Theorem 2.13, and we refer to [Mac95, Chapter I, Section 5, (5.4)] for the proof; see also Problem 7 at the end of this chapter. The formula (2.30) identifies $s_{\lambda/\mu}$ with minors of an infinite triangular Toeplitz (*i.e.*, constant along the diagonals) matrix:

$$\begin{bmatrix} \ddots & & & & & & \\ & 1 & h_1 & h_2 & h_3 & h_4 & \\ & 0 & 1 & h_1 & h_2 & h_3 & \\ & 0 & 0 & 1 & h_1 & h_2 & \\ & 0 & 0 & 0 & 1 & h_1 & \\ & 0 & 0 & 0 & 0 & 1 & \\ & & & & & & \ddots \end{bmatrix}. \tag{2.31}$$

Toeplitz matrices are studied through their *symbols*, cf. [BS99, BS06], which are generating functions of matrix elements. In our case the symbol is

$$\sum_{n=-\infty}^{\infty} h_n z^n = \prod_{i\geq 1} \frac{1}{1-x_i z}.$$

Then Propositions 2.16 and 2.17 can be viewed together as an evaluation of minors of a product of two Toeplitz matrices. Indeed, such a product is again an infinite Toeplitz matrix with a symbol given by the product of the symbols.

We summarize without proofs several other important properties of the skew Schur functions. Many of them can be obtained from the Jacobi-Trudi formula, and we refer to the classical treatments in [Mac95, Chapter 1] and [Sta99, Chapter 7] for further details.

Theorem 2.18. *Properties of the skew Schur functions:*

1. $s_{\lambda/\emptyset}(x) = s_\lambda(x)$ *and* $s_{\emptyset/\nu}(x) = \begin{cases} 1 & \text{if } \nu = \emptyset, \\ 0 & \text{otherwise.} \end{cases}$
2. $s_{\lambda/\mu} = 0$ *unless* $\mu \subset \lambda$, i.e., $\mu_i \leq \lambda_i$ *for all* $i \geq 1$.

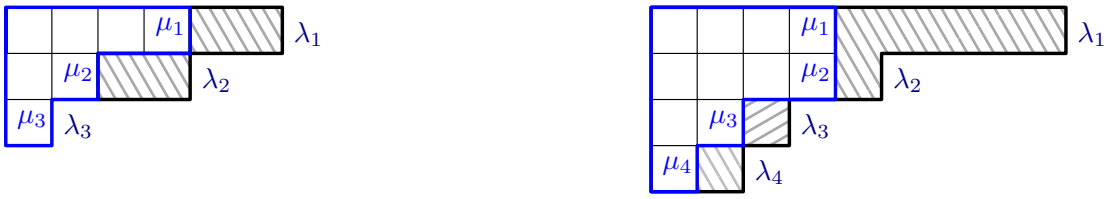


Figure 2.1: Left panel: a horizontal strip λ/μ, shown with gray hatching. Right panel: a skew diagram with three connected components, shown with gray hatching.

3. *If $\mu \subset \lambda$, let $\theta = \lambda/\mu$, viewed as a skew diagram, defined as the set-theoretical difference of Young diagrams corresponding to λ and μ. Suppose that θ is a disjoint union of (finitely many) connected components θ^i. Then*

$$s_{\lambda/\mu} = \prod_i s_{\theta^i}. \tag{2.32}$$

*In particular, $s_{\lambda/\mu}$ depends only on the shape of the skew-diagram λ/μ, but not on its positioning (*e.g.*, increasing all rows of λ and μ by 1 keeps $s_{\lambda/\mu}$ unchanged).*

4. *Set $x_2 = x_3 = \cdots = 0$ by considering the one-variable coordinate in the definition of a symmetric function and let α denote the remaining variable x_1. Then $s_{\lambda/\mu} = 0$, unless λ/μ is a* horizontal strip, i.e.*, a diagram with at most one box per column, cf. Figure 2.1. This is also equivalent to interlacing inequalities:*

$$\lambda_1 \geq \mu_1 \geq \lambda_2 \geq \mu_2 \geq \lambda_3 \ldots, \tag{2.33}$$

denoted $\mu \prec \lambda$. In the latter case, $s_{\lambda/\mu}(\alpha) = \alpha^{|\lambda|-|\mu|}$, cf. Section 2.5.

5. *The involution ω of* (2.12) *transposes both diagrams: $\omega(s_{\lambda/\mu}) = s_{\lambda'/\mu'}$.*

Let us give an example to illustrate the third property in Theorem 2.18. Consider $\lambda = (9, 5, 3, 2)$, $\mu = (4, 4, 2, 1)$, as in the right panel of Figure 2.1. The skew diagram is given by $\theta^1 = (5, 1)$, $\theta^2 = (1)$, $\theta^3 = (1)$. The table of indices $\lambda_i - \mu_j - i + j$ inside the matrix (2.30) is

i \ j	1	2	3	4
1	5	6	9	11
2	0	1	4	6
3	-3	-2	1	3
4	-5	-4	-1	1

and $s_{\lambda/\mu}$ is given by

$$s_{\lambda/\mu} = \det \begin{bmatrix} h_5 & h_6 & h_9 & h_{11} \\ 1 & h_1 & h_4 & h_6 \\ 0 & 0 & h_1 & h_3 \\ 0 & 0 & 0 & h_1 \end{bmatrix} = \det \begin{bmatrix} h_5 & h_6 \\ 1 & h_1 \end{bmatrix} \cdot h_1^2.$$

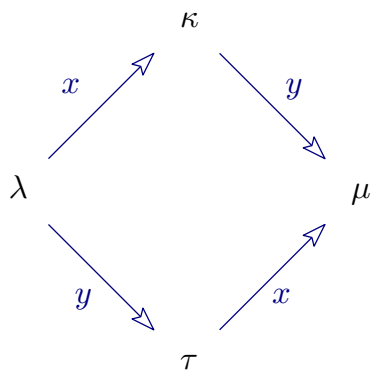


Figure 2.2: Flipping the arrows in the skew Cauchy identity.

We recall that $s_\lambda = \det\left[h_{\lambda_i - i + j}\right]_{1 \le i,j \le \ell(\lambda)}$. So $s_{\theta^1} = \det \begin{bmatrix} h_5 & h_6 \\ 1 & h_1 \end{bmatrix}$, $s_{\theta^2} = s_{\theta^3} = h_1$ and we have $s_{\lambda/\mu} = s_{\theta^1} \cdot s_{\theta^2} \cdot s_{\theta^3}$.

The following generalization of the Cauchy identity will play an important role in identification of stochastic models with Schur measures, and threfore we include a proof.

Theorem 2.19 (Skew Cauchy identity)**.** *For any $\lambda, \mu \in \mathbb{Y}$ and two sets of variables $x = (x_1, x_2, \dots)$ and $y = (y_1, y_2, \dots)$, we have (see Figure 2.2 for a visual representation)*

$$\sum_{\kappa \in \mathbb{Y}} s_{\kappa/\lambda}(x) s_{\kappa/\mu}(y) = \prod_{i,j \ge 1} \frac{1}{1 - x_i y_j} \sum_{\tau \in \mathbb{Y}} s_{\lambda/\tau}(y) s_{\mu/\tau}(x). \tag{2.34}$$

The proof relies on another relation.

Lemma 2.20. *Let* Littlewood–Richardson coefficients $c^\lambda_{\mu\nu}$ *be defined through the expansion*

$$s_{\lambda/\mu}(x) = \sum_{\nu \in \mathbb{Y}} c^\lambda_{\mu\nu} s_\nu(x), \qquad \lambda, \mu \in \mathbb{Y}. \tag{2.35}$$

Then we also have

$$s_\mu(x) s_\nu(x) = \sum_{\lambda \in \mathbb{Y}} c^\lambda_{\mu\nu} s_\lambda(x), \qquad \nu \in \mathbb{Y}. \tag{2.36}$$

In particular, this implies $c^\lambda_{\mu\nu} = c^\lambda_{\nu\mu}$, for any $\lambda, \mu, \nu \in \mathbb{Y}$.

Proof. Define $d^\lambda_{\mu\nu}$ as the coefficients in the expansion $s_\mu(z) s_\nu(z) = \sum_{\lambda \in \mathbb{Y}} d^\lambda_{\mu\nu} s_\lambda(z)$. We set $H(x; y) = \prod_{i,j \ge 1} \frac{1}{1 - x_i y_j}$ and use the Cauchy identity (2.17) for the sets of variables x, y, z:

$$H(x; z) H(y; z) = H(x, y; z) = \sum_{\lambda \in \mathbb{Y}} s_\lambda(x, y) s_\lambda(z) = \sum_{\lambda, \mu \in \mathbb{Y}} s_{\lambda/\mu}(x) s_\mu(y) s_\lambda(z)$$
$$= \sum_{\lambda, \mu, \nu \in \mathbb{Y}} c^\lambda_{\mu\nu} s_\nu(x) s_\mu(y) s_\lambda(z).$$

But also

$$H(x;z)H(y;z) = \sum_{\mu,\nu\in\mathbb{Y}} s_\mu(y)s_\mu(z)s_\nu(x)s_\nu(z) = \sum_{\lambda,\mu,\nu\in\mathbb{Y}} d^\lambda_{\mu\nu} s_\nu(x)s_\mu(y)s_\lambda(z).$$

Hence, $d^\lambda_{\mu\nu} \equiv c^\lambda_{\mu\nu}$. □

Proof of Theorem 2.19. We again start with $H(x;y) = \prod_{i,j\geq 1} \frac{1}{1-x_iy_j}$. Applying the Cauchy identity (2.17), we get

$$H(x;y)H(x;u)H(z;y)H(z;u) = H(x,z;y,u) = \sum_{\kappa\in\mathbb{Y}} s_\kappa(x,z)s_\kappa(y,u)$$
$$= \sum_{\kappa,\lambda,\mu\in\mathbb{Y}} s_{\kappa/\lambda}(x)s_\lambda(z)s_{\kappa/\mu}(y)s_\mu(u). \quad (2.37)$$

On the other hand, applying the Cauchy identity three times, the same expression is also equal to

$$H(x;y)\sum_{\sigma,\nu,\tau\in\mathbb{Y}} s_\sigma(x)s_\sigma(u)s_\nu(y)s_\nu(z)s_\tau(z)s_\tau(u) = H(x;y)\sum_{\substack{\sigma,\nu,\tau\in\mathbb{Y}\\ \lambda,\mu\in\mathbb{Y}}} s_\sigma(x)s_\nu(y)c^\mu_{\sigma\tau}s_\mu(u)c^\lambda_{\nu\tau}s_\lambda(z)$$
$$= H(x;y)\sum_{\tau,\lambda,\mu\in\mathbb{Y}} s_{\mu/\tau}(x)s_{\lambda/\tau}(y)s_\mu(u)s_\lambda(z), \quad (2.38)$$

where we used (2.36) in the first equality and (2.35) in the second one. Comparing the coefficient of $s_\mu(u)s_\lambda(z)$ in (2.37) and (2.38), we arrive at (2.34). □

2.4 Specializations

Schur functions and identities concerning them involve elements of an abstract algebra Λ of symmetric functions. In contrast, stochastic models involve real numbers, which also should be positive in order to define probabilities. A bridge between these viewpoints is provided by the notion of a specialization.

Definition 2.21. *An algebra homomorphism $\rho : \Lambda \to \mathbb{C},\ f \mapsto f(\rho)$, is called a* specialization. *In other words, ρ must satisfy the following properties:*

$$(f+g)(\rho) = f(\rho) + g(\rho), \qquad (fg)(\rho) = f(\rho)g(\rho), \qquad (cf)(\rho) = cf(\rho), \quad c\in\mathbb{C}.$$

Take any sequence of complex numbers $u_1, u_2, \dots$ satisfying $\sum_i |u_i| < \infty$. Then the *substitution* map $\Lambda \to \mathbb{C},\ x_i \mapsto u_i$ is a specialization. More generally, any specialization is uniquely determined by its values on any set of generators of Λ. Furthermore, if the generators are algebraically independent, then these values can be chosen arbitrarily. What this means is that defining ρ is equivalent to specifying the set of numbers $p_1(\rho)$, $p_2(\rho)$,..., *or* the set of numbers $e_1(\rho)$, $e_2(\rho)$,..., *or* the set of numbers $h_1(\rho)$, $h_2(\rho)$,.... In particular, if ρ is the substitution of complex numbers u_i, then

$$p_k \mapsto p_k(\rho) = \sum_{i=1}^{\infty} (u_i)^k. \quad (2.39)$$

Note that the condition $\sum_i |u_i| < \infty$ implies that the series in (2.39) converges for every $k \geq 1$.

In order to use specializations to define probabilities, it is important to know which ones are *positive* in a certain sense.

Definition 2.22. *We call a specialization ρ* Schur–positive *if for every Young diagram $\lambda \in \mathbb{Y}$ we have*

$$s_\lambda(\rho) \geq 0.$$

There is an explicit classification for Schur–positive specializations.

Theorem 2.23. *The Schur–positive specializations are parameterized by pairs of sequences of non-negative reals $\alpha = (\alpha_1 \geq \alpha_2 \geq \cdots \geq 0)$ and $\beta = (\beta_1 \geq \beta_2 \geq \cdots \geq 0)$ satisfying $\sum_i(\alpha_i + \beta_i) < \infty$ and an additional parameter $\gamma \geq 0$. The specialization with parameters $(\alpha;\beta;\gamma)$ can be described by its values on power sums*

$$p_1 \mapsto p_1(\alpha;\beta;\gamma) = \gamma + \sum_i(\alpha_i + \beta_i), \tag{2.40}$$
$$p_k \mapsto p_k(\alpha;\beta;\gamma) = \sum_i(\alpha_i^k + (-1)^{k-1}\beta_i^k), \quad k \geq 2$$

or, equivalently, via the generating function

$$\sum_{k=0}^{\infty} h_k(\alpha;\beta;\gamma)z^k = \exp\left(\sum_{k\geq 1}\frac{p_k(\alpha;\beta;\gamma)\ z^k}{k}\right) = e^{\gamma z}\prod_{i\geq 1}\frac{1+\beta_i z}{1-\alpha_i z}. \tag{2.41}$$

If ρ is a Schur–positive specialization, then also $s_{\lambda/\mu}(\rho) \geq 0$ for every $\lambda, \mu \in \mathbb{Y}$.

Theorem 2.23 has a number of equivalent reformulations, in particular, it is equivalent to the description of all characters of the infinite symmetric group $S(\infty)$ and to the classification of *totally positive* triangular Toeplitz matrices, as can be seen from (2.30) and (2.31). The first proofs of Theorem 2.23 were obtained independently by Thoma [Tho64] and Edrei [Edr53]. A proof by a different method can be found in [VK81, Ker03, KOO98] — this approach also gives an interpretation for α_i and β_j as normalized row and column lengths of growing Young diagrams, so that the corresponding (normalized) characters of finite symmetric groups approximate the $(\alpha;\beta;\gamma)$-character of $S(\infty)$. Its detailed exposition can be found in [BO17a]. Two other proofs are in [Oko99] and [BG15].

Partial proof of Theorem 2.23. The hardest part of the argument is to show that the list is exhaustive, *i.e.*, that there are no further specializations beyond (2.40), (2.41). We do not give this proof, and only explain that each specialization from the list satisfies $s_{\lambda/\mu}(\rho) \geq 0$ for all $\lambda, \mu \in \mathbb{Y}$.

We start with a specialization with a single α: $\alpha_1 = \alpha > 0$ and all other parameters are 0. In this case $p_k(\rho) = \alpha^k$, and $\sum\limits_{k=0}^{\infty} h_k(\rho)z^k = (1-\alpha z)^{-1}$, and this specialization is simply a substitution $x_1 = \alpha$, $x_2 = \cdots = 0$ in a symmetric function of $(x_1, x_2, \dots)$. The fourth property in Theorem 2.18 implies $s_{\lambda/\mu}(\rho) \geq 0$.

Next, consider a specialization ρ with a single β: $\beta_1 = \beta > 0$ and all other parameters are 0. In this case, $p_k(\rho) = (-1)^{k-1}\beta^k$ and $\sum\limits_{k=0}^{\infty} h_k(\rho)z^k = 1 + \beta z$. Note that $1 + \beta z$ is also $\sum\limits_{k=0}^{\infty} e_k(\rho')z^k$, where ρ' is the specialization with $\alpha_1 = \beta$ and all other parameters 0. Therefore, comparing with (2.12), we conclude that

$$\rho(f) = \rho'(\omega(f)). \tag{2.42}$$

Hence, $s_{\lambda/\mu}(\rho) \geq 0$ follows from $s_{\lambda'/\mu'}(\rho') \geq 0$ and the fifth property in Theorem 2.18.

In order to reach the general case from the two basic ones, we use the following operation:

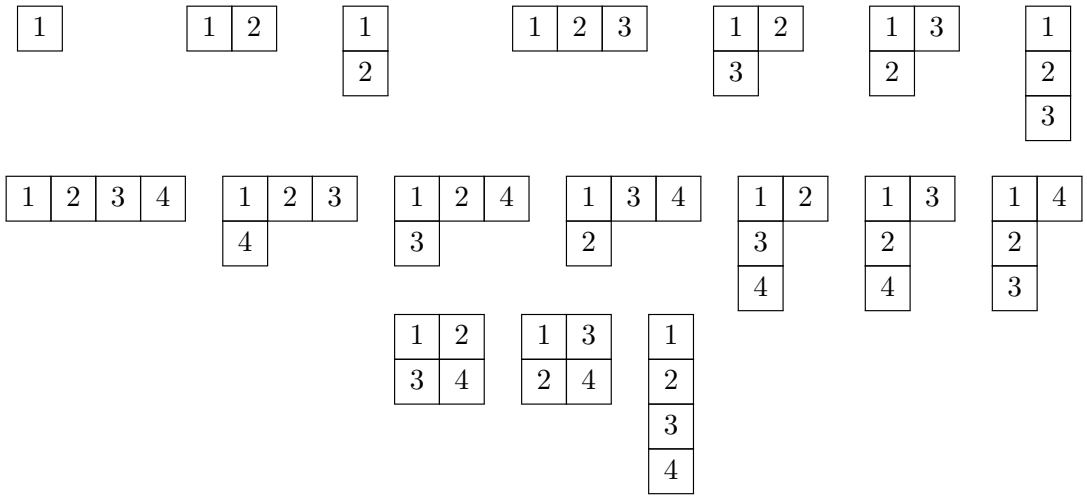


Figure 2.3: Top row: all SYT of shapes λ with $|\lambda| = 1, 2, 3$. Bottom two rows: $|\lambda| = 4$.

Definition 2.24. *Given two specializations ρ_1, ρ_2, their union (ρ_1, ρ_2) is defined through its values on the power sums p_k:*

$$p_k(\rho_1, \rho_2) = p_k(\rho_1) + p_k(\rho_2). \tag{2.43}$$

We claim that if ρ_1 and ρ_2 are such that $s_{\lambda/\mu}(\rho_1) \geq 0$ and $s_{\lambda/\mu}(\rho_2) \geq 0$ for all $\lambda, \mu \in \mathbb{Y}$, then also $s_{\lambda/\mu}(\rho_1, \rho_2) \geq 0$. Indeed, (2.27) and (2.29) imply that

$$s_{\lambda/\mu}(\rho_1, \rho_2) = \sum_{\nu \in \mathbb{Y}} s_{\lambda/\nu}(\rho_1) s_{\nu/\mu}(\rho_2) \geq 0.$$

Using the unions, starting from a single α and a single β, we reach any finite collections of non-zero α_i and β_i parameters. Next, notice that all $s_{\lambda/\mu}$ are polynomials in p_k, and therefore, $s_{\lambda/\mu}(\rho)$ continuously depend on $\{p_k(\rho)\}_{k\geq 1}$. Therefore, we can pass to the limits and reach arbitrary infinite collection of parameters α_i and β_i subject to $\sum_i (\alpha_i + \beta_i) < \infty$.

For the γ–parameter, we notice

$$p_k(0; 0; \gamma) = \lim_{N\to\infty} p_k\left(\tfrac{\gamma}{N}, \dots, \tfrac{\gamma}{N}; 0, 0\right), \qquad k = 1, 2, \dots, \tag{2.44}$$

where the used specialization has non-zero parameters $\alpha_1 = \alpha_2 = \cdots = \alpha_N = \frac{\gamma}{N}$. Hence, the γ–specialization can also be obtained by a limit transition from positive specializations and, therefore, is Schur-positive. Finally, we combine γ with α's and β's by another union. □

The specialization with non-zero γ and all other parameters set to 0 is called the *Plancherel specialization*. It is the most famous one, and we discuss it in more detail.

Definition 2.25. *Given a Young diagram $\lambda \in \mathbb{Y}$ with $|\lambda| = n$, a* Standard Young Tableau *(SYT) of shape λ, is a filling of boxes of λ with numbers $1, 2, \dots, n$, in such a way that entries grow along the rows and columns. The total number of SYT of a fixed shape λ is called the dimension of λ and denoted*[1] $\dim \lambda$.

All Standard Young Tableaux of shapes λ with $|\lambda| \leq 4$ are shown in Figure 2.3.

[1] Algebraic combinatorics literature typically uses f^λ for the same quantity. Our $\dim \lambda$ notation emphasizes that this is the dimension of the irreducible representation of the symmetric group $\mathcal{S}_n$ indexed by λ, cf. Theorem 2.27 below.

Proposition 2.26. *The Plancherel specialization* $(0;0;\gamma)$ *in Theorem 2.23 leads to*

$$s_\lambda(0;0;\gamma) = \frac{\gamma^{|\lambda|}}{|\lambda|!}\dim\lambda, \qquad \lambda \in \mathbb{Y}. \tag{2.45}$$

Proof. Recall the Cauchy identity (2.17) in the form

$$\sum_{\lambda\in\mathbb{Y}} s_\lambda(x)s_\lambda(y) = \exp\left(\sum_{k\geq 1}\frac{p_k(x)p_k(y)}{k}\right)$$

and apply in variables (y) the specialization with a fixed γ and all other parameters set to 0. We obtain

$$\sum_{\lambda\in\mathbb{Y}} s_\lambda(x)s_\lambda(0;0;\gamma) = \exp\bigl(p_1(x)\gamma\bigr) = \sum_{n=0}^{\infty}\frac{\gamma^n}{n!}\bigl[p_1(x)\bigr]^n. \tag{2.46}$$

Noting that $s_\lambda(0;0;\gamma) = \gamma^{|\lambda|}s_\lambda(0;0;1)$ from homogeneity of Schur polynomials, we conclude that $s_\lambda(0;0;\gamma)|\lambda|!\gamma^{-|\lambda|}$ is equal to the coefficient of $s_\lambda(x)$ in the decomposition of $\bigl[p_1(x)\bigr]^n$ in the basis of Schur functions; here $n = |\lambda|$. In order to compute this coefficient, we note the recurrence on Schur polynomials:

$$s_\lambda(x)p_1(x) = \sum_{\mu=\lambda+\square} s_\mu(x),$$

where the summation goes over all μ obtained from λ by adding one box. This recurrence is proven directly from the definition (2.14), and we leave it as an exercise for Section 2.5. Iterating the recurrence, we arrive at

$$\bigl[p_1(x)\bigr]^n = \sum_{\lambda\colon |\lambda|=n} \dim\lambda\cdot s_\lambda(x).$$

Picking the coefficient of $s_\lambda(x)$, we conclude that $s_\lambda(0;0;\gamma)|\lambda|!\gamma^{-|\lambda|} = \dim\lambda$, as desired. □

Let us study the numbers $\dim\lambda$ more carefully. From Figure 2.3, it is clear that:

- For $|\lambda| = 1$ the only dimension is 1;
- For $|\lambda| = 2$ the dimensions are 1 and 1;
- For $|\lambda| = 3$ the dimensions are 1, and 2, and 1;
- For $|\lambda| = 4$ the dimensions are 1, and 3, and 3, and 2, and 1.

Let us sum the squares of these numbers, getting 1, $1+1=2$, $1+4+1=6$, and $1+9+9+4+1=24$. One can see the pattern here, which generalizes to the *Burnside identity*.

Theorem 2.27. *For each* $n = 1, 2, \ldots,$ *we have* $\displaystyle\sum_{\lambda\colon |\lambda|=n} \dim^2\lambda = n!.$

This identity has a representation-theoretic meaning. The irreducible representations of the symmetric group $\mathcal{S}_n$ are parameterized by partitions of n, with the representation corresponding to λ having dimension precisely $\dim\lambda$, see, *e.g.*, [Mac95, Section I.7] or [Sag01]. On the other hand, $n!$ is the dimension of the regular representation of $\mathcal{S}_n$ in the linear space $\mathbb{C}[\mathcal{S}_N]$. Hence, the Burnside identity can be obtained by evaluating dimensions in the statement "each irreducible representation of a finite group enters into the decomposition of the regular representation of the same group with multiplicity equal to its dimension", see *e.g.*, [Ser77, Section 2.4].

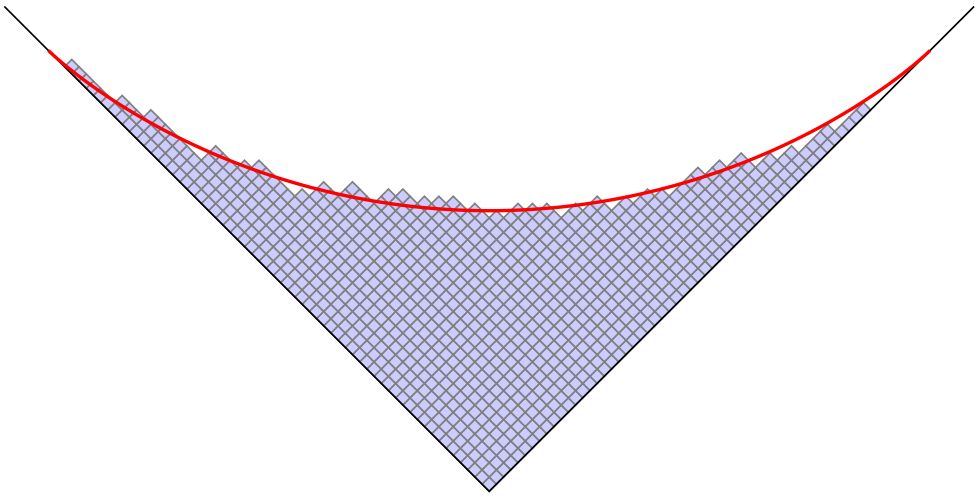


Figure 2.4: Plancherel-random partition of $n = 1000$ and Vershik-Kerov-Logan-Shepp limit shape.

Proof of Theorem 2.27. We again start from the Cauchy identity

$$\sum_{\lambda\in\mathbb{Y}} s_\lambda(x)s_\lambda(y) = \exp\left(\sum_{k\geq 1}\frac{p_k(x)p_k(y)}{k}\right).$$

Let us apply the γ–specialization in (x)–variables and the $\gamma = 1$ specialization in (y) variables. Taking into account Proposition 2.26, we obtain

$$\sum_{\lambda\in\mathbb{Y}} \gamma^{|\lambda|}\frac{\dim^2\lambda}{(n!)^2} = \exp(\gamma) = \sum_{n=0}^{\infty}\frac{\gamma^n}{n!}.$$

Comparing the coefficient of γ^n in both sides, we arrive at the desired identity. □

Theorem 2.27 implies that the formula

$$\mathbb{P}(\lambda) = \frac{\dim^2\lambda}{n!} \tag{2.47}$$

defines a probability distribution on the set of all partitions of n. This distribution is known as the *Plancherel measure* and it has been extensively studied in the literature, see, for example, [VK77, LS77, Joh01a, BOO00, Oko00, IO02, JS16, Rap25]. We will return to this measure in future sections, and for now refer to the teaser in Figure 2.4, where a large Plancherel-random Young diagram and the corresponding limit shape are shown.

Let us explain the origin of the name of the Plancherel measure. The classical Plancherel theorem [Pla10] is a statement on preservation of the norm of a function under the Fourier transform:

$$\int_{-\infty}^{\infty}|f(x)|^2\mathrm{d}x = \int_{-\infty}^{\infty}|\hat{f}(\xi)|^2\mathrm{d}x, \qquad \hat{f}(\xi) = \int_{\mathbb{R}} f(x)e^{-2\pi\mathbf{i}x\xi}\mathrm{d}x. \tag{2.48}$$

This theorem has a non-commutative analogue, valid for all finite groups and beyond. We state it for the symmetric group $\mathcal{S}_n$, whose irreducible representations are parameterized by partitions of n. For $\lambda\in\mathbb{Y}_n$, let χ^λ be the *normalized* trace of the representation T_λ:

$$\chi^\lambda(g) = \frac{\mathrm{Trace}\big(T_\lambda(g)\big)}{\dim\lambda}, \qquad g\in\mathcal{S}_n, \qquad \chi^\lambda\big(\mathrm{Id}\big) = 1.$$

Consider the space of all *central* functions $F : \mathcal{S}_n \to \mathbb{C}$, *i.e.*, such that $F(ab) = F(ba)$ for any $a, b \in \mathcal{S}_N$, and equip it with the scalar product

$$\big\langle F, H \big\rangle = \sum_{g \in \mathcal{S}_N} F(g)\overline{H}(g).$$

An analogue of the Fourier transform then becomes

$$\widehat{F}(\lambda) = \big\langle F, \chi^\lambda \big\rangle, \qquad \lambda \in \mathbb{Y}_n.$$

Orthogonality relations for the characters (see, *e.g.*, [Ser77, Section 2.3]) imply the identity:

$$\big\langle F, F \big\rangle = \sum_{\lambda \in \mathbb{Y}_N} \frac{\dim^2 \lambda}{n!} \left|\widehat{F}(\lambda)\right|^2. \tag{2.49}$$

In contrast to the Plancherel theorem (2.48), where both sides of the identity involved integration against the Lebesgue measure, in the right-hand side of (2.49) we see a non-uniform measure with weights $\frac{\dim^2 \lambda}{n!}$ — this is precisely the Plancherel measure for the symmetric group $\mathcal{S}_n$.

The identity (2.48) can be also given a representation theoretic meaning by looking at the additive group $\mathbb{R}$ and interpreting exponents $x \mapsto e^{-2\pi \mathbf{i} x\xi}$ as characters of all possible one-dimensional representations parameterized by ξ. Formulas (2.48) and (2.49) admit a common generalization covering locally compact topological groups, see, *e.g.*, [Dix77, Section 18.8].

2.5 Exercises

Problem 1. Take $\lambda \in \mathbb{Y}_n$ and consider the expansion of $e_\lambda = \prod_i e_{\lambda_i}$ in the basis of monomial symmetric functions in Λ:

$$e_\lambda = \sum_{\mu \in \mathbb{Y}_n} M_\lambda^\mu m_\mu.$$

Prove that the coefficient M_λ^μ is equal to the number of matrices $A = [a_{ij}]$ which are large enough (*e.g.*, of size $n \times n$), and which satisfy:

$$a_{ij} \in \{0, 1\}, \quad \sum_j a_{ij} = \lambda_i, \quad \sum_i a_{ij} = \mu_j.$$

Problem 2. Show that in Λ

$$p_n = \det \begin{pmatrix} e_1 & 1 & 0 & 0 & \dots & 0 \\ 2e_2 & e_1 & 1 & 0 & \dots & 0 \\ 3e_3 & e_2 & e_1 & 1 & \dots & 0 \\ \vdots & \vdots & \vdots & \ddots & & \vdots \\ ne_n & e_{n-1} & e_{n-2} & e_{n-3} & \dots & e_1 \end{pmatrix}.$$

Problem 3. Working directly with the definition of $s_\lambda(x_1, \dots, x_N)$ and sending $N \to \infty$, prove that

$$s_\lambda p_1 = \sum_{\mu = \lambda + \square} s_\mu.$$

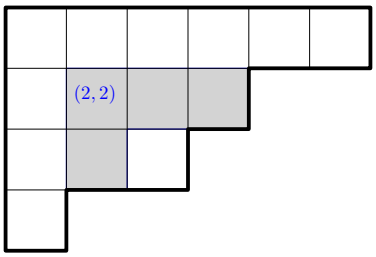


Figure 2.5: Hook at $(2,2)$ with the hook length $h(2,2) = 4$.

Extend the argument to compute the expansion in s_μ of the product $s_\lambda e_k$ for any $k \geq 1$.

Problem 4. Working directly with the definition of $s_\lambda(x_1, \ldots, x_N)$, prove that

$$s_\lambda(x_1, \ldots, x_{N-1}, \alpha) = \sum_{\mu \prec \lambda} \alpha^{\sum_i \lambda_i - \sum_i \mu_i} s_\mu(x_1, \ldots, x_{N-1}), \tag{2.50}$$

where $\mu \prec \lambda$ means the interlacement condition (compare with property 4 in Theorem 2.18):

$$\lambda_1 \geq \mu_1 \geq \lambda_2 \geq \cdots \geq \mu_{N-1} \geq \lambda_N.$$

.

Problem 5.

A. Working directly with the definition and using the Vandermonde determinant, evaluate $s_\lambda(1, q, \ldots, q^{N-1})$ for $\lambda = (\lambda_1 \geq \cdots \geq \lambda_N)$.

B. Sending $q \to 1$, prove that

$$s_\lambda(1, \ldots, 1) = \prod_{1 \leq i < j \leq N} \frac{\lambda_i - i - \lambda_j + j}{j - i}. \tag{2.51}$$

This is the dimension of the irreducible representation of the unitary group $U(N)$ with highest weight λ. In this interpretation, (2.51) is the *Weyl dimension formula.*

C. Recall from Proposition 2.26 that $\dim \lambda$ can be expressed through the Plancherel specialization and the limits of specializations in N equal variables:

$$\dim \lambda = \frac{|\lambda|!}{\gamma^{|\lambda|}} s_\lambda(0; 0; \gamma) = \frac{|\lambda|!}{\gamma^{|\lambda|}} \lim_{N \to \infty} s_\lambda\left(\frac{\gamma}{N}, \frac{\gamma}{N}, \ldots, \frac{\gamma}{N}\right).$$

Use this and the result of part **B** to get *some* formula for $\dim \lambda$

D. Prove that your formula from part **C** is equivalent to the hook length formula

$$\dim \lambda = \frac{|\lambda|!}{\prod_{(i,j) \in \lambda} h(i,j)},$$

where for a box (i,j) inside the Young diagram λ, its hook length $h(i,j)$ is $\lambda_i + \lambda'_j - i - j + 1$, illustrated graphically as the number of boxes in the gray hook area in Figure 2.5.

Problem 6. Let N and M be two natural numbers and let M^N be the rectangular Young diagram with N rows of length M. For $\lambda \in M^N$, denote $\hat{\lambda} = (\hat{\lambda}_1, \dots, \hat{\lambda}_N) = (M - \lambda_N, M - \lambda_{N-1}, \dots, M - \lambda_1)$.

A. Use Jacobi-Trudi formula to prove that $s_{M^N/\lambda} = s_{\hat{\lambda}}$.

B. Prove that for any $n = 0, 1, 2 \dots, NM$,

$$\sum_{\lambda \subset M^N : |\lambda| = n} \dim \lambda \cdot \dim \hat{\lambda} = \dim M^N.$$

Hint. Apply the specialization $(0; 0; \gamma_1 + \gamma_2)$ to s_{M^N}.

Problem 7. Consider up-right monotone lattice paths on $\mathbb{Z}^2$, which follow the lattice edges and connect $(1, 0)$ with (N, K). We encode a path γ as a non-decreasing sequence of integers

$$0 = \gamma(0) \le \gamma(1) \le \gamma(2) \le \dots \le \gamma(N) = K$$

via

$$\gamma = [(1, \gamma(0)) \to (1, \gamma(1)) \to (2, \gamma(1)) \to (2, \gamma(2)) \to \dots \to (N, \gamma(N))].$$

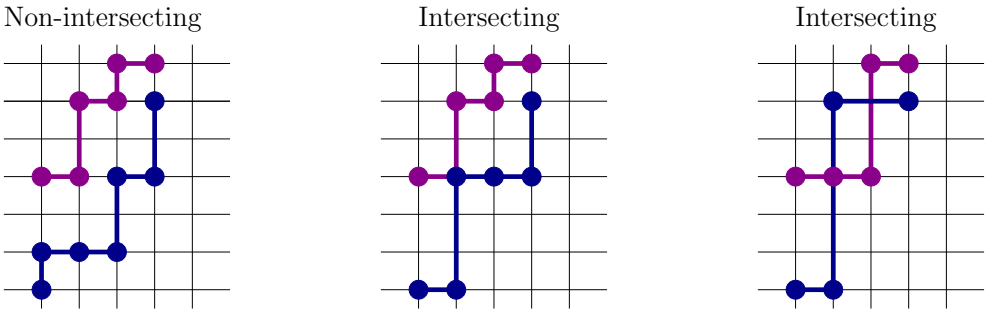
Choose positive parameters $\alpha_1, \dots, \alpha_N$ and assign to a path γ the weight

$$w(\gamma) = \prod_{i=1}^{N} \alpha_i^{\gamma(i) - \gamma(i-1)}.$$

A. Using complete homogeneous symmetric functions, prove that

$$\sum_{\gamma : (1,0) \to (N,K)} w(\gamma) = h_K(\alpha_1, \alpha_2, \dots, \alpha_N).$$

B. Consider pairs of paths $\gamma_1 : (1, J_1) \to (N, K_1)$, $\gamma_2 : (1, J_2) \to (N, K_2)$ which do not intersect:



Prove by direct count that the sum of $w(\gamma_1)w(\gamma_2)$ over such pairs of non-intersecting paths is equal to

$$h_{K_1 - J_1}(\alpha_1, \dots, \alpha_N) h_{K_2 - J_2}(\alpha_1, \dots, \alpha_N) - h_{K_1 - J_2}(\alpha_1, \dots, \alpha_N) h_{K_2 - J_1}(\alpha_1, \dots, \alpha_N).$$

Hint. The two terms being subtracted correspond to all paths and paths with intersections.

C. Extend the argument of part **B** to m–tuples of non-intersecting paths and prove

$$\sum_{\substack{\gamma_1 : (1,J_1) \to (N,K_1), \\ \dots \\ \gamma_m : (1,J_m) \to (N,K_m), \\ \gamma_1, \dots, \gamma_m \text{ do not intersect}}} w(\gamma_1) w(\gamma_2) \cdots w(\gamma_m) = \det \Big[h_{K_a - J_b}(\alpha_1, \dots, \alpha_N) \Big]_{a,b=1}^{m}.$$

D. Use part **C** to prove Proposition 2.17, by verifying that the right-hand side of (2.30) satisfies (2.28).

E. A generalization of part **C** is known as Lindström–Gessel–Viennot (LGV) lemma, which we now present. Consider a finite[2] directed acyclic graph and denote by V and E the sets of its vertices and edges. Let $w : E \to \mathbb{C}$ be an arbitrary weight function. For any path γ denote by $w(\gamma)$ the product of weights over the edges in the path: $w(\gamma) = \prod_{e \in \gamma} w(e)$. We say that two paths γ_1 and γ_2 do not intersect (notation $\gamma_1 \cap \gamma_2 = \varnothing$) if they have no common vertices.

For any $u, v \in V$, let $\Upsilon(u, v)$ be the set of all (directed) paths from u to v. Set

$$\mathcal{T}(u, v) = \sum_{\gamma \in \Upsilon(u,v)} w(\gamma). \tag{2.52}$$

Let $(u_1, \dots, u_m)$ and $(v_1, \dots, v_m)$ be two m-tuples of vertices of our graph, and assume that for any nonidentical permutation $\sigma \in \mathcal{S}_n$,

$$\left\{(\gamma_1, \dots, \gamma_m) \mid \gamma_i \in \Upsilon\left(u_i, v_{\sigma(i)}\right),\ \gamma_i \cap \gamma_j = \varnothing,\ 1 \le i < j \le m\right\} = \varnothing.$$

Prove that

$$\sum_{\substack{\gamma_1 \in \Upsilon(u_1, v_1), \dots, \gamma_m \in \Upsilon(u_m, v_m) \\ \gamma_i \cap \gamma_j = \varnothing,\ 1 \le i < j \le m}} w(\gamma_1) \cdots w(\gamma_m) = \det\left[\mathcal{T}(u_i, v_j)\right]_{i,j=1}^{m}.$$

Literature. We used the following sources for composing problems and refer to them for more information, references, and connections: [Mac95], [ZJ08], and [BO17a].

[2] The assumption of finiteness is not necessary as long as the sums in (2.52) converge.

Chapter 3

Schur measures, PNG, and increasing subsequences

In this chapter, we first introduce another interface growth model in the KPZ universality class that is closely related to lattice models of 2d statistical mechanics. Then we connect this model to Schur measures and Schur processes (which are also introduced here). A degeneration of the constuction provides a link to the Plancherel measure, last passage percolation, and longest increasing subsequences of random permutations.

3.1 The discrete PNG

The *discrete polynuclear growth model* (PNG) is a growth model with discrete space, $x \in \mathbb{Z}$, and discrete time, $t \in \mathbb{Z}_{\geq 0}$. The height function h is integer-valued, $h(x,t) \in \mathbb{Z}$ for any $x \in \mathbb{Z}, t \in \mathbb{Z}_{\geq 0}$. We consider the PNG model in the droplet geometry, which corresponds to the initial condition $h(x,0) = 0$, for any $x \in \mathbb{Z}$, and the dynamics

$$h(x,t+1) = \max\{h(x-1,t), h(x,t), h(x+1,t)\} + \omega(x,t+1), \tag{3.1}$$

where the noise $\omega(x,t)$ is defined using auxiliary i.i.d. random geometric weights $w_{i,j}$, $i,j \in \mathbb{Z}_{\geq 1}$ with

$$\mathbb{P}(w_{i,j} = k) = (1-a_ib_j)(a_ib_j)^k, \qquad k \geq 0,$$

and a_i, b_j are parameters satisfying $0 < a_ib_j < 1$ for all $i,j = 1,2,\ldots$. We have

$$\omega(x,t) = \begin{cases} 0, & \text{if } t-x \text{ is even or } |x| > t, \\ w_{\frac{t+x+1}{2}, \frac{t-x+1}{2}}, & \text{if } t-x \text{ is odd and } |x| \leq t. \end{cases} \tag{3.2}$$

Equivalently, $\omega(i-j, i+j-1) = w_{i,j}$, $i,j \in \mathbb{Z}_{\geq 1}$, and all other $\omega(x,t)$ are 0, see Figure 3.1.[1] We use the set of parameters $\{a_i, b_j\}$ in order to observe more clearly the algebraic structure underlying the model; later, when we study large time asymptotics, we fix $a_i = b_j = \sqrt{q} \in (0,1)$, so that the parameter in the geometric distribution is always q.

The procedure (3.1) for evolving $h(x,t)$ into $h(x,t+1)$ can be described by the three rules shown in Figure 3.2. For a better graphical visualization we view the function $h(\cdot,t)$ as a continuous interface: instead of a single point at position $(x, h(x,t))$, we draw a horizontal segment of size 1 centered at x at the vertical position $h(x,t)$, and join the ends of the horizontal segments by vertical ones. Then the rules are:

[1] The droplet geometry corresponds to $\omega(x,t)$ vanishing outside the cone, $|x| > t$; the droplet itself is visible in Figure 3.10.

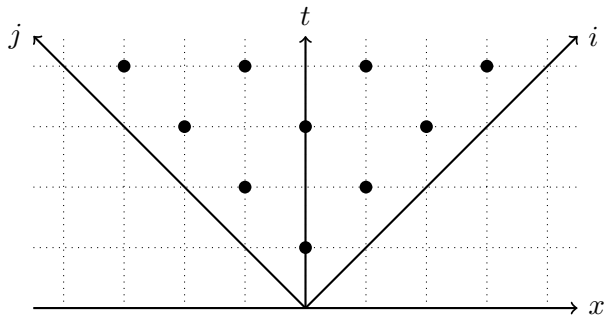


Figure 3.1: Setting for the discrete PNG model. $\omega(x,t)$ are independent geometric random variables at black dots and zeros everywhere else.

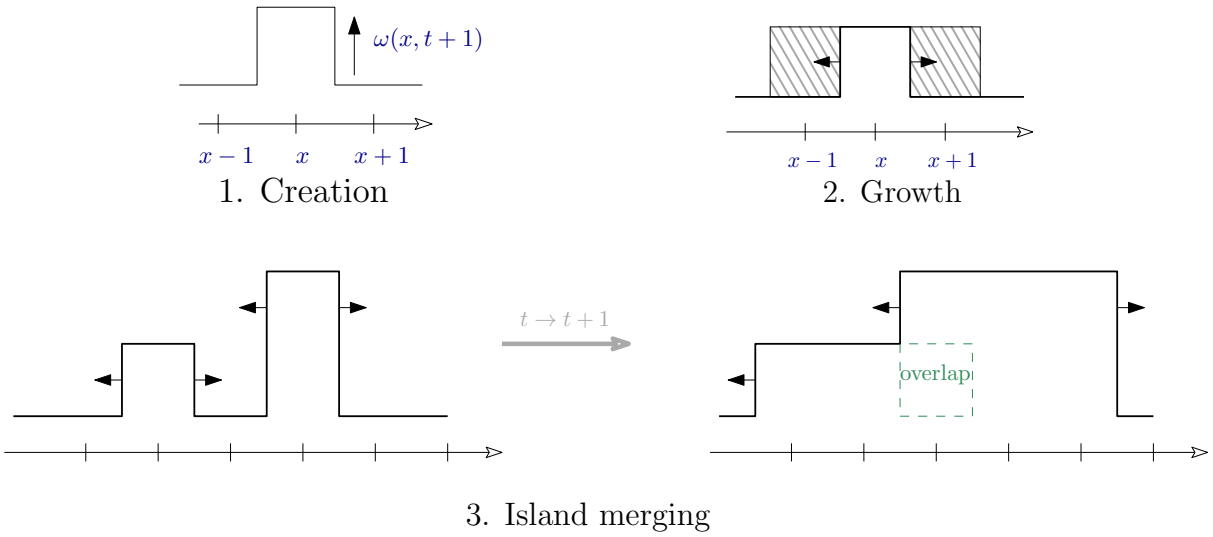


Figure 3.2: Rules in discrete PNG.

1. The weight $\omega(x,t+1)$ leads to creation of an island of width 1, spanning $[x-\frac{1}{2}, x+\frac{1}{2}]$, and of height $\omega(x,t+1)$, placed on top of $h(x,t)$.

2. The existing islands grow by 1 both in negative and in positive x–directions.

3. When two islands merge, they both continue growing, but their overlap becomes invisible and is removed from the picture.

Let us consider an explicit example of Figure 3.3 for times $t = 1, 2, 3$. At time $t = 0$ we have a flat interface. At time $t = 1$ an island of width 1 and height 2 appears because of $w_{1,1}$ random variable taking the value 2. At time $t = 2$, this island grows to width 3, and two new islands are appended on top of it, of heights 1 and 3, corresponding to values of $w_{1,2}$ and $w_{2,1}$. At time 3, the islands centered at -1 and 1 merge together, with the overlap removed, and then three more islands are appended on top.

It is clear from the example that for times $t = 1, 2$ we can recover from the graph of the height function the values of the $w_{i,j}$ used so far (*i.e.*, for $i + j - 1 \le t$): $h(\cdot, 1)$ contains full information on $w_{1,1}$; $h(\cdot, 2)$ contains full information on $w_{1,1}$, $w_{1,2}$, $w_{2,1}$. However this is no longer possible for times $t \ge 3$, and the mapping from $\{w_{i,j}, i + j - 1 \le t\}$ to $\{h(x,t), |x| \le t\}$ is not a bijection anymore: in our

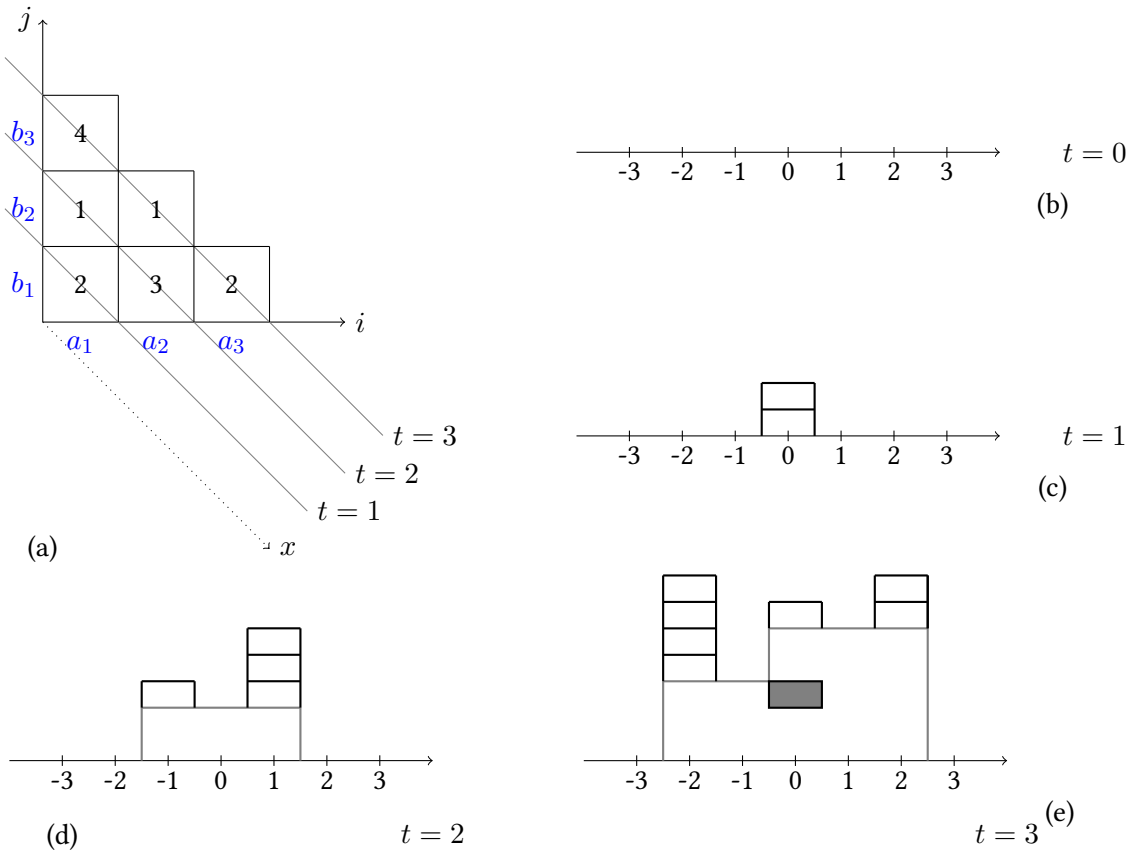


Figure 3.3: Example of the volution of the PNG model. In figure (a) the values of the random variables w are represented on the plane (i, j). From (b) to (e) are the graphs of the height function at times $t = 0, 1, 2, 3$. At $t = 3$ two islands meet and we have the formation of an overlap (in gray), which is removed with no trace.

example, given $h(\cdot, 3)$, it is impossible to distinguish the two cases

$$\big(w_{1,1}, w_{1,2}, w_{2,1}\big) = (2, 1, 3) \quad \text{or} \quad \big(w_{1,1}, w_{1,2}, w_{2,1}\big) = (1, 2, 4).$$

Due to this loss of information, even a nice measure on the array $w_{i,j}$ does not translate to a simple measure on $\{h(x, t), |x| \leq t\}$, which complicates the analysis.

In order to maintain a bijection between the growth model and the underlying random variables $w_{i,j}$, we need to extend the model. This extension is know as the *multilayer PNG model*.

3.2 The multilayer PNG

The multilayer PNG is an evolution of the family of height functions $\{h_\ell, \ell \geq 1\}$, where $h_\ell(x, t)$ is the ℓth line of the model at time t, and h_1 is the PNG height function from the previous section. By construction, the lines are non-intersecting, *i.e.*, $h_1(x, t) > h_2(x, t) > h_3(x, t) > \dots$ for each x and t. At time 0 the evolution is initialized by horizontal lines $h_\ell(x, 0) = 1 - \ell$, for each $\ell = 1, 2, \dots$.

The evolution is defined as follows: first of all, $h_1(x, t) := h(x, t)$ (this is the function we actually want to study). For the other lines, the dynamics of h_ℓ, $\ell \geq 1$, is given by the following recursion:

$$h_\ell(x, t + 1) = \max\{h_\ell(x - 1, t), h_\ell(x, t), h_\ell(x + 1, t)\} + \omega_\ell(x, t + 1), \tag{3.3}$$

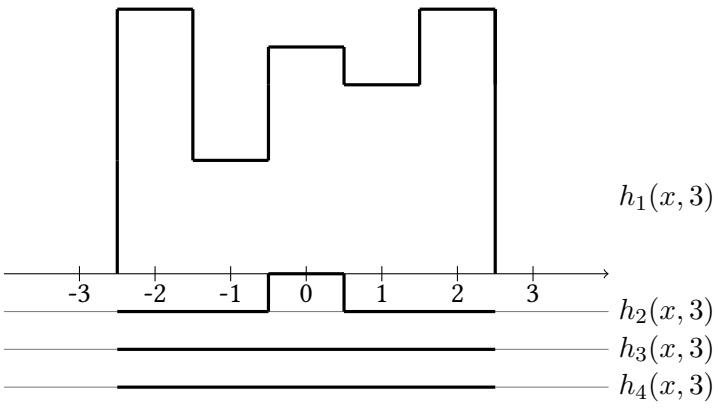


Figure 3.4: The multilayer PNG for the example in Figure 3.3 at time $t = 3$.

where for $\ell = 1$ the noise $\omega_\ell(x, t+1)$ is the same as $\omega(x, t+1)$ in (3.1), while for $\ell \geq 2$, $w_\ell(x, t+1)$ is given by the new overlap on the site x at level $\ell - 1$ when updating $h_{\ell-1}(\cdot, t) \mapsto h_{\ell-1}(\cdot, t+1)$. Let us spell out the meaning of the overlap more formally. For $t - x$ odd and $\ell = 1, 2 \dots$ we define the *jumps*,

$$\begin{aligned} \eta_\ell^+(x,t) &= h_\ell(x,t) - h_\ell(x-1,t), \\ \eta_\ell^-(x,t) &= h_\ell(x,t) - h_\ell(x+1,t). \end{aligned} \tag{3.4}$$

Geometrically, $\eta_\ell^\pm$ are the lengths of the vertical segments in the interface h_ℓ to the left (at $x - \frac{1}{2}$) and to the right (at $x + \frac{1}{2}$) of x. The parity is chosen so that both of these segments go down from the horizontal segments at height $h_\ell(x,t)$, and consequently $\eta^+, \eta^- \geq 0$. In terms of $\eta_\ell^\pm$, the new overlap at the site x is computed for $\ell = 2, 3, \dots$ as

$$\omega_\ell(x,t) = \begin{cases} \min\left\{\eta_{\ell-1}^+(x+1,t-1), \eta_{\ell-1}^-(x-1,t-1)\right\} & \text{if } t-x \text{ is odd}, \\ 0 & \text{if } t-x \text{ is even}. \end{cases} \tag{3.5}$$

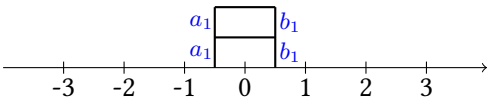
Due to the shift of indices, $\eta_{\ell-1}^+(x \pm 1, t-1)$ are the lengths of the vertical segments going up from the horizontal segment at height $h_{\ell-1}(x,t)$. Hence, when updating from time $t-1$ to time t, these two segments collide, leading to island merging and readily matching $\omega_\ell(x,t)$ with the previous intuitive definition of the overlap and the last panel in Figure 3.3.

We leave as an exercise to the reader to check that the evolution rules (3.3), (3.5) imply that the interfaces corresponding to h_ℓ, $\ell = 1, 2, \dots$, remain non-intersecting (and do not share corners) at each time $t = 0, 1, 2, \dots$, see [Joh03, Claim 3.7] for further details. In the example of Figure 3.3, the interfaces h_ℓ, $\ell > 1$, stay constant at times $t = 1$ and $t = 2$, and the first growth is at time $t = 3$, leading to the interfaces of Figure 3.4.

In contrast to the top interface $h_1(\cdot, t) = h(\cdot, t)$, the joint law of the family $\{h_\ell(\cdot, t)\}_{\ell \geq 1}$ turns out to be explicit at each time $t = 0, 1, 2, \dots$, as recorded in the following theorem.

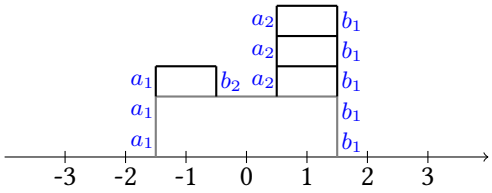
Theorem 3.1. *Suppose that h_ℓ evolve according to* (3.3)–(3.5)*, with initial condition $h_\ell(x, 0) \equiv -\ell + 1$ and the driving noises $\omega_1 = \omega$ given by* (3.2)*. Then at time t, the interfaces $\{h_\ell(\cdot, t)\}_{\ell \geq 1}$ almost surely satisfy the following:*

1. *$h_\ell(x,t) \equiv 1 - \ell$ whenever $|x| \geq t$ (droplet geometry);*
2. *The interfaces $\{h_\ell(\cdot, t)\}_{\ell \geq 1}$ do not intersect and do not share corners;*



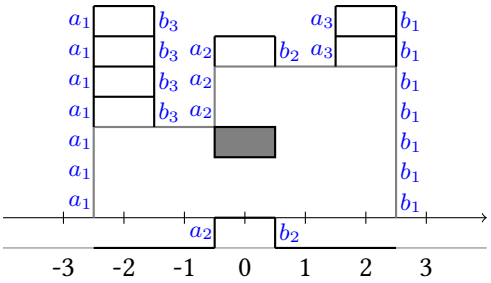
$$(1-a_1b_1)\cdot(a_1b_1)^2$$

$$\mathbf{t=1}$$



$$(1-a_1b_1)(1-a_1b_2)(1-a_2b_1)\cdot(a_1b_1)^2(a_1b_2)^1(a_2b_1)^3$$

$$\mathbf{t=2}$$



$$\prod_{i+j\le 4}(1-a_ib_j)\cdot(a_1b_1)^2(a_1b_2)^1(a_2b_1)^3(a_1b_3)^4(a_2b_2)^1(a_3b_1)^2$$

$$\mathbf{t=3}$$

Figure 3.5: Illustration of Theorem 3.1 for the example in Figure 3.3.

3. *The jumps* $\eta_\ell^{\pm}$ *of* (3.4) *are all non-negative.*

The probability $\{h_\ell\}_{\ell\ge 1}$ *of a family satisfying the above three conditions is*

$$\prod_{i+j\le t+1}(1-a_ib_j)\prod_{\ell=1}^{\infty}\prod_{x\,:\,t-x\text{ is odd}}\left[a_{(t+x+1)/2}^{\eta_\ell^+(x,t)}\cdot b_{(t-x+1)/2}^{\eta_\ell^-(x,t)}\right]. \tag{3.6}$$

Proof. An illustration for the theorem is given in Figure 3.5. The three properties satisfied by the interfaces were all discussed in the construction. Note that the law of $\{h_\ell(\cdot,t)\}_{\ell\ge 1}$ depends only on $w_{i,j}$ with $i+j\le t+1$. In fact, the algorithm for constructing $\{h_\ell(\cdot,t)\}_{\ell\ge 1}$ implies that the possible families $\{h_\ell(\cdot,t)\}_{\ell\ge 1}$ are in bijection with $\mathbb{Z}^{t(t+1)/2}$ realized as values of $w_{i,j}$, $i+j\le t+1$. This is because all these values are encoded as heights of the islands in the interfaces — the bijectivity was precisely the reason to introduce h_ℓ for $\ell>1$, and we refer to [Joh03, Section 3] for more details.

In the rest of the argument we prove the formula (3.6) by induction in t and analyze the change of the weight of the collection of interfaces as t grows. As we transition from t to $t+1$, the random growth of $h_1(\cdot,t+1)$ is governed by $t+1$ random variables $w_{i,j}$ with $i+j=t+2$.

When an island is created at point x at time $t+1$ as in the first rule of Figure 3.2, the value of $w_{(t+1+x+1)/2,(t+1-x+1)/2}$ governs this creation. If we assume this value (height of the created island) to be k, then we collect the weight of geometric distribution

$$\left(1-a_{(t+1+x+1)/2}b_{(t+1-x+1)/2}\right)\cdot a_{(t+1+x+1)/2}^k\cdot b_{(t+1-x+1)/2}^k. \tag{3.7}$$

On the other hand, both $\eta_1^{\pm}(x, t+1)$ grow by k from the island creation, leading to multiplication by the same factor (3.7) in (3.6).

All the remaining rules in $t \to t+1$ multilayer PNG evolution are deterministic, and we only need to check that they keep the value of (3.6) unchanged. For the growth of an island in the second rule of Figure 3.2 (and similar rule for h_ℓ with $\ell > 1$), note that the a-parameters correspond to the left vertical borders of islands. These borders move to the left, so that x decreases by 1 as t increases by 1. Hence, the $(t+x+1)/2$ index in a-parameter in (3.6) corresponding to a given vertical border remains unchanged. The b–parameters correspond to the right borders of islands, which move to the right with x increasing by 1 as t increases by 1. Hence, the $(t-x+1)/2$ index in b-parameter in (3.6) is also unchanged.

For the island merging in the third rule of Figure 3.2 and similar rule for h_ℓ with $\ell > 1$, note that $\eta_\ell^{\pm}$ decrease by the overlap $\omega_{\ell+1}$ (cf. (3.5)), compared to if there were no overlap. But simultaneously the island of the height $\omega_{\ell+1}$ is created in $h_{\ell+1}$ leading to the increase of $\eta_{\ell+1}^{\pm}$ by the same amount. Hence, the overlap leads to transfer of factors between ℓ and $\ell+1$ parts of (3.6), with overall product unchanged. □

3.3 From PNG to skew Schur functions

Our next task is to connect the PNG to Schur symmetric functions. We look at the fixed time distribution of the multilayer PNG and encode the interfaces $\{h_\ell(\cdot, t)\}_{\ell \geq 1}$ as a sequence of Young diagrams or partitions. For fixed t, we have $2t-1$ diagrams split into two groups $\lambda^{(1)}, \dots, \lambda^{(t)}$ and $\mu^{(1)}, \dots, \mu^{(t-1)}$. One group corresponds to even positions x and the other one to odd positions:

- $\big(\lambda_i^{(m)} + 1 - i\big)_{i \geq 1} = \big(h_i(-t-1+2m, t)\big)_{i \geq 1}, \quad m = 1, 2, \dots, t.$
- $\big(\mu_i^{(m)} + 1 - i\big)_{i \geq 1} = \big(h_i(-t+2m, t)\big)_{i \geq 1}, \quad m = 1, 2, \dots, t-1.$

The correspondence for $t = 3$ is illustrated in Figure 3.6. There the configuration of Figure 3.4 is matched to a sequence of Young diagrams $\emptyset \prec (6) \succ (3) \prec (5,1) \succ (4) \prec (6) \succ \emptyset$, where we recall the interlacement condition (2.33).

Proposition 3.2. *The interfaces $\{h_\ell(\cdot, t)\}_{\ell \geq 1}$ of the multilayer PNG at time t are in one-to-one correspondence with sequences of interlacing Young diagrams:*

$$\varnothing \prec \lambda^{(1)} \succ \mu^{(1)} \prec \lambda^{(2)} \succ \mu^{(2)} \prec \cdots \succ \mu^{(t-1)} \prec \lambda^{(t)} \succ \varnothing. \tag{3.8}$$

The distribution of $\{h_\ell(\cdot, t)\}_{\ell \geq 1}$ induced by the PNG is recast in terms of Young diagrams as

$$\left[\prod_{i+j \leq t+1} (1 - a_i b_j) \right] \cdot s_{\lambda^{(1)}}(a_1) \cdot s_{\lambda^{(1)}/\mu^{(1)}}(b_t) \cdot s_{\lambda^{(2)}/\mu^{(1)}}(a_2) \cdots s_{\lambda^{(t)}/\mu^{(t-1)}}(a_t) \cdot s_{\lambda^{(t)}}(b_1). \tag{3.9}$$

Proof. Recall that the interlacement condition $\mu \prec \lambda$ reads

$$\lambda_1 \geq \mu_1 \geq \lambda_2 \geq \mu_2 \geq \dots.$$

Hence, interlacement in (3.1) is a restatement of the second and third points in Theorem 3.1. The first point in the same theorem implies that the sequence in (3.8) starts and ends with $\varnothing$. In view of the evaluation of the skew Schur functions in one variable presented in the fourth point of Theorem 2.18,

$$s_{\lambda/\mu}(\alpha) = \begin{cases} \alpha^{\sum_{i \geq 1} (\lambda_i - \mu_i)}, & \mu \prec \lambda, \\ 0, & \text{otherwise}, \end{cases}$$

the weight (3.9) is the same as the PNG weight computed in (3.6). □

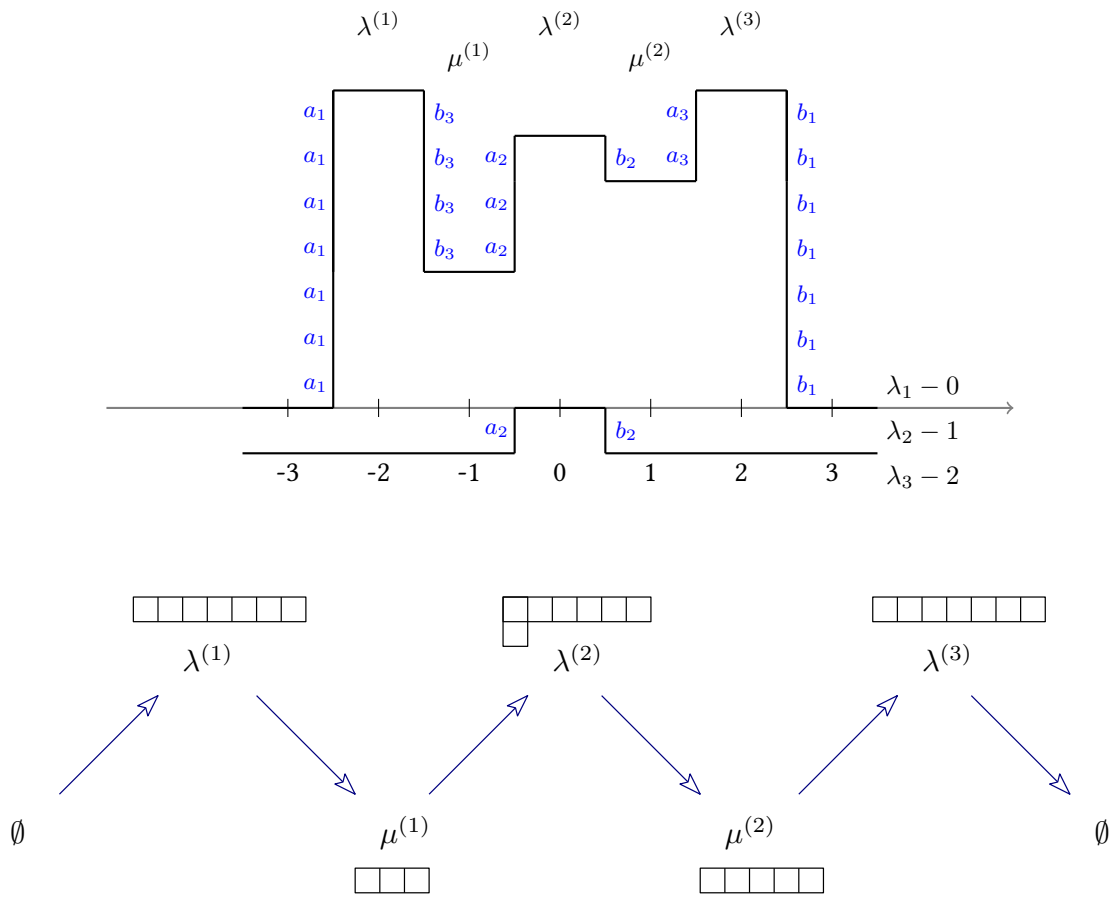


Figure 3.6: From interfaces to Young diagrams in multilayer PNG.

3.4 Schur measures and Schur processes

Inspired by Proposition 3.2, we present a generalization of a probability distribution on Young diagrams (3.9). The resulting Schur measure and Schur process were first introduced in [Oko01a, OR03].

Definition 3.3. *We call two specializations ρ_1 and ρ_2 (as in Section 2.4)* admissible *if they are both Schur-positive, and the series $\sum_{k=1}^{\infty} \frac{p_k(\rho_1)p_k(\rho_2)}{k}$ is absolutely convergent. In this situation we denote*

$$H(\rho_1;\rho_2) := \exp\left(\sum_{k=1}^{\infty} \frac{p_k(\rho_1)p_k(\rho_2)}{k}\right). \tag{3.10}$$

Definition 3.4. *Given two admissible specializations ρ_1, ρ_2, the Schur measure is a probability measure on $\mathbb{Y}$ with weights*

$$\mathbb{P}(\lambda) = \frac{s_\lambda(\rho_1)s_\lambda(\rho_2)}{H(\rho_1;\rho_2)}, \qquad \lambda \in \mathbb{Y}. \tag{3.11}$$

The Schur-positivity of ρ_1 and ρ_2 implies that $\mathbb{P}(\lambda) \geq 0$ for any $\lambda \in \mathbb{Y}$. Applying ρ_1 and ρ_2 in variables (x) and (y), respectively, to the Cauchy identity of Theorem 2.9 and justifying the convergence

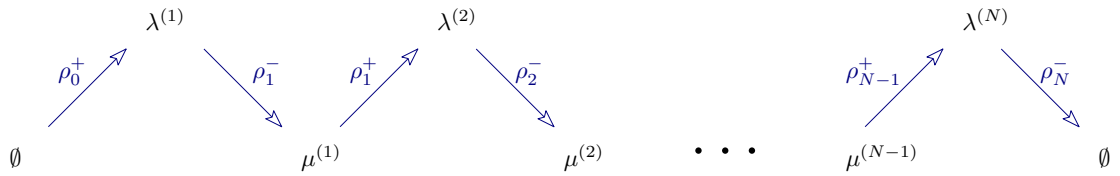


Figure 3.7: Diagram of a Schur process.

by using the absolute convergence of $\sum_{k=1}^{\infty} \frac{p_k(\rho_1)p_k(\rho_2)}{k}$, we get $\sum_{\lambda} \mathbb{P}(\lambda) = 1$. Hence, (3.11) indeed defines a probability measure on $\mathbb{Y}$.

Definition 3.5. *Given $N = 1, 2, \ldots$ and $2N$ specializations $\rho_0^+, \rho_1^+, \ldots, \rho_{N-1}^+, \rho_1^-, \rho_2^-, \ldots, \rho_N^-$, such that for each $i < j$, the pair $(\rho_i^+; \rho_j^-)$ is admissible, the* Schur process *(of rank N) is a probability measure on sequences of Young diagram $\lambda^{(1)}, \mu^{(1)}, \lambda^{(2)}, \mu^{(2)}, \ldots, \mu^{(N-1)}, \lambda^{(N)}$ with weights*

$$\begin{aligned}&\mathbb{P}\left(\lambda^{(1)}, \mu^{(1)}, \lambda^{(2)}, \mu^{(2)}, \ldots, \mu^{(N-1)}, \lambda^{(N)}\right)\\ &= \frac{1}{\prod\limits_{0 \le i < j \le N} H(\rho_i^+; \rho_j^-)} \cdot s_{\lambda^{(1)}}(\rho_0^+) \cdot s_{\lambda^{(1)}/\mu^{(1)}}(\rho_1^-) \cdot s_{\lambda^{(2)}/\mu^{(1)}}(\rho_1^+) \cdots s_{\lambda^{(N)}/\mu^{(N-1)}}(\rho_{N-1}^+) \cdot s_{\lambda^{(N)}}(\rho_N^-).\end{aligned} \tag{3.12}$$

An illustration of the Schur process with a diagram is in Figure 3.7. Several remarks are in order:

- Due to the second property in Theorem 2.18, almost surely
$$\lambda^{(1)} \supset \mu^{(1)} \subset \lambda^{(2)} \supset \cdots \supset \mu^{(N-1)} \subset \lambda^{(N)};$$
- For $N = t$, ρ_i^+ being one-α specialization with a_{i+1}, $0 \le i \le t-1$, and ρ_i^- being one-α specialization with b_{t+1-i}, $1 \le i \le t$, we return to the multilayer PNG measure of Proposition 3.2;
- By choosing some specialization to be empty $(0; 0; 0)$, we can enforce neighboring Young diagrams to coincide. For instance, $\rho_1^- = (0; 0; 0)$ implies $\lambda^{(1)} = \mu^{(1)}$ almost surely, because
$$s_{\lambda/\mu}(0; 0; 0) = \begin{cases} 1, & \lambda = \mu, \\ 0, & \lambda \ne \mu. \end{cases}.$$
- For $N = 1$, the Schur process turns into a Schur measure.

For general N, Schur measures can be obtained from a Schur process as its marginals.

Theorem 3.6. *The distribution of $\lambda^{(k)}$, obtained by summing* (3.12) *over all Young diagrams other than $\lambda^{(k)}$, coincides with the Schur measure* (3.11) *with specializations $\rho_1 = (\rho_0^+, \rho_1^+, \ldots, \rho_{k-1}^+)$ and $\rho_2 = (\rho_k^-, \rho_{k+1}^-, \ldots, \rho_N^-)$.*

Remark 3.7. Since we already know that the weights of the Schur measure (3.11) sum up to 1, a corollary is that (3.12) is a probability distribution, *i.e.*, the total sum over all $\lambda^{(1)}, \ldots, \lambda^{(N)}, \mu^{(1)} \ldots, \mu^{(N-1)}$ is 1.

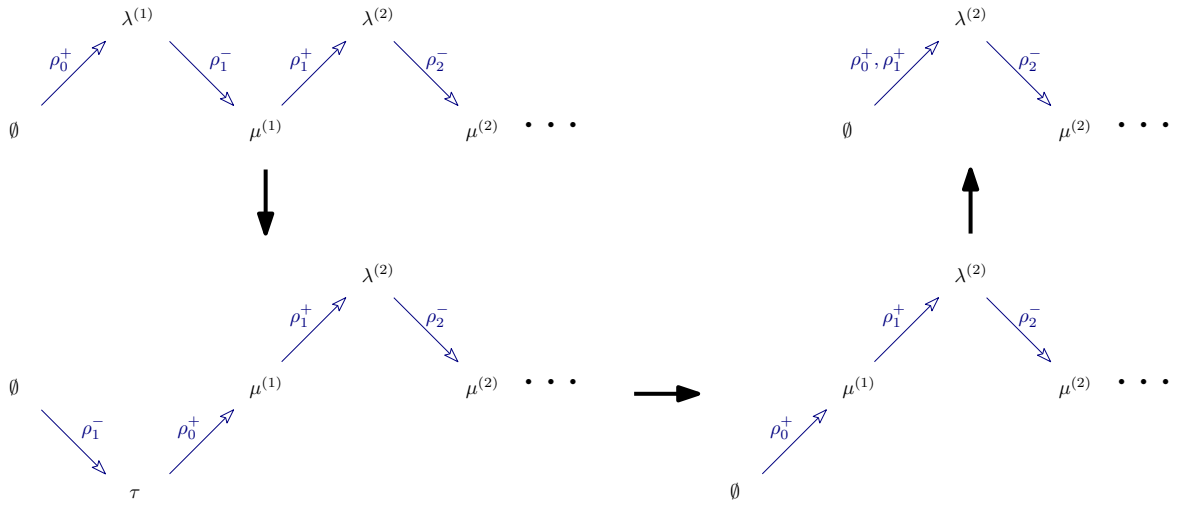


Figure 3.8: Transformation of Schur process (top-left → bottom-left → bottom-right → top-right).

Proof of Theorem 3.6. The proof is induction in N. Let us show how to sum over $\lambda^{(1)}$ and $\mu^{(1)}$ to reduce to the Schur process of rank $N-1$. The argument is schematically shown in Figure 3.8. We denote

$$\mathfrak{S} = s_{\lambda^{(2)}/\mu^{(2)}}(\rho_2^-) \cdot s_{\lambda^{(3)}/\mu^{(2)}}(\rho_2^+) \cdots s_{\lambda^{(N)}/\mu^{(N-1)}}(\rho_{N-1}^+) \cdot s_{\lambda^{(N)}}(\rho_N^-).$$

This part is kept unchanged in the induction step. Applying two specializations to the skew Cauchy identity (2.34), we get

$$\sum_{\kappa \in \mathbb{Y}} s_{\kappa/\lambda}(\rho_0^+) s_{\kappa/\mu}(\rho_1^-) = H(\rho_0^+; \rho_1^-) \sum_{\tau \in \mathbb{Y}} s_{\lambda/\tau}(\rho_1^-) s_{\mu/\tau}(\rho_0^+). \tag{3.13}$$

Hence, choosing $\lambda = \varnothing$, $\mu = \mu^{(1)}$, $\kappa = \lambda^{(1)}$, we have

$$\begin{aligned} \sum_{\lambda^{(1)}, \mu^{(1)}} & \frac{1}{\prod\limits_{0 \le i < j \le N} H(\rho_i^+; \rho_j^-)} \cdot s_{\lambda^{(1)}}(\rho_0^+) \cdot s_{\lambda^{(1)}/\mu^{(1)}}(\rho_1^-) \cdot s_{\lambda^{(2)}/\mu^{(1)}}(\rho_1^+) \cdot \mathfrak{S} \\ & = \sum_{\tau, \mu^{(1)}} \frac{H(\rho_0^+; \rho_1^-)}{\prod\limits_{0 \le i < j \le N} H(\rho_i^+; \rho_j^-)} \cdot s_{\varnothing/\tau}(\rho_1^-) \cdot s_{\mu^{(1)}/\tau}(\rho_0^+) \cdot s_{\lambda^{(2)}/\mu^{(1)}}(\rho_1^+) \cdot \mathfrak{S}. \end{aligned} \tag{3.14}$$

The presence of $s_{\varnothing/\tau}(\rho_1^-)$ forces $\tau = \varnothing$, and this factors turns into 1. Summation over $\mu^{(1)}$ can then be done using the definition of the skew Schur functions (2.28). Therefore, (5.27) transforms into

$$\frac{H(\rho_0^+; \rho_1^-)}{\prod\limits_{0 \le i < j \le N} H(\rho_i^+; \rho_j^-)} \cdot s_{\lambda^{(2)}}(\rho_0^+, \rho_1^+) \cdot \mathfrak{S}.$$

Cancelling $H(\rho_0^+; \rho_1^-)$ in the numerator and denominator, we recognize a rank $(N-1)$ Schur process, in which the ρ_1^- specialization disappeared, and the left-most specialization became the union (ρ_0^+, ρ_1^+).

A similar argument shows how to sum over $\lambda^{(N)}$ and $\mu^{(N-1)}$. Iterating both arguments $N-1$ times in total, we arrive at rank 1 Schur process, with specializations $\rho_0^+, \rho_1^+, \dots, \rho_{k-1}^+$ in the left half and $\rho_k^-, \rho_{k+1}^-, \dots, \rho_N^-$ in the right half. This is the desired Schur measure. □

Remark 3.8. Exploiting the same argument based on the skew Cauchy identity as in the proof of Theorem 3.6, one can arrive at many more identities between marginals of Schur processes of different ranks N whose specializations are related by taking unions.

Corollary 3.9. *Fix $t \in \mathbb{Z}_{\geq 1}$ and $x \in \mathbb{Z}$, such that $t + x$ is odd and $t - |x| \geq 1$, and identify the multilayer PNG configuration $\{h_\ell(x,t)\}_{\ell \geq 1}$ with $\{\lambda_1, \lambda_2 - 1, \lambda_3 - 2, \dots\}$ for a partition λ. Then λ is distributed as a Schur measure* (3.11) *with two α–specializations $\rho_1 = \big(a_1, a_2, \dots, a_{(t+x+1)/2}\big)$ and $\rho_2 = \big(b_1, b_2, \dots, b_{(t-x+1)/2}\big)$.*

In the particular case when t is odd, $x = 0$, and all a_i and all b_i parameters are equal to $\sqrt{q}$, the resulting distribution is the same as in Theorem 1.4 with $t = 2N - 1$.

3.5 Continuous PNG

3.5.1 Poisson limit

The discrete PNG becomes a simpler (and arguably more attractive) model in the continuous limit, which we now describe. The tradeoff is that the combinatorics and connections to Schur polynomials are harder to spot and prove after this limit is taken.

Consider the discrete multilayer PNG model with all a_i and b_j parameters equal to $\sqrt{q}$ so that $w_{i,j}$, $i, j \in \mathbb{Z}_{\geq 1}$ are i.i.d. with distribution

$$\mathbb{P}\left(w_{i,j} = k\right) = (1-q)q^k, \qquad k \geq 0. \tag{3.15}$$

Let us consider its $q \to 0$ limit, simultaneously rescaling all the coordinates $(i,\, j,\, x,\, t)$ by $\sqrt{q}$. In this regime, the vast majority of $w_{i,j}$ are equal to 0, some of them are equal to 1, and a negligible amount of $w_{i,j}$ are larger than one. We keep track of (i,j) where $w_{i,j} = 1$, call such (i,j) points or particles, and discard the remaining information.

Theorem 3.10. *In the limit $q \to 0$, the random set of points*

$$\left\{\left(i\sqrt{q}, j\sqrt{q}\right) : w_{i,j} = 1\right\} \tag{3.16}$$

converges to the Poisson point process of intensity 1 in the positive quadrant. Simultaneously, for each fixed $(A,B) \in \mathbb{R}^2_{>0}$,

$$\lim_{q\to 0} \#\left\{\left(i\sqrt{q}, j\sqrt{q}\right) \in [0,A] \times [0,B] : w_{i,j} \geq 2\right\} = 0, \qquad \textit{in probability.} \tag{3.17}$$

If we instead use the (t,x) coordinate system, then we arrive at the Poisson point process of intensity $\frac{1}{2}$ in the rotated quadrant $\{(t,x) \in \mathbb{R}^2 \mid t \geq 0, |x| \leq t\}$.

Proof. We delay the detailed discussion of point process till the next chapter. For now, we only need to know the fact that the Poisson point process of intensity ϱ is characterized by joint distributions of particle counts in (good enough) sets. For disjoint sets those are independent. For a set $\mathcal{A}$, the number of points in $\mathcal{A}$ is distributed as a Poisson random variable $\mathrm{Poi}(\varrho \mathrm{Area}(\mathcal{A}))$:

$$\mathbb{P}\big(\mathrm{Poi}(\varrho\mathrm{Area}(\mathcal{A})) = m\big) = e^{-\varrho\mathrm{Area}(\mathcal{A})}\frac{(\varrho\mathrm{Area}(\mathcal{A}))^m}{m!}, \qquad m = 0,1,2\dots. \tag{3.18}$$

The independence is a direct corollary of the independence of the random variables $w_{i,j}$. In order to see (3.17), note that $\mathbb{P}(w_{i,j} \leq 1) = 1 - q^2$. Hence, for a set with $O(q^{-1})$ elements, probability that $w_{i,j} \leq 1$ for all (i,j) in this set is

$$(1-q^2)^{O(q^{-1})} = 1 + O(q).$$

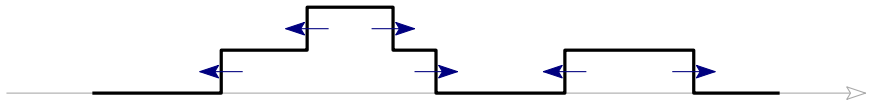


Figure 3.9: Height function of PNG model after the birth of 3 seeds.

Hence, probability of the complementary event is $O(q)$ and tends to 0 as $q \to 0$. In view of (3.17), counting the points (3.16) belonging to a set $\mathcal{A}$ is (asymptotically) the same as summing $w_{i,j}$ over all $\big(i\sqrt{q}, j\sqrt{q}\big)$ in $\mathcal{A}$. In order to compute the distribution of this sum, we recall that if $\xi_1, \xi_2, \dots, \xi_r$ are i.i.d. geometric random variables, as in (3.15), then $\xi_1 + \cdots + \xi_r$ is negative binomial[2]:

$$\mathbb{P}\big(\xi_1 + \cdots + \xi_r = m\big) = (1-q)^r q^m \binom{m+r-1}{m}, \qquad m = 0, 1, 2, \dots. \tag{3.19}$$

Setting $r = q^{-1}\mathrm{Area}(\mathcal{A})$ and sending $q \to 0$, (3.19) turns into (3.18) with $\varrho = 1$.

The statement in (x,t)–plane is obtained by a rotation, as in (3.2). □

3.5.2 Continuous PNG: singlelayer and multilayer versions

Let us spell out explicitly the process obtained in the limit $q \to 0$ from the constructions of Sections 3.1 and 3.2. This is a continuous-space, continuous-time polynuclear growth model, which combines nucleation events with growth in all directions. The origins of the model in chemistry and physics can be traced back to the Kolmogorov–Johnson–Mehl–Avrami (KJMA) framework [Kol37, JM39, Avr39, Avr40, Avr41], which provides a statistical kinetic description of phase transformations based on random nucleation events and subsequent isotropic growth. Later, the study of polymer crystal growth models led to formulations closely related to the PNG model; see, for instance, [SD71, Fra74, Gol84]. In modern theoretical physics and mathematics, the PNG model and its exact solvability were brought into focus by [PS00].

More precisely, we consider the following growth model, driven by a Poisson point process of intensity $\frac{1}{2}$ in the quadrant $t \geq 0$, $|x| < t$ of the (x,t)–plane, and illustrated in Figure 3.9.[3] At time $t \in \mathbb{R}_{\geq 0}$, the height profile is given by an integer-valued random function $h(x,t)$, $x \in \mathbb{R}$. At time zero, $h(x,0) \equiv 0$.

At any given time t and any space point x, the left and right limits of the function $h(x,t)$ differ by at most 1; in other words, $h(x,t)$ is almost surely a step function with steps of size $+1$ (an "up step", when reading the function from left to right) and -1 (a "down step"). If there is a point of the Poisson process at (z,t), then a nucleation event occurs: at time t, a *seed* is born at position $x = z$, consisting of an up step and a down step, that is, $h(z,t)$ increases by 1. After that, the down step moves to the right with speed 1, while the up step moves to the left with the same speed. When a subsequent seed is born, another pair of up and down steps appears and also begins to expand. When up and down steps (originating from different seeds) meet, they annihilate and both disappear.

For the multilayer continuous PNG, we call the above evolution $h_1(x,t)$, and more generally introduce $h_\ell(x,t)$, $\ell \geq 2$. The evolution rule for h_ℓ is exactly the same as for $h_1(x,t)$, expect for the origin of the seeds: a seed on level ℓ, $\ell \geq 2$, is born at time t and position x when the up and down steps collide at level $\ell - 1$ at the same (x,t) position. A simulation is provided in Figure 3.10.

Theorem 3.11. *For a fixed $t \geq 0$, we identify the continuous multilayer PNG configuration $\{h_\ell(0,t)\}_{\ell \geq 1}$ with $\{\lambda_1, \lambda_2 - 1, \lambda_3 - 2, \dots\}$ for a partition λ. Then λ is distributed as a Schur measure* (3.11) *with two*

[2] A direct proof can be obtained by induction in r.

[3] As in the discrete setup, placing the nucleations into the cone $|x| < t$ corresponds to the droplet geometry, cf. Figure 3.10.

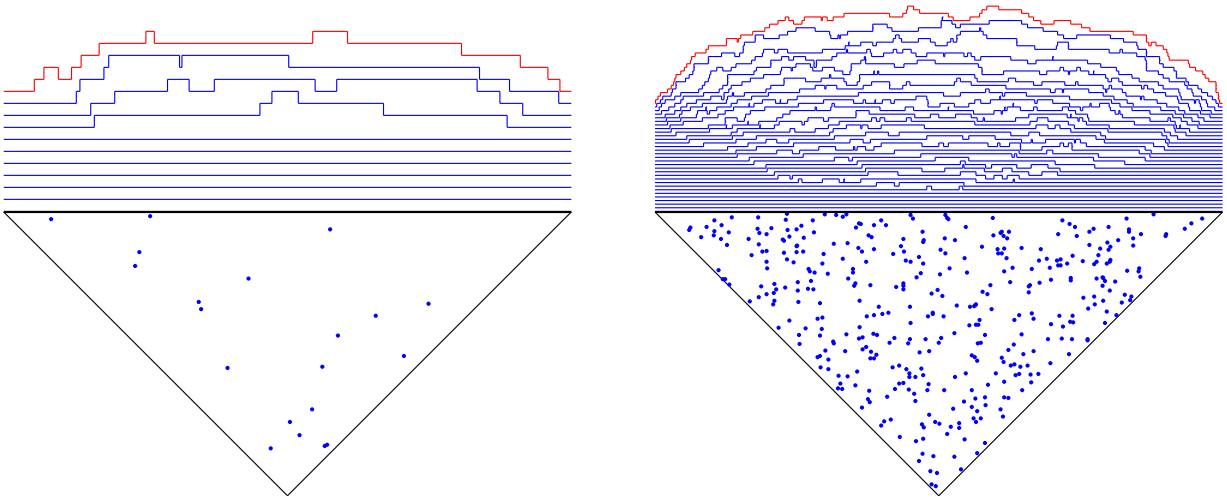


Figure 3.10: Multilayer PNG simulations. Left panel: after 20 nucleation events. Right panel: after 400 nucleation events.

Plancherel specializations $\rho_1 = \rho_2 = (0; 0, t/2)$. *This is also known as the* Poissonized Plancherel measure *of weight*

$$\mathbb{P}(\lambda) = e^{-\theta} \frac{\theta^{|\lambda|} \dim^2(\lambda)}{(|\lambda|!)^2}, \qquad \theta = \frac{t^2}{4}. \tag{3.20}$$

Proof. We start from Corollary 3.9 for odd t, $x = 0$, and all $a_i = b_j = \sqrt{q}$. We rescale t by $\sqrt{q}$, so that the specializations ρ_1 and ρ_2 become $(\frac{t}{\sqrt{q}} + 1)/2$ tuples of $\sqrt{q}$. Taking the limit to Plancherel, as in (2.44), we get two specializations $(0; 0; \frac{t}{2})$. The Schur measure with these specializations was identified with (3.20) by Proposition 2.26. □

Note the difference between (3.20) and the Plancherel measure of (2.47): in the latter the number of boxes $n = |\lambda|$ was fixed, while in the former it fluctuates according to the Poisson distribution with parameter (mean) $\theta = t^2/4$. An analogue of Theorem 3.11 can be also obtained by a very similar argument for the distribution of $\{h_\ell(x, t)\}_{\ell \geq 1}$ for any fixed (x, t).

3.5.3 From PNG to LPP

An alternative way to view the continuous time PNG is via a graphical construction involving Poisson points. Take a realization of the Poisson point process of intensity $\frac{1}{2}$ in the quadrant $t \geq 0$, $|x| < t$ of the (x, t)–plane, and draw two rays from each nucleation event in the up direction of slopes $+1$ and -1. A ray ends upon crossing another ray. The union of all parts of (pieces of) rays obtained in this way forms a collection of broken lines, see Figure 3.11. The height $h_1(x, t)$ is then the number of lines crossed along the path from $(x, 0)$ to (x, t). We leave it as an exercise to the reader to check that this construction leads to exactly the same process as $h_1(x, t)$ in the previous section.[4]

As a consequence, we can interpret the PNG height as the last passage time in the *Poissonian last passage percolation model*, cf. Section 1.4 and Figure 3.11.

Proposition 3.12. *Consider the points of the Poisson process from the definition of continuous PNG. The value* $h_1(x, t)$ *is equal to the maximal number of points one can collect along a path* $(0, 0) \to (x, t)$*, which*

[4]Hint: the rays represent the space-time trajectories of up and down steps.

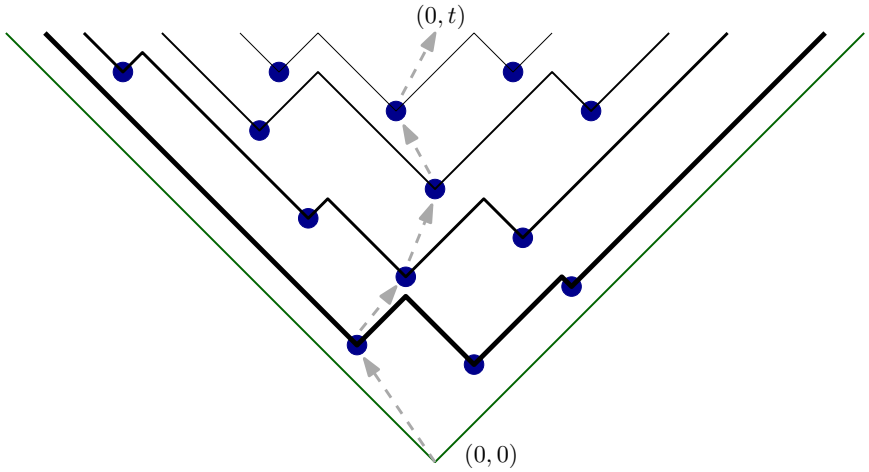


Figure 3.11: Graphical construction of generating the interface height from the Poisson points, broken lines and a monotone path collecting maximal number of points.

*is monotone in the sense that x coordinate grows slower than t coordinate (*i.e.*, the absolute value of the path slope is larger than 1).*

Proof. Note that each point on the monotone path necessarily belongs to a different broken line. Hence, the maximal number of points on a monotone path is at most $h_1(x,t)$. For the opposite inequality, one proves by induction in k that each (x,t) between the kth (from the bottom) and the $(k+1)$st broken line can be connected to $(0,0)$ by a monotone path going through k points of the process. □

3.6 Longest increasing subsequences in a random permutation

Poissonian LPP naturally connects to a combinatorial question about permutations of $\{1,\dots,n\}$.

Definition 3.13. *Let $\sigma = (\sigma(1),\dots,\sigma(n)) \in \mathcal{S}_n$ be a permutation of $\{1,\dots,n\}$. We say that σ has an increasing subsequence of length k, $(n_1,\dots,n_k) \subset (\sigma(1),\dots,\sigma(n))$, if $1 \le n_1 < n_2 < \cdots < n_k \le n$.*

For example, $(3,4,5,6)$ is an increasing subsequence of length 4 for the permutation

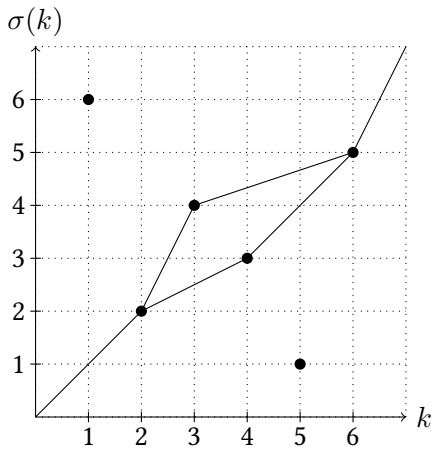
$$\sigma = \begin{pmatrix} 1 & 2 & 3 & 4 & 5 & 6 & 7 \\ 3 & 4 & 1 & 7 & 5 & 2 & 6 \end{pmatrix}. \tag{3.21}$$

Definition 3.14. *We denote by $L(\sigma)$ the length of the longest increasing subsequence (or one of them) for the permutation σ.*

In order to connect to LPP, let us give a geometric interpretation of $L(\sigma)$. Represent a permutation σ as N points $(k,\sigma(k))$, $k = 1,2,\dots$. Then $L(\sigma)$ is identified with the maximal number of points collected along a top-right monotone (*i.e.*, with both coordinates increasing) path joining $(0,0)$ with $(n+1,n+1)$, see Figure 3.12 for an example with $n = 6$.

We see a clear analogy with the construction of Section 3.5.3 which can be formalized by introducing two different random variables:

- For $n = 1,2,3,\dots$, we let L_n be the length of the longest increasing subsequence in a uniformly random permutation of n letters.



$$\sigma = \begin{pmatrix} 1 & 2 & 3 & 4 & 5 & 6 \\ 6 & 2 & 4 & 3 & 1 & 5 \end{pmatrix}$$

Figure 3.12: Permutation (624315) with two longest increasing subsequences $(2, 4, 5)$ and $(2, 3, 5)$.

- For $\theta \in \mathbb{R}_{>0}$ we let L^θ be obtained through a two-step sampling algorithm: first choose n to be Poisson-distributed with parameter (mean) equal to θ. Then set $L^\theta = L_n$, where we agree that $L_0 = 0$.

Theorem 3.15. *The following distributional identities hold:*

1. $L^\theta \stackrel{d}{=} h_1(0, t)$, *where* $h_1(x, t)$ *is the interface of the continuous PNG and* $\theta = \frac{t^2}{4}$.
2. $L^\theta \stackrel{d}{=} \lambda_1$, *where* $\lambda \in \mathbb{Y}$ *is sampled from the Poissonized Plancherel measure* (3.20).
3. $L_n \stackrel{d}{=} \tilde{\lambda}_1$, *where* $\tilde{\lambda} \in \mathbb{Y}_n$ *is sampled from the Plancherel measure* (2.47).

Proof. We prove the equalities in the order they are listed. Using Proposition 3.12 and rotating by $\pi/4$, we see that $h_1(0, t)$ has the same law as the maximal number of points of the Poisson point process of intensity $\frac{1}{2}$ in the square $\left[0, \frac{t}{\sqrt{2}}\right] \times \left[0, \frac{t}{\sqrt{2}}\right]$ which can be collected among a monotone path connecting $(0, 0)$ with $\left(\frac{t}{\sqrt{2}}, \frac{t}{\sqrt{2}}\right)$. Let the total number of points in this square be n, and let their coordinates be (u_1, v_1),..., (u_n, v_n). Then we are looking for the maximal length of a sequence $1 \le n_1 < n_2 < \cdots < n_\ell \le n$ such that

$$u_{n_1} \le u_{n_2} \le \cdots \le u_{n_\ell}, \qquad \text{and} \qquad v_{n_1} \le v_{n_2} \le \cdots \le v_{n_\ell}.$$

Note two facts, which follow from the basic properties of the Poisson point process of intensity $\frac{1}{2}$, cf. [Kin93, DVJ03]:

- The distribution of n is Poisson with mean equal to half the area of $\left[0, \frac{t}{\sqrt{2}}\right] \times \left[0, \frac{t}{\sqrt{2}}\right]$, *i.e.*, with mean $\frac{t^2}{4}$.
- Conditional on the value of n, the points (u_i, v_i) are uniformly distributed in $\left[0, \frac{t}{\sqrt{2}}\right] \times \left[0, \frac{t}{\sqrt{2}}\right]$. Hence, all their relative orders are equiprobable, and the maximal length of a monotone subsequence has the same distribution as L_n.

Comparing to the definition of L^θ with $\theta = \frac{t^2}{4}$, we obtain the first equality. The second identity follows from the first one and Theorem 3.11.

For the third equality note that distributions in the both sides of the second equality are convergent power series in θ. Their coincidence for all $\theta > 0$ implies that the coefficients of these power series must be the same. The coefficient of θ^n gives the desired equality. □

The problem of the asymptotic behavior of L_n as $n \to \infty$ was formulated and promoted by Ulam in the early 1960s [Ula61] in the context of Monte Carlo methods. The simulations (attributed by Ulam to E. Neighbor) seemed to indicate $L_n = O(\sqrt{n})$ and Gaussian fluctuations. Early mathematical progress was made by Hammersley, who introduced a formulation through Poisson points on the plane and proved a law of large numbers $L_n \sim c\sqrt{n}$ using subadditivity [Ham72]. The exact asymptotic constant was predicted to be 2 based on simulations in [BB68] and heuristics in [Ham72]. Subsequently, Logan and Shepp [LS77] showed $c \geq 2$ and independently Vershik and Kerov [VK77] showed $c = 2$. These papers exploited the interplay between L_n and the limit shape of Young diagrams under Plancherel measure (cf. Figure 2.4) via the Robinson–Schensted correspondence, which is a variation of our approach here, but without the detour through discrete PNG.

A central open question — the nature of the fluctuations — remained open until a breakthrough of Baik, Deift, and Johansson [BDJ99], who showed that the asymptotic distribution of $n^{1/6}(L_n - 2\sqrt{n})$ is Tracy-Widom distribution F_2; thus, Gaussian predictions from [Ula61] were wrong. Three influential extensions of this result soon followed in [Joh01a, BOO00, Oko00]. We will also arrive at this asymptotic statement in the next chapter. The book [Rom15] gives a very nice introduction to the mathematics surrounding the longest increasing subsequences.

The problem of determining the asymptotics of L_n admits two real life interpretations. In the *airplane boarding problem*, one imagines passengers with numbered seats arriving in random order along a single aisle. A passenger can proceed to their seat only if all smaller-numbered passengers ahead of them are already seated; once this condition is met, seating takes one unit of time. In this interpretation, L_n represents the total time required to board the airplane. Further details on modeling the boarding process can be found in [BBS$^+$06].

Another popular viewpoint is provided by *patience sorting*, a solitaire card game whose greedy sorting algorithm, introduced by Mallows [Mal73] and analyzed by Aldous and Diaconis [AD99], decomposes a permutation into decreasing subsequences ("piles"), with the number of piles equal to the length of the longest increasing subsequence. The mathematical model studied in these works involves a single card suit, corresponding to a permutation of distinct numbers; the actual card game uses four suits and is substantially more complex and far less understood.

3.7 Exercises

Problem 1. Consider the Schur process of Definition 3.5 and choose $1 \leq k < m \leq N$. By generalizing the proof of Theorem 3.6, show that the joint distribution of $\lambda^{(k)}$ and $\lambda^{(m)}$ is the same as the joint distribution of two λs in the rank 2 Schur process

$$\lambda^{(k)} \supset \mu \subset \lambda^{(m)}$$

with probability distribution

$$\mathbb{P}\big(\lambda^{(k)}, \mu, \lambda^{(m)}\big) = \frac{1}{H(\tilde{\rho}_0^+; \tilde{\rho}_1^-) H(\tilde{\rho}_0^+; \tilde{\rho}_2^-) H(\tilde{\rho}_1^+; \tilde{\rho}_2^-)} s_{\lambda^{(k)}}(\tilde{\rho}_0^+) s_{\lambda^{(k)}/\mu}(\tilde{\rho}_1^-) s_{\lambda^{(m)}/\mu}(\rho_1^+) s_{\lambda^{(m)}}(\tilde{\rho}_2^-), \tag{3.22}$$

$$\tilde{\rho}_0^+ = (\rho_0^+, \rho_1^+, \ldots, \rho_{k-1}^+), \quad \tilde{\rho}_1^+ = (\rho_k^+, \ldots, \rho_{m-1}^+), \quad \tilde{\rho}_1^- = (\rho_k^-, \ldots, \rho_{m-1}^-), \quad \tilde{\rho}_2^- = (\rho_m^-, \ldots, \rho_N^-).$$

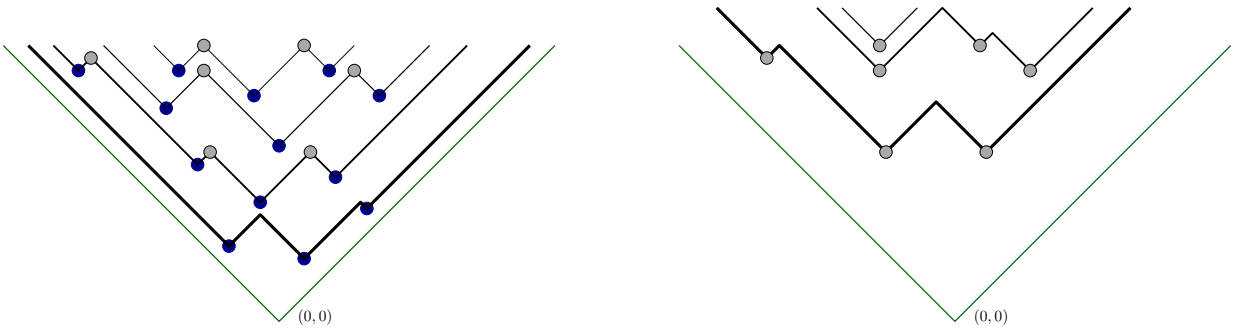
Problem 2. Consider the Schur process of Definition 3.5 and choose $1 \leq k \leq N-1$. Prove that the marginal distribution of $\mu^{(k)}$ is a Schur measure. What are the specializations?

Problem 3. Let σ be a permutation of n letters. Show that σ necessarily either has an increasing subsequence of length $\sqrt{n}$ or a decreasing subsequence of length $\sqrt{n}$. Recall that L_n is the length of the longest increasing subsequence in a uniformly random permutation, and deduce the lower bound $\mathbb{E}L_n \geq \frac{1}{2}\sqrt{n}$.

Problem 4. Consider the unit square $[0,1] \times [0,1]$, take n points in the lower triangle $0 < y < x < 1$, other n points which are mirror-images with respect to the diagonal $x = y$, and yet other m points on the diagonal $x = y$. If we order the resulting $2n + m$ points by their first coordinates, then the order of second coordinates encodes a permutation σ. Assuming all x–coordinates and all y–coordinates to be distinct, show that σ is an involution, *i.e.*, $\sigma^2 = \mathrm{Id}$.

Problem 5. Our goal is to generalize the correspondence of Theorem 3.15 to $h_k(x,t)$, λ_k, $\tilde{\lambda}_k$ with $k > 1$.

A. The broken lines of Figure 3.11 have down-corners corresponding to the Poisson point process, and up-corners corresponding to the new set of points. Erase all Poisson points and draw a new collection of broken lines, by starting two new rays with slope ± 1 from each new point and ending them upon crossing. Here is an example:



Prove that the shifted height $(h_2(x,t)+1)$ is equal to the number of new broken lines crossed along the path from $(x,0)$ to (x,t) and is also equal to the maximal number of new points one can collect along a monotone path $(0,0) \to (x,t)$.

B. Extend the procedure of part **A** to a similar geometric way to compute $h_k(x,t)$, for each $k \geq 1$.

C***.** Prove that for each $k \geq 1$, the sum $h_1(x,t) + (h_2(x,t)+1) + \cdots + (h_k(x,t)+k-1)$ equals the maximal number of the points of the Poisson process of Section 3.5.3, which can be collected by k paths $(0,0) \to (x,t)$, which are monotone in the sense that x coordinate grows slower than t coordinate.

D. Prove Greene's theorem: The distribution of $\lambda_1 + \cdots + \lambda_k$, for $\lambda \in \mathbb{Y}_n$ distributed according to the Plancherel measure, is the same as the maximal total length of k disjoint increasing subsequences in a uniformly random permutation in $\mathcal{S}_n$.

Problem 6. A semistandard Young tableaux of shape λ and rank N is a filling of a boxes of a Young diagram λ with integers between 1 and N, in such a way that the entries are non-decreasing along the rows and (strictly) increasing along the columns. Here are some examples for rank $N = 5$:

1	1	2	2
3	4		

1	1	1	1
2	3		

1	3	3	4
4	4		
5			

Denote by $M^n_{K,L}$ the set of matrices of size $K \times L$ with nonnegative integral entries, total sum of entries equal to n. The Robinson-Schensted-Knuth correspondence[5] (RSK) establishes a bijection between $M^n_{K,L}$ and the set of ordered pairs of semistandard Young tableaux of the same shape with n boxes, the first tableau of rank K, while the second of rank L.

A. Let $0 < q < 1$. Consider a random $K \times L$ matrix with nonnegative integral entries that are independent identically distributed random variables with geometric distribution $\mathbb{P}(\xi = m) = (1-q)q^m$, $m = 0, 1, \dots$. Via the RSK, this random matrix induces a probability distribution on $\mathbb{Y}$; the random Young diagram is the shape of the tableaux associated to the random matrix. Show that this distribution is a Schur measure. What are the specializations?

B. Let W^n_K denote the set of all words of length n in the alphabet $\{1, 2, \dots, K\}$. Each such word can be identified with an element of $M^n_{K,n}$, in which each column j has exacly one non-zero element, which is equal to 1. Denoting the row of this element by $w(j) \in \{1, 2 \dots, n\}$, the matrix corresponds to the word $w(1)w(2) \dots w(n)$. Hence, RSK restricts onto W^n_K. Consider the following continuous time Markov chain on the set of all words $\bigsqcup_{n=0}^{\infty} W^n_K$, depending on K real parameters $a_1, \dots, a_K \geq 0$: the initial condition is the empty word of length 0; new letters are appended at the end of the word with intensity a_k for appending k, $1 \leq k \leq K$ (equivalently, a new letter k is appended after independent exponential waiting time of mean a_k^{-1}). Applying the RSK and keeping track of the shape of the Young tableau, we get a stochastic process on Young diagrams λ^t, $t \geq 0$. Prove that for each fixed t, the law of λ^t is a Schur measure. What are the specializations?

Hint. You can use without proof that for the restriction of RSK onto W^n_K, the second Young tableau is standard, while the entries (with multiplicities) of the first one are the letters of the word.

C. Each permutation $\sigma \in \mathcal{S}_n$ can be represented as a word in W^n_n, and therefore as a matrix in $M^n_{n,n}$, in which each row and each column have exactly one non-zero element equal to 1. Hence, we can apply the RSK to permutations. Prove that the RSK pusforward of the uniform measure on $\mathcal{S}_n$ is the Plancherel measure.

Literature. We used the following sources for composing problems and refer to them for more information, references, and connections: [Rob38], [Sch61], [Knu70], [Vie77], [Gre74], [Sag01], [BR01], [PS02], and [OR03].

[5] You can use RSK a black box in this problem or read about it in [Ful97, Sag01].

Chapter 4

Determinantal point processes

In the previous chapter we discussed a connection between growth models and combinatorics of Schur polynomials. It is not yet clear how this is going to help us in investigating the asymptotic questions. The answer originates in the determinantal structures. Many results in integrable probability rely on manipulations with determinants in various ways. The definitions and properties of Schur functions already involved determinants in (2.14), (2.12), (2.24), (2.30). In this chapter we will see how determinants appear in the probabilistic context of random point processes.

We start from abstract point processes, then specialize to determinantal point processes, and finally show how the Schur measures fit into this formalism.

4.1 Point processes and correlation functions

Consider a reasonable "state space" or "one particle space" $\mathfrak{X}$, say the real line $\mathbb{R}$, or the Euclidean space $\mathbb{R}^d$, or a discrete space such as the set $\mathbb{Z}$ of integers, or its subset. We assume that $\mathfrak{X}$ is a topological space, *i.e.*, there are open sets, compact sets, convergence, etc. A *point configuration* X in $\mathfrak{X}$ is a locally finite (*i.e.*, without accumulation points) collection of points of the space $\mathfrak{X}$. For our purposes it suffices to assume that the points of X are always pairwise distinct. The set of all point configurations in $\mathfrak{X}$ will be denoted as $\mathrm{Conf}(\mathfrak{X})$.

A compact subset $A \subset \mathfrak{X}$ is called *a window*. For a window A and $X \in \mathrm{Conf}(\mathfrak{X})$, set $N_A(X) = |A \cap X|$ (number of points of X in the window). Thus, N_A is a function on $\mathrm{Conf}(\mathfrak{X})$. We equip $\mathrm{Conf}(\mathfrak{X})$ with the Borel structure generated by functions N_A for all windows A. In other words, we consider the smallest σ–algebra, which makes all functions N_A measurable.

Definition 4.1. *A random point process on $\mathfrak{X}$ is a probability measure on $\mathrm{Conf}(\mathfrak{X})$.*

We will often use the term *particles* for the elements of a random point configuration. Thus, we will speak about particle configurations[1].

For the first example we take $\mathfrak{X}$ to be the lattice $\mathbb{Z}$ of integers. A particle configuration on $\mathbb{Z}$ is simply an arbitrary subset $X \subset \mathbb{Z}$, the assumption of absence of accumulation points holds automatically.

Fix a real number $p \in (0, 1)$. The *Bernoulli point process* with parameter p on $\mathbb{Z}$ is constructed as follows: for each integer $i \in \mathbb{Z}$ we put a particle at the node i with probability p, independently of other nodes. This procedure leads to a random particle configuration. Equivalently, the Bernoulli process is a doubly infinite sequence ξ_i, $i \in \mathbb{Z}$, of binary independent random variables, such that each ξ_i takes value

[1] Another point of view is to consider random point processes as random point measures, where the measure is the sum of Dirac unit mass measures supported by the particle positions.

1 or 0 with probability p or $1-p$, respectively. Then the random configuration X consists of those i's for which $\xi_i = 1$.

Lemma 4.2. *For the Bernoulli point process, for each finite $A \subset \mathbb{Z}$ with $|A| = n$, the random variable N_A is distributed as a binomial random variable* $\mathrm{Bin}(n, p)$*:*

$$\mathbb{P}(N_A = k) = p^k (1-p)^{n-k} \binom{n}{k}, \qquad 0 \le k \le n.$$

For disjoint sets $A_1, \ldots, A_m$ the random variables $\{N_{A_j}\}_{j=1}^m$ are independent.

Proof. The proof follows by observing that N_A can be represented as a sum of n independent Bernoulli random variables. Independence of N_{A_j} follows from the independence of ξ_i. □

Our second example is the homogeneous Poisson process on $\mathbb{R}$.

Definition 4.3. *The Poisson point process on $\mathbb{R}$ of (constant) intensity ϱ is determined by random variables N_A for each compact set A of Lebesgue measure $|A|$ having a Poisson distribution of mean $\varrho|A|$,* i.e.*,* $\mathrm{Poi}(\varrho|A|)$*:*

$$\mathbb{P}(N_A = k) = e^{-\varrho\chi} \frac{(\varrho|A|)^k}{k!}, \qquad k = 0, 1, 2, \ldots.$$

For disjoint sets $A_1, \ldots, A_m$ the random variables $\{N_{A_j}\}_{j=1}^m$ are independent.

Remark 4.4. In the same way we can define the Poisson point process on $\mathbb{R}^d$, with the only difference being that A is now a compact subset of $\mathbb{R}^d$. We stick to $d = 1$ throughout this section, but all the constructions have direct analogues for $d > 1$.

The consistency of this definition follows from the fact that the sum of independent Poisson random variables is again Poisson: $\mathrm{Poi}(a) + \mathrm{Poi}(b) = \mathrm{Poi}(a+b)$.

If one wishes to construct the Poisson point process from a collection of i.i.d. random variables, there are several ways to do so. The most classical construction proceed through the observation that spacings between adjacent particles are independent exponential random variables of mean ϱ^{-1}, see, *e.g.*, [Bil12, Section 23]. Alternatively, one can take a limit from the Bernoulli point process:

Lemma 4.5. *Take $\varepsilon > 0$ and embed the integer lattice into $\mathbb{R}$ as $\varepsilon\mathbb{Z}$. Then the Bernoulli point process of parameter $p = \varepsilon\varrho$ converges in distribution as $\varepsilon \to 0$ to the Poisson process of intensity ϱ.*

Proof. Let us start by decoding what "convergence in distribution" means. Since we defined the point process through the random variables N_A, we should also use them here. Hence, we say that point processes converge in distribution whenever all finite-dimensional distributions of random variables N_A (where A is a compact subset of $\mathfrak{X}$) converge.

Take an interval $[u, v] \subset \mathbb{R}$ and let m_ε denote the number of points of $\varepsilon\mathbb{Z}$ belonging to the interval. Clearly, $\varepsilon m_\varepsilon \to v - u = \mathrm{length}([u, v])$ as $\varepsilon \to 0$. Hence, by a straightforward computation, for $A = [u, v]$

$$\lim_{\varepsilon\to 0} \mathbb{P}\left(N_A^{\text{Bernoulli}} = k\right) = \lim_{\varepsilon\to 0} \left[(\varepsilon\varrho)^k (1-\varepsilon\varrho)^{m_\varepsilon - k} \frac{(m_\varepsilon)!}{(m_\varepsilon - k)!} \cdot \frac{1}{k!}\right]$$
$$= e^{-\varrho(v-u)} \frac{(\varrho(v-u))^k}{k!} = \mathbb{P}\left(N_A^{\text{Poisson}} = k\right).$$

Hence, for $A = [u, v]$ we have the desired convergence in distribution for N_A. The same argument also works for open intervals. Using independence for disjoint N_A, which is true both for Bernoulli

and Poisson cases, we extend the convergence to A being a union of intervals, and to joint distributions over finite collections $A_1, A_2, \dots A_l$. Representing open sets as unions of disjoint open intervals, we can further extend to an arbitrary open and bounded A and to finite collections of those.

For a general compact A, we can always choose r large enough, so that $A \subset [-r, r]$. Then $[-r, r] \setminus A$ is open, and using the joint convergence for this set and for the segment $[-r, r]$, we also get $\varepsilon \to 0$ convergence for such N_A. □

Here is a different construction of the Poisson process:

Lemma 4.6. *Let $M = 1, 2, 3, \dots$. Take the interval $\left[-\frac{M}{2\varrho}, \frac{M}{2\varrho}\right]$ and place M particles in it, uniformly and independently of each other. In the limit as $M \to \infty$, these collections converge in distribution to the Poisson point process of intensity ϱ.*

Proof. Take two disjoint intervals: $[x, y], [u, v] \subset \mathbb{R}$. For large enough M, we have

$$\mathbb{P}\big(k \text{ particles in } [x, y] \text{ and } l \text{ particles in } [u, v]\big) = \frac{M!}{k!l!(M-k-l)!} \left(\varrho\frac{y-x}{M}\right)^k \left(\varrho\frac{v-u}{M}\right)^l \left(1 - \varrho\frac{y-x}{M} - \varrho\frac{v-u}{M}\right)^{M-k-l}.$$

Sending $M \to \infty$, we get the probabilities corresponding to the Poisson point process of intensity ϱ:

$$\frac{1}{k!l!} \left(\varrho(y-x)\right)^k \left(\varrho(v-u)\right)^l \exp\big(-\varrho(y-x) - \varrho(v-u)\big).$$

The same argument works for any collection of disjoint intervals, and we arrive at Definition 4.3. □

The limits of Lemmas 4.5 and 4.6 contain a few important ideas:

- First, the idea of a limit transition: starting from a discrete ensemble one can get a continuous ensemble; starting from M–particle configurations one can get infinite particle configurations.
- Second, the limit transition may lead to a simplification. The structure of the joint distribution of $N_{A_1}, \dots, N_{A_k}$ simplifies in the limit of Lemma 4.6: dependencies between particle counts disappear as $M \to \infty$.
- Third, we observe a hint of the universality: very different object are leading to exactly the same scaling limit in both lemmas.

How to describe a point process that would be more complicated than Poisson? The problem here comes from the fact that the space of particle configurations $\mathrm{Conf}(\mathfrak{X})$ is, typically, infinite–dimensional and, thus, there is no natural "Lebesgue measure" which could be used for writing densities. One solution is to use *correlation functions*.

Let us temporarily restrict ourselves to point processes on a finite or countable discrete space $\mathfrak{X}$ (for instance, the reader may assume $\mathfrak{X} = \mathbb{Z}$). Such a process is the same as a collection $\{\xi_x\}$ of binary random variables, indexed by elements $x \in \mathfrak{X}$, which indicate the presence of a particle at x. (They are often called *occupancy variables*.) The Bernoulli process was a simple example. Now we no longer assume that these variables are independent and identically distributed; they may have an arbitrary law. Their law is simply an arbitrary probability measure $\mathbb{P}$ on the space of all configurations. This is a large space, it can be described as the infinite product space $\{0, 1\}^{\mathfrak{X}}$. Thus, defining a point process on $\mathfrak{X}$ amounts to specifying a probability measure $\mathbb{P}$ on $\{0, 1\}^{\mathfrak{X}}$.

Definition 4.7. *Let A range over* finite *subsets of discrete $\mathfrak{X}$. The correlation function of a point process X on $\mathfrak{X}$ is the function $\rho(A)$ defined by*

$$\rho(A) = \mathbb{P}(A \subset X).$$

If A has n points, $A = \{x_1, \dots, x_n\}$, then we also employ the alternative notation

$$\rho(A) = \rho_n(x_1, \dots, x_n).$$

In this notation, the single function ρ splits into a sequence of functions $\rho_1, \rho_2, \dots$, where ρ_n is a symmetric function in n distinct arguments from $\mathfrak{X}$, called the *nth correlation function.*

Equivalently, in terms of occupation random variables $\{\xi_x\}$, we have

$$\rho_n(x_1, \dots, x_n) = \mathbb{P}(\xi_{x_1} = \dots = \xi_{x_n} = 1). \tag{4.1}$$

For example, for the Bernoulli process one easily sees that $\rho(A) = p^{|A|}$.

Lemma 4.8. *A random point process on a discrete set $\mathfrak{X}$ is uniquely determined by its correlation functions.*

Proof. The law of a point process on $\mathfrak{X}$ is determined by the probabilities of all cylindrical events, describing the positions of particles. Those can be encoded using the following sets:

$$U_A^B = \{X : X \cap B = A\} \subset \operatorname{Conf}(\mathfrak{X})$$

where $A \subset B$ is a pair of finite sets. The sets U_A^B generate the same σ–algebra on $\operatorname{Conf}(\mathfrak{X})$ as functions N_A. A probability measure $\mathbb{P}$ on $\{0,1\}^{\mathfrak{X}}$ is uniquely determined by its values $\mathbb{P}(U_A^B)$ on such sets. Thus, it suffices to show that the correlation function determines these values. This follows from the formula

$$\mathbb{P}(U_A^B) = \sum_{C : A \subseteq C \subseteq B} (-1)^{|C|-|A|} \rho(C),$$

which is a direct corollary of the inclusion–exclusion principle. □

Let us now extend the definition of the correlation functions to arbitrary, not necessarily discrete state spaces $\mathfrak{X}$. If the space is continuous, then the probabilities in Definition 4.7 might all be zeros, and we need to adjust our point of view.

Definition 4.9. *Given a random point process on $\mathfrak{X}$, we define a sequence $\{\rho_n\}_{n=1}^{\infty}$, where ρ_n is a symmetric measure on $\mathfrak{X}^n$ called the nth* correlation measure. *The correlation measures are characterized by the following property: for any $n \geq 1$ and a compactly supported bounded Borel function f on $\mathfrak{X}^n$, one has*

$$\int_{\mathfrak{X}^n} f \mathrm{d}\rho_n = \mathbb{E}\left(\sum_{x_{i_1}, \dots, x_{i_n} \in X} f(x_{i_1}, \dots, x_{i_n}) \right), \tag{4.2}$$

where $\mathbb{E}$ denotes averaging with respect to our point process, and the sum on the right is taken over all n-tuples of pairwise distinct points of the random point configuration X.

In particular, for $n = 1$ we have

$$\int_{\mathfrak{X}} f(x) \rho_1(\mathrm{d}x) = \mathbb{E}\left(\sum_{x \in X} f(x) \right),$$

and ρ_1 is often called the *density measure* or *intensity measure* of a point process.

Proposition 4.10. *If $\mathfrak{X}$ is discrete, then Definitions 4.7 and 4.9 coincide.*

Proof. Given correlation functions in the discrete setting as in (4.1), we extend their definitions to possibly coinciding x_i by setting $\rho(x_1, \dots, x_n) = 0$ whenever $x_i = x_j$. Then $\rho(x_1, \dots, x_n)$ can be treated as weights of a measure on $\mathfrak{X}^n$. Let us check that (4.2) holds. Note that both sides are linear in f, and therefore it is sufficient to choose some $y_1, \dots, y_n \in \mathfrak{X}$ and verify the identity for

$$f(x_1, \dots, x_n) = \begin{cases} 1, & (x_1, \dots, x_n) = (y_1, \dots, y_n), \\ 0, & \text{otherwise.} \end{cases}$$

If $y_i = y_j$, for some $i \neq j$, then both sides of (4.2) are zeros and, therefore, coincide. If all y_i are distinct, then the left-hand side is $\rho_n(y_1, \dots, y_n)$, while the right-hand side is the expectation of the indicator function for the event $\{y_1 \in X, \dots, y_n \in X\}$, *i.e.*, it is the probability of that event. Comparing with Definition 4.7, this is also $\rho_n(y_1, \dots, y_n)$. □

Definition 4.11. *Suppose that for a measure μ on $\mathfrak{X}$ (called* reference measure*), all the correlation measures have densities with respect to $\mu^{\otimes n}$, $n = 1, 2, \dots$. Then the density of ρ_n is called the nth* correlation function *and it is usually denoted by the same symbol ρ_n.*

Often $\mathfrak{X} = \mathbb{R}$ and μ is the Lebesgue measure, so that the definition becomes:

$$\rho_n = \rho_n(x_1, \dots, x_n) \mathrm{d}x_1 \cdots \mathrm{d}x_n.$$

In this case the probabilistic meaning of the nth correlation function is that of the density of probability to find a particle in each of the infinitesimal intervals around points $x_1, x_2, \dots x_n$:

$$\rho_n(x_1, x_2, \dots x_n) \mathrm{d}x_1 \cdots \mathrm{d}x_n \approx \mathbb{P}\left(\text{there is a particle of } X \text{ in each interval } [x_i, x_i + \mathrm{d}x_i]\right).$$

As an exercise, the reader might check directly from Definition 4.9 that the nth correlation function of intensity ϱ Poisson point process (with respect to Lebesgue measure) is identically equal to ϱ^n:

$$\rho_n \equiv \varrho^n, \quad n \geq 1.$$

Vaguely, correlation measures for the point processes play the same role as moments for the random variables: under mild technical conditions they exist and uniquely determine the distribution. We refer to [DVJ08, Section 9.5] for further discussions. The analogy with the moments becomes more transparent in the following statement.

Theorem 4.12. *Let ρ_n be correlation measures for a point process $X \in \mathfrak{X}$. For any compact set $A \subset \mathfrak{X}$, we have*

$$\mathbb{E} N_A = \int_A \rho_1(\mathrm{d}x), \tag{4.3}$$

and, more generally, for each $n \geq 1$

$$\mathbb{E}\big[N_A(N_A - 1) \cdots (N_A - n + 1)\big] = \int_{A^n} \rho_n(\mathrm{d}x_1, \dots, \mathrm{d}x_n). \tag{4.4}$$

Proof. We take $f = \mathbf{1}_A(x_1)\mathbf{1}_A(x_2) \cdots \mathbf{1}_A(x_n)$ in (4.2). The left-hand side becomes $\int_{A^n} \rho_n(\mathrm{d}x_1, \dots, \mathrm{d}x_n)$. The right-hand side is

$$\mathbb{E}\big[\#\{\text{distinct } x_{i_1}, \dots, x_{i_n} \in X, \text{ such that they are all in } A\}\big].$$

The expression under expectation is precisely $N_A(N_A - 1) \cdots (N_A - n + 1)$: we have N_A options for choosing x_{i_1}, $N_A - 1$ options for choosing x_{i_2}, etc. □

Similar formulas exist for joint distributions of N_A with several different sets A. Comparing with the classical moment problem (cf. [Akh65] or [Bil12, Section 30]), the conclusion is that as long as the correlation functions do not grow too fast (e.g. $\rho_n(x_1, \dots, x_n) \le n^{2n} C^n$ for some $C > 0$ is sufficient), they uniquely determine the joint distribution of N_A and therefore of the point process. [Len73] contains the exact necessary growth conditions. In all examples of our interest these conditions are straightforward to check.

Here is one way to compute correlation functions when the total number of particles is fixed.

Proposition 4.13. *For a random point process with a fixed number of particles N, described by a joint probability distribution $P(\mathrm{d}x_1, \dots, \mathrm{d}x_N)$, symmetric with respect to permutations of the arguments and assigning probability 0 to the diagonals $x_i = x_j$, the correlation measures for $n \le N$ are given by*

$$\rho_n(dx_1, \dots, dx_n) = \frac{N!}{(N-n)!} \int_{x_{n+1}, \dots, x_N \in \mathfrak{X}} P(dx_1, \dots, dx_N), \qquad n \le N. \tag{4.5}$$

For $n > N$ the correlation measures ρ_n vanish identically.

Proof. The statement for $n > N$ is immediate from the definition. For $n \le N$ we have

$$\mathbb{E}\left(\sum_{\substack{x_{i_1}, \dots, x_{i_n} \\ \text{pairwise distinct}}} f(x_{i_1}, \dots, x_{i_n}) \right) = \int_{\mathfrak{X}^N} \sum_{\substack{x_{i_1}, \dots, x_{i_n} \\ \text{pairwise distinct}}} f(x_{i_1}, \dots, x_{i_n}) P(\mathrm{d}x_1, \dots, \mathrm{d}x_N)$$
$$= \frac{N!}{(N-n)!} \int_{\mathfrak{X}^N} f(x_1, \dots, x_n) P(\mathrm{d}x_1, \dots, \mathrm{d}x_N),$$

where we used the symmetry of $P(\mathrm{d}x_1, \dots, \mathrm{d}x_N)$ in the last equality. □

4.2 Determinantal point processes

We now proceed to defining an important class of random point processes.

Definition 4.14. *A point process on $\mathfrak{X}$ is said to be* determinantal *if there exists a function $K(x, y)$ on $\mathfrak{X} \times \mathfrak{X}$ such that the correlation functions (with respect to some reference measure) are given by the determinantal formula*

$$\rho_n(x_1, \dots, x_n) = \det[K(x_i, x_j)]_{i,j=1}^n$$

for all $n = 1, 2, \dots$. The function K is called the correlation kernel.

In particular, we have

$$\rho_1(x_1) = K(x_1, x_1), \quad \rho_2(x_1, x_2) = \det \begin{bmatrix} K(x_1, x_1) & K(x_1, x_2) \\ K(x_2, x_1) & K(x_2, x_2) \end{bmatrix},$$
$$\rho_3(x_1, x_2, x_3) = \det \begin{bmatrix} K(x_1, x_1) & K(x_1, x_2) & K(x_1, x_3), \\ K(x_2, x_1) & K(x_2, x_2) & K(x_2, x_3) \\ K(x_3, x_1) & K(x_3, x_2) & K(x_3, x_3) \end{bmatrix}.$$

Note that the values of determinants $\det[K(x_i, x_j)]$ do not depend on the ordering of the arguments x_i and vanish at $x_i = x_j$. Also the correlation kernel is not unique — gauge transformations of the form

$$K(x, y) \mapsto \frac{f(x)}{f(y)} K(x, y) \tag{4.6}$$

with a non-vanishing $f : \mathfrak{X} \to \mathbb{C}$ do not affect the correlation functions. Another freedom is in the choice of the reference measure: if we simultaneously multiply the density of the reference measure by a positive function $f(x)$ and divide $K(x, y)$ by the same function, then the correlation functions are unchanged.

The main benefit of the determinantal structure is complexity reduction. The correlation kernel is a single function of two variables while the correlation functions form an infinite sequence of functions of growing number of variables. Thus, if a point process happens to be determinantal, it can be described by a substantially reduced amount of data. This is parallel to Gaussian processes for which all the information is encoded in a single covariance function.

Example 4.15. *The Bernoulli point process is determinantal with respect to the counting measure on $\mathbb{Z}$ with*

$$K(x, y) = \begin{cases} p, & x = y, \\ 0, & x \neq y. \end{cases}$$

The Poisson point process of intensity ϱ is determinantal with respect to the Lebesgue measure on $\mathbb{R}$ with

$$K(x, y) = \begin{cases} \varrho, & x = y, \\ 0, & x \neq y. \end{cases}$$

Determinantal processes first appeared in the 1960s in the context of random matrix theory, with the first examples going back to the work of Dyson [Dys62a, Dys62b, Dys62c]; see also the monograph of Mehta [Meh04], first edition published in 1967, where the determinantal structure of eigenvalue correlations became a standard tool. As a class, such processes were first distinguished in 1975 by Macchi [Mac75], who considered the case when the correlation kernel is Hermitian ($K(x, y) = \overline{K(y, x)}$) and called them "Fermion processes". In this case

$$\rho_2(x, y) = \rho_1(x)\rho_1(y) - |K(x, y)|^2 \leq \rho_1(x)\rho_1(y),$$

which, from a probabilistic point of view, means that particles repel.

The term "determinantal point process" first appeared in [BO00b], together with the first natural examples of such processes with *non-Hermitian* kernels. A systematic probabilistic study of determinantal point processes, including general existence results and limit theorems, was carried out by Soshnikov [Sos00a]. Today the term is widespread, and determinantal point processes play a central role in random matrix theory and integrable probability; there is a Wikipedia article devoted to them. Other foundational papers and influential reviews include [Lyo03, BR05, HKPV09, Bor11a, KT12].

An important class of determinantal random point processes is formed by *biorthogonal ensembles*.

Definition 4.16. *Consider a state space $\mathfrak{X}$ with a reference measure μ. An N–point biorthogonal ensemble on $\mathfrak{X}$ is a probability measure on $\mathfrak{X}^N$ of the form*

$$P_N(dx_1, \dots, dx_N) = c_N \cdot \det\big[\phi_i(x_j)\big]_{i,j=1}^N \det\big[\psi_i(x_j)\big]_{i,j=1}^N \cdot \mu(\mathrm{d}x_1) \cdots \mu(\mathrm{d}x_N)$$

for a normalization constant $c_N > 0$ and functions $\phi_1, \psi_1, \dots, \phi_N, \psi_N$ on $\mathfrak{X}$ such that all integrals of the form $\int_{\mathfrak{X}} \phi_i(x)\psi_j(x)\mu(\mathrm{d}x)$ are finite.

Theorem 4.17. *Mapping $(x_1, \dots, x_N) \in \mathfrak{X}^N$ to a point configuration $\{x_1, \dots, x_N\} \subset \mathfrak{X}$, any biorthogonal ensemble gives rise to a determinantal point process. Its correlation kernel has the form*

$$K(x, y) = \sum_{i,j=1}^N \phi_i(x)\psi_j(y)\big[G^{-\mathsf{T}}\big]_{ij}, \tag{4.7}$$

where $^{-\mathsf{T}}$ *means inverse transpose, and* $G = \big[G_{ij}\big]_{i,j=1}^{N}$ *is the Gram matrix defined by*

$$G_{ij} = \int_{\mathfrak{X}} \phi_i(x)\psi_j(x)\mu(\mathrm{d}x).$$

Remark 4.18. When the functions $\phi_i(x)$ and $\psi_j(y)$ are biorthogonal, the Gram matrix is diagonal and can be easily inverted. This is the origin of the name "biorthogonal ensemble".

Proof of Theorem 4.17. Applying the Cauchy-Binet formula (in the context of integrals it is also known as the Andréief identity [And86]) of Proposition 2.10 :

$$\int_{\mathfrak{X}^N} \det\big[\phi_i(x_j)\big]_{i,j=1}^{N} \det\big[\psi_i(x_j)\big]_{i,j=1}^{N} \cdot \mu(\mathrm{d}x_1)\cdots\mu(\mathrm{d}x_N) = N!\det G.$$

This implies that the normalization constant c_N in the definition of the biorthogonal ensemble above is equal to $(N!\det G)^{-1}$, and that the matrix G is invertible.

We need to prove that $\rho_n(x_1,\dots,x_n) = \det\big[K(x_i,x_j)\big]_{i,j=1}^{n}$ for any $n \geq 1$. For $n > N$ both sides vanish: the right-hand side is zero because the matrix under determinant has rank no more than N due to the explicit formula for K.

Assume $n \leq N$. By formula (4.5) for the correlation functions,

$$\rho_n(x_1,\dots,x_n) = \frac{N!c_N}{(N-n)!}\int_{\mathfrak{X}^{N-n}} \det\big[\phi_i(x_j)\big]_{i,j=1}^{N} \det\big[\psi_i(x_j)\big]_{i,j=1}^{N} \mu(\mathrm{d}x_{n+1})\cdots\mu(\mathrm{d}x_N).$$

Let A and B be two $N\times N$ matrices such that $AGB^{\mathsf{T}} = \mathrm{Id}$. Due to invertibility of G such two matrices exist, but they are not unique. Set

$$\Phi_k = \sum_{l=1}^{N} A_{kl}\phi_l, \qquad \Psi_k = \sum_{l=1}^{N} B_{kl}\psi_l, \qquad k = 1,\dots,N.$$

Then

$$\langle \Phi_i, \Psi_j\rangle_{L^2(\mathfrak{X},\mu)} = [AGB^{\mathsf{T}}]_{ij} = \mathbf{1}_{i=j}.$$

On the other hand, for any $x_1,\dots,x_N$,

$$\det\big[\Phi_i(x_j)\big]_{i,j=1}^{N} = \det A \det\big[\phi_i(x_j)\big]_{i,j=1}^{N},$$
$$\det\big[\Psi_i(x_j)\big]_{i,j=1}^{N} = \det B \det\big[\psi_i(x_j)\big]_{i,j=1}^{N}.$$

Also $AGB^{\mathsf{T}} = \mathrm{Id}$ implies $\det A \det B \det G = 1$. Hence, the formula for the correlation functions can be rewritten as

$$\rho_n(x_1,\dots,x_n) = \frac{1}{(N-n)!}\int_{\mathfrak{X}^{N-n}} \det\big[\Phi_i(x_j)\big]_{i,j=1}^{N} \det\big[\Psi_i(x_j)\big]_{i,j=1}^{N} \mu(\mathrm{d}x_{n+1})\cdots\mu(\mathrm{d}x_N).$$

Opening up the determinants and using the fact that Φ_i's and Ψ_j's are biorthogonal, we obtain

$$\begin{aligned}\rho_n(x_1,\dots,x_n) &= \frac{1}{(N-n)!}\int_{\mathfrak{X}^{N-n}} \sum_{\sigma,\tau\in\mathcal{S}_N} (-1)^{\sigma\tau}\left[\prod_{i=1}^{N}\Phi_{\sigma(i)}(x_i)\Psi_{\tau(i)}(x_i)\right]\mu(\mathrm{d}x_{n+1})\cdots\mu(\mathrm{d}x_N)\\ &= \frac{1}{(N-n)!}\sum_{\sigma,\tau\in\mathcal{S}_N\,\sigma(k)=\tau(k),\,k>n} (-1)^{\sigma\tau}\prod_{i=1}^{n}\Phi_{\sigma(i)}(x_i)\Psi_{\tau(i)}(x_i)\\ &= \sum_{1\leq j_1<\dots<j_n\leq N} \det\Phi^{j_1,\dots,j_n}\det\Psi^{j_1,\dots,j_n},\end{aligned}$$

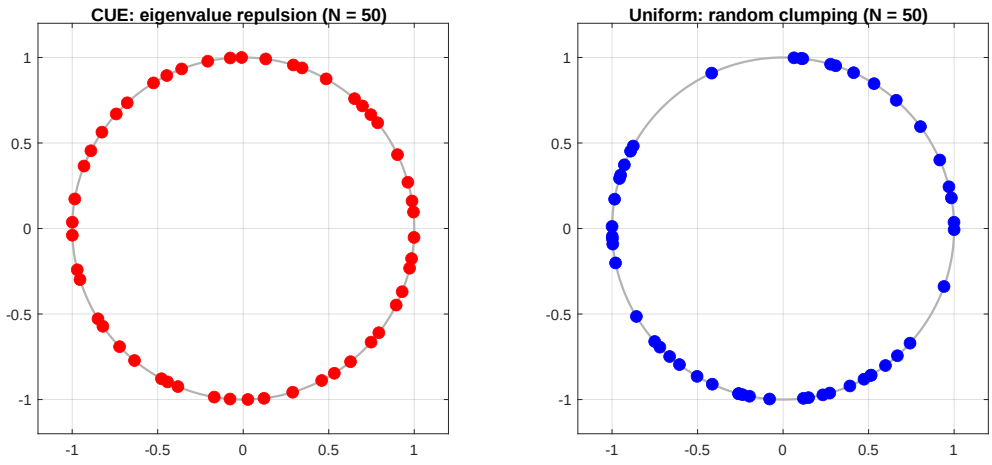


Figure 4.1: Left panel: points from Circular Unitary Ensemble. Right panel: uniformly random points.

where $\Phi^{j_1,\dots,j_n}$ is the submatrix of $\Phi := [\Phi_j(x_i)]_{\substack{i=1,\dots,n\\ j=1,\dots,n}}$ formed by columns $j_1,\dots,j_n$, and similarly for $\Psi^{j_1,\dots,j_n}$. The Cauchy-Binet formula now yields $\rho_n(x_1,\dots,x_n) = \det \Phi\Psi^{\mathsf{T}}$, and

$$[\Phi\Psi^{\mathsf{T}}]_{ij} = \sum_{k,l,m=1}^{N} A_{kl}B_{km}\phi_l(x_i)\psi_m(x_j) = \sum_{l,m=1}^{N} [A^{\mathsf{T}}B]_{lm}\phi_l(x_i)\psi_m(x_j).$$

The right-hand side is equal to $K(x_i,x_j)$ because $AGB^{\mathsf{T}} = \mathrm{Id}$ is equivalent to $A^{\mathsf{T}}B = G^{-\mathsf{T}}$. □

Important examples of biorthogonal ensembles come from the random matrix theory. One case is the measure on N–particle configurations on the unit circle, $|z| = 1$, with density with respect to the Lebesgue measure given by

$$\frac{1}{(2\pi)^N N!} \prod_{1\le i<j\le N} |z_i - z_j|^2, \qquad |z_i| = 1, \quad i = 1,2,\dots,N. \tag{4.8}$$

It can be identified with the distribution of eigenvalues of the $N \times N$ random unitary matrices sampled from the uniform measure, see *e.g.*, [Meh04, Chapters 10,11] or [For10, Chapter 2]. This N–point process is known as the Circular Unitary Ensemble or CUE. The CUE eigenvalue density is the spectral representation of the Haar measure, formally expressed by the Weyl Integration Formula [Wey26, Wey39]. This result provides the analytical form for the geometric structures discovered in Cartan's classification of Lie groups [Car94], later adapted by Dyson [Dys62a] to model quantum level statistics.

Figures 4.1 and 4.2 reveal striking differences between the behavior of points of CUE, as compared to the uniformly random points on the unit circle. The eigenvalues exhibit much more rigidity, caused by their repulsion expressed through $|z_i - z_j|$ factors in (4.8).

Proposition 4.19. *CUE* (4.8) *is a determinantal point process with correlation kernel with respect to the Lebesgue measure on the unit circle (of total mass* 2π*) given by*

$$K(z,w) = \frac{1}{2\pi} \cdot \frac{1-(z\bar{w})^N}{1-z\bar{w}}, \qquad |z| = |w| = 1, \tag{4.9}$$

where $\bar{w}$ *denotes the complex conjugate of* w.

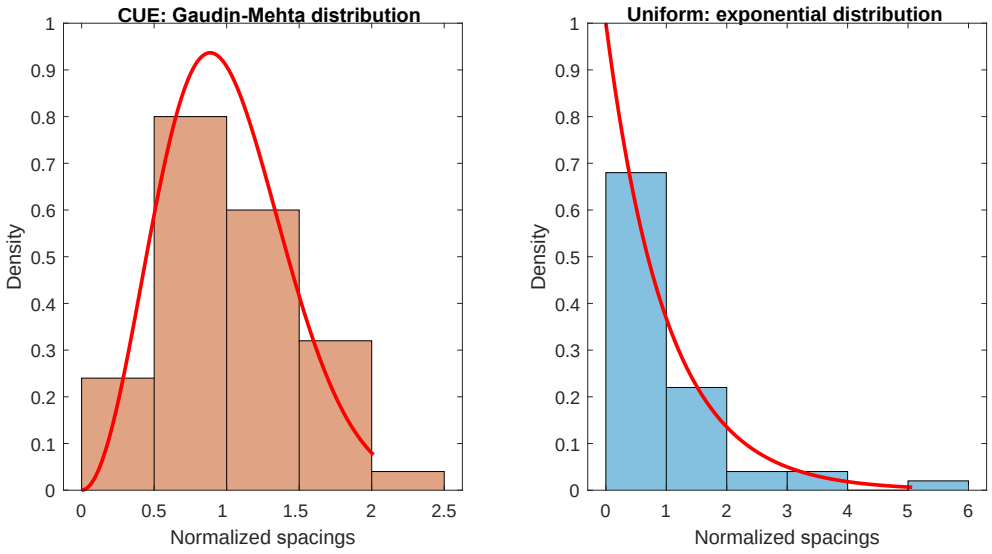


Figure 4.2: Histograms for adjacent spacings for points in Figure 4.1. Red curves are theoretical asymptotic distributions for the spacings as $N \to \infty$, which is the exponential distribution for the right panel and is called the Gaudin-Mehta distribution for the left panel.

Proof. Using the Vandermonde determinant (2.15), we rewrite (4.8) as

$$\frac{1}{(2\pi)^N N!} \det\left[z_j^{i-1}\right]_{i,j=1}^N \det\left[\bar{z}_j^{i-1}\right]_{i,j=1}^N |\mathrm{d}z_1| \cdots |\mathrm{d}z_N|. \tag{4.10}$$

Hence, we are in the framework of Theorem 4.17 with the Gram matrix

$$G_{ij} = \int_{|z|=1} z^{i-1}\bar{z}^{j-1}|\mathrm{d}z| = \frac{1}{\mathbf{i}} \oint_{\text{around } 0} z^{i-j-1}\mathrm{d}z = \begin{cases} 2\pi, & i = j, \\ 0, & \text{otherwise.} \end{cases} \tag{4.11}$$

Inverting G is straightforward, and (4.7) turns into

$$K(z,w) = \frac{1}{2\pi}\sum_{i=1}^N (z\bar{w})^{i-1} = \frac{1}{2\pi}\cdot\frac{1-(z\bar{w})^N}{1-z\bar{w}}. \quad \square$$

Another case of a biorthogonal ensemble is the measure on N–particle configurations $x_1 > x_2 > \cdots > x_N$ in $\mathbb{R}$ with density

$$\frac{1}{(2\pi)^{N/2}\prod_{j=1}^{N-1} j!} \prod_{i<j}(x_i - x_j)^2 \prod_i e^{-\frac{1}{2}x_i^2}, \tag{4.12}$$

which is the distribution of eigenvalues of a random Hermitian matrix M from Gaussian Unitary Ensemble (GUE), *i.e.*, $M = \frac{1}{2}(Y + Y^*)$, where Y is a matrix of i.i.d. $\mathcal{N}(0,1) + \mathbf{i}\mathcal{N}(0,1)$ elements, and Y^* its transpose-conjugate matrix, see *e.g.*, [**?**, For10, AGZ10, ABDF11] for further details. The correlation kernel of (4.12) is often written down in terms of the Hermite orthogonal polynomials (see exercises), making it one of the instances of an *orthogonal polynomial ensemble*. An alternative contour integral expression for the correlation functions of (4.12) will be presented in Section 5.8.

4.3 Correlation functions of the Schur measure

Our next goal is to show that any Schur measure is a determinantal point process. We will split the discussion into two steps. In the first step, we deal with Schur measures with two specializations into finitely many α–parameters. In other words, we consider the probability measure

$$\mathbb{P}(\lambda) = \prod_{i,j=1}^{N} (1 - x_i y_j) \cdot s_\lambda(x_1, \dots, x_N) s_\lambda(y_1, \dots, y_N). \tag{4.13}$$

Directly from Definition 2.8, the Schur functions $s_\lambda(x_1, \dots, x_N)$ are non-zero only if $\ell(\lambda) \le N$. We encode such λ through a finite point configuration

$$X_N(\lambda) = \{\lambda_j + N - j\}_{j=1}^{N} \subset \mathbb{Z}_{\ge 0}.$$

Theorem 4.20. *Let λ be distributed as in* (4.13)*, where x_i and y_j are non-negative real numbers, such that $|x_i y_j| < 1$ for each $i, j = 1, \dots, N$. Then the point process $X_N(\lambda)$ is determinantal, with correlation kernel (with respect to the counting measure) given by a double contour integral:*

$$K(\ell_1, \ell_2) = \frac{1}{(2\pi \mathbf{i})^2} \oint\!\!\oint \prod_{k=1}^{N} \frac{(v - y_k)(1 - w x_k)}{(1 - v x_k)(w - y_k)} \cdot \frac{v^{-\ell_1 - 1} w^{\ell_2}}{w - v} \mathrm{d}v \mathrm{d}w, \qquad \ell_1, \ell_2 \in \mathbb{Z}_{\ge 0}, \tag{4.14}$$

where the integration is over positively-oriented contours which enclose the singularities at $v = (x_k)^{-1}$ and $w = y_k$, but leave out the singularities at $v = w$ or $v = 0$. In particular, the contours do not intersect, cf. Corollary 4.22 and Figure 4.4 below.

Proof. The definition of Schur functions (1.6) and definition of $\mathbb{P}(\lambda)$ in (4.13) imply that

$$\mathbb{P}(\lambda) = \frac{1}{Z} \det\left[x_i^{\lambda_j + N - j}\right]_{i,j=1}^{N} \det\left[y_i^{\lambda_j + N - j}\right]_{i,j=1}^{N}. \tag{4.15}$$

We recognize a biorthogonal ensemble on $\mathbb{Z}_{\ge 0}$ in the right–hand side of (4.15). Therefore, we can use Theorem 4.17 which yields that $X_N(\lambda)$ is a determinantal point process with correlation kernel

$$\widetilde{K}(\ell_1, \ell_2) = \sum_{i,j=1}^{N} x_i^{\ell_1} y_j^{\ell_2} G^{-\mathsf{T}}_{ij},$$

where $G^{-\mathsf{T}}_{ij}$ is the inverse–transpose matrix of the $N \times N$ Gram matrix

$$G_{ij} = \sum_{\ell \ge 0} x_i^\ell y_j^\ell = \frac{1}{1 - x_i y_j}.$$

The determinant of G was computed in Proposition 2.12:

$$\det\left[G_{ij}\right]_{i,j=1}^{N} = \det\left[\frac{1}{1 - x_i y_j}\right]_{i,j=1}^{N} = \frac{\prod_{i<j}(x_i - x_j) \prod_{i<j}(y_i - y_j)}{\prod_{i,j=1}^{N}(1 - x_i y_j)}. \tag{4.16}$$

By Cramer's rule, we have

$$\left(G^{-\mathsf{T}}\right)_{k\ell} = \frac{(-1)^{k+\ell} \det[G_{ij}]_{i \ne k, j \ne \ell}}{\det[G_{ij}]_{i,j=1}^{N}}.$$

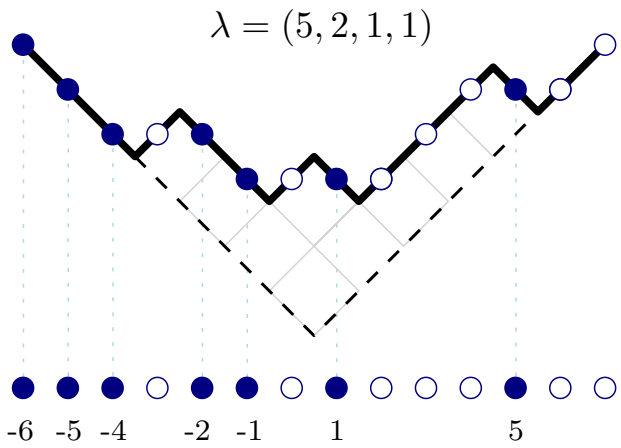


Figure 4.3: Particle configuration $X(\lambda)$.

Using the fact that submatrices of G_{ij} are matrices of the same type, and their determinants can be evaluated using (4.16), we obtain

$$\left(G^{-\mathsf{T}}\right)_{k\ell} = \frac{\prod_{a=1}^{N}(1-x_a y_\ell)(1-x_k y_a)}{(1-x_k y_\ell)\prod_{b\neq k}(x_k-x_b)\prod_{c\neq \ell}(y_\ell - y_c)}. \tag{4.17}$$

We claim that

$$\widetilde{K}(\ell_1,\ell_2) = \sum_{i,j=1}^{N} x_i^{\ell_1} y_j^{\ell_2} G^{-\mathsf{T}}_{ij} = \frac{1}{(2\pi\mathbf{i})^2}\oiint \prod_{k=1}^{N}\frac{(1-zy_k)(1-wx_k)}{(z-x_k)(w-y_k)}\cdot\frac{z^{\ell_1}w^{\ell_2}}{1-zw}\mathrm{d}z\mathrm{d}w, \tag{4.18}$$

with contours chosen so that they enclose the singularities at $z = x_k$ and $w = y_k$, but do not enclose the singularity at $zw = 1$. Indeed, (4.18) is just the evaluation of the double integral as the sum of the residues. Changing the variables $z = 1/v$ in (4.18) we arrive at (4.14). □

For more general specializations in the Schur measure, the particle configuration $X_N(\lambda)$ no longer works, and there is no N that makes $\lambda_i + N - i$ non-negative for all i. Hence, we introduce *infinite* particle configurations in $\mathbb{Z}$ instead. Given a Young diagram λ, we associate to it a point configuration

$$X(\lambda) = \left\{\lambda_i - i + 1\right\}_{i=1}^{\infty} \subset \mathbb{Z}. \tag{4.19}$$

Note that $X(\lambda)$ is semi–infinite, *i.e.*, there are finitely many points to the right of the origin, and all but finitely many points to the left of the origin belong to $X(\lambda)$. The construction of $X(\lambda)$ is illustrated in Figure 4.3.

We recall the most general Schur measure of Definition 3.4 and introduce the notation

$$H(\rho;z) = \sum_{k=0}^{\infty} h_k(\rho) z^k = \exp\left(\sum_{k=1}^{\infty} p_k(\rho)\frac{z^k}{k}\right).$$

Theorem 4.21. *Suppose that $\lambda \in \mathbb{Y}$ is distributed according to the Schur measure with two admissible specializations ρ_1, ρ_2. Then $X(\lambda)$ is a determinantal point process on $\mathbb{Z}$ with correlation kernel $K(\ell_1,\ell_2)$ defined by*

$$K(\ell_1,\ell_2) = \frac{1}{(2\pi\mathbf{i})^2}\oiint \frac{H(\rho_1;v)H(\rho_2;w^{-1})}{H(\rho_2;v^{-1})H(\rho_1;w)}\frac{v^{-\ell_1}w^{\ell_2-1}}{v-w}\,\mathrm{d}v\mathrm{d}w, \qquad \ell_1,\ell_2\in\mathbb{Z}, \tag{4.20}$$

with integration over two positively oriented circles around the origin $|w| = R_1$, $|v| = R_2$ such that $R_1 < R_2$ and the functions $\sum_{k=1}^{\infty} p_k(\rho_1)\frac{u^k}{k}$, $\sum_{k=1}^{\infty} p_k(\rho_1)\frac{u^{-k}}{k}$, $\sum_{k=1}^{\infty} p_k(\rho_2)\frac{u^k}{k}$, $\sum_{k=1}^{\infty} p_k(\rho_2)\frac{u^{-k}}{k}$, are holomorphic in the annulus $R_1 - \varepsilon < |u| < R_2 + \varepsilon$. In particular, if $|p_k(\rho_1)| < Cr^k$ and $|p_k(\rho_2)| < Cr^k$ with some constants $C > 0$ and $0 < r < 1$, then any $r < R_1 < R_2 < r^{-1}$ are suitable.[2]

We included Schur positivity of ρ_1 and ρ_2 in the conditions of the theorem, yet it is a purely algebraic statement which holds more generally, as long as all the series arising in the statement are absolutely convergent. An important example going beyond our admissible specializations is given by the *z–measures on partitions*, for which $s_\lambda(\rho_1)$ and $s_\lambda(\rho_2)$ do not have to be real numbers, but their product is real nonnegative, see [BO06, Theorem A, $s = t$ case] for a direct analogue of (4.20) and references therein for the earlier literature on the z-measures

Determinantal structure of Schur measures was discovered in [Oko01a], following an earlier developments for z–measures in [Oko01b]; his approach through the Fock space is outlined in the exercises for this chapter. Our proof through Theorem 4.20 is very different from that paper and is closer to [Joh01b].

Proof of Theorem 4.21. We have to prove that for any finite set $A = \{a_1, \dots, a_m\} \subset \mathbb{Z}$ we have

$$\sum_{\lambda : A \subset X(\lambda)} \frac{s_\lambda(\rho_1) s_\lambda(\rho_2)}{H(\rho_1;\rho_2)} = \det\bigl[K(a_i, a_j)\bigr]_{i,j=1}^{m}. \tag{4.21}$$

Let us first prove the following identity of formal power series. Let $x = (x_1, x_2, \dots)$ and $y = (y_1, y_2, \dots)$ be two infinite sets of variables; then

$$\prod_{i,j=1}^{\infty} (1 - x_i y_j) \sum_{\lambda : A \subset X(\lambda)} s_\lambda(x) s_\lambda(y) \stackrel{?}{=} \det\left[\widehat{K}(a_i, a_j)\right]_{i,j=1}^{m}, \tag{4.22}$$

where the kernel $\widehat{K}$ is a power series defined through,

$$\widehat{K}(\ell_1, \ell_2) = \frac{1}{(2\pi \mathbf{i})^2} \oiint \frac{\left(\sum_{k=0}^{\infty} h_k(x) v^k\right)\left(\sum_{k=0}^{\infty} h_k(y) w^{-k}\right)}{\left(\sum_{k=0}^{\infty} h_k(y) v^{-k}\right)\left(\sum_{k=0}^{\infty} h_k(x) w^{k}\right)} \frac{v^{-\ell_1 - 1} w^{\ell_2 - 1}}{1 - \frac{w}{v}} \, \mathrm{d}v \mathrm{d}w. \tag{4.23}$$

Here the integral should be understood in the following sense: we expand

$$\frac{1}{1 - \frac{w}{v}} = 1 + \frac{w}{v} + \frac{w^2}{v^2} + \frac{w^3}{v^3} + \dots, \tag{4.24}$$

convert the integrand in (4.23) into a (Laurent) power series in w and v, and collect the coefficient of $v^{-1}w^{-1}$. In this way the integral becomes a power series in $h_k(x)$ and $h_k(y)$ with integer coefficients. We choose some $d = 0, 1, 2, \dots$ and consider the degree d (with respect to x and y) component of this series — this is an element of $\Lambda \otimes \Lambda$.

The left-hand side of (4.22) is also a power series in $h_k(x)$ and $h_k(y)$ with integer coefficients. Again, we can consider the degree d component of this series as an element of $\Lambda \otimes \Lambda$.

Hence, the meaning of (4.22) is that for each d the corresponding elements of $\Lambda \otimes \Lambda$ in both sides coincide. In order to check that, we choose N and project onto finite sets of variables by setting $x_{N+1} =$

[2] Generally speaking, such R_1, R_2 and the corresponding integration contours do not have to exist. However, in all interesting examples we know of, either they exist, or contours can be deformed so that (4.20) still holds.

$x_{N+2} = \cdots = 0$ and $y_{N+1} = y_{N+2} = \cdots = 0$. An identity in $\Lambda \otimes \Lambda$ turns into an identity in $\Lambda_N \otimes \Lambda_N$; if we manage to prove it for each large enough N, then we would be done, because $\Lambda = \varprojlim \Lambda_N$.

For finite N, we start from the result of Theorem 4.20, and rewrite the kernel for $X_N(\overleftarrow{\lambda})$ as

$$\frac{1}{(2\pi\mathbf{i})^2} \oiint \prod_{k=1}^{N} \frac{(1-v^{-1}y_k)(1-wx_k)}{(1-vx_k)(1-w^{-1}y_k)} \cdot \frac{v^{N-\ell_1-1}w^{\ell_2-N}}{w-v}\,\mathrm{d}v\mathrm{d}w, \qquad \ell_1,\ell_2 \in \mathbb{Z}_{\geq 0}.$$

We now specify x_i and y_i to be small positive numbers, choose the v–contour to be a *negatively oriented* circle of radius 2 (we absorbed ∞ into the contour, which is allowed because of the decay of the integrand) and w–contour to be a *positively oriented* circle of radius $\frac{1}{2}$, both centered at the origin. In the next step we will flip the orientation of the v–contour changing the sign of the integral simultaneously.

Note that $X_N(\lambda)$ differs from $X(\lambda)$ by shift by $(N-1)$ and addition of particles extending to $-\infty$. The latter does not matter, because for large enough N, the set $A = \{a_1, \dots, a_m\}$ of our interest does not have any of these additional particles. Absorbing the shift and using the H–notations, the kernel for $X(\lambda)$ becomes

$$\frac{1}{(2\pi\mathbf{i})^2} \oiint \frac{H(x_1,\dots,x_N;\, v)H(y_1,\dots,y_N;\, w^{-1})}{H(x_1,\dots,x_N;\, w)H(y_1,\dots,y_N;\, v^{-1})} \cdot \frac{v^{-\ell_1-1}w^{\ell_2-1}}{1-\frac{w}{v}}\,\mathrm{d}v\mathrm{d}w, \qquad \ell_1,\ell_2 \in \mathbb{Z}_{>-N}.$$

Because $\left|\frac{w}{v}\right| < 1$, we can use the expansion (4.24), and then compute the v–integral as the residue at ∞ and w–integral as the residue at 0. This gives the same meaning to the integral as in (4.23). Since x_k and y_k can take arbitrarily small values, and we deal with power series in these variables, the evaluation of the correlation functions can be viewed as a power series identity in $(x_1, \dots, x_N)$ and $(y_1, \dots, y_N)$. This proves a finite N version of (4.22). Sending $N \to \infty$, we get (4.22) itself.

From (4.22) we obtain (4.21) by applying specializations ρ_1 and ρ_2 and choosing the contours on which all four $H(\rho_1; v)$, $H(\rho_2; w^{-1})$, $H(\rho_2; v^{-1})$, $H(\rho_1; w)$ are given by converging series in terms of the specialized h_k. □

Let us specialize Theorems 4.20 and 4.21 to our running examples. The first one is the Schur measure with α–specializations (4.13) with $x_1 = x_2 = \cdots = x_N = y_1 = y_2 = \cdots = y_N = \sqrt{q}$, which is relevant to the last passage percolation (Theorem 1.4) and discrete PNG (Corollary 3.9).

Corollary 4.22. *For $0 < q < 1$, let $\lambda = (\lambda_1 \geq \cdots \geq \lambda_N \geq 0)$ be distributed according to (see* (2.51) *for the equivalence of two forms)*

$$\mathbb{P}(\lambda) = (1-q)^{N^2}\left[s_\lambda(\sqrt{q},\dots,\sqrt{q})\right]^2 = (1-q)^{N^2}q^{|\lambda|}\left[\prod_{1\leq i<j\leq N}\frac{\lambda_i - i - \lambda_j + j}{j-i}\right]^2.$$

Then $X_N(\lambda) = \{\lambda_i + N - i\}_{i=1}^N \subset \mathbb{Z}_{\geq 0}$ is a determinantal point process with kernel

$$K(\ell_1,\ell_2) = \frac{1}{(2\pi\mathbf{i})^2} \oiint \left[\frac{(v-\sqrt{q})(1-w\sqrt{q})}{(1-v\sqrt{q})(w-\sqrt{q})}\right]^N \cdot \frac{v^{-\ell_1-1}w^{\ell_2}}{w-v}\,\mathrm{d}v\mathrm{d}w, \qquad \ell_1,\ell_2 \in \mathbb{Z}_{\geq 0}, \tag{4.25}$$

where the v–contour is a small positively oriented loop around $\frac{1}{\sqrt{q}}$ and w–contour is a small positively oriented loop around $\sqrt{q}$, see the left panel of Figure 4.4.

We remark that the integrand has no residue at $v = \infty$. Hence, the v–contour can be modified into a circle of radius 1 around the origin, at the expense of changing the sign of the integral. The integrand also has no residue at $w = 0$, hence, this point can be included in the w–contour.

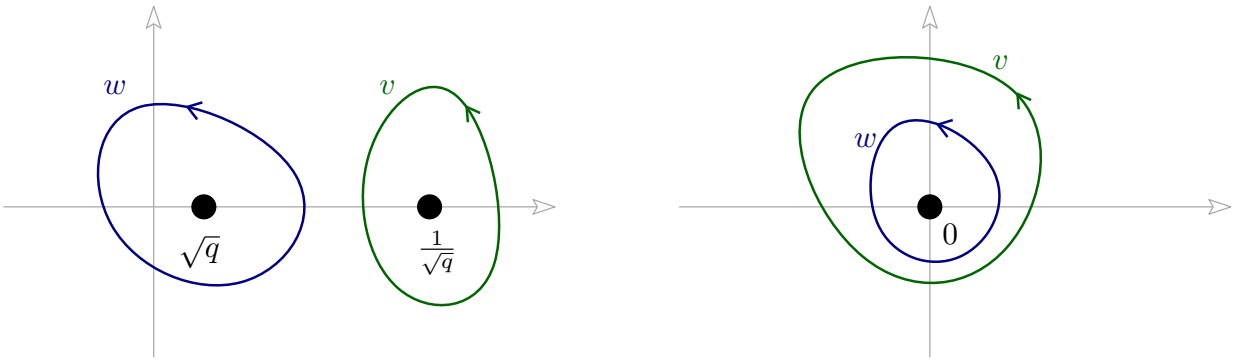


Figure 4.4: Integration contours in Corollary 4.22 on the left and Corollary 4.23 on the right.

The second example is relevant to continuous PNG (Theorem 3.11) and longest increasing subsequences in random permutations (Theorem 3.15). In this situation we use the Plancherel specialization $\rho = (0; 0; \gamma)$ of Proposition 2.26 with

$$H\big((0;0;\gamma);z\big) = \exp(\gamma z)$$

and apply Theorem 4.21 with $\gamma = \sqrt{\theta}$.

Corollary 4.23. *For $\theta > 0$, let $\lambda \in \mathbb{Y}$ be distributed according to the Poissonized Plancherel measure:*

$$\mathbb{P}(\lambda) = e^{-\theta}\big[s_\lambda(0;0;\sqrt{\theta})\big]^2 = e^{-\theta}\frac{\theta^{|\lambda|}\dim^2(\lambda)}{(|\lambda|!)^2}. \tag{4.26}$$

Then $X(\lambda) = \{\lambda_i + 1 - i\}_{i=1}^{\infty} \subset \mathbb{Z}$ is a determinantal point process with kernel

$$K(\ell_1,\ell_2) = \frac{1}{(2\pi\mathbf{i})^2}\oiint \exp\left(\sqrt{\theta}\left(v-\frac{1}{v}\right) - \sqrt{\theta}\left(w-\frac{1}{w}\right)\right)\cdot\frac{v^{-\ell_1}w^{\ell_2-1}}{v-w}\,\mathrm{d}v\mathrm{d}w, \qquad \ell_1,\ell_2\in\mathbb{Z} \tag{4.27}$$

where the $v-$ and $w-$contours are positively oriented loops around 0; the $w-$contour is inside the $v-$contour, as in the right panel of Figure 4.4.

Note the sign differences: $w-v$ in (4.25) vs $v-w$ in (4.27) caused by different choices of the contours. If we deform the v-contour in (4.25) trough the infinity to enclose the w-contour, then it becomes negatively oriented. Changing the orientation and taking appropriate $q \to 0$, $N \to \infty$ limits of (4.25) leads to (4.27).

4.4 Gap probabilities and Fredholm determinants

The correlation kernel contains a lot of information about a determinantal point process, and we need to learn how to extract this information. We start from *gap probabilities*.

Theorem 4.24. *Let X be a determinantal point process on $\mathfrak{X}$ with correlation kernel $K(x,y)$ with respect to a reference measure ν. For a measurable set A, we have*

$$\mathbb{P}(\textit{no points in } A) = \det\big(\mathrm{Id}-K\big)_{L^2(A,\nu)} = \sum_{n\geq 0}\frac{(-1)^n}{n!}\int_{A^n}\det\big[K(x_i,x_j)\big]_{i,j=1}^n \nu(\mathrm{d}x_1)\cdots\nu(\mathrm{d}x_n), \tag{4.28}$$

assuming that the right-hand side is well-defined, i.e., *that the series is absolutely convergent.*

The notation $\det\big(\mathrm{Id}-K\big)_{L^2(A,\mu)}$ is a Fredholm determinant for the trace-class integral operator with kernel $K(x,y)$ acting in $L^2(A,\mu)$. The $\sum_{n=0}^{\infty}$ expression is the Fredholm expansion for this determinant, which can be taken as a definition, see, *e.g.*, [Lax02] or [Sim05b]. An alternative definition could be $\det\big(\mathrm{Id}-K\big)=\prod_{i=1}^{\infty}(1-\lambda_i)$, where λ_i are eigenvalues of K in $L^2(A,\mu)$.

For finite matrices the Fredholm determinant is the same as the usual determinant and matches other definitions. In particular, expanding the determinant by multilinearity, for $N\times N$ matrix K_{ab}, we have

$$\det\Big[\mathbf{1}_{a=b}-K_{ab}\Big]_{a,b=1}^{N}=\sum_{n=0}^{N}\frac{(-1)^n}{n!}\sum_{a_1,\ldots,a_n=1}^{N}\det\Big[K_{a_i,a_j}\Big]_{i,j=1}^{n},$$

where only the terms with all distinct a_i are non-zero and correspond to various principal minors of the matrix $[K_{ab}]_{a,b=1}^{N}$.

Absolute convergence of the series (4.28) is related to the unique determination of the random variable N_A by its moments, cf. discussion after Theorem 4.12. Indeed, by this theorem the $n-$tuple integral in (4.28) is the nth factorial moment of N_A and it is smaller than the nth standard moment $\mathbb{E}N_A^n$. Convergence of the series $\sum_{n\geq 0}\frac{n\text{th moment}}{n!}$ implies the uniqueness in the moments problem. Determinants $\det\big[K(x_i,x_j)\big]_{i,j=1}^{n}$ are typically bounded by Hadamard's inequality (see Lemma 5.15 below), leading both to the unique determination of the process by its determinantal correlation measures, and to convergence of the series (4.28) for "nice" sets A.

Proof of Theorem 4.24. Directly from Theorem 4.12, the right-hand side of (4.28) is

$$\sum_{n\geq 0}\frac{(-1)^n}{n!}\mathbb{E}\big[N_A(N_A-1)\cdots(N_A-n+1)\big]$$
$$=\mathbb{E}\left[\sum_{n=0}^{N_A}(-1)^n\binom{N_A}{n}\right]=\mathbb{E}\left[(1-1)^{N_A}\right]=\mathbb{P}(N_A=0).\quad\square$$

A generalization of Theorem 4.24 is a computation of expectation of a *multiplicative functional.*

Theorem 4.25. *Let X be a determinantal point process on $\mathfrak{X}$ with correlation kernel $K(x,y)$ with respect to a reference measure ν. Let ϕ be a function on $\mathfrak{X}$, such that the kernel $(1-\phi(x))K(x,y)$ defines a trace class operator $(1-\phi)K$ in $L^2(\mathfrak{X},\nu)$. Then*

$$\mathbb{E}\left[\prod_{x\in X}\phi(x)\right]=\det\big(\mathrm{Id}-(1-\phi)K\big)_{L^2(\mathfrak{X},\nu)}.$$

Sketch of the proof. We only outline the case of discrete $\mathfrak{X}$ and counting measure ν, see, *e.g.*, [Sos00a, Joh06] for further discussions. We have

$$\mathbb{E}\left[\prod_{x\in X}\phi(x)\right]=\mathbb{E}\left[\prod_{x\in\mathfrak{X}}\big(1-\mathbf{1}_{x\in X}(1-\phi(x))\big)\right]$$
$$=1-\sum_{x\in\mathfrak{X}}\mathbb{P}(x\in X)\cdot(1-\phi(x))+\frac{1}{2!}\sum_{\substack{x,y\in\mathfrak{X}\\ x\neq y}}\mathbb{P}(x,y\in X)\cdot(1-\phi(x))(1-\phi(y))-\cdots.$$

Plugging in the probabilities as determinants of the correlation kernel, we recognize the expansion of $\det\big[\mathbf{1}_{x=y}-(1-\phi(x))K(x,y)\big]_{x,y\in\mathfrak{X}}$. $\square$

Another generalization is the computation of the distribution of N_A.

Theorem 4.26. *Let X be a determinantal point process on $\mathfrak{X}$ with correlation kernel $K(x,y)$ with respect to a reference measure ν. For a measurable set A, we have*

$$\mathbb{P}(m \text{ points in } A) = \frac{(-1)^m}{m!}\frac{\partial^m}{\partial z^m}\det\bigl(\mathrm{Id} - zK\bigr)_{L^2(A,\nu)}\Big|_{z=1} = \sum_{n\geq m}\frac{(-1)^{n-m}}{m!(n-m)!}\int_{A^n}\det\bigl[K(x_i,x_j)\bigr]_{i,j=1}^{n}\nu(\mathrm{d}x_1)\cdots\nu(\mathrm{d}x_n), \quad (4.29)$$

assuming that the right-hand side is well-defined, i.e.*, that the series is absolutely convergent.*

Proof. The second equality in (4.29) is obtained by term-by-term differentiation of the Fredholm expansion for $\det\bigl(\mathrm{Id} - zK\bigr)_{L^2(A,\nu)}$. A possible proof of the first equality is to interpret $\det\bigl(\mathrm{Id} - zK\bigr)$ as $\mathbb{E}\left[\prod_{x\in X\cap A}(1-z)\right]$ using Theorem 4.25, then differentiate m times, and set $z=1$ under the expectation sign. Alternatively, we can match the left-hand side of (4.29) with the right-hand side by repeating the proof of Theorem 4.24 and transforming the right-hand side into

$$\sum_{n\geq m}\frac{(-1)^{n-m}}{m!(n-m)!}\mathbb{E}\bigl[N_A(N_A-1)\cdots(N_A-n+1)\bigr]$$
$$= \mathbb{E}\left[\frac{N_A(N_A-1)\cdots(N_A-m+1)}{m!}\sum_{n=m}^{N_A}\frac{(-1)^{n-m}(N_A-m)(N_A-m-1)\cdots(N_A-n+1)}{(n-m)!}\right]$$
$$= \mathbb{E}\left[\frac{N_A(N_A-1)\cdots(N_A-m+1)}{m!}\cdot(1-1)^{N_A-m}\right] = \mathbb{P}(N_a = m). \quad \square$$

A typical application of Theorem 4.24 is to compute the distribution of the largest particle in the point process (which we need for the analysis of many systems due to Theorem 1.4, Theorem 1.6, Corollary 3.9, Theorem 3.11, or Theorem 3.15).

Theorem 4.27. *Let X be a configuration of a determinantal point process on $\mathfrak{X}\subset\mathbb{R}$ with correlation kernel $K(x,y)$ with respect to a reference measure ν. The law of the largest particle x_1 in X is*

$$\mathbb{P}(x_1 \leq s) = \det\bigl(\mathrm{Id} - K\bigr)_{L^2((s,+\infty),\nu)}, \quad (4.30)$$

and the largest particle exists almost surely if and only the last determinant tends to 1 as $s\to+\infty$.

Proof. The event $\{x_1\leq s\}$ is the same as the event that all points of X belong to $(-\infty,s]$, and is the same as the event that no points of X belong to $(s,+\infty)$. The probability of the last one is a gap probability computed in Theorem 4.24. This proves (4.30).

For the existence of the largest particle, note that then event "there exists the largest particle" is the union of the growing sequence of events "all particles of X are at most s" as $s\to+\infty$. Hence, the probability of the former is the limit of the probabilities of the latter, computed by the right-hand side of (4.30). $\square$

Application of Theorem 4.27 to the Schur measure gives a curious result in functional analysis, saying, essentially, that *every Toeplitz determinant can be written as a Fredholm determinant*, and known as the Borodin-Okounkov-Geronimo-Case formula.

In order to establish this connection we start from a result hidden inside [Ges90] and [TW01].

Proposition 4.28. *Let $x = (x_1, x_2, \dots)$ and $y = (y_1, y_2, \dots)$ be two sets of variables. For each $n = 1, 2, \dots$ we have*

$$\sum_{\lambda\in\mathbb{Y}:\, \lambda_1\le n} s_\lambda(x)s_\lambda(y) = \det\bigl[f_{i-j}\bigr]_{i,j=1}^{n}, \tag{4.31}$$

where f_m are series of elements of $\Lambda\otimes\Lambda$:

$$f_m = \sum_{\ell=-\infty}^{\infty} e_\ell(x)e_{m+\ell}(y). \tag{4.32}$$

Proof. We use Nagelbach-Kostka formula (2.24) in the form

$$s_\lambda = \det\bigl[e_{\ell_i-n+j}\bigr]_{i,j=1}^{n}, \qquad \ell_i = \lambda_i' + n - i.$$

We have, using the Cauchy-Binet formula in the third equality:

$$\begin{aligned}\sum_{\lambda\in\mathbb{Y}:\, \lambda_1\le n} s_\lambda(x)s_\lambda(y) &= \sum_{\ell_1>\dots>\ell_n\ge 0} \det\bigl[e_{\ell_i-n+j}(x)\bigr]_{i,j=1}^{n} \det\bigl[e_{\ell_i-n+j}(y)\bigr]_{i,j=1}^{n}\\ &= \sum_{\ell_1>\dots>\ell_n\ge 0} \det\bigl[e_{\ell_i+1-j}(x)\bigr]_{i,j=1}^{n} \det\bigl[e_{\ell_i+1-j}(y)\bigr]_{i,j=1}^{n} = \det\left[\sum_{\ell=0}^{\infty} e_{\ell-i}(x)e_{\ell-j}(y)\right]_{i,j=1}^{n}.\end{aligned}$$

The summation in the last formula can be extended to $\ell\in\mathbb{Z}$, because $e_k = 0$ for $k < 0$. Since (4.32) is equivalent to

$$f_{i-j} = \sum_{\ell=-\infty}^{\infty} e_{\ell-i}(x)e_{\ell-j}(y),$$

we arrive at (4.21). □

Combining with Theorem 4.21, Theorem 4.27, and (4.23), we get the Toeplitz-to-Fredholm formula:

Proposition 4.29. *Let $x = (x_1, x_2, \dots)$ and $y = (y_1, y_2, \dots)$ be two sets of variables and let f_m be from* (4.32)*. We have*

$$\det\Bigl[f_{i-j}\Bigr]_{i,j=1}^{n} = \exp\left(\sum_{k=1}^{\infty}\frac{p_k(x)p_k(y)}{k}\right)\cdot\det\Bigl(\mathrm{Id}-\widehat{K}\Bigr)_{\ell_2(n+1,n+2,\dots)}, \tag{4.33}$$

where $\widehat{K}$ is given by the double contour integral in (4.23)*.*

Applying various specializations ρ in (x) and (y), we can get arbitrary Toeplitz determinant (of a matrix with complex entries) in the left-hand side of (4.33). The formula (4.33) has been widely used in functional analysis and integrable probability communities, following the paper of Borodin and Okounkov [BO00a], but, in fact, the result was sitting unnoticed in the literature for many years before that, since the article of Geronimo and Case [GC79]. Several alternative and much more direct (*i.e.*, not using Schur functions) proofs of the identity are known by now, see [BW00, Böt01, Böt02, BS06]. The first factor in the right-hand side of (4.33) governs the large n asymptotics of the Toeplitz determinants known as the *Strong Szegö theorem*, see [Sze52, Sim05a, Sim11].

4.5 Rescaling a determinantal point process

Our main application of the determinantal point processes is for the study of scaling limits. Hence, we need to know how rescaling of particle positions changes the correlation kernel.

Lemma 4.30. *Let X be a determinantal point process on $\mathfrak{X}$ with particles $\{x_i\}$ and correlation kernel $K(x,y)$ with respect to a reference measure μ. Fix $a \in \mathbb{R} \setminus \{0\}$ and $b \in \mathbb{R}$, consider the transformed process with particles $\{ax_i + b\}$, and define*

$$\widetilde{K}(x,y) = \frac{1}{|a|} K\left(\frac{x-b}{a}, \frac{y-b}{a}\right). \tag{4.34}$$

1. *If $\mathfrak{X} = \mathbb{R}$ and μ is the Lebesgue measure, then the transformed process is determinantal with respect to Lebesgue measure, with transformed correlation kernel $\widetilde{K}$.*
2. *Suppose that $\mathfrak{X} = \mathbb{Z}$ and μ is the counting measure assigning mass 1 to each point of $\mathbb{Z}$. Then the transformed process is determinantal on $a\mathbb{Z}+b$ with respect to the rescaled counting measure assigning mass $|a|$ to each point of $a\mathbb{Z}+b$, with transformed correlation kernel $\widetilde{K}$.*

The motivation to have mass $|a|$ per point in the discrete situation is that the resulting measure approximates the Lebesgue measure on $\mathbb{R}$ as $a \to 0$.

Proof of Lemma 4.30. In the continuous case, by the definition of correlation functions, for any $n \geq 1$ and any compactly supported Borel function f,

$$\mathbb{E}\left(\sum_{\substack{x_{i_1},\dots,x_{i_n} \\ \text{pairwise distinct}}} f(ax_{i_1}+b,\, \dots,\, ax_{i_n}+b)\right) = \int_{\mathbb{R}^n} f(at_1+b,\dots,at_n+b) \det\big[K(t_i,t_j)\big]_{i,j=1}^n \,\mathrm{d}t_1 \cdots \mathrm{d}t_n.$$

Making the substitution $u_j = at_j + b$, with Jacobian factor $|a|^{-n}$, turns the right-hand side into

$$\int_{\mathbb{R}^n} f(u_1,\dots,u_n) \det\left[\frac{1}{|a|} K\left(\frac{u_i-b}{a}, \frac{u_j-b}{a}\right)\right]_{i,j=1}^n \mathrm{d}u_1 \cdots \mathrm{d}u_n.$$

In the discrete case, the analogous identity is

$$\begin{aligned}\mathbb{E}\left(\sum_{\substack{x_{i_1},\dots,x_{i_n} \\ \text{pairwise distinct}}} f(ax_{i_1}+b,\, \dots,\, ax_{i_n}+b)\right) &= \sum_{t_1,\dots,t_n \in \mathbb{Z}} f(at_1+b,\dots,at_n+b)\, \det\big[K(t_i,t_j)\big]_{j,j=1}^n \\ &= \sum_{u_1,\dots,u_n \in a\mathbb{Z}+b} f(u_1,\dots,u_n) \det\left[\frac{1}{|a|} K\left(\frac{u_i-b}{a}, \frac{u_j-b}{a}\right)\right]_{i,j=1}^n \cdot |a|^n.\end{aligned}$$

Thus, in both cases the transformed correlation kernel is $\widetilde{K}$. □

4.6 Exercises

Problem 1. Directly using Definition 4.9, show that the nth correlation function ρ_n (with respect to the Lebesgue measure) of the Poisson point process on $\mathbb{R}$ of intensity ϱ is ϱ^n.

Problem 2. Generalize Theorem 4.12 to joint factorial moments of $N_{A_1},\ldots,N_{A_r}$ for several disjoint sets $A_1,\ldots, A_r$: prove that

$$\mathbb{E}\left[\prod_{i=1}^{r} N_A(N_A-1)\cdots(N_A-n_i+1)\right] = \int_{A^{n_1}\times A^{n_2}\times\cdots\times A^{n_r}} \rho_n(\mathrm{d}x_1,\ldots,\mathrm{d}x_n), \tag{4.35}$$

where $n_i \in \mathbb{Z}_{\geq 0}$ and $n = n_1 + n_2 + \cdots + n_r$.

Problem 3. Prove a generalization of Theorem 4.26 to several sets: for a determinantal point process with kernel K with respect to a measure ν and disjoint measurable sets $A_1,\ldots, A_m$, we have

$$\begin{aligned}&\mathbb{P}(N_{A_1}=m_1,\ldots,N_{A_r}=m_r)\\ &=\frac{(-1)^{m_1+\cdots+m_r}}{m!}\frac{\partial^{m_1+\cdots+m_r}}{\partial z_1^{m_1}\cdots\partial z_r^{m_r}}\det\bigl(\mathrm{Id}-z_1[K]_{A_1}-\cdots-z_r[K]_{A_r}\bigr)_{L^2(A_1\cup A_2\cup\cdots\cup A_r,\nu)}\Big|_{z_1=\cdots=z_r=1},\end{aligned} \tag{4.36}$$

where $[K]_A$ is the restriction of the kernel K to the set A: $[K]_A(x,y) = K(x,y)\mathbf{1}_A(x)\mathbf{1}_A(y)$. The derivatives of the Fredholm determinant should be understood as differentiating the Fredholm expansion term-by-term.

Problem 4. Consider the Circular Unitary Ensemble: N particles on the circle with density

$$\frac{1}{(2\pi)^N N!}\prod_{1\leq i<j\leq N}|z_i-z_j|^2, \qquad |z_i|=1, \quad i=1,2,\ldots,N. \tag{4.37}$$

A. Take an arbitrary point $\mathfrak{z} = \exp(\mathbf{i}\phi) \neq -1$ on the unit circle and change the coordinates $z_j = \exp(\mathbf{i}\phi_j)$, so that $-\pi < \phi_j, \phi \leq \pi$. Show that the point process

$$\left\{\frac{N}{2\pi}(\phi_j-\phi)\right\}_{j=1}^{N},$$

converges to a translationally-invariant determinantal point process[3] on $\mathbb{R}$ with the first correlation function identically equal to 1. In the literature this is known as the (continuous) Sine process. What is the correlation kernel for the process?

B. For $0 \leq t \leq N$ consider the gap probability:

$$G(t) = \lim_{N\to\infty}\mathbb{P}\left(\text{there are no particles } z_j \text{ with complex argument between } 0 \text{ and } \frac{2\pi t}{N}\right).$$

Using part A this is equal to a Fredholm determinant involving the limiting correlation kernel. Write down this Fredholm determinant. Computing the Fredholm expansion numerically on *your* computer, plot $G(t)$.

[3]The case $\mathfrak{z} = -1$ works equally well, if we redefine the angles ϕ_i and ϕ to be in $[0, 2\pi)$.

C. Now approximate $G(t)$ by choosing a large N (You can take $N = 100$ or $N = 1000$.), and sampling CUE many times to approximate the probability in question. Plot the result and compare with the graph from part B.

D. It is possible to express the distribution of the asymptotic spacing (*i.e.*, the distribution of the first positive particle in the Sine process, conditional on the event that there is a particle at 0) through $G(t)$? What is the expression? No need to be fully rigorous here (but one can check whatever answer one gets on the computer, as in parts B and C).

Problem 5. Consider the GUE–eigenvalue distribution, which is a probability distribution on $x_1 > x_2 > \cdots > x_N$ with density

$$\frac{1}{(2\pi)^{N/2}\prod_{j=1}^{N-1} j!}\prod_{i<j}(x_i - x_j)^2 \prod_i e^{-\frac{1}{2}x_i^2}. \tag{4.38}$$

A. Passing to unordered configurations and using Theorem 4.17, show that the corresponding particle configuration forms a determinantal point process on $\mathbb{R}$ with correlation kernel with respect to the Lebesgue measure given by

$$K_N^{\mathrm{GUE}}(x,y) = \sum_{k=0}^{N-1} \frac{H_k(x)H_k(y)}{\langle H_k, H_k\rangle} \exp\left(-\frac{x^2}{4} - \frac{y^2}{4}\right), \tag{4.39}$$

Where $H_k(x) = x^k$+(lower degree terms), $k = 0, 1, 2, \ldots$, is the kth degree monic Hermite orthogonal polynomial, so that

$$\langle H_k,\, H_\ell\rangle := \int_{-\infty}^{\infty} H_k(x)H_\ell(y)\exp\left(-\frac{x^2}{2}\right)\mathrm{d}x = 0, \qquad \text{for any } k \neq \ell.$$

Hint. Rewrite the Vandermonde determinant (2.15) as a determinant involving $H_k(x)$.

B. Integrating by parts in the expression for scalar product with x^m, deduce expressions for the Hermite polynomials and their norm:

$$H_n(x) = (-1)^n \exp\left(\frac{x^2}{2}\right)\frac{\partial^n}{\partial x^n}\exp\left(-\frac{x^2}{2}\right), \qquad \langle H_k(x),\, H_\ell(x)\rangle = \mathbf{1}_{k=\ell}k!\sqrt{2\pi}. \tag{4.40}$$

C. Show that Hermite polynomials satisfy a three-term recurrence:

$$H_{n+1}(x) - xH_n(x) + nH_{n-1}(x) = 0.$$

Hint. One way is by converting the expression in part B into a contour integral around 0.

D. Deduce from part C an alternative expression for the correlation kernel:

$$K_N^{\mathrm{GUE}}(x,y) = \frac{1}{(N-1)!\sqrt{2\pi}}\frac{H_N(x)H_{N-1}(y) - H_N(y)H_{N-1}(x)}{x-y}\exp\left(-\frac{x^2}{4} - \frac{y^2}{4}\right). \tag{4.41}$$

Problem 6. Our goal is to give another proof of Theorem 4.21 by using the *Fock space* $\mathfrak{F}$. Let V be a linear space with basis $\{\underline{k} \mid k \in \mathbb{Z}\}$. The semi-infinite exterior power is a linear space $\mathfrak{F}$ spanned by infinite wedge products of elements of V of the form

$$v_S = \underline{s_1} \wedge \underline{s_2} \wedge \underline{s_3} \wedge \ldots, \tag{4.42}$$

where $S = \{s_1 > s_2 > \dots\} \subset \mathbb{Z}$ is such that both sets $S_+ = S \setminus \mathbb{Z}_{\le 0}$ and $S_- = \mathbb{Z}_{\le 0} \setminus S$ are finite. We equip $\mathfrak{F}$ with the inner product $\langle \cdot, \cdot \rangle$ in which the basis $\{v_S\}$ is orthonormal. *Creation* and *annihilation* operators in $\mathfrak{F}$ are introduced as follows. The creation operator ψ_k is the exterior multiplication[4] by $\underline{k}$: $\psi_k(f) = \underline{k} \wedge f$. The annihilation operator ψ_k^* is its adjoint. Observe that

$$\psi_k \psi_k^* \, v_S = \begin{cases} v_S \,, & k \in S \,, \\ 0 \,, & k \notin S \,. \end{cases} \tag{4.43}$$

Let C be the *charge operator*: $Cv_S = (|S_+| - |S_-|)v_S$. Using (4.19), the zero-charge subspace $\ker C \subset \mathfrak{F}$ is spanned by the vectors $v_{X(\lambda)}$ with λ varying over all partitions. The *vacuum vector*

$$v_{\mathrm{vac}} = \underline{0} \wedge \underline{-1} \wedge \underline{-2} \wedge \dots$$

corresponds to the empty partition. Define the operators

$$\alpha_n = \sum_{k \in \mathbb{Z}} \psi_{k-n} \psi_k^*, \qquad n \in \mathbb{Z} \setminus \{0\}.$$

Note that the application of α_n to any v_S yields a finite linear combination of basis vectors.

A. Show that operators ψ_k and ψ_k^* satisfy the canonical anti-commutation relations

$$\psi_k \psi_l + \psi_l \psi_k = 0, \qquad \psi_k^* \psi_l^* + \psi_l^* \psi_k^* = 0, \qquad \psi_k \psi_l^* + \psi_l^* \psi_k = \mathbf{1}_{k=l} \,, \qquad k, l \in \mathbb{Z}.$$

B. Show that operators α_n satisfy the Heisenberg commutation relations

$$\alpha_m \alpha_n - \alpha_n \alpha_m = m \, \mathbf{1}_{n=-m} \,, \qquad m, n \in \mathbb{Z} \setminus \{0\}.$$

C. Fix two admissible specializations ρ_1, ρ_2, as in Definition 3.3, and set

$$\Gamma_\pm(\rho_j) = \exp\left(\sum_{k \ge 1}^{\infty} \frac{p_k(\rho_j)}{k} \, \alpha_{\pm k} \right), \qquad j = 1, 2,$$

where the exponential is understood through its series expansion. Prove the relations:

$$\Gamma_\pm^*(\rho_j) = \Gamma_\mp(\rho_j), \qquad \Gamma_+(\rho_j) v_{\mathrm{vac}} = v_{\mathrm{vac}}, \qquad \Gamma_-(\rho_j) v_{\mathrm{vac}} = \sum_{\lambda \in \mathbb{Y}} s_\lambda(\rho_j) \cdot v_{X(\lambda)}, \qquad j = 1, 2,$$

$$\Gamma_+(\rho_1)\Gamma_-(\rho_2) = H(\rho_1; \rho_2) \cdot \Gamma_-(\rho_2)\Gamma_+(\rho_1).$$

D. Use part **C** and (4.43) to derive the following formulas for the correlation functions of $X(\lambda)$, with λ distributed as the Schur measure of Definition 3.4:

$$\rho_n(x_1, \dots, x_n) = \frac{1}{H(\rho_1; \rho_2)} \left\langle \left(\prod_{i=1}^{n} \psi_{x_i} \psi_{x_i}^* \right) \Gamma_-(\rho_1) \, v_{\mathrm{vac}}, \, \Gamma_-(\rho_2) v_{\mathrm{vac}} \right\rangle = \left\langle \prod_{i=1}^{n} \Psi_{x_i} \Psi_{x_i}^* \, v_{\mathrm{vac}}, \, v_{\mathrm{vac}} \right\rangle, \tag{4.44}$$

where

$$\Psi_k = G \, \psi_k \, G^{-1} \,, \quad \Psi_k^* = G \, \psi_k^* \, G^{-1} \,, \quad G = \Gamma_+(\rho_1) \, \Gamma_-(\rho_2)^{-1}.$$

[4] If f contains $\underline{k}$, then $\underline{k} \wedge f = 0$. Otherwise, we multiply by $\underline{k}$ on the left, and then reorder the coordinates as in (4.42) using $x \wedge y = -y \wedge x$ on each step.

E. Show that Ψ_a and Ψ_b^* are linear combinations of ψ_k's and ψ_l^*'s respectively. Use part **A** to deduce

$$\rho_n(x_1,\dots,x_n)=\det\left[K(x_i,x_j)\right]_{i,j=1}^n, \qquad K(x,y)=\left\langle \Psi_x\Psi_y^*\, v_{\mathrm{vac}},\, v_{\mathrm{vac}}\right\rangle. \tag{4.45}$$

The passage from (4.44) to (4.45) is an instance of the *fermionic Wick theorem*.

F. Denote $\psi(z)=\sum_{m\in\mathbb{Z}}\psi_m z^m,\ \psi^*(z)=\sum_{m\in\mathbb{Z}}\psi_m^* z^{-m}$. Prove the commutation relations

$$\Gamma_\pm(\rho_j)\psi(z)=H(\rho_j;\,z^{\pm1})\psi(z)\Gamma_\pm(\rho_j), \qquad \Gamma_\pm(\rho_j)\psi^*(z)=\frac{1}{H(\rho_j;\,z^{\pm1})}\psi^*(z)\Gamma_\pm(\rho_j), \qquad j=1,2.$$

Use them to match (4.45) with (4.20).

Problem 7. Our goal is to prove a generalization of Theorem 4.17 known as the *Eynard–Mehta theorem*. Fix integers $k,n\ge 1$ and let $\mathfrak{X}^{(1)},\dots,\mathfrak{X}^{(k)}$ be finite sets. We choose n functions $\phi_1,\dots,\phi_n$ on $\mathfrak{X}^{(1)}$ and n functions $\psi_1,\dots,\psi_n$ on $\mathfrak{X}^{(k)}$ organized into matrices

$$\Phi=\big[\phi_i(x)\big]_{1\le i\le n,\,x\in\mathfrak{X}^{(1)}}, \qquad \Psi=\big[\psi_j(x)\big]_{x\in\mathfrak{X}^{(k)},\,1\le j\le n}.$$

We also choose transition matrices

$$W_m:\mathfrak{X}^{(m)}\times\mathfrak{X}^{(m+1)}\to\mathbb{C}, \qquad m=1,\dots,k-1.$$

For $1\le i,j\le k$, we introduce ordered products of these matrices:

$$\mathcal{W}_{[i,j)}=\begin{cases} W_iW_{i+1}\cdots W_{j-1}, & i<j,\\ \mathrm{Id}_{\mathfrak{X}^{(i)}}, & i=j,\\ 0, & i>j,\end{cases} \qquad W_{[i,j)}=\begin{cases} W_iW_{i+1}\cdots W_{j-1}, & i<j,\\ 0, & i\ge j.\end{cases} \tag{4.46}$$

These two types of products differ only when $i=j$. We consider nk–point configurations

$$\left\{x_i^{(1)}\right\}_{i=1}^n\cup\left\{x_i^{(2)}\right\}_{i=1}^n\cup\dots\cup\left\{x_i^{(k)}\right\}_{i=1}^n\subset\mathfrak{X}^{(1)}\sqcup\mathfrak{X}^{(2)}\sqcup\dots\sqcup\mathfrak{X}^{(k)},$$

with $\left\{x_i^{(m)}\right\}_{i=1}^n\subset\mathfrak{X}^{(m)}$ for each $1\le m\le k$, and assign them a weight

$$\mathrm{wt}(\{x_i^{(m)}\})=\det\big[\phi_i(x_j^{(1)})\big]_{i,j=1}^n\left(\prod_{m=1}^{k-1}\det\big[W_m(x_i^{(m)},x_j^{(m+1)})\big]_{i,j=1}^n\right)\det\big[\psi_i(x_j^{(k)})\big]_{i,j=1}^n. \tag{4.47}$$

A. Set $M=\Phi\mathcal{W}_{[1,k)}\Psi$ and compute the normalization constant for (4.47) as:

$$\sum_{\{x_i^{(m)}\}}\mathrm{wt}(\{x_i^{(m)}\})=\det M. \tag{4.48}$$

B. Let Ω be a finite set and let L be a matrix with rows and columns indexed by Ω. Fix a subset $\mathbb{Y}\subset\Omega$ with complement $\overline{\mathbb{Y}}=\Omega\setminus\mathbb{Y}$. The conditional L-ensemble on $\mathbb{Y}$ is a probability measure on subsets of $\mathbb{Y}$ given by

$$\mathbb{P}(Y)=\frac{\det L_{Y\cup\overline{\mathbb{Y}}}}{\det(\mathrm{Id}_{\mathbb{Y}}+L)}, \qquad Y\subset\mathbb{Y}, \tag{4.49}$$

where the determinant in numerator involves a matrix of size $|Y|+|\overline{\mathbb{Y}}|$, while the determinant in denominator involves a matrix of size $|\Omega|$, in which $\mathrm{Id}_{\mathbb{Y}}$ is viewed as an orthogonal projection onto $\mathbb{Y}$. Show that the weights (4.49) sum up to 1.

Remark. When $\mathbb{Y} = \Omega$, (4.49) is called L–ensemble (without "conditional"). The statements below and their proofs also make sense for complex measures, without imposing positivity of the weights (4.49).

C. Prove that the conditional L-ensemble is a determinantal point process with correlation kernel

$$K = \mathrm{Id}_{\mathbb{Y}} - (\mathrm{Id}_{\mathbb{Y}} + L)^{-1}\big|_{\mathbb{Y}\times\mathbb{Y}}. \tag{4.50}$$

Hint. Use inclusion–exclusion and the following identity (see *e.g.*, [Pra94, Section 2.5.2]):

$$\det(A^{-1})_S = \frac{\det A_{\Omega\setminus S}}{\det A}.$$

D. Now set

$$\Omega = \{1,\dots,n\} \sqcup \mathfrak{X}^{(1)} \sqcup \cdots \sqcup \mathfrak{X}^{(k)}, \qquad \mathbb{Y} = \mathfrak{X}^{(1)} \sqcup \cdots \sqcup \mathfrak{X}^{(k)}, \qquad \overline{\mathbb{Y}} = \{1,\dots,n\}.$$

Define the block matrix

$$L = \begin{bmatrix} 0 & \Phi & 0 & 0 & \cdots & 0 \\ 0 & 0 & -W_1 & 0 & \cdots & 0 \\ 0 & 0 & 0 & -W_2 & \cdots & 0 \\ \vdots & \vdots & \vdots & \vdots & \ddots & \vdots \\ 0 & 0 & 0 & 0 & \cdots & -W_{k-1} \\ \Psi & 0 & 0 & 0 & \cdots & 0 \end{bmatrix}, \tag{4.51}$$

where the block rows and columns are ordered as

$$\{1,\dots,n\},\ \mathfrak{X}^{(1)},\ \mathfrak{X}^{(2)},\ \dots,\mathfrak{X}^{(k)}.$$

Show that the conditional L-ensemble (4.49) is exactly the point process with weights (4.47). More precisely, show that $\det L_{Y\cup\overline{\mathbb{Y}}}$ vanishes unless Y contains exactly n points on each level $\mathfrak{X}^{(m)}$, and that in the nonzero case it is equal to (4.47) up to a sign depending only on n and k, but not on the configuration.

E. Prove the block inversion formula (assuming all inverses that appear exist):

$$\begin{bmatrix} A & B \\ C & D \end{bmatrix}^{-1} = \begin{bmatrix} -\mathcal{M}^{-1} & \mathcal{M}^{-1}BD^{-1} \\ D^{-1}C\mathcal{M}^{-1} & D^{-1} - D^{-1}C\mathcal{M}^{-1}BD^{-1} \end{bmatrix}, \qquad \mathcal{M} = BD^{-1}C - A. \tag{4.52}$$

F. Continuing part **D**, split the matrix $\mathrm{Id}_{\mathbb{Y}} + L$ into blocks according to the decomposition $\Omega = \overline{\mathbb{Y}} \sqcup \mathbb{Y}$. Use (4.52): identify the blocks A, B, C, D, check that

$$D^{-1} = \begin{bmatrix} I & \mathcal{W}_{[1,2)} & \mathcal{W}_{[1,3)} & \cdots & \mathcal{W}_{[1,k)} \\ 0 & I & \mathcal{W}_{[2,3)} & \cdots & \mathcal{W}_{[2,k)} \\ 0 & 0 & I & \cdots & \mathcal{W}_{[3,k)} \\ \vdots & \vdots & \vdots & \ddots & \vdots \\ 0 & 0 & 0 & \cdots & I \end{bmatrix},$$

and prove that the *Schur complement* $\mathcal{M}$ in (4.52) matches M in part **A**.

G. Using part **C**, prove the following statement.

Theorem 4.31. *The process with weights* (4.47), i.e.,

$$\mathbb{P}(\{x_i^{(m)}\}) = \frac{1}{\det M}\mathrm{wt}(\{x_i^{(m)}\}),$$

is a determinantal point process (with respect to the counting measure) on

$$\mathfrak{X}^{(1)} \sqcup \cdots \sqcup \mathfrak{X}^{(k)},$$

such that its correlation kernel has (i,j) block (in which we used both types of products (4.46)*)*

$$K_{ij} = \mathcal{W}_{[i,k)} \Psi M^{-1} \Phi \mathcal{W}_{[1,j)} - W_{[i,j)}, \qquad 1 \le i,j \le k. \tag{4.53}$$

Equivalently, for pairwise distinct space-time points (m_a, x_a),

$$\mathbb{P}\big((m_1,x_1),\dots,(m_r,x_r) \in \{x_i^{(m)}\}\big) = \det\big[K_{m_a m_b}(x_a,x_b)\big]_{a,b=1}^{r}.$$

H. Check that for $k=1$, the result of part **G** matches Theorem 4.17 up to transposition.

Remark. Problem 7.E in Section 2.5 delivers examples for the Eynard-Mehta theorem. If, in a suitable weighted oriented graph, we have nonintersecting paths with fixed starting and ending vertices, then the distributions of the intersection points of these paths with any chosen "sections" have the same structure as (4.47), and thus we obtain a determinantal point process.

Problem 8. We deal with a Schur process of Definition 3.5: we pick a natural number T and consider sequences of partitions

$$\varnothing \subset \lambda^{(1)} \supset \mu^{(1)} \subset \lambda^{(2)} \supset \mu^{(2)} \subset \cdots \supset \mu^{(T-1)} \subset \lambda^{(T)} \supset \varnothing,$$

equipped with probability measure (for the normalization constant Z, see (3.12))

$$\mathbb{P}\left(\lambda^{(1)},\mu^{(1)},\dots,\lambda^{(T)}\right) = \frac{1}{Z} s_{\lambda^{(1)}}(\rho_0^+)\, s_{\lambda^{(1)}/\mu^{(1)}}(\rho_1^-) s_{\lambda^{(2)}/\mu^{(1)}}(\rho_1^+)\, \cdots s_{\lambda^{(T)}/\mu^{(T-1)}}(\rho_{T-1}^+)\, s_{\lambda^{(T)}}(\rho_T^-).$$

We consider a random point process on $\{1,\dots,T\}\times\mathbb{Z}$ given by

$$\mathcal{L}(\lambda^{(1)},\dots,\lambda^{(T)}) = \left\{\big(1,\lambda_i^{(1)}-i+1\big)\right\}_{i\ge1} \cup \cdots \cup \left\{\big(T,\lambda_i^{(T)}-i+1\big)\right\}_{i\ge1}. \tag{4.54}$$

In this problem we extend Theorem 4.21 to Schur processes by proving the following statement.

Theorem 4.32. *The random point process $\mathcal{L}$ of* (4.54) *is determinantal*[5]*: for any pairwise distinct pairs $\{(t_i,\ell_i)\}_{i=1}^m$ of $\{1,\dots,T\}\times\mathbb{Z}$, we have*

$$\sum_{\{(t_1,\ell_1),\dots,(t_m,\ell_m)\}\subset\mathcal{L}(\lambda^{(1)},\dots,\lambda^{(T)})} \mathbb{P}\left(\lambda^{(1)},\mu^{(1)},\dots,\lambda^{(T)}\right) = \det\big[K(t_i,\ell_i;t_j,\ell_j)\big]_{i,j=1}^m, \qquad \textit{where}$$

$$K(t_1,\ell_1;t_2,\ell_2) = \frac{1}{(2\pi\mathbf{i})^2} \oiint \frac{H(\rho^+_{[0,t_1)};v) H(\rho^-_{[t_2,T]};w^{-1})}{H(\rho^-_{[t_1,T]};v^{-1}) H(\rho^+_{[0,t_2)};w)} \frac{v^{-\ell_1} w^{\ell_2-1}}{(v-w)}\,\mathrm{d}w\mathrm{d}v. \tag{4.55}$$

The contours for w and v go around 0 in the positive direction. $H(\cdot)$ must have uniformly convergent series expansions on the contours (cf. Theorem 4.21). For $t_2 \ge t_1$, we require $|v/w|>1$, so that

$$\frac{1}{v-w} = \frac{1}{v}\cdot\frac{1}{1-w/v} = \frac{1}{v}\left(1+\frac{w}{v}+\left(\frac{w}{v}\right)^2+\dots\right)$$

[5] We can also add diagrams $\mu^{(t)}$ to consideration. Such an extension can be proven by choosing some of the specializations to be $(0;0;0)$ leading to almost sure equality of μ and λ coordinates.

For $t_2 < t_1$, we require $|v/w| < 1$ on the contours, thus allowing the expansion

$$\frac{1}{v-w} = -\frac{1}{w}\cdot\frac{1}{1-v/w} = -\frac{1}{w}\left(1+\frac{v}{w}+\left(\frac{v}{w}\right)^2+\dots\right).$$

In (4.55) *we use the notation ρ_A for the union (as in Definition 2.24) of specializations $\{\rho_a\}_{a\in A}$.*

A. Check that the case $t_1 = t_2 = \cdots = t_m$ in the theorem and (4.55) coincides with Theorem 4.21.

B. Consider the case when ρ_0^+ and ρ_T^- are specializations into finitely many variables:

$$\rho_0^+ = (x_1,\dots,x_N), \qquad \rho_T^- = (y_1,\dots,y_N). \tag{4.56}$$

Using the Jacobi-Trudi formula of Proposition 2.17, show that the joint law of $\lambda^{(1)},\lambda^{(2)},\dots,\lambda^{(T)}$ has weights proportional to

$$\det\left[x_i^{\ell_j^{(1)}}\right]_{i,j=1}^N \det\left[W_1(\ell_i^{(1)},\ell_j^{(2)})\right]_{i,j=1}^N \cdots \det\left[W_{T-1}(\ell_i^{(T-1)},\ell_j^{(T)})\right]_{i,j=1}^N \det\left[y_i^{\ell_j^{(T)}}\right]_{i,j=1}^N, \tag{4.57}$$

where $\ell_j^{(t)} = \lambda_j^{(t)} - j + 1$ for all meaningful values of t, j; N is assumed to be larger than the number of rows in each $\lambda^{(t)}$, $1 \le t \le T$; and $[W_t(x,y)]_{x,y\in\mathbb{Z}}$ are Toeplitz matrices with symbols

$$\sum_{m\in\mathbb{Z}} W_i(x+m,x)z^m = H(\rho_i^-;z)H(\rho_i^+;z^{-1}).$$

C. The formula (4.57) is similar to the setting of Problem 7, but with two important differences: the sizes N of intermediate determinants in (4.57) depend on $\lambda^{(t)}$ and the variables $\ell_j^{(t)}$ may vary over the infinite set of all integers, not over a finite set $\mathfrak{X}$. Show that nevertheless one can apply the Eynard-Mehta theorem of Problem 7 to (4.57) and deduce that (4.54) is a determinantal point process.
Hint. Recall how we deduced Theorem 4.21 from Theorem 4.20.

D. Compute $(M^{-\mathsf{T}})_{k\ell}$ for M as in Problem 7.A, corresponding to (4.57). Your expression should be reminiscent of (4.17), but multiplied by a power of $x_k y_\ell$ due to a shift by $(N-1)$ in the definition of the point process, and should include additional $H(\cdot)$–factors

E. Plug the result of part **D** into (4.53) and convert the resulting sum into a contour integral for the correlation kernel of the Schur process. What are the contours?

F. Extend the contour integral expression of part **E** from specific ρ_0^+ and ρ_T^- of (4.56) to general specializations. Match with (4.55).

Literature. We used the following sources for composing problems and refer to them for more information, references, and connections: [Kac90], [Sos00a], [Oko01a], [Meh04], [OR06], [Bor11a], and [BR05].

Chapter 5

Steepest descent and its applications to local limits

The contour integrals we encountered in the formulas for correlation kernels, such as (4.25) or (4.26), can often be written in the form $\int \exp[Nf(z)]\mathrm{d}z$, where N is a relevant large parameter. In this chapter we learn how to study $N \to \infty$ asymptotics of such integrals. The integrals which we need are fairly advanced, so we start with much simpler examples.

5.1 Real integral: Stirling's formula

As a warm up, we prove Stirling's formula for $N!$.

Proposition 5.1. *As $N \to \infty$, we have*

$$N! = \sqrt{2\pi N}\left(\frac{N}{e}\right)^N \big(1 + o(1)\big). \tag{5.1}$$

Proof. We start from the representation of $N!$ through the Gamma function: $N! = \Gamma(N+1)$, *i.e.*,

$$N! = \int_0^\infty x^N e^{-x}\mathrm{d}x. \tag{5.2}$$

This identity is readily proven by induction, using integration by parts. The asymptotic analysis of the real integral (5.2) can be performed using *Laplace's method*, whose origins date back to [Lap74, Lap86].

Changing variables $x = Ny$, we study the integral

$$N^{N+1}\int_0^\infty \exp\left(N(\log(y) - y)\right)\mathrm{d}y. \tag{5.3}$$

The key idea is that the integral is dominated by a small neighborhood of the maximum of the integrand, or, equivalently, of the maximum of $\log(y) - y$. The maximum is a critical point, *i.e.*, the first derivative vanishes at this point:

$$0 = \frac{\partial}{\partial y}\big(\log(y) - y\big) = \frac{1}{y} - 1.$$

Because $\log(y) - y \to -\infty$, as $y \to +0$ and $y \to +\infty$, the critical point $y = 1$ is the global maximum.

We choose small $\varepsilon > 0$ and split the integral into two parts, $y \in [0, 1-\varepsilon] \cup [1+\varepsilon, +\infty)$ and $y \in (1-\varepsilon, 1+\varepsilon)$. Inside the ε–neighborhood of 1 we Taylor-expand the function in the exponent. The second derivative is

$$\frac{\partial^2}{\partial y^2}(\log(y) - y) = \frac{\partial}{\partial y}\left(\frac{1}{y} - 1\right) = -\frac{1}{y^2}.$$

Hence,

$$\log(y) - y = -1 - \frac{(y-1)^2}{2} + O\left((y-1)^3\right).$$

With $y = 1 + \frac{z}{\sqrt{N}}$, the integral over $y \in [1-\varepsilon, 1+\varepsilon]$ becomes

$$N^{N+1}\frac{1}{\sqrt{N}}\int_{-\varepsilon\sqrt{N}}^{\varepsilon\sqrt{N}} \exp\left(-N - \frac{z^2}{2} + N\cdot O(\varepsilon^3)\right) \mathrm{d}z \tag{5.4}$$

Let us choose[1] $\varepsilon = N^{-2/5}$, so that $N\varepsilon^3 \to 0$ as $N \to \infty$. Then, via the Gaussian integral $\int_{-\infty}^{\infty} \exp\left(-\frac{z^2}{2}\right) \mathrm{d}z = \sqrt{2\pi}$, the expression (5.4) becomes

$$\sqrt{N}\left(\frac{N}{e}\right)^N \int_{-\varepsilon\sqrt{N}}^{\varepsilon\sqrt{N}} \exp\left(-\frac{z^2}{2}\right)\mathrm{d}z \cdot \big(1 + o(1)\big) = \sqrt{2\pi N}\left(\frac{N}{e}\right)^N \big(1 + o(1)\big).$$

It remains to show that the integral over $y \in (0, 1-\varepsilon] \cup [1+\varepsilon, +\infty)$ is negligible. We upper-bound this part by:

$$\begin{aligned} N^{N+1}\left[\int_0^{1-\varepsilon} + \int_{1+\varepsilon}^{2} + \int_2^{\infty}\right] \exp\left(N(\log(y) - y)\right)\mathrm{d}y \\ \le CN^{N+1}\left[\exp\big(-N(1+\delta)\big) + \exp\big(-N(1+\delta)\big) + \exp\big(N(\log(2)-2)\big)\right], \end{aligned} \tag{5.5}$$

where C is a constant which does not depend on ε or N, and

$$\delta = -1 - \max\big(\log(1+\varepsilon) - (1+\varepsilon),\, \log(1-\varepsilon) - (1-\varepsilon)\big) > 0.$$

In order to get the third term in the right-hand side of (5.5), one notices that the integrand decays fast enough as $y \to +\infty$, so that the integral can be upper-bounded by a constant times the value of the integrand in the left-most point of the integration segment. Since we chose $\varepsilon = N^{-2/5}$, we can lower bound $\delta > cN^{-4/5}$ for some $c > 0$. Then (5.5) becomes

$$\left(\frac{N}{e}\right)^N \cdot C'N\exp\left(-cN^{1/5}\right),$$

which can be absorbed into $o(1)$ term in (5.1)[2]. □

We conclude that the integral is computed by localizing and Taylor expanding near the critical point.

[1] Any $N^{-\xi}$ with $\frac{1}{3} < \xi < \frac{1}{2}$ will work.

[2] The $o(1)$ term in (5.1) is, actually, $\frac{1}{12n} + O\left(\frac{1}{n^2}\right)$, see, e.g., [Olv97, Section 8.4].

5.2 Contour integral: local CLT for binomial random variables

In the next example we use a contour integral to establish asymptotics of binomial coefficients.

Proposition 5.2. *Choose $0 < p < 1$ and $x \in \mathbb{R}$. For $N = 1, 2, \ldots$, set K to be the nearest integer to $pN + x\sqrt{N}$. Then*

$$p^K(1-p)^{N-K}\binom{N}{K} = \frac{1}{\sqrt{2\pi N p(1-p)}} \exp\left(-\frac{x^2}{2p(1-p)}\right) \cdot \big(1 + o(1)\big), \qquad N \to \infty. \tag{5.6}$$

The left-hand side of (5.6) is the weight of the binomial random variable, equal to the sum of N i.i.d. Bernoulli random variables $\xi_1 + \cdots + \xi_N$, with $\mathbb{P}(\xi = 1) = p$, $\mathbb{P}(\xi = 0) = 1 - p$. pN in our choice of K is the mean of this random variable, $Np(1-p)$ is its variance. The right-hand side of (5.6) is $N^{-1/2}$ times the density of the Gaussian random variable $\mathcal{N}\big(0, p(1-p)\big)$. The asymptotic identity is a manifestation of the *local central limit theorem*, where the word local means that we deal with individual weights, rather than sums of those required for the (weaker) convergence in distribution in the usual CLT, which we recalled in Chapter 1 as Theorem 1.1.

Proof of Proposition 5.2. Using the binomial theorem and computing the residue at 0 as coefficient of $\frac{1}{z}$:

$$p^K(1-p)^{N-K}\binom{N}{K} = \frac{1}{2\pi\mathbf{i}} \oint_{\text{around } 0} \frac{\big(zp + (1-p)\big)^N}{z^{K+1}} \mathrm{d}z, \tag{5.7}$$

where the contour can be an arbitrary positively-oriented loop enclosing the singularity at $z = 0$.

Comparing to the previous case, a new difficulty appears: if we want to localize near a maximum of the modulus of the integrand, then that depends on the choice of the contour around 0. In addition, oscillations of the complex integrand (caused by variations in the phase) may lead to cancellations near the maximum. Yet, it turns out that we should still look for the critical point.

We recast the integral in the form:

$$\frac{1}{2\pi\mathbf{i}} \oint_{\text{around } 0} \exp\big(Nf(z)\big) z^{pN-K-1} \mathrm{d}z, \tag{5.8}$$

where

$$f(z) = \ln\big(pz + (1-p)\big) - p\ln(z). \tag{5.9}$$

We treat z^{pN-K-1} separately, because its power grows as $O\left(N^{1/2}\right)$, *i.e.*, much slower than $Nf(z)$. One might be uneasy about the choice of the branches for $\ln(z)$ in the definition of $f(z)$, since this is a multivalued function — eventually, this is not going to matter, and any consistent choice of branches is going to work, because the modulus of the integrand is controlled by $\mathrm{Re} f(z)$ which is independent of the branch. Throughout this proof we use the branch of $\ln(z)$ with a cut along the negative real axis, so that $\ln(\exp(\mathbf{i}\phi)) = \mathbf{i}\phi$ for $-\pi < \phi < \pi$.

We compute the derivative

$$f'(z) = \frac{p}{pz + (1-p)} - \frac{p}{z}.$$

Setting the above expression to zero gives us the unique critical point $z_c = 1$. We observe that

$$f''(z_c) = -\frac{p^2}{(pz_c + (1-p))^2} + \frac{p}{z_c^2} = p(1-p) > 0.$$

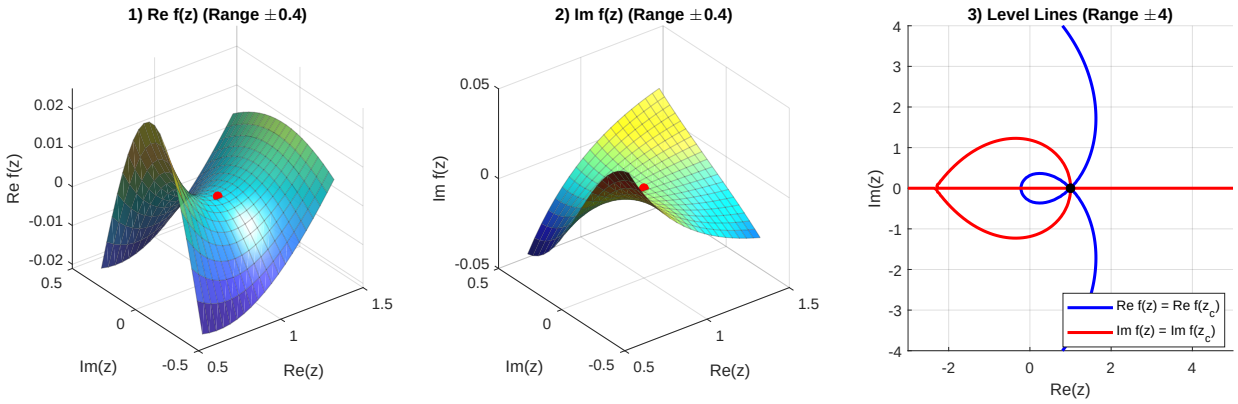


Figure 5.1: Real and imaginary parts of $f(z) = \ln(pz + (1-p)) - p\ln(z)$ near the critical point $z_c = 1$.

Hence, the Taylor expansion yields

$$f(z) = f(z_c) + \frac{f''(z_c)}{2}(z - z_c)^2 + O\big((z - z_c)^3\big) = \frac{p(1-p)}{2}(z-1)^2 + O\big((z-1)^3\big). \tag{5.10}$$

For a holomorphic function, its critical points are also known as *saddle points*, for the reasons best seen by examining the graphs of $\mathrm{Re} f(z)$ and $\mathrm{Im} f(z)$ near such point, as in Figure 5.1. The graphs locally look like two saddles, rotated by $\frac{\pi}{4}$ with respect to each other. In particular, locally near critical point z_c there is a contour passing through it and such that on this contour $\mathrm{Re} f(z)$ is maximized at z_c, while $\mathrm{Im} f(z)$ stays constant — this is the contour we need for studying the asymptotics of the integral. In a more general situation (*i.e.*, for more complicated $f(z)$), it might be tricky to figure out the *global* geometry of the desired contour of integration, because there is no *a priory* information on $\mathrm{Re} f(z)$ or $\mathrm{Im} f(z)$ far from the critical points.

However, for our particular choice of $f(z)$ given by (5.9) this is straightforward: we deform the integration contour into the closed loop $\mathrm{Im} f(z) = \mathrm{Im} f(1)$ passing through 1 and enclosing 0, as in the right panel of Figure 5.1. We claim that along this loop the real part $\mathrm{Re} f(z)$ is maximized at $z = 1$. Indeed, locally near 1 this is true directly from (5.10): $\mathrm{Re} f(z)$ is monotone decreasing as we move away from $z = 1$. We claim that monotonicity continues until the contour reaches the real axis at the left tip[3] again. Indeed, otherwise, $\mathrm{Re} f(z)$ would have a local minimum on the contour at a point $\tilde{z}$. But then $\tilde{z}$ would have to be another critical point of $f(z)$: at a non-critical point a holomorphic function is locally linear and simultaneous vanishing of directional derivatives of $\mathrm{Re} f(z)$ and $\mathrm{Im} f(z)$ is impossible. Since there are no other critical points, the claim is proven.

We split the integral over the contour $\mathrm{Im} f(z) = \mathrm{Im} f(1)$ into two parts, as in the proof of Proposition 5.1: a small neighborhood of $z = 1$ and the rest. The latter part does not contribute to the asymptotics by the same argument as before. In an ε–neighborhood of $z = 1$ we approximate the contour by the vertical line and make a change of variables:

$$z = 1 + \mathbf{i}\frac{v}{\sqrt{N}},$$

[3] At the left tip $\mathrm{Im} f(z)$ has a discontinuity along the contour due to branching of $\ln(z)$.

which converts, as $N \to \infty$, the integral (5.8) into a Gaussian integral:

$$\frac{1+o(1)}{2\pi\sqrt{N}} \int_{-\varepsilon\sqrt{N}}^{\varepsilon\sqrt{N}} \exp\left(-\frac{p(1-p)}{2}v^2 + o(1)\right)\left(1+\mathbf{i}\frac{v}{\sqrt{N}}\right)^{pN-k-1} \mathrm{d}v$$
$$= \frac{1+o(1)}{2\pi\sqrt{N}} \int_{-\infty}^{\infty} \exp\left(-\frac{p(1-p)}{2}v^2\right)\exp(-\mathbf{i}vx)\mathrm{d}v = \frac{1+o(1)}{\sqrt{2\pi N p(1-p)}}\exp\left(-\frac{x^2}{2p(1-p)}\right),$$

where the last equality is a computation of the characteristic function (Fourier transform) of the Gaussian random variable $\mathcal{N}\left(0, \frac{1}{p(1-p)}\right)$, which can be justified, *e.g.*, by completing the square in the exponent. □

The lesson from this integral is that we still need to localize near a critical point, but we have to be careful about the contour along which we are integrating. This method is known since the 19th century as the "steepest descent method" or alternatively "saddle point method", and we refer, *e.g.*, to [Cop65, BH86, BO99] for detailed expositions.

5.3 Edges of the Plancherel measure

Our next goal is to apply the steepest descent method to the correlation kernel of the Poissonized Plancherel measure

$$\mathbb{P}(\lambda) = e^{-\theta}\frac{\theta^{|\lambda|}\dim^2(\lambda)}{(|\lambda|!)^2}, \tag{5.11}$$

as recorded in Corollary 4.23, *i.e.*, to

$$K(\ell_1,\ell_2) = \frac{1}{(2\pi\mathbf{i})^2}\oiint \exp\left(\sqrt{\theta}\left(v-\frac{1}{v}\right)-\sqrt{\theta}\left(w-\frac{1}{w}\right)\right)\frac{v^{-\ell_1}w^{\ell_2-1}}{v-w}\mathrm{d}v\mathrm{d}w, \tag{5.12}$$

where both contours enclose 0 and w–contour is inside the v–contour, as in Figure 4.4.

We are interested in $\theta \to \infty$ limit with ℓ_1 and ℓ_2 staying close to $\chi\sqrt{\theta}$. The asymptotics of the kernel (5.12) is going to be drastically different in three regimes, cf. Figure 5.2:

- If $|\chi| < 2$, then we are inside the Vershik-Kerov-Logan-Shepp curve of Figure 2.4, and the first correlation function $\rho_1(\chi\sqrt{\theta}) = K(\chi\sqrt{\theta},\chi\sqrt{\theta})$ remains strictly between 0 and 1. The asymptotics here is referred to as the *bulk limit*.
- If $\chi > 2$, then we are in the *void* region, where no particles are present with high probability, and the first correlation function $\rho_1(\chi\sqrt{\theta})$ approaches 0. If $\chi < -2$, then we are in the *saturated* region where all positions are occupied by particles with high probability, and the first correlation function approaches 1. The $\chi > 2$ and $\chi < -2$ cases are related to each other by the particle-hole involution, which swaps the particles with empty sites.
- If $|\chi| = 2$, then we are in the critical regime, which governs the asymptotic distribution of the longest rows and longest columns of Plancherel-random Young diagrams. This asymptotics is referred to as the (soft) *edge limit*

We start our analysis from the critical regime $\chi = 2$, which connects us to a new special function.

Definition 5.3. *The Airy function* $\mathrm{Ai} : \mathbb{R} \to \mathbb{R}$ *is a function satisfying the following three properties*

$$\mathrm{Ai}''(x) = x\,\mathrm{Ai}(x), \qquad \mathrm{Ai}(0) = \frac{\Gamma(\frac{1}{3})}{2\pi\cdot 3^{1/6}}, \qquad \lim_{x\to+\infty}\mathrm{Ai}(x) = 0.$$

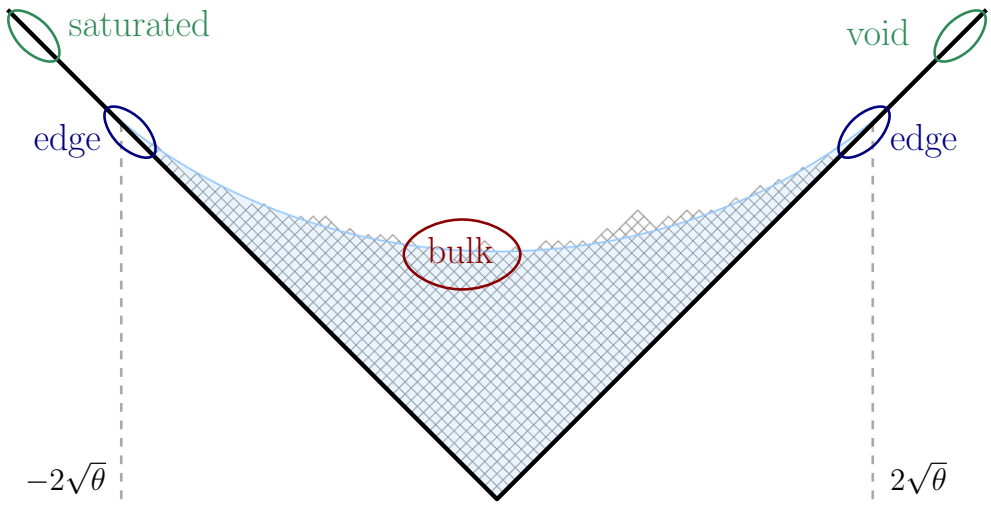


Figure 5.2: Three limit regimes for the asymptotics of the Plancherel measure.

The Airy function serves as the canonical solution to the Airy equation $y'' - xy = 0$, representing the simplest dynamical system exhibiting a transition from oscillatory to exponential behavior across a turning point, see Figure 5.3. Its second solution, denoted as Bi, grows at $+\infty$. Originally derived by George Biddell Airy in 1838 [Air38] to resolve the intensity singularity predicted by geometric optics at the caustic of a rainbow, the function's deep analytic structure was later revealed by Stokes. In his seminal 1850 work [Sto50], Stokes utilized the Airy integral to discover the "Stokes phenomenon" – the discontinuous change in the constants of asymptotic expansions across specific rays in the complex plane. In modern mathematical physics, the Airy function remains ubiquitous; for a comprehensive tabulation of its properties, integral representations, and zeros, [OLBC10] is a definitive standard.

The Airy function vanishes at both infinities, but the speed of decay is very different:

$$\mathrm{Ai}(x) \sim \frac{1}{\sqrt{\pi}\,|x|^{1/4}} \sin\left(\frac{2}{3}|x|^{3/2} + \frac{\pi}{4}\right), \qquad x \to -\infty; \tag{5.13}$$

$$\mathrm{Ai}(x) \sim \frac{e^{-\frac{2}{3}x^{3/2}}}{2\sqrt{\pi}\,x^{1/4}}, \qquad x \to +\infty. \tag{5.14}$$

The normalization condition written in terms of $\mathrm{Ai}(0)$ in Definition 5.3 ensures orthonormality (which we are not going to prove or use, but which can be deduced by applying the Plancherel theorem (2.48) to the Fourier representation (5.17) below):

$$\int_{-\infty}^{\infty} \mathrm{Ai}(x+a)\,\mathrm{Ai}(x+b)\mathrm{d}x = \delta(a-b).$$

Definition 5.4. *The* Airy point process *is a determinantal point process on $\mathbb{R}$ with correlation kernel with respect to the Lebesgue measure given by:*

$$K^{Airy}(x,y) = \frac{\mathrm{Ai}(x)\,\mathrm{Ai}'(y) - \mathrm{Ai}(y)\,\mathrm{Ai}'(x)}{x-y}, \tag{5.15}$$

where the value on the diagonal $x = y$ is understood as the limit of the ratio as $y \to x$.

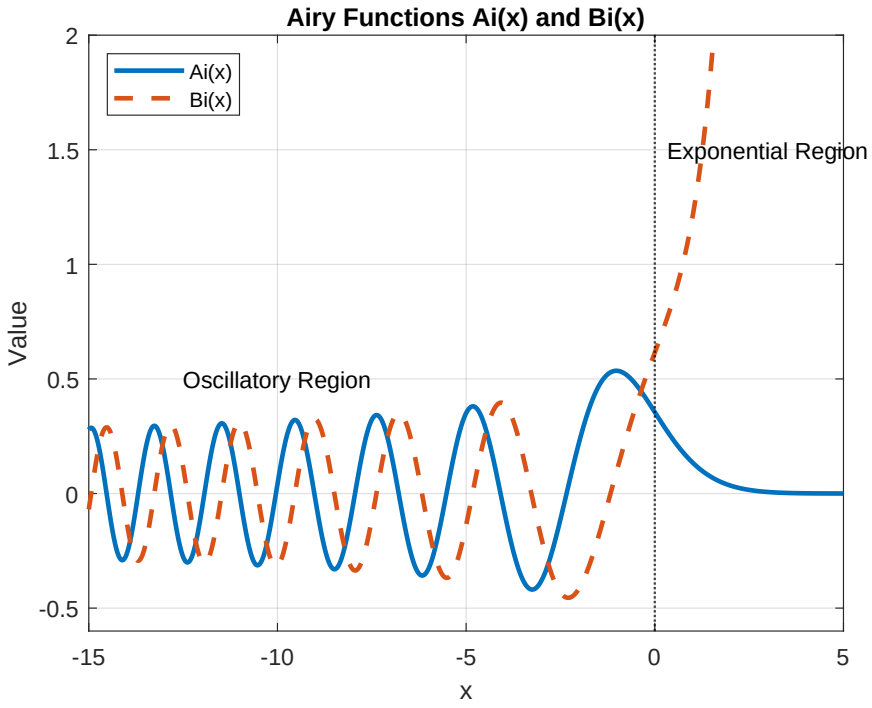


Figure 5.3: Two independent solutions of the equation $y'' - xy = 0$.

If one wants to be more precise, one should use the name Airy_2 point process, as this is a $\beta = 2$ representative of a one-parametric family of Airy_β point processes, in which $\beta > 0$ corresponds to the strength of repulsion between the particles, see, *e.g.*, [RRV11, GS18, GXZ24].

There are two ways to show that the Airy point process exists. First, one can rely on the Macchi–Soshnikov theorem saying that any kernel corresponding to a Hermitian locally trace class operator K satisfying $0 \le K \le \mathrm{Id}$ defines a determinantal point process, see [Mac75] and [Sos00a, Theorem 3]. Alternatively, we get the Airy point process via a limit transition from the objects already known to us.[4] The following statement first appeared in [Oko00, BOO00, Joh01a].

Theorem 5.5. *Let $\lambda = (\lambda_1 \ge \lambda_2 \ge \dots)$ be distributed as the Poissonized Plancherel measure* (5.11) *with parameter θ. Consider the point process on $\mathbb{R}$ defined as*

$$\left\{\theta^{-1/6}\left(\lambda_i + 1 - i - 2\sqrt{\theta}\right)\right\}_{i=1}^{\infty}. \tag{5.16}$$

As $\theta \to \infty$, the correlation measures of (5.16) *converge to those of the Airy point process, in the sense that all integrals over compact sets converge.*

Remark 5.6. Since $\lim\limits_{\theta\to\infty} \theta^{-1/6}(1-i) = 0$, the shifts by $1-i$ in (5.16) can be omitted.

In Section 5.6 we show that Theorem 5.5, together with tail estimates, lead to convergence in distribution of $\theta^{-1/6}(\lambda_1 - 2\sqrt{\theta})$ to the position of the largest particle in the Airy point process. The probability distribution of the latter is precisely the Tracy-Widom distribution.

[4] Theorem 5.5 obtains the correlation functions of the Airy point process as limits, while Theorem 5.14 explains how to deduce convergence of the joint distributions of the random variables N_A for various windows A. The existence of N_A consistent with the correlation functions of Definition 5.4 is precisely the statement of the existence of the Airy point process.



Figure 5.4: Integration contours in (5.17) and (5.18).

Before proceeding to the proof, let us present integral formulas both for the Airy function and for the Airy kernel (5.15).

Lemma 5.7. *The Airy function* $\mathrm{Ai}(x)$ *admits integral representations:*

$$\mathrm{Ai}(x) = \frac{1}{\pi}\int_0^{+\infty} \cos\left(\frac{z^3}{3}+zx\right)\mathrm{d}z = \frac{1}{2\pi}\int_{-\infty}^{\infty}\exp\left(\mathbf{i}\frac{z^3}{3}+\mathbf{i}xz\right)\mathrm{d}z$$
$$= \frac{1}{2\pi\mathbf{i}}\int_{e^{-\mathbf{i}\frac{\pi}{3}}\infty}^{e^{\mathbf{i}\frac{\pi}{3}}\infty}\exp\left(\frac{z^3}{3}-xz\right)\mathrm{d}z. \quad (5.17)$$

The Airy kernel (5.15) *admits an integral representation:*

$$K^{Airy}(x,y) = \frac{1}{(2\pi\mathbf{i})^2}\int_{e^{-\mathbf{i}\frac{\pi}{3}}\infty}^{e^{\mathbf{i}\frac{\pi}{3}}\infty}\mathrm{d}v\int_{e^{-2\mathbf{i}\frac{\pi}{3}}\infty}^{e^{2\mathbf{i}\frac{\pi}{3}}\infty}\mathrm{d}w\exp\left(\left[\frac{v^3}{3}-vx\right]-\left[\frac{w^3}{3}-wy\right]\right)\frac{1}{v-w}, \quad (5.18)$$

where the contours for the second line in (5.17) *and for* (5.18) *are as in Figure 5.4.*

The first two integrals in (5.17) are conditionally convergent improper Riemann integrals. The last integral is a version of the first two on a deformed contour, which leads to fast decay at the infinities and absolute convergence of the integral. Instead of $\pi/3$ angles anything between $\pi/6$ and $\pi/2$ works equally well.

Proof of Lemma 5.7. We start from the integral formula in the second line of (5.17) and denote it $f(x)$. Note that on the integration contours z^3 is a negative real number, and therefore the integrand decays very fast as $z\to\infty$. Differentiating under the integral sign, we have

$$f''(x)-xf(x) = \frac{1}{2\pi\mathbf{i}}\int_{e^{-\mathbf{i}\frac{\pi}{3}}\infty}^{e^{\mathbf{i}\frac{\pi}{3}}\infty}(z^2-x)\exp\left(\frac{z^3}{3}-xz\right)\mathrm{d}z = \frac{1}{2\pi\mathbf{i}}\exp\left(\frac{z^3}{3}-xz\right)\Big|_{e^{-\mathbf{i}\frac{\pi}{3}}\infty}^{e^{\mathbf{i}\frac{\pi}{3}}\infty} = 0.$$

In addition, changing the variables $x=z^3$ and comparing with the definition of the Γ function, we conclude $f(0)=\frac{\Gamma\left(\frac{1}{3}\right)}{2\pi\cdot 3^{1/6}}$. Further, directly from the definition it is clear that $\lim_{x\to+\infty}f(x)=0$. These three properties uniquely determine $\mathrm{Ai}(x)$, and we conclude that $f(x)=\mathrm{Ai}(x)$. The integrals in the first line of (5.17) are obtained from those in the second line by contour deformation and replacement of z with $-\mathbf{i}z$.

For (5.18) with $x \neq y$, we integrate by parts, use $\left(\frac{\partial}{\partial v} + \frac{\partial}{\partial w}\right)\frac{1}{v-w} = 0$, and the second line in (5.17) with $z = v$ and $z = -w$:

$$\begin{aligned}
&\frac{1}{(2\pi\mathbf{i})^2}\iint \exp\left(\frac{v^3}{3} - vx - \frac{w^3}{3} + wy\right)\frac{\mathrm{d}v\mathrm{d}w}{v-w} \\
&\qquad = \frac{1}{y-x}\frac{1}{(2\pi\mathbf{i})^2}\iint\left[\left(\frac{\partial}{\partial v} + \frac{\partial}{\partial w}\right)\exp(-vx+wy)\right]\exp\left(\frac{v^3}{3} - \frac{w^3}{3}\right)\frac{\mathrm{d}v\mathrm{d}w}{v-w} \\
&\qquad\qquad = \frac{1}{x-y}\frac{1}{(2\pi\mathbf{i})^2}\iint \exp\left(\frac{v^3}{3} - \frac{w^3}{3} - vx + wy\right)\frac{(v^2-w^2)\mathrm{d}v\mathrm{d}w}{v-w} \\
&= \frac{1}{x-y}\frac{1}{(2\pi\mathbf{i})^2}\iint \exp\left(\frac{v^3}{3} - \frac{w^3}{3} - vx + wy\right)(w+v)\mathrm{d}v\mathrm{d}w = \frac{\mathrm{Ai}(x)\,\mathrm{Ai}'(y) - \mathrm{Ai}'(x)\,\mathrm{Ai}(y)}{x-y}.
\end{aligned}$$

The diagonal values at $x = y$ follow by continuity of both sides. □

Proof of Theorem 5.5. We choose[5]

$$\ell_1 = 2\sqrt{\theta} + \theta^{1/6}x_1, \qquad \ell_2 = 2\sqrt{\theta} + \theta^{1/6}x_2,$$

and rewrite $K(\ell_1, \ell_2)$ in (5.12) as

$$K(\ell_1,\ell_2) = \frac{1}{(2\pi\mathbf{i})^2}\oiint \exp\left(\sqrt{\theta}\big(f(v) - f(w)\big)\right)\frac{v^{-\theta^{1/6}x_1}w^{\theta^{1/6}x_2-1}}{v-w}\,\mathrm{d}v\mathrm{d}w, \tag{5.19}$$

where

$$f(z) = z - \frac{1}{z} - 2\ln(z), \tag{5.20}$$

and we use the branch of $\ln(z)$ with a cut along the negative real axis, so that $\ln(\exp(\mathbf{i}\phi)) = \mathbf{i}\phi$ for $-\pi < \phi < \pi$. The integral (5.19) has a similar form to the cases studied in the two previous sections with $\sqrt{\theta}$ playing the role of a large parameter. Hence, the steepest descent method suggests to deform the integration contours to pass through a critical point. Differentiating f, we have

$$f'(z) = 1 + \frac{1}{z^2} - \frac{2}{z},$$

and we observe that $z_c = 1$ is a *double critical point*, *i.e.*, a double zero of $f'(z)$. (If ℓ_i are close to $\chi\sqrt{\theta}$ with $|\chi| \neq 2$, then $f(z)$ would instead have two single critical points leading to a very different asymptotic behavior of the kernel which we are also going to study below.)

We compute $f(1) = f'(1) = f''(1) = 0$, $f'''(1) = 2$ and conclude that near 1 the function $f(z)$ has an asymptotic expansion

$$f(z) = \frac{(z-1)^3}{3} + O\left((z-1)^4\right).$$

The double critical point leads to a more complicated behavior of $\mathrm{Re}f$ and $\mathrm{Im}f$, as compared to the single critical point in Figure 5.1. This is shown in Figure 5.5. This time there are six, rather than four rays of constant $\mathrm{Im}f$ emanating from the critical point $z_c = 1$; they are inclined by angles $0, \pm\frac{\pi}{3}, \pm\frac{2\pi}{3}$ to the real axis. On the $\pm\frac{\pi}{3}$ rays, $z = 1$ is a local maximum of $\mathrm{Re}f(z)$, while on the $\pm\frac{2\pi}{3}$ rays, $z = 1$ is a local minimum of $\mathrm{Re}f(z)$[6]. Hence, we deform the contours in the following way, see the left panel in Figure 5.6:

[5] As we will see from the proof, the $\theta^{1/6}$ prefactor is chosen so that the eventual asymptotic formula keeps non-trivial dependence on x_1 and x_2. For another explanation of this scaling see the end of Section 5.4.

[6] Such local behavior is sometimes referred to as a "monkey saddle" with three downward parts suitable for monkey's two legs and the tail.

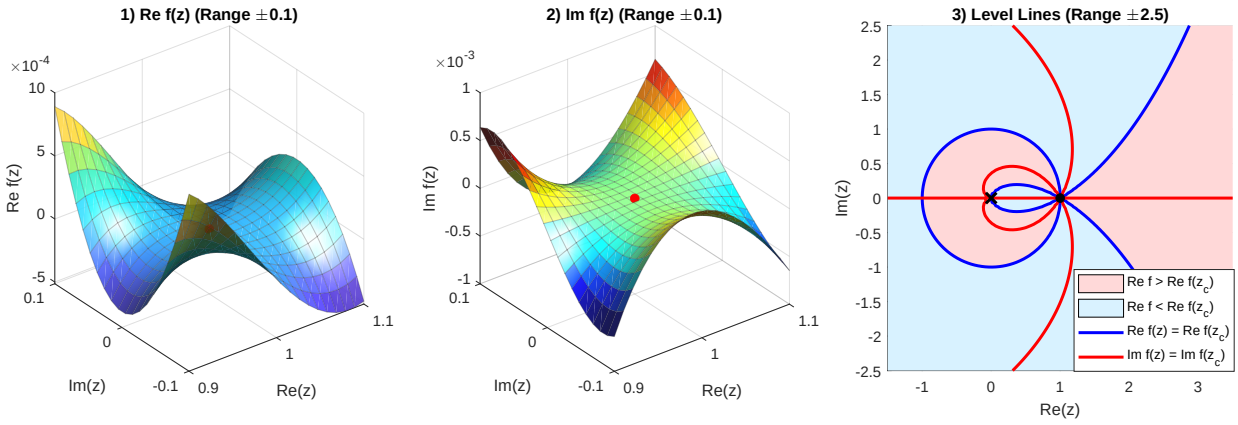


Figure 5.5: Real and imaginary parts of $f(z) = z - \frac{1}{z} - 2\ln z$ near the double critical point $z_c = 1$.

- The new w–contour is the closed loop $\mathrm{Im} f(z) = \mathrm{Im} f(1)$ around 0 starting from 1 at angles $\pm\frac{2\pi}{3}$.
- The new v–contour is a closed loop around 0 starting from 1 at angles $\pm\frac{\pi}{3}$ and following the level line $\mathrm{Im} f(z) = \mathrm{Im} f(1)$ until reaching $\mathrm{Re}(z) = -2$, at which point upper and lower parts are connected by a vertical line.

The important features are: first, the w–contour is inside the v–contour, so that there is no residue at $v = w$ gained while deforming the old contours in (5.12) into the new ones. Second, $\mathrm{Re} f(v) - \mathrm{Re} f(w)$ is maximized on the new contours at the point $v = w = 1$. The latter follows from $\mathrm{Re} f(z)$ being harmonic, and therefore not having any local maxima/minima, implying the constant sign of $\mathrm{Re} f(z) - \mathrm{Re} f(1)$ in the domains bounded by $\mathrm{Re} f(z) = \mathrm{Re} f(1)$ curves.

The conclusion is that only a small neighborhood of $v = w = 1$ contributes to the asymptotics of the double integral on the new contours. In this neighborhood we make a change of variables

$$v = 1 + \theta^{-1/6}\tilde{v}, \qquad w = 1 + \theta^{-1/6}\tilde{w},$$

so that the integral becomes:

$$\frac{\theta^{-1/6}}{(2\pi \mathbf{i})^2} \iint \exp\left(\frac{\tilde{v}^3}{3} - \frac{\tilde{w}^3}{3}\right) \left(1 + \theta^{-1/6}\tilde{v}\right)^{-\theta^{1/6}x_1} \left(1 + \theta^{-1/6}\tilde{w}\right)^{\theta^{1/6}x_2 - 1} \frac{\mathrm{d}\tilde{v}\mathrm{d}\tilde{w}}{\tilde{v} - \tilde{w}} \big(1 + o(1)\big)$$
$$= \frac{\theta^{-1/6}}{(2\pi \mathbf{i})^2} \iint \exp\left(\frac{\tilde{v}^3}{3} - \tilde{v}x_1 - \frac{\tilde{w}^3}{3} + \tilde{w}x_2\right) \frac{\mathrm{d}\tilde{v}\mathrm{d}\tilde{w}}{\tilde{v} - \tilde{w}} \big(1 + o(1)\big), \quad (5.21)$$

where the contour transformations are shown in Figure 5.6. The answer matches (5.18), with the $\theta^{-1/6}$ prefactor in the asymptotics appearing because of the lattice rescaling by $\theta^{1/6}$, as in Section 4.5. The asymptotics (5.21) implies weak convergence of the correlation measures. For instance, the expected number of points in an interval $[a, b]$ for the point process (5.16) is computed as the sum or integral of the first correlation function

$$\sum_{x \in [a,b]} K\big(2\sqrt{\theta} + \theta^{1/6}x, 2\sqrt{\theta} + \theta^{1/6}x\big),$$

where the summation goes only over such $x \in [a, b]$ that the argument of $K(\cdot, \cdot)$ is an integer. The locally-uniform in x convergence in (5.21) guarantee that this (Riemann) sum approximates $\int_a^b K^{\mathrm{Airy}}(x, x)\mathrm{d}x$

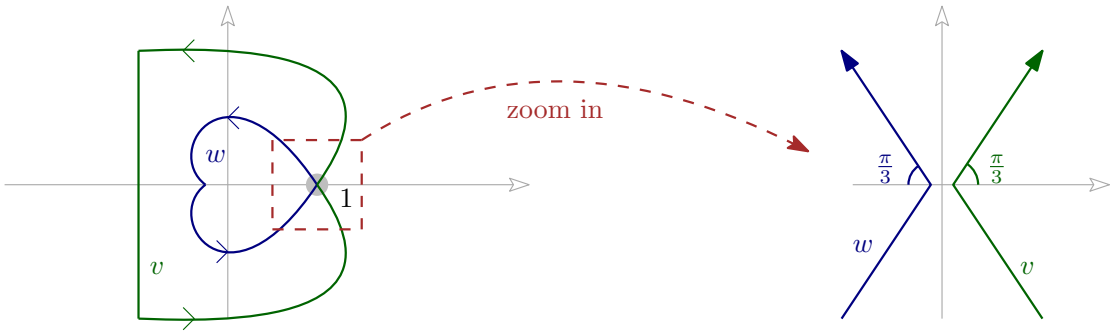


Figure 5.6: Global and local shape of the integration contours.

as $\theta \to \infty$. Since this is true for all intervals $[a, b]$, it follows that the first correlation measure of (5.16) weakly converges to the first correlation measure of the Airy point process.

For the kth correlation measure, we instead plug the asymptotics of (5.21) into the $k \times k$ determinant for the correlation function and integrate over $[a_1, b_1] \times [a_2, b_2] \times \cdots \times [a_k, b_k]$. □

5.4 Bulk limit for the Poissonized Plancherel measure

We proceed to the bulk limit regime and study the middle portion of Figure 5.2 corresponding to $\ell_i \approx \chi\sqrt{\theta}$ with $|\chi| < 2$.

Definition 5.8. *The* discrete Sine process *of density* $\frac{\phi}{\pi} \in (0, 1)$ *is a determinantal point process on* $\mathbb{Z}$ *with correlation kernel with respect to the counting measure given by*

$$K^{\text{Sine}}(x, y) = \begin{cases} \dfrac{\sin(\phi(x-y))}{\pi(x-y)}, & \text{if } x \neq y, \\ \dfrac{\phi}{\pi}, & \text{otherwise.} \end{cases} \tag{5.22}$$

Theorem 5.9. *Let* $\lambda = (\lambda_1 \geq \lambda_2 \geq \dots)$ *be distributed as the Poissonized Plancherel measure* (5.11) *with parameter* θ*. For any* $-2 < \chi < 2$*, consider the point process on* $\mathbb{Z}$ *formed by*[7]

$$\left\{\lambda_i + 1 - i - \lfloor \chi\sqrt{\theta} \rfloor\right\}_{i=1}^{\infty}. \tag{5.23}$$

As $\theta \to \infty$*, the correlation functions of* (5.23) *converge to those of the discrete Sine process with* $\phi = \arccos(\chi/2)$.

Note that while (5.23) seems to capture all particles together, the limiting correlation functions only capture probabilistic information at the finite distance from the origin. Hence, as $\theta \to \infty$, only the particles which have $\lambda_i - i$ close to $\chi\sqrt{\theta}$ remain visible in this limit.

In contrast to the Bernoulli point process of Section 4.1, in the discrete Sine process particles repel each other, as can be seen from the inequality

$$\rho_2^{\text{Sine}}(x, y) = \rho_1^{\text{Sine}}(x)\rho_1^{\text{Sine}}(y) - K^{\text{sine}}(x, y)^2 < \rho_1^{\text{Sine}}(x)\rho_1^{\text{Sine}}(y).$$

[7]We define the floor $\lfloor y \rfloor = \max\{k \in \mathbb{Z} \mid k \leq y\}$.

The correlations functions give all probabilities of various local patterns in the discrete Sine process. For instance, if $\phi = \frac{\pi}{2}$, then the probability to observe two particles at two fixed adjacent positions is:

$$\rho_2^{\text{Sine}}(0,1) = \frac{1}{4} - \frac{1}{\pi^2},$$

and the probability to have no particles at these locations is also

$$1 - \rho_1^{\text{Sine}}(0) - \rho_1^{\text{Sine}}(1) + \rho_2^{\text{Sine}}(0,1) = \frac{1}{4} - \frac{1}{\pi^2}.$$

Corollary 5.10. *In the setting of Theorem 5.9, the point process* (5.23) *converges in distribution to the discrete Sine process.*

Proof. Convergence in distribution means convergence of finite-dimensional distributions of the random variables N_A for all finite sets $A \subset \mathbb{Z}$. As we saw in Lemma 4.8, the probabilities of the events $\{N_{A_1} = k_1, N_{A_2} = k_2, \dots, N_{A_m} = k_m\}$ can be written as finite linear combinations of correlation functions of the process. Hence, convergence of the latter in Theorem 5.9 implies convergence of the former. □

Proof of Theorem 5.9. We choose

$$\ell_1 = \chi\sqrt{\theta} + x_1, \qquad \ell_2 = \chi\sqrt{\theta} + x_2,$$

and rewrite $K(\ell_1, \ell_2)$ in (5.12) as

$$K(\ell_1, \ell_2) = \frac{1}{(2\pi\mathbf{i})^2} \oiint \exp\Big(\sqrt{\theta}\big(f(v) - f(w)\big)\Big) \frac{v^{-x_1} w^{x_2 - 1}}{v - w} \mathrm{d}v \mathrm{d}w, \tag{5.24}$$

where

$$f(z) = z - \frac{1}{z} - \chi \ln(z), \tag{5.25}$$

and we use the branch of $\ln(z)$ with a cut along the negative real axis. The critical point equation has two solutions this time:

$$0 = f'(z_c) = 1 + \frac{1}{z_c^2} - \frac{\chi}{z_c}, \qquad z_c = \frac{\chi \pm \mathbf{i}\sqrt{4 - \chi^2}}{2}. \tag{5.26}$$

Since we assumed $|\chi| < 2$, the two critical points are complex conjugate and lie on the unit circle. We denote them $\exp(\pm\mathbf{i}\phi)$ and note that $2\cos\phi = \chi$, matching the definition of ϕ in the statement of the theorem. $\mathrm{Re} f(z)$ and its level lines are plotted in Figure 5.7.

According to the general principles, we deform the contours to pass through the critical points. The new feature is that there are two rather than one such point, and the contours need to go through both. Let us deform the contours so that both of them pass through the critical points and look as shown in Figure 5.8 — in this argument there is a lot of flexibility in choosing the contours without affecting the final asymptotics. We claim that now $\mathrm{Re} f(v) < 0$ everywhere on its contour except at critical points $e^{\pm i\phi}$, and $\mathrm{Re} f(w) > 0$ everywhere on its contour except at critical points $e^{\pm i\phi}$, and $\mathrm{Re} f(v) = \mathrm{Re} f(w) = 0$ at $e^{\pm\phi}$. Indeed, observe that $\mathrm{Re} f(z) = 0$ for z on the unit circle $|z| = 1$ and compute the gradient of $\mathrm{Re} f(z) = \mathrm{Re} f(a + b\mathbf{i})$ on the unit circle $a^2 + b^2 = 1$:

$$\mathrm{Re} f(a + b\mathbf{i}) = a - \frac{a}{a^2 + b^2} - \frac{\chi}{2} \ln(a^2 + b^2),$$

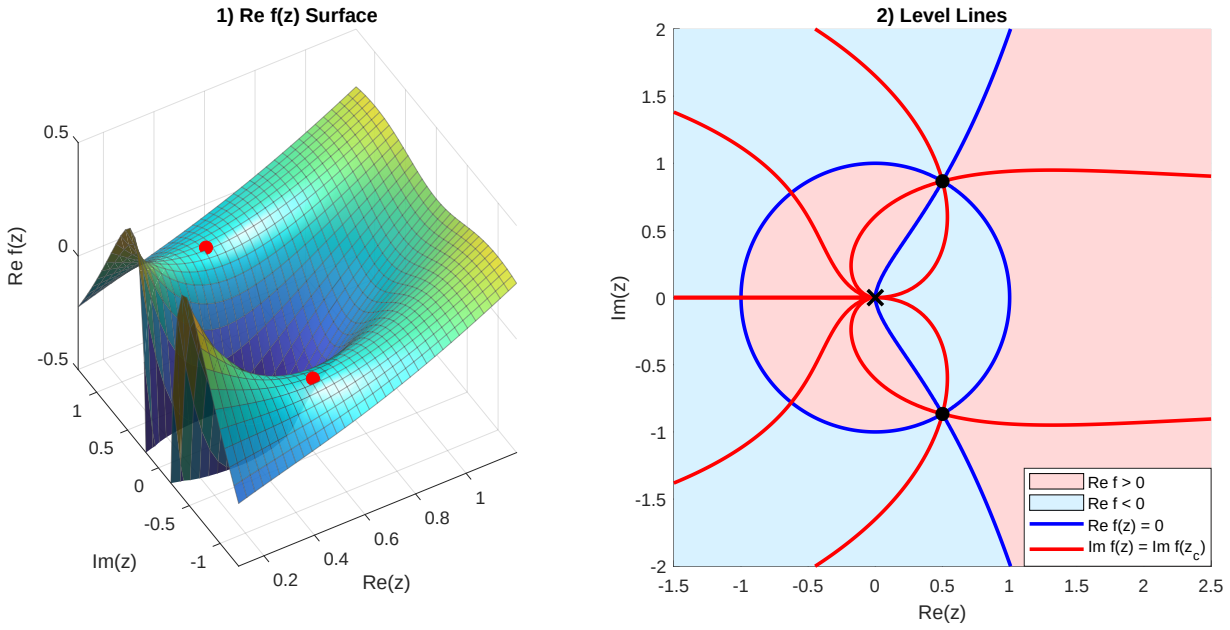


Figure 5.7: $\mathrm{Re} f(z)$ and $\mathrm{Im} f(z)$ for $f(z) = z - \frac{1}{z} - \ln(z)$, *i.e.*, $\chi = 1$.

$$\nabla \mathrm{Re} f(a+b\mathbf{i}) = \left(1 - \frac{b^2-a^2}{(a^2+b^2)^2} - \frac{a\chi}{a^2+b^2}\,,\, \frac{2ab}{(a^2+b^2)^2} - \frac{b\chi}{a^2+b^2}\right)$$
$$= \left(1 - b^2 + a^2 - a\chi\,, 2ab - b\chi\right) = \left(2a^2 - a\chi\,, 2ab - b\chi\right) = (2a-\chi)\cdot(a,b). \quad (5.27)$$

Identity (5.27) implies that the gradient vanishes at points $e^{\pm i\phi}$, points outwards the unit circle on the right arc joining the critical points, and points inwards on the left arc. This implies our inequalities for $\mathrm{Re} f(z)$ on the contours, as long as we assume that the contours are fairly close to the unit circle so that the gradient approximation works.

After the deformation of the contours the integral vanishes as $\theta \to \infty$: by the same arguments as in the previous sections, it decays as $\theta^{-1/4}$. However, this does *not* imply vanishing of the correlation functions. The reason is that the integrand in (5.24) has a singularity at $v = w$. Therefore, when we deform the contours from the contour configuration with $|w| < |v|$, as we had in (5.12), to the contours of Figure 5.8, we get a residue of the integrand in (5.24) at $w = v$ along the arc of the unit circle joining $e^{\pm \mathbf{i}\phi}$. This residue is

$$\frac{1}{2\pi\mathbf{i}} \int_{e^{-\mathbf{i}\phi}}^{e^{\mathbf{i}\phi}} v^{x_2 - x_1 - 1} \mathrm{d}v = \begin{cases} \dfrac{\sin(\phi(x_1 - x_2))}{\pi(x_1 - x_2)}, & \text{if } x_1 \neq x_2, \\ \dfrac{\phi}{\pi}, & \text{if } x_1 = x_2. \end{cases}$$

This matches (5.22) and finishes the proof. □

A particular case of Theorem 5.9 is that for $\chi = 2\cos(\phi)$ with $0 < \phi < \pi$, we have the limit of the first correlation function:

$$\lim_{\theta \to \infty} \rho_1(\chi\sqrt{\theta}) = \frac{\phi}{\pi}.$$

Thus, the asymptotic density of particles at point $\chi\sqrt{\theta}$ decreases from 1 when $\chi = -2$ down to 0 when

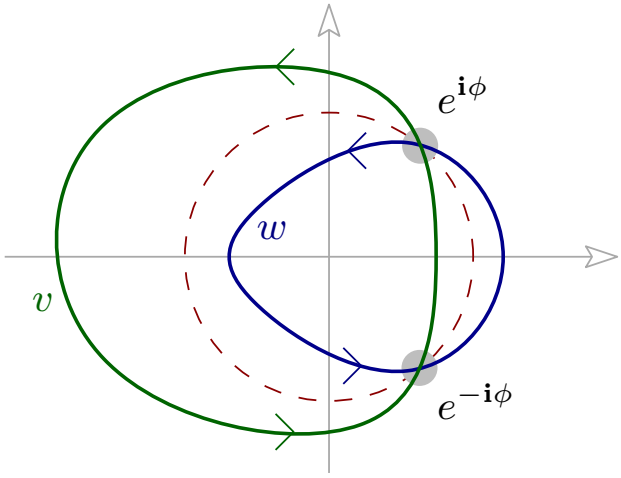


Figure 5.8: Deformed v and w contours, the dashed unit circle, and gray dots for critical points of $f(z)$.

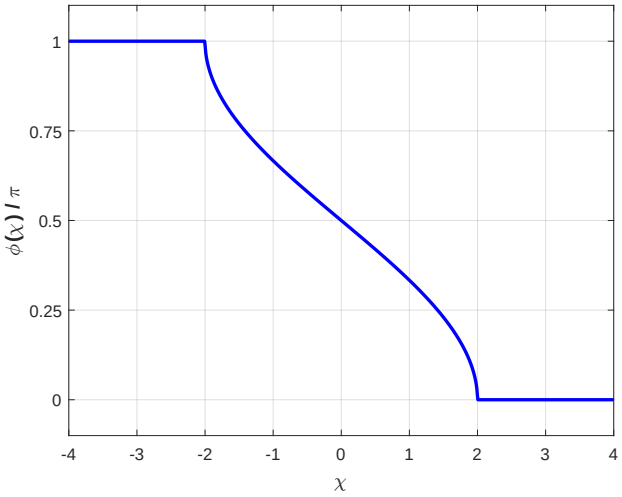


Figure 5.9: Graph of $\lim_{\theta\to\infty} \rho_1(\chi\sqrt{\theta})$ for the Poissonized Plancherel measure.

$\chi = 2$, as in Figure 5.9. Integrating this expression, we obtain the Vershik–Kerov–Logan–Shepp curve [VK77, LS77] describing the limit shape of the Plancherel random Young diagrams. It is the curve shown in Figure 5.2 and explicitly given by

$$\Omega(\chi) = \begin{cases} \frac{2}{\pi}\left(\chi \arcsin\left(\frac{\chi}{2}\right) + \sqrt{4-\chi^2}\right), & |\chi| \le 2, \\ |\chi|, & |\chi| \ge 2, \end{cases}$$

which satisfies[8]

$$\frac{1-\Omega'(\chi)}{2} = \lim_{\theta\to\infty} \rho_1(\chi\sqrt{\theta}) = \begin{cases} \frac{\arccos\left(\frac{\chi}{2}\right)}{\pi}, & |\chi| < 2, \\ 0, & \chi \ge 2, \\ 1, & \chi \le -2. \end{cases}$$

[8]We have not yet established the result for $|\chi| \ge 2$, but it will be addressed in the next section.

An important feature of the asymptotic density $\lim_{\theta\to\infty}\rho_1(\chi\sqrt{\theta})$ is its $\sqrt{x}$–type behavior at -2 and 2. The unusual $\theta^{1/6}$ rescaling in the edge limit of Theorem 5.5 can be attributed to this $\sqrt{x}$ by the following heuristics: If the kth largest particle of the process is close to some $x_k\in\mathbb{R}$, then we expect $\sum_{x\geq x_k}\rho_1(x)\approx k$. Hence,

$$k\approx\sum_{x=x_k}^{2\sqrt{\theta}}\frac{1}{\pi}\sqrt{2-\frac{x}{\sqrt{\theta}}}\approx\sqrt{\theta}\int_{\frac{x_k}{\sqrt{\theta}}}^{2}\frac{\sqrt{2-y}}{\pi}\mathrm{d}y=\sqrt{\theta}\frac{2}{3\pi}\left(2-\frac{x_k}{\sqrt{\theta}}\right)^{3/2},$$

which leads to

$$x_k\approx 2\sqrt{\theta}-k^{2/3}\theta^{1/6}\left(\frac{3\pi}{2}\right)^{2/3}$$

and yields the desired $\theta^{1/6}$ prefactor.

5.5 Decay of the Poissonized Plancherel measure outside the support

We proceed to analyzing the last case $|\chi|>2$ in Figure 5.8. We will only deal with $\chi>2$. Similar bounds for $\chi<-2$ can be obtained by transposing the Young diagram λ, corresponding to replacing all particles by holes and then flipping by $x\mapsto -x$ the point configuration $X(\lambda)$.

Theorem 5.11. *Let $\lambda=(\lambda_1\geq\lambda_2\geq\dots)$ be distributed as the Poissonized Plancherel measure* (5.11) *with parameter θ. Let $\rho_1=\mathbb{P}\big(x\in\{\lambda_i+1-i\}_{i=1}^{\infty}\big)$ be the first correlation function of the point process $X(\lambda)$. There exists $C>0$, such that for each $\theta>1$ and each $x>2\sqrt{\theta}+\theta^{1/6}$, we have*

$$\rho_1(x)\leq C\theta^{-1/6}\exp\left[-\min\left(x-2\sqrt{\theta},\ \frac{(x-2\sqrt{\theta})^{3/2}}{\theta^{1/4}}\right)\right]. \tag{5.28}$$

When x is close to $2\sqrt{\theta}$, the $\min$ equals to its second argument, and the power of $3/2$ matches the large x decay of the diagonal of the Airy kernel $K^{\mathrm{Airy}}(x,x)$ of (5.15), which can be established using the known asymptotics of the Airy function. The prefactor 1 in front of $\min$ is not optimal, but the exact decay constant $\frac{4}{3}$ can be extracted from our proof.

When $x-2\sqrt{\theta}$ is large, the $\min$ is equal to its first argument. This bound is not optimal, but rather a simplification of the exact estimate (5.32) we obtain in the proof. As x grows, the bound (5.28) quickly decays to 0, thus indicating the absence of the particles far to the right from the $x=2\sqrt{\theta}$ point.

Proof of Theorem 5.11. The values of the constants $C>0$ may change from line to line in this proof. For a given $x>2\sqrt{\theta}+\theta^{1/6}$, let χ be such that $x=\chi\sqrt{\theta}$. We rewrite $K(x,x)$ in (5.12) as

$$\rho_1(x)=K(x,x)=\frac{1}{(2\pi\mathbf{i})^2}\oiint\exp\Big(\sqrt{\theta}\big(f(v)-f(w)\big)\Big)\frac{\mathrm{d}v\mathrm{d}w}{w(v-w)}, \tag{5.29}$$

where $|w|<|v|$,

$$f(z)=z-\frac{1}{z}-\chi\ln(z), \tag{5.30}$$

and we use the branch of $\ln(z)$ with a cut along the negative real axis. The quadratic critical point equation has two positive real roots this time, because of $\chi>2$:

$$0=f'(z_c)=1+\frac{1}{z_c^2}-\frac{\chi}{z_c},\qquad z_c^{\pm}=\frac{\chi\pm\sqrt{\chi^2-4}}{2}. \tag{5.31}$$

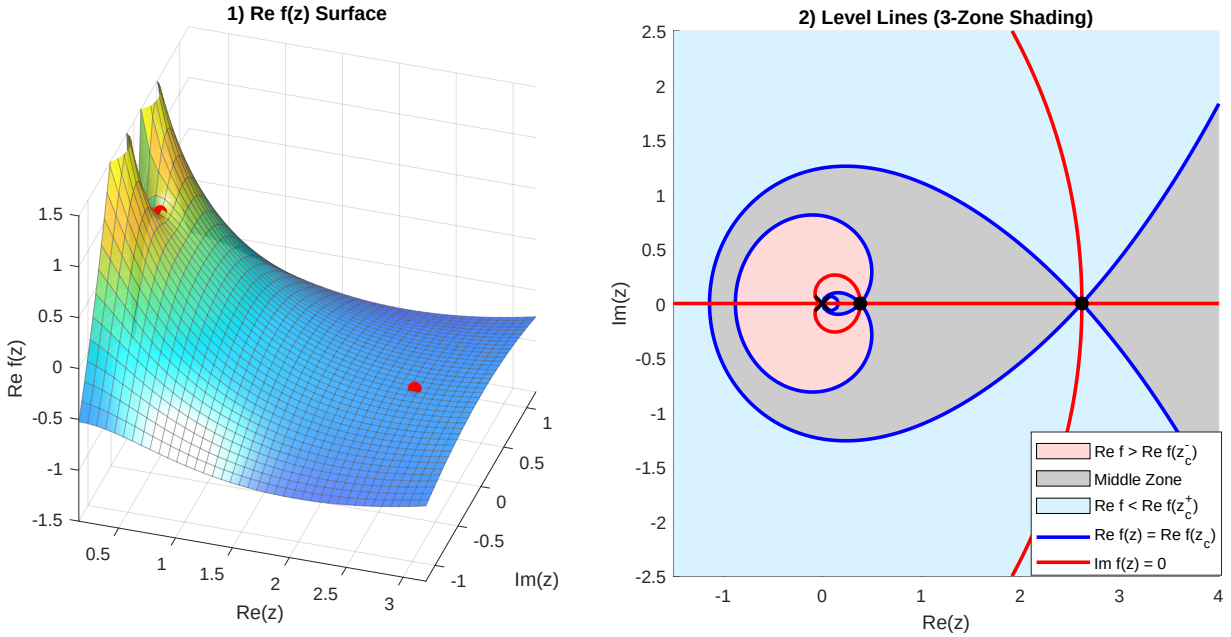


Figure 5.10: $\mathrm{Re} f(z)$ and $\mathrm{Im} f(z)$ for $f(z) = z - \frac{1}{z} - 3\ln(z)$, *i.e.*, $\chi = 3$.

$\mathrm{Re} f(z)$ and its level lines are plotted in Figure 5.10. Note that the two critical points are inverses of each other, and $\mathrm{Re} f(z_c^-) = -\mathrm{Re} f(z_c^+) > 0$. The second derivative is computed using (5.31) as:

$$f''(z_c) = -\frac{2}{z_c^3} + \frac{\chi}{z_c^2} = \frac{1}{z_c} - \frac{1}{z_c^3},$$

which is positive at the larger critical point and negative at the smaller one. We deform the $w-$contour to pass through the smaller critical point and the $v-$contour to pass through the larger critical point. Both contours cross the real axis perpendicularly to the axis itself and then circle around the origin in such a way that $\mathrm{Re} f(w)$ is minimized along its contour at the critical point z_c^-, and $\mathrm{Re} f(v)$ is maximized along its contour at the critical point z_c^+. As before, this allows us to localize the integral near the critical points by making a change of variables:

$$w = z_c^- + \mathbf{i}\theta^{-1/4} \frac{1}{\sqrt{-f''(z_c^-)}} \tilde{w}, \qquad v = z_c^+ + \mathbf{i}\theta^{-1/4} \frac{1}{\sqrt{f''(z_c^+)}} \tilde{v}.$$

The double integral in (5.29) turns into a product of two Gaussian integrals in $\tilde{v}$ and $\tilde{w}$, each evaluated as $\sqrt{2\pi}$. Hence, for some $C > 0$

$$\rho_1(x) \le C \frac{\theta^{-1/2}}{\sqrt{-f''(z_c^-)}\sqrt{f''(z_c^+)}} \frac{\exp\left[\sqrt{\theta}(f(z_c^+) - f(z_c^-))\right]}{z_c^-(z_c^+ - z_c^-)}. \tag{5.32}$$

For the analysis of this expression, we note that f is real and monotone decreasing between z_c^- and z_c^+, with $z_c^- < 1 < z_c^+$ and $f(1) = 0$. We assumed $x > 2\sqrt{\theta} + \theta^{1/6}$, which implies $\chi > 2 + \theta^{-1/3}$ and consequently $|z_c^\pm - 1| \ge \frac{1}{C}\theta^{-1/6}$ for some $C > 0$. Elementary computations lead to further bounds:

$$|z_c^+ - z_c^-| > \frac{\theta^{-1/6}}{C}, \qquad z_c^- > \frac{1}{C\chi}, \qquad -f''(z_c^-) > \frac{\theta^{-1/6}}{C}, \qquad f''(z_c^+) > \frac{\theta^{-1/6}}{C} \cdot \frac{1}{\chi}.$$

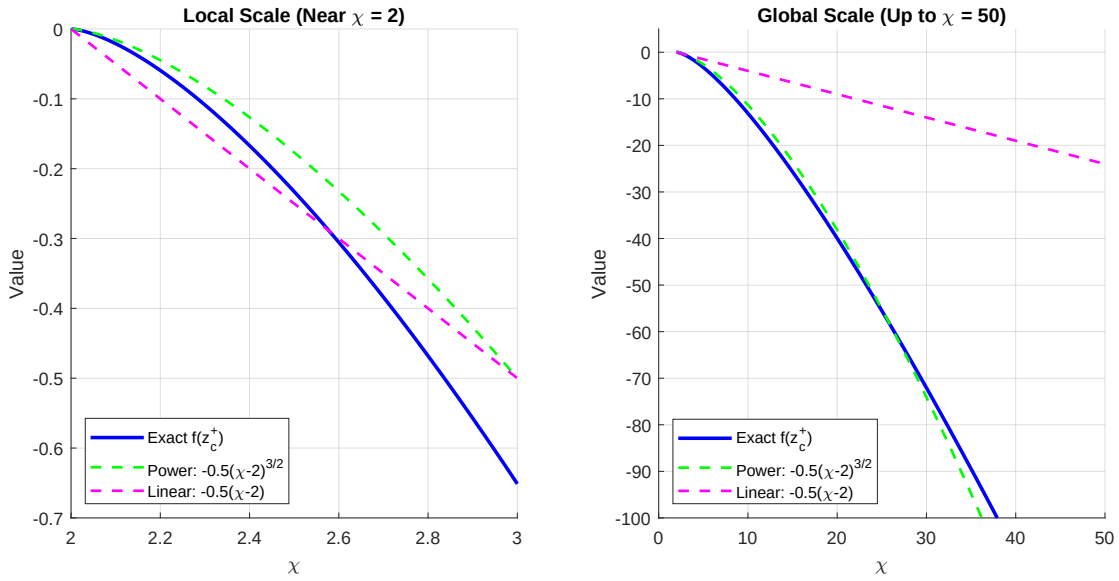


Figure 5.11: Upper bound for $f(z_c^+)$ as a function of χ.

Plugging these inequalities into (5.32), we get an upper bound

$$\rho_1(x) \le C\theta^{-1/6}\chi^{3/2}\exp\bigl[\sqrt{\theta}(f(z_c^+)-f(z_c^-))\bigr] = C\theta^{-1/6}\chi^{3/2}\exp\bigl[2\sqrt{\theta}f(z_c^+)\bigr]$$
$$\le C\theta^{-1/6}\exp\Bigl[-\sqrt{\theta}\min\Bigl(\chi-2,\ (\chi-2)^{3/2}\Bigr)\Bigr], \quad (5.33)$$

where the last inequality is obtained from the exact formulas for f and z_c^+: the left panel in Figure 5.11 shows the values of χ for which $(\chi-2)^{3/2}$ bound is relevant and the right panel corresponds to the values for which $(\chi-2)$ is important. Plugging $\chi = x\theta^{-1/2}$, we obtain (5.28). □

Corollary 5.12. *Let $\lambda = (\lambda_1 \ge \lambda_2 \ge \dots)$ be distributed as the Poissonized Plancherel measure* (5.11) *with parameter θ. Then*

$$\lim_{y\to+\infty}\sup_{\theta>1}\mathbb{P}(\lambda_1 > 2\sqrt{\theta}+\theta^{1/6}y) = 0. \quad (5.34)$$

Remark 5.13. Note that the Plancherel measure is symmetric under the transposition $\lambda \mapsto \lambda'$. Hence, exactly the same statement also holds for $\lambda_1' = \ell(\lambda)$.

Proof of Corollary 5.12. We have

$$\mathbb{P}(\lambda_1 > 2\sqrt{\theta}+\theta^{1/6}y) = \mathbb{P}\bigl(X(\lambda) \text{ has at least one particle larger than } 2\sqrt{\theta}+\theta^{1/6}y\bigr)$$
$$\le \mathbb{E}\Bigl[\text{number of particles of } X(\lambda) \text{ larger than } 2\sqrt{\theta}+\theta^{1/6}y\Bigr] = \sum_{x\in\mathbb{Z}:\,x>2\sqrt{\theta}+\theta^{1/6}y}\rho_1(x). \quad (5.35)$$

We bound the right-hand side using (5.28). For that we let z the point where the value of min in (5.28) switches: *i.e.*, it solves

$$z-2\sqrt{\theta} = \frac{(z-2\sqrt{\theta})^{3/2}}{\theta^{1/4}}, \qquad z = 3\sqrt{\theta}.$$

The sub-sum in (5.35) over $x > z$ is upper-bounded as

$$C\theta^{-1/6}\exp\Bigl(-\sqrt{\theta}\Bigr)\Bigl(1+\frac{1}{e}+\frac{1}{e^2}+\frac{1}{e^3}+\dots\Bigr) \to 0, \qquad \theta\to\infty. \quad (5.36)$$

The sub-sum in (5.35) over $2\sqrt{\theta}+\theta^{1/6}y<x<z$ is upper-bounded as

$$\begin{aligned} C\theta^{-1/6} \sum_{2\sqrt{\theta}+\theta^{1/6}y<x<z} \exp\left[-\frac{(x-2\sqrt{\theta})^{3/2}}{\theta^{1/4}}\right] \\ \le C\theta^{-1/6} \sum_{2\sqrt{\theta}+\theta^{1/6}y<x<z} \exp\left[-y^{1/2}\frac{(x-2\sqrt{\theta})}{\theta^{1/6}}\right] \\ \le C\theta^{-1/6}\exp\left[-y^{3/2}\right]\left(1+\exp\left(-\frac{y^{1/2}}{\theta^{1/6}}\right)+\exp\left(-2\frac{y^{1/2}}{\theta^{1/6}}\right)+\exp\left(-3\frac{y^{1/2}}{\theta^{1/6}}\right)+\dots\right) \\ = C\exp\left[-y^{3/2}\right]\frac{\theta^{-1/6}}{1-\exp\left(-\frac{y^{1/2}}{\theta^{1/6}}\right)}. \end{aligned} \tag{5.37}$$

Assuming $y>1$, $\theta>1$, the last expression is upper-bounded by $C'\exp\left[-y^{3/2}\right]$ and tends to 0 as $y\to\infty$, uniformly in θ.

We now prove (5.34). For any $\varepsilon>0$, we can choose θ_0 such that (5.36) is smaller than $\varepsilon/2$ for all $\theta>\theta_0$. Combining with (5.37), we conclude that

$$\limsup_{y\to+\infty}\sup_{\theta>\theta_0}\mathbb{P}(\lambda_1>2\sqrt{\theta}+\theta^{1/6}y)\le\varepsilon. \tag{5.38}$$

On the other hand, since the distribution of λ_1 continuously depends on θ, we also have

$$\limsup_{y\to+\infty}\sup_{1\le\theta\le\theta_0}\mathbb{P}(\lambda_1>2\sqrt{\theta}+\theta^{1/6}y)\le\varepsilon. \tag{5.39}$$

Since $\varepsilon>0$ can be arbitrary small, (5.38) and (5.39) imply (5.34). □

5.6 Solution to the Ulam problem

Theorem 5.5 presents asymptotic behavior of the correlation measures and we would like to deduce probabilistic consequence regarding individual particles λ_i.

Theorem 5.14. *Let $\lambda=(\lambda_1\ge\lambda_2\ge\dots)$ be distributed as the Poissonized Plancherel measure* (5.11) *with parameter θ. Let $\mathfrak{a}_1\ge\mathfrak{a}_2\ge\dots$ denote the points of the Airy point process of Definition 5.4. Then, in the sense of convergence in finite-dimensional distributions, we have*

$$\lim_{\theta\to\infty}\theta^{-1/6}\left(\lambda_i-2\sqrt{\theta}\right)\overset{d}{=}\mathfrak{a}_i,\qquad i=1,2,\dots. \tag{5.40}$$

The definition of $\mathfrak{a}_1$ implicitly uses the fact that the Airy point process almost surely has finitely many particles to the right from the origin. One way to prove it is by noticing that the expected number of particles to the right from the origin is computed via the first correlation function as

$$\int_0^\infty K^{\text{Airy}}(x,x)\mathrm{d}x,$$

and the last integral is finite because of the fast decay of $\mathrm{Ai}(x)$ and its derivatives as $x\to+\infty$.

Proof of Theorem 5.14. We start from individual distributions of the coordinates λ_i. Note that

$$\mathbb{P}\big(\theta^{-1/6}(\lambda_i + 1 - i - 2\sqrt{\theta}) \le s\big) = \mathbb{P}\big(N^{\theta}_{(s,+\infty)} \le i\big),$$

where $N^{\theta}_{(s,+\infty)}$ is the number of particles in $(s,+\infty)$ interval for the point process

$$\left\{\theta^{-1/6}\left(\lambda_i + 1 - i - 2\sqrt{\theta}\right)\right\}_{i=1}^{\infty}. \tag{5.41}$$

Hence, all we need to prove is that the random variables $N^{\theta}_{(s,+\infty)}$ converge in distribution to similar random variables for the Airy point process.

Instead of dealing with $(s,+\infty)$, we deal with finite intervals (s,t). This is sufficient, because if t is large enough, then $N^{\theta}_{(t,+\infty)} = 0$ with probability close to 1 uniformly in θ by Corollary 5.12; same is true for the Airy point process due to super-exponential decay of $K^{\text{Airy}}(x,x)$ as $x \to +\infty$. For $N^{\theta}_{(s,t)}$ we write, using Theorem 4.26:

$$\mathbb{P}\left(N^{\theta}_{(s,t)} = m\right) = \sum_{n \ge m} \frac{(-1)^{n-m}}{m!(n-m)!} \sum_{\substack{x_1,\dots,x_m \in \theta^{-1/6}\mathbb{Z} \\ s<x_1,\dots,x_n<t}} \det\big[K^{\theta}(x_i,x_j)\big]_{i,j=1}^{n}, \tag{5.42}$$

where $K^{\theta}(x,y)$ is the correlation kernel of the point process (5.41). We want to show that as $\theta \to \infty$, (5.42) converges to a similar expression for the Airy point process, *i.e.*, to

$$\mathbb{P}\left(N^{\text{Airy}}_{(s,t)} = m\right) = \sum_{n \ge m} \frac{(-1)^{n-m}}{m!(n-m)!} \int \dots \int_{s<x_1,\dots,x_n<t} \det\big[K^{\text{Airy}}(x_i,x_j)\big]_{i,j=1}^{n} \mathrm{d}x_1 \cdots \mathrm{d}x_n. \tag{5.43}$$

By Theorem 5.5, the series (5.42) converges to (5.43) term-by-term, and it remains to develop a tail bound. For that we use the classical Hadamard's inequality, whose proof is given below:

Lemma 5.15. *For any $n \times n$ complex matrix A with matrix elements A_{ij} we have*

$$|\det(A)| \le \prod_{i=1}^{n} \sqrt{|A_{1i}|^2 + |A_{2i}|^2 + \dots + |A^2_{ni}|}. \tag{5.44}$$

Applying (5.44), we see that the magnitude of the nth term in (5.42) is upper-bounded by

$$C \cdot \frac{n^{n/2}}{(n-m)!} \big[\theta^{1/6}(t-s)\big]^n \left[\max_{\substack{x,y \in \theta^{-1/6}\mathbb{Z} \\ s<x,y<t}} \left|K^{\theta}(x,y)\right|\right]^n, \tag{5.45}$$

for some $C > 0$ not depending on n. By the asymptotics for K^{θ} established in (5.21), the maximum is upper-bounded by $C\theta^{-1/6}$ for some other $C > 0$. Since $(n-m)!$ grows faster than $\left(\frac{n-m}{e}\right)^{n-m}$ by Proposition 5.1, the term (5.45) decays to 0 very fast, giving the desired convergent upper bound. Hence, by the dominated convergence theorem, (5.42) converges to (5.43).

For the joint distribution of several λ_i, a similar argument leads us to proving the joint convergence in distribution of $N^{\theta}_{(s,t)}$ for several segments (s,t). This is done in the same way as for one interval,

using a generalization of (5.42) provided by (4.36) in Section 4.6: for a determinantal point process with kernel K with respect to a reference measure ν and disjoint intervals $A_1,\dots, A_m$, we have

$$\begin{aligned}&\mathbb{P}(N_{A_1}=m_1,\dots,N_{A_r}=m_r)\\&=\frac{(-1)^{m_1+\dots+m_r}}{m!}\frac{\partial^{m_1+\dots+m_r}}{\partial z_1^{m_1}\dots\partial z_r^{m_r}}\det\bigl(\mathrm{Id}-z_1[K]_{A_1}-\dots-z_r[K]_{A_r}\bigr)_{L^2(A_1\cup A_2\cup\dots\cup A_r,\nu)}\Big|_{z_1=\dots=z_r=1},\end{aligned}\tag{5.46}$$

where $[K]_A$ is the restriction of the kernel K to the set A: $[K]_A(x,y)=K(x,y)\mathbf{1}_A(x)\mathbf{1}_A(y)$. □

Proof of Lemma 5.15. Geometrically, Hadamard's inequality (5.44) upper-bounds the volume of the parallelepiped spanned by columns of A by the product of lengths of its sides. The inequality can be reduced to the classical relation between arithmetic and geometric means by writing

$$|\det A|^2=\det[AA^*]=\det\left[\sum_{k=1}^n A_{ik}\bar{A}_{kj}\right]_{i,j=1}^n.$$

Normalizing the columns of the matrix A, we can assume without loss of generality that the diagonal matrix elements of the last (Hermitian, non-negative definite) matrix AA^* are all equal to 1, and the same for the right-hand side of (5.44). Denoting by $\lambda_1,\dots,\lambda_n\ge 0$ its eigenvalues, we have

$$|\det A|^2=\prod_{i=1}^n\lambda_i\le\left(\frac{\lambda_1+\dots+\lambda_n}{n}\right)^n=\left(\frac{\mathrm{Trace}(AA^*)}{n}\right)^n=1.\quad\square$$

As a corollary of Theorem 5.14, we can now completely solve Ulam's problem on the length of the longest increasing subsequences.

Theorem 5.16. *Let L_n denote the length of the longest increasing subsequence in a uniformly random permutation of n letters, as in Section 3.6. Then, in distribution*

$$\lim_{n\to\infty}n^{-1/6}\bigl(L_n-2\sqrt{n}\bigr)\stackrel{d}{=}\mathfrak{a}_1,\tag{5.47}$$

where $\mathfrak{a}_1$ is the largest particle of the Airy point process.

The law of $\mathfrak{a}_1$ is the *Tracy-Widom distribution*, discussed in further detail in Section 5.9.

Theorem 5.14 is the same statement as Theorem 5.16 but for the Poissonized version of L^θ, obtained by Poisson-randomizing n in L_n. Note that a Poisson random variable ξ^θ with mean θ is sharply concentrated around θ. In fact, by the Central Limit Theorem (note that for integer θ, ξ^θ is a sum of θ i.i.d. Poisson random variables of mean 1 and variance 1):

$$\lim_{\theta\to\infty}\frac{\xi^\theta-\theta}{\sqrt{\theta}}\stackrel{d}{=}\mathcal{N}(0,1).\tag{5.48}$$

Hence, it is reasobable to expect that (5.40) implies (5.47). However, a technical difficulty is that *a priory* Poissonization might have had a smoothing effect: hypothetically one could imagine L_n having the asymptotics (5.47) for generic n, but some completely different behavior for special rare values of n (say, $L_N=0$ for $N=m^2$, $m\in\mathbb{Z}$). In such a situation the Poissonized version of the theorem could still hold, but the de-Poissonized one would fail.

The difficulty can be overcome by observing the following monotonicity property; for a systematic study of the *Plancherel growth process* underlying it, see [Ker98][9].

[9] See `https://vilas.us/simulations/` for a simulation.

Lemma 5.17. *One can define all random variables L_n, $n = 1, 2, \dots$ on the same probability space in such a way that almost surely*

$$L_1 \le L_2 \le L_3 \le \dots. \tag{5.49}$$

Proof. We define a Markov chain $\lambda^{(n)}$, $n = 0, 1, 2, \dots$, on Young diagrams, such that $\lambda^{(n)} \in \mathbb{Y}_n$, $\lambda^{(0)} = \varnothing$, and $\lambda^{(n+1)}$ differs from $\lambda^{(n)}$ by addition of one box:

$$\mathbb{P}\bigl(\lambda^{(n+1)} = \mu \mid \lambda^{(n)} = \lambda\bigr) = \begin{cases} \dfrac{1}{n+1} \cdot \dfrac{\dim \mu}{\dim \lambda}, & \mu = \lambda + \square, \\ 0, & \text{otherwise.} \end{cases} \tag{5.50}$$

We prove two identities:

$$\sum_{\mu\colon \mu = \lambda + \square} \frac{1}{n+1} \cdot \frac{\dim \mu}{\dim \lambda} = 1, \qquad \sum_{\lambda\colon \mu = \lambda + \square} \frac{1}{n+1} \cdot \frac{\dim \mu}{\dim \lambda} \cdot \frac{\dim^2 \lambda}{n!} = \frac{\dim^2 \mu}{(n+1)!}. \tag{5.51}$$

Together these identities imply that $\lambda^{(n)}$ is a Markov chain of growing Young diagrams whose fixed time distribution is Plancherel, and therefore $\lambda_1^{(1)} \le \lambda_1^{(2)} \le \lambda_1^{(3)} \le \dots$ is the desired coupling (5.49) by Theorem 3.15.

The second identity in (5.51) is essentially the definition of $\dim \mu$. For the first identity we recall

$$s_\lambda(x) p_1(x) = \sum_{\mu = \lambda + \square} s_\mu(x)$$

from Section 2.5, and apply the specialization $(0; 0; 1)$ to both sides using Proposition 2.26. □

We also use the following elementary probabilistic statement whose proof we leave as an exercise.

Lemma 5.18. *Let b_n, c_n, d_n, $n = 1, 2, \dots$, be three sequences of random variables on the same probability space, such that for some random variable ξ we have $\lim\limits_{n\to\infty} b_n \overset{d}{=} \lim\limits_{n\to\infty} d_n \overset{d}{=} \xi$ in distribution and $\lim\limits_{n\to\infty} \mathbb{P}(b_n \le c_n \le d_n) = 1$. Then also $\lim\limits_{n\to\infty} c_n \overset{d}{=} \xi$.*

Proof of Theorem 5.16. We put on the same probability space $L_1 \le L_2 \le \dots$ as in Lemma 5.17 and an auxiliary independent sequence $\xi_1, \xi_2, \dots$ of i.i.d. Poisson random variables of mean 1. Set $p(t) = \xi_1 + \dots + \xi_{\lfloor t \rfloor}$ and note that $p(t)$ is a Poisson random variable of mean $\lfloor t \rfloor$. Define the following three sequences of random variables:

$$b_n = n^{-1/6}\bigl(L_{p(n-\sqrt{n}\ln n)} - 2\sqrt{n}\bigr), \quad c_n = n^{-1/6}\bigl(L_n - 2\sqrt{n}\bigr), \quad d_n = n^{-1/6}\bigl(L_{p(n+\sqrt{n}\ln n)} - 2\sqrt{n}\bigr).$$

Applying Theorems 3.15 and 5.14 with $\theta = \lfloor n \pm \sqrt{n}\ln n \rfloor$, and noting that replacements of $\sqrt{\theta}$ with $\sqrt{n}$ and $\theta^{-1/6}$ with $n^{-1/6}$ lead to negligible errors, we conclude that $\lim\limits_{n\to\infty} b_n = \lim\limits_{n\to\infty} d_n \overset{d}{=} \mathfrak{a}_1$. On the other hand, by the CLT for Poisson random variables (5.48) and monotonicity of L_n, the probability of the inequality $b_n \le c_n \le d_n$ tends to 1 as $n \to \infty$. It remains to use Lemma 5.18. □

5.7 Shape and fluctuations of the continuous PNG droplet

Since the continuous PNG model of Section 3.5 was tightly linked to the Poissonized Plancherel measure, another corollary of our developments is identification of the shape and one-point fluctuations of the PNG droplet.

Theorem 5.19. *Let $h(x,t)$ denote the height profile of the continuous PNG model of Section 3.5.2. For each $-1<\chi<1$, we have*

$$\lim_{t\to\infty}\frac{h(\chi t,t)-t\sqrt{1-\chi^2}}{t^{1/3}}\stackrel{d}{=}\mathfrak{a}_1\cdot\left(\frac{1-\chi^2}{4}\right)^{1/6}, \tag{5.52}$$

where $\mathfrak{a}_1$ is the first point of the Airy point process (that has Tracy–Widom distribution).

At $\chi=0$ the scalings simplify to $\lim_{t\to\infty}\left(\frac{t}{2}\right)^{-1/3}\left(h(0,t)-t\right)\stackrel{d}{=}\mathfrak{a}_1$. While we do not prove it here, for distinct values of χ the limits in (5.52) are independent. In order to reconstruct the spatial dependencies and see a random function in the limit, one should study the large t fluctuations of $h(\chi t+yt^{2/3},t)$ as a function of $y\in\mathbb{R}$, see [PS02][10].

The limit shape and rescaling are illustrated in Figure 5.12. It is instructive to compare it against Figure 5.2 giving the shape for Plancherel-random Young diagrams. In both situations a non-random limit shape appears. However, the structure of fluctuations is very different. For the PNG, fluctuations are of order $t^{1/3}$ with Tracy-Widom limit for all $-1<\chi<1$. In contrast, for the Plancherel-random Young diagrams, the Tracy-Widom limit appears only at the critical transition points $\chi=\pm2$, while in between we saw a very different local limit governed by the discrete sine kernel. The discrepancy between the Vershik-Kerov-Logan-Shepp limit shape and the border of the Young diagram in Figure 5.2 is much smaller than for the PNG in Figure 5.12. In fact, the former discrepancy grows at most logarithmically in θ, cf. [Ker93, IO02], a simulation in Figure 5.18, and related statements in Sections 6.5-6.7 below. The conclusion is that the two growth processes — PNG and Plancherel growth — exhibit different asymptotic phenomenology, despite being related to the same algebraic objects and being two different projections of the same multilayer PNG. Heuristically, this can be traced back to transition probabilities (5.51) for the Plancherel growth which, in contrast to the PNG, are very non-local and lead to additional smoothing effects.

Proof of Theorem 5.19. We recall the identification of $h(x,t)$ with λ_1 for a random partition $\lambda\in\mathbb{Y}$ distributed according to the Poissonized Plancherel measure

$$\mathbb{P}(\lambda)=e^{-\theta}\frac{\theta^{|\lambda|}\dim^2(\lambda)}{(|\lambda|!)^2},\qquad \theta=\frac{t^2-x^2}{4}. \tag{5.53}$$

For $x=0$, this is Theorem 3.11. For other x one can repeat the same proof. Alternatively, one can use Proposition 3.12 identifying $h(t,x)$ with a maximal number of Poisson points collected along $(0,0)\mapsto(x,t)$ monotone path and notice that the latter problem (due to invariance of the Poisson process under area-preserving rescalings) depends only on the area of the rectangle with vertices $(0,0)$, $(\frac{t+x}{2},\frac{t+x}{2})$, $(\frac{t-x}{2},\frac{t+x}{2})$, (x,t), rather than on its individual side lengths.

It remains to apply Theorem 5.14 with $i=1$ and $\theta=t^2\frac{1-\chi^2}{4}$. □

5.8 Edge limits for GUE

From the proofs in Sections 5.3 and 5.4, it becomes clear that not much is being used from the exact double contour integral expression for the correlation kernel that we had. The qualitative form of the integrand was important, but the precise features of the function $f(z)$ in the exponent $\sqrt{\theta}f(v)-\sqrt{\theta}f(w)$ much less so. The asymptotics is determined by the critical points, and the behavior of $f(z)$ near them. These behaviors are universal in the sense that up to scaling constants they do not depend on the choice of

[10]Note that we use the Poisson process of intensity $\frac{1}{2}$, while [PS02] uses intensity 2 instead, leading to different scaling constants.

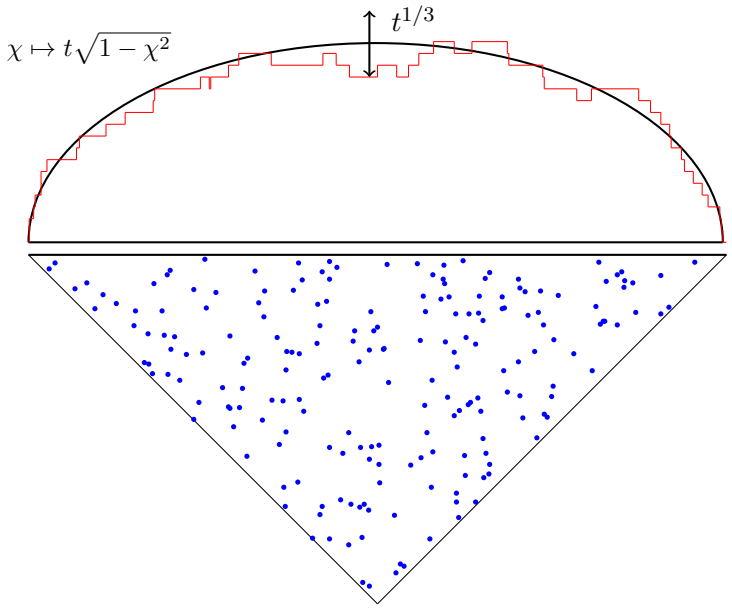


Figure 5.12: Continuous PNG profile after 200 nucleation event vs asymptotic predictions.

f. This suggests that the asymptototic behaviors can also be universal. In this section and Section 5.10 we confirm this prediction by showing that a few other models have exactly the same edge asymptotics as Poissonized Plancherel measure, leading to the Airy point process. We omit some technical details, which are parallel to the previous sections.

The following theorem (proven by another method) can be found in the paper of Tracy and Widom [TW94] and was the origin for the name "Tracy–Widom distribution" attached to the law of $\mathfrak{a}_1$.

Theorem 5.20. *For $N = 1, 2, \ldots$, let $x_1^N \geq x_2^N \geq \cdots \geq x_N^N \in \mathbb{R}$ be distributed with density*

$$\frac{1}{(2\pi)^{N/2}\prod_{j=1}^{N-1} j!} \prod_{1\leq i<j\leq N} \left(x_i^N - x_j^N\right)^2 \prod_{i=1}^{N} \exp\left(-\frac{1}{2}(x_i^N)^2\right), \tag{5.54}$$

and let $\mathfrak{a}_1 \geq \mathfrak{a}_2 \geq \ldots$ be the points of the Airy point process. Then, in finite-dimensional distributions

$$\lim_{N\to\infty} N^{1/6}\left(x_i^N - 2\sqrt{N}\right) \stackrel{d}{=} \mathfrak{a}_i, \qquad i = 1, 2, \ldots. \tag{5.55}$$

The N particles (5.54) can be identified with eigenvalues of the random matrix from Gaussian Unitary Ensemble (GUE), *i.e.*, $M = \frac{1}{2}(Y + Y^*)$, where Y is a matrix of i.i.d. $\mathcal{N}(0,1) + \mathbf{i}\mathcal{N}(0,1)$ elements, see [**?**, For10, AGZ10, ABDF11]. Hence, the $i = 1$ case of (5.55) has already been announced in the introduction in Theorem 1.5.

Our proof of Theorem 5.20 is based on explicit evaluation of the correlation functions. We obtain them as a scaling limit of the correlation functions for a Schur measure. There is a lot of flexibility which measure to choose — many of them rescale to GUE eigenvalues. Our particular choice relates to the binomial distributions (cf. Proposition 5.2) and to the Aztec diamond (cf. Theorem 1.6).

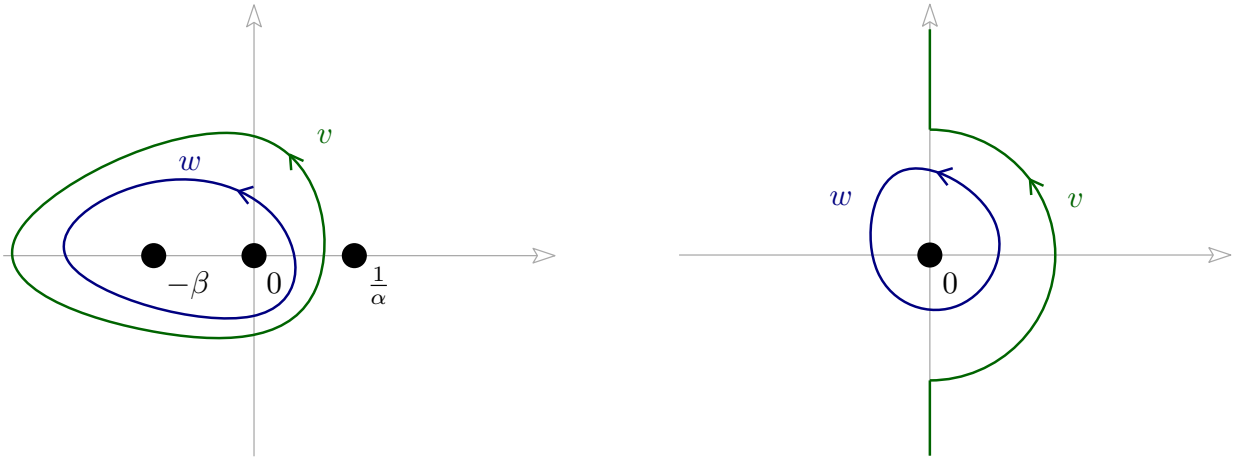


Figure 5.13: Integration contours for Schur measure's correlation kernel (5.57) on the left and for the GUE kernel (5.62) on the right.

Proposition 5.21. *For $N, M = 1, 2, \dots$ and $\alpha, \beta > 0$ consider the distribution on Young diagrams λ with at most N rows and at most M columns, given by*

$$\mathbb{P}(\lambda) = (1+\alpha\beta)^{-NM} s_\lambda(\alpha^N) s_{\lambda'}(\beta^M) = (1+\alpha\beta)^{-MN} \prod_{i=1}^{N} \left[\frac{(\alpha\beta)^{i-N}(M+i-1)!}{(i-1)!(M+N-1)!} \right] \times \prod_{1 \le i < j \le N} \Big[(\lambda_i + N - i) - (\lambda_j + N - j) \Big]^2 \prod_{i=1}^{N} \left[(\alpha\beta)^{\lambda_i + N - i} \binom{M+N-1}{\lambda_i + N - i} \right], \quad (5.56)$$

where α^N and β^M are specializations in N and M variables equal to α and β, respectively. Then the point process $X_N(\lambda) = \{\lambda_i + N - i\}_{i=1}^N$ is determinantal with kernel

$$K_{N,M}(\ell_1, \ell_2) = \frac{1}{(2\pi \mathbf{i})^2} \oiint \frac{(1-\alpha w)^N (1+\beta w^{-1})^M}{(1+\beta v^{-1})^M (1-\alpha v)^N} \frac{v^{N-1-\ell_1} w^{\ell_2 - N}}{v - w} \mathrm{d}v \mathrm{d}w, \quad (5.57)$$

where both contours enclose $-\beta$ and 0, but not α^{-1}, w–contour is inside the v–contour (see Figure 5.13), and $\ell_1, \ell_2 \in \{0, 1, \dots, M+N-1\}$.

Proof. Let us treat the first equality in (5.56) as a definition of $\mathbb{P}(\lambda)$. Then the determinantal structure and (5.57) are corollaries of Theorem 4.21, in which we take:

$$\rho_1 = (\alpha^N; 0; 0), \quad H(\rho_1; z) = (1-\alpha z)^{-N}, \qquad \rho_2 = (0; \beta^M; 0), \quad H(\rho_2; z) = (1+\beta z)^M.$$

For the choice of contours first note that for the case $0 < \alpha < 1, 0 < \beta < 1$, integrating w over the circle $|w| = 1 - \varepsilon$ and integrating v over the circle $|v| = 1 + \varepsilon$ with $0 < \varepsilon < \min(1-\alpha, 1-\beta)$ fits both the description in Theorem 4.21 and the description in Proposition 5.21. For the cases $\alpha > 1$ or $\beta > 1$, we note that the desired evaluation of the correlation functions is equivalent to the following identity: for any finite set $A = \{a_1, \dots, a_m\} \subset \{0, 1, \dots, M+N-1\}$ we have

$$\sum_{\lambda : A \subset X_N(\lambda)} \frac{s_\lambda(\alpha^N) s_{\lambda'}(\beta^M)}{(1+\alpha\beta)^{MN}} = \det\big[K_{N,M}(a_i, a_j)\big]_{i,j=1}^m. \quad (5.58)$$

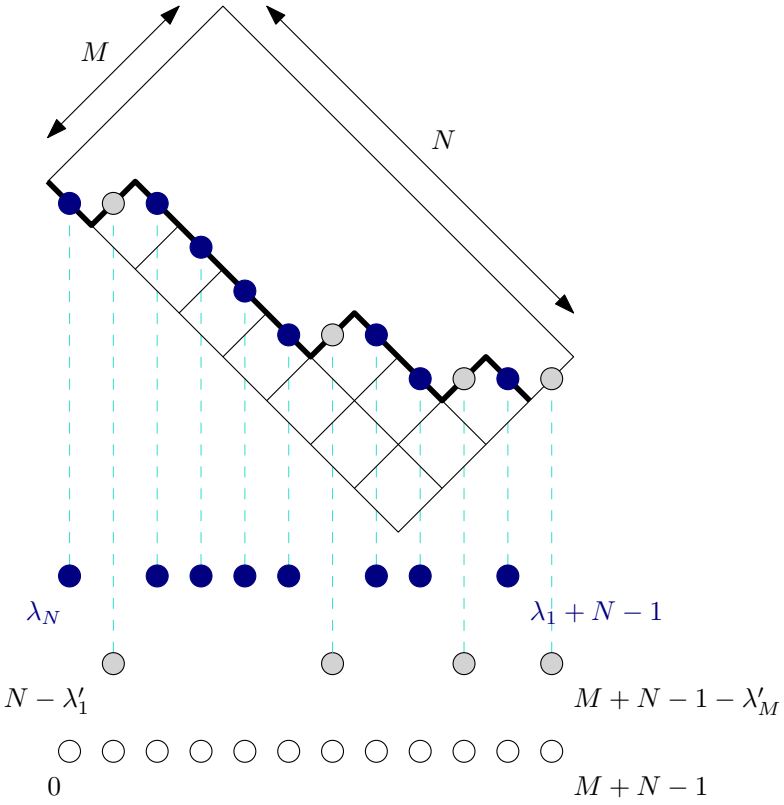


Figure 5.14: Particle-hole involution and transposition of a Young diagram.

Both sides are analytic (even rational) functions of α and β, and therefore the identity (5.58) for small α and β implies the same identity for all $\alpha > 0$ and $\beta > 0$ (as long as the contours are chosen so that no singularity occurs in deforming α and β) by uniqueness of an analytic continuation.

In addition, we would like to show that the two different formulas for $\mathbb{P}(\lambda)$ in (5.56) are the same. For that we recall (2.51), which implies

$$s_\lambda(\alpha^N) = \alpha^{|\lambda|} \prod_{1 \le i < j \le N} \frac{\lambda_i - i - \lambda_j + j}{j - i}, \qquad s_{\lambda'}(\beta^M) = \beta^{|\lambda|} \prod_{1 \le i < j \le M} \frac{\lambda'_i - i - \lambda'_j + j}{j - i}. \tag{5.59}$$

The second formula is given in terms of column lengths, and we need to transform it into an expression involving row lengths. For that we use the following observation, best seen geometrically in Figure 5.14: we have a disjoint union

$$\{\lambda_i + N - i\}_{i=1}^N \bigsqcup \{-\lambda'_j + j + N - 1\}_{j=1}^M = \{0, 1, \dots, M + N - 1\}. \tag{5.60}$$

We combine this observation with the following enumeration lemma.

Lemma 5.22. *Suppose that $A = \{a_1 > \cdots > a_N\}$ and $B = \{b_1 > \cdots > b_M\}$ are two disjoint subsets of $\mathbb{R}$ and denote $A \sqcup B = \{c_1 > \cdots > c_{N+M}\}$. Then we have*

$$\prod_{1 \le i < j \le M} (b_i - b_j) = \prod_{1 \le i < j \le N} (a_i - a_j) \cdot \left[\prod_{i=1}^N \prod_{\substack{1 \le j \le N+M \\ c_j \ne a_i}} \frac{1}{|a_i - c_j|} \right] \cdot \prod_{1 \le i < j < N+M} (c_i - c_j). \tag{5.61}$$

Proof. The proof is a direct count of various $c_i - c_j$ factors in both sides of the identity. We say that a factor appears with $+1$ multiplicity if it is in the numerator and with -1 multiplicity if it is in the denominator. If both c_i and c_j belong to A, then $c_i - c_j$ appears zero times in the left-hand side and $1 - 2 + 1 = 0$ times in the right-hand side. If both c_i and c_j belong to B then $c_i - c_j$ appears one time in the left-hand side and one time in the right-hand side. If one of c_i, c_j belongs to A and the other one belongs to B, then $c_i - c_j$ appears zero times in the left-hand side and $-1+1 = 0$ times in the right-hand side. □

Applying the lemma to $s_{\lambda'}(\beta^M)$ given by (5.59), we get

$$s_{\lambda'}(\beta^M) = C \cdot \beta^{|\lambda|} \prod_{i<j} \big((\lambda_i + N - i) - (\lambda_j + N - j)\big) \prod_{i=1}^{N} \frac{1}{(\lambda_i + N - i)!\big(M + N - 1 - (\lambda_i + N - i)\big)!},$$

where C does not depend on λ. Plugging in this formula and the expression for $s_\lambda(\alpha^N)$, we arrive at the second line of (5.56). The normalization constant is obtained either by carefully keeping track of C and other factors, or by substituting $\lambda = \varnothing$ and noting that $(1+\alpha\beta)^{-NM} s_\lambda(\alpha^N) s_{\lambda'}(\beta^M) = (1+\alpha\beta)^{-NM}$ in this case. □

Proposition 5.23. *For fixed $N \geq 1$, the N–point process $\{x_i^N\}_{i=1}^N$ of GUE eigenvalues* (5.54) *is a determinantal point process with correlation kernel with respect to the Lebesgue measure given by*

$$K_N^{\mathrm{GUE}}(x,y) = \frac{1}{(2\pi\mathbf{i})^2} \iint \exp\left(\frac{v^2}{2} - vy - \frac{w^2}{2} + wx\right) \frac{v^N}{w^N} \frac{\mathrm{d}w\mathrm{d}v}{v-w}, \tag{5.62}$$

where the integration contours are shown in Figure 5.13: the w-contour encloses 0 with positive orientation and the v-contour goes from $-\mathbf{i}\infty$ to $+\mathbf{i}\infty$ leaving the w–contour on the left.

Proof. In the setting of Proposition 5.21, set $\alpha = \beta = 1$ and

$$x_i^N(M) = \frac{\lambda_i - \frac{M}{2}}{\frac{1}{2}\sqrt{M}}, \qquad 1 \leq i \leq N. \tag{5.63}$$

Directly from the local CLT, as in Proposition 5.2, in the limit $M \to \infty$, the binomial weights in the second line of (5.56) turn into the Gaussian weights (N is kept finite here, and therefore the shifts by $N - i$ disappear in the limit), and we observe distributional convergence to the GUE:

$$\lim_{M\to\infty} \big[x_i^N(M)\big]_{i=1}^N \overset{d}{=} \big[x_i^N\big]_{i=1}^N.$$

We make the same limit transition in the correlation kernel (5.57), *i.e.*, using the rescaling of Lemma 4.30, we consider the asymptotics of

$$\frac{\sqrt{M}}{2} K_{N,M}\left(\frac{M}{2} + \frac{1}{2}\sqrt{M}x,\ \frac{M}{2} + \frac{1}{2}\sqrt{M}y\right), \qquad M \to \infty,$$

where we should have inserted integer part in the arguments, but we will omit it to simplify the notations; this does not affect the proof. The last expression is

$$\frac{\sqrt{M}}{2 \cdot (2\pi\mathbf{i})^2} \oiint \frac{(1+w^{-1})^M w^{M/2}}{(1+v^{-1})^M v^{M/2}} \cdot v^{-\frac{1}{2}\sqrt{M}x} w^{\frac{1}{2}\sqrt{M}y} \cdot \frac{v^{N-1}(1-w)^N}{w^N(1-v)^N} \frac{\mathrm{d}v\mathrm{d}w}{v-w}. \tag{5.64}$$

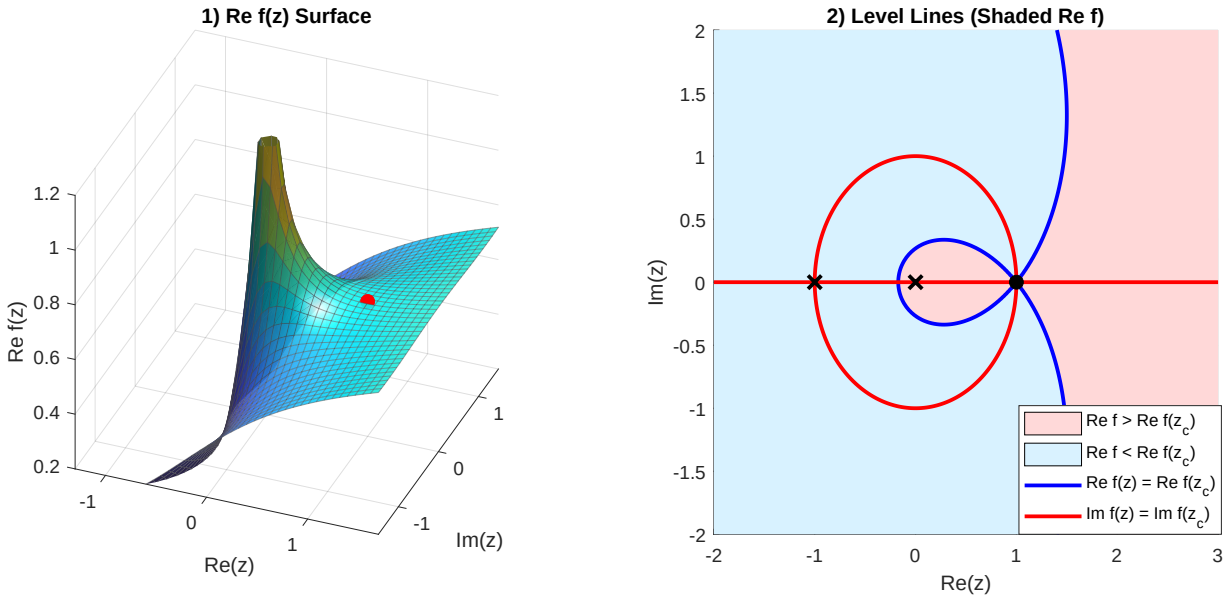


Figure 5.15: $\mathrm{Re} f(z)$ and $\mathrm{Im} f(z)$ for $f(z) = \ln\bigl(1+z^{-1}\bigr) + \frac{1}{2}\ln z$.

The steepest descent method suggests to deform the contours to pass through the critical points of

$$f(z) = \frac{1}{M}\ln\bigl[(1+z^{-1})^M z^{M/2}\bigr] = \ln\bigl(1+z^{-1}\bigr) + \tfrac{1}{2}\ln z.$$

We compute:

$$f'(z) = -\frac{1}{z^2(1+z^{-1})} + \frac{1}{2z} = \frac{1}{z+1} - \frac{1}{z} + \frac{1}{2z} = \frac{1}{z+1} - \frac{1}{2z}, \qquad f''(z) = -\frac{1}{(z+1)^2} + \frac{1}{2z^2}.$$

Hence, $z_c = 1$, $f''(z_c) = \frac{1}{4}$, and $f(z) = \ln 2 + \frac{1}{8}(z-1)^2 + O\bigl((z-1)^3\bigr)$ locally near z_c. Figure 5.15 plots $\mathrm{Re} f(z)$ and corresponding level lines.

There is a new feature compared to the previous examples: we can no longer deform the contours to pass directly through the critical point $z_c = 1$, because the integrand in (5.64) has a singularity at $v = 1$. Instead, the contours will have to stay at finite distance from the critical point after rescaling. Hence, we deform the v–contour to be a small loop of radius $\frac{1}{\sqrt{M}}$ around 1: this involves pushing the contour through $v = \infty$, which is possible because the integrand in (5.64) decays fast enough as $v \to \infty$, so that there is no residue there. The w–contour is essentially a vertical line slightly pushed to the left near $w = 1$, and then circling around the singularity at $w = 0$, see Figure 5.16.

The part of the w–integral away from the critical point has a vanishing contribution as $M \to \infty$. In contrast, the entire v–integral contributes to the leading asymptotics. We make a change of variables

$$v = 1 + \frac{2}{\sqrt{M}}\tilde{v}, \qquad w = 1 + \frac{2}{\sqrt{M}}\tilde{w}.$$

This transforms (5.64) into

$$\frac{1+o(1)}{(2\pi \mathbf{i})^2} \iint \frac{\exp\left(\frac{\tilde{w}^2}{2} + \tilde{w}y\right)}{\exp\left(\frac{\tilde{v}^2}{2} + \tilde{v}x\right)} \cdot \frac{\mathrm{d}v\mathrm{d}w}{\tilde{v} - \tilde{w}}, \qquad M \to \infty.$$

We arrive at (5.62) after renaming $\tilde{v} \mapsto -w$, $\tilde{w} \mapsto -v$ and adjusting the contour orientations. □

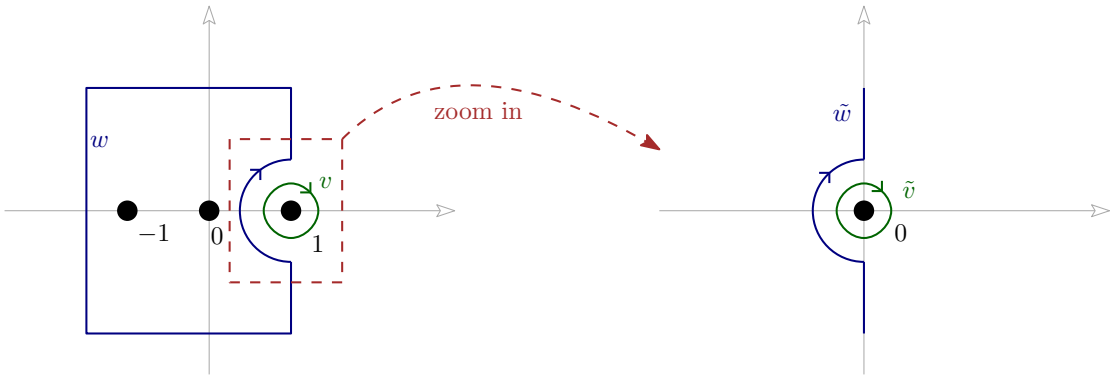


Figure 5.16: The steepest descent contours for the GUE limit.

Another, more traditional approach to GUE correlation kernel via Hermite orthogonal polynomials is outlined in Problem 5 in Chapter 4 and in Problem 4 at the end of this chapter.

Proof of Theorem 5.20. We study $N^{-1/6}K_N^{\mathrm{GUE}}(\chi\sqrt{N}+xN^{-1/6},\chi\sqrt{N}+yN^{-1/6})$ as $N\to\infty$, where we will eventually take $\chi=2$, but at first keep it is a parameter. Plugging into (5.62), we get

$$\frac{N^{-1/6}}{(2\pi\mathbf{i})^2}\iint \exp\left(\frac{v^2}{2}-v\left(\chi\sqrt{N}+yN^{-1/6}\right)-\frac{w^2}{2}+w\left(\chi\sqrt{N}+xN^{-1/6}\right)\right)\frac{v^N}{w^N}\frac{\mathrm{d}w\mathrm{d}v}{v-w}. \tag{5.65}$$

In order to balance different terms in the exponent and bring the integral into the form amenable to the steepest descent analysis, we replace w by $w\sqrt{N}$ and v by $v\sqrt{N}$, which leads to

$$\frac{N^{1/3}}{(2\pi\mathbf{i})^2}\iint \exp\left(N\left[\frac{v^2}{2}-\chi v+\ln v-\frac{w^2}{2}+\chi w-\ln w\right]\right)\exp\left(N^{1/3}\left[wx-vy\right]\right)\frac{\mathrm{d}w\mathrm{d}v}{v-w}. \tag{5.66}$$

We need to look at the critical points of the function

$$f(z)=\frac{z^2}{2}-\chi z+\ln z,\qquad f'(z)=z-\chi+\frac{1}{z}.$$

For generic χ, the equation $f'(z)=0$ is quadratic. As we learned in Section 5.3, the Airy asymptotics arises when the equation has a double root, which happens for $\chi=\pm 2$ (corresponding to the largest and smallest eigenvalues of GUE). We focus on $\chi=2$ case with the critical point $z_c=1$, so that for z close to 1

$$f(z)=-\frac{3}{2}+\frac{(z-1)^3}{3}+O\big((z-1)^4\big).$$

Let us zoom in near the critical point and change the variables

$$v=1+N^{-1/3}\tilde{v},\qquad w=1+N^{-1/3}\tilde{w}.$$

Recognizing the Airy kernel in the integral form of (5.18), but with swapped x and y, we conclude that as $N\to\infty$

$$N^{-1/6}K_N^{\mathrm{GUE}}\big(2\sqrt{N}+xN^{-1/6},2\sqrt{N}+yN^{-1/6}\big)=\exp\left(N^{1/3}\left[x-y\right]\right)K^{\mathrm{Airy}}(y,x)\cdot\big(1+o(1)\big). \tag{5.67}$$

The $N^{-1/6}$ factors match the rescaling in (5.55), as in Lemma 4.30. The $\exp\left(N^{1/3}\left[x-y\right]\right)$ prefactor cancels out from the determinants in the definition of correlation functions and therefore can be omitted.

The swap $x \leftrightarrow y$ does not matter, because the Airy kernel is symmetric. Hence, (5.67) implies that the point process $\left\{N^{1/6}\left(x_i^N - 2\sqrt{N}\right)\right\}_{i=1}^{N}$ converges to the Airy point process. Supplementing this with the asymptotic decay of $K_N^{\mathrm{GUE}}\big(\chi\sqrt{N}, \chi\sqrt{N}\big)$ for $\chi > 2$, which is proven very similarly to Theorem 5.11, we deduce (5.55) by repeating the argument of Theorem 5.14. □

5.9 Properties of the Tracy-Widom distribution

We have already established the appearance of the Tracy–Widom distribution in asymptotic fluctuations for three problems: length of the longest increasing subsequence (5.47), PNG interface (5.52), and GUE's largest eigenvalue (5.55). But what is this distribution, how to deal with it and think about it?

At least five different definitions of the Tracy–Widom distribution can be used for studying it:

1. $F_2(s)$ is the distribution function of the random variable $\mathfrak{a}_1$, which is the right-most particle of the Airy point process of Definition 5.4: $F_2(s) = \mathbb{P}(\mathfrak{a}_1 \le s)$.

2. $F_2(s)$ is given by a Fredholm determinant:

$$F_2(s) = \det\big(\mathrm{Id} - K^{\mathrm{Airy}}(x,y)\big)_{L^2((s,+\infty)} = \sum_{n\ge 0} \frac{(-1)^n}{n!} \int_{[s,+\infty)^n} \det\big[K^{\mathrm{Airy}}(x_i,x_j)\big]_{i,j=1}^n \mathrm{d}x_1 \cdots \mathrm{d}x_n, \quad (5.68)$$

   where the Airy kernel is given by either of the equivalent formulas (5.15) or (5.18).

3. Using the Hastings-McLeod [HM80] solution to the Painlevé II differential equation:

$$q''(x) = xq(x) + 2q(x)^3 \quad (5.69)$$

   with the boundary condition $q(x) \sim \mathrm{Ai}(x)$ as $x \to \infty$, we have (see [TW94] or [BD02, Section 9])

$$F_2(s) = \exp\left(-\int_s^\infty (x-s)q(x)^2\,\mathrm{d}x\right). \quad (5.70)$$

4. $F_2(s)$ is the distribution function for the largest eigenvalue of the $\beta = 2$ version of the *Stochastic Airy Operator* of [ES07, RRV11]. The operator is defined for $\beta > 0$ parameter via:

$$\frac{\partial^2}{\partial x^2} - x + \frac{2}{\sqrt{\beta}}W'(x), \qquad W(x) \text{ is a Brownian motion}, \qquad x \ge 0, \quad (5.71)$$

   acting on functions in $L^2(\mathbb{R}_{\ge 0})$ vanishing at the origin $x = 0$. Explaining the proper mathematical meaning of the operator (5.71) and its eigenfunctions goes beyond the scope of this book and we refer to [RRV11].

5. One can take one of the asymptotic theorems (5.47), (5.52), (5.55) as a definition. *E.g.*, one can define the Tracy-Widom distribution as the scaling limit of the largest eigenvalue of $N \times N$ GUE random matrices after subtracting $2\sqrt{N}$ and multiplying by $N^{1/6}$ as $N \to \infty$.

The fourth approach shows that F_2 is a $\beta = 2$ representative of general β Tracy-Widom distributions F_β, defined as the law of the largest eigenvalue of (5.71). This connects us to the topic of general β random matrices, and we refer to [ES07, RRV11, GS18, GXZ24] for related developments. Beyond $\beta = 2$, the cases

$\beta = 1, 4$ are of central importance: F_1 and F_4 are limits of largest eigenvalues for real symmetric and Hermitian quaternionic matrices, respectively, see [TW96, Meh04, For10]; they also appear in interface growth models and $2d$ statistical mechanics, as in [PS00, BR01, Fer04, SI04, BBCS18]. As $\beta \to \infty$, F_β becomes a δ–mass on the largest root of the Airy function (cf. Figure 5.3), with Gaussian limit after $\sqrt{\beta}$ rescaling — this approximation from $\beta = \infty$ is surprisingly good even for $\beta = 1$, see [DE05, EPS14, GK24].

Each of the five definitions above can be used to produce a sampler of the Tracy-Widom distribution F_2 and to numerically compute its density $F_2'(s)$:

- One can sample a determinantal point process with a given kernel by diagonalizing its correlation kernel and then using a sequence of independent Bernoulli random variables, as described in [HKPV06]. The only caveat is that this approach works the best for the processes with finitely many points, hence, one should first choose a large negative $-R$ and restrict the Airy point process to $(-R, +\infty)$ interval, which does not matter that much, because we are interested in $\mathfrak{a}_1$.

- One can numerically approximate the Fredholm determinant in (5.68) using finite quadrature formulas, similar to those used in approximating integrals, as discussed in detail in [Bor10b].

- Starting from a large value of s (where we set $q(s)$ and its first derivative to match the Airy function), and then numerically integrating (5.69) backward in time, we get an approximation of $q(s)$, which subsequently leads to $F_2(s)$ through (5.70); this is how we produced Figure 5.17 below. Bornemann in [Bor10a] compares the numeric efficiency of the Painleve and Fredholm approaches, arguing that (when implemented properly) the latter is preferable.

- One can approximate the operator (5.71) with a discrete version, which is a random tridiagonal matrix. The limit of the largest eigenvalue of these matrices gives a direct access to the largest eigenvalue of (5.71); one advantage of this approach is that it extends to all β and to other marginals of the Airy point process (say, to $\mathfrak{a}_1 + \mathfrak{a}_2$). In particular, for $\beta = 2$, we consider the matrix

$$M_N = \begin{pmatrix} d(N) & u(N-1) & 0 & \cdots & 0 \\ u(N-1) & d(N-1) & u(N-2) & \ddots & \vdots \\ 0 & u(N-2) & d(N-3) & \ddots & 0 \\ \vdots & \ddots & \ddots & \ddots & u(1) \\ 0 & \cdots & 0 & u(1) & d(1) \end{pmatrix},$$

  where $d(k)$ are i.i.d. Gaussian $\mathcal{N}(0,1)$ random variables and $u(k)$ are independent χ_{2k} random variables of density

$$\frac{2^{1-k}}{\Gamma(k)}\, x^{2k-1}\, e^{-x^2/2}, \quad x > 0.$$

  Alternatively, ξ_{2k}^2 is a sum of squares of $2k$ i.i.d. $\mathcal{N}(0,1)$ random variables. M_N can be obtained as a result of tridiagonalization (*i.e.*, sequential rotation of columns to make the matrix tridiagonal) of a GUE matrix, see [Tro84, DE02], which keeps the eigenvalues unchanged, and therefore Theorem 5.20 applies with x_1^N being the largest eigenvalue of M_N.

  One technical detail is that one needs to take a very large N (say, $N = 10^6$) to get a good approximation of $F_2(s)$, and computing eigenvalues of such huge matrices can be prohibitively slow. This can be fixed by replacing M_N with its top-left $\sqrt{N} \times \sqrt{N}$ corner, see [BGK25, Section 2.3] for the implementation details and further references for other approaches.

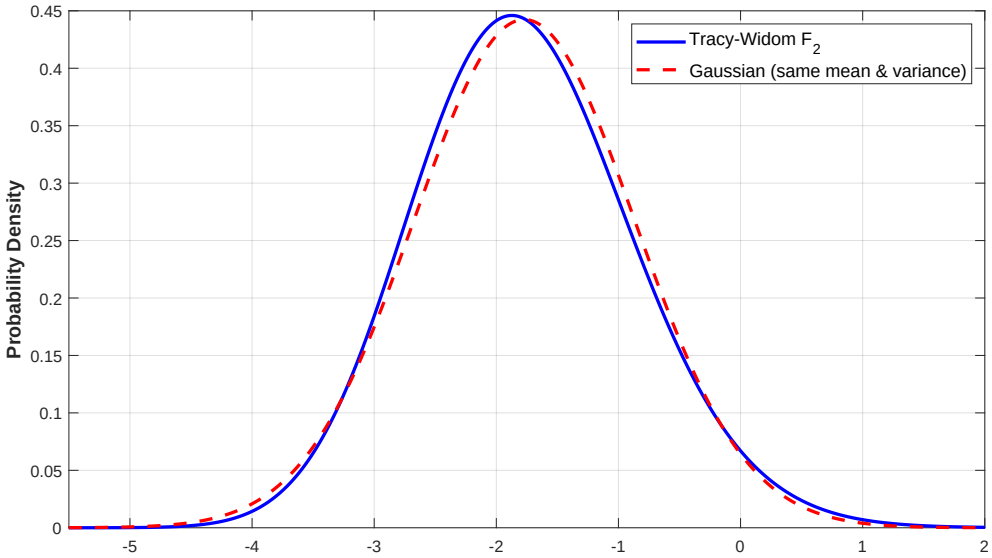


Figure 5.17: Density for Tracy-Widom distribution F_2 and Gaussian of the same mean and variance.

Figure 5.17 present a numeric plot of the density $F_2'(s)$ and compares it to the Gaussian density of the same mean (≈ -1.77) and variance (≈ 0.81). For historic reasons, the Tracy-Widom distribution is not normalized: rather than rescaling it to have mean 0 and variance 1, the community keeps the current notations whose advantage is the simpler form of the formulas, such as (5.55), (5.68), (5.70), (5.71).

Beyond centering, Figure 5.17 reveals two other features of the Tracy-Widom distribution: it is asymmetric (skewness ≈ 0.22), and its tails differ from the Gaussian ones (the excess kurtosis is ≈ 0.09). The latter property was investigated and exact tails are known. The right tail is heavier than Gaussian and exhibits the exponential decay exponent $3/2$, which we already saw in (5.28):

$$1 - F_\beta(s) = \exp\left(-\frac{2\beta}{3} s^{3/2}\bigl(1+o(1)\bigr)\right), \qquad s \to +\infty. \tag{5.72}$$

The left tail is lighter than Gaussian and exhibits the exponential decay exponent 3:

$$F_\beta(s) = \exp\left(-\frac{\beta}{24}(-s)^3\bigl(1+o(1)\bigr)\right), \qquad s \to -\infty. \tag{5.73}$$

Precise understanding of $o(1)$ error terms in (5.72), (5.73) is also available in the literature, see [BBD08, BN12, DV13] and references therein.

5.10 Edge limits for discrete PNG and geometric LPP

We end this chapter by producing large-time asymptotics of discrete PNG of Section 3.1 and delivering a proof of the long-announced Theorem 1.4 about the last passage percolation with geometric weights.

Theorem 5.24. *Consider the multilayer discrete PNG model as in Sections 3.1, 3.2 with all a_i and all b_i parameters equal to $0 < q^{\frac{1}{2}} < 1$. Let $\mathfrak{a}_1 \geq \mathfrak{a}_2 \geq \dots$ denote the points of the Airy point process. Then, in the sense of convergence of finite-dimensional distributions, we have*

$$\lim_{t\to\infty} t^{-1/3}\left(h_i(0,t) - \frac{q^{\frac{1}{2}}}{1-q^{\frac{1}{2}}}t\right) \stackrel{d}{=} \mathfrak{a}_i \cdot \left(\frac{q+q^{\frac{1}{2}}}{2}\right)^{1/3} \frac{1}{1-q^{\frac{1}{2}}}, \qquad i = 1,2,\dots. \tag{5.74}$$

Remark 5.25. One can extend this analysis to find the $t \to \infty$ asymptotics of $h_i(\chi t, t)$ as $t \to \infty$, with $-1 < \chi < 1$. All steps remain the same, but computations are heavier, see [Joh00, Thereom 1.2]. For $t \to \infty$ functional convergence of the rescaled interface $x \mapsto h(xt^{2/3}, t)$, we refer to [Joh03].

Proof of Theorem 5.24. By Corollary 3.9, for odd t, $\{h_\ell(0,t)\}_{\ell \geq 1} \stackrel{d}{=} \{\lambda_1, \lambda_2 - 1, \lambda_3 - 2, \dots\}$, where λ is distributed according to the Schur measure

$$\mathbb{P}(\lambda) = (1-q)^{(t+1)^2/4} \cdot s_\lambda^2 \left(\left[q^{\frac{1}{2}} \right]^{(t+1)/2} \right),$$

where $\left[q^{\frac{1}{2}} \right]^{(t+1)/2}$ means $(t+1)/2$ variables equal to $q^{\frac{1}{2}}$. In the following steps we will ignore the parity restrictions: due to monotonicity of the heights $h_\ell(0, t-1) \leq h_\ell(0,t) \leq h_\ell(0, t+1)$, we can always reduce even t case to the odd t case. Applying Theorem 4.21, $X(\lambda) = \{\lambda_i + 1 - i\}_{i=1}^\infty$ is a determinantal point process with kernel

$$K(\ell_1, \ell_2) = \frac{1}{(2\pi \mathbf{i})^2} \oiint \left[\frac{\left(1 - q^{\frac{1}{2}} w\right)\left(1 - q^{\frac{1}{2}} v^{-1}\right)}{\left(1 - q^{\frac{1}{2}} v\right)\left(1 - q^{\frac{1}{2}} w^{-1}\right)} \right]^{(t+1)/2} \frac{v^{-\ell_1} w^{\ell_2 - 1}}{v - w} \mathrm{d}v \mathrm{d}w, \qquad \ell_1, \ell_2 \in \mathbb{Z},$$

with integration over two positively oriented circles around the origin $|w| = R_1$, $|v| = R_2$ such that $q^{\frac{1}{2}} < R_1 < R_2 < q^{-\frac{1}{2}}$. We set

$$\ell_1 = \zeta t + x t^{1/3}, \qquad \ell_2 = \zeta t + y t^{1/3},$$

in which ζ is not yet known. Ignoring parity, integer parts, and shift by 1 in $(t+1)/2$ (none of that is important for the eventual asymptotics), we rewrite the kernel as

$$\frac{1}{(2\pi \mathbf{i})^2} \oiint \exp\big(t f(v) - t f(w)\big) \frac{v^{-x t^{1/3}} w^{y t^{1/3}}}{(v-w)w} \, \mathrm{d}v \mathrm{d}w, \tag{5.75}$$

with

$$f(z) = \frac{1}{2} \ln\big(1 - q^{\frac{1}{2}} z^{-1}\big) - \frac{1}{2} \ln\big(1 - q^{\frac{1}{2}} z\big) - \zeta \ln z$$
$$= \frac{1}{2} \left(\ln\left(z - q^{\frac{1}{2}}\right) - \ln\left(q^{-\frac{1}{2}} - z\right) - (2\zeta + 1) \ln z - \ln q^{\frac{1}{2}} \right).$$

The equation for the critical point becomes

$$0 = 2f'(z) = \frac{1}{z - q^{\frac{1}{2}}} - \frac{1}{z - q^{-\frac{1}{2}}} - \frac{2\zeta + 1}{z} = \frac{z(z - q^{-\frac{1}{2}}) - z(z - q^{\frac{1}{2}}) - (2\zeta+1)(z - q^{-\frac{1}{2}})(z - q^{\frac{1}{2}})}{z(z - q^{\frac{1}{2}})(z - q^{-\frac{1}{2}})},$$
$$= - \frac{(2\zeta+1) z^2 + z\big(q^{-\frac{1}{2}} - q^{\frac{1}{2}} - (2\zeta+1)(q^{-\frac{1}{2}} + q^{\frac{1}{2}})\big) + (2\zeta+1)}{z(z - q^{\frac{1}{2}})(z - q^{-\frac{1}{2}})}.$$

We know that the Airy asymptotics arises when we have a double root, which corresponds to the vanishing discriminant of the quadratic polynomial in z in the numerator and gives

$$\zeta = \frac{q \pm q^{\frac{1}{2}}}{1 - q}. \tag{5.76}$$

Since we are interested in the upper edge, corresponding to λ_1, we choose the plus sign

$$\zeta = \frac{q+q^{\frac12}}{1-q} = \frac{q^{\frac12}}{1-q^{\frac12}}, \qquad 2\zeta+1 = \frac{1+q^{\frac12}}{1-q^{\frac12}}, \qquad z_c = 1.$$

The reader might be surprised by observing critical point $z_c = 1$ yet again, but it does not mean that the same critical point appears in *all* problems. Rather, we keep choosing the simplest cases to highlight the ideas, but avoid heavy computations. At the critical point:

$$f''(1) = 0, \qquad f'''(1) = -\frac{2\zeta+1}{(1-q^{\frac12})(1-q^{-\frac12})} = \frac{q+q^{\frac12}}{(1-q^{\frac12})^3} > 0.$$

Hence, we do the usual deformation of the contours to pass through the critical point and local change of variables

$$v = 1 + \left(\frac{2}{q+q^{\frac12}}\right)^{1/3} (1-q^{\frac12}) t^{-1/3}\tilde{v}, \qquad w = 1 + \left(\frac{2}{q+q^{\frac12}}\right)^{1/3} (1-q^{\frac12}) t^{-1/3} t^{-1/3}\tilde{w}.$$

Hence, plugging into (5.75), we conclude that as $t \to \infty$, the kernel $K(\ell_1, \ell_2)$ becomes

$$\frac{\left(\frac{2}{q+q^{\frac12}}\right)^{1/3}(1-q^{\frac12})t^{-1/3}}{(2\pi \mathbf{i})^2} \iint \exp\left(\frac{\tilde{v}^3}{3} - \frac{\tilde{w}^3}{3} - \left(\frac{2}{q+q^{\frac12}}\right)^{1/3}(1-q^{\frac12})(x\tilde{v} - y\tilde{w})\right) \frac{\mathrm{d}\tilde{v}\mathrm{d}\tilde{w}}{\tilde{v}-\tilde{w}}. \quad (5.77)$$

We recognize the Airy kernel in the double integral form (5.18) and with x and y variables rescaled by $\left(\frac{2}{q+q^{\frac12}}\right)^{1/3}(1-q^{\frac12})$ factor. Supplementing this computation with a tail bound (omitted), as in the proof of Theorem 5.14, we arrive at (5.74). □

We now go back to the setting of Section 1.4.

Corollary 5.26. *Let $w_{i,j}$ be i.i.d. geometric random variables $\mathbb{P}(w_{i,j} = k) = (1-q)q^k$, $k = 0, 1, 2, \ldots$. Consider the last passage time*

$$t_{i,j} = \max_{\pi:(1,1)\to(i,j)} \sum_{(k,l)\in\pi} w_{k,l}, \quad (5.78)$$

where π is a path with $(1,0)$ and $(0,1)$ increments. Then, in distribution

$$\lim_{N\to\infty} N^{-1/3}\left(t_{N,N} - N\frac{2q^{\frac12}}{1-q^{\frac12}}\right) \stackrel{d}{=} \mathfrak{a}_1 \cdot \frac{\left(q+q^{\frac12}\right)^{\frac13}}{1-q^{\frac12}}, \quad (5.79)$$

where the distribution of $\mathfrak{a}_1$ is Tracy-Widom F_2.

Proof. We claim that $t_{N,N}$ has the same distribution as $h_1(0, 2N-1)$, *i.e.*, the height at 0 for discrete PNG at time $t = 2N-1$. This can be seen by looking at the PNG recursive rule (3.1)

$$h_1(x, t+1) = \max\{h_1(x-1,t), h_1(x,t), h_1(x+1,t)\} + \omega(x, t+1), \quad (5.80)$$

in which weights ω vanish at ever second point and are i.i.d. geometric at the black dots:

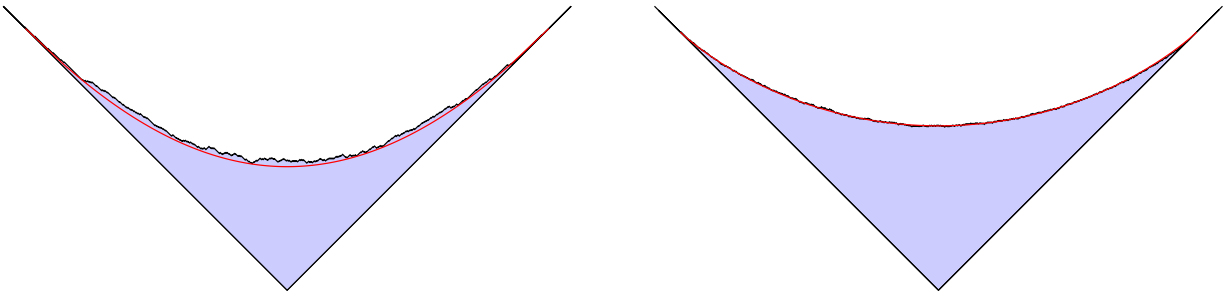
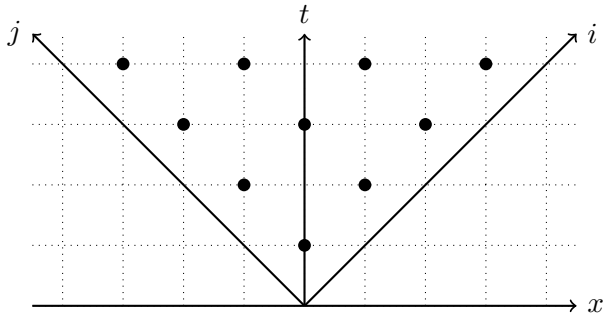


Figure 5.18: Left panel: the Young diagram $\{(i,j) \mid t_{i,j} \le t\}$ for geometric LPP with parameter $q = 0.8$ and $t = 2400$, so that the first row is approximately $t(1-q)/q = 600$. Right panel: Plancherel-random Young diagram with $n = 90000$, so that the first row is approximately $2\sqrt{n} = 600$.



Due to up-down shape of the interface, *i.e.*, positivity of the jumps defined in (3.4), the value of the height at a black dotted point (x,t) is always at least as large as $h(x+1,t)$ and $h(x-1,t)$. Hence, if we restrict our attention to the values of $h(x,t)$ only at these points, then the recurrence (5.80) becomes simpler

$$h_1(x,t+1) = \max\{h_1(x-1,t), h_1(x+1,t)\} + \omega(x,t+1). \tag{5.81}$$

Upon rotation of the coordinate system, this is the same recurrence as the one satisfied by the last passage times: $t_{i,j} = \max(t_{i-1,j}, t_{i,j-1}) + w_{i,j}$. The claim follows.

Therefore, (5.79) is obtained from (5.74) by plugging in $t = 2N-1$. □

The same methodology can be used to understand the asymptotics of $t_{i,j}$ for arbitrary large i and j. One way to interpret the result is by looking at the Young diagram $\lambda(t) = \{(i,j) \mid t_{i,j} \le t\}$ – its evolution in time t was discussed in Section 1.4. The order $t^{1/3}$ for the fluctuations of the boundary of this Young diagram can be contrasted with much smaller fluctuations for the Plancherel-random Young diagram, as is clearly visible from the simulation in Figure 5.18.

In Theorem 5.24 we analyzed the first rows of the Schur measure, but in the same way we can also get the result for the first column. We record the answer — it will turn out to be useful later, when studying the six-vertex model in Chapter 8.

Theorem 5.27. *For $N = 1, 2, \ldots$, let $\lambda \in \mathbb{Y}$ be distributed as the Schur measure*

$$\mathbb{P}(\lambda) = (1-q)^{N^2} \cdot s_\lambda^2\left(\left[q^{\frac{1}{2}}\right]^N\right).$$

Then the lengths of the first columns of λ converge to particles of the Airy point process:

$$\lim_{N\to\infty} N^{-1/3}\left(\lambda_i' - \frac{2q^{\frac{1}{2}}}{1+q^{\frac{1}{2}}}N\right) \stackrel{d}{=} \mathfrak{a}_i \cdot \frac{\left(q^{\frac{1}{2}}-q\right)^{\frac{1}{3}}}{1+q^{\frac{1}{2}}}, \qquad i = 1, 2, \ldots. \tag{5.82}$$

Proof. We continue the analysis in the proof of Theorem 5.27. For the longest columns we need the second value of ζ with minus sign in (5.76),

$$\zeta = \frac{q-q^{\frac12}}{1-q} = -\frac{q^{\frac12}}{1+q^{\frac12}}, \qquad 2\zeta+1 = \frac{1-q^{\frac12}}{1+q^{\frac12}}, \qquad z_c = -1.$$

At the critical point:

$$f''(-1)=0, \qquad f'''(-1) = \frac{2\zeta+1}{(1+q^{\frac12})(1+q^{-\frac12})} = \frac{q^{\frac12}-q}{(1+q^{\frac12})^3} > 0.$$

As we saw many times before, when the third derivative is positive, locally near the critical point, the v–contour should be to the right from the w–contour. Since our original contour arrangement is two circles around 0 with $|w|<|v|$, in the contour deformation we would need to push one contour entirely through another one, collecting the $v=w$ residue equal to:

$$\frac{1}{2\pi\mathbf{i}}\oint_{\text{around }0} v^{\ell_2-\ell_1-1}\mathrm{d}v = \mathbf{1}_{\ell_1=\ell_2} = \begin{cases}1, & \ell_1=\ell_2,\\ 0, & \ell_1\neq\ell_2.\end{cases}$$

Hence, the analogue of (5.77) becomes

$$\begin{aligned}&\mathbf{1}_{\ell_1=\ell_2} - K(\ell_1,\ell_2) = \bigl(1+o(1)\bigr)\\ &\times\left(\frac{2}{q^{\frac12}-q}\right)^{\frac13}\bigl(1+q^{\frac12}\bigr)t^{-1/3}K^{\text{Airy}}\left(-\left(\frac{2}{q^{\frac12}-q}\right)^{\frac13}\bigl(1+q^{\frac12}\bigr)\cdot x, -\left(\frac{2}{q^{\frac12}-q}\right)^{\frac13}\bigl(1+q^{\frac12}\bigr)\cdot y\right),\end{aligned} \tag{5.83}$$

where the minus signs appeared because of $z_c=1$ being replaced with $z_c=-1$ in the argument. Plugging in $t=2N-1$, we get the rescalings of (5.82), and it remains to explain why subtracting the kernel from the identity operator $\mathbf{1}_{\ell_1=\ell_2}$ is equivalent to passing from rows to columns. This is based on two observations. First, the $N=\infty$ version of (5.60) is the identity valid for any $\lambda\in\mathbb{Y}$ and easily seen from Figure 4.3:

$$\bigl\{\lambda_i-i+1\bigr\}_{i=1}^{\infty}\bigsqcup\bigl\{-\lambda'_j+j\bigr\}_{j=1}^{\infty} = \mathbb{Z}. \tag{5.84}$$

Second, the following complementation principle is proven immediately after we finish the current proof:

Lemma 5.28. *Let X be a determinantal point process on $\mathbb{Z}$ with correlation kernel $K(\ell_1,\ell_2)$ with respect to the counting measure. Then $\mathbb{Z}\setminus X$ is a determinantal point process on $\mathbb{Z}$ with correlation kernel $\mathbf{1}_{\ell_1=\ell_2}-K(\ell_1,\ell_2)$.*

Given the lemma, we see that negative signs in front of λ'_i in (5.84) match the negative signs in front of x and y in (5.83). Hence, using also a tail bound, whose proof we again omit, we arrive at (5.82). □

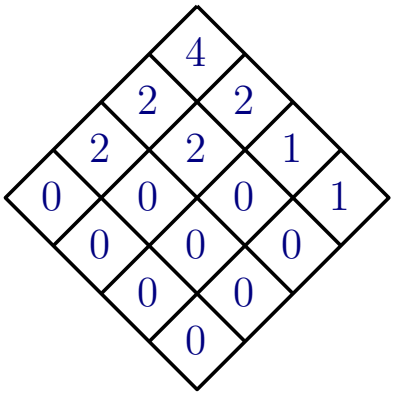
Proof of Lemma 5.28. We take an m–element subset $A=\{a_1,\dots,a_m\}\subset\mathbb{Z}$ and compute the probability of the event $A\subset(\mathbb{Z}\setminus X)$ using the gap probability formula of Theorem 4.24:

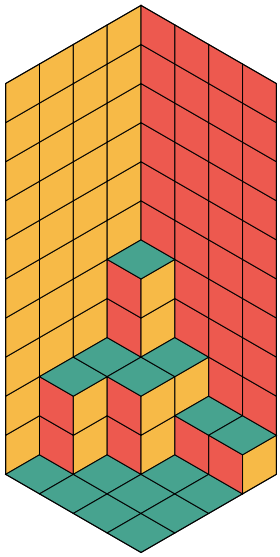
$$\mathbb{P}\bigl(A\subset(\mathbb{Z}\setminus X)\bigr) = \mathbb{P}\bigl(\text{no points of } X \text{ in } A\bigr) = \det\bigl(\mathrm{Id}-K\bigr)_{\ell_2(A)} = \det\left[\mathbf{1}_{a_i=a_j}-K(a_i,a_j)\right]_{i,j=1}^{m}.$$

Comparing with the definition of a determinantal point process with kernel $\mathbf{1}_{\ell_1=\ell_2}-K(\ell_1,\ell_2)$, we are done. □

5.11 Exercises

Problem 1. A *plane partition* is an array $\pi = (\pi_{i,j})$, $i,j = 1,2,\dots$ of non-negative integers, such that the numbers are monotone ($\pi_{i+1,j} \le \pi_{i,j}$ and $\pi_{i,j+1} \le \pi_{i,j}$) and their sum (or "volume") is finite: $\sum_{i,j=1}^{\infty} \pi_{i,j} = \mathrm{Vol}(\pi) < \infty$. Plane partitions are in bijection with $3d$ Young diagrams (put k unit cubes on entry k), lozenge tilings, and with interlacing sequences of Young diagrams (diagonal slices of the plane partition), as shown on the picture below:





$$(0) \prec (2,0) \prec (2,0,0) \prec (4,2,0,0) \succ (2,0) \succ (1,0) \succ (1)$$

A. Fix $N = 1,2,\dots$ and consider probability measure with weights $q^{\mathrm{Vol}(\pi)}$ on plane partitions inside $N \times N$ square (*i.e.*, such that $\pi_{i,j} = 0$ whenever $\max(i,j) > N$). Prove that the corresponding sequence of Young diagrams forms a Schur process.

B. Deduce from part **A** the formula for

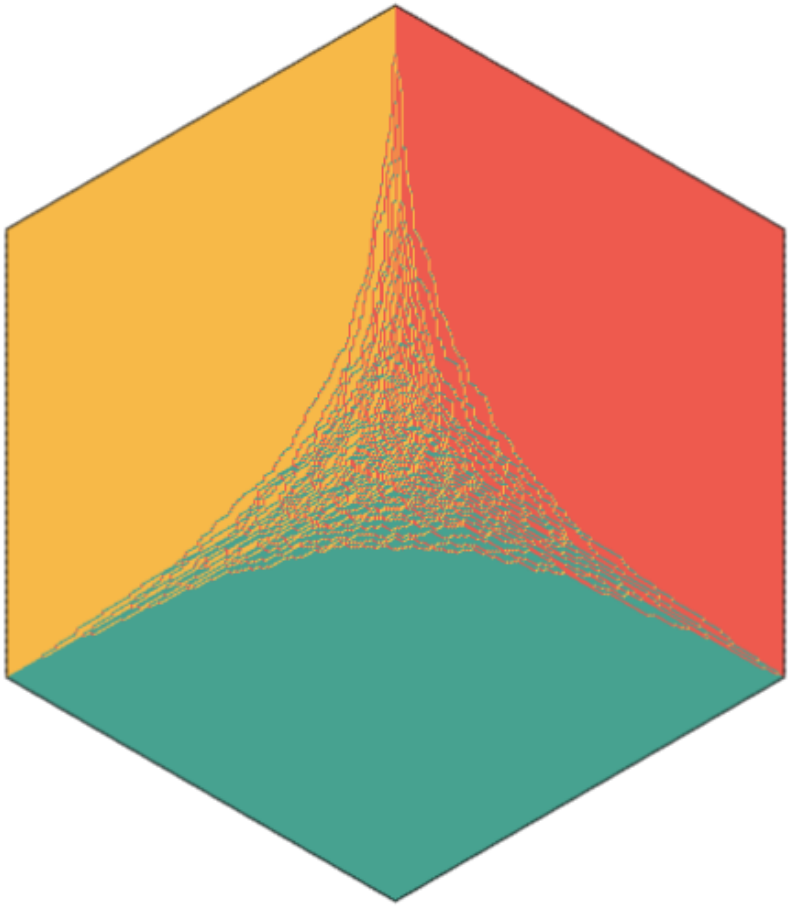
$$\sum_{\pi=\text{plane partition inside } N\times N \text{ square}} q^{\mathrm{Vol}(\pi)}.$$

Send $N \to \infty$ and deduce the MacMahon generating function:

$$\sum_{\pi=\text{plane partition}} q^{\mathrm{Vol}(\pi)} = \prod_{n=1}^{\infty} \frac{1}{(1-q^n)^n}.$$

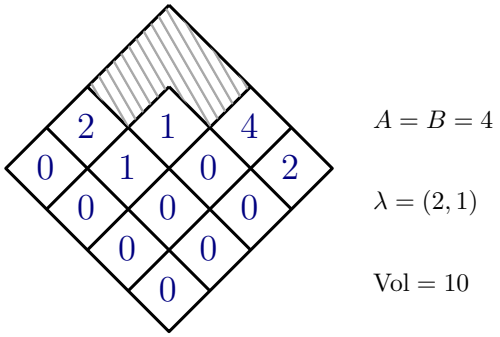
C. Sending $N \to \infty$ in part **A** deduce that Young diagram λ^t corresponding to the tth diagonal slice of the q^{Vol}–distributed plane partition, forms a Schur measure. Hence, the point process $\{\lambda_i^t + 1 - i\}_{i=1}^{\infty}$ is determinantal. Write down the double contour integral representation for its correlation kernel.

D. Send $q \to 1$ in the result of part **C** and compute (using the steepest descent method) the limit of the first correlation function $\rho_1(x)$ with x rescaled as $x = \chi/\ln q$ and t rescaled as $t = \tau/\ln q$. The result is the density of the green color in the image below (which has $q = 0.97$ and $200 \times 200 \times 200$ bounding hexagon).



E. Find a limit leading to the Tracy-Widom distribution.

F. For a Young diagram λ inside an $A \times B$ rectangle, let $\overline{\lambda}$ be a collection of unit boxes complementing λ to the rectangle. A skew plane partition $\pi = (\pi_{i,j})$ of shape $\overline{\lambda}$ is a filling of boxes of $\overline{\lambda}$ with non-negative integers, such that the numbers are monotone ($\pi_{i+1,j} \le \pi_{i,j}$ and $\pi_{i,j+1} \le \pi_{i,j}$) and their sum is finite: $\sum_{i,j=1}^{\infty} \pi_{i,j} = \mathrm{Vol}(\pi) < \infty$. Here is an example:



Extending part **A**, show that random skew plane partitions of shape $\overline{\lambda}$ equipped with weight $q^{\mathrm{Vol}(\pi)}$, $0 < q < 1$, can be identified with a Schur process. Use this to compute $\sum q^{\mathrm{Vol}(\pi)}$ over the skew plane partitions of shape $\overline{\lambda}$.

Problem 2. Consider the measure (5.56) on Young diagrams λ and suppose that $N, M \to \infty$, in such a way $\frac{M}{N+M} \to \mathbf{m} \in (0,1)$.

A. Compute the bulk limit for the point process $\{\lambda_i + N - i\}_{i=1}^{N}$ using the steepest descent, leading to the discrete sine kernel of Definition 5.8. How does ϕ depend on $\mathbf{m}$ and the point where you zoom in?

B. Find the scaling limit of λ_1.

C. Find the scaling limit of λ_1'.

Problem 3. Taking geometric distribution $\mathbb{P}(w=k) = (1-q)q^k,\ k = 0, 1, \ldots$, setting $q = 1-\varepsilon$, and sending $\varepsilon \to 0$, one sees that εw converges towards an exponential distribution. By performing this limit transition in the geometric last passage percolation of Section 1.4, one arrives at the exponential last passage percolation. Reformulate the resulting system as time evolution rules for an interface $h(x,t)$. Using encoding of Figure 4.3, you should be getting Totally Asymmetric Simple Exclusion Process (TASEP) with step initial condition as the evolution of particle configurations: at time 0 all particles are to the left from the origin; each particle has an independent exponential clock, which rings at Poisson process times. When the clock rings, the particle jumps to the right, unless it is blocked by a neighbor, in which case it does nothing. Repeating the proof of Corollary 5.26, compute the distributional scaling limit

$$\lim_{t\to\infty} \frac{h(\alpha t, t) - c(\alpha) t}{t^{1/3}} \stackrel{d}{=} \xi(\alpha) \cdot \mathfrak{a}_1. \tag{5.85}$$

Find how $c(\alpha)$ and $\xi(\alpha)$ depend on $-1 < \alpha < 1$.

Problem 4. Our goal is to match two expressions for the correlation kernel of GUE: (4.39) in Chapter 4 and (5.62) in this chapter. This is done in tree steps:

A. Starting from (4.40) deduce two contour integral representations for Hermite polynomials:

$$H_n(x) = \frac{n!}{2\pi\mathbf{i}} \oint_0 \exp\left(-\frac{z^2}{2} + zx\right) \frac{\mathrm{d}z}{z^{n+1}} = \frac{1}{\mathbf{i}\sqrt{2\pi}} \int_{-\mathbf{i}\infty}^{\mathbf{i}\infty} w^n \exp\left(\frac{(x-w)^2}{2}\right) \mathrm{d}w.$$

B. Using the contour integrals from part **A**, and extending the sum to $k = -\infty, \ldots, N-1$, convert (4.39) into a double contour integral.

C. Find a gauge transformation (4.6) of the form $K(x,y) \mapsto \frac{f(x)}{f(y)} K(x,y)$, to match the result of part B with (5.62).

Problem 5. Prove the integral representation for the Airy kernel:

$$K^{\mathrm{Airy}}(x,y) = \int_0^\infty \mathrm{Ai}(x+z)\,\mathrm{Ai}(y+z)\mathrm{d}z, \qquad x, y \in \mathbb{R}. \tag{5.86}$$

Problem 6. Let $\mathfrak{a}_1 \geq \mathfrak{a}_2 \geq \ldots$ be the points of the Airy point process. Prove that for each $T > 0$,

$$\mathbb{E}\left[\sum_{i=1}^{\infty} \exp(T\mathfrak{a}_i)\right] = \frac{1}{2\sqrt{\pi}} T^{-3/2} \exp\left(\frac{T^3}{12}\right). \tag{5.87}$$

Hint. Express the expectation through the first correlation function and compute the resulting integrals. If you encounter divergences, then $\exp(Tx) = \lim_{\varepsilon\to 0} \exp(Tx - \varepsilon x^2)$ might help.

Problem 7. Consider $N \times N$ table filled with independent geometric random variables $w_{i,j}$, with parameter $0 < q < 1$ for $i > 1$ and with parameter $0 < \widetilde{q} < 1$ for $i = 1$. As in (1.5), define

$$t_{N,N} = \max_{\pi:(1,1)\to(N,N)} \sum_{(k,l)\in\pi} w_{k,l}. \tag{5.88}$$

A. As in Theorem 1.4, identify $t_{N,N}$ with the length of the first row λ_1 for a Schur measure. How does the specialization change compared to Theorem 1.4?

B. Fix $0 < q < 1$ and $0 < \widetilde{q} < 1$. Show that as $N \to \infty$ for all $\widetilde{q}$, except for one choice $\widetilde{q} = q_c$ (which depends on q), the correlation kernel of the Schur process has exactly the same limit as in (5.77). Find the value of q_c.

C. Show that for $\widetilde{q} < q_c$, an analogue of Corollary 5.26 holds, with exactly the same limit.

D. Show that for $\widetilde{q} > q_c$, the scaling limit of $t_{N,N}$ is no longer given by the Tracy-Widom distribution, but instead it is Gaussian. What centering and rescaling of $t_{N,N}$ do you need?
Hint. You need to redo the steepest descent analysis: *another* critical point is relevant, compared to **B**.

E. Compute the distributional limit of $t_{N,N}$ for the case $\widetilde{q} = q_c$. It is neither Gaussian, nor Tracy-Widom; it is sometimes called the Baik-Ben Arous-Peche (BBP) transitional distribution.

Remark. In the language of the maximization problem (5.88) the transition we observe has a simple probabilistic interpretation. For small $\widetilde{q}$, the optimal path collects only a few weights $w_{1,l}$, their distribution is washed out in the sum and does not affect its fluctuations. In contrast, for large $\widetilde{q}$, the optimal path collects linear in N number of weights $w_{1,l}$ and the Gaussian CLT for their sum dominates in the fluctuations. Optimizing over the number of collected weights $w_{1,l}$, one can get alternative proofs for parts **C** and **D**.

Literature. We used the following sources for composing problems and refer to them for more information, references, and connections: [Joh00], [Joh01a], [Joh02], [Oko02], [OR03], [BBAP05], [FS03], [Bor11b], and [BG16].

Chapter 6

Domino tilings of the Aztec diamond

In this chapter we introduce domino tilings, connect them to the Schur processes, and produce three types of results: construction of a stochastic dynamics which produces random tilings from a sequence of Bernoulli coin flips; law of large numbers for tilings leading to the appearance of the Artic circle; central limit theorem for tilings leading to the Gaussian free field describing the fluctuations of the height function.

6.1 Combinatorics of tilings

For any $n = 1, 2, \dots$, we define the Aztec diamond A_n of size n as the union of all lattice squares $[m, m+1] \times [n, n+1]$, $m, n \in \mathbb{Z}$, such that they are fully inside the region $\{(x, y) : |x| + |y| \le n + 1\}$. A tiling of the Aztec diamond is a configurations of $n(n+1)$ disjoint dominoes (*i.e.*, 2×1 rectangles) such that the Aztec diamond A_n is fully covered by dominoes, see Figure 6.1 for an example.

We introduce the checkerboard coloring on the squares of the grid in such a way that among the two bottommost squares in the diamond, the left one is white and the right one is gray: . Hence, among the two leftmost squares the top one is gray: . Among the two topmost squares the left one is gray: . Among the two rightmost squares the bottom one is gray: . We distinguish four domino types according to the checkerboard coloring: a horizontal domino with gray on the left is called *North*, while the other one is called *South*; a vertical domino with gray on top is called *West*, while the other one is called *East*. Left panel of Figure 6.1 illustrates the notation and Figure 1.8 in the introduction motivates the names. The group of symmetries of the Aztec diamond (rotations and reflections) has eight elements, and these symmetries reshuffle the four types of dominos.

Domino tilings of the Aztec diamond are in bijection with certain sequences of partitions. In order to see that, we distinguish two types of dominos out of four — we choose West and South — and put green particles on the gray squares of those and orange particles on the white squares of those, resulting in  and , respectively. Let us keep track of the particles along the diagonal slices of Figure 6.1. We call the zeroth white layer the n white squares along the South-West (bottom-left) border of the diamond. More generally, the mth white layer is formed by n white squares at distance m from the bottom-left border. Similarly, the mth gray layer is formed by $n+1$ gray squares adjacent to the $(m-1)$st and mth white layers. Clearly, the orange particles belong to white layers, and green particles belong to gray layers, as in the right panel of Figure 6.1.

Proposition 6.1. *For $m = 0, 1, 2 \dots, n$, the mth white layer has $(n-m)$ orange particles with coordinates*

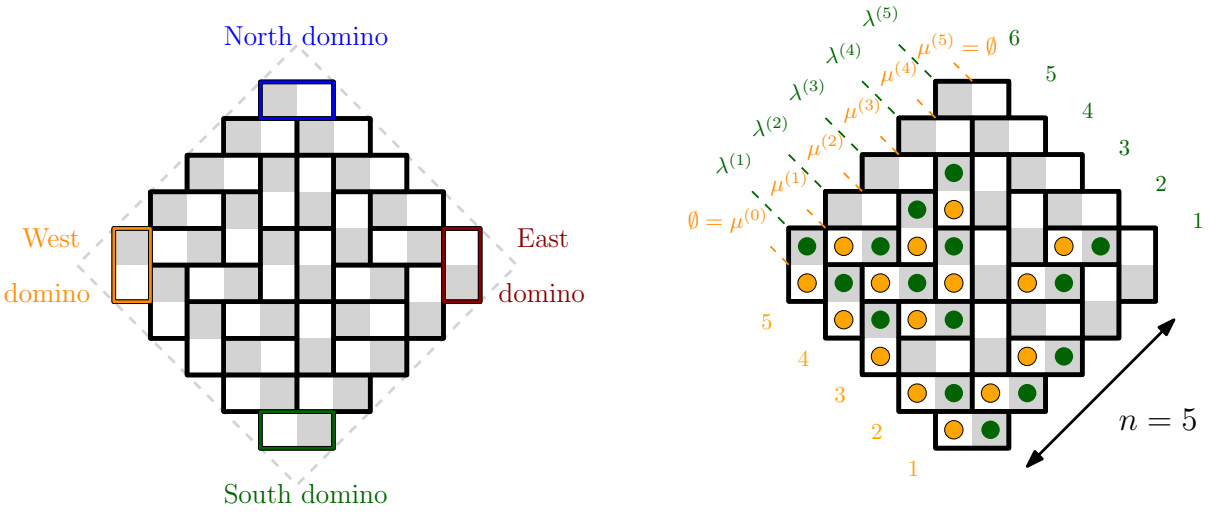


Figure 6.1: A domino tiling of the Aztec diamond, four types of dominos, and encoding via partitions.

inside $\{1, 2, \ldots, n\}$*, which can be encoded by a partition* $\mu^{(m)} \in \mathbb{Y}$ *via*

$$\left\{\mu_i^{(m)} - i + n - m + 1\right\}_{i=1}^{n-m}.$$

For $m = 1, 2, \ldots, n$*, the* m*th gray layer has* $(n + 1 - m)$ *green particles inside* $\{1, 2, \ldots, n + 1\}$*, which can be encoded by a partition* $\lambda^{(m)} \in \mathbb{Y}$ *via*

$$\left\{\lambda_i^{(m)} - i + n - m + 2\right\}_{i=1}^{n+1-m}.$$

The partitions satisfy the following properties:

1. $\mu^{(0)} = \mu^{(n)} = \varnothing$;
2. *For each* $m = 0, 1, \ldots, n - 1$*, the skew partition* $\lambda^{(m+1)}/\mu^{(m)}$ *is a vertical strip,* i.e.,
$$\lambda_i^{(m+1)} - \mu_i^{(m)} \in \{0, 1\};$$
3. *For each* $m = 1, 2 \ldots, n$*, the skew partition* $\lambda^{(m)}/\mu^{(m)}$ *is a horizontal strip,* i.e.,
$$\lambda_1^{(m)} \geq \mu_1^{(m)} \geq \lambda_2^{(m)} \geq \cdots \geq \mu_{n-m}^{(m)} \geq \lambda_{n-m+1}^{(m)}.$$

The correspondence between tilings and partitions of the corresponding lengths satisfying the above three properties is a bijection.

Using the notations $\mu \prec \lambda$ and $\mu \prec' \lambda$ for a pair of partitions which differ by horizontal and vertical strips, respectively, the tiling in Figure 6.1 is encoded by the following sequence of partitions:

$$\varnothing \prec' (1,1,1,0,0) \succ (1,1,1,0) \prec' (1,1,1,0) \succ (1,1,0) \prec' (2,2,0) \succ (2,1) \prec' (3,1) \succ (1) \prec' (1) \succ \varnothing.$$

$$\varnothing = \mu^{(0)} \prec' \lambda^{(1)} \succ \mu^{(1)} \prec' \lambda^{(2)} \succ \mu^{(2)} \prec' \lambda^{(3)} \succ \mu^{(3)} \prec' \lambda^{(4)} \succ \mu^{(4)} \prec' \lambda^{(5)} \succ \mu^{(5)} = \varnothing. \tag{6.1}$$

Proof of Proposition 6.1. We keep track of particles recursively layer-by-layer. For the 0th white layer, each of the n white squares must be covered with a domino, and this domino is necessarily of either South or West type. It follows that the 0th white layer has n orange particles, and the 1st gray layer has n green particles. The green particles have to be adjacent to orange particles (because they belong to the same domino), which is equivalent to $\lambda_i^{(1)} - \mu_i^{(0)} \in \{0,1\}$, $i = 1, 2, \ldots, n$.

Since the total number of gray squares in a layer is $n+1$, the 1st gray layer has one gray square without a particle. This square is covered by a domino, which leads to a white square in the 1st white layer without a particle. All other squares in the 1st white layer must necessarily have particles, and therefore there are $n-1$ orange particles in this layer, corresponding to the partition $\mu^{(1)}$. We learned in the previous chapter (see (5.60) and (5.84)) that passing from particles to holes is equivalent to transposing the Young diagram. Hence, the fact that the single hole in the first gray layer is adjacent to the single hole in the first white layer (they are covered by North or East domino) means that $(\lambda^{(1)})'/(\mu^{(1)})'$ is a vertical strip, which implies that $\lambda^{(1)}/\mu^{(1)}$ is a horizontal strip.

We continue this counting argument: $n-1$ orange particles in the 1st white layer are adjacent to $n-1$ green particles in the 2nd gray layer, leading to $\lambda^{(2)}/\mu^{(1)}$ being a vertical strip. Two holes in the 2nd gray layer are adjacent to two holes in the 2nd white layer, leading to $\lambda^{(2)}/\mu^{(2)}$ being a horizontal strip, etc.

We conclude that all the stated properties of the partitions $\mu^{(j)}$ and $\lambda^{(j)}$ hold. It remains to note that by the above constructions, $\lambda_i^{(j+1)} - \mu_i^{(j)} \in \{0,1\}$ and $(\lambda^{(j)})'_i - (\mu^j)'_i \in \{0,1\}$ precisely encode the South/West and North/East dominos, and therefore the correspondence between tilings and sequences of partitions is a bijection. □

Corollary 6.2. *In each tiling the number of East dominos equals the number of West dominos, and the number of North dominos equals the number of South dominos.*

Proof. Let $\mathcal{E}, \mathcal{N}, \mathcal{W}, \mathcal{S}$ denote the numbers of East, North, West, and South dominos, respectively. Then $\mathcal{W} + \mathcal{S}$ equals the total number of orange particles, *i.e.*, $n + (n-1) + \cdots + 1 = \frac{n(n+1)}{2}$. Flipping the tiling vertically, $\mathcal{W} + \mathcal{N}$ equals the same number. Hence, $\mathcal{S} = \mathcal{N}$. Flipping the tiling horizontally, we also have $\mathcal{E} + \mathcal{S} = \frac{n(n+1)}{2}$. Therefore, $\mathcal{W} = \mathcal{E}$. □

We would like to introduce randomness to the tilings, and to that end we choose two weights: $\alpha > 0$ corresponding to the East dominos and $\beta > 0$ corresponding to the West dominos. Let

$$\mathbb{P}\big(\text{tiling}\big) = \frac{1}{Z}\alpha^{\#\{\text{East dominos}\}}\beta^{\#\{\text{West dominos}\}} = \frac{1}{Z}(\alpha\beta)^{\frac{1}{2}\#\{\text{vertical dominos}\}}, \tag{6.2}$$

where the equality between two forms of weights is Corollary 6.2, and Z is a normalization constant which makes (6.2) a probability distribution. In words, we assign weight α to each East domino, assign weight β to each West domino and multiply all the weights in a tiling.

Theorem 6.3. *Under the measure* (6.2)*, via the bijection of Proposition 6.1, the sequence of partitions*

$$\varnothing \prec' \lambda^{(1)} \succ \mu^{(1)} \prec' \lambda^{(2)} \succ \cdots \succ \mu^{(n-1)} \prec' \lambda^{(n)} \succ \varnothing \tag{6.3}$$

becomes a Schur process of Definition 3.5 with $\succ$ *corresponding to one variable specializations* $(\alpha; 0; 0)$ *and* $\prec'$ *corresponding to one dual variable specializations* $(0; \beta; 0)$*.*

Proof. Specializing Definition 3.5 and using (2.42) and the fifth property in Theorem 2.18, we would like to prove that (6.3) has distribution

$$(1+\alpha\beta)^{-\frac{n(n+1)}{2}} \cdot s_{(\lambda^{(1)})'}(\beta) \cdot s_{\lambda^{(1)}/\mu^{(1)}}(\alpha) \cdot s_{(\lambda^{(2)})'/(\mu^{(1)})'}(\beta) \cdots s_{(\lambda^{(n)})'/(\mu^{(n-1)})'}(\beta) \cdot s_{\lambda^{(n)}}(\alpha), \tag{6.4}$$

where all (α) and (β) are one-variable specializations. Recall from the fourth property in Theorem 2.18 that

$$s_{\lambda/\mu}(\alpha) = \begin{cases} \alpha^{|\lambda|-|\mu|}, & \mu \prec \lambda, \\ 0, & \text{otherwise;} \end{cases} \qquad s_{\lambda'/\mu'}(\beta) = \begin{cases} \beta^{|\lambda|-|\mu|}, & \mu \prec' \lambda, \\ 0, & \text{otherwise.} \end{cases}$$

Hence, (6.4) is nonzero if and only if the sequence of λ's and μ's satisfies the conditions of Proposition 6.1, *i.e.*, (6.3). It remains to match the weights between (6.4) and (6.2), which follows from observing that for each $m = 1, 2, \ldots, n$:

- $\beta^{|\lambda^{(m)}|-|\mu^{(m-1)}|}$ is the total weight of all West dominos joining white squares of layer $m-1$ with gray squares of layer m;
- $\alpha^{|\lambda^{(m)}|-|\mu^{(m)}|}$ is the total weight of all East dominos joining gray squares of layer m with white squares of layer m. □

Corollary 6.4. *The normalization constant in* (6.2) *is*

$$Z = (1+\alpha\beta)^{\frac{n(n+1)}{2}}.$$

In particular, the total number of domino tilings of the Aztec diamond of size n is $2^{\frac{n(n+1)}{2}}$.

Proof. Each $(1+\alpha\beta)$ factor in (6.4) is $H(\rho_i^+; \rho_j^-)$ from (3.10), (3.12). The normalization constant Z in (6.2) is computed from (6.4) by $\frac{1}{Z} = (1+\alpha\beta)^{-\frac{n(n+1)}{2}}$. When we substitute $\alpha = \beta = 1$, the probability of an individual tilings becomes $\frac{1}{Z}$, where Z is the total number of tilings. □

Corollary 6.5. *Under the measure* (6.2) *and using the bijection of Proposition 6.1, the partition $\lambda^{(m)}$, $1 \le m \le n$, is distributed as a Schur measure of Definition 3.4 with $\rho_1 = (0; \beta^m; 0)$ and $\rho_2 = (\alpha^{n+1-m}; 0; 0)$:*

$$\mathbb{P}(\lambda^{(m)} = \lambda) = (1+\alpha\beta)^{-m(n+1-m)} s_{\lambda'}\bigl(\beta^m\bigr) s_{\lambda}\bigl(\alpha^{n+1-m}\bigr). \tag{6.5}$$

Proof. This is a combination of Theorem 6.3 and Theorem 3.6. □

In particular, (6.5) is the same object as the one in the earlier Theorem 1.6 and Proposition 5.21.

Let us compare the Schur process arising from the Aztec diamond with the one we had for multilayer discrete PNG in Proposition 3.2. In both situations the process can be encoded as a family of non-intersecting paths, but the combinatorics is slightly different. Following the construction of Section 3.3, let us identity the partitions (6.3) with integer-valued interfaces $\{h_\ell^{\text{Aztec}}(\cdot, n)\}_{\ell \ge 1}$:

- For fixed n, we have $2n-1$ partitions split into two groups $\lambda^{(1)}, \ldots, \lambda^{(n)}$ and $\mu^{(1)}, \ldots, \mu^{(n-1)}$. One group corresponds to even positions x and another one to odd positions.
- $\bigl(\lambda_i^{(m)} + 1 - i\bigr)_{i \ge 1} = \bigl(h_i^{\text{Aztec}}(-n-1+2m, n)\bigr)_{i \ge 1}, \quad m = 1, 2, \ldots, n.$
- $\bigl(\mu_i^{(m)} + 1 - i\bigr)_{i \ge 1} = \bigl(h_i^{\text{Aztec}}(-n+2m, n)\bigr)_{i \ge 1}, \quad m = 1, 2, \ldots, n-1.$

If we follow the picture with interfaces from the left to the right, then the up-steps are now allowed only to be of size 1, but several adjacent paths can go up simultaneously (which was not possible for the discrete PNG paths). The down-steps are of the same kind, as for the PNG. Figure 6.2 gives an example corresponding to the domino tiling of Figure 6.1.

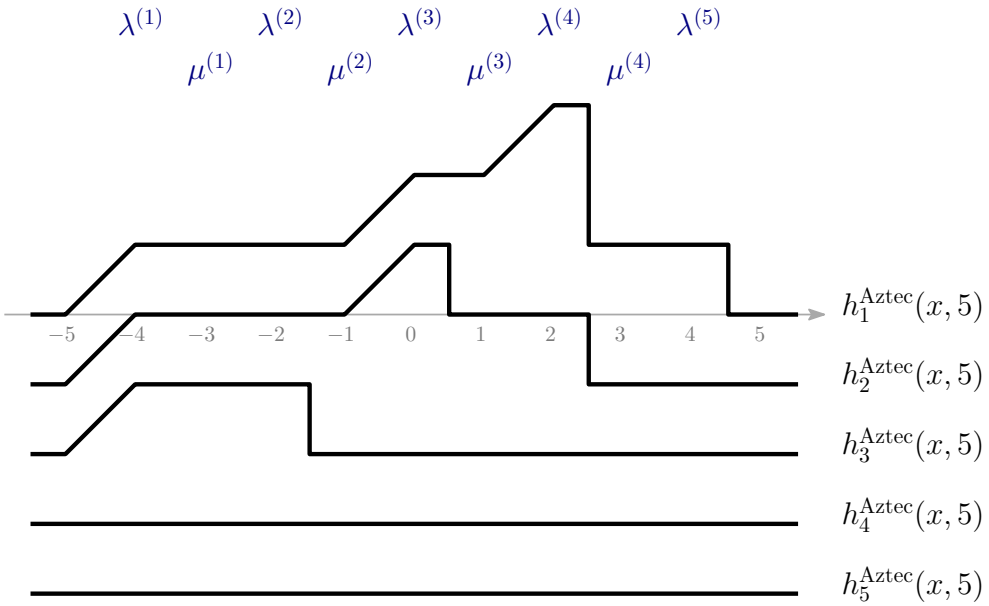


Figure 6.2: Non-intersecting paths corresponding to the tiling in Figure 6.1 and partitions (6.1).

6.2 Shuffling algorithm

For the polynuclear growth in Section 3, we started from a stochastic interface growth model and arrived at a 2d statistical mechanics model — ensemble of non-intersecting paths encoded by a Schur process — as a tool for studying the growth. For domino tilings we go in opposite direction, and a 2d statistical mechanics model becomes our starting point. Inspired by the PNG analogy, one might wonder whether there exists a simple stochastic dynamics, for which the size of the Aztec diamond, n, plays the role of time, and for fixed n one obtains random tilings, weighted as in (6.2). Such dynamics was introduced simultaneously with the very first studies of the Aztec diamond by Elkies, Cohn, Larsen, and Propp, see [EKLP92, Pro03], under the name of *shuffling algorithm*. We present a treatment based on the Schur processes, as in [Nor10, Bor11b, BF18].

6.2.1 Growth of Schur processes

The central idea is to revisit the transformations of the Schur processes which we used in computing its marginals and partition function (arrow flip of Figure 3.8 used in Theorem 3.6) and treat them in a stochastic fashion as steps of a Markov dynamics. The transformations were based on the skew Cauchy identity (2.34), (3.13), which reads (for one α–variable and one dual β–variable specializations):

$$\sum_{\kappa\in\mathbb{Y}} s_{\kappa/\lambda}(0;\beta;0)s_{\kappa/\mu}(\alpha;0;0) = (1+\alpha\beta)\sum_{\tau\in\mathbb{Y}} s_{\lambda/\tau}(\alpha;0;0)s_{\mu/\tau}(0;\beta;0). \tag{6.6}$$

One can place identities such as (6.6) in two different contexts. Diaconis and Fill [DF90] might think about (6.6) as of a commutation relation between "Up" and "Down" Markov transition probabilities: in this point of view partitions κ and τ are completely independent. In contrast, Fomin [Fom88, Fom95],[Sta99, Section 7.13 and Appendix][1] suggested that one could treat (6.6) as a correspondence between κ's and

[1] See also [FSA24] and references therein for recent developments.

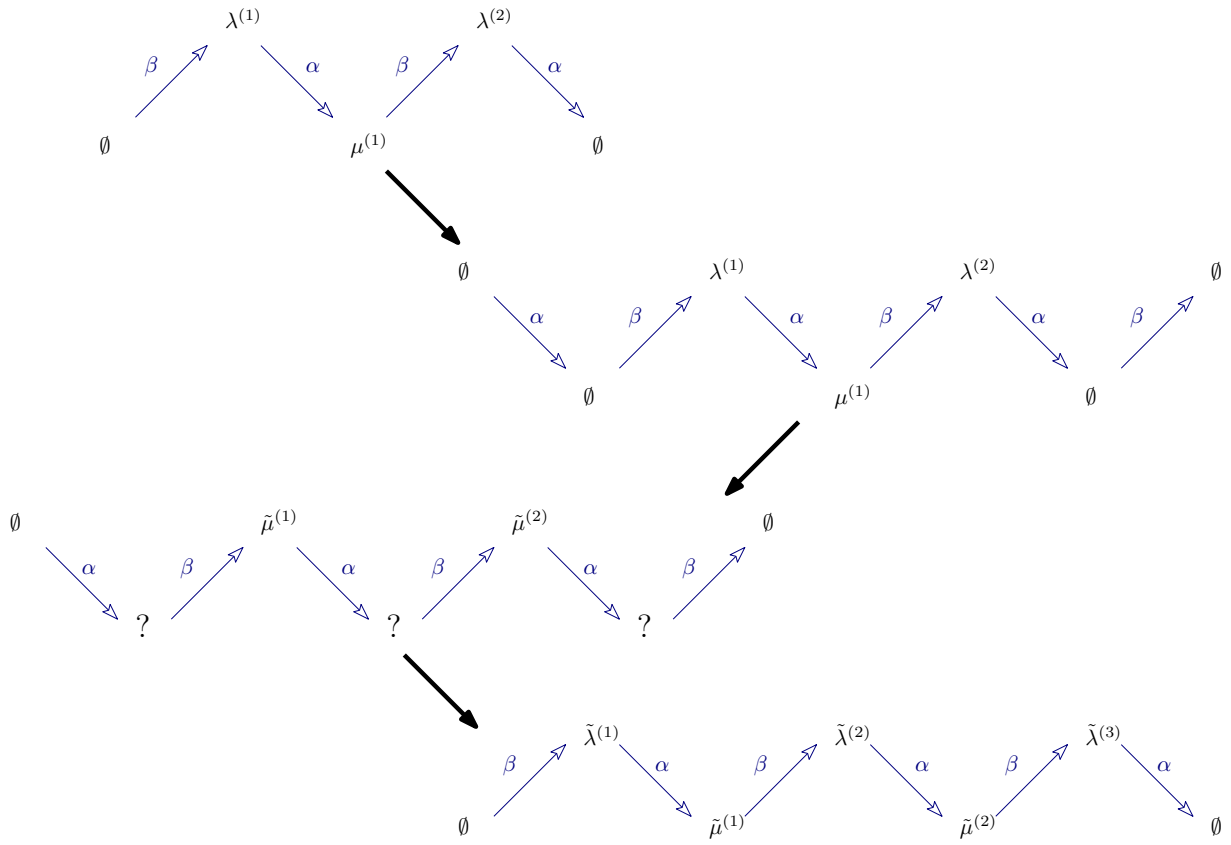


Figure 6.3: Schematics of one step of the shuffling algorithm

τ's which underlies the Robinson-Schensted–Knuth correspondence between integer-valued rectangular matrices and pairs of semistandard Young tableaux. These two different viewpoints lead to two different stochastic dynamics and generalize in different directions. We explore the first point of view here and the second one in the exercises.

We present the stochastic dynamics in an algorithmic form. One time step of the dynamics takes as its input a domino tiling of the size n Aztec diamond represented as a collection of partitions

$$\varnothing \prec' \lambda^{(1)} \succ \mu^{(1)} \prec' \lambda^{(2)} \succ \cdots \succ \mu^{(n-1)} \prec' \lambda^{(n)} \succ \varnothing \tag{6.7}$$

and outputs a domino tiling of the size $n+1$ Aztec diamond represented as a collection of partitions

$$\varnothing \prec' \tilde{\lambda}^{(1)} \succ \tilde{\mu}^{(1)} \prec' \tilde{\lambda}^{(2)} \succ \cdots \prec' \tilde{\lambda}^{(n)} \succ \tilde{\mu}^{(n)} \prec' \tilde{\lambda}^{(n+1)} \succ \varnothing. \tag{6.8}$$

This is done in four stages, illustrated in Figure 6.3:
Stage 1. Add two dummy empty partitions to the ends of (6.7) resulting in

$$\varnothing \succ \varnothing \prec' \lambda^{(1)} \succ \mu^{(1)} \prec' \lambda^{(2)} \succ \cdots \succ \mu^{(n-1)} \prec' \lambda^{(n)} \succ \varnothing \prec' \varnothing. \tag{6.9}$$

Stage 2. Erase all $\mu^{(m)}$, $1 \le m \le n-1$, as well as two $\varnothing$ adjacent to the ends, turning all of them into ?. Rename $\lambda^{(m)}$ into $\tilde{\mu}^{(m)}$ for all $1 \le m \le n$ resulting in:

$$\varnothing \succ ? \prec' \tilde{\mu}^{(1)} \succ ? \prec' \tilde{\mu}^{(2)} \succ \cdots \succ ? \prec' \tilde{\mu}^{(n)} \succ ? \prec' \varnothing. \tag{6.10}$$

Stage 3. Swap all $\succ$ and $\prec'$ signs, resulting in:

$$\varnothing \prec' ? \succ \tilde{\mu}^{(1)} \prec' ? \succ \tilde{\mu}^{(2)} \prec' \cdots \prec' ? \succ \tilde{\mu}^{(n)} \prec' ? \succ \varnothing. \tag{6.11}$$

Stage 4. Denoting $\tilde{\mu}^{(0)} = \varnothing = \tilde{\mu}^{(n-1)}$, sample each ? independently as $\tilde{\lambda}^{(m)}$, $1 \le m \le n+1$, in the triple $\tilde{\mu}^{(m-1)} \prec' \tilde{\lambda}^{(m)} \succ \tilde{\mu}^{(m)}$, according to the weight of κ in the left-hand side of (6.6), *i.e.*:

$$\mathbb{P}\Bigl(\tilde{\lambda}^{(m)} = \kappa \mid \tilde{\mu}^{(m-1)}, \tilde{\mu}^{(m)}\Bigr) = \frac{s_{\kappa/\tilde{\mu}^{(m-1)}}(0;\beta;0)\, s_{\kappa/\tilde{\mu}^{(m)}}(\alpha;0;0)}{\sum_{\hat{\kappa}\in\mathbb{Y}} s_{\hat{\kappa}/\tilde{\mu}^{(m-1)}}(0;\beta;0)\, s_{\hat{\kappa}/\tilde{\mu}^{(m)}}(\alpha;0;0)}, \qquad 1 \le m \le n+1. \tag{6.12}$$

Output the resulting sequence

$$\varnothing \prec' \tilde{\lambda}^{(1)} \succ \tilde{\mu}^{(1)} \prec' \tilde{\lambda}^{(2)} \succ \cdots \prec' \tilde{\lambda}^{(n)} \succ \tilde{\mu}^{(n)} \prec' \tilde{\lambda}^{(n+1)} \succ \varnothing. \tag{6.13}$$

Theorem 6.6. *If the input* (6.7) *is the Schur process* (6.4) *corresponding to the weights* (6.2) *for domino tilings of the Aztec diamond of size n, then the output* (6.11) *is the Schur process corresponding to the weights* (6.2) *for domino tilings of the Aztec diamond of size $n+1$.*

Proof. We analyze the procedure stage by stage. In Stage 1, the addition of empty partitions does not change anything, because a subdiagram of $\varnothing$ is necessarily $\varnothing$ again. Stages 2 and 3 are based on the observation that for the Schur process of Theorem 6.3, the distribution of the n–tuple of partitions $\lambda^{(1)}$, $\lambda^{(2)}, \ldots, \lambda^{(n)}$ is the same as the distribution of the n-tuple of partitions $\tilde{\mu}^{(1)}, \tilde{\mu}^{(2)}, \ldots, \tilde{\mu}^{(n)}$. The latter fact is proven by comparing the sums defining these distributions as marginals of the full Schur processes, and noting that these sums are the same by the skew Cauchy identity in the form (6.6).

In Stage 4 we already know that $\tilde{\mu}^{(m)}$, $1 \le m \le n$, have the desired distribution of a marginal of the Schur process. Conditional on them, the definition of the Schur process readily implies the formula for the conditional distributions of $\tilde{\lambda}^{(m)}$, $1 \le m \le n+1$. □

The four stage procedure outlined above can be performed for any Schur process: one takes a rank n Schur process and outputs a rank $n+1$ Schur process. For the algorithmic implementation, the hardest stage is sampling from the distribution (6.12). This can be a convoluted procedure for general specializations. However, for the particular one-variable specializations in (6.12), this stage reduces to flipping several (biased) independent coins.

Proposition 6.7. *Choose two Young diagrams μ, ν such that the sum over $\tilde{\kappa}$ in* (6.14) *below is non-empty. Then sampling λ from the distribution*

$$\frac{s_{\lambda/\mu}(0;\beta;0)\, s_{\lambda/\nu}(\alpha;0;0)}{\sum_{\hat{\kappa}\in\mathbb{Y}} s_{\hat{\kappa}/\mu}(0;\beta;0)\, s_{\hat{\kappa}/\nu}(\alpha;0;0)} \tag{6.14}$$

amounts to three cases for each $i = 1, 2, \ldots$:

1. *If $\nu_{i-1} = \mu_i$, then set $\lambda_i = \mu_i$;*
2. *If $\nu_i = \mu_i + 1$, then set $\lambda_i = \mu_i + 1$;*
3. *Otherwise, flip a coin: with probability $\frac{\alpha\beta}{1+\alpha\beta}$ set $\lambda_i = \mu_i + 1$, and with probability $\frac{1}{1+\alpha\beta}$ set $\lambda_i = \mu_i$.*

Proof. Due to factor $s_{\lambda/\mu}(0;\beta;0)$ in (6.14), $\lambda_i - \mu_i \in \{0, 1\}$, in order for the probability to be non-zero. In the first two cases, $\lambda_i - \mu_i$ is forced to have one of the two values, in order for $s_{\kappa/\nu}(\alpha;0;0)$ to be non-zero. In the remaining case both options are possible, and their weights differ by the factor of $\alpha\beta$. Since the choices for each i are independent, so are the coin flips. □

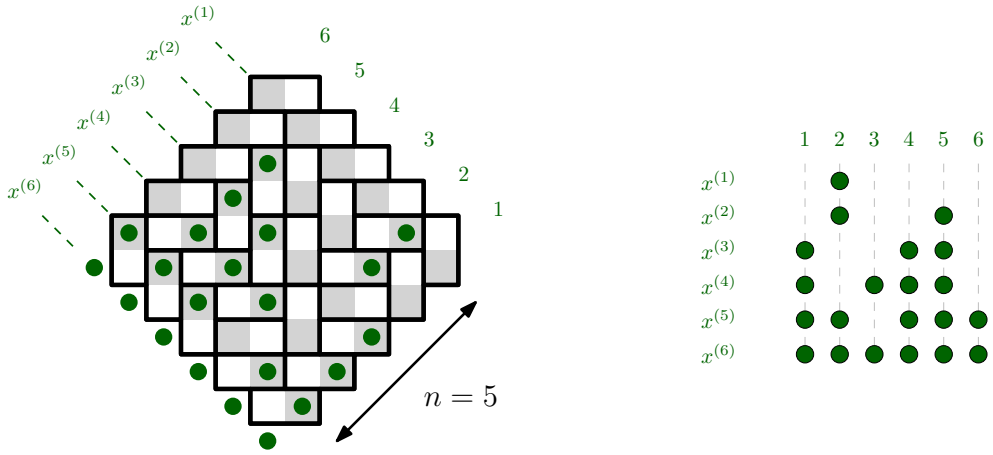


Figure 6.4: Green particles for domino tiling. $x_1^{(1)}, x_1^{(2)},\ldots, x_1^{(6)}$ have the largest coordinates in the corresponding rows $1, 2, \ldots, 6$ and $x_1^{(1)}, x_2^{(2)},\ldots, x_6^{(6)}$ have the smallest ones.

6.2.2 Push-block dynamics

The four stage procedure together with Proposition 6.7 have two visually different interpretations, depending on whether we deal with particles or with dominos. Let us present both. We will keep track of only green particles on gray squares, as in Figure 6.4. This is sufficient for reconstructing tilings, since in Stage 2 the orange particles are directly obtained from the green particles at the previous time step. We slightly adjust the notations compared to $\lambda^{(1)}$, …, $\lambda^{(n)}$ of Figure 6.1: we do not perform shifts $\lambda_i^{(m)} \mapsto \lambda_i^{(m)} - i + n - m + 2$ anymore and replace (m) with $(n + 1 - m)$. Hence, the upper-right-most gray layer now has one green particle encoded by $x_1^{(1)} \in \{1, 2, \ldots, n + 1\}$. The second upper-right-most layer has two green particles encoded by $x_1^{(2)} > x_2^{(2)} \in \{1, 2, \ldots, n + 1\}$, etc. The bottom-left-most gray layer inside the Aztec diamond of size n has n green particles encoded by $x_1^{(n)} > x_2^{(n)} > \cdots > x_n^{(n)} \in \{1, 2, \ldots, n + 1\}$. We will also need a deterministic particle configuration $x^{(n+1)} = (n + 1 > n > n - 1 > \cdots > 1)$.

The particles $x_i^{(m)}$, $1 \le i \le m \le n + 1$, satisfy the following combination of strict and weak inequalities for all meaningful indices:

$$x_i^{(m)} < x_{i-1}^{(m)}, \qquad x_i^{(m-1)} \le x_i^{(m)} \le x_{i-1}^{(m-1)}. \tag{6.15}$$

In the literature such configurations are sometimes called *monotone triangles*.

Proposition 6.8. *In terms of the monotone triangle* $\left\{x_i^{(m)}[n]\right\}_{1\le i\le n+1}$ *the four stage time step procedure* $n \mapsto n + 1$ *is recast as follows. We set* $p = \frac{\alpha\beta}{1+\alpha\beta}$ *and construct* $x^{(m)}[n + 1]$, $m = 1, 2, \ldots n + 1$, *by doing the following for each* $1 \le i \le m$ *independently:*

1. **Blocking:** *If* $x_i^{(m)}[n] = x_{i-1}^{(m-1)}[n]$, *then set* $x_i^{(m)}[n + 1] = x_i^{(m)}[n]$;
2. **Pushing:** *If* $x_i^{(m)}[n] = x_i^{(m-1)}[n]$, *then set* $x_i^{(m)}[n + 1] = x_i^{(m)}[n] + 1$;
3. **Bernoulli move:** *If* $x_{i-1}^{(m-1)} > x_i^{(m)} > x_i^{(m-1)}$, *then with probability* p *set* $x_i^{(m)}[n+1] = x_i^{(m)}[n]+1$ *and with probability* $1 - p$ *set* $x_i^{(m)}[n + 1] = x_i^{(m)}[n]$.

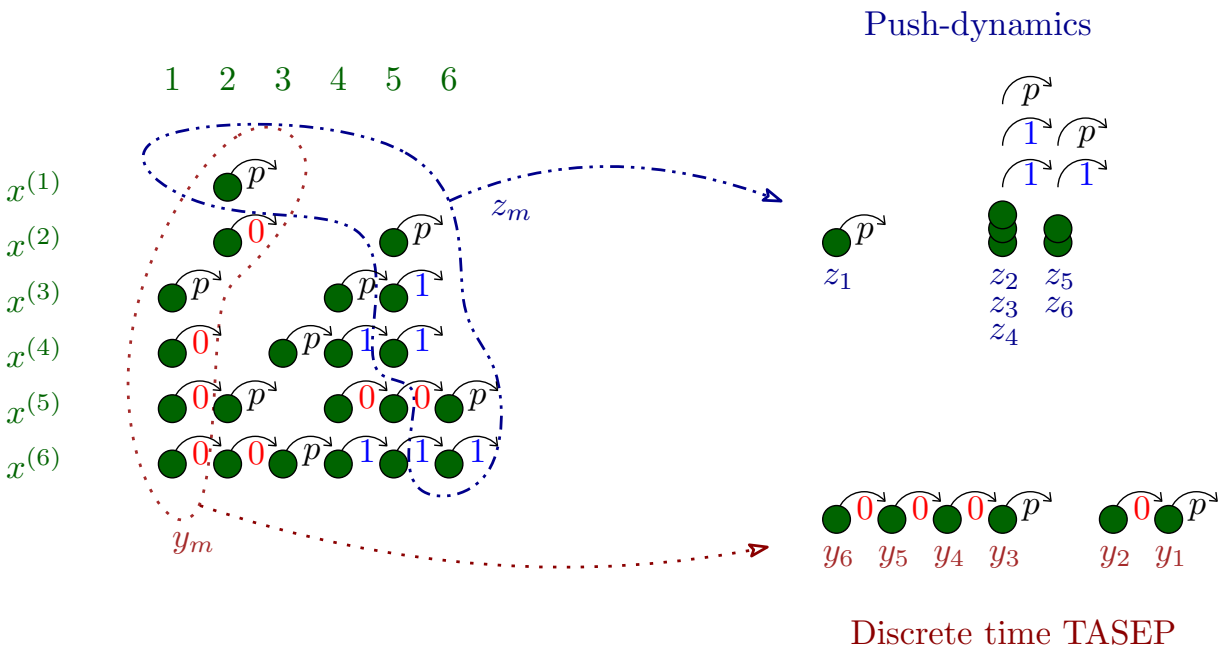


Figure 6.5: Jump probabilities for different particles and projections to first and last particles.

Once all $m \leq n+1$ *have been updated, we set* $x^{(n+2)}[n+1] = (n+2 > n+1 > \cdots > 1)$.

In words, each particle at level m and time n checks whether it is blocked by a particle at the previous level $m-1$ (then necessarily do nothing) or pushed by a particle at the previous level (then necessarily jump forward). If neither, then the particle either stays or moves one step forward according to a p–biased coin flip, see Figure 6.5 for an illustration. The description of the dynamics in Proposition 6.8 is equivalent to that of [Nor10].

Proof of Proposition 6.8. These three cases are a rewording of the three cases in Proposition 6.7. □

There are a few projections of this Markov chain which are still Markov chains. Observe that the solo particle in the first row, $x_1^{(1)}[n]$ evolves as a Bernoulli random walk with probability of jump p and initial condition $x_1^{(1)}[0] = 1$.

Remarkably, the evolution of the last (smallest) particles decouples. If we set $y_m = x_m^{(m)} - m$, so that $y_1 > y_2 > y_3 > \ldots$, then the particles $y_1, y_2, \ldots$, evolve by the *discrete time TASEP with parallel update* (or Bernoulli TASEP). At time zero $y_m[0] = 1-m$ for all $m = 1, 2, \ldots$. At time n each particle y_m independently and in parallel checks whether it is blocked by a particle in front (*i.e.*, $y_m[n] = y_{m-1}[n]-1$) in which case it does nothing. Otherwise, it jumps one step forward with probability p. If we identify particle configurations with Young diagrams, as in Figure 5.14, then the evolution of $\{y_m\}_{m\geq 1}$ can be linked to the last passage percolation by the same mechanism as in Section 1.4. The weights w_{ij}, as in (1.5), are again i.i.d. geometric random variables, but this time supported on $\mathbb{Z}_{\geq 1}$, *i.e.*, $\mathbb{P}(w_{i,j} = k) = p(1-p)^{k-1}$, $k = 1, 2, \ldots$.

Evolution of the first (largest) particles also decouples, leading to a discrete time push-dynamics (Bernoulli Push-TASEP), in which more than one particle can occupy a lattice spot. If we set $z_m = x_1^{(m)}$, so that $z_1 \leq z_2 \leq z_3 \leq \ldots$, then at time 0, we have $z_m = m$ for all $m = 1, 2, \ldots$. At time n, only the particles with $m \leq n+1$ are allowed to move. Such a particle z_m, checks if it is pushed by a particle

in the back (*i.e.*, $z_m[n] = z_{m-1}[n]$), in which case it necessarily jumps one step forward. Otherwise, it jumps one step forward with probability p.

One can further simplify the dynamics by taking a continuous time limit, similar to the one we saw in Bernoulli to Poisson limit of Lemma 4.5:

$$p \to 0, \qquad np \to t. \tag{6.16}$$

As the result, the Bernoulli TASEP evolution for y_m becomes the classical continuous time totally asymmetric simple exclusion process (or simply TASEP), in which each particle has an independent exponential clock. When the clock rings, the particle checks whether there is a free spot directly in front of it. If so, then the particle moves one step forwards. The study of such processes goes back to the work of Spitzer [Spi70] in 1970, see also [MGP68] for biology motivations and [Lig85, Lig99] for overviews. The integrability of TASEP and its Tracy-Widom fluctuations were discovered in [Sch97] and [Joh00].

Simultaneously, the Bernoulli Push-TASEP becomes a continuous time Push-TASEP, in which each particle has an independent exponential clock. When the clock rings, the particle moves one step forward and pushes any group of particles directly in front of it, in order to preserve the condition of at most one particle per lattice spot. Here we see a simplification: while the discrete time version allowed several particles to occupy the same lattice spot, this no longer happens in the continuous time. The interest to PushTASEP as a particular case of the Toom model goes back to [DLSS91]. Its integrability and Tracy-Widom limits were discovered in [AKK99] and [BF08], see also [BFLS14].

The full 2d-dynamics of the array of green particles in the Aztec diamond converges under (6.16) to the multilevel TASEP, which combines block and push interactions, see [BF09, BF14, GS15, Ton18] for its various aspects. Closely related variations of these processes were discussed in [War07, DW08]. For further developments of these techniques see [Bor11b, BO12, BC14, BP14, BP16, Cue18, Ass18, Ass20].

6.2.3 Shuffling of dominos

Alternatively, one can restate the growth of the Aztec diamond in the language of dominos, avoiding the mention of any particles. This is the form in which the dynamics first appeared in the literature in [EKLP92, Pro03] under the name "shuffling algorithm".

The procedure starts from drawing an arrow on each domino, pointing to the right for East dominos, to the left for West dominos, upward for North dominos and downward for South dominos. Then the procedure for obtaining a domino tiling of size $n+1$ Aztec diamond from a domino tiling of size n Aztec diamond proceeds in three steps, see Figure 6.6 for an illustration:

1. Each pair of adjacent dominos with arrows pointing towards each other (either East-West or South-North) is declared a "bad box" and removed. The empty 2×2 square stays in place.

2. All other dominos move distance 1 at the direction of their arrows.

3. The complement of the resulting collection of dominos inside the Aztec diamond of size $n+1$ is uniquely represented as a disjoint union of 2×2 boxes; we call each a "box to fill". Independently, we fill each box by two vertical dominos with probability $p = \frac{\alpha\beta}{1+\alpha\beta}$ and by two horizontal dominos with probability $1-p$.

Note that the Aztec diamond itself grows by 1 in all directions under this operation and, therefore, the checkerboard coloring convention changes: it is no longer true that the bottommost part of the diamond is white-gray ▭. We need to invert the checkerboard coloring at the end of the procedure in order to restore the conventions.

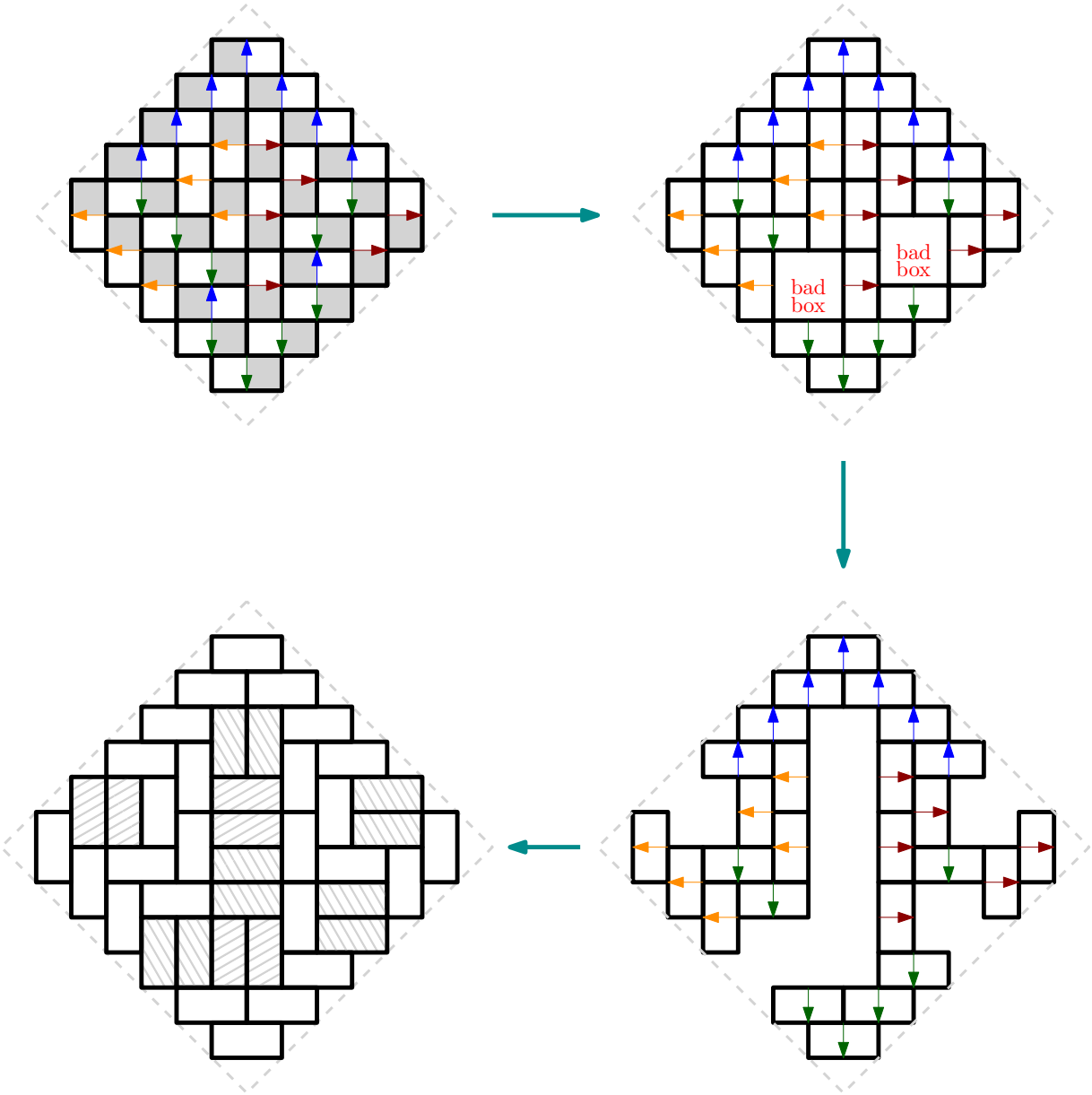


Figure 6.6: One step of the shuffling algorithm, size changes $5 \to 6$.

Proposition 6.9. *The just described shuffling algorithm is the same as the Schur process dynamics of Theorem 6.6 and the push-block dynamics of Proposition 6.8.*

Proof. In order to see the correspondence with the algorithms of the previous sections, we reconstruct the green and orange particles on dominos, as shown in Figure 6.7.

We first look at bad boxes and notice that those necessarily have a green particle in the top-right corner, while the orange particle can be either in bottom-right or top-left.

Next, we analyze sliding. Observe that the slide is always possible, *i.e.*, leads to no overlaps of dominos: for instance, if we are looking at a south domino moving down, then the obstacles to its move could have been a pair East-South directly below or a North domino directly below; however, both of these

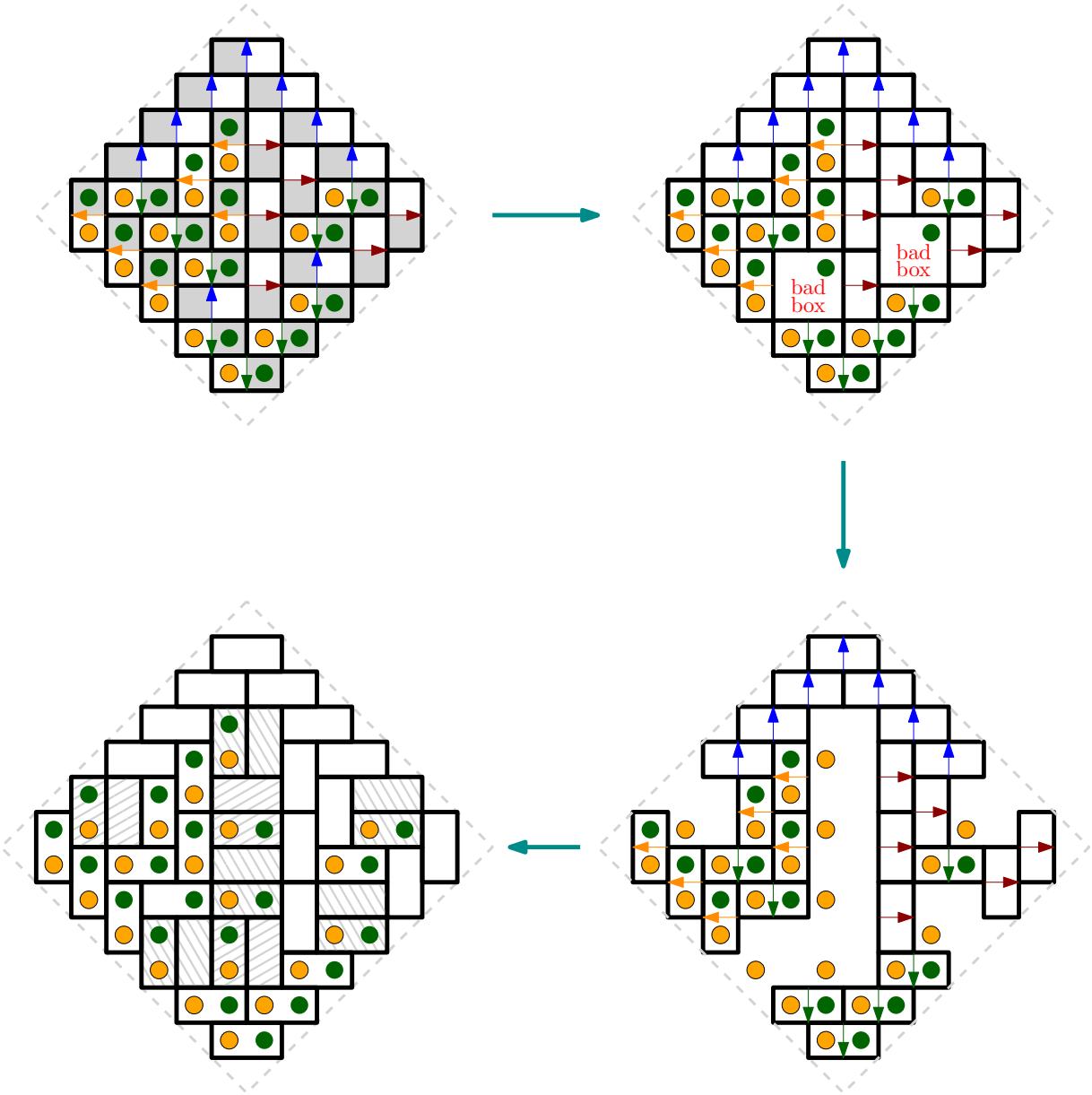


Figure 6.7: One step of the shuffling algorithm, with green and orange particles shown.

cases would have led to a removal of these dominos in bad boxes and therefore do not happen.

Furthermore, South dominos moving down correspond to the green particles blocking each other, *i.e.*, the case $x_i^{(m)}[n] = x_{i-1}^{(m-1)}[n]$ in Proposition 6.8 (otherwise, there would have been a North domino or a East-South pair right below, corresponding to the absence of the particle). The moving green particle itself corresponds to $x_{i-1}^{(m-1)}[n]$ turning into $x_i^{(m)}[n+1]$.

Similarly, West dominos moving left correspond to the green particles pushing each other, *i.e.*, the case $x_i^{(m)}[n] = x_i^{(m-1)}[n]$ in Proposition 6.8. The moving green particle itself corresponds to $x_i^{(m-1)}[n]$ turning into $x_i^{(m)}[n+1]$ with coordinate increasing by 1.

All the remaining particle (neither blocked, nor pushed) correspond to the Bernoulli move case in

Proposition 6.8 and to the 2×2 boxes to fill in the third step of the shuffling algorithm. Note that the number of dominos in the Aztec diamond grows by $2 \cdot (n+1)$ and therefore the total number of 2×2 boxes to fill is $n+1$ plus the number of bad boxes at the first step. Since each bad box corresponds to a green particle not causing blocks or pushes, we conclude that the number of Bernoulli coin flips matches between the description in Proposition 6.8 and the one in the current section.

In order to convince ourselves that these flips correspond to exactly the same jumps between two descriptions, it is helpful to keep track of green particles in the Aztec diamond of size n and orange particles in the Aztec diamond of size $n+1$. We know from the description in Theorem 6.6 (equivalent to the one in Proposition 6.8) that green particles should be turning into orange particles, and in addition $n+1$ new orange particles are appearing along the bottom-left boundary. Let us do this recoloring/adding operation in the description of the present section and convince ourselves that this matches the South/West moves and creation of dominos in the shuffling algorithm description. (East and North dominos do not carry particles. Hence, because we already know that particles uniquely determine the tiling, we do not have to directly track the moves of East and North dominos.)

A West domino moving to the left corresponds to two orange particles: one is at the bottom of the domino after the move and another one is at the old position of the green particle (equivalently, to the right from the green particle after the move); these correspond precisely to $x_i^{(m)}[n] = x_{i-1}^{(m-1)}[n]$. In this way, the move of the West domino is just a reflection of the fact that this situation necessarily leads to the green particle landing at top-left position with regard to these two orange particles.

Similarly, a South domino moving down corresponds to two orange particles: one is at the left of the domino after the move and another one is at the old position of the green particle (equivalently, above the green particle after the move); these correspond precisely to $x_i^{(m)}[n] = x_i^{(m-1)}[n]$. In this way, the move of the South domino is just a reflection of the fact that this situation necessarily leads to the green particle landing at the bottom-right position with regard to these two orange particles.

After the move was done, some orange particles are not yet covered by dominos; those become bottom-left corners of boxes to fill. The new green particle adjacent to them is not subject to a block or push, and therefore can be chosen freely between two options, reflecting the choice between two vertical and two horizontal dominos covering the box. □

Figure 6.8 shows two samples for $n = 200$ Aztec diamond obtained by running the shuffling algorithm. One intriguing feature of the pictures is the appearance of the *Arctic circle* on the left and *Arctic ellipse* on the right, separating the pictures into five separates regions: in the four *frozen* regions only one type of dominos survive asymptotically; in the fifth *liquid* (or *rough*) region all four types are present. The possibility of coexistence of different phases in a single domain is a prominent feature of random tilings, cf. [Ken09, Gor21]. We come back to the asymptotics of tilings in the next several sections.

Introduction of the shuffling algorithm into the study of random domino tilings has two conceptual consequences. First, we now have a direct probabilistic bridge between 2d statistical mechanics (represented by tilings) and interface growth models (represented by the interacting particle system with push/block interactions). Hence, we can import tools from one area into another one (*e.g.*, [JPS26] used hydrodynamics of TASEP in order to find the shape of the Arctic curves visible in Figure 6.8). Second, a complicated measure on domino tilings got split into elementary building blocks (coin flips) — this powerful idea will be further explored in the context of the six-vertex model and Yang-Baxter equation in Chapters 7 and 8.

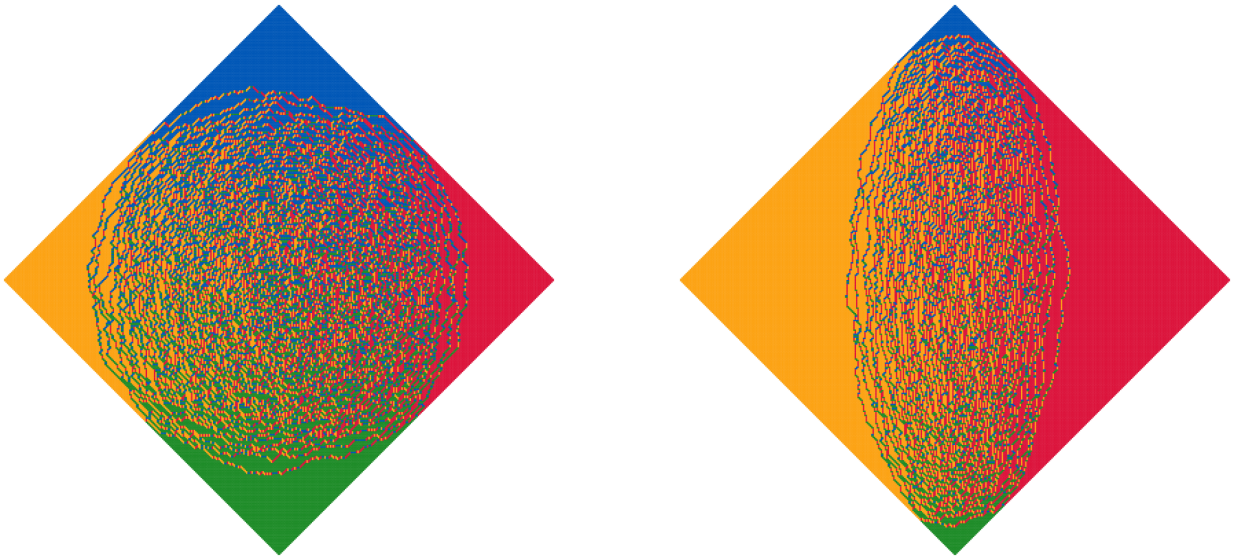


Figure 6.8: Random tilings of $n = 200$ Aztec diamond: $\alpha\beta = 1$ on the left and $\alpha\beta = 5$ on the right.

6.3 Observables through operators

Our next goal is asymptotic analysis of the domino tilings of the Aztec diamond. We build on Corollary 6.5 linking us to the Schur processes. In principle, we can use here all the machinery of the determinantal point processes and contour integrals, as developed in the previous chapter — this approach will be postponed till the exercises at the end of this chapter. Instead, we describe and apply another influential method of integrable probability: the use of differential and difference operators for the extraction of the asymptotic information.

The idea underlying the method has roots in classical probability. Suppose that one would like to compute the moments of a random variable ξ, $\mathbb{E}\xi^n$, but what one knows is its characteristic function, $\chi(s) = \mathbb{E}\exp(\mathbf{i}s\xi)$. Then one can extract the moments by differentiation:

$$\mathbb{E}\xi^n = \frac{1}{\mathbf{i}^n}\frac{\partial^n}{\partial s^n}\chi(s)\Big|_{s=0}.$$

For Schur measures, the evaluation of analogues of characteristics functions is delivered by the Cauchy summation identity, while $\frac{\partial}{\partial s}$ is replaced by more complicated operators which we now introduce.

We deal with operators acting on functions $f(x_1, \dots, x_N)$ in N variables. The q–shift operator $\mathcal{T}_i^q$ multiplies x_i by q:

$$\left[\mathcal{T}_i^q f\right](x_1, \dots, x_N) = f\big(x_1, \dots, x_{i-1}, qx_i, x_{i+1}, \dots, x_N\big).$$

The following operator $\mathcal{D}_q$ is the $q = t$ version of the celebrated Macdonald (first order) operator[2]:

$$\mathcal{D}_q = \sum_{i=1}^{N}\left[\prod_{j\neq i}\frac{qx_i - x_j}{x_i - x_j}\right]\mathcal{T}_i^q. \tag{6.17}$$

[2]For higher order and $q \neq t$ cases important for the study of Macdonald symmetric polynomials, see [Mac95, Section VI.3].

Theorem 6.10. *The operator $\mathcal{D}_q : \Lambda_N \to \Lambda_N$ maps symmetric polynomials to themselves and preserves degrees. Operators $\mathcal{D}_q$ with different values of q commute. Schur polynomials are their common eigenfunctions: for any $\lambda = (\lambda_1, \dots, \lambda_N)$*

$$\mathcal{D}_q s_\lambda = \left(\sum_{i=1}^N q^{\lambda_i + N - i} \right) s_\lambda. \tag{6.18}$$

Proof. Definition (6.17) implies that $\mathcal{D}_q$ can be represented as a conjugation of $\sum_{i=1}^N \mathcal{T}_i^q$ by the operator of multiplication with $\prod_{i<j}(x_i - x_j)$:

$$\mathcal{D}_q f = \frac{1}{\prod\limits_{1 \le i < j \le N} (x_i - x_j)} \left(\sum_{i=1}^N \mathcal{T}_i^q \right) \left[\prod_{1 \le i < j \le N} (x_i - x_j) \cdot f \right]. \tag{6.19}$$

Multiplication by $\prod_{i<j}(x_i - x_j)$ maps a degree n symmetric polynomials to a degree $n + N(N-1)/2$ skew-symmetric polynomial; action by $\sum_{i=1}^N \mathcal{T}_i^q$ preserves skew-symmetry, polynomiality, and degree; division by $\prod_{i<j}(x_i - x_j)$ maps a degree $n + N(N-1)/2$ skew-symmetric polynomial to a degree n symmetric polynomial. Hence, $\mathcal{D}_q$ maps Λ_N^n to Λ_N^n. For the eigenrelation we combine (6.19) with the definition of Schur polynomials via (1.6), (2.14):

$$\begin{aligned} \mathcal{D}_q s_\lambda &= \frac{1}{\prod\limits_{1 \le i < j \le N} (x_i - x_j)} \left(\sum_{i=1}^N \mathcal{T}_i^q \right) \operatorname{Alt}_{\lambda + \delta_N}(x_1, \dots, x_N) \\ &= \frac{1}{\prod\limits_{1 \le i < j \le N} (x_i - x_j)} \left(\sum_{i=1}^N q^{\lambda_i + N - i} \right) \operatorname{Alt}_{\lambda + \delta_N}(x_1, \dots, x_N) = \left(\sum_{i=1}^N q^{\lambda_i + N - i} \right) s_\lambda. \end{aligned} \tag{6.20}$$

Finally, commutativity of the operators holds either from (6.19) or because they share an eigenbasis. □

The relevance of the operators to the study of Schur measures is based on the following observation.

Theorem 6.11. *Fix any complex numbers $q_1, \dots, q_K$, and a Schur measure with one pure-α specialization $\rho_1 = (\alpha_1, \dots, \alpha_N;\, 0;\, 0)$ and an arbitrary specialization $\rho_2 = \rho$,* i.e.,

$$\mathbb{P}(\lambda) = \prod_{i=1}^N \frac{1}{H(\rho;\, \alpha_i)} s_\lambda(\alpha_1, \dots, \alpha_N) s_\lambda(\rho), \qquad \lambda \in \mathbb{Y}.$$

Then, assuming the series defining the expectation is absolutely convergent, we have

$$\mathbb{E}\left[\prod_{k=1}^K \sum_{i=1}^N q_k^{\lambda_i + N - i} \right] = \prod_{i=1}^N \frac{1}{H(\rho;\, \alpha_i)} \left[\prod_{k=1}^K \mathcal{D}_{q_k} \prod_{i=1}^N H(\rho;\, x_i) \right]_{x_1 = \alpha_1, \dots, x_N = \alpha_N}. \tag{6.21}$$

Proof. We start from $K = 1$ case. Specializing the second set of variables into ρ in the Cauchy identity of Theorem 2.9, we have

$$\sum_\lambda s_\lambda(x_1, \dots, x_N) s_\lambda(\rho) = \prod_{i=1}^N H(\rho;\, x_i).$$

Acting by $\mathcal{D}_q$ and using (6.18), we get

$$\sum_\lambda \left(\sum_{i=1}^N q^{\lambda_i + N - i} \right) s_\lambda(x_1, \dots, x_N) s_\lambda(\rho) = \mathcal{D}_q \prod_{i=1}^N H(\rho;\, x_i).$$

Specializing $(x_1, \dots, x_N) = (\alpha_1, \dots, \alpha_N)$ and then dividing by $\prod_{i=1}^N H(\rho;\, \alpha_i)$ yields (6.21) for $K = 1$ and $q_1 = q$.

The case $K > 1$ is obtained in the same way by applying $\prod_{k=1}^K \mathcal{D}_{q_k}$ instead of a single $\mathcal{D}_q$. Note that the order of the operators does not matter because they commute. □

The following lemma helps us to rewrite (6.21) in a form suitable for asymptotic analysis. The key feature is that while it is tricky to plug $x_1 = \cdots = x_N$ into (6.17), this becomes straightforward in the integral representation.

Lemma 6.12. *Choose an open set $\mathcal{A} \subset \mathbb{C}$ and let $f(z)$ be a function such that $\frac{f(qz)}{f(z)}$ is holomorphic in $z \in \mathcal{A}$. Then for any $x_1, \dots, x_N \in \mathcal{A}$*

$$\mathcal{D}_q \prod_{i=1}^N f(x_i) = \frac{1}{2\pi\mathbf{i}(q-1)} \prod_{i=1}^N f(x_i) \oint_{\{x_i\}} \prod_{i=1}^N \frac{qz - x_i}{z - x_i} \cdot \frac{f(qz)}{f(z)} \frac{\mathrm{d}z}{z}, \tag{6.22}$$

where the integration goes over a positively-oriented contour enclosing all x_i, $1 \le i \le N$, but not 0. The contour and its interior are required to be inside $\mathcal{A}$.

Proof. Since both sides of (6.22) are continuous in x_i, it is sufficient to prove the identity for the case of all distinct x_i. Then the integral in the right-hand side of (6.22) is computed as the sum of N residues at points $x_1, \dots, x_N$:

$$\frac{1}{2\pi\mathbf{i}} \oint_{\{x_i\}} \prod_{i=1}^N \frac{qz - x_i}{z - x_i} \cdot \frac{f(qz)}{f(z)} \frac{\mathrm{d}z}{z} = \sum_{i=1}^N \prod_{j \ne i} \frac{qx_i - x_j}{x_i - x_j} \cdot \frac{f(qx_i)}{f(x_i)} \cdot \frac{(q-1)x_i}{x_i}.$$

Multiplying by $\frac{1}{q-1} \prod_{i=1}^N f(x_i)$ and comparing with (6.17), we obtain the desired formula. □

Theorem 6.13. *Fix any complex numbers $q_1, \dots, q_K$, and a Schur measure with one pure-α specialization $\rho_1 = (\alpha_1, \dots, \alpha_N;\, 0;\, 0)$ and an arbitrary specialization $\rho_2 = \rho$,* i.e.*,*

$$\mathbb{P}(\lambda) = \prod_{i=1}^N \frac{1}{H(\rho;\, \alpha_i)} s_\lambda(\alpha_1, \dots, \alpha_N) s_\lambda(\rho), \qquad \lambda \in \mathbb{Y}.$$

Then, assuming the series defining the expectation is absolutely convergent, we have

$$\mathbb{E}\left[\prod_{k=1}^K \sum_{i=1}^N q_k^{\lambda_i + N - i}\right] = \oiint \prod_{1 \le k < l \le K} \frac{(q_k z_k - q_l z_l)(z_k - z_l)}{(z_k - q_l z_l)(q_k z_k - z_l)} \times \prod_{k=1}^K \left[\prod_{i=1}^N \frac{q_k z_k - \alpha_i}{z_k - \alpha_i} \cdot \frac{H(\rho; q_k z_k)}{H(\rho; z_k)} \cdot \frac{\mathrm{d}z_k}{2\pi\mathbf{i}(q_k - 1) z_k}\right], \tag{6.23}$$

where $z_1, \dots z_K$ are integrated over positively-oriented contours such that:

- *Each z_k contour, $1 \le k \le K$, encloses the points $\{\alpha_1, \dots, \alpha_N\}$, but not 0. The contour is inside the disk around the origin in which the series $\sum_{n=1}^\infty p_k(\rho) \frac{z_k^n}{n}$ and $\sum_{n=1}^\infty p_k(\rho) \frac{(q_k z_k)^n}{n}$ are convergent.*
- *For each pair $k < l$, the z_l contour does* not *enclose points $\{q_k z_k, q_l^{-1} z_k\}$.*

Remark 6.14. In the theorem we silently assume that the desired contours exist, cf. Figure 6.9. Once the theorem is proven for this particular choice of the contours, one can further deform them into various other arrangements without changing the value of the integral. Generalizations of (6.23) exist both for the case when ρ_1 specialization is arbitrary and for the joint distribution of several Young diagrams in the Schur process, see [BCGS16]. Contour integrals (6.23) can be related to the contour integrals for the correlation functions of the Schur measure in Theorems 4.20 and 4.21, see [Agg15].

Proof of Theorem 6.13. Throughout the proof we assume that all q_k, $1 \le k \le K$, are sufficiently close to 1, which guarantees the existence of the contours satisfying the stated conditions. The theorem can be extended to other q_k by either repeating the argument and paying more attention to contours, or by analytic continuation in q_k.

We use (6.21) and apply the operators in the following order: first $\mathcal{D}_{q_1}$, then $\mathcal{D}_{q_2}$, etc. Applying the first operator via Lemma 6.12 we have

$$\mathcal{D}_{q_1} \prod_{i=1}^{N} H(\rho;\, x_i) = \prod_{i=1}^{N} H(\rho;\, x_i) \oint_{\{x_i\}} \prod_{i=1}^{N} \frac{q_1 z_1 - x_i}{z_1 - x_i} \cdot \frac{H(\rho;\, q_1 z_1)}{H(\rho;\, z_1)} \cdot \frac{\mathrm{d}z_1}{2\pi \mathbf{i}(q_1 - 1) z_1}, \tag{6.24}$$

where the contour should be chosen inside the disk around the origin where $H(\rho;\, z_1) = \exp\left(\sum_{n=1}^{\infty} p_k(\rho) \frac{z_k^n}{n}\right)$ and $H(\rho;\, q_1 z_1)$ are converging. We will apply the next operator $\mathcal{D}_{q_2}$ under the integral sign in (6.24); note that this requires fixing the same contour for all the choices of x_i in the next steps.[3] Omitting the factors not depending on x_i, the function to which we are applying $\mathcal{D}_{q_2}$ becomes $\prod_{i=1}^{N} f(x_i)$ with

$$f(z) = \frac{q_1 z_1 - z}{z_1 - z} \cdot H(\rho;\, z), \qquad \frac{f(q_2 z)}{f(z)} = \frac{(q_1 z_1 - q_2 z)(z_1 - z)}{(z_1 - q_2 z)(q_1 z_1 - z)} \cdot \frac{H(\rho;\, q_2 z)}{H(\rho;\, z)}.$$

Hence, using Lemma 6.12, renaming $z = z_2$ and noting the restriction on the contours needed to ensure that $\frac{f(q_2 z_2)}{f(z_2)}$ is holomorphic, we get

$$\begin{aligned} \mathcal{D}_{q_2} \mathcal{D}_{q_1} \prod_{i=1}^{N} H(\rho;\, x_i) = \prod_{i=1}^{N} H(\rho;\, x_i) \\ \times \oiint \frac{(q_1 z_1 - q_2 z_2)(z_1 - z_2)}{(z_1 - q_2 z_2)(q_1 z_1 - z_2)} \prod_{k=1}^{2} \left[\prod_{i=1}^{N} \frac{q_k z_k - x_i}{z_k - x_i} \cdot \frac{H(\rho;\, q_k z_k)}{H(\rho;\, z_k)} \cdot \frac{\mathrm{d}z_k}{2\pi \mathbf{i}(q_k - 1) z_k} \right]. \end{aligned}$$

Applying further operators $\mathcal{D}_{q_3}, \dots, \mathcal{D}_{q_K}$, setting $(x_1, \dots, x_N) = (\alpha_1, \dots, \alpha_N)$, and dividing by $\prod_{i=1}^{N} H(\rho;\, \alpha_i)$, we arrive at (6.23). □

Let us now specialize to the measures relevant for the Aztec diamond.

Corollary 6.15. *Consider the Schur measure of Corollary 6.5:*

$$\mathbb{P}(\lambda^{(m)} = \lambda) = (1 + \alpha\beta)^{-m(n+1-m)} s_{\lambda'}\big(\beta^m\big) s_{\lambda}\big(\alpha^{n+1-m}\big). \tag{6.25}$$

[3] Since we further apply various $\mathcal{T}_i^q$ operators, this is where it is convenient to assume that q's are close to 1.

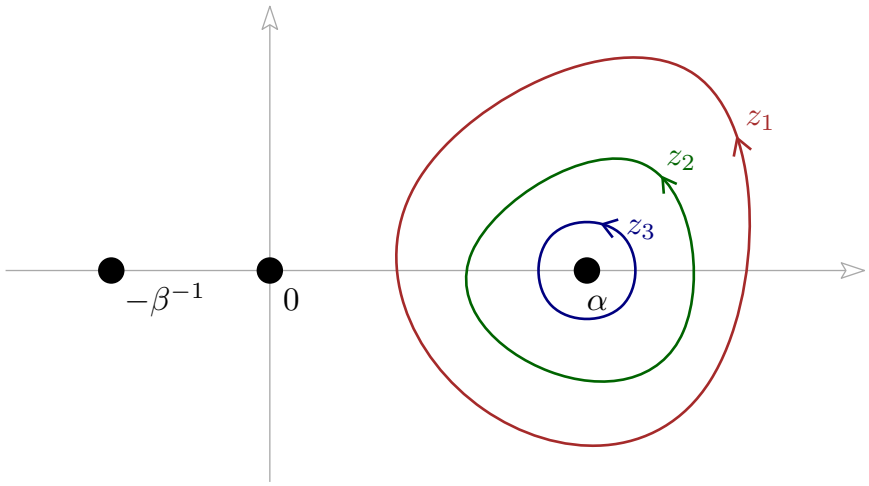


Figure 6.9: Contours in Corollary 6.15 for $K = 3$ and q_1, q_2, q_3 close to 1.

Then, for any complex numbers $q_1, \dots, q_K$ we have

$$\mathbb{E}\left[\prod_{k=1}^{K}\sum_{i=1}^{n+1-m} q_k^{\lambda_i^{(m)}+n+1-m-i}\right] = \oint\!\!\oint \prod_{1\le k<l\le K}\frac{(q_k z_k - q_l z_l)(z_k - z_l)}{(z_k - q_l z_l)(q_k z_k - z_l)} \times \prod_{k=1}^{K}\left[\frac{(q_k z_k-\alpha)^{n+1-m}}{(z_k-\alpha)^{n+1-m}}\cdot\frac{(1+\beta q_k z_k)^m}{(1+\beta z_k)^m}\cdot\frac{\mathrm{d}z_k}{2\pi\mathbf{i}(q_k-1)z_k}\right], \quad (6.26)$$

where $z_1, \dots z_K$ are integrated over positively-oriented loops around α (each of them encloses α, but neither 0, nor $-\beta^{-1}$), which are nested, as in Figure 6.9: for each pair $k < l$, the z_l contour does not *enclose points $\{q_k z_k, q_l^{-1} z_k\}$.*

Proof. For small α, β and q_k close to 1 we directly apply Theorem 6.13. As contours we can choose concentric circles around α, which become smaller with growing k. Note that the measure (6.25) has finite support, hence, we do not have to check convergence of the expectations. Also the condition on convergence of $\sum_{n=1}^{\infty} p_k(\rho)\frac{z_k^n}{n}$ and $\sum_{n=1}^{\infty} p_k(\rho)\frac{(q_k z_k)^n}{n}$ is automatically true. For other values of α, β, and q_k we use an analytic continuation argument, as in the proof of Proposition 5.21. □

6.4 Law of large numbers and the Arctic ellipse

We introduce an encoding of green particles in domino tilings via the height function $h(x, m)$, $m = 1, 2, \dots, n$, $x = 0, 1, 2, \dots, n+1$, defined on the gray squares of the grid and counting the number of particles at (x, m) or below it in the South–East direction along the gray layer m, as in Figure 6.10. Using the bijection with partitions of Proposition 6.1, we have the following.

Definition 6.16. *In the coordinate system, in which x grows North-West and m grows North-East, we define*

$$h(x,m) = \left|(-\infty, x]\bigcap\left\{\lambda_i^{(m)} - i + n - m + 2\right\}_{i=1}^{n+1-m}\right|, \qquad 1 \le m \le n, \quad 0 \le x \le n+1. \quad (6.27)$$

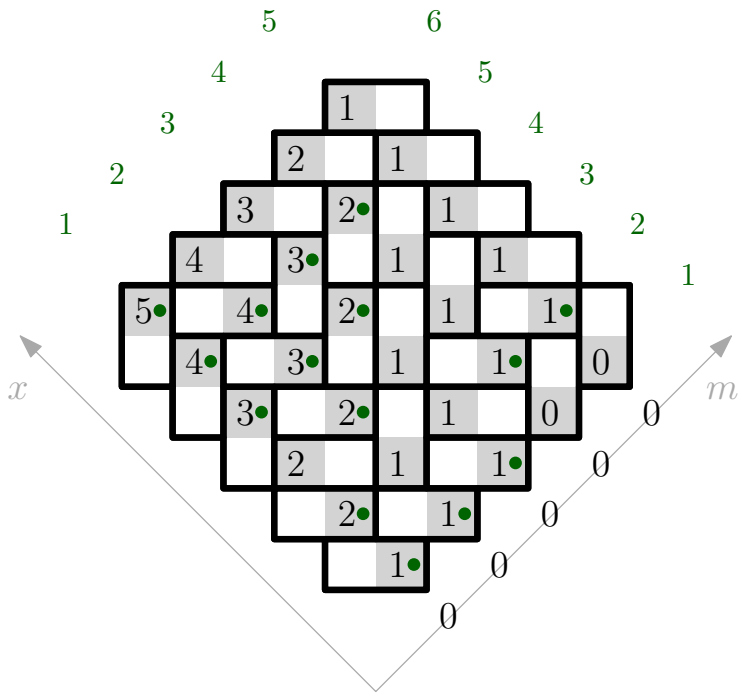


Figure 6.10: Height function encoding green particles.

Clearly, $h(0,m)=0,\ h(n+1,m)=n+1-m$, and

$$h(x,m)-h(x-1,m)=\begin{cases}1, & \text{there is a green particle at } (x,m),\\ 0, & \text{otherwise.}\end{cases} \tag{6.28}$$

We remark that there are several equivalent definitions of the height function in the literature, cf. [Thu90, Ken00, BK18]. All of them differ by explicit deterministic (*i.e.*, not depending on a particular tiling) transformations. The height function contains most (but not all) information about the tiling, as we can reconstruct only green but not orange particles out of it. As $n\to\infty$, the height function concentrates around a deterministic limit.

Theorem 6.17. *Let $h^n(\cdot,\cdot)$ be the height function of $(\alpha\beta)$-weighted random domino tilings of the Aztec diamond of size n, as in* (6.2)*. Then there exists a deterministic 1–Lipshitz function $\mathfrak{h}(\mathbf{x},\mathbf{m})$, $0\le\mathbf{x},\mathbf{m}\le 1$, such that, in probability,*

$$\lim_{n\to\infty}\sup_{\substack{1\le m\le n\\ 0\le x\le n+1}}\left|\frac{1}{n}\,h^n(x,m)-\mathfrak{h}\left(\frac{x}{n},\frac{m}{n}\right)\right|=0. \tag{6.29}$$

The function $\mathfrak{h}(\mathbf{x},\mathbf{m})$ is called the limit shape for the random tilings. It is smooth inside a particular ellipse inscribed in the diamond and linear outside. Let us introduce the ellipse

$$\frac{(\mathbf{x}+\mathbf{m}-1)^2}{p}+\frac{(\mathbf{x}-\mathbf{m})^2}{1-p}=1,\qquad p=\frac{\alpha\beta}{1+\alpha\beta}. \tag{6.30}$$

The center of the ellipse is $(\frac12,\frac12)$ and it is inscribed into the (scaling limit of the) Aztec diamond represented as a unit square with vertices $(0,0)$, $(0,1)$, $(1,0)$, $(1,1)$. Inside the ellipse, we define the density function $0<\rho<1$ (see Figures 6.11 and 6.12) through

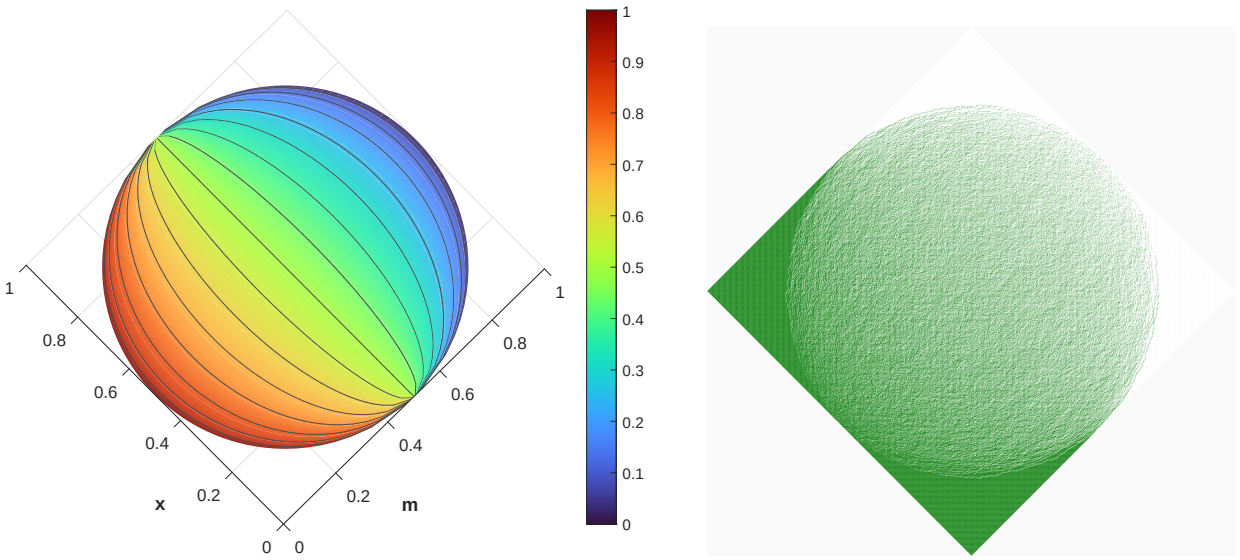


Figure 6.11: Density of green particles for $\alpha\beta = 1$: (6.31) and $n = 1000$ simulation.

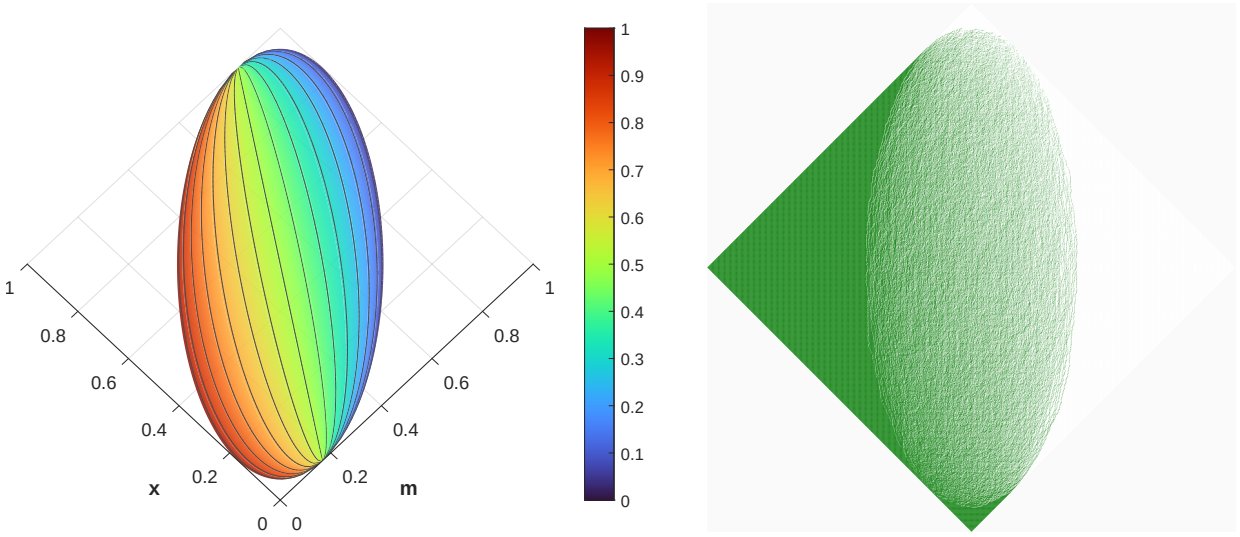


Figure 6.12: Density of green particles for $\alpha\beta = 5$: (6.31) and $n = 1000$ simulation.

$$\rho(\mathbf{x},\mathbf{m}) = \frac{1}{\pi}\,\mathrm{arccot}\left(\frac{\mathbf{m}+\mathbf{x}-1+\alpha\beta(\mathbf{m}-\mathbf{x})}{\sqrt{4\,\alpha\beta\,\mathbf{x}(1-\mathbf{x})-\big[\mathbf{m}+\mathbf{x}-1+\alpha\beta(\mathbf{m}-\mathbf{x})\big]^2}}\right), \tag{6.31}$$

where arccot is the inverse cotangent taking values in $[0,\pi)$.

Theorem 6.18. *The limit shape* $\mathfrak{h}(\mathbf{x},\mathbf{m})$ *of Theorem 6.17 is explicitly determined by boundary conditions*

$\mathfrak{h}(0,\mathbf{m})=0$, $\mathfrak{h}(1,\mathbf{m})=1-\mathbf{m}$, *and its derivative*

$$\frac{\partial}{\partial \mathbf{x}}\mathfrak{h}(\mathbf{x},\mathbf{m})=\begin{cases}\rho(\mathbf{x},\mathbf{m}) & \text{inside the ellipse (6.30),}\\ 0 & \text{near North and East corners outside the ellipse,}\\ 1 & \text{near South and West corners outside the ellipse.}\end{cases} \tag{6.32}$$

The reader might be wondering why we even need to introduce the height function, if eventually all the answers are stated in terms of its x–derivative, which is the density of the green particles. One reason is topological: in terms of the height functions we can have uniform convergence, as in (6.29). In contrast, the discrete x–derivative of $h^n(x,m)$ takes two values $\{0,1\}$, and, therefore, can not converge in probability to a non-trivial limit[4]. When we study fluctuations in the next section, height functions also lead to more transparent asymptotic statements.

We are going to deduce Theorems 6.17 and 6.18 from the expectations delivered by Corollary 6.15 and whose asymptotics is summarized in the following two statements.

Proposition 6.19. *For any* $0<\mathbf{m}<1$ *and* $s\in\mathbb{R}$*, we have*

$$\begin{aligned}\lim_{\substack{m,n\to\infty\\ m/n\to\mathbf{m}}}\mathbb{E}\left[\frac{1}{n}\sum_{i=1}^{n+1-m}\exp\left(s\cdot\frac{1}{n}\left(\lambda_i^{(m)}+n+1-m-i\right)\right)\right]&\\ =\frac{1}{2\pi\mathbf{i}s}\oint\exp\left(s\cdot\left(\frac{(1-\mathbf{m})z}{z-\alpha}+\frac{\beta\mathbf{m}z}{1+\beta z}\right)\right)\frac{\mathrm{d}z}{z}&\\ =\frac{1}{2\pi\mathbf{i}}\oint\left(\frac{\alpha(1-\mathbf{m})}{(z-\alpha)^2}-\frac{\beta\mathbf{m}}{(1+\beta z)^2}\right)\exp\left(s\cdot\left(\frac{(1-\mathbf{m})z}{z-\alpha}+\frac{\beta\mathbf{m}z}{1+\beta z}\right)\right)\ln(z)\mathrm{d}z,&\end{aligned} \tag{6.33}$$

where the integration goes over a positively oriented small loop around α*.*

Proof. Using Corollary 6.15, we study

$$\mathbb{E}\left[\sum_{i=1}^{n+1-m}q^{\lambda_i^{(m)}+n+1-m-i}\right]=\oint\frac{(qz-\alpha)^{n+1-m}}{(z-\alpha)^{n+1-m}}\cdot\frac{(1+\beta qz)^m}{(1+\beta z)^m}\cdot\frac{\mathrm{d}z}{2\pi\mathbf{i}(q-1)z}.$$

We plug in $q=\exp(\frac{s}{n})$ and simplify the integral as $n\to\infty$:

$$\oint\left(1+\frac{\frac{s}{n}z}{z-\alpha}+O\left(\frac{1}{n^2}\right)\right)^{n+1-m}\cdot\left(1+\frac{\beta\frac{s}{n}z}{1+\beta z}+O\left(\frac{1}{n^2}\right)\right)^{m}\cdot\frac{\mathrm{d}z}{2\pi\mathbf{i}\left(\frac{s}{n}+O\left(\frac{1}{n^2}\right)\right)z}. \tag{6.34}$$

Directly taking the $n\to\infty$ limit of the integrand, we arrive at the second line of (6.33). Note that $\frac{s}{n}$ in the last denominator of (6.34) results in $\frac{1}{n}$ normalization in the left-hand side of (6.33). The third line is obtained from the second line via integration by parts. □

Proposition 6.20. *For any* $0<\mathbf{m}<1$ *and* $s\in\mathbb{R}$*, we have*

$$\lim_{\substack{m,n\to\infty\\ m/n\to\mathbf{m}}}\mathrm{Variance}\left[\frac{1}{n}\sum_{i=1}^{n+1-m}\exp\left(s\cdot\frac{1}{n}\left(\lambda_i^{(m)}+n+1-m-i\right)\right)\right]=0.$$

[4]The expectation of the discrete x-derivative, which is the density function of the associated point process, does converge to (6.32), as can be deduced from Proposition 6.19.

Proof. Using Corollary 6.15, we have

$$\mathbb{E}\left[\left(\sum_{i=1}^{n+1-m} q^{\lambda_i^{(m)}+n+1-m-i}\right)^2\right] = \oiint \frac{(qz_1-qz_2)(z_1-z_2)}{(z_1-qz_2)(qz_1-z_2)} \times \prod_{k=1}^{2}\left[\frac{(qz_k-\alpha)^{n+1-m}}{(z_k-\alpha)^{n+1-m}}\cdot\frac{(1+\beta q z_k)^m}{(1+\beta z_k)^m}\cdot\frac{\mathrm{d}z_k}{2\pi\mathbf{i}(q-1)z_k}\right]. \quad (6.35)$$

As $q=\exp(\frac{s}{n})\to 1$ the fraction in the first line of (6.35) goes to 1, and two integration variables z_1 and z_2 decouple. Therefore, the double integral approximates the square of the single integral computed in Proposition 6.19, which implies asymptotic vanishing of the variance. □

The next step is to explain how (6.33) is equivalent to (6.32). For that we rewrite the prelimit expectations in (6.33) in terms of the prelimit height function (6.28):

$$\sum_{i=1}^{n+1-m} q^{\lambda_i^{(m)}+n+1-m-i} = \sum_{x=1}^{n+1} q^x\big[h(x,m)-h(x-1,m)\big]. \quad (6.36)$$

Taking the limit as $n\to\infty$ using (6.33), and omitting a justification for now (it is given at the end of the section), (6.36) becomes

$$\frac{1}{2\pi\mathbf{i}}\oint\left(\frac{\alpha(1-\mathbf{m})}{(z-\alpha)^2}-\frac{\beta\mathbf{m}}{(1+\beta z)^2}\right)\exp\left(s\cdot\left(\frac{(1-\mathbf{m})z}{z-\alpha}+\frac{\beta\mathbf{m}z}{1+\beta z}\right)\right)\ln(z)\mathrm{d}z = \int_0^1 \exp(s\mathbf{x})\frac{\partial}{\partial\mathbf{x}}\mathfrak{h}(\mathbf{x},\mathbf{m})\mathrm{d}x. \quad (6.37)$$

Hence, the left-hand side of (6.37) is a Laplace transform of the function $\frac{\partial}{\partial\mathbf{x}}\mathfrak{h}(\mathbf{x},\mathbf{m})$. In order to reconstruct the function itself, we need to invert the Laplace transform. One way to do it is by using the *Stieltjes transform*, which can be obtained from the Laplace transform by integration:

$$G(u) := \int_0^1 \frac{1}{u-\mathbf{x}}\frac{\partial}{\partial\mathbf{x}}\mathfrak{h}(\mathbf{x},\mathbf{m})\,\mathrm{d}\mathbf{x} = \int_0^1\left[\int_0^\infty \exp(s(\mathbf{x}-u))\mathrm{d}s\right]\frac{\partial}{\partial\mathbf{x}}\mathfrak{h}(\mathbf{x},\mathbf{m})\,\mathrm{d}\mathbf{x}. \quad (6.38)$$

In the last identity, we should assume $\mathrm{Re}(u)>1$ in order to have convergence. However, since $G(u)$ is a holomorphic function of $u\in\mathbb{C}\setminus[0,1]$, once we find a formula for this function for $\mathrm{Re}(u)>1$, we can extend to other z by uniqueness of analytic continuation.

Lemma 6.21. *Assuming* (6.37)*, we have for* $u\in\mathbb{C}\setminus[0,1]$

$$G(u)=\ln\left[\frac{\mathbf{m}+u-1+\alpha\beta(\mathbf{m}-u)-\sqrt{\big[\mathbf{m}+u-1+\alpha\beta(\mathbf{m}-u)\big]^2-4\,\alpha\beta\,u(1-u)}}{2\alpha\beta(1-u)}\right], \quad (6.39)$$

where we choose the branches of $\sqrt{\cdot}$ *and* $\ln(\cdot)$ *mapping large positive numbers to large positive numbers.*

Proof. Changing the order of integration in (6.38) and using (6.37), we get an integral formula for $G(u)$:

$$\frac{1}{2\pi\mathbf{i}}\oint\left[\int_0^\infty\left(\frac{\alpha(1-\mathbf{m})}{(z-\alpha)^2}-\frac{\beta\mathbf{m}}{(1+\beta z)^2}\right)\exp\left(s\cdot\left(\frac{(1-\mathbf{m})z}{z-\alpha}+\frac{\beta\mathbf{m}z}{1+\beta z}-u\right)\right)\mathrm{d}s\right]\ln(z)\mathrm{d}z = \frac{1}{2\pi\mathbf{i}}\oint\frac{-\frac{\alpha(1-\mathbf{m})}{(z-\alpha)^2}+\frac{\beta\mathbf{m}}{(1+\beta z)^2}}{\frac{(1-\mathbf{m})z}{z-\alpha}+\frac{\beta\mathbf{m}z}{1+\beta z}-u}\ln(z)\mathrm{d}z. \quad (6.40)$$

Let us explain the proper choice of the integration contour, which makes the last formula valid. If we choose the contour to be a very small loop around α, as in (6.33), then $\operatorname{Re}\left(\frac{(1-\mathbf{m})z}{z-\alpha}+\frac{\beta\mathbf{m}z}{1+\beta z}-u\right)$ would have different signs on different parts of the contour, and the integral $\int_0^\infty$ in (6.40) would be divergent. Instead, we choose some small $0<\varepsilon<\alpha$ and let the contour be a vertical line $\operatorname{Re}(z)=\varepsilon$, oriented from top to bottom — we make transformations (6.40) on this contour. The formula in the last line of (6.33) is still valid on such a contour, because the integrand decays when $z\to\infty$ as $\frac{\ln|z|}{|z|^2}$ and therefore has no residue at $z=\infty$. On this new contour, as long as $\operatorname{Re}(u)$ is large enough, we would have

$$\operatorname{Re}\left(\frac{(1-\mathbf{m})z}{z-\alpha}+\frac{\beta\mathbf{m}z}{1+\beta z}-u\right)<0,$$

and therefore the evaluation in (6.40) is valid. The contour integral in (6.40) then evaluates as the sum of the residues at two simple poles: at $z=\alpha$ and at z solving the equation

$$\frac{(1-\mathbf{m})z}{z-\alpha}+\frac{\beta\mathbf{m}z}{1+\beta z}-u=0. \tag{6.41}$$

Note that this is a quadratic equation. For large u the equation has two solutions, one is close to $-\frac{1}{\beta}$ and the other one is close to α. We need the latter one. Denoting this solution

$$z(u):=\frac{\mathbf{m}+u-1+\alpha\beta(\mathbf{m}-u)-\sqrt{\big[\mathbf{m}+u-1+\alpha\beta(\mathbf{m}-u)\big]^2-4\,\alpha\beta\,u(1-u)}}{2\beta(1-u)},$$

the final answer is

$$G(u)=-\ln(\alpha)+\ln(z(u)).$$

As a consistency check, note that $G(u)\to 0$ as $u\to\infty$, as it should from the definition (6.38). □

The Stieltjes transform can be used to reconstruct the underlying density by a direct limit.

Lemma 6.22. *Let $0\le\mu(x)\le 1$ be a density of a finite measure μ on the interval $x\in[0,1]$ and let $G_\mu(u)$ be its Stieltjes transform:*

$$G_\mu(u)=\int_0^1\frac{\mu(x)}{u-x}\mathrm{d}x. \tag{6.42}$$

Define, for each $\varepsilon>0$, a measure μ_ε on $\mathbb{R}$ with density

$$\mu_\varepsilon(x)=-\frac{1}{\pi}\operatorname{Im}\big(G_\mu(x+\mathbf{i}\varepsilon)\big),\qquad x\in\mathbb{R}. \tag{6.43}$$

Then as $\varepsilon\to 0$ the measures μ_ε weakly converge to μ.

Remark 6.23. When all the densities are continuous functions of x, we have $\mu(x)=\lim\limits_{\varepsilon\to 0+}\mu_\varepsilon(x)$.

Proof of Lemma 6.22. Rescaling the measure, if necessary, we can assume that $\int_0^1\mu(x)\mathrm{d}x=1$, *i.e.*, μ is a probability measure. Directly from definition, we have

$$-\frac{1}{\pi}\operatorname{Im}\big(G(x+\mathbf{i}\varepsilon)\big)=\int_0^1\frac{1}{\pi}\cdot\frac{\varepsilon}{\varepsilon^2+(x-y)^2}\mu(y)\mathrm{d}y. \tag{6.44}$$

Let ξ be a Cauchy–distributed random variable (*i.e.*, of density $\frac{1}{\pi(1+x^2)}\mathrm{d}x$), and let η be μ–distributed. Then the right-hand side of (6.44) can be interpreted as the convolution of η and $\varepsilon\xi$, *i.e.*, the density of the sum of independent $\eta+\varepsilon\xi$. Hence, the statement becomes a straightforward $\lim_{\varepsilon\to 0}(\eta+\varepsilon\xi)=\eta$.

Alternatively, note that the function $y\mapsto\frac{1}{\pi}\cdot\frac{\varepsilon}{\varepsilon^2+(x-y)^2}$ is sharply concentrated near $y=x$ and integrates to 1. Hence, at each point x of continuity of $\mu(\cdot)$, (6.44) converges towards $\mu(x)$ as $\varepsilon\to 0+$. □

Corollary 6.24. *If $G(u)$ is given by* (6.38), (6.39)*, then the corresponding $\frac{\partial}{\partial \mathbf{x}}\mathfrak{h}(\mathbf{x},\mathbf{m})$ is given by* (6.32).

Proof. By Lemma 6.22, we need to compute $-\frac{1}{\pi}\lim_{\varepsilon\to 0+}\operatorname{Im}\big(G(x+\mathbf{i}\varepsilon)\big)$. This boils down to plugging into (6.39) the real value of $u=x$ leading to three cases:

- If the argument of $\ln[\cdot]$ is non-real, then the imaginary part of the logarithm is the complex argument, computed via cotangent in (6.31).
- If the argument of $\ln[\cdot]$ is real positive, then the imaginary part vanishes.
- If the argument of $\ln[\cdot]$ is real negative, then the imaginary part is $-\pi$.

These are precisely the three cases in (6.32). □

Proof of Theorems 6.17 and 6.18. For a fixed m, we let $\nu^{(m)}$ denote the empirical measure of green particles at layer m, shifted by 1 and rescaled by n:

$$\nu^{(m)}=\frac{1}{n}\sum_{i=1}^{n+1-m}\delta_{\frac{1}{n}[\lambda_i^{(m)}+n+1-m-i]}$$

The height function can be identified with the distribution function of $\nu^{(m)}$ shifted by $\frac{1}{n}$:

$$\frac{1}{n}h^n(x,m)=\nu^{(m)}\left(\left(-\infty,\frac{x-1}{n}\right]\right). \tag{6.45}$$

On the other hand, the random variables in Proposition 6.19 and 6.20 are integrals against these measures:

$$\frac{1}{n}\sum_{i=1}^{n+1-m}\exp\left(s\cdot\frac{1}{n}\left(\lambda_i^{(m)}+n+1-m-i\right)\right)=\int_0^1\exp(sx)\,\nu^{(m)}(\mathrm{d}x). \tag{6.46}$$

By Propositions 6.19 and 6.20, all expectations (6.46) converge to deterministic limits. Hence (*e.g.*, because the functions $x\to\exp(sx)$ are dense in the space of all continuous function on $[0,1]$), the random empirical measures $\nu^{(\mathbf{m}n)}$ converge as $n\to\infty$ (weakly, in probability) to deterministic limits $\tilde{\nu}^{(\mathbf{m})}$. Since $\nu^{(m)}$ satisfy

$$\nu^{(m)}([a,b])\le b-a+\frac{1}{n},$$

the limits $\tilde{\nu}^{(\mathbf{m})}$ are non-negative measures absolutely continuous with respect to the Lebesgue measure and of density at most 1. The Laplace transform of the limiting measure is computed by (6.37), and therefore Corollary 6.24 identifies the density of $\tilde{\nu}^{(\mathbf{m})}$ with $\frac{\partial}{\partial \mathbf{x}}\mathfrak{h}(\mathbf{x},\mathbf{m})$ computed by (6.32).

Since convergence of measures implies convergence of their distribution functions (at the points of continuity of the limiting functions but in our case the limit is differentiable and therefore continuous), we conclude that, in probability,

$$\lim_{n\to\infty}\frac{1}{n}h^n\left(\lfloor n\mathbf{x}\rfloor,\lfloor n\mathbf{m}\rfloor\right)=\mathfrak{h}(\mathbf{x},\mathbf{m}). \tag{6.47}$$

Because the right-hand side is deterministic, (6.47) also holds jointly over finitely many pairs $(\mathbf{x},\mathbf{m})$. In order to get (6.29), we need to upgrade to joint convergence over *all* $(\mathbf{x},\mathbf{m})\in[0,1]^2$. For this, we observe that $h(x,m)$ is a Lipshitz function, in the sense that

$$\left|\frac{1}{n}h^n(x,m)-\frac{1}{n}h^n(x',m')\right|\le\left|\frac{x}{n}-\frac{x'}{n}\right|+\left|\frac{m}{n}-\frac{m'}{n}\right|.$$

Hence, covering $[0,1]^2$ by a finite net of arbitrary small mesh-size, (6.47) implies (6.29). □

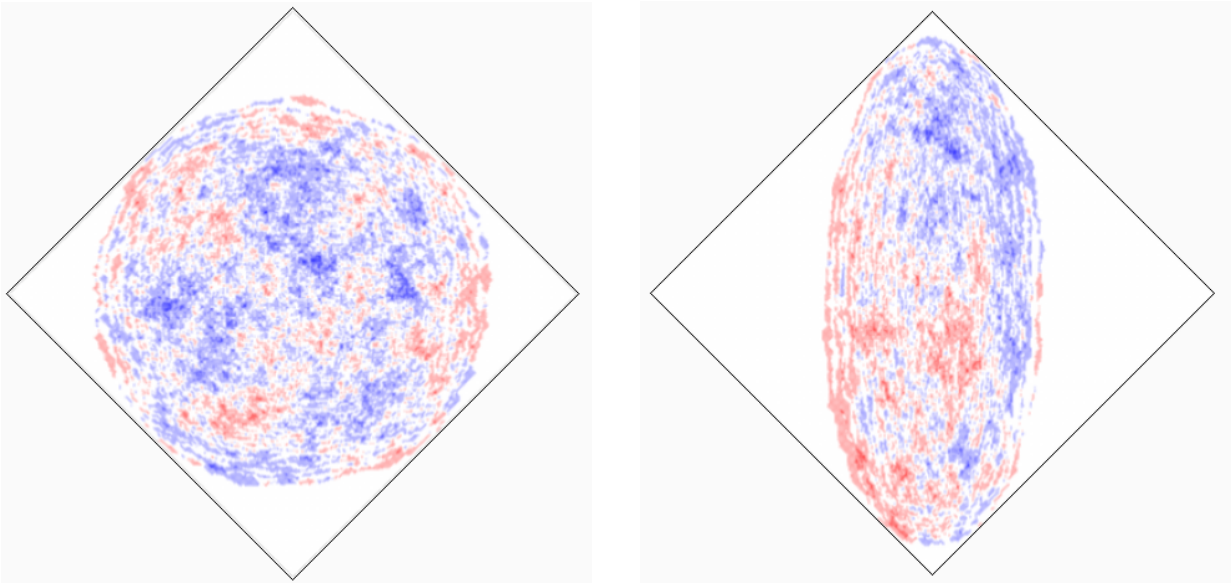


Figure 6.13: Field of height fluctuations for $n = 200$ Aztec diamond for $\alpha\beta = 1$ and $\alpha\beta = 5$. Red and blue colors indicate positive and negative values, respectively.

6.5 Field of fluctuations for the height function

Theorem 6.17 tells us that the height functions $\frac{1}{n}h(x, m)$ concentrate near a deterministic limit as $n \to \infty$, and therefore the fluctuations of $h(x, m)$ are $o(n)$. In fact, these fluctuations are much smaller — they are essentially finite. Figure 6.13 is an approximation of the field of fluctuations $h(\mathbf{x}n, \mathbf{m}n) - \mathbb{E}h(\mathbf{x}n, \mathbf{m}n)$, $(\mathbf{x}, \mathbf{m}) \in [0, 1]^2$, obtained by sampling two independent copies h, h' of the height function and drawing $\frac{1}{\sqrt{2}}(h(\mathbf{x}n, \mathbf{m}n) - h'(\mathbf{x}n, \mathbf{m}n))$. The subtraction achieves cancelling of the (large) expectation term, while division by $\sqrt{2}$ guarantees that the covariance structure of the difference is the same as for the individual fields.

It is clear from the simulation that the field of fluctuations is non-trivial only in the liquid region inside the inscribed ellipse (6.30). In the frozen regions outside the ellipse fluctuations vanish. The field of asymptotic fluctuations is known as the two-dimensional *Gaussian free field* (GFF) — a remarkable conformally invariant object. GFF is a *generalized* field: its covariance function has $\ln(z - w)$–type singularity on the diagonal $z = w$, and the values of GFF at individual points are not well-defined. Instead, a proper object of study is integrals of GFF against sufficiently smooth test-measures: such integrals for the field $h(\mathbf{x}n, \mathbf{m}n) - \mathbb{E}h(\mathbf{x}n, \mathbf{m}n)$ are asympotically Gaussian and converge in distribution towards similar integrals for GFF. In contrast, the individual values of $h(\mathbf{x}n, \mathbf{m}n) - \mathbb{E}h(\mathbf{x}n, \mathbf{m}n)$ can be shown to grow as $\sqrt{\ln(n)}$ and become asymptotically Gaussian and independent (over distinct values of $(\mathbf{x}, \mathbf{m})$) upon proper rescaling, see [BF14] for a similar theorem and [CL95, Sos00b] for a general CLT often used for proving such results.

We first provide one partial result about the convergence towards the Gaussian free field, which captures the marginal of the field for fixed $\mathbf{m}$. In the next two sections we discuss what GFF is and upgrade this result to a convergence statement for the full 2d field.

Theorem 6.25. *Under the measure* (6.2)*, and using the bijection of Proposition 6.1, consider the partition* $\lambda^{(m)}$ *encoding the green particles in the* m*th gray layer. For any* $0 < \mathbf{m} < 1$ *and* $s_1, \dots, s_K \in \mathbb{R}$*, the*

random variables

$$\sum_{i=1}^{n+1-m} \exp\left(s_k \cdot \frac{1}{n}\left(\lambda_i^{(m)} + n + 1 - m - i\right)\right) - \mathbb{E}\sum_{i=1}^{n+1-m} \exp\left(s_k \cdot \frac{1}{n}\left(\lambda_i^{(m)} + n + 1 - m - i\right)\right), \tag{6.48}$$

converge (in joint distribution over $1 \le k \le K$ and in the sense of moments) as $m, n \to \infty$ in such a way that $\frac{m}{n} \to \mathbf{m}$, to a mean 0 Gaussian vector with covariance of the kth and lth coordinates given by

$$\frac{1}{(2\pi\mathbf{i})^2} \oiint \exp\left(s_k\left(\frac{(1-\mathbf{m})z_k}{z_k - \alpha} + \frac{\beta\mathbf{m}z_k}{1+\beta z_k}\right)\right) \exp\left(s_l\left(\frac{(1-\mathbf{m})z_l}{z_l - \alpha} + \frac{\beta\mathbf{m}z_l}{1+\beta z_l}\right)\right) \frac{\mathrm{d}z_k \mathrm{d}z_l}{(z_k - z_l)^2}, \tag{6.49}$$

where both contours are small positively oriented loops around α, with one being inside another one.

Using (6.36) or (6.45), (6.46) we can rewrite (6.48) as integrals against an x-derivative (or its difference version) of the height function $h(x, m)$. Integration by parts then converts (6.48) into an integral of $h(x, m) - \mathbb{E}h(x, m)$ against a test-measure, which is supported on the line of fixed m and has exponential density in x–direction. Hence, Theorem 6.25 can be interpreted as convergence of pairings of the centered height function with such specific test-measures.

Integrating (6.48) over s_k with various weights, one can see that Theorem 6.25 implies asymptotic Gaussianity and formulas for the covariance for a wide class of centered linear statistics

$$\sum_{i=1}^{n+1-m} f\left(\frac{1}{n}\left(\lambda_i^{(m)} + n + 1 - m - i\right)\right) - \mathbb{E}\sum_{i=1}^{n+1-m} f\left(\frac{1}{n}\left(\lambda_i^{(m)} + n + 1 - m - i\right)\right)$$

for smooth test-functions $f(x)$.

Similar asymptotic phenomenology can be found for other stochastic systems considered in this book. For instance, the distance between the broken line describing the boundary of Plancherel-random Young diagrams and Vershik-Kerov-Logan-Schepp limit shape can also be described (in the bulk, cf. Figure 5.2) by a generalized Gaussian field, see [Ker93, IO02]. The full two-dimensional Gaussian free field can be seen by considering the Plancherel growth process (5.51), see [Rap25] for further details.

Proof of Theorem 6.25. We start by analyzing the covariance. Using Corollary 6.15, we have

$$\mathbb{E}\left[\sum_{i=1}^{n+1-m} q_k^{\lambda_i^{(m)}+n+1-m-i} \sum_{i=1}^{n+1-m} q_l^{\lambda_i^{(m)}+n+1-m-i}\right] = \oiint \frac{(q_k z_k - q_l z_l)(z_k - z_l)}{(z_k - q_l z_l)(q_k z_k - z_l)}$$
$$\times \frac{(q_k z_k - \alpha)^{n+1-m}}{(z_k - \alpha)^{n+1-m}} \cdot \frac{(1+\beta q_k z_k)^m}{(1+\beta z_k)^m} \cdot \frac{(q_l z_l - \alpha)^{n+1-m}}{(z_l - \alpha)^{n+1-m}} \cdot \frac{(1+\beta q_l z_l)^m}{(1+\beta z_l)^m} \cdot \frac{\mathrm{d}z_k}{2\pi\mathbf{i}(q_k - 1)z_k} \cdot \frac{\mathrm{d}z_l}{2\pi\mathbf{i}(q_l - 1)z_l}. \tag{6.50}$$

We plug in $q_l = \exp\left(\frac{s_k}{n}\right)$, $q_l = \exp\left(\frac{s_l}{n}\right)$ and notice that

$$\frac{(q_k z_k - q_l z_l)(z_k - z_l)}{(z_k - q_l z_l)(q_k z_k - z_l)} = 1 + \frac{z_k z_l (1 - q_k)(1 - q_l)}{(z_k - q_l z_l)(q_k z_k - z_l)} = 1 + \frac{s_k s_l}{n^2} \cdot \frac{z_k z_l}{(z_k - z_l)^2} + O\left(\frac{1}{n^3}\right). \tag{6.51}$$

Hence, subtracting the product of two applications of Corollary 6.15 with $K = 1$ and using the same

asymptotic expansion as in (6.34), we get, as $n \to \infty$,

$$\operatorname{Cov}\left[\sum_{i=1}^{n+1-m} q_k^{\lambda_i^{(m)}+n+1-m-i}, \sum_{i=1}^{n+1-m} q_l^{\lambda_i^{(m)}+n+1-m-i}\right] \to C_{k,l}$$
$$= \frac{1}{(2\pi\mathbf{i})^2} \oiint \exp\left(s_k\left(\frac{(1-\mathbf{m})z_k}{z_k-\alpha}+\frac{\beta\mathbf{m}z_k}{1+\beta z_k}\right)\right)\exp\left(s_l\left(\frac{(1-\mathbf{m})z_l}{z_l-\alpha}+\frac{\beta\mathbf{m}z_l}{1+\beta z_l}\right)\right)\frac{\mathrm{d}z_k\mathrm{d}z_l}{(z_k-z_l)^2}. \tag{6.52}$$

For the asymptotic Gaussianity, we compute higher moments of centered random variables (6.48). We take some $s_1, \dots, s_K$, which are allowed to coincide with each other, and let $q_k = \exp\left(\frac{s_k}{n}\right)$, $1 \le k \le K$. Using Corollary 6.15 for each of 2^K terms in the expansion of the product,

$$\mathbb{E}\prod_{k=1}^{K}\left[\sum_{i=1}^{n+1-m}\left[\exp\left(s_k\cdot\frac{1}{n}\left(\lambda_i^{(m)}+n+1-m-i\right)\right)-\mathbb{E}\exp\left(s_k\cdot\frac{1}{n}\left(\lambda_i^{(m)}+n+1-m-i\right)\right)\right]\right]$$
$$= \oint\dots\oint \sum_{A\subset\{1,2,\dots,K\}}(-1)^{K-|A|}\prod_{k<l:\,k,l\in A}\frac{(q_kz_k-q_lz_l)(z_k-z_l)}{(z_k-q_lz_l)(q_kz_k-z_l)}$$
$$\times\prod_{k=1}^{K}\left[\frac{(q_kz_k-\alpha)^{n+1-m}}{(z_k-\alpha)^{n+1-m}}\cdot\frac{(1+\beta q_kz_k)^m}{(1+\beta z_k)^m}\cdot\frac{\mathrm{d}z_k}{2\pi\mathbf{i}(q_k-1)z_k}\right], \tag{6.53}$$

where the subset A corresponds to the indices in the product in the first line for which we choose the first rather than the second term in the factor, and therefore only for the indices in A we have the crossterm $\prod_{k<l:k,l\in A}$. Using the first equality in (6.51), the sum in the second line of (6.53) further becomes

$$\sum_{A\subset\{1,2,\dots,K\}}\sum_{B\subset A^{(2)}}(-1)^{K-|A|}\prod_{(k,l)\in B}\frac{z_kz_l(1-q_k)(1-q_l)}{(z_k-q_lz_l)(q_kz_k-z_l)}, \tag{6.54}$$

where $A^{(2)}$ is the set of ordered pairs of elements of A: $A^{(2)} = \{(i,j) \mid i<j,\ \ i,j\in A\}$. We change the order of summation in (6.54) — sum over A for a fixed B and then send $n\to\infty$. We claim that the only surviving terms are those where $|B| = K/2$ and B is a perfect matching of A, *i.e.*, a set partition representing it as a disjoint union of two element sets; in particular, for odd K the limit is 0. In order to see that, we denote by $B^{(1)} \subset \{1,\dots,K\}$ the subset of all elements which appear as either first or second coordinates in pairs of B and observe:

- If $|B^{(1)}| < K$ then, after factoring out common terms, the sum over A becomes a sum of ±1 over all $B^{(1)} \subset A \subset \{1,\dots,K\}$, which evaluates, via the binomial theorem, to $(1-1)^{K-|B^{(1)}|} = 0$.
- If $|B| < \frac{K}{2}$, then necessarily $|B^{(1)}| < K$ and the corresponding term vanishes.
- If $|B| > \frac{K}{2}$, then $\prod$ in the corresponding (6.54) term is $o(n^{-K})$ because of the $(1-q_j)$ factors. Since the third line of (6.53) is $O(n^K)$ because of the (q_k-1) denominators, the overall contribution vanishes as $n\to\infty$.
- If $|B| = \frac{K}{2}$ and $|B^{(1)}| = K$, then K has to be even, B must be a perfect matching, hence, $A = \{1,2,\dots,K\}$.

When B is a perfect matching, the K–dimensional integral in (6.53) splits into a product of $K/2$ two-dimensional integrals of the form (6.52). Therefore, the $n \to \infty$ limit of (6.53) evaluates as

$$\sum_{\substack{B \text{ is a perfect matching} \\ \text{of } \{1,2,\dots,K\}}} \prod_{(k,l)\in B} C_{k,l}.$$

We arrive at the expression for the higher moments of mean zero Gaussian random variables in terms of their covariance known as Isserlis theorem or Wick's formula, see [Iss18, Wic50, MS17]. Hence, the random variables (6.48) converge in the sense of moments to Gaussian random variables. Convergence of moments also implies convergence in distribution, since Gaussians are uniquely determined by their moments, see, *e.g.*, [Bil12, Section 30]. □

6.6 Multilevel observables

The goal of this and the next section is prove the convergence of the centered height function to the Gaussian free field by generalizing Theorem 6.25 to joint fluctuations for several $\mathbf{m}$ and interpreting the result in terms of GFF.

Note that up to now we have never dealt with joint fluctuations of more than one Young diagram: we could analyze Schur measures of Definition 3.4, but not Schur processes of Definition 3.5. In fact, many of our tools can be generalized in this direction. For instance, if we combine all partitions of the Schur process into a point process in the plane (or, rather, in $\mathbb{Z}\times\mathbb{Z}$), it is going to be determinantal with a correlation kernel given by a double contour integral, see [OR03, BR05] and Problem 8 in Section 4.6. Same is true for the expectations of observables in Theorem 6.13. We demonstrate this on the example of the Schur process corresponding to the Aztec diamond and refer to [BCGS16] for the most general Schur processes.

Theorem 6.26. *Consider the $(\alpha\beta)$-weighted measure on domino tilings* (6.2) *corresponding to the Schur process as in Theorem 6.3:*

$$\varnothing \prec' \lambda^{(1)} \succ \mu^{(1)} \prec' \lambda^{(2)} \succ \cdots \succ \mu^{(n-1)} \prec' \lambda^{(n)} \succ \varnothing. \tag{6.55}$$

Then, for any $1 \le m_1 \le m_2 \le \cdots \le m_K \le n$ and complex numbers $q_1, \dots, q_K$ we have

$$\mathbb{E}\left[\prod_{k=1}^{K}\sum_{i=1}^{n+1-m_k} q_k^{\lambda_i^{(m_k)}+n+1-m_k-i}\right] = \oint\cdots\oint \prod_{1\le k<l\le K}\frac{(q_k z_k - q_l z_l)(z_k - z_l)}{(z_k - q_l z_l)(q_k z_k - z_l)} \times \prod_{k=1}^{K}\left[\frac{(q_k z_k-\alpha)^{n+1-m_k}}{(z_k-\alpha)^{n+1-m_k}}\cdot\frac{(1+\beta q_k z_k)^{m_k}}{(1+\beta z_k)^{m_k}}\cdot\frac{\mathrm{d}z_k}{2\pi\mathbf{i}(q_k-1)z_k}\right], \tag{6.56}$$

where $z_1, \dots, z_K$ are integrated over positively-oriented loops around α (each of them encloses α, but neither 0, nor $-\beta^{-1}$), which are nested: for each pair $k<l$, the z_l contour does not *enclose points $\{q_k z_k, q_l^{-1} z_k\}$.*

Compared to Corollary 6.15, each m got replaced by m_k, but we emphasize the ordering of m_k: in the proof we apply operators in different collections of variables; these operators do not commute and the exact sequence of applications matters.

Proof of Theorem 6.26. We need a generalization of the expectation identity (6.21) based on operators acting in varying numbers of variables. We introduce an N–variable version of (6.17), with only $x_1, \dots, x_N$

variables involved in the formula, but allowing this operator to act on functions in a greater number of variables:

$$\mathcal{D}_q^N = \sum_{i=1}^{N} \left[\prod_{\substack{j\in\{1,\dots,N\}\\ j\neq i}} \frac{qx_i - x_j}{x_i - x_j} \right] \mathcal{T}_i^q. \tag{6.57}$$

Then the key identity is that for ordered $1 \leq m_1 \leq m_2 \leq \cdots \leq m_K \leq n$,

$$\mathbb{E}\left[\prod_{k=1}^{K} \sum_{i=1}^{n+1-m_k} q_k^{\lambda_i^{(m_k)}+n+1-m_k-i} \right] = \left[\mathcal{D}_{q_K}^{n+1-m_K} \prod_{i=1}^{n} \left(\frac{1+\beta x_i}{1+\alpha\beta} \right)^{m_K-m_{K-1}} \mathcal{D}_{q_{K-1}}^{n+1-m_{K-1}} \cdots \right.$$
$$\left. \cdots \mathcal{D}_{q_2}^{n+1-m_2} \prod_{i=1}^{n} \left(\frac{1+\beta x_i}{1+\alpha\beta} \right)^{m_2-m_1} \mathcal{D}_{q_1}^{n+1-m_1} \prod_{i=1}^{n} \left(\frac{1+\beta x_i}{1+\alpha\beta} \right)^{m_1} \right]_{x_1=\cdots=x_n=\alpha}. \tag{6.58}$$

Once (6.58) is proven, (6.56) is obtained from it by recursive applications of Lemma 6.12 in exactly the same way as in the proof of Theorem 6.13. Hence, in the rest of the proof we only explain (6.58). The idea is that in the up-down chain encoding the Schur process (6.55), in the language of symmetric functions the $\prec'$ steps get encoded by multiplication with $\prod_i \left(\frac{1+\beta x_i}{1+\alpha\beta}\right)$, while $\succ$ steps get encoded by plugging in one variable equal to α. The argument is the same for any $K > 1$, and we detail it for $K = 2$, *i.e.*, we show

$$\mathbb{E}\left[\sum_{i=1}^{n+1-m_2} q_2^{\lambda_i^{(m_2)}+n_2+1-m-i} \sum_{i=1}^{n+1-m_1} q_1^{\lambda_i^{(m_1)}+n+1-m_1-i} \right]$$
$$= \left[\mathcal{D}_{q_2}^{n+1-m_2} \prod_{i=1}^{n} \left(\frac{1+\beta x_i}{1+\alpha\beta} \right)^{m_2-m_1} \mathcal{D}_{q_1}^{n+1-m_1} \prod_{i=1}^{n} \left(\frac{1+\beta x_i}{1+\alpha\beta} \right)^{m_1} \right]_{x_1=\cdots=x_n=\alpha}. \tag{6.59}$$

We start by using the Cauchy identity (2.17) in $x_1, \dots, x_{n+1-m_1}$ and with y–variables specialized using $\rho = (0; \beta^{m_1}; 0)$:

$$\prod_{i=1}^{n} \left(\frac{1+\beta x_i}{1+\alpha\beta} \right)^{m_1} = \prod_{i=n+2-m_1}^{n} \left(\frac{1+\beta x_i}{1+\alpha\beta} \right)^{m_1}$$
$$\times (1+\alpha\beta)^{-m_1(n+1-m_1)} \left[\sum_{\lambda^{(m_1)}} s_{\lambda^{(m_1)}}(x_1, \dots, x_{n+1-m_1}) s_{\lambda^{(m_1)}}(0; \beta^{m_1}; 0) \right].$$

None of the operators will act on the variables in $\prod_{i=n+2-m_1}^{n}$, this factor will disappear when we plug in $x_i = \alpha$, and we can ignore it. Hence, using the eigenrelation (6.18), we have

$$\mathcal{D}_{q_1}^{n+1-m_1} \prod_{i=1}^{n} \left(\frac{1+\beta x_i}{1+\alpha\beta} \right)^{m_1} = \prod_{i=n+2-m_1}^{n} \left(\frac{1+\beta x_i}{1+\alpha\beta} \right)^{m_1}$$
$$\times (1+\alpha\beta)^{-m_1(n+1-m_1)} \left[\sum_{\lambda^{(m_1)}} \left(\sum_{i=1}^{n+1-m_1} q_1^{\lambda_i^{(m_1)}+n+1-m_1-i} \right) s_{\lambda^{(m_1)}}(x_1, \dots, x_{n+1-m_1}) s_{\lambda^{(m_1)}}(0; \beta^{m_1}; 0) \right]. \tag{6.60}$$

We proceed by using the definition of the skew Schur functions (2.28) and skew Cauchy identity (2.34) with y–variables specialized using $\rho = (0; \beta^{m_2-m_1}; 0)$ in the form:

$$s_{\lambda^{(m_1)}}(x_1, \dots, x_{n+1-m_1}) = \sum_{\mu} s_{\mu}(x_1, \dots, x_{n+1-m_2}) s_{\lambda^{(m_1)}/\mu}(x_{n+2-m_2}, \dots, x_{n+1-m_1}),$$

$$\prod_{i=1}^{n+1-m_2} (1+\beta x_i)^{m_2-m_1} s_{\mu}(x_1, \dots, x_{n+1-m_2}) = \sum_{\lambda^{(m_2)}} s_{\lambda^{(m_2)}}(x_1, \dots, x_{n+1-m_2}) s_{\lambda^{(m_2)}/\mu}(0; \beta^{m_2-m_1}; 0).$$

We plug these two identities into the right-hand side of (6.60), apply $\mathcal{D}_{q_2}^{n+1-m_2}$ using the eigenrelation (6.18), and set all x_i equal to α to get:

$$\begin{aligned}
&\left[\mathcal{D}_{q_2}^{n+1-m_2} \prod_{i=1}^{n} \left(\frac{1+\beta x_i}{1+\alpha\beta} \right)^{m_2-m_1} \mathcal{D}_{q_1}^{n+1-m_1} \prod_{i=1}^{n} \left(\frac{1+\beta x_i}{1+\alpha\beta} \right)^{m_1} \right]_{x_1=\cdots=x_n=\alpha} \\
&\qquad = \sum_{\lambda^{(m_2)},\, \mu,\, \lambda^{(m_1)}} \left[\sum_{i=1}^{n+1-m_2} q_2^{\lambda_i^{(m_2)}+n+1-m_2-i} \sum_{i=1}^{n+1-m_1} q_1^{\lambda_i^{(m_1)}+n+1-m_1-i} \right] \\
&\qquad \times \frac{s_{\lambda^{(m_1)}}(0; \beta^{m_1}; 0) s_{\lambda^{(m_1)}/\mu}(\alpha^{m_2-m_1}; 0; 0) s_{\lambda^{(m_2)}/\mu}(0; \beta^{m_2-m_1}; 0) s_{\lambda^{(m_2)}}(\alpha^{n+1-m_2}; 0; 0)}{(1+\alpha\beta)^{m_1(n+1-m_1)+(m_2-m_1)(n+1-m_2)}}.
\end{aligned}$$

Comparing with (3.22) from the exercises in Chapter 3, we recognize the expectation from the left-hand side of (6.59). □

We can now prove a multilevel version of Theorem 6.25.

Theorem 6.27. *Under the measure* (6.2) *and using the bijection of Proposition 6.1, consider the partition* $\lambda^{(m)}$ *encoding the green particles in the* m*th gray layer. For any* $0 < \mathbf{m}_1 \le \mathbf{m}_2 \le \cdots \le \mathbf{m}_K < 1$ *and* $s_1, \dots, s_K \in \mathbb{R}$*, the random variables*

$$\sum_{i=1}^{n+1-m_k} \exp\left(s_k \cdot \frac{1}{n} \left(\lambda_i^{(m_k)} + n + 1 - m_k - i \right) \right) - \mathbb{E} \sum_{i=1}^{n+1-m_k} \exp\left(s_k \cdot \frac{1}{n} \left(\lambda_i^{(m_k)} + n + 1 - m_k - i \right) \right) \tag{6.61}$$

converge (in joint distribution over $1 \le k \le K$ *and in the sense of moments) as* $m_1, \dots, m_K, n \to \infty$ *in such a way that* $\frac{m_k}{n} \to \mathbf{m}_k$*,* $1 \le k \le K$*, to a mean* 0 *Gaussian vector with covariance of the* k*th and* l*th coordinates given for* $k < l$ *by*

$$\frac{1}{(2\pi\mathbf{i})^2} \oiint \exp\left(s_k \left(\frac{(1-\mathbf{m}_k) z_k}{z_k - \alpha} + \frac{\beta \mathbf{m}_k z_k}{1+\beta z_k} \right) \right) \exp\left(s_l \left(\frac{(1-\mathbf{m}_l) z_l}{z_l - \alpha} + \frac{\beta \mathbf{m}_l z_l}{1+\beta z_l} \right) \right) \frac{\mathrm{d}z_k \mathrm{d}z_l}{(z_k - z_l)^2}, \tag{6.62}$$

where both contours are small positively oriented loops around α*, with* z_l *contour inside* z_k *contour.*

Proof. The argument in exactly the same as in Theorem 6.25, and we only verify the formula for the asymptotic covariance. Using Theorem 6.26, we have

$$\begin{aligned}
&\mathbb{E}\left[\sum_{i=1}^{n+1-m_k} q_k^{\lambda_i^{(m_k)}+n+1-m_k-i} \sum_{i=1}^{n+1-m_l} q_l^{\lambda_i^{(m_l)}+n+1-m_l-i} \right] = \oiint \frac{(q_k z_k - q_l z_l)(z_k - z_l)}{(z_k - q_l z_l)(q_k z_k - z_l)} \\
&\frac{(q_k z_k - \alpha)^{n+1-m_k}}{(z_k - \alpha)^{n+1-m_k}} \cdot \frac{(1+\beta q_k z_k)^{m_k}}{(1+\beta z_k)^{m_k}} \cdot \frac{(q_l z_l - \alpha)^{n+1-m_l}}{(z_l - \alpha)^{n+1-m_l}} \cdot \frac{(1+\beta q_l z_l)_l^m}{(1+\beta z_l)_l^m} \cdot \frac{\mathrm{d}z_k}{2\pi\mathbf{i}(q_k - 1) z_k} \cdot \frac{\mathrm{d}z_l}{2\pi\mathbf{i}(q_l - 1) z_l},
\end{aligned} \tag{6.63}$$

where both integration contours are small loops around α and z_k contour is slightly larger. We plug in $q_l = \exp\left(\frac{s_k}{n}\right)$, $q_l = \exp\left(\frac{s_l}{n}\right)$ and use (6.51). Hence, subtracting the product of two applications of Corollary 6.15 with $K = 1$ and using the same asymptotic expansion as in (6.34), we get (6.62) as $n \to \infty$ limit of the covariance. The nesting of the final contours comes from the nesting of the contours in (6.63), while in Theorem 6.25 the nesting was arbitrary since we could apply $\mathcal{D}_q$ operators in any order. □

6.7 The Gaussian free field

In this section we interpret Theorem 6.27 as convergence of the fluctuations of the height function of domino tilings to the Gaussian free field.

6.7.1 Definition of GFF

We start our discussion of convergence towards the Gaussian free field by defining this object. Generally speaking, the definition uses two pieces of data: a two-dimensional domain (more generally, a two-dimensional surface with boundary) and a complex structure on this domain. On the first step we define the (two-dimensional) Gaussian free field in a domain $\mathbb{V} \subset \mathbb{C}$ in the *standard* complex structure of $\mathbb{C}$.

Take the Laplace operator on $\mathbb{V}$

$$\triangle = \frac{\partial^2}{\partial x^2} + \frac{\partial^2}{\partial y^2}\Big|_{x+\mathbf{i}y\in\mathbb{V}}.$$

We consider the inverse operator $(-\triangle^{-1})$ taken with Dirichlet, *i.e.*, identical zero, boundary conditions on the boundary $\partial\mathbb{V}$. $\triangle^{-1}$ is an integral operator with respect to the Lebesgue measure on $\mathbb{V}$, and its kernel is known as the *Green's function*, given by the following definition.

Definition 6.28. *The Green's function $\mathcal{G}_{\mathbb{V}}(z, z')$ on $\mathbb{V}$ with Dirichlet boundary condition is a function $\mathcal{G} : \mathbb{V} \times \mathbb{V} \to \mathbb{R}$ of two complex arguments $z = x + \mathbf{i}y$, $z' = x' + \mathbf{i}y'$, such that*

$$\triangle\mathcal{G}_{\mathbb{V}}(z, z') = -\delta(z - z'),$$

where $\delta(z - z')$ is the Delta-function[5]*, $\triangle$ can be applied either in z or in z' variables, and*

$$\lim_{z\to z_0} \mathcal{G}_{\mathbb{V}}(z, z') = \lim_{z'\to z_0} \mathcal{G}_{\mathbb{V}}(z, z') = 0, \quad \text{for any } z_0 \in \partial\mathbb{V}.$$

We remark without proof that (for non-pathological $\mathbb{V}$) the Green's function exists, is unique and symmetric, *i.e.*, $\mathcal{G}_{\mathbb{V}}(z, z') = \mathcal{G}_{\mathbb{V}}(z', z)$. When $\mathbb{V}$ is unbounded, one should add an at most logarithmic growth condition at ∞ to the definition of the Green's function. An important property of $\mathcal{G}_{\mathbb{V}}$ is its conformal invariance: if we map $\mathbb{V} \subset \mathbb{C}$ to another domain $\mathbb{V}' \subset \mathbb{C}$ by a conformal bijection[6] ϕ, then the Green's functions of the domains are related by a simple composition with ϕ. In particular, if we conformally map $\mathbb{V}$ to itself, then $\mathcal{G}_{\mathbb{V}}$ is kept unchanged; this is restated as the conformal-invariance property (6.68) below.

By the Riemann uniformization theorem, all simply-connected domains in $\mathbb{C}$ which do not coincide with $\mathbb{C}$ itself, can be conformally mapped to each other. Hence, it suffices to understand the Green's function in a single model domain, and we use the upper halfplane $\mathbb{U} = \{z \in \mathbb{C} \mid \mathrm{Im}(z) > 0\}$ for that.

[5] Equivalently, this means that for every smooth test-function $f(z)$, supported in a compact subset of the interior of $\mathbb{V}$, the double integral $\iint_{\mathbb{V}} \triangle\mathcal{G}_{\mathbb{V}}(z, z')f(z)\mathrm{d}x\mathrm{d}y$ with $z = x + \mathbf{i}y$, which should be computed via integration by parts as $\iint_{\mathbb{V}} \mathcal{G}_{\mathbb{V}}(z, z')\triangle f(z)\mathrm{d}x\mathrm{d}y$, evaluates to $-f(z')$.

[6] A map $\phi : \mathbb{V} \to \mathbb{V}'$ is called *conformal* if it is holomorphic, bijective and its inverse is also holomorphic.

Lemma 6.29. *The Green's function on the upper halfplane $\mathbb{U}$ is defined by*

$$\mathcal{G}_{\mathbb{U}}(z,z') = -\frac{1}{2\pi}\ln\left|\frac{z-z'}{z-\bar{z}'}\right|, \qquad \operatorname{Im}(z),\, \operatorname{Im}(z') > 0. \tag{6.64}$$

We leave it as an exercise to check that (6.64) agrees with Definition 6.28. The conformal invariance property can be directly verified for (6.64): the conformal bijections of $\mathbb{U}$ are Moebius transformations

$$z \mapsto \frac{az+b}{cz+d}, \qquad a,b,c,d \in \mathbb{R},$$

and one readily checks that the formula (6.64) is unchanged under such transformations.

For general domains, there is often no explicit formula for the Green's function, but locally such function always grows like a logarithm of the distance:

$$\mathcal{G}_{\mathbb{V}}(z,z') \sim -\frac{1}{2\pi}\ln|z-z'| \quad \text{for } z \approx z'. \tag{6.65}$$

Informally, the Gaussian free field is a Gaussian field with covariance given by the Green's function.

Definition 6.30. *The Gaussian free field on $\mathbb{V}$ is a random Gaussian function $\mathrm{GFF}_{\mathbb{V}} : \mathbb{V} \to \mathbb{R}$ such that*

$$\mathbb{E}\big[\mathrm{GFF}_{\mathbb{V}}(z)\big] = 0, \qquad \textit{and} \qquad \mathbb{E}\big[\mathrm{GFF}_{\mathbb{V}}(z)\mathrm{GFF}_{\mathbb{V}}(z')\big] = \mathcal{G}_{\mathbb{V}}(z,z'), \qquad z,z' \in \mathbb{V}.$$

Making the above definition mathematically precise requires some care. Indeed, if $z = z'$, then $\mathcal{G}_{\mathbb{V}}(z,z') = +\infty$, hence, the values of $\mathrm{GFF}_{\mathbb{V}}$ at individual points have infinite variance and are not well-defined as random variables. Therefore, $\mathrm{GFF}_{\mathbb{V}}$ is not a function, but a *generalized function*: we cannot ask about the values of this random function at a point, but we can compute its integrals (or pairings) with reasonably smooth *test measures*. Omitting the description of the required smoothness of measures, we record this property in the following two special cases for $\mathbb{V} = \mathbb{U}$ that we present without proofs.

Lemma 6.31. *Let μ be an absolutely continuous (with respect to the Lebesgue measure) measure on $\mathbb{U}$ whose density is a smooth function $g(z)$ with compact support. Then*

$$\int_{\mathbb{U}} \mathrm{GFF}_{\mathbb{U}} d\mu = \int_{\mathbb{U}} \mathrm{GFF}_{\mathbb{U}}(u) g(u)\, \mathrm{dRe}(u)\, \mathrm{dIm}(u)$$

is a well-defined centered Gaussian random variable. Moreover, if we have two such measures μ_1, μ_2 with densities g_1, g_2, then

$$\mathbb{E}\left[\Big(\int_{\mathbb{U}} \mathrm{GFF}_{\mathbb{U}}(u) g_1(u)\, \mathrm{dRe}(u)\, \mathrm{dIm}(u)\Big) \cdot \Big(\int_{\mathbb{U}} \mathrm{GFF}_{\mathbb{U}} g_2(u)\, \mathrm{dRe}(u)\, \mathrm{dIm}(u)\Big)\right]$$
$$= \int_{\mathbb{U}^2} g_1(z) \left(-\frac{1}{2\pi}\ln\left|\frac{z-w}{z-\overline{w}}\right|\right) g_2(w)\, \mathrm{dRe}(z)\, \mathrm{dIm}(z)\, \mathrm{dRe}(w)\, \mathrm{dIm}(w). \tag{6.66}$$

Lemma 6.32. *Let μ be a measure on $\mathbb{U}$ whose support is a smooth curve γ and whose density with respect to the natural arc-length measure on γ is given by a smooth function $g(z)$ such that*

$$\int\int_{\gamma\times\gamma} g(z) \left(-\frac{1}{2\pi}\ln\left|\frac{z-w}{z-\overline{w}}\right|\right) g(w)\, |\mathrm{d}z|\, |\mathrm{d}w| < \infty, \tag{6.67}$$

where $|\mathrm{d}z|$ indicates the integral with respect to the arc-length measure. Then

$$\int_{\mathbb{U}} \mathrm{GFF}_{\mathbb{U}} d\mu = \int_{\gamma} \mathrm{GFF}_{\mathbb{U}}(u) g(u)\, |\mathrm{d}u|$$

is a well-defined Gaussian centered random variable of variance given by (6.67)*. Moreover, if we have two such measures μ_1, μ_2 (with two curves γ_1, γ_2 and two densities g_1, g_2), then*

$$\mathbb{E}\left[\Big(\int_{\gamma_1} \mathrm{GFF}_{\mathbb{U}}(u)g_1(u)|\mathrm{d}u|\Big)\cdot\Big(\int_{\gamma_2} \mathrm{GFF}_{\mathbb{U}}(u)g_2(u)\,|\mathrm{d}u|\Big)\right] = \int\int_{\gamma_1\times\gamma_2} g_1(z)\left(-\frac{1}{2\pi}\ln\left|\frac{z-w}{z-\overline{w}}\right|\right)g_2(w)\,|\mathrm{d}z|\,|\mathrm{d}w|.$$

In principle, the above two lemmas can be taken as an alternative definition of the Gaussian free field as a random functional on smooth enough measures. By invoking the Kolmogorov consistency theorem, $\mathrm{GFF}_{\mathbb{V}}$ would be well-defined as a stochastic process, if we show that the joint distributions appearing in this definition are consistent. Since they are all mean 0 Gaussians, it suffices to check that the covariance is positive-definite. We make this check only in the context of Lemma 6.31 and leave a similar check involving Lemma 6.32 as an exercise.

Lemma 6.33. *The covariance of $\int \mathrm{GFF}_{\mathbb{U}}\mathrm{d}\mu$ given by* (6.66) *is positive-definite.*

Proof. We need to check that the operator with kernel $\mathcal{G}_{\mathbb{U}}$ is positive-definite, which is equivalent to $-\triangle$ being positive definite. The latter can be checked via integration by parts to reduce to the norm of the gradient:

$$\langle -\triangle g, g\rangle = \iint_{\mathbb{U}} \big(-\triangle g(x+\mathbf{i}y)\big)g(x+\mathbf{i}y)\,\mathrm{d}x\,\mathrm{d}y = \iint_{\mathbb{U}} \big\|\nabla g(x+\mathbf{i}y)\big\|^2_{L^2}\,\mathrm{d}x\,\mathrm{d}y \geq 0. \quad \square$$

A better alternative to using Lemmas 6.31 and 6.32 as a definition would be to define a functional space (like the space of continuous functions in the definition of the Brownian motion) to which the field $\mathrm{GFF}_{\mathbb{U}}$ belongs. We refer to [She07, WP21] for more details on the definition of the Gaussian free field.

If we extend the definition of GFF from $\mathbb{U}$ to general domains $\mathbb{V}\subset\mathbb{C}$, then the conformal invariance of the Green's function leads to the conformal invariance of the resulting fields: if ϕ is a conformal bijection of $\mathbb{V}\subset\mathbb{C}$ with $\mathbb{V}'\subset\mathbb{C}$, then

$$\{\mathrm{GFF}_{\mathbb{V}'}(\phi(z))\}_{z\in\mathbb{V}'} \overset{d}{=} \{\mathrm{GFF}_{\mathbb{V}}(z)\}_{z\in\mathbb{V}}. \tag{6.68}$$

Here is another informal definition of the Gaussian free field in a domain $\mathbb{V}$. According to it, $\mathrm{GFF}_{\mathbb{V}}$ is a probability measure on functions f on $\mathbb{V}$ with 0 boundary conditions with density

$$\rho(f) \sim \exp\left(-\frac{1}{2}\int_{\mathbb{V}} ||\nabla f||^2\,dx\,dy\right). \tag{6.69}$$

The formula (6.69) is based on the well-known computation for the finite-dimensional Gaussian vectors: for a Gaussian vector $v\in\mathbb{R}^N$ with probability density

$$\rho(v) = \frac{\sqrt{\det B}}{\sqrt{(2\pi)^N}}\exp\left(-\frac{1}{2}\langle v, Bv\rangle\right),$$

the covariance matrix $\mathbb{E}[vv^T]$ is equal to B^{-1}. Since the covariance for the $\mathrm{GFF}_{\mathbb{V}}$ is given by the minus inverse Laplace operator, the matrix B appearing in its density should be identified with $-\triangle$, and integration by parts leads to (6.69). The precise mathematical meaning of (6.69) is even trickier than Definition 6.30: it is unclear with respect to which underlying measure the density is computed, and also the

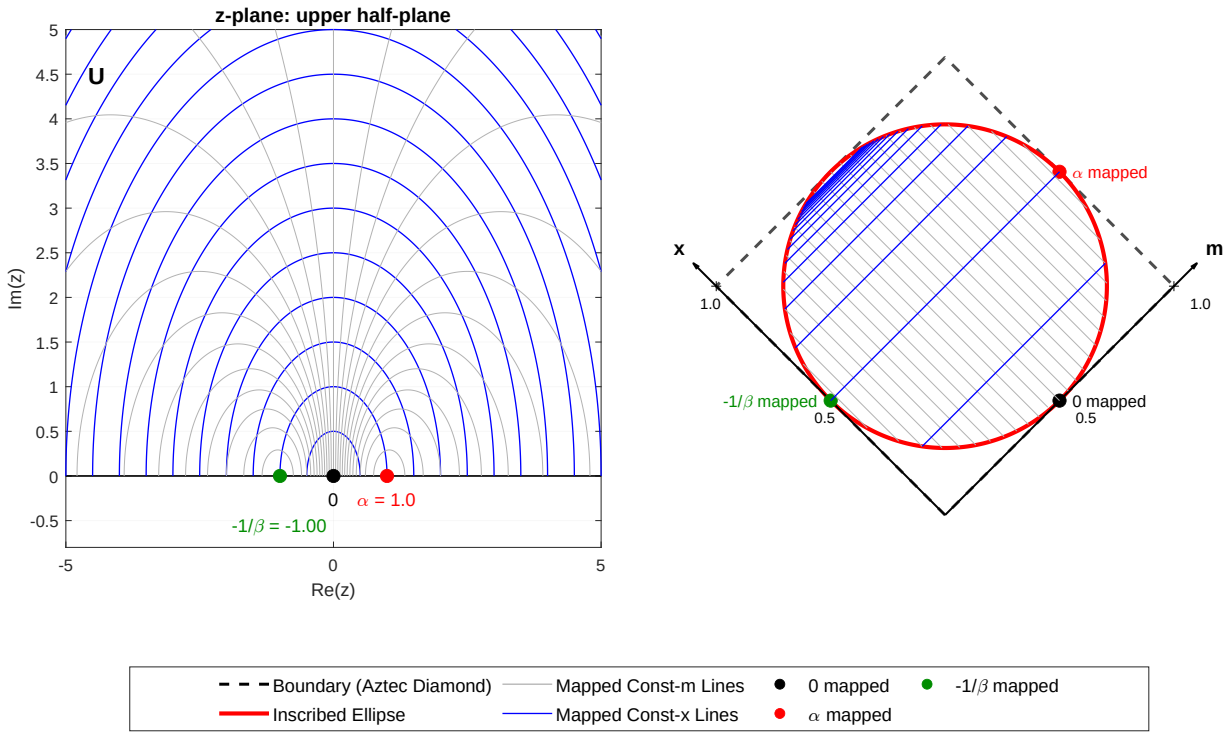


Figure 6.14: The bijection of Proposition 6.34 for $\alpha = \beta = 1$.

symbol $||\nabla f||_{L^2}^2$ is not well-defined for non-smooth f, while we already know that GFF is not smooth, even its values at points are not properly defined.

Finally, one can construct the Gaussian free field from a sequence of i.i.d. Gaussian random variables, by using the decomposition

$$\mathrm{GFF}_{\mathbb{V}}(z) = \sum_{k=1}^{\infty} \xi_k \frac{\phi_k(z)}{\sqrt{\lambda_k}}, \qquad \xi_k \sim \text{i.i.d. } \mathcal{N}(0,1), \tag{6.70}$$

where $0 < \lambda_1 < \lambda_2 < \dots$ are eigenvalues of minus the Laplace operator, $-\triangle$, in $\mathbb{V}$ with corresponding L^2–orthonormal eigenvectors $\phi_1, \phi_2, \dots$, vanishing on $\partial\mathbb{V}$. The convergence of the series (6.70) is delicate: the sum diverges for a fixed $z \in \mathbb{V}$, but its term-wise integrals against test-measures (as in Lemmas 6.31 and 6.32) converge.

6.7.2 Complex structure and pullback for GFF

The next step towards describing the height fluctuations of the domino tilings is to identify the liquid region (interior of the inscribed ellipse in the Aztec diamond) with the upper half-plane $\mathbb{U}$, appropriate for the $\mathrm{GFF}_{\mathbb{U}}$. The bijective map that we are about to introduce *is not conformal*; in other words, the desired Gaussian free field comes not from the standard complex structure of the plane on which the (scaled) Aztec diamond is drawn, but through more involved definitions.

Proposition 6.34. *For any* $0 \le \mathbf{x}, \mathbf{m} \le 1$, *the equation*

$$\frac{(1-\mathbf{m})z}{z-\alpha} + \frac{\beta \mathbf{m} z}{1+\beta z} - \mathbf{x} = 0, \qquad z \in \mathbb{C}, \quad \mathrm{Im}(z) > 0, \tag{6.71}$$

has at most one root z in the upper halfplane $\mathbb{U} = \{z \in \mathbb{C} \mid \mathrm{Im}(z) > 0\}$. It has such a root if and only if $(\mathbf{x}, \mathbf{m})$ is inside the ellipse inscribed in the Aztec diamond and given by

$$\frac{(\mathbf{x}+\mathbf{m}-1)^2}{p} + \frac{(\mathbf{x}-\mathbf{m})^2}{1-p} = 1, \qquad p = \frac{\alpha\beta}{1+\alpha\beta}. \tag{6.72}$$

The map $(\mathbf{x}, \mathbf{m}) \mapsto z$ is a bijection between the interior of the ellipse and $\mathbb{U}$.

Proof. The equation (6.71) has already appeared before in the proof of Lemma 6.21, see (6.41). This is a quadratic equation in z, which has a pair of complex conjugate roots inside the ellipse (6.72) and two real roots outside the ellipse. Hence, the map $(\mathbf{x}, \mathbf{m}) \mapsto z$ is well-defined inside the ellipse. For the bijectivity, we study the inverse map by interpreting the real and imaginary parts of (6.71) as two linear equations on $(\mathbf{x}, \mathbf{m})$. The imaginary part gives:

$$0 = \mathrm{Im}\left[(1-\mathbf{m})\left(1+\frac{\alpha}{z-\alpha}\right) + \mathbf{m}\left(1-\frac{1}{1+\beta z}\right)\right] = (1-\mathbf{m})\alpha\frac{-\mathrm{Im}(z)}{|z-\alpha|^2} + \mathbf{m}\beta\frac{\mathrm{Im}(z)}{|1+\beta z|^2},$$

which has solution

$$\mathbf{m} = \frac{1}{1+\frac{\beta}{\alpha}\frac{|z-\alpha|^2}{|1+\beta z|^2}} \in (0,1).$$

Plugging back into the equation, we get

$$\begin{aligned}\mathbf{x} = 1 + \left(\frac{(1-\mathbf{m})\alpha}{z-\alpha} - \frac{\mathbf{m}}{1+\beta z}\right) &= 1 + \frac{1}{|1+\beta z|^2 + \frac{\beta}{\alpha}|z-\alpha|^2} \cdot \left(\beta\frac{|z-\alpha|^2}{z-\alpha} - \frac{|1+\beta z|^2}{1+\beta z}\right) \\ &= 1 - \frac{1+\alpha\beta}{|1+\beta z|^2 + \frac{\beta}{\alpha}|z-\alpha|^2} = 1 - \frac{1}{1+\frac{\beta}{\alpha}|z|^2} \in (0,1). \quad \square\end{aligned} \tag{6.73}$$

Figures 6.14 and 6.15 illustrate the correspondence $z \leftrightarrow (\mathbf{x}, \mathbf{m})$: the lines of constant $\mathbf{x}$ in the ellipse are mapped to half-circles centered at 0 in $\mathbb{U}$, while the lines of constant $\mathbf{m}$ are mapped to half-circles separating α from $-1/\beta$ (and to a vertical ray for $\mathbf{m} = p$).

We use the map $(\mathbf{x}, \mathbf{m}) \mapsto z$ to pullback GFF on $\mathbb{U}$ into the interior of the ellipse by using the following definition.

Definition 6.35. *Given a domain $\mathbb{V}$ and a map $\Omega : \mathbb{V} \to \mathbb{U}$, the pullback $\mathrm{GFF}_{\mathbb{U}} \circ \Omega$ is a generalized centered Gaussian Field on $\mathbb{V}$ with covariance*

$$\mathbb{E}\big[\mathrm{GFF}_{\mathbb{U}}(\Omega(z))\mathrm{GFF}_{\mathbb{U}}(\Omega(w))\big] = -\frac{1}{2\pi}\ln\left|\frac{\Omega(z)-\Omega(w)}{\Omega(z)-\overline{\Omega}(w)}\right|, \quad z, w \in \mathbb{V}.$$

Integrals of $\mathrm{GFF}_{\mathbb{U}} \circ \Omega$ with respect to measures are computed through

$$\int_{\mathbb{V}} (\mathrm{GFF}_{\mathbb{U}} \circ \Omega)\, \mathrm{d}\mu = \int_{\mathbb{U}} \mathrm{GFF}_{\mathbb{U}}\, \mathrm{d}(\Omega_*\mu),$$

where $\mathrm{d}(\Omega_*\mu)$ stands for the pushforward of measure μ.

Remark 6.36. The difference from (6.68) is that Ω is not conformal (*e.g.*, in Figure 6.14 and 6.15 the angles between gray and blue lines are not preserved under the map), in contrast with ϕ.

The above definition implies the following analogue of Lemma 6.32, and there is a similar analogue of Lemma 6.31.

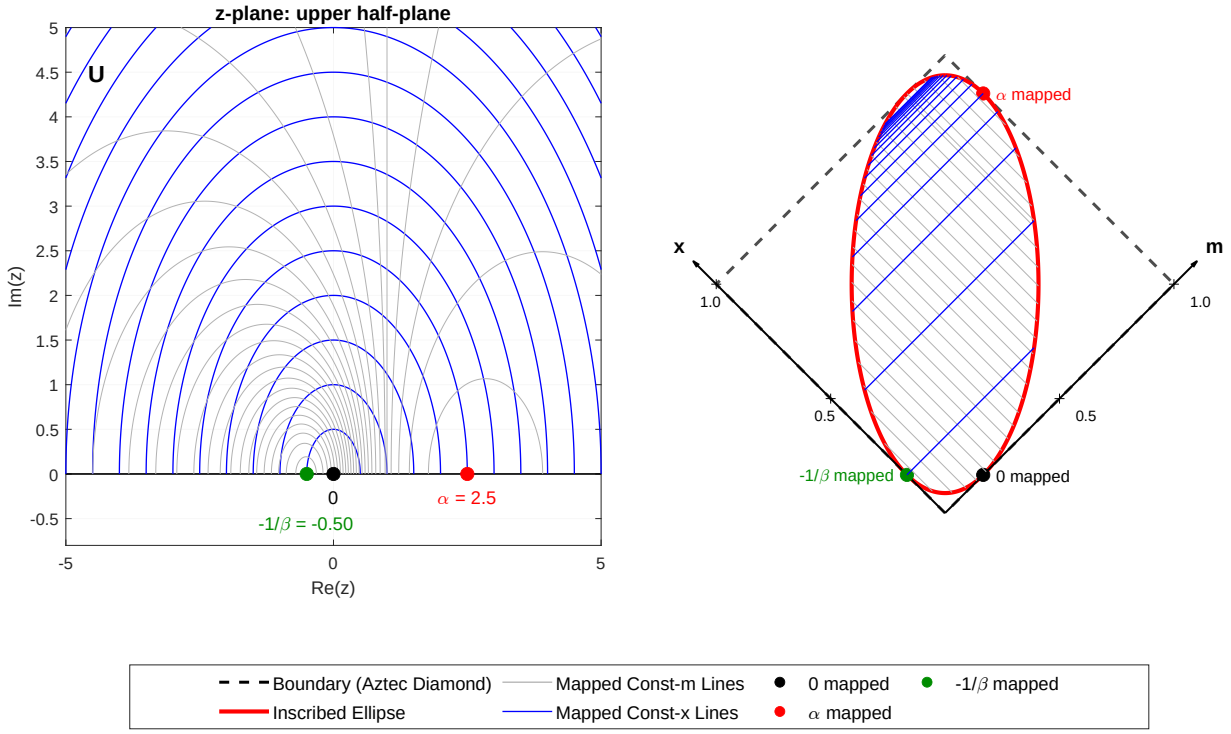


Figure 6.15: The bijection of Proposition 6.34 for $\alpha = 2.5$, $\beta = 2$.

Lemma 6.37. *In the notation of Definition 6.35, let μ be a measure on $\mathbb{V}$ supported on a smooth curve γ and whose density with respect to the natural length measure on γ is given by a smooth function $g(z)$ such that*

$$\int\int_{\gamma\times\gamma} g(z)\left(-\frac{1}{2\pi}\ln\left|\frac{\Omega(z)-\Omega(w)}{\Omega(z)-\overline{\Omega}(w)}\right|\right)g(w)\,|\mathrm{d}z||\mathrm{d}w| < \infty. \tag{6.74}$$

Then

$$\int_{\mathbb{V}} (\mathrm{GFF}_{\mathbb{U}}\circ\Omega)\,\mathrm{d}\mu = \int_{\gamma}\mathrm{GFF}_{\mathbb{U}}(\Omega(u))g(u)|\mathrm{d}u|$$

is a well-defined Gaussian centered random variable of variance given by (6.74)*. Moreover, if we have two such measures μ_1, μ_2 (with two curves γ_1, γ_2 and two functions g_1, g_2), then*

$$\mathbb{E}\left[\left(\int_{\gamma_1}\mathrm{GFF}_{\mathbb{U}}(\Omega(u))g_1(u)|\mathrm{d}u|\right)\cdot\left(\int_{\gamma_2}\mathrm{GFF}_{\mathbb{U}}(\Omega(u))g_2(u)\,|\mathrm{d}u|\right)\right]$$
$$= \int\int_{\gamma_1\times\gamma_2} g_1(z)\left(-\frac{1}{2\pi}\ln\left|\frac{\Omega(z)-\Omega(w)}{\Omega(z)-\overline{\Omega}(w)}\right|\right)g_2(w)\,|\mathrm{d}z|\,|\mathrm{d}w|. \tag{6.75}$$

6.7.3 Matching the Aztec fluctuations with GFF

We recall Definition 6.16 for the height function and extend it from integer arguments to a piece-wise constant, right-continuous function of real arguments. Using $\lfloor m\rfloor$ for the largest integer not greater than m, we introduce the following definition of the extended height function.

Definition 6.38. *With x growing towards North-West and m towards growing North-East, we define the extended height function:*

$$h^n(x,m) = \left|(-\infty,x]\bigcap\left\{\lambda_i^{(\lfloor m\rfloor)} - i + n - \lfloor m\rfloor + 2\right\}_{i=1}^{n+1-\lfloor m\rfloor}\right|. \tag{6.76}$$

We have $h^n(0,m) = 0,\ h^n(n+1,m) = n+1-\lfloor m\rfloor$, and

$$h^n(x,m) - \lim_{\varepsilon\to 0+} h^n(x-\varepsilon,m) = \begin{cases} 1, & \text{there is a green particle at } (x,m),\\ 0, & \text{otherwise.}\end{cases} \tag{6.77}$$

Theorem 6.39. *Let $h^n(\cdot,\cdot)$ be the extended height function of Definition 6.38 for $(\alpha\beta)$-weighted random domino tilings of the Aztec diamond of size n, as in* (6.2)*. Then*

$$\lim_{n\to\infty}\sqrt{\pi}\Big[h^n(n\mathbf{x},n\mathbf{m}) - \mathbb{E}h^n(n\mathbf{x},n\mathbf{m})\Big] = \Theta(\mathbf{x},\mathbf{m}), \qquad 0\le\mathbf{x},\mathbf{m}\le 1, \tag{6.78}$$

where $\Theta(\cdot,\cdot)$ is a generalized Gaussian field, which is identically zero outside the ellipse (6.72)*, and is the pullback of the Gaussian free field $\mathrm{GFF}_{\mathbb{U}}$ with respect to the map $(\mathbf{x},\mathbf{m})\mapsto z$ of Proposition 6.34 inside the ellipse. The convergence in* (6.78) *is in joint moments for integrals of the two-dimensional field along the fixed $\mathbf{m}$ lines and with density $\exp(s\mathbf{x})$ in the $\mathbf{x}$ direction.*

Our proof of Theorem 6.39 is a direct verification: we are going to check that the result of Theorem 6.27 matches the covariance of a pullback of GFF. Other proofs can be found in [CJY15, Section 6], [BG18, Section 3.6], [BK18], [CR24], [BNR24]. A conceptual reason for the appearance of the Gaussian free field in this problem can be seen through the informal definition of GFF in (6.69). As proven in [CKP01], for random domino tilings one can approximate the logarithm of the probability of seeing a particular realization of the height function h as a double integral of a certain functional ("surface tension") of the gradient of h. The Law of Large Numbers in Theorem 6.17 can be achieved by maximizing this integral, and the fluctuations are governed by an expansion of the functional near its maximum. After a proper change of the coordinate system, this expansion leads to the integral of the squared gradient, as in (6.69). In the related case of random lozenge tilings, this heuristics is explained in more detail in [Gor21, Lectures 11, 12, and 23]. The same heuristics predicts universal appearance of GFF in many other models of random two-dimensional surfaces in three-dimensional space. Making it mathematically rigorous for domino tilings of general domains is beyond the currently existing methods, and one needs to use other approaches to prove the convergence to the Gaussian free field.

Proof of Theorem 6.39. For a fixed $0<\mathbf{m}<1$ and $s\in\mathbb{R}$, we analyze the integral of the left-hand side of (6.78) against $\exp(s\mathbf{x})$. The goal is to show that

$$\lim_{n\to\infty}\int_{\mathbb{R}}\sqrt{\pi}\Big[h^n(n\mathbf{x},n\mathbf{m}) - \mathbb{E}h^n(n\mathbf{x},n\mathbf{m})\Big]\exp(s\mathbf{x})\mathrm{d}\mathbf{x} = \int_{\mathbb{R}}\Theta(\mathbf{x},\mathbf{m})\exp(s\mathbf{x})\mathrm{d}\mathbf{x}, \tag{6.79}$$

where the convergence is in joint moments over finite collections of pairs $(\mathbf{m},s)$. The right-hand side is an integral of a pullback of $\mathrm{GFF}_{\mathbb{U}}$ and its covariance is given by (6.75). For the left-hand side we integrate

by parts using Definition 6.38 and that $h^n(n\mathbf{x}, n\mathbf{m}) - \mathbb{E}h^n(n\mathbf{x}, n\mathbf{m}) = 0$ whenever $\mathbf{x} < 0$ or $\mathbf{x} > 1 + \frac{1}{n}$:

$$\int_{\mathbb{R}} \Big[h^n(n\mathbf{x}, n\mathbf{m}) - \mathbb{E}h^n(n\mathbf{x}, n\mathbf{m})\Big] \exp(s\mathbf{x}) \mathrm{d}\mathbf{x} = -\frac{1}{s} \int_{\mathbb{R}} \frac{\partial}{\partial \mathbf{x}} \Big[h^n(n\mathbf{x}, n\mathbf{m}) - \mathbb{E}h^n(n\mathbf{x}, n\mathbf{m})\Big] \exp(s\mathbf{x}) \mathrm{d}\mathbf{x}$$
$$= -\frac{1}{s} \Bigg[\sum_{i=1}^{n+1-\lfloor n\mathbf{m} \rfloor} \exp\left(\frac{s}{n}\left(\lambda_i^{(\lfloor n\mathbf{m} \rfloor)} - i + n - \lfloor n\mathbf{m} \rfloor + 2\right)\right)$$
$$- \mathbb{E} \sum_{i=1}^{n+1-\lfloor n\mathbf{m} \rfloor} \exp\left(\frac{s}{n}\left(\lambda_i^{(\lfloor n\mathbf{m} \rfloor)} - i + n - \lfloor n\mathbf{m} \rfloor + 2\right)\right)\Bigg]. \quad (6.80)$$

We recognize the expressions analyzed in Theorem 6.27, up to multiplication by $\exp\left(\frac{s}{n}\right)$, which does not change the conclusion of the theorem. Applying it, we conclude that the limit in the left-hand side of (6.79) is Gaussian and mean 0, with covariance between $(\mathbf{m}, s) = (\mathbf{m}_k, s_k)$ and $(\mathbf{m}, s) = (\mathbf{m}_l, s_l)$ cases given by (6.62), *i.e.*:

$$\frac{\pi}{(2\pi\mathbf{i})^2 s_k s_l} \oiint \exp\left(s_k \left(\frac{(1-\mathbf{m}_k)z_k}{z_k - \alpha} + \frac{\beta \mathbf{m}_k z_k}{1 + \beta z_k}\right)\right) \exp\left(s_l \left(\frac{(1-\mathbf{m}_l)z_l}{z_l - \alpha} + \frac{\beta \mathbf{m}_l z_l}{1 + \beta z_l}\right)\right) \frac{\mathrm{d}z_k \mathrm{d}z_l}{(z_k - z_l)^2}. \quad (6.81)$$

What remains is to match this expression with the covariance of the integrals in the right-hand side of (6.79). We assume without loss of generality that $\mathbf{m}_k \neq \mathbf{m}_l$; the case of equal parameters is achieved by a limit transition. We deform the integration contours in (6.81): the z_l–contour is deformed to the circle, whose upper half-plane part is the image of the $\mathbf{m} = \mathbf{m}_l$ section of the interior of the ellipse under $(\mathbf{x}, \mathbf{m}) \mapsto z$ map of Proposition 6.34, and the z_k–contour is deformed to the circle whose upper half-plane part is the image of the $\mathbf{m} = \mathbf{m}_k$ section of the interior of the ellipse. Note that on the original contours in Theorem 6.27, the ordering $\mathbf{m}_k \leq \mathbf{m}_l$ implies that z_k–contour is outside the z_l–contour, with both contours being small loops around α. The ordering of the images of the constant $\mathbf{m}$ sections of the ellipse (cf. Figures 6.14 and 6.15) and the fact that integral has no residue at $z = \infty$, allows the desired deformation of the contours without picking up any additional residues.

On the new contours, we split the double integral into four parts corresponding to upper and lower halves of the circles. Parameterizing the $\mathbb{U}$–parts as the z–images of $\mathbf{m} = \mathbf{m}_k$ and $\mathbf{m} = \mathbf{m}_l$ sections of the ellipse, we convert (6.81) into

$$\frac{\pi}{(2\pi\mathbf{i})^2 s_k s_l} \iint \exp\left(s_k \mathbf{x}_k\right) \exp\left(s_l \mathbf{x}_l\right) \mathrm{d}\mathbf{x}_k \mathrm{d}\mathbf{x}_l \Bigg[\frac{\frac{\partial z(\mathbf{m}_k, \mathbf{x}_k)}{\partial \mathbf{x}_k} \frac{\partial z(\mathbf{m}_l, \mathbf{x}_l)}{\partial \mathbf{x}_l}}{(z(\mathbf{m}_k, \mathbf{x}_k) - z(\mathbf{m}_l, \mathbf{x}_l))^2}$$
$$- \frac{\frac{\partial \bar{z}(\mathbf{m}_k, \mathbf{x}_k)}{\partial \mathbf{x}_k} \frac{\partial z(\mathbf{m}_l, \mathbf{x}_l)}{\partial \mathbf{x}_l}}{(\bar{z}(\mathbf{m}_k, \mathbf{x}_k) - z(\mathbf{m}_l, \mathbf{x}_l))^2} - \frac{\frac{\partial z(\mathbf{m}_k, \mathbf{x}_k)}{\partial \mathbf{x}_k} \frac{\partial \bar{z}(\mathbf{m}_l, \mathbf{x}_l)}{\partial \mathbf{x}_l}}{(z(\mathbf{m}_k, \mathbf{x}_k) - \bar{z}(\mathbf{m}_l, \mathbf{x}_l))^2} + \frac{\frac{\partial \bar{z}(\mathbf{m}_k, \mathbf{x}_k)}{\partial \mathbf{x}_k} \frac{\partial \bar{z}(\mathbf{m}_l, \mathbf{x}_l)}{\partial \mathbf{x}_l}}{(\bar{z}(\mathbf{m}_k, \mathbf{x}_k) - \bar{z}(\mathbf{m}_l, \mathbf{x}_l))^2} \Bigg].$$

We further integrate by parts in $\mathbf{x}_k$ and $\mathbf{x}_l$, noting that the boundary terms cancel because $z(\mathbf{m}, \mathbf{x})$ is real on the ellipse, which corresponds to the end-points of the integration segment. We obtain

$$\frac{\pi}{(2\pi\mathbf{i})^2} \iint \exp\left(s_k \mathbf{x}_k\right) \exp\left(s_l \mathbf{x}_l\right) \mathrm{d}\mathbf{x}_k \mathrm{d}\mathbf{x}_l \Bigg[\ln\big(z(\mathbf{m}_k, \mathbf{x}_k) - z(\mathbf{m}_l, \mathbf{x}_l)\big)$$
$$- \ln\big(\bar{z}(\mathbf{m}_k, \mathbf{x}_k) - z(\mathbf{m}_l, \mathbf{x}_l)\big) - \ln\big(z(\mathbf{m}_k, \mathbf{x}_k) - \bar{z}(\mathbf{m}_l, \mathbf{x}_l)\big) + \ln\big(\bar{z}(\mathbf{m}_k, \mathbf{x}_k) - \bar{z}(\mathbf{m}_l, \mathbf{x}_l)\big) \Bigg]$$
$$= \iint \exp\left(s_k \mathbf{x}_k\right) \exp\left(s_l \mathbf{x}_l\right) \left[-\frac{1}{2\pi} \ln \left| \frac{z(\mathbf{m}_k, \mathbf{x}_k) - z(\mathbf{m}_l, \mathbf{x}_l)}{z(\mathbf{m}_k, \mathbf{x}_k) - \bar{z}(\mathbf{m}_l, \mathbf{x}_l)} \right| \right] \mathrm{d}\mathbf{x}_k \mathrm{d}\mathbf{x}_l.$$

The last expression matches (6.75) with Ω-map being the z-map and γ–contours being the fixed $\mathbf{m}$ sections of the interior of the ellipse (6.72) inscribed into the Aztec diamond. □

6.8 Exercises

Problem 1. Compare (6.32) with the result of Problem 2 in Section 5.11. Explain the similarities.

Problem 2. Continuing the connection of Problem 1 and developing the exact tail bounds as in Section 5.5, show that the random domino tiling is completely frozen outside the frozen ellipse: for each $\varepsilon > 0$, with probability tending to 1 as $n \to \infty$, all the dominos in the South/West/North/East corners of the diamond, outside the ε–neighborhood of the ellipse (6.30), are of South/West/North/East types, respectively.

Problem 3. By taking $q \to 1$ as $n \to \infty$ in Corollary 6.15 with $K = 1$, develop the edge limit version of Proposition 6.19, in which the asymptotic behavior is determined by the first rows of λ and the limit relates to the Airy point process. Compare the result with (5.87).

Problem 4. Repeating the limit of Problem 3 for the multilevel observables of Theorem 6.26, and assuming $m_{k+1} - m_k = n^{2/3}\Delta_k$, find the multilevel joint edge limit for the domino tilings. The limiting object is a random collection of continuous curves known as the *Airy$_2$ line ensemble*; the top-most curve (describing the boundary of the frozen region for random domino tilings) is called the *Airy$_2$ process*. The subscript $_2$ is sometimes omitted from the names.

Problem 5. Given three interlacing partitions λ, τ, μ with $\lambda \succ \tau \prec \mu$ (*i.e.*, λ/τ and μ/τ are horizontal strips), and a nonnegative integer $W = 0, 1, 2, \dots$, we define another partition κ through

$$\kappa_i = \begin{cases} \max(\lambda_1, \mu_1) + W, & i = 1, \\ \max(\lambda_i, \mu_i) + \min(\lambda_{i-1}, \mu_{i-1}) - \tau_{i-1}, & i > 1. \end{cases} \tag{6.82}$$

A. Prove that $|\lambda| + |\mu| + W = |\tau| + |\kappa|$.

B. Prove that for fixed λ and μ, (6.82) is a *bijection* between the sets:

$$\{(\tau, W) \in \mathbb{Y} \times \mathbb{Z}_{\geq 0} \mid \lambda \succ \tau \prec \mu\} \quad \text{and} \quad \{\kappa \in \mathbb{Y} \mid \lambda \prec \kappa \succ \mu\}.$$

C. Apply this bijection to prove the one-variable version of the skew Cauchy identity:

$$\sum_{\kappa \in \mathbb{Y}} s_{\kappa/\lambda}(x) s_{\kappa/\mu}(y) = \frac{1}{1 - xy} \sum_{\tau \in \mathbb{Y}} s_{\lambda/\tau}(y) s_{\mu/\tau}(x).$$

(You can use the vanishing property of skew Schur functions, which implies $\lambda \succ \tau \prec \mu$ and $\lambda \prec \kappa \succ \mu$ in the sums.)

Problem 6. Given an array of nonnegative integers $W(i, j)$, $i, j = 1, 2, \dots$, the bijection (6.82) can be used to create an array of partitions $\lambda(i, j)$, $i, j = 0, 1, 2, \dots$, in the following way:

- We postulate $\lambda(i, 0) = \lambda(0, j) = \varnothing$ for all i and j.
- The array satisfies $\lambda(i - 1, j) \prec \lambda(i, j)$ and $\lambda(i, j - 1) \prec \lambda(i, j)$ for all $i, j = 1, 2, \dots$.
- Given $\lambda(i - 1, j)$ and $\lambda(i, j - 1)$, we construct $\lambda(i, j)$ as κ in (6.82) based on $\tau = \lambda(i - 1, j - 1)$ and $W = W(i, j)$.

For each $t = 1, 2, \dots$, we consider a sequence of partitions along right-down path from $(0, t)$ to $(t, 0)$:

$$\varnothing = \lambda(0,t) \prec \lambda(1,t) \succ \lambda(1,t-1) \prec \lambda(2,t-1) \succ \cdots \succ \lambda(t-1,1) \prec \lambda(t,1) \succ \lambda(t,0) = \varnothing.$$

We view t as time, so that we get time evolving sequence of partitions.

A. What choice of *random* $W(i, j)$ (other than just all $W(i, j) = 0$) will turn this sequence (t is fixed) into a Schur process?
Hint. Start with $t = 1$, then argue inductively in t. You do not need to find all possible $W(i, j)$ — at least one non-trivial example would be sufficient.

B. Prove that one can choose $W(i, j)$ to be random variables in a particular way (how?), so that the evolution (in time t) of the first rows of the partitions in this sequence is the same as the discrete PNG of Section 3.1.

Problem 7. In the framework of Problem 6, choose $n = 1, 2, \dots$ and suppose that array $W(i, j)$ has exactly n elements equal to 1 and all others are equal to 0. The positions of 1s are encoded by a permutation $\sigma \in \mathcal{S}_n$ via $W(i, \sigma(i)) = 1$.

A. Show that the sequence

$$\lambda(1,n) \prec \lambda(2,n) \prec \cdots \prec \lambda(n-1,n) \prec \lambda(n,n) \succ \lambda(n,n-1) \succ \cdots \succ \lambda(n,2) \succ \lambda(n,1)$$

can be identified with a pair of Standard Young Tableaux of the same shape $\lambda(n, n)$ with $|\lambda(n, n)| = n$.

B. Prove that the correspondence between σ and the above pairs of SYT is a bijection. Therefore, we arrive at a bijective proof of the Burnside identity $\sum_{|\lambda|=n} \dim^2 \lambda = n!$.

C. Read about the row insertions and Robinson-Schensted correspondence in [Ful97, Sag01] or in Wikipedia. Prove that this is the same correspondence as in part **B**.

Problem 8. Read about Robinson-Schensted-Knuth (RSK) correspondence between integer matrices and pairs of semistandard Young tableaux (*e.g.*, in [Ful97, Sag01] or `https://www.symmetricfunctions.com/rsk.htm`). Prove that in the framework of Problem 7 this is the same as the correspondence between $W(i, j)$, $1 \le i \le N$, $1 \le j \le K$ and sequences

$$\lambda(1,K) \prec \lambda(2,K) \prec \cdots \prec \lambda(N-1,K) \prec \lambda(N,K) \succ \lambda(N,K-1) \succ \cdots \succ \lambda(N,2) \succ \lambda(N,1).$$

Compare with Problem 6 in Section 3.7.

Problem 9. Our goal is to study more complicated measures on tilings than (6.2). We introduce a graph, whose vertices are $2n(n + 1)$ squares of the Aztec diamond with edges connecting squares sharing a side. Domino tilings are in bijection with perfect matchings or dimer configurations on this graph.

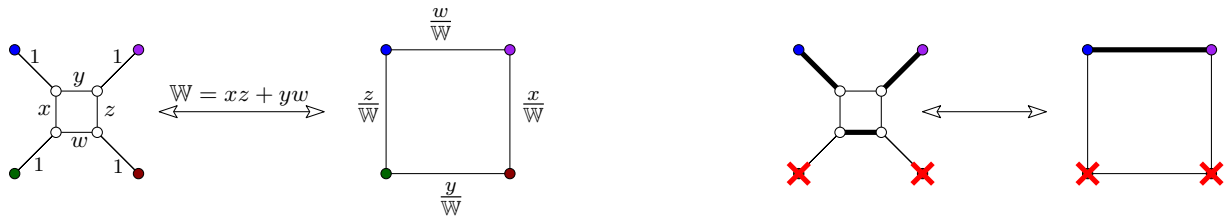
A. Check that the graph has $4n^2$ edges.

B. Take $n = 2$ and introduce 16 variables corresponding to the 16 edges. Call variables corresponding to left-most and right-most vertical edges v_L and v_R. Call variables corresponding to top-most and bottom-most horizontal edges h_T and h_B. Assign to a perfect matching the weight equal to the product of variables of matched edges. Compute the sum Z_2 over all 8 matchings and prove its factorization:

$$Z_2 = v_L v_R \cdot A \cdot B + h_T h_B \cdot C \cdot D, \qquad \text{for degree 2 polynomials } A, B, C, D.$$

Compare with Corollary 6.4.

C. We introduce the *urban renewal* or the *spider move* graphically as shown below:



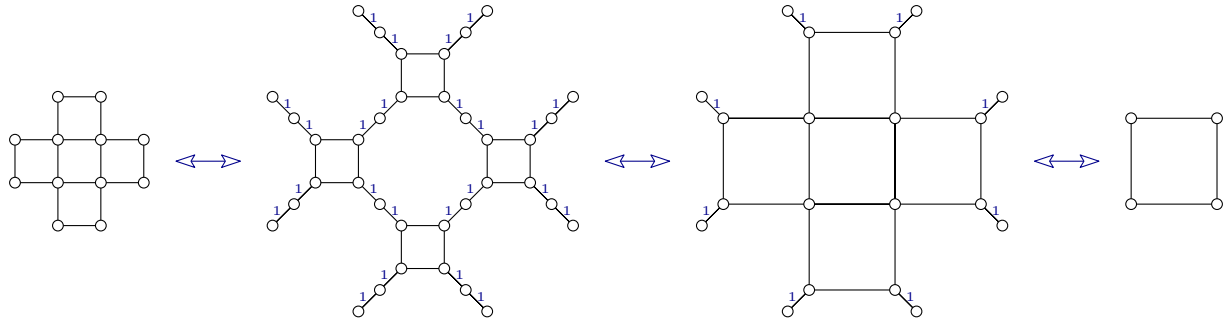
This drawing is an identity of $2^4 = 16$ pairs of partition functions, *i.e.*, sums of products of weights of edges over all perfect matchings of a graph. The weights of edges are shown in the left picture. In each identity, some of the exterior four vertices are present in the graph, while other are removed. Prove that in all 16 cases (one case is shown on the right) the partition functions differ by the same factor:

$$Z_{\text{left picture}} = \mathbb{W} \cdot Z_{\text{right picture}}.$$

D. For each n we take $2n^2$ variables on edges of the graph corresponding to the Aztec diamond and let Z_n be the corresponding partition function, *i.e.*, sum over all perfect matchings of products of variables of the matched edges. Using part **C** prove the recurrence:

$$Z_n = (??) \cdot Z_{n-1}. \tag{6.83}$$

Find what the $(??)$ factor is and how the variables for Z_n are related to the variables for Z_{n-1}.
Hint. For $n = 2$ you need the following sequence of transformations of graphs and four urban renewals.



E. Prove that the following recursive algorithm samples perfect matchings from the distribution

$$\mathbb{P}(\text{matching } \sigma) = \frac{1}{Z_n} \prod_{e \in \sigma} \text{variable}(e).$$

Step 1: given target weights (variables) for size n Aztec diamond, compute the corresponding variables for size $n-1$ diamond entering (6.83). Assume that a perfect matching for size $n-1$ (and corresponding weights) has already been sampled.
Step 2: Interpret the urban renewal identity of part **C** as a random mapping from right to left: forget about the particular perfect matching on the right; for each of the 16 cases on the left one has either one possible matching, or two. In the former case output that matching; in the latter case, flip an independent coin to ouput one of the two matchings with probabilities proportional to their weights.
Step 3: Interpret the transformation of the graphs in part **D** as a random mapping from perfect matchings of size $n-1$ diamond to perfect matchings of size n diamond.

F. Show that if all variables of edges corresponding to East dominos are set to α, all variables of edges corresponding to West dominos are set to β, and all variables of horizontal edges are set to 1, then the algorithm of part **E** is the same as the shuffling algorithm of Section 6.2.

Problem 10. Check that $\mathcal{G}_{\mathbb{U}}(z, z')$ given by (6.64) satisfies Definition 6.28. In more detail, you need to check that for each fixed $z' \in \mathbb{U}$, $\mathcal{G}_{\mathbb{U}}(z, z')$ tends to 0 as z becomes real or goes to infinity. Also you need to check that for any smooth $f(z)$ whose support is a compact subset of $\mathbb{U}$, and any $z' \in \mathbb{U}$, we have:

$$\iint_{\mathbb{U}} f(z) \triangle \mathcal{G}_{\mathbb{U}}(z, z') \mathrm{d}x\mathrm{d}y = \iint_{\mathbb{U}} \triangle f(z) \mathcal{G}_{\mathbb{U}}(z, z') \mathrm{d}x\mathrm{d}y = -f(z'), \qquad z = x + \mathbf{i}y. \tag{6.84}$$

Remark. These properties uniquely determine a continuous outside $\{z = z'\}$ function given by (6.64).

Problem 11. Verify the conformal-invariance of GFF given by (6.68).

Problem 12. Consider the standard Brownian bridge: $B : [0, 1] \to \mathbb{R}$, $B(0) = B(1) = 0$, which can be defined as the Brownian motion conditioned to be at 0 at time 1, or as a centered Gaussian process with covariance function

$$\mathbb{E} B_s B_t = \mathcal{C}(s, t) = \min(t, s)(1 - \max(t, s)), \qquad 0 \le t, s \le 1. \tag{6.85}$$

Prove that the function $\mathcal{C}(s, t)$ is the kernel of the minus inverse Laplace operator[7] on the interval $[0, 1]$ with Dirichlet boundary conditions at 0 and 1. Hence, the Brownian bridge is the one-dimensional version of the Gaussian free field.

Literature. We used the following sources for composing problems and refer to them for more information, references, and connections: [Fom99], [Sag01], [Pro03], [Joh05], [CJY15], [Ahn22], [GN25], and [WP21].

[7] The one dimensional Laplace operator is $\frac{\partial^2}{\partial x^2}$.

Chapter 7

Six-vertex model with domain wall boundary conditions

7.1 Definition of the six-vertex model in a planar domain

Our next stop is the six-vertex or square-ice model. It has several equivalent combinatorial interpretations, with the most convenient one for developing mathematical theory being a representation as a collection of lattice paths.

A configuration of the six-vertex model in a finite domain $\Omega \subset \mathbb{Z}^2$ is an assignment to the vertices of this domain of one of the six types of configurations of the top panel Figure 7.1 in a consistent way, *i.e.*, so that the outcome is a collection of lattice paths which travel in the up-right direction along the edges of the grid. The paths are allowed to touch each other but not to cross (see vertex of Type (2) in Figure 7.1), and connect points on the boundary of Ω. Let $\partial\Omega$ be the collection of all edges of the grid connecting Ω to its complement $\mathbb{Z}^2 \setminus \Omega$. By a *boundary condition* we mean a choice of a $\{0,1\}$-sequence of length $|\partial\Omega|$, where each 1 indicates that the corresponding edge of Ω is occupied by a path and 0 indicates that the edge is not occupied. A configuration is consistent with boundary conditions if the paths leave/enter domain Ω through the edges of $\partial\Omega$ labeled with 1's and only through them.

As a simple example, take Ω to be the $N \times N$ square, $\Omega = \{1,\dots,N\} \times \{1,\dots,N\}$, with $|\partial\Omega| = 4N$ and the boundary condition such that all the edges along the left and top boundaries are occupied and all the edges along the bottom and right boundaries are not occupied, see Figure 7.2. This situation is usually called the "Domain Wall Boundary Condition". A more complicated example of a domain Ω is shown in Figure 7.3.

We introduce a weight $w_i > 0$ for each vertex type $i = 1, 2, \dots, 6$ and define the probability of a configuration σ of the six-vertex model in domain Ω as

$$\mathbb{P}(\sigma) = \frac{1}{Z} \prod_{i=1}^{6} w_i^{N_i(\sigma)}, \tag{7.1}$$

where $N_i(\sigma)$ is the number of vertices of Type i in the configuration σ. The normalization Z in (7.1) is chosen so that the sum over all σ in Ω is 1, and this Z is referred to as the *partition function*. The measure itself is sometimes called a Boltzmann distribution and sometimes a Gibbs distribution. It is convenient to split the six vertices into three pairs, such that the two configurations in a pair are complementary to each other, *i.e.*, differ by paths-no-paths involution. The pairs will be referred to as Type a vertices (Type (1) and Type (2) in Figure 7.1), Type b vertices (Type (3) and Type (4)), Type c vertices (Type (5) and

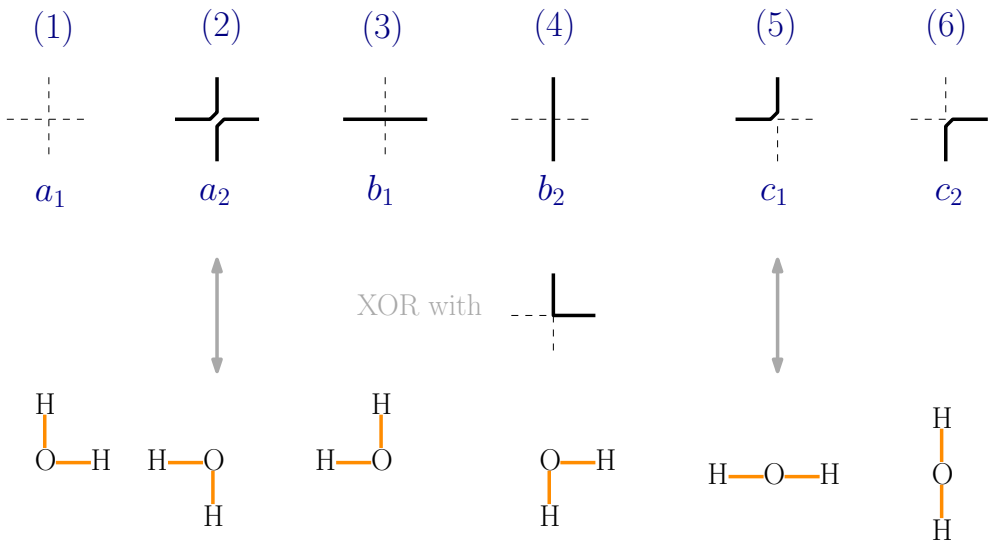


Figure 7.1: The six types of vertices and their weights.

Type (6)); their weights are denoted $a_1, a_2; b_1, b_2; c_1, c_2$, respectively. Hence, the partition function Z is a function of these weights and domain Ω: $Z = Z(a_1, a_2, b_1, b_2, c_1, c_2; \Omega)$.

The six-vertex model is also known as *square ice*, due to the bijection between the local configurations of paths and configurations of H_2O molecules on the grid, shown in Figure 7.1. The bijection can be described by placing O in the middle, connecting O to H to the left if a path enters the vertex from the left, connecting to H to the right, if a path *does not* leave the vertex to the right, connecting to H downward if a path enters from the bottom, and connecting to H in upward direction if a path *does not* leave through the top. Puting it otherwise, H_2O connectivity is obtained by XOR-ing the paths' connectivity with up and right directions. The result of applying the bijection to configurations in a 5×5 square is shown in Figure 7.2.

Equivalently, the definition of the square ice model on the lattice $\mathbb{Z}^2$ begins with the placement of atoms "O" at the vertices and atoms "H" at the edges connecting adjacent vertices of the grid. A configuration of the model is a matching of these atoms into molecules of water, H_2O, such that each atom is matched and each O is matched to two neighboring H's out of four. Note that there are $\binom{4}{2} = 6$ ways to choose two neighbors out of the four, hence, there are six possible local configurations of a molecule at a vertex, leading to the name "six-vertex model".

In this way we arrive at a model of statistical mechanics introduced by Pauling in 1935 [Pau35] with the goal of computing numeric characteristics (*e.g.*, the residual entropy) of the real-world ice; the six-vertex model can be seen as a model for "two-dimensional ice" because its state space can be defined as allowed configurations of water molecules arranged in a finite piece of the square lattice. There are thousands of papers in mathematical and theoretical physics literature devoted to the study of the six-vertex model. The early influential results concerned the computation of the partition function Z for the model on the torus going back to the seminal work of Lieb in 1967 [Lie67a]; see also the extensive survey of Lieb and Wu [LW72]. Many other developments in the study of the six-vertex model are covered in the classical 1982 textbook by Baxter [Bax07], and we also refer to [Res10] for a more recent review. There were attempts to observe planar six-vertex model experimentally, although with mixed success, see [ASLW$^+$15], discussion in [ZYW$^+$15], and another setting in [JB25].

From the probabilistic point of view, we are interested in the properties of the probability distribution

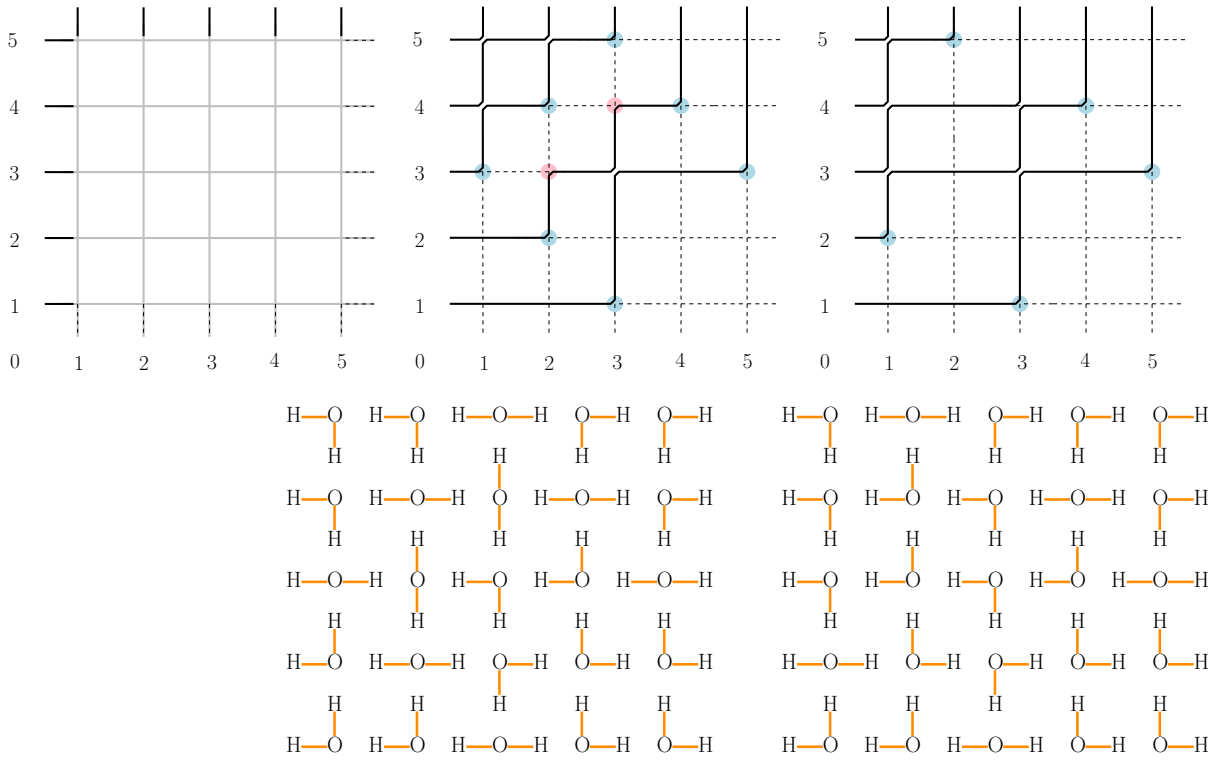


Figure 7.2: $N \times N$ square with Domain Wall Boundary Conditions for $N = 5$, two possible configurations of paths with Type c vertices highlighted, and the same configurations in H_2O representation

(7.1). It turns out that it depends on two, rather than six parameters $a_1, a_2, b_1, b_2, c_1, c_2$.

Proposition 7.1. *For any finite domain $\Omega \subset \mathbb{Z}^2$, equipped with boundary conditions for the six-vertex model along $\partial\Omega$ and six weights $(w_1, \ldots, w_6) = (a_1, a_2, b_1, b_2, c_1, c_2)$ (which are the same for all vertices (i, j)), the Gibbs measure* (7.1) *only depends on the two parameters $\frac{b_1 b_2}{a_1 a_2}$ and $\frac{c_1 c_2}{a_1 a_2}$.*

Proof. Given a configuration σ, we denote by $N_i(\sigma)$ the number of vertices Type i, accorging to Figure 7.1. Each linear combination of the N_i's whose value is independent of the configuration, leads to a one parameter family of transformations of the weights that preserve the Gibbs measure. We have the following conserved quantities and corresponding transformations:

1. Since the number of vertices in the domain equals $\sum_{i=1}^{6} N_i$ and does not depend on the configuration, multiplying all six weighs by a constant preserves the measure (7.1).

2. Since all paths have fixed entry and exit points, the number of times a particular path turns up minus the number of times it turns right is prescribed by the boundary conditions to be one of the three numbers $\{-1, 0, 1\}$. This implies that $N_5 - N_6$ does not depend on a configuration. Hence, $(c_1, c_2) \to (\alpha c_1, \frac{1}{\alpha} c_2)$ preserves the measure (7.1).

3. The total number of edges occupied by a path is determined by the boundary conditions (*i.e.*, its entrance and exit points along $\partial\Omega$), which implies that $2N_2 + N_3 + N_4 + N_5 + N_6$ does not depend on the configuration. Together with the first conserved quantity, this implies a fixed value of $N_1 - N_2$. Thus, $(a_1, a_2) \to (\alpha a_1, \frac{1}{\alpha} a_2)$ preserves the measure (7.1).

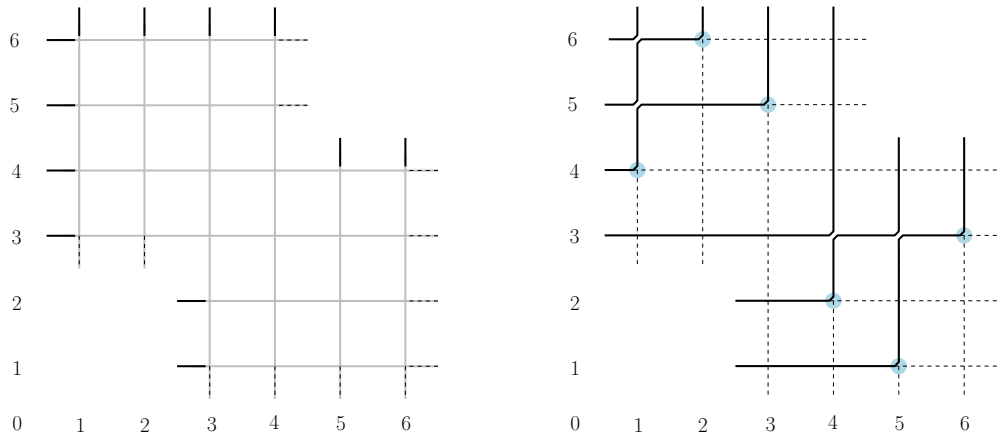


Figure 7.3: A domain with 24 vertices and a possible configuration of the six vertex model.

4. The total number of edges occupied by a path can be split into vertical and horizontal ones, and both are determined by the boundary conditions. The horizontal edges give fixed $N_2+N_3+\frac{1}{2}N_5+\frac{1}{2}N_6$. Subtracting $\frac{1}{2}$ of the previous conserved quantity, we get that $N_3 - N_4$ does not depend on a configurtion. So $(b_1, b_2) \to (\alpha b_1, \frac{1}{\alpha} b_2)$ preserves the measure (7.1).

Using these four transformation we can get any six-tuple $a_1, a_2, b_1, b_2, c_1, c_2$ from any other six-tuple with the same values of $\frac{b_1 b_2}{a_1 a_2}$ and $\frac{c_1 c_2}{a_1 a_2}$. □

7.2 Domain Wall Boundary Conditions

For the rest of this chapter we focus on Ω being an $N \times N$ square equipped with domain wall boundary conditions, as in Figure 7.2. This situation has fruitful combinatorics connecting us to the alternating sign matrices and the domino tilings of the Aztec diamond.

Let us record the positions of c_1 and c_2 vertices in a configuration as 1's and -1's in an $N \times N$ matrix, with all other matrix elements being zeros. In this way, the configurations in Figure 7.2 become 6×6 matrices:

$$\begin{pmatrix} 0 & 0 & 1 & 0 & 0 \\ 0 & 1 & -1 & 1 & 0 \\ 1 & -1 & 0 & 0 & 1 \\ 0 & 1 & 0 & 0 & 0 \\ 0 & 0 & 1 & 0 & 0 \end{pmatrix} \qquad \begin{pmatrix} 0 & 1 & 0 & 0 & 0 \\ 0 & 0 & 0 & 1 & 0 \\ 0 & 0 & 0 & 0 & 1 \\ 1 & 0 & 0 & 0 & 0 \\ 0 & 0 & 1 & 0 & 0 \end{pmatrix} \tag{7.2}$$

Proposition 7.2. *The matrices encoding the positions of* 1*'s and* -1*'s are* alternating sign matrices *(ASM): the* 1*'s and* -1*'s in each row alternate; the* 1*'s and* -1*'s in each column alternate; the sum in each row is* 1*; the sum in each column is* 1*. The correspondence between the configurations of the six-vertex model with domain wall boundary conditions and ASMs is a bijection.*

Proof. Let us change the meaning of a Type (2), *i.e.*, a_2 vertex from paths touching each other to paths crossing, as shown in Figure 7.4. Then the paths only turn at Type c vertices: as we follow them in up-right direction, the horizontal-to-vertical turns happen at Type (5), *i.e.*, c_1 vertices and vertical-to-horizontal turns happen at Type (6), *i.e.*, c_2 vertices. In this way, each c_1 vertex corresponds to two rays going up and left from it, until reaching a c_2 vertex or exiting the domain. Each c_2 vertex correspond



Figure 7.4: The change of meaning of Type (2) vertices.

to two rays going right and down from it until reaching a c_1 vertex (since no paths exit/enter through the right or bottom boundaries, exiting the domain is impossible for these paths). Together with the fact that rays must exit at every grid line on the left and at the top, this implies that each c_2 vertex must be between two c_1 vertices both in horizontal and in vertical directions. In addition, the first and last Type c vertex in each row and column is necessarily of Type c_1 (again, otherwise a path would have to enter/exit through bottom/right boundary or there would be no path somewhere along left/top boundary). Hence, positions of 1s and -1s alternate and the row/column sums in the matrix are equal to 1.

Once we fixed the positions of all c_1 and c_2 vertices according to an ASM, all paths are uniquely determined by drawing the above rays. If we know the paths, then we know the vertex types for the rest of the configuration. This proves the bijectivity. □

Note that each permutation $\sigma \in \mathcal{S}_N$ gives rise to an ASM with 1's at positions $(i, \sigma(i))$, $1 \le i \le N$, and no -1's. The ASM on the right in (7.2) is like that. This implies that the total number of ASMs is at least $N!$. In fact, there are many more, as first conjectured in [MRR83], and proven in [Zei96, Kup96].

Theorem 7.3. *The total number of $N \times N$ alternating sign matrices is*

$$\#\{N \times N \text{ ASMs}\} = \prod_{i=0}^{N-1} \frac{(3i+1)!}{(N+i)!}. \tag{7.3}$$

These numbers are $1, 2, 7, 42, 429, 7436, 218348, \ldots$. For instance, here are seven ASMs for $N = 3$:

$$\begin{pmatrix} 1 & 0 & 0 \\ 0 & 1 & 0 \\ 0 & 0 & 1 \end{pmatrix}, \begin{pmatrix} 1 & 0 & 0 \\ 0 & 0 & 1 \\ 0 & 1 & 0 \end{pmatrix}, \begin{pmatrix} 0 & 1 & 0 \\ 1 & 0 & 0 \\ 0 & 0 & 1 \end{pmatrix}, \begin{pmatrix} 0 & 0 & 1 \\ 0 & 1 & 0 \\ 1 & 0 & 0 \end{pmatrix}, \begin{pmatrix} 0 & 1 & 0 \\ 0 & 0 & 1 \\ 1 & 0 & 0 \end{pmatrix}, \begin{pmatrix} 0 & 0 & 1 \\ 1 & 0 & 0 \\ 0 & 1 & 0 \end{pmatrix}, \begin{pmatrix} 0 & 1 & 0 \\ 1 & -1 & 1 \\ 0 & 1 & 0 \end{pmatrix}.$$

We deduce Theorem 7.3 in Section 7.5 from the evaluation of the *Izergin-Korepin determinant*, which we are soon to introduce. The formula (7.3) is complicated, but a simpler answer exists for a weighted count:

Theorem 7.4. *The total number of $N \times N$ alternating sign matrices weighted as $2^{\#\{-1\}}$ is*

$$\sum_{\sigma \text{ is an } N \times N \text{ ASM}} 2^{\#\{-1 \text{ in } \sigma\}} = 2^{N(N-1)/2}. \tag{7.4}$$

We again deduce Theorem 7.4 in Section 7.5 from the evaluation of the Izergin-Korepin determinant.

Comparing (7.4) to the enumeration of domino tilings in Corollary 6.4, one suspects a connection between tilings of $n \times n$ Aztec diamond and 2–weighted $N \times N$ ASMs if we set $N = n + 1$. Beyond the partition functions, this connection manifests as a non-bijective correspondence which we now describe, see Figure 7.5.

1. Given a domino tiling of the size n Aztec diamond, construct the corresponding set of green particles at gray squares of West and South dominos, as in Section 6.1.

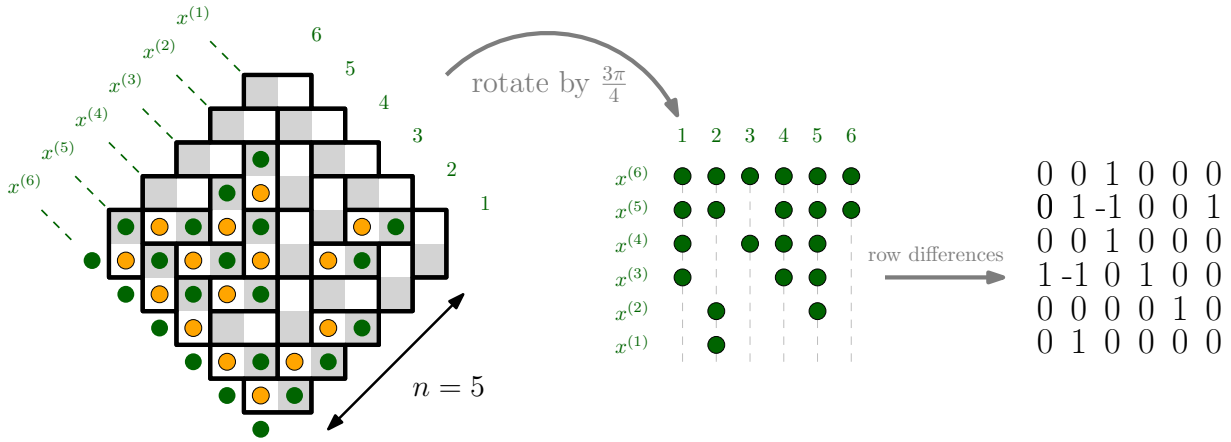


Figure 7.5: The mapping from domino tilings to ASMs.

2. Rotate the particle configuration by $\frac{3\pi}{4}$ clockwise, and represent the configuration as an $(n+1) \times (n+1)$ matrix of 1's and 0's, where 1's encode the green particles. The matrix has k 1's in the kth row from below.

3. Compute the differences of the kth and $(k-1)$st rows from below for $k = 1, 2, \ldots, n+1$, assuming the 0th row to be filled with 0's.

Theorem 7.5. *The output of this procedure is an $(n+1) \times (n+1)$ ASM. The preimage of an ASM with $m \geq 0$ entries equal to -1 consists of 2^m different domino tilings.*

Proof. The properties of partitions in Proposition 6.1 are recast as inequalities for the green particle positions:

$$n+1 \geq x_1^{(m)} > x_2^{(m)} > \cdots > x_m^{(m)} \geq 1, \qquad x_i^{(m+1)} \geq x_i^{(m)} \geq x_{i+1}^{(m+1)}. \tag{7.5}$$

When we subtract the row $(k-1)$ from the row k, we are subtracting two $0/1$ arrays, and therefore are getting $0/1/-1$ array. Because of the inequalities (7.5), the 1's and -1's interlace along the resulting row. Because the sums of the differences of rows are non-negative, the 1's and -1's also interlace along each column. We conclude that the output is indeed an ASM.

In order to construct the preimage, note that the ASM uniquely determines positions of green particles: the particles in the mth layer are 1's in the sum of the m bottom rows of the ASM. Using Proposition 6.1, in order to reconstruct the tiling we need to also determine the positions of yellow particles. Those are always adjacent to the green particles (they are covered by the same domino), and for each green particle there is either a unique choice of the yellow one adjacent to it, or there are two options. The second case corresponds to a green particle $x_i^{(m)}$ such that strict inequalities $x_i^{(m+1)} > x_i^{(m)} > x_{i+1}^{(m+1)}$ hold, and the first case arises when $x_i^{(m)}$ is equal to either $x_i^{(m+1)}$ or $x_{i+1}^{(m+1)}$. Hence, in the second case we have a green particle in row m with no particle at the same position in row $m+1$, which leads to the appearance of the -1 in row $m+1$ (from the bottom) in the ASM. We conclude that each -1 in the ASM creates a choice between two cases for the preimage, and all choices are independent. □

7.3 The Yang-Baxter equation

Theorems 7.3 and 7.4 are computations of the partition function Z for the six-vertex model in a particular domain, as in (7.1). Many other such computations are important building blocks for the investigations

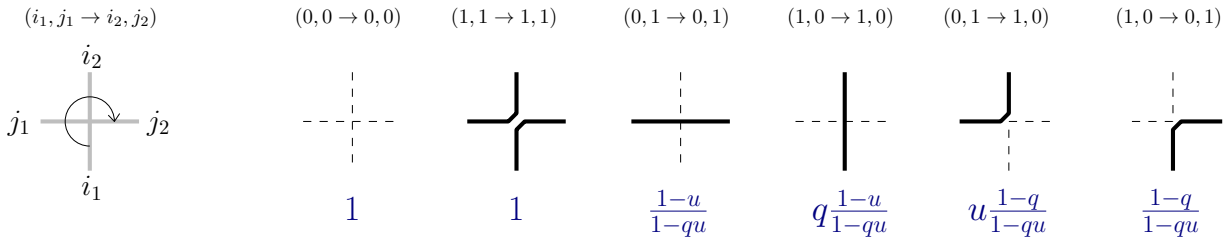


Figure 7.6: The six stochastic weights parameterized by q and u.

of the asymptotics of the model. In turn, the evaluations of the partition functions are often based on modifications of the domain Ω. The simplest of such modifications operates with a domain containing three vertices and is the celebrated *Yang-Baxter equation.*

We parameterize a vertex through two inputs denoted $i_1, j_1 \in \{0, 1\}$ and two outputs $i_2, j_2 \in \{0, 1\}$, subject to the condition $i_1 + j_1 = i_2 + j_2$. The indices are arranged in i_1, j_1, i_2, j_2 order in clockwise direction, starting from the bottom. Hence, $i_1 = 1$ means that there is an edge entering in the vertex from below, while $i_2 = 1$ means that there is an edge exiting the vertex at the top. In the Yang-Baxter equation the six possible weights are not the same for the three vertices, but vary in a particular way. The weights we use are based on two parameters, rather than six, which can be motivated by Proposition 7.1. They depend on the *quantization parameter* q and *spectral parameter* u through the following formulas, also shown in Figure 7.6:

$$\begin{aligned} &w_u(0,0 \to 0,0) = a_1 = 1, && w_u(1,1 \to 1,1) = a_2 = 1, \\ &w_u(0,1 \to 0,1) = b_1 = \frac{1-u}{1-qu}, && w_u(1,0 \to 1,0) = b_2 = q\frac{1-u}{1-qu}, \\ &w_u(0,1 \to 1,0) = c_1 = \frac{u(1-q)}{1-qu}, && w_u(1,0 \to 0,1) = c_2 = \frac{1-q}{1-qu}. \end{aligned} \tag{7.6}$$

These weights are called *stochastic*, because of the $a_1 = a_2 = b_1 + c_1 = b_2 + c_2 = 1$ relations, which will get a probabilistic meaning in the next chapter. For all our domains Ω, the parameter q is going to be fixed (and therefore we omit it from the notations), while u might be varying from vertex to vertex (and therefore kept in the notation). It is convenient to extend the definition also to (i_1, j_1, i_2, j_2) not satisfying $i_1 + j_1 = i_2 + j_2$, by setting the remaining weights to 0:

$$\begin{aligned} &w_u(0,0 \to 0,1) = w_u(0,0 \to 1,0) = w_u(0,0 \to 1,1) = w_u(1,0 \to 0,0) = w_u(1,0 \to 1,1) = 0, \\ &w_u(0,1 \to 0,0) = w_u(0,1 \to 1,1) = w_u(1,1 \to 0,0) = w_u(1,1 \to 1,0) = w_u(1,1 \to 0,1) = 0. \end{aligned} \tag{7.7}$$

In this way, w_u can be treated as a 4×4 matrix with rows parameterized by (i_1, j_1) and columns parameterized by (i_2, j_2). This is usually called the R–matrix, and we use $(0,0)$, $(0,1)$, $(1,0)$, $(1,1)$ ordering for its rows and columns:

$$R(u) = \begin{pmatrix} 1 & 0 & 0 & 0 \\ 0 & \frac{1-u}{1-qu} & u\frac{1-q}{1-qu} & 0 \\ 0 & \frac{1-q}{1-qu} & q\frac{1-u}{1-qu} & 0 \\ 0 & 0 & 0 & 1 \end{pmatrix}. \tag{7.8}$$

The stochasticity of the weights means that the R–matrix is stochastic: the sum along each row is 1. Note, however, that at this point q and u are arbitrary complex numbers, and therefore we do not claim any positivity of the weights.

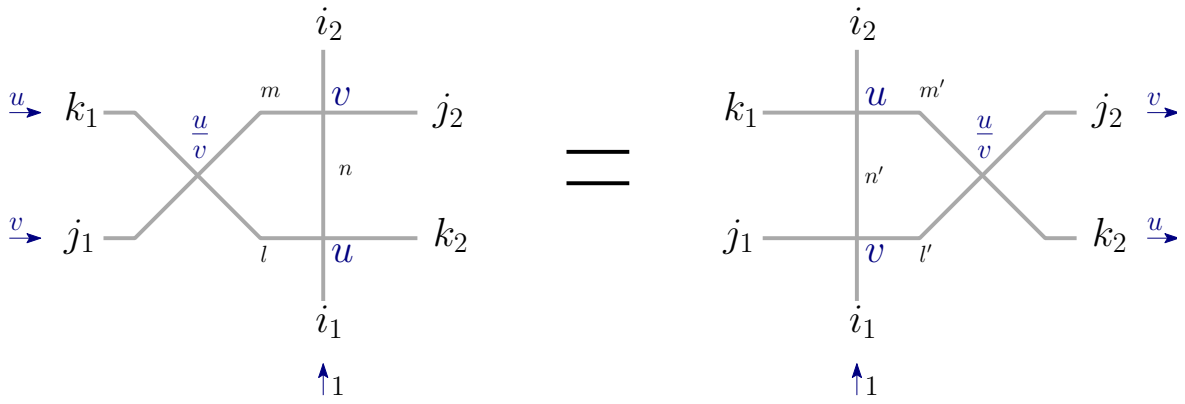


Figure 7.7: The Yang-Baxter equation as a move of the cross.

Theorem 7.6 (Yang–Baxter Equation). *For each $i_1, j_1, k_1, i_2, j_2, k_2 \in \{0,1\}$, the following identity of rational functions of u, v, and q holds:*

$$\sum_{l,m,n\in\{0,1\}} w_{u/v}(j_1, k_1 \to m, l) w_u(i_1, l \to n, k_2) w_v(n, m \to i_2, j_2)$$
$$= \sum_{l',m',n'\in\{0,1\}} w_v(i_1, j_1 \to n', l') w_u(n', k_1 \to i_2, m') w_{u/v}(l', m' \to j_2, k_2). \tag{7.9}$$

Graphically, Theorem 7.6 is an identity between partition functions of the six-vertex model in two three–vertex domains with two different assignments of the spectral parameters and matching boundary conditions, with incoming paths encoded as $(i_1, j_1, k_1) \in \{0,1\}^3$ and exiting paths encoded by $(i_2, j_2, k_2) \in \{0,1\}^3$, as in Figure 7.7. The summation variables l, m, n and l', m', n' encode the types of three vertices in the domains, and the sums are partition functions. A delicate point is that these domains are not in $\mathbb{Z}^2$. Instead, we connect the inputs and outputs of each vertex in such a way that three vertices form a triangle, so that the u and v vertices are exactly as they were in Figure 7.6, while the u/v vertex is rotated by $\frac{\pi}{4}$ in clockwise direction so that paths flow from left to right, as in Figure 7.8. We are going to refer to such a rotated vertex as a *cross*. In this way, (7.9) is an identity allowing to move a cross through a vertical line connecting two vertices at the expense of swapping the spectral parameters u and v of these vertices. The hidden rule for assigning the spectral parameters to the vertices is as follows: there are three braids/threads/lines in the picture (which intersect at the vertices) with assigned *rapidities* u ($k_1 - k_2$ braid), v ($j_1 - j_2$ braid), and 1 ($i_1 - i_2$ braid), as in Figure 7.7; the spectral parameter at a vertex is the ratio of the rapidities of the two meeting braids[1].

An alternative representation of Theorem 7.6 is shown in Figure 7.9. Now the inputs (i_1, j_1, k_1) are on the left, the outputs (i_2, j_2, k_2) are on the right, and all vertices are crosses. In this way, reading presence/absence of paths in the vertical coordinate system from top to bottom, (7.9) becomes an identity between two chains of transformations: $(k_1, j_1, i_1) \to (m, l, i_1) \to (m, n, k_2) \to (i_2, j_2, k_2)$ and $(k_1, j_1, i_1) \to (k_1, n', l') \to (i_2, m', l') \to (i_2, j_2, k_2)$. Alternatively, if we read the presence/absence of paths along the i-braid, j-braid, and k–braid (treating the gray lines in Figure 7.9 as three braids intersecting at the crosses), (7.9) becomes an identity between two related chains of transformations: $(i_1, j_1, k_1) \to (i_1, m, l) \to (n, m, k_2) \to (i_2, j_2, k_2)$ and $(i_1, j_1, k_2) \to (n', l', k_2) \to (i_2, l', m') \to (i_2, j_2, k_2)$. Figure 7.10 illustrates these two different points of view.

[1] If rapidity 1 were replaced by w, then the spectral parameters of the vertices would had a more symmetric form $\frac{u}{v}$, $\frac{v}{w}$, $\frac{u}{w}$.

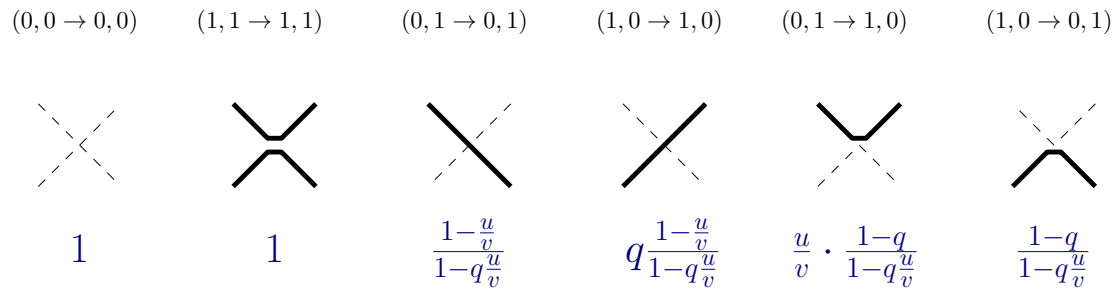


Figure 7.8: A rotated vertex (cross) with spectral parameter $\frac{u}{v}$.

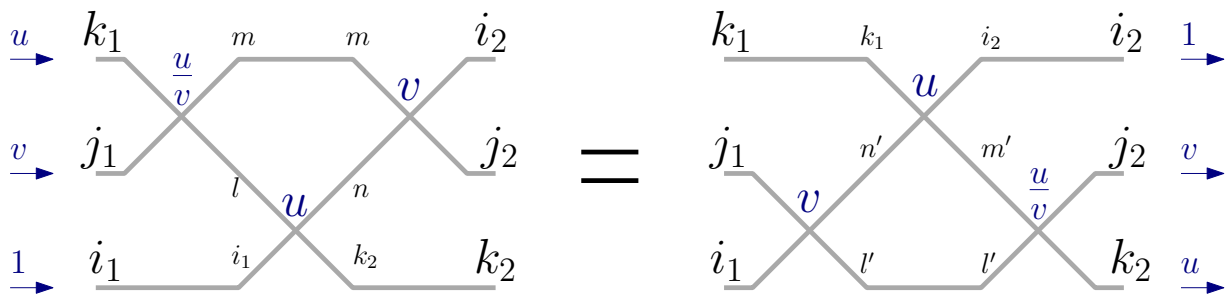


Figure 7.9: The Yang-Baxter equation as a braid relation.

We can also represent a transformation of a length three $0-1$ vector as a $2^3\times 2^3=8\times 8$ transition matrix. This matrix is constructed from the R–matrix (7.8). The latter is acting on length two $0-1$ vectors and can be represented as a 8×8 matrix acting on length three vectors in different ways. Using the vertical coordinate system, (7.9) turns into an identity of 8×8 matrices

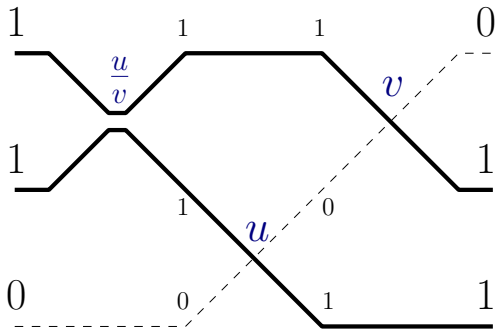
$$\check{R}_{12}\big(\tfrac{u}{v}\big)\check{R}_{23}(u)\check{R}_{12}(v)=\check{R}_{23}(v)\check{R}_{12}(u)\check{R}_{23}\big(\tfrac{u}{v}\big), \tag{7.10}$$

known as the *braided Yang-Baxter relation*. On the other hand, in the coordinate system relative to i, j, and k braids, (7.9) turns into a different identity of 8×8 matrices

$$R_{jk}\big(\tfrac{u}{v}\big)R_{ik}(u)R_{ij}(v)=R_{ij}(v)R_{ik}(u)R_{jk}\big(\tfrac{u}{v}\big). \tag{7.11}$$

The difference between (7.10) and (7.11) is in the way the 4×4 R–matrix (7.8) is represented as an 8×8 matrix in the factors. In (7.11), we identify rows/columns of the matrix with length three $0-1$ vectors with coordinates named i, j, and k corresponding to the three braids. R_{ij}, R_{ik}, R_{jk} act as (7.8) on the corresponding two coordinates and as the identity on the remaining coordinate. Hence, the $(i_1,j_1,k_1)\to(i_2,j_2,k_2)$ matrix element for $R_{ij}(u)$ is $\mathbf{1}_{k_1=k_2}w_u(i_1,j_1\to i_2,j_2)$, for $R_{ik}(u)$ is $\mathbf{1}_{j_1=j_2}w_u(i_1,k_1\to i_2,k_2)$, and for $R_{jk}(u)$ is $\mathbf{1}_{i_1=i_2}w_u(j_1,k_1\to j_2,k_2)$. In contrast, in (7.10), the row/columns of the matrix are identified with length three vectors with coordinates named 1, 2, 3, corresponding to the vertical coordinate in Figure 7.10. Hence, $(x^1,x^2,x^3)\to(y^1,y^2,y^3)$ matrix element for $\check{R}_{12}(u)$ is $\mathbf{1}_{x^3=y^3}w_u(x^2,x^1\to y^1,y^2)$, for $\check{R}_{13}(u)$ is $\mathbf{1}_{x^2=y^2}w_u(x^3,x^1\to y^1,y^3)$, and for $\check{R}_{23}(u)$ is $\mathbf{1}_{x^1=y^1}w_u(x^3,x^2\to y^2,y^3)$. If we identify i,j,k with $3,2,1$ (as they are in the left-most column of Figure 7.9), then $\check{R}$ matrices differ from R matrices by multiplication with the transposition matrices.

In particular, in the *classical limit* $q=1$, $u=v=u/v=0$, $R(u)=R(v)=R(u/v)=\mathrm{Id}$, and (7.11) becomes a trivial equality of the products of three identity matrices. However, $\check{R}$ matrices turn



Vertical coordinate system:
$(1,1,0) \to (1,1,0) \to (1,0,1) \to (0,1,1)$

Coordinate system relative to braids:
$(0,1,1) \to (0,1,1) \to (0,1,1) \to (0,1,1)$

Figure 7.10: One configuration of three vertices encoded in two different coordinate systems.

into transpositions and (7.10) becomes the braid or Coxeter relation for transpositions in $\mathcal{S}_3$:

$$(1,2)(2,3)(1,2) = (2,3)(1,2)(2,3). \tag{7.12}$$

The name "Yang–Baxter equation" originates from a 1967 paper of Yang [Yan67] (who studied quantum many-body systems, see also McGuire [McG64], Brezin–Zinn-Justin [BZJ66]), and a 1972 paper of Baxter [Bax72] (who studied lattice models and used the name "star-triangle relation" — terminology going back to the 1944 work of Onsager [Ons44] on the Ising model).

An exploration of families of the R-matrices, which can satisfy the equations (7.10) or (7.11), and formalization of a procedure for construction of new solutions from existing ones, led to the introduction and study of quantum groups. Another connection is to the study of Young operators in the group algebra of symmetric group initiated by Jucys in 1966 in [Juc66]. The surveys and books [Jim94, GRAS96, Bax07, Res10, Lam15] give a more detailed account of quantum integrability and the Yang–Baxter equation.

Proof of Theorem 7.6. This is a direct check for all $64 = 2^6$ cases. In principle, any modern mathematical software can directly verify the required 8×8 matrix identity in either of the forms (7.10) or (7.11). Nevertheless, let us break it down into simpler ingredients, in order to see the structure of the identity.

We first note that if $i_1 + j_1 + k_1 \neq i_2 + j_2 + k_2$, then both sides of (7.9) vanish — there are no configurations satisfying such boundary conditions. Next, notice that simultaneous inversion of q and u swaps the pairs of the weights $a_1 \leftrightarrow a_2$, $b_1 \leftrightarrow b_2$, $c_1 \leftrightarrow c_2$. Hence, by paths/no paths involution, (7.9) for $(i_1, j_1, k_1, i_2, j_2, k_2)$ is equivalent to the identity for $(1-i_1, 1-j_1, 1-k_1, 1-i_2, 1-j_2, 1-k_2)$, and we may check only one identity from each pair. For $(0,0,0,0,0,0)$ there is only one non-zero term in each of the sides of (7.9), and it is equal to 1. Nine cases remain: each of (i_1, j_1, k_1) and (i_2, j_2, k_2) can be equal to $(1,0,0)$, or $(0,1,0)$, or $(0,0,1)$; the configurations for such boundary conditions consist of a single path.

We verify the 3×3 block of the identity (7.10) for $\check{R}$ corresponding to these nine cases. Hence, we trace the single path from the left boundary to the right boundary. In the following matrices the three

rows correspond to $(1,0,0)$, $(0,1,0)$, $(0,0,1)$, in the top to bottom order. Then we need to check

$$\begin{pmatrix} \frac{u}{v}\cdot\frac{1-q}{1-q\frac{u}{v}} & \frac{1-\frac{u}{v}}{1-q\frac{u}{v}} & 0 \\ q\frac{1-\frac{u}{v}}{1-q\frac{u}{v}} & \frac{1-q}{1-q\frac{u}{v}} & 0 \\ 0 & 0 & 1 \end{pmatrix} \begin{pmatrix} 1 & 0 & 0 \\ 0 & u\frac{1-q}{1-qu} & \frac{1-u}{1-qu} \\ 0 & q\frac{1-u}{1-qu} & \frac{1-q}{1-qu} \end{pmatrix} \begin{pmatrix} v\frac{1-q}{1-qv} & \frac{1-v}{1-qv} & 0 \\ q\frac{1-v}{1-qv} & \frac{1-q}{1-qv} & 0 \\ 0 & 0 & 1 \end{pmatrix}$$

$$\stackrel{?}{=} \begin{pmatrix} 1 & 0 & 0 \\ 0 & v\frac{1-q}{1-qv} & \frac{1-v}{1-qv} \\ 0 & q\frac{1-v}{1-qv} & \frac{1-q}{1-qv} \end{pmatrix} \begin{pmatrix} u\frac{1-q}{1-qu} & \frac{1-u}{1-qu} & 0 \\ q\frac{1-u}{1-qu} & \frac{1-q}{1-qu} & 0 \\ 0 & 0 & 1 \end{pmatrix} \begin{pmatrix} 1 & 0 & 0 \\ 0 & \frac{u}{v}\cdot\frac{1-q}{1-q\frac{u}{v}} & \frac{1-\frac{u}{v}}{1-q\frac{u}{v}} \\ 0 & q\frac{1-\frac{u}{v}}{1-q\frac{u}{v}} & \frac{1-q}{1-q\frac{u}{v}} \end{pmatrix}. \quad (7.13)$$

At $q=1$, $u=v=u/v=0$, all matrices become permutations, and we are back to (7.12). The q–version of (7.13) is a direct verification: there is no further shortcut here and one needs to compare all matrix elements on both sides. The $(1,1)$ matrix element match is the identity:

$$\frac{u}{v}\cdot\frac{1-q}{1-q\frac{u}{v}}\cdot v\frac{1-q}{1-qv}+\frac{1-\frac{u}{v}}{1-q\frac{u}{v}}\cdot u\frac{1-q}{1-qu}\cdot q\frac{1-v}{1-qv}\stackrel{?}{=}u\frac{1-q}{1-qu}, \quad (7.14)$$

which becomes, after clearing the denominators, a basic polynomial identity

$$v(1-q)(1-qu)+q(v-u)(1-v)=(v-qu)(1-qv). \quad (7.15)$$

The $(2,2)$ matrix element match is the identity:

$$\frac{1-q}{1-q\frac{u}{v}}\cdot u\frac{1-q}{1-qu}\cdot\frac{1-q}{1-qv}+q\frac{1-\frac{u}{v}}{1-q\frac{u}{v}}\cdot\frac{1-v}{1-qv}\stackrel{?}{=}v\frac{1-q}{1-qv}\cdot\frac{1-q}{1-qu}\cdot\frac{u}{v}\cdot\frac{1-q}{1-q\frac{u}{v}}+\frac{1-v}{1-qv}\cdot q\frac{1-\frac{u}{v}}{1-q\frac{u}{v}}, \quad (7.16)$$

which is trivially true by the matching of terms. The $(1,3)$ and $(3,1)$ matrix elements are trivially equal, as there is the same single term on both sides. The match for each of the remaining five matrix elements is a similar computation to (7.14), (7.15). □

7.4 Izergin-Korepin determinant

Let us return to the $N\times N$ square $[1,N]\times[1,N]\cap\mathbb{Z}^2$ equipped with domain wall boundary conditions: paths entering at every site of the left boundary and exiting at every site of the top boundary, as in Figure 7.2. We introduce *inhomogeneous weights*, which depend on the quantization parameter q and $2N$ rapidities $x_1,\dots,x_N,y_1,\dots,y_N$.

We attach rapidities x_i to column i and y_j to row j, $1\le i,j\le N$, and assign the weight $\mathrm{wt}(i,j;\sigma)$ of a vertex (i,j) in configuration σ by using the weight function $w_{x_iy_j}$, *i.e.*, we rely on (7.6) with spectral parameter $u=x_iy_j$, as in Figure 7.11. We denote by $Z_N(x_1,\dots,x_N;y_1,\dots,y_N;\,q)$ the inhomogeneous partition function for this model:

$$Z_N(x_1,\dots,x_N;y_1,\dots,y_N;\,q)=\sum_{\sigma}\prod_{i=1}^{N}\prod_{j=1}^{N}\mathrm{wt}(i,j;\,\sigma). \quad (7.17)$$

Theorem 7.7 (Izergin-Korepin Determinant, [Kor82], [Ize87])**.** *The inhomogenous partition function for domain wall boundary conditions is given by the determinant*

$$Z_N(x_1,\dots,x_N;y_1,\dots,y_N;\,q)=\frac{\prod_{i,j=1}^{N}(1-x_iy_j)}{\prod_{i<j}(x_i-x_j)(y_i-y_j)}\det\left[\frac{(1-q)x_iy_j}{(1-x_iy_j)(1-qx_iy_j)}\right]_{i,j=1}^{N}. \quad (7.18)$$

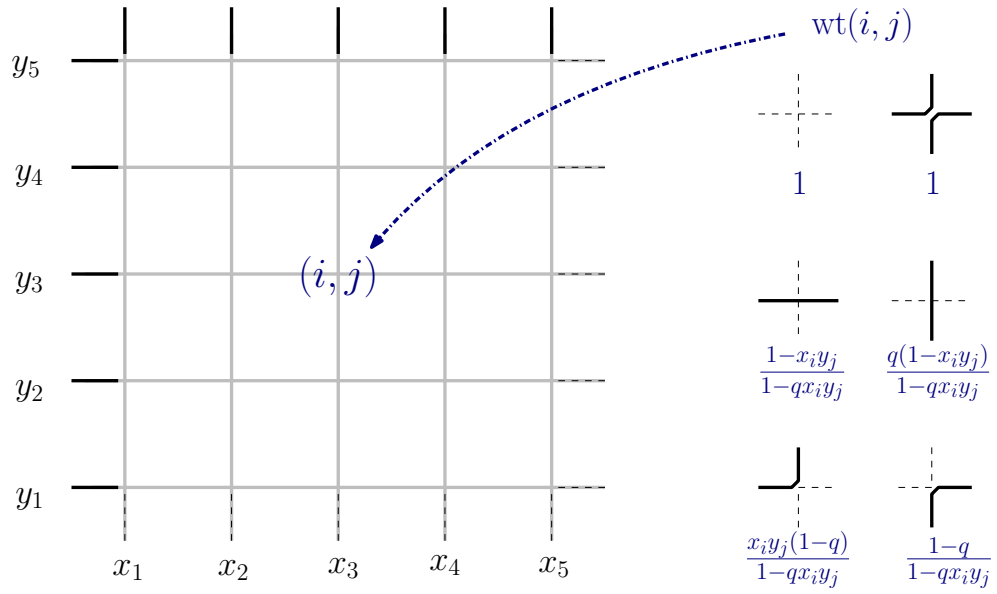


Figure 7.11: Assignment of inhomogeneous weights in $N \times N$ square.

We are going to present a proof by verification, following historic developments. The purpose of Korepin's original paper [Kor82] was to compute norms of Bethe Ansatz eigenfunctions, and a recurrence in N for $Z_N(y_1, \dots, y_N; x_1, \dots, x_N;\, q)$ was introduced there. The recurrence was solved in terms of a determinant by Izergin [Ize87]. It seems that [Ize87] was an educated guess inspired by frequent appearances of the determinants in theoretical physics literature of that era. We are not aware of more conceptual explanations of why the partition function for this instance of the six-vertex model should be a determinant.

An important ingredient of the proof of Theorem 7.7 is the following symmetry lemma, which we need to prove without relying on (7.18).

Lemma 7.8. *The partition function $Z_N(x_1, \dots, x_N; y_1, \dots, y_N;\, q)$ of* (7.17) *is symmetric in $x_1, \dots, x_N$ and in $y_1, \dots, y_N$ (separately in two groups of likewise rapidities).*

Proof. We choose $1 \le i \le N-1$ and aim to prove that

$$Z_N(x_1, \dots, x_N;\, y_1, \dots, y_i, y_{i+1}, \dots, y_N;\, q) = Z_N(x_1, \dots, x_N;\, y_1, \dots, y_{i+1}, y_i, \dots, y_N;\, q).$$

We present a graphical argument based on the Yang-Baxter equation and schematically shown in Figure 7.12. Let us append a cross on the right to the N^2 vertices of the domain, between the ith and $(i+1)$st layers. The boundary condition is that no paths exit through the right ends of the cross, which implies that the cross must be occupied by a Type (1) vertex whose weight is $a_1 = 1$. The partition function of the enlarged domain is the same and equals $Z_N(x_1, \dots, x_N; y_1, \dots, y_N;\, q)$. Next, we iterate Theorem 7.6 N times using the graphic representation of Figure 7.7. On each step the cross is moved to the left by one, the spectral parameters next to it are swapped, but the partition function of the (N^2+1)–vertex domain stays the same. At the very end, the cross ends up at the leftmost possible position, and the boundary condition is that paths are entering into both its left ends. Hence, in any configuration the cross ends up being occupied by a Type (2) vertex whose weight is $a_2 = 1$. Therefore, we can remove the cross, and the final domain is again the $N \times N$ square with domain wall boundary conditions, but with rapiditis y_i and y_{i+1} swapped. The arguments for swapping x_j and x_{j+1} is similar. □

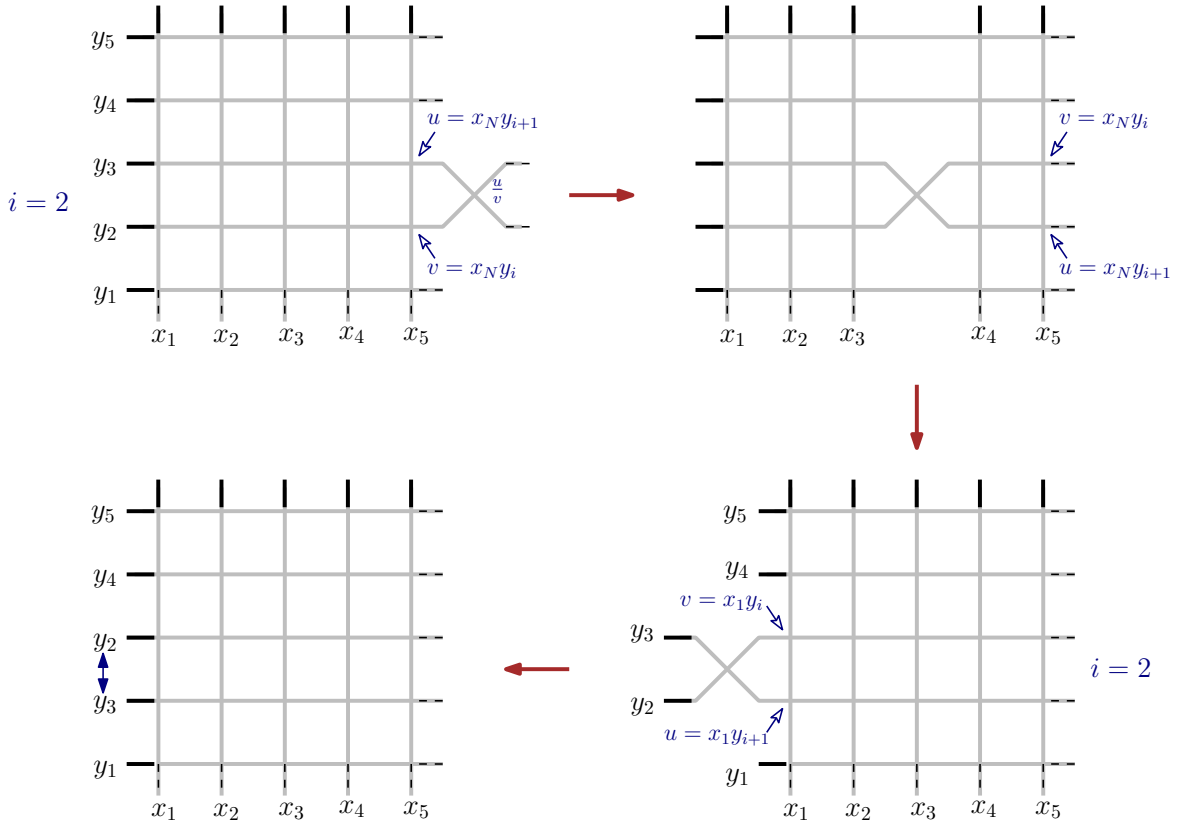


Figure 7.12: Yang-Baxter transformations of the domain manifesting the $y_i \leftrightarrow y_{i+1}$ symmetry.

Proof of Theorem 7.7. We proceed by induction on N.

Base case. For $N = 1$, we directly check the equality. There is only one possible configuration, which contains a single c_1 vertex, and the partition function equals the weight of this vertex

$$c_1 = x_1 y_1 \frac{1-q}{1-q x_1 y_1} = (1 - x_1 y_1) \left[\frac{(1-q) x_1 y_1}{(1 - x_1 y_1)(1 - q x_1 y_1)} \right].$$

Inductive step. Denote $\boldsymbol{x} = (x_1, \ldots, x_N), \boldsymbol{y} = (y_1, \ldots, y_N)$. First we argue that it suffices to show that the left-hand and right-hand sides in (7.18), denoted $Z_N(x_1, \ldots, x_N; y_1, \ldots, y_N; q)$ and $R_N(y_1, \ldots, y_N; x_1, \ldots, x_N; q)$, respectively, are rational functions satisfying the following properties:

(a) Symmetry in variables $(x_1, \ldots, x_N)$, and in variables $(y_1, \ldots, y_N)$.

(b) The functions $Z_N(\boldsymbol{x}; \boldsymbol{y}; q) \cdot \prod_{i,j}(1 - q x_i y_j)$ and $R_N(\boldsymbol{x}; \boldsymbol{y}; q) \cdot \prod_{i,j}(1 - q x_i y_j)$ are polynomials in $x_1, \ldots, x_N, y_1, \ldots, y_N$, such that the degree in each variable is at most N.

(c) If $x_N = \frac{1}{y_N}$, then

$$Z_N(\boldsymbol{x}; \boldsymbol{y}; q) = Z_{N-1}(x_1, \ldots, x_{N-1}; y_1, \ldots, y_{N-1}; q) \qquad \text{and}$$
$$R_N(\boldsymbol{x}; \boldsymbol{y}; q) = R_{N-1}(x_1, \ldots, x_{N-1}; y_1, \ldots, y_{N-1}; q).$$

(d) If $x_i = 0$ for some i, then $Z_N(\boldsymbol{x}; \boldsymbol{y}; q) = 0$ and $R_N(\boldsymbol{x}; \boldsymbol{y}; q) = 0$.

If P_N represents either Z_N or R_N and satisfies these four properties, then $x_N \mapsto \prod_{i,j}(1-qx_iy_j)P_N(x_1,\dots,x_N;y_1,\dots,y_N;\,q)$ is a degree N polynomial in x_N, and at the $N+1$ values of x_N

$$0, \quad 1/y_1, \quad 1/y_2, \quad \dots, \quad 1/y_N,$$

its values are determined by properties (c) and (d) and by the induction assumption. A degree N polynomial is uniquely determined by its values at $N+1$ points, therefore, $Z_N \equiv R_N$.

It remains to prove that Z_N and R_N satisfy the four properties.

Proof that the right-hand side R_N satisfies (a)-(d).

(a) We argue for symmetry in $(x_1,\dots,x_N)$, as the symmetry in y's is similar. The product $\prod_{i,j}(1-x_iy_j)$ is clearly symmetric. The function $\prod_{i<j}(x_i-x_j)$ is skew-symmetric in $(x_1,\dots,x_N)$. In the determinant term, the swap $x_i \leftrightarrow x_j$ interchanges rows i and j in the matrix, and thus the determinant is also skew-symmetric. Therefore, R_N is symmetric in the x_i.

(b) The function

$$\left(\prod_{i,j=1}^{N}(1-x_iy_j)\right)\left(\prod_{i,j=1}^{N}(1-qx_iy_j)\right)\det\left[\frac{(1-q)x_iy_j}{(1-x_iy_j)(1-qx_iy_j)}\right]_{i,j=1}^{N}$$

is a polynomial which is skew-symmetric in $(x_1,\dots,x_N)$ and in $(y_1,\dots,y_N)$. Thus, it is divisible by $\prod_{i<j}(x_i-x_j)(y_i-y_j)$. It is easy to see that the degree of

$$\frac{\left(\prod_{i,j=1}^{N}(1-x_iy_j)\right)\left(\prod_{i,j=1}^{N}(1-qx_iy_j)\right)}{\prod_{i<j}(x_i-x_j)(y_i-y_j)}\det\left[\frac{(1-q)x_iy_j}{(1-x_iy_j)(1-qx_iy_j)}\right]_{i,j=1}^{N}$$

in any variable is equal to N — say, if we send $x_1\to\infty$, it grows proportionally to x_1^N.

(c) Before sending $x_N \mapsto y_N^{-1}$, we multiply the bottom row of the determinant in R_N by $(1-x_Ny_N)$. Then when we set $x_N = y_N^{-1}$, the bottom row has a single nonzero entry, equal to 1, in the bottom right corner. Thus, the determinant reduces to the one corresponding to $R_{N-1}(x_1,\dots,x_{N-1};y_1,\dots,y_{N-1};q)$. The extra pre-factors containing x_N and y_N in the numerator and denominator cancel out cleanly, so the entire expression evaluates to $R_{N-1}(x_1,\dots,x_{N-1};y_1,\dots,y_{N-1};q)$.

(d) This follows from the fact that a row of the determinant becomes 0 if $x_i=0$.

Proof that the left-hand side Z_N satisfies (a)-(d).

(a) Symmetry of the partition function Z_N is Lemma 7.8.

(b) The function $Z_N(\boldsymbol{x};\boldsymbol{y};q)\cdot\prod_{i,j=1}^{N}(1-qx_iy_j)$ is a polynomial because the factor $\prod_{i,j}^{N}(1-qx_iy_j)$ clears the denominators of vertex weights (7.6). The degree in x_i is at most N because $(1-qx_iy_j)\mathrm{wt}(i,j;\sigma)$ has degree 1 in x_i for any $i,j=1,\dots,N$ and any configuration σ.

(c) The vertex weights (7.6), shown in Figure 7.11 imply that if $x_N=y_N^{-1}$, leading to $u=1$, then the vertex at (N,N) must be of Type (5). Therefore, each vertex at (i,N) for $i<N$ has to be of Type (1), and each vertex (N,j) for $j<N$ has to be of Type (2), as in Figure 7.13. Thus, each configuration with nonzero weight is determined by the configuration of paths in the square $[1,N-1]\times[1,N-1]$, and, furthermore, the weight of the configuration is equal to the weight of the vertices in this smaller square.

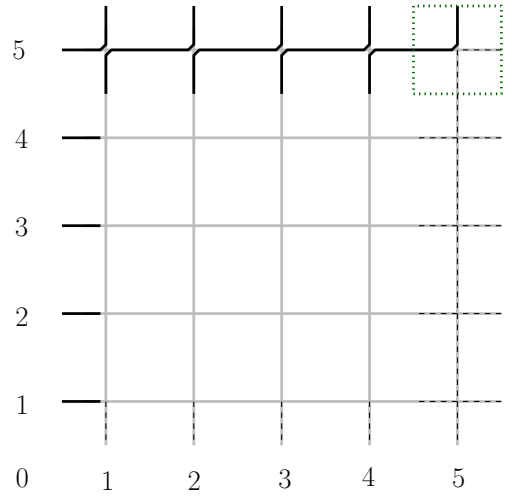


Figure 7.13: Vertex of Type (5) in the top-right corner uniquely fixes the top row and the leftmost column.

(d) By symmetry of part (a), it suffices to prove that $Z_N = 0$ whenever $x_N = 0$. This can be deduced by observing that at least one vertex in the right-most column must have Type (5) and its weight c_1 vanishes in the right-most column if $x_N = 0$, cf. Figure 7.11. □

7.5 ASM count and 2-count

In this section we deduce the ASM counts in Theorems 7.3 and 7.4 from the Izergin-Korepin determinant. For that we need to set all x_i and y_j equal to each other in Theorem 7.7, which requires care because the determinant vanishes and so do the denominators $x_i - x_j$ and $y_i - y_j$.

We start from Theorem 7.4, whose proof is based on a significant simplification of (7.18) at $q = -1$.

Theorem 7.9. *The partition function* (7.17) *at* $q = -1$ *evaluates to:*

$$Z_N(x_1, \dots, x_N; y_1, \dots, y_N; -1) = \prod_{i=1}^{N} (2x_i y_i) \cdot \frac{\prod_{i<j} (x_i + x_j)(y_i + y_j)}{\prod_{i,j=1}^{N} (1 + x_i y_j)}. \tag{7.19}$$

Proof. At $q = -1$, the determinant in the right-hand side of (7.18) becomes the Cauchy determinant and evaluates using Proposition 2.12:

$$\det \left[\frac{(1-q)x_i y_j}{(1 - x_i y_j)(1 - q x_i y_j)} \right]_{i,j=1}^{N} = \prod_{i=1}^{N} (2x_i y_i) \cdot \det \left[\frac{1}{1 - x_i^2 y_j^2} \right]_{i,j=1}^{N}$$
$$= \prod_{i=1}^{N} (2x_i y_i) \cdot \frac{\prod_{1 \le i < j \le N} (x_i^2 - x_j^2)(y_i^2 - y_j^2)}{\prod_{i,j=1}^{N} (1 - x_i^2 y_j^2)}.$$

Plugging into the result of Theorem 7.7, we are arrive at (7.19). □

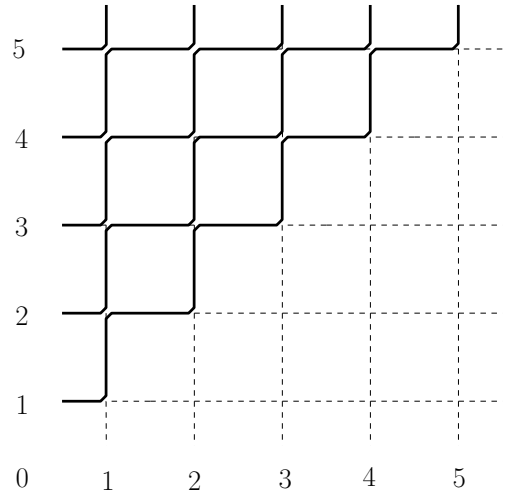


Figure 7.14: A configuration with N vertices of Type (5), and no vertices of Types (3), (4), or (6).

Proof of Theorem 7.4. In order to obtain the desired sum $\sum_{\sigma \text{ is an } N\times N \text{ ASM}} 2^{\#\{-1 \text{ in } \sigma\}}$, we would like to make the weights homogeneous by choosing all x_i and y_j to be the same in the Izergin-Korepin determinant, so that $x_i y_j = u$. Since -1's correspond to vertices of weight c_2, we further want to choose weights so that

$$(a_1, a_2, b_1, b_2, c_1, c_2) = (1, 1, 1, 1, 1, 2), \tag{7.20}$$

while the available six-tuples of the weights (7.6) have the form:

$$\left(1,\, 1,\, \frac{1-u}{1-qu},\, q\frac{1-u}{1-qu},\, \frac{u(1-q)}{1-qu},\, \frac{1-q}{1-qu}\right). \tag{7.21}$$

If we naively try to choose q and u so that (7.20) is identified with (7.21), we quickly find this to be impossible. The situation becomes much better if we recall Proposition 7.1, which says that the non-trivial dependence of the weight of a configuration on parameters is based on two ratios $\frac{b_1 b_2}{a_1 a_2}$ and $\frac{c_1 c_2}{a_1 a_2}$. In other words, if we manage to match the ratios, then the partition functions would differ by multiplication with explicit products of weights. Hence, we would like to match:

$$1 = \frac{b_1 b_2}{a_1 a_2} = q\left[\frac{1-u}{1-qu}\right]^2, \qquad 2 = \frac{c_1 c_2}{a_1 a_2} = u\left[\frac{(1-q)}{1-qu}\right]^2. \tag{7.22}$$

A quick computation reveals that $q = -1$, $u = \mathbf{i}$ leads to (7.22) being true. For this choice of parameters the six stochastic weights (7.21) become

$$(a_1, a_2, b_1, b_2, c_1, c_2) = (1,\, 1,\, -\mathbf{i},\, \mathbf{i},\, 1+\mathbf{i},\, 1-\mathbf{i}). \tag{7.23}$$

From the proof of Proposition 7.1 (see item 2 and item 4 there), the differences $N_5 - N_6$ for the counts of vertices of Type (5) and Type (6) and $N_3 - N_4$ for the counts of vertices of Type (3) and Type (4), do not depend on the configuration. Looking at the configuration of Figure 7.14, we conclude that these differences are $N_3 - N_4 = 0$ and $N_5 - N_6 = N$. Therefore,

$$Z_N\big(1^N; \mathbf{i}^N; -1\big) = \sum_\sigma (-\mathbf{i})^{N_3} (\mathbf{i})^{N_4} (1+\mathbf{i})^{N_5} (1-\mathbf{i})^{N_6} = \sum_\sigma (-\mathbf{i}\cdot\mathbf{i})^{N_3} (1+\mathbf{i})^{N_5-N_6} [(1+\mathbf{i})(1-\mathbf{i})]^{N_6}$$
$$= (1+\mathbf{i})^N \sum_\sigma 2^{N_6}. \tag{7.24}$$

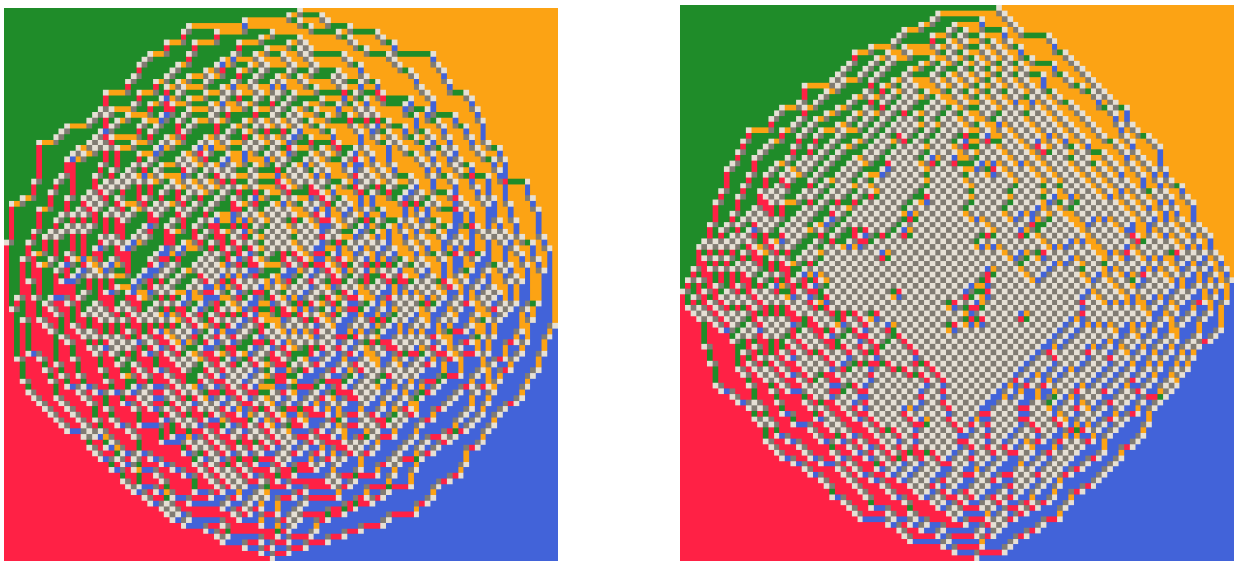


Figure 7.15: Two samples of six-vertex configurations in 100×100 square with domain-wall boundary conditions using vertex colors (blue, green, red, orange, light gray, dark gray) matching the domino coloring in Figure 6.8. Left: weights $(1, 1, 1, 1, 1, 2)$, $\Delta = 0$. Right: weights $(1, 1, 1, 1, \sqrt{8}, \sqrt{8})$, $\Delta = -3$.

On the other hand, (7.19) yields

$$Z_N\big(1^N; \mathbf{i}^N; -1\big) = (2\mathbf{i})^N \frac{(4\mathbf{i})^{N(N-1)/2}}{(1+\mathbf{i})^{N^2}} = (1+\mathbf{i})^N 2^{N^2} \mathbf{i}^{N(N+1)/2} [(1+\mathbf{i})^2]^{-N(N+1)/2}$$
$$= (1+\mathbf{i})^N 2^{N(N-1)/2}. \quad (7.25)$$

Comparing (7.24) with (7.25) and recalling that Type (6) vertices correspond to -1's in ASMs, we conclude the proof. □

The weights (7.6) of Figure 7.6 at $q = -1$ satisfy a special property:

$$\Delta := \frac{a_1 a_2 + b_1 b_2 - c_1 c_2}{2\sqrt{a_1 a_2 b_1 b_2}} = \frac{1+q}{2\sqrt{q}} = 0. \quad (7.26)$$

The parameter Δ plays a central role in many studies of the six-vertex model, and the $\Delta = 0$ situation is called *the free fermion point*. One reason is that in this situation a map to random domino tilings exists (as in Theorem 7.5), and tilings can be studied using the determinantal point processes, Schur measures, and non-interacting (free) fermions, see [Lie67b] for the latter. Generally speaking, the $\Delta = 0$ case is considered to be simpler; much more is known about the asymptotic behavior of the six-vertex model in this situation. The asymptotic phenomenology can be also richer for $\Delta \neq 0$, as can be seen by comparing two panels in Figure 7.15.

We chose $u = \mathbf{i}$ in the proof of Theorem 7.4, but (at $q = -1$) any complex number u with $|u| = 1$, $u \neq -1$, will also give rise to a positive probability measure (7.1) on the configurations of the six-vertex model via Proposition 7.1. We leave as an exercise to the reader to figure out the correspondence between these measures and $(\alpha\beta)$-weighted domino tilings (6.2).

The choice $q = -1$ can be rephrased as q being a square root of unity. We saw in Section 7.3 that $q = 1$ also leads to a dramatic simplification of the weights, cf. (7.12). The next case to try would be

the cube root of unity, $q = \exp\left(\frac{2\pi\mathbf{i}}{3}\right)$, and, indeed, the Izergin-Korepin determinant again has special properties. This is also the case which leads to the uniform weights $a_1 = a_2 = b_1 = b_2 = c_1 = c_2 = 1$.

Theorem 7.10. *Let $q = \exp\left(\frac{2\pi\mathbf{i}}{3}\right)$ and $\lambda[N] = (N-1, N-1, N-2, N-2, \dots, 1, 1, 0, 0)$. Then, denoting $y_j = q/z_j$, the partition function* (7.17) *evaluates as*

$$Z_N\left(x_1,\dots,x_N; y_1,\dots,y_N; \exp\left(\frac{2\pi\mathbf{i}}{3}\right)\right)$$
$$= (-1)^{N(N-1)/2}(1-q)^N q^{-N(N-3)/2}\frac{\prod_{i=1}^N x_i}{\prod_{i,j=1}^N (z_j - q^2 x_i)} s_{\lambda[N]}(x_1,\dots,x_N,z_1,\dots,z_N), \quad (7.27)$$

where $s_{\lambda[N]}$ is the Schur polynomial.

The most striking feature of Theorem 7.10 is that a modification of the partition function is fully symmetric in all $2N$ parameters $x_1,\dots,x_N,z_1,\dots,z_N$. This symmetry was noticed by Stroganov [Str06], see also [Oka06, FZJ08]. We present a proof based on a determinantal identity generalizing the Cauchy determinant (2.20) and coming from [Oka98, Theorem 4.2], where it was developed in connection with decompositions into irreducibles for certain natural representations of classical Lie groups.

Theorem 7.11. *For any $u_1,\dots,u_N, v_1,\dots,v_N, a_1,\dots,a_N, b_1,\dots,b_N$, we have*

$$\det\left[\frac{a_i - b_j}{u_i - v_j}\right]_{i,j=1}^N = \frac{(-1)^{N(N+1)/2}}{\prod_{i,j=1}^N (u_i - v_j)} \det\left[V^{N,N}(u,v;a,b)\right], \quad (7.28)$$

where $V^{N,N}(u,v;a,b)$ is a $2N\times 2N$ matrix written in the 2×2 block form as

$$\begin{pmatrix} \left[u_i^{j-1}\right]_{i,j=1}^N & \left[a_i u_i^{j-1}\right]_{i,j=1}^N \\ \left[v_i^{j-1}\right]_{i,j=1}^N & \left[b_i v_i^{j-1}\right]_{i,j=1}^N \end{pmatrix}.$$

As a check, if $a_1 = \dots = a_N = a$ and $b_1 = \dots = b_1 = b$, then the left-hand side, using (2.20), is

$$(a-b)^N \cdot \frac{\prod_{1\le i<j\le N}(u_i - u_j)(v_j - v_i)}{\prod_{i,j=1}^N (u_i - v_j)}.$$

In the matrix V_N we can multiply the left $2N\times N$ block by a and subtract from the right $2N\times N$ block, after which the determinant splits into the product of two $N\times N$ Vandermonde determinants (2.15) and evaluates as (note the discrepancy of signs in $(b-a)$ and $(v_i - v_j)$)

$$(b-a)^N \prod_{i<j}(u_i - u_j)(v_i - v_j).$$

Proof of Theorem 7.11. The determinant in the left-hand side of (7.28) is a homogenous polynomial in $a_1,\dots,a_N$, $b_1,\dots,b_N$ of total degree N and with each variable having degree at most 1. We take two sets $I, J \subset \{1,2,\dots,N\}$ such that $|I| + |J| = N$, and evaluate the coefficient of the monomial

$\prod_{i\in I} a_i \prod_{j\in J} b_j$. This coefficient is equal to the determinant of the $N\times N$ matrix whose (i,j)th element is

$$\begin{cases} \dfrac{1}{u_i-v_j}, & \text{if } i\in I,\ j\notin J,\\ -\dfrac{1}{u_i-v_j}, & \text{if } i\notin I,\ j\in J,\\ 0, & \text{if } i\in I,\ j\in J \quad \text{or} \quad i\notin I,\ j\notin J. \end{cases}$$

This is a block matrix whose determinant splits into the product of two determinants, each one of the Cauchy type (2.20). Denoting $\overline{I}=\{1,\dots,N\}\setminus I$ and $\overline{J}=\{1,\dots,N\}\setminus J$, the coefficient becomes

$$\pm\det\left[\frac{1}{u_i-v_j}\right]_{i\in I,\,j\in\overline{J}}\det\left[\frac{1}{u_i-v_j}\right]_{i\in\overline{I},\,j\in J} = \pm\frac{\prod_{i<i'\in I}(u_i-u_{i'})\prod_{i<i'\in\overline{I}}(u_i-u_{i'})\prod_{j<j'\in J}(v_j-v_{j'})\prod_{j<j'\in\overline{J}}(v_j-v_{j'})}{\prod_{i\in I}\prod_{j\in\overline{J}}(u_i-v_j)\prod_{i\in\overline{I}}\prod_{j\in J}(u_i-v_j)}. \quad (7.29)$$

On the other hand, the coefficient of the same monomial $\prod_{i\in I} a_i\prod_{j\in J} b_j$ in $\det\bigl[V^{N,N}(u,v;a,b)\bigr]$ is the determinant of the $2N\times 2N$ matrix whose ith row is

$$\begin{cases} 0,\dots,0,\ 1,u_i,u_i^2,\dots,u_i^{N-1}, & \text{if } 1\le i\le N,\ i\in I,\\ 1,u_i,u_i^2,\dots,u_i^{N-1},\ 0,\dots,0, & \text{if } 1\le i\le N,\ i\in\overline{I},\\ 0,\dots,0,\ 1,v_{i-N},v_{i-N}^2,\dots,v_{i-N}^{N-1}, & \text{if } N+1\le i\le 2N,\ i-N\in J,\\ 1,v_{i-N},v_{i-N}^2,\dots,v_{i-N}^{N-1},\ 0,\dots,0, & \text{if } N+1\le i\le 2N,\ i-N\in\overline{J}. \end{cases}$$

This determinant splits into the product of two Vandermonde determinants (2.15), corresponding to nonzero rows in the $2N\times N$ submatrices formed by the first and last N columns. Hence, it is equal to

$$\pm\prod_{i<i'\in I}(u_i-u_{i'})\prod_{i<i'\in\overline{I}}(u_i-u_{i'})\prod_{j<j'\in J}(v_j-v_{j'})\prod_{j<j'\in\overline{J}}(v_j-v_{j'})\prod_{i\in I}\prod_{j\in J}(u_i-v_j)\prod_{i\in\overline{I}}\prod_{j\in\overline{J}}(u_i-v_j). \quad (7.30)$$

Dividing by $\prod_{i=1}^N\prod_{j=1}^N(u_i-v_j)$ we arrive at (7.29), and it only remains to show that the signs match. Keeping track of all the steps, in the right-hand side of (7.29), the power of (-1) is

$$\sum_{i\in I} i+\sum_{j\in\overline{J}} j+|\overline{I}|+\frac{|I|(|I|-1)}{2}+\frac{|J|(|J|-1)}{2}. \quad (7.31)$$

In (7.30) the power of (-1) is

$$\sum_{i\in\overline{I}} i+\sum_{j\in\overline{J}} j+N|\overline{J}|+\frac{N(N+1)}{2}. \quad (7.32)$$

In addition, we have (-1) to the power $N(N+1)/2$ in (7.28) that we are proving. Adding all the powers together, dropping the terms which are obviously even, and recalling that $|\overline{I}|=|J|=N-|I|=N-|\overline{J}|$, we need to show that the following number is even:

$$\sum_{i=1}^N i+(N-|I|)+\frac{|I|(|I|-1)}{2}+\frac{(N-|I|)(N-|I|-1)}{2}+N|I|.$$

We leave this straightforward verification to the reader. □

The following corollary of Theorem 7.11 is used to prove Theorem7.10 below.

Corollary 7.12. *Let $\lambda[N] = (N-1, N-1, N-2, N-2, \dots, 1, 1, 0, 0)$. Then we have*

$$\det\left[\frac{z_j - x_i}{z_j^3 - x_i^3}\right]_{i,j=1}^{N} = \det\left[\frac{1}{z_j^2 + z_j x_i + x_i^2}\right]_{i,j=1}^{N} = \frac{\prod_{i<j}(x_i - x_j)(z_i - z_j)}{\prod_{i,j=1}^{N}(x_i^2 + x_i z_j + z_j^2)} s_{\lambda[N]}(x_1, \dots, x_N, z_1, \dots, z_N). \quad (7.33)$$

Proof. We apply (7.28) with $u_i = x_i^3$, $v_j = z_j^3$, $a_i = x_i$, $b_j = z_j$ and observe that the matrix $V^{N,N}$ becomes

$$\begin{pmatrix} \left[x_i^{3j-3}\right] & \left[x_i^{3j-2}\right] \\ \left[z_i^{3j-3}\right] & \left[z_i^{3j-2}\right] \end{pmatrix}, \qquad i, j = 1, \dots, N.$$

The top and bottom halves have the same forms as the matrix appearing in the definition of the Schur function $s_{\lambda(N)}$ via ratio of determinants (2.14), *i.e.*, $\left[x_i^{\lambda_j + 2N - j}\right]$, $1 \le j \le 2N$, up to permutation of the columns. The permutation of the columns in determinant introduces the sign $(-1)^{N(N+1)}$, which cancels out the sign in (7.28). In order to recognize the right-hand side of (7.33), it remains to note that

$$\frac{z_j - x_i}{z_j^3 - x_i^3} = \frac{1}{x_i^2 + x_i z_j + z_j^2}. \quad \square$$

Proof of Theorem 7.10. At $q = \exp\left(\frac{2\pi \mathbf{i}}{3}\right)$, we have

$$\frac{1}{(z_j - q x_i)(z_j - q^2 x_i)} = \frac{z_j - x_i}{z_j^3 - x_i^3} = \frac{1}{z_j^2 + z_j x_i + x_i^2}.$$

Hence, denoting $z_i = q/y_i$ we transform (7.18) as

$$\frac{\prod_{i,j=1}^{N}(1 - x_i y_j)}{\prod_{i<j}(x_i - x_j)(y_i - y_j)} \det\left[\frac{(1-q) x_i y_j}{(1 - x_i y_j)(1 - q x_i y_j)}\right]_{i,j=1}^{N} = (1-q)^N q^{N - N(N-1)/2} \frac{\prod_{i,j=1}^{N}(z_j - q x_i) \prod_{i=1}^{N} x_i}{\prod_{i<j}(x_i - x_j)(z_j - z_i)} \det\left[\frac{1}{z_j^2 + z_j x_i + x_i^2}\right]_{i,j=1}^{N}. \quad (7.34)$$

For the last determinant, we apply Corollary 7.12 and note that the sign $(-1)^{N(N-1)/2}$ arises from the transformation $(z_i - z_j) \mapsto (z_j - z_i)$. $\square$

Choosing in Theorem 7.11 all variables equal to each other, we compute the total number of ASMs.

Proof of Theorem 7.3. In order to obtain the total number of ASMs we would like to make the six weights homogeneous by choosing all x_i and y_j to be the same in the Izergin-Korepin determinant, so that $x_i y_j = u$, and further choose u and q in such a way as to make the six weights equivalent (in the sense of Proposition 7.1) to the uniform weights $(1, 1, 1, 1, 1, 1)$. The available six-tuples of the weights (7.6) have the form:

$$\left(1,\, 1,\, \frac{1-u}{1-qu},\, q\frac{1-u}{1-qu},\, \frac{u(1-q)}{1-qu},\, \frac{1-q}{1-qu}\right), \quad (7.35)$$

and therefore we would like to have u and q such that

$$\frac{b_1 b_2}{a_1 a_2} = q\left[\frac{1-u}{1-qu}\right]^2 = 1, \qquad \frac{c_1 c_2}{a_1 a_2} = u\left[\frac{1-q}{1-qu}\right]^2 = 1.$$

This is achieved by choosing $q = u = \exp\left(\frac{2\pi \mathbf{i}}{3}\right)$. Therefore, by Proposition 7.1, we obtain

$$Z_N\left(1^N; \left[\exp\left(\frac{2\pi\mathbf{i}}{3}\right)\right]^N; \exp\left(\frac{2\pi\mathbf{i}}{3}\right)\right) = \left[\frac{\exp\left(\frac{2\pi\mathbf{i}}{3}\right) - \exp\left(\frac{4\pi\mathbf{i}}{3}\right)}{1-\exp\left(\frac{4\pi\mathbf{i}}{3}\right)}\right]^N \cdot \#\{N\times N \text{ ASMs}\},$$

where the prefactor is the weight of the configuration in Figure 7.14 (and, hence, also of every other configuration). Using Theorem 7.10, we conclude

$$\begin{aligned}\#\{N\times N \text{ ASMs}\} &= \frac{(-1)^{N(N-1)/2}\left(1-\exp\left(\frac{2\pi\mathbf{i}}{3}\right)\right)^N}{\left(1-\exp\left(\frac{4\pi\mathbf{i}}{3}\right)\right)^{N^2}\left(\exp\left(\frac{2\pi\mathbf{i}}{3}\right)\right)^{N(N-3)/2}}\left[\frac{1-\exp\left(\frac{4\pi\mathbf{i}}{3}\right)}{\exp\left(\frac{2\pi\mathbf{i}}{3}\right)-\exp\left(\frac{4\pi\mathbf{i}}{3}\right)}\right]^N s_{\lambda[N]}(1^{2N}) \\ &= \left[\frac{-1}{\left[\exp\left(\frac{2\pi\mathbf{i}}{3}\right)-\exp\left(\frac{-2\pi\mathbf{i}}{3}\right)\right]^2}\right]^{N(N-1)/2} s_{\lambda[N]}(1^{2N}) = 3^{-N(N-1)/2}\cdot s_{\lambda[N]}(1^{2N}).\end{aligned}$$

Recalling $\lambda[N] = (N-1, N-1, \ldots, 1, 1, 0, 0)$ and using (2.51), we transform this expression into

$$3^{-N(N-1)/2}\cdot \prod_{i=1}^{2N-1}\frac{1}{i!}\prod_{i=1}^{N-1}\Big([1\cdot 4\cdot 7\cdots(3i+1)]\cdot[3\cdot 6\cdot 9\cdots(3i)]^2\cdot[2\cdot 5\cdots(3i-1)]\Big) = \prod_{i=1}^{N-1}\frac{(3i+1)!}{(N+i)!}. \quad \square$$

The cube root of unity choice of q in Theorems 7.3 and 7.10 again leads to the special value of the Δ parameter, namely

$$\Delta = \frac{a_1a_2 + b_1b_2 - c_1c_2}{2\sqrt{a_1a_2b_1b_2}} = \frac{1+q}{2\sqrt{q}} = \frac{1}{2}.$$

This is usually referred to as the *combinatorial point* precisely because of the connection to combinatorial enumeration of ASMs.

Various enumerations of the ASMs go beyond Theorems 7.3 and 7.4. One direction is to count the ASMs with symmetries, another one is to introduce more advanced weights beyond uniform and $2^{\#\{-1\}}$; the latter direction, in particular, involves taking q to be other roots of unity. For instance, [Kup02] and [Oka06] have many such enumerations.

7.6 Gaussian and GUE limits at the boundary

The inhomogeneous partition function $Z_N(x_1, \ldots, x_N; y_1, \ldots, y_N;\, q)$ contains much more information about the six-vertex model than only the total count of configurations, yet extracting this information may be delicate. We demonstrate how to compute the asymptotics of the random ASMs (equivalently, uniformly random domino tilings of the Aztec diamond) near the boundary of the domain.

Theorem 7.13. *Consider a random $N\times N$ alternating sign matrix σ sampled from the distribution*

$$\mathbb{P}(\sigma) = \frac{2^{\#\{-1 \text{ in } \sigma\}}}{2^{N(N-1)/2}}. \tag{7.36}$$

Let $\xi[N] \in \{1, 2, \ldots, N\}$ be the position of the (unique) 1 in the bottom row of σ. Then centered and scaled $\xi[N]$ has a Gaussian limit in distribution:

$$\lim_{N\to\infty}\frac{\xi[N] - \frac{N}{2}}{\frac{1}{2}\sqrt{N}} \overset{d}{=} \mathcal{N}(0,1). \tag{7.37}$$

The idea of the proof is to interpret inhomogeneous partition function Z_N as an expectation of an observable involving ξ_N with respect to the measure (7.36), based on the following computation.

Lemma 7.14. *Consider the six-vertex model in the $N \times N$ square with domain-wall boundary conditions and six weights $\left(1,\, 1,\, \frac{1-u}{1-qu},\, q\frac{1-u}{1-qu},\, \frac{u(1-q)}{1-qu},\, \frac{1-q}{1-qu}\right)$. Let $\xi[N]$ be the position of the Type (5) vertex in the bottom row (=position of 1 in the bottom row of the corresponding ASM) in the random configuration* (7.1). *Then*

$$\mathbb{E}\left[\left(\frac{1-uz}{1-u}\cdot\frac{1-qu}{1-quz}\right)^{\xi[N]-1}\right] = \frac{z-quz}{1-quz}\cdot\frac{Z_N(u^N; z, 1^{N-1};\, q)}{Z_N(u^N; 1^N;\, q)}. \tag{7.38}$$

Proof. Let σ be a configuration in the $N\times N$ square and let $w(\sigma;\, x_1, \dots, x_N; y_1; \dots, y_N; q)$ be its weight with respect to the inhomogeneous vertex weights, as in (7.17) and Figure 7.11. Then

$$\begin{aligned}\frac{Z_N(u^N; z, 1^{N-1};\, q)}{Z_N(u^N; 1^N;\, q)} = \frac{\sum_\sigma w(\sigma;\, u^N; z, 1^{N-1};\, q)}{\sum_\sigma w(\sigma;\, u^N; 1^N;\, q)} &= \frac{\sum_\sigma \frac{w(\sigma; u^N; z, 1^{N-1}; q)}{w(\sigma; u^N; 1^N; q)} w(\sigma;\, u^N; 1^N;\, q)}{\sum_\sigma w(\sigma;\, u^N; 1^N;\, q)} \\ &= \mathbb{E}\left[\frac{w(\sigma;\, u^N; z, 1^{N-1};\, q)}{w(\sigma;\, u^N; 1^N;\, q)}\right].\end{aligned} \tag{7.39}$$

Note that $w(\sigma;\, u^N; z, 1^{N-1};\, q)$ differs from $w(\sigma;\, u^N; 1^N;\, q)$ by the weight of the vertices in the bottom. In this row there are $\xi[N]-1$ vertices of Type (3), of weight b_1, one vertex of Type (5), of weight c_1, and $N-\xi[N]-1$ vertices of Type (1), of weight a_1. Computing the ratios of the weights, we arrive at (7.38). □

Proof of Theorem 7.13. We deduce convergence of (7.37) from convergence of the Laplace transform of the rescaled $\xi[N]$. Denote

$$\eta[N] = \frac{\xi[N] - \frac{N}{2}}{\frac{1}{2}\sqrt{N}}, \qquad \xi[N] = \frac{N}{2} + \frac{1}{2}\eta[N]\sqrt{N}.$$

Recalling from the proof of Theorem 7.4 that we need to set $q=-1$ and $u=\mathbf{i}$, for the left-hand side of (7.38) we obtain

$$\left(\frac{1-\mathbf{i}z}{1-\mathbf{i}}\cdot\frac{1+\mathbf{i}}{1+\mathbf{i}z}\right)^{\frac{N}{2}-1} \mathbb{E}\left[\left(\frac{1-\mathbf{i}z}{1-\mathbf{i}}\cdot\frac{1+\mathbf{i}}{1+\mathbf{i}z}\right)^{\frac{1}{2}\eta[N]\sqrt{N}}\right]. \tag{7.40}$$

We would like to choose z in such a way that the expression under expectation turns into the Laplace transform as $N\to\infty$. For that z should be close to 1 and we set

$$z = \exp\left(\mathbf{i}\frac{2s}{\sqrt{N}}\right), \qquad s\in\mathbb{R}. \tag{7.41}$$

In principle, any other choice of z of the form $1+O\left(\frac{1}{\sqrt{N}}\right)$ would also work, but choosing z on the unit circle leads to a positive expression under the expectation in (7.40), which makes justification of the limit transition more straightforward. The factor of 2 in front of s was chosen to simplify later formulas. We have

$$\frac{1-\mathbf{i}z}{1-\mathbf{i}}\cdot\frac{1+\mathbf{i}}{1+\mathbf{i}z} = \exp\left(\frac{2s}{\sqrt{N}} + O\left(N^{-3/2}\right)\right), \tag{7.42}$$

where the remainder is real. In particular, the N^{-1} term in the asymptotic expansion vanishes. For the ratio in the right-hand side of (7.38) we recall Theorem 7.9, which gives

$$\frac{Z_N(\mathbf{i}^N; z, 1^{N-1};\, -1)}{Z_N(\mathbf{i}^N; 1^N;\, -1)} = z\frac{(1+z)^{N-1}(1+\mathbf{i})^N}{2^{N-1}(1+\mathbf{i}z)^N}.$$

We plug (7.41) in and Taylor expand to get

$$\frac{Z_N(\mathbf{i}^N; z, 1^{N-1}; -1)}{Z_N(\mathbf{i}^N; 1^N; -1)} = \exp\left(\sqrt{N}s + \frac{s^2}{2} + O\left(N^{-1/2}\right)\right). \tag{7.43}$$

Combining (7.40), (7.41), and (7.42), we conclude that (7.38) becomes, as $N \to \infty$,

$$\exp\left(\sqrt{N}s + O\left(N^{-1/2}\right)\right) \mathbb{E}\left[\exp\left(s \cdot \eta[N] + O\left(N^{-1}\right)\right)\right] = \exp\left(\sqrt{N}s + \frac{s^2}{2} + O\left(N^{-1/2}\right)\right).$$

We conclude that

$$\lim_{N\to\infty} \mathbb{E}\Big[\exp\left(s \cdot \eta[N] + O\left(N^{-1}\right)\right)\Big] = \exp\left(\frac{s^2}{2}\right). \tag{7.44}$$

In order to deduce the distributional convergence, we note that (7.44) with $s = 1$ and $s = -1$ imply tightness of random variables $\eta[N]$ as $N \to \infty$: by the Markov inequality applied to $\exp(\pm\eta[N])$, the tail probability $\mathbb{P}(|\eta[N]| > L)$ tends to 0 as $L \to \infty$, uniformly in N. This is the step which would have been slightly more complicated if the $O(N^{-1})$ remainder were not real. Tightness implies that random variables $\eta[N]$ have subsequential distributional limits as $N \to \infty$. Every such limit η satisfies $\mathbb{E}(\exp(s\eta)) = \exp\left(\frac{s^2}{2}\right)$, which uniquely determines η to be the standard Gaussian $\mathcal{N}(0,1)$. □

Theorem 7.13 has an extension capturing the kth from the bottom row in the ASM.

Theorem 7.15. *Consider a random $N \times N$ alternating sign matrix σ sampled from the distribution*

$$\mathbb{P}(\sigma) = \frac{2^{\#\{-1 \text{ in } \sigma\}}}{2^{N(N-1)/2}}. \tag{7.45}$$

Let $\left(\xi_1[N] > \xi_2[N] > \cdots > \xi_k[N]\right)$ be the positions of the 1's in the kth bottom row of σ. Then this random vector has a GUE limit in distribution:

$$\lim_{N\to\infty} \left(\frac{\xi_i[N] - \frac{N}{2}}{\frac{1}{2}\sqrt{N}}\right)_{i=1}^{k} \stackrel{d}{=} \left(x_1^k, x_2^k, \ldots, x_k^k\right), \tag{7.46}$$

where the right-hand side is the GUE distribution of (5.54)*,* i.e.*, the eigenvalues of $M = \frac{1}{2}(Y + Y^*)$, where Y is a $k \times k$ matrix of i.i.d. $\mathcal{N}(0,1) + \mathbf{i}\mathcal{N}(0,1)$. In particular,* (7.46) *means that the probability to have exactly k elements 1 in the kth row of ASM tends to 1 as $N \to \infty$.*

One can develop a proof of Theorem 7.15 along the lines of Theorem 7.13 using the Izergin-Korepin determinant. We outline a part of the argument in the exercises and refer to [GN25] for further details. Instead, we present here another argument emphasizing the link to the Aztec diamond and Schur measures. This argument and its modifications work only for $\Delta = 0$, while the ultimate statement (7.46) is valid for any six-vertex weights satisfying $\Delta < 1$, with the only weight-dependent part being the constant $\frac{1}{2}$ in the denominator. Such a more general statement can be still proven using the Izergin-Korepin determinant, but the asymptotic analysis becomes more delicate, because the factorization of Theorem 7.9 is no longer available, and one has to study the $N \times N$ determinant as $N \to \infty$. This was done in [GL25], and the same article showed the limits of GUE-universality: for $\Delta > 1$, the limit of ASMs is instead described by the stochastic six-vertex model, which we explore in the next chapter.

Proof of Theorem 7.15. We recall the mapping of Theorem 7.5. Under that correspondence, the uniform measure on the tilings of the $(N-1)\times(N-1)$ Aztec diamond becomes the 2–weighted measure (7.45) on the $N\times N$ ASMs. The k green particles in the $(N-k)$th gray layer of the tiling are identified with positions of 1's in the sum of the bottom k rows of the ASM.

By Proposition 6.1 and Corollary 6.5, these k particles are $\{\lambda_i^{(k)}-i+1+k\}_{i=1}^k$, where $\lambda^{(k)}$ is the Schur measure with weights

$$\mathbb{P}(\lambda^{(k)}=\lambda)=2^{-k(N-k)}s_{\lambda'}\big(1^{N-k}\big)s_{\lambda}\big(1^k\big).$$

This measure was made more explicit in Proposition 5.21; it is given by (5.56) with (N,M) in that formula replaced by present $(k,N-k)$, that is:

$$\mathbb{P}(\lambda^{(k)}=\lambda)=\frac{1}{Z}\prod_{1\le i<j\le N}\big(\lambda_i-i-\lambda_j+j\big)^2\prod_{i=1}^k\binom{N-1}{\lambda_i+k-i},$$

where Z is a normalization constant. Using the Local CLT in the form of Proposition 5.2, we compute the limit of the last formula as $N\to\infty$, concluding that

$$\lim_{N\to\infty}\left(\frac{\lambda_i^{(k)}-\frac{N}{2}}{\frac{1}{2}\sqrt{N}}\right)_{i=1}^k\overset{d}{=}\big(x_1^k,x_2^k,\dots,x_k^k\big),\tag{7.47}$$

where the right-hand side is the vector of GUE eigenvalues of density

$$\frac{1}{(2\pi)^{k/2}\prod_{j=1}^{k-1}j!}\prod_{1\le i<j\le k}\left(x_i^k-x_j^k\right)^2\prod_{i=1}^k\exp\left(-\frac{1}{2}(x_i^k)^2\right).\tag{7.48}$$

In particular, the scaling limit is absolutely continuous, the probability of taking any particular values vanishes asymptotically, and, therefore, the individual distances between green particles tend to infinity as $N\to\infty$. Since this is true for each k, the probability of green particles in the first k levels having any coinciding coordinates tends to 0 as $N\to\infty$ (one way to see that is by looking at the distribution of the first $k-1$ levels of green particles, conditional on the kth level). Since the 1's in the ASM encode the difference between green particles in adjacent rows (treated as $0-1$ vectors), it follows that as $N\to\infty$, the 1's in the kth row of ASMs are the same as the green particles, whose asymptotics is given by (7.47). Hence, (7.46) follows from (7.47). □

An intriguing open question (at the time when this book is being written) is to learn how to extract more asymptotic information from the Izergin-Korepin determinant. The authors of [CP10, CS16, Agg20] explain how the frozen boundary can be found from it, *i.e.*, an analogue of the Arctic ellipse of Section 6.4 (which is recast as the same ellipse in terms of random ASMs with $\Delta=0$) for $\Delta\neq 0$, cf. Figure 1.13. In contrast to the dominos case, for general values of Δ the boundary is no longer an algebraic curve, it is only piecewise analytic. In Section 6.4 we saw how inhomogeneous partition functions can be used to extract asymptotic densities and limit shapes for dominos through the action of operators. It is unknown how to mimic such an approach for $\Delta\neq 0$. For the asymptotic density of 1's in the ASM, Tracy-Widom fluctuations of the frozen boundary, or GFF fluctuations of the heights, we are just starting to understand what is happening outside of $\Delta=0$, cf. [ACJ23, CP26, Li26, Lia26, BO26, Buf26, ADCH$^+$26].

7.7 Exercises

Problem 1. Write down the 8×8 matrices involved in the Yang-Baxter equation and use mathematical software to directly verify that both (7.10) and (7.11) hold.

Problem 2. Extending Theorem 7.5, show that the $\Delta = 0$ case of the six-vertex model with domain wall boundary conditions leads to $(\alpha\beta)$-weighted domino tilings (6.2). How is $\alpha\beta$ related to the six weights?

Problem 3. Find a version of the Gaussian limit of Theorem 7.13 for the setting of Problem 2.

Problem 4. Choose $K \geq 1$ and K real numbers $s_1, \ldots, s_K$. Compute the limit

$$\lim_{N\to\infty} \left[\frac{Z_N(\mathbf{i}^N; z_1, \ldots, z_K, 1^{N-k}; -1)}{Z_N(\mathbf{i}^N; 1^N; -1)} \exp\left(-\frac{\sqrt{N}}{2} \sum_{k=1}^{K} s_k \right) \right], \qquad z_k = \exp\left(\mathbf{i} \frac{s_k}{\sqrt{N}} \right), \quad 1 \leq k \leq K.$$

As in the proof of Theorem 7.13, deduce convergence of certain K random variables describing a random 2–weighted ASMs.

Problem 5. The GUE-corners process of rank K is the joint distribution of $K(K-1)/2$ random variables describing the eigenvalues of the top-left $k \times k$ corners ($1 \leq k \leq K$) of $M = \frac{1}{2}(Y + Y^*)$, where Y is a $k \times k$ matrix of i.i.d. $\mathcal{N}(0,1) + \mathbf{i}\mathcal{N}(0,1)$. From either of Problem 4 or Theorem 7.15 one can deduce convergence of the positions of 1's in the bottom K rows of a 2–weighted ASM towards the GUE-corners process. Figure out the exact statement and explain how Problem 4 matches Theorem 7.15 in this statement.
Remark. In order to *prove it*, one uses a certain Gibbs property and unitary invariance of GUE, see [GN25] and references therein.

Problem 5. By row-expanding the definition of Schur polynomial as a determinant (divided by Vandermonde determinant) along the last row, and using the explicit formula for $s_\lambda(1^M)$, prove that

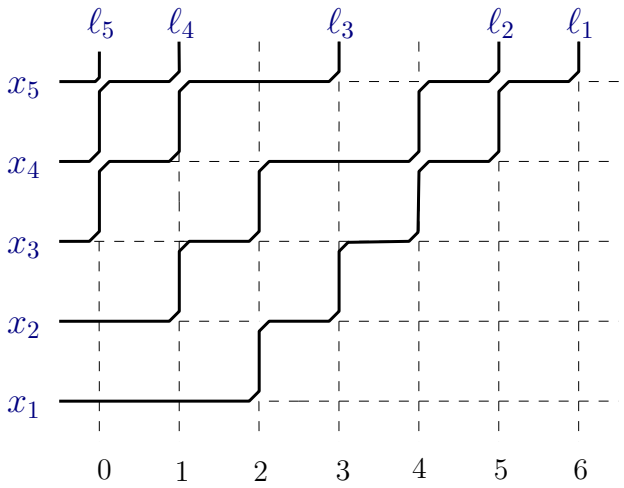
$$\frac{s_\lambda(x, 1^{M-1})}{s_\lambda(1^M)} = \frac{(M-1)!}{(x-1)^{M-1}} \frac{1}{2\pi\mathbf{i}} \oint \frac{x^z}{\prod_{i=1}^{M} \bigl(z - (\lambda_i + M - i)\bigr)} \mathrm{d}z, \qquad \lambda = (\lambda_1 \geq \lambda_2 \geq \cdots \geq \lambda_M),$$

with integration around all poles of the integrand. Use the steepest descent method to deduce the asymptotic behavior as $N \to \infty$ for $x = \exp(s/\sqrt{N})$ and $\lambda[N] = (N-1, N-1, N-2, N-2, \ldots, 1, 1, 0, 0)$. Here $M = 2N$. Conclude that for the uniformly random $N \times N$ ASMs, the position of the 1 in the bottom row satisfies

$$\lim_{N\to\infty} \frac{\xi[N] - \frac{N}{2}}{c\sqrt{N}} \overset{d}{=} \mathcal{N}(0,1).$$

How does c change compared to (7.37)?

Problem 6. Consider the five-vertex model obtained by specializing the weights of Figure 7.1 as follows: $a_1 = a_2 = 1$, $b_1 = x$, $b_2 = 0$, $c_1 = c_2 = 1$. In other words, we prohibit Type (4) vertices and assign weight x to each Type (3) vertex. Consider the model in the domain $\mathbb{Z}_{\geq 0} \times \{1, 2, \ldots, N\}$ with the following boundary conditions: paths enter at every single position on the left and exit at positions $\ell_1 > \ell_2 > \cdots > \ell_N \geq 0$ on top. Assume that the weight x depends on the row and equals x_1, x_2,…, x_N. Let $Z(x_1, \ldots, x_N; \ell_1, \ldots, \ell_N)$ denote the partition function of the resulting vertex model. Here is one possible configuration:



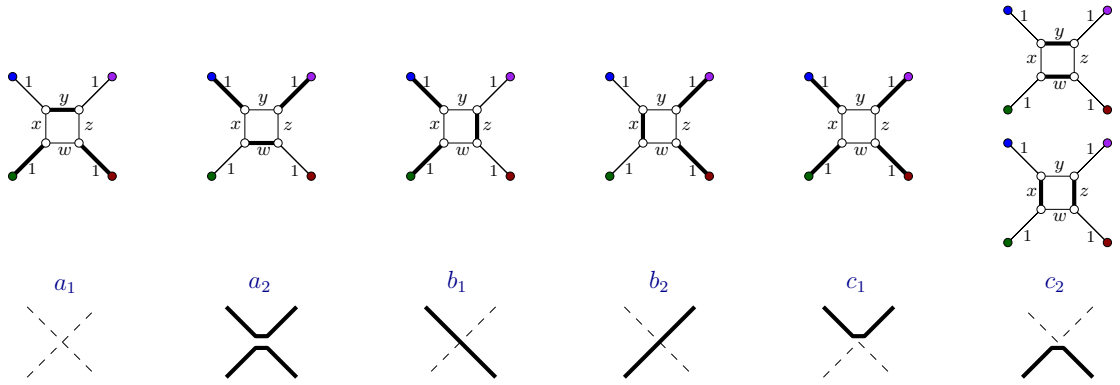
A. Using an appropriate version of the Yang-Baxter equation as in Lemma 7.8, show that $Z(x_1, \dots, x_N;\, \ell_1, \dots, \ell_N)$ is symmetric in $x_1, \dots, x_N$.

B. Comparing with (2.50), prove that

$$Z(x_1, \dots, x_N; \lambda_1 + N - 1, \lambda_2 + N - 2, \dots, \lambda_N) = s_\lambda(x_1, \dots, x_N),$$

where s_λ is the Schur polynomial.

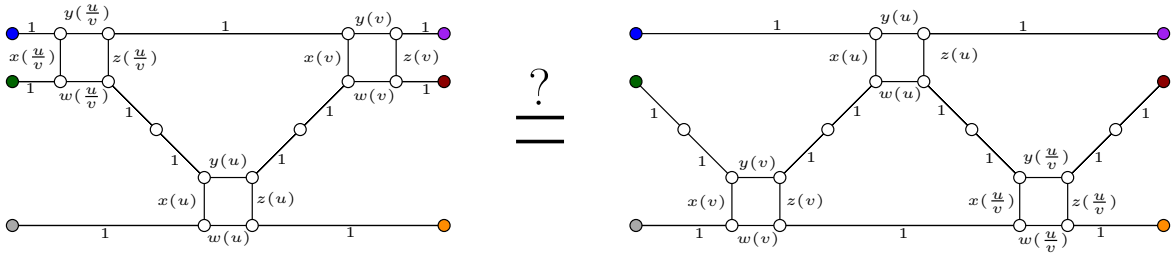
Problem 7. The goal of this problem is to connect the urban renewal of Problem 9 in Section 6.8 with the Yang-Baxter equation for $\Delta = 0$. We consider (partial) dimer configurations on the four-legged graph of Problem 9 such that all four vertices of the internal graph are covered. There are seven of them:



We equip each configuration with product of the weights of covered edges, where the central square edges have weights x, y, z, w, and the four legs have weight 1. We further map the seven dimer configurations into the vertices (rotated, as in Figure 7.8) of the six-vertex model by forgetting the edges in the middle square and inverting the types of the two bottom legs. The dimer weights are mapped to the six-vertex weights: $(a_1, a_2, b_1, b_2, c_1, c_2) = (y, w, z, x, 1, xz + yw)$.

A. Prove that the resulting six-vertex weights satisfy $a_1a_2 + b_1b_2 = c_1c_2$, and any six weights $(a_1, a_2, b_1, b_2, c_1, c_2)$ satisfying $a_1a_2 + b_1b_2 = c_1c_2$ and $c_1 = 1$ can be obtained from some x, y, z, w.

B. We glue three vertices together in two different ways, as in the setup of the Yang-Baxter equation:



Note that we added one vertex in the middle of each diagonal edges, but not on the horizontal edges. The boundary condition on these pictures is a choice for each boundary vertex of the graph, whether it is present or absent. There are 2^6 boundary conditions. Verify that for each boundary condition: either the dimer configurations are mapped to the valid six-vertex configurations entering Theorem 7.6; or neither dimer covers nor six-vertex configurations exist.

C. For each boundary condition in part **B** define the partition function as the sum over all perfect matchings of the graph of products of weights of covered edges. Specialize the six-vertex weights of Figure 7.8 to $\Delta = 0$, divide all six weights by c_1, and determine how $x(u)$, $y(u)$, $z(u)$, $w(u)$ should depend on the spectral parameter u under the correspondence with dimers. Show that the equality of the two dimer partition functions is then exactly Theorem 7.6 at $\Delta = 0$.

D. *Do not* use Theorem 7.6. Deduce the identity of part **C** by local transformations of the graphs which change the partition functions in a controlled way: urban renewal of Problem 9 in Section 6.8 and vertex splitting, which adds/removes two vertices and two edges of weight 1 to the graph.



Hint. You need to apply six urban renewals together with a few vertex splittings.

Literature. We used the following sources for composing problems and refer to them for more information, references, and connections: [FS06], [JN06], [ZJ08], [GP15], [KP16], and [GN25].

Chapter 8

Stochastic six-vertex model in the quadrant

8.1 Model in the quadrant and link to ASEP

In this chapter we continue studying the six-vertex model with stochastic weights of (7.6) and Figure 7.6, which satisfy $a_1 = a_2 = b_1 + c_1 = b_2 + c_2 = 1$. In contrast to the previous chapter, we now use different u and q and different boundary conditions. Previously, we were focusing on u and q being roots of unity, and here we instead look at the case when they are both positive: either $0 < u, q < 1$ or $u, q > 1$. In both situations, the weights become *bona fide* stochastic: they are given by *positive numbers* smaller than 1, cf. Figure 8.1. We still look at the model in an $N \times N$ square, and the boundary conditions along the left and bottom boundaries are the same domain wall case: paths enter from the left and nothing enters from the bottom. However, on the right and top boundary we now consider *free* boundary conditions, *i.e.*, we do not fix the end-points of the paths, and each of the N paths can exit the square either to the right or upward, cf. Figure 8.2. Note that in this setting Proposition 7.1 no longer applies, and the model depends on five rather then two parameters: the only surviving conserved quantity is the total number of vertices in the domain. Due to the stochastic weights, the measure is consistent when increasing the size N and one can see it also as a model on the quadrant, see Proposition 8.1 below.

This new boundary condition can be obtained as $N \to \infty$ limit of the domain wall boundary conditions of the previous chapter. However, in contrast to enumerations and asymptotic theorems developed in Chapter 7 or Figure 1.13 in Section 1.6, the parameter Δ is in a different range for the stochastic six-vertex model:

$$\Delta = \frac{a_1 a_2 + b_1 b_2 - c_1 c_2}{2\sqrt{a_1 a_2 b_1 b_2}} = \frac{1+q}{2\sqrt{q}} > 1.$$

Proposition 8.1. *Consider the six-vertex model in the $N \times N$ square with domain wall boundary conditions on the left and bottom boundaries, and free boundary conditions on the top and right boundaries, and stochastic weights of Figure 8.1. Then*

- *The partition function of the Gibbs measures* (7.1) *is equal to* 1.
- *For any $N > M$, the restriction of the model in the $N \times N$ square onto the bottom-left $M \times M$ subsquare is the same model in the $M \times M$ square. Taking $N = \infty$, we obtain a model in the quadrant $\mathbb{Z}_{>0} \times \mathbb{Z}_{>0}$.*
- *The model can be sampled sequentially for the vertices (i, j) in the order of growing $i + j$, by forced choices of vertices of Type* (1) *or Type* (2) *and by independent biased coin flips to choose between Type*

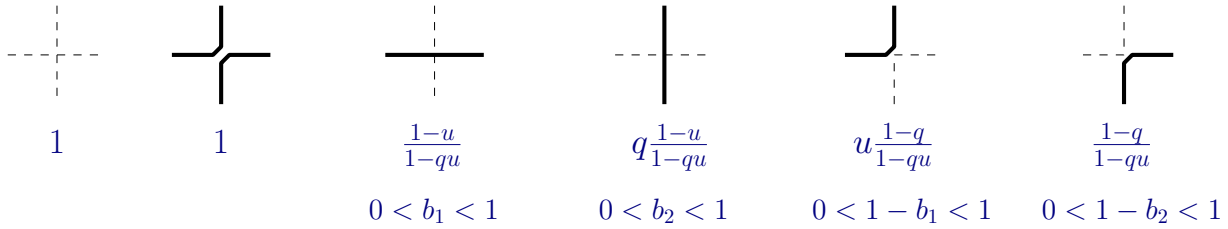


Figure 8.1: The six stochastic weights for $0 < u, q < 1$ or $u, q > 1$.

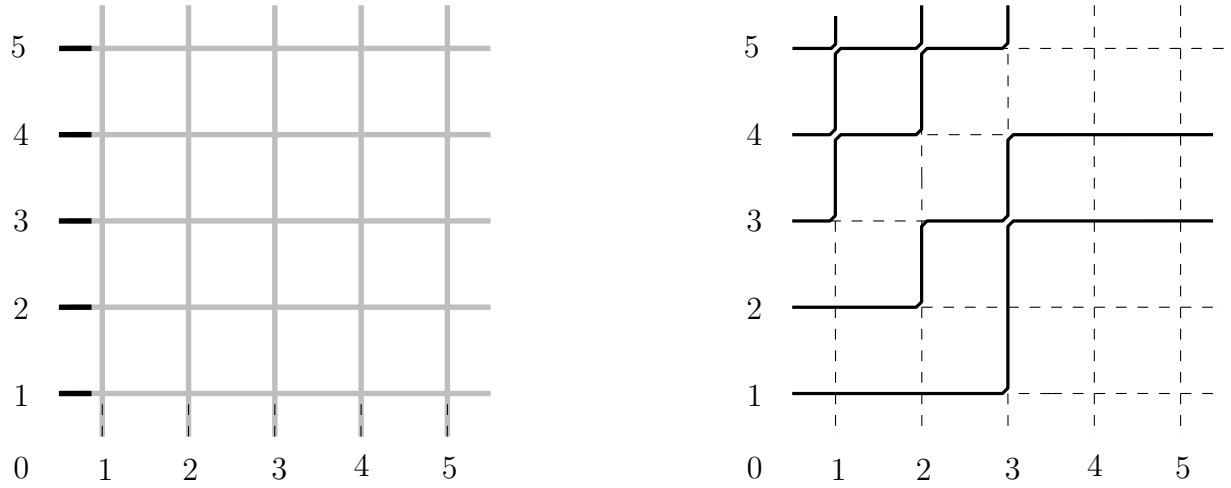


Figure 8.2: Free boundary conditions and one possible configuration.

(3), *of weight* b_1 *and Type* (5), *of weight* $c_1 = 1 - b_1$, *or between Type* (4), *of weight* b_2, *and Type* (6), *of weight* $c_2 = 1 - b_2$.

Note that the statement does not require the weights b_1 and b_2 to be fixed, they can depend on the vertex (i, j) in an arbitrary way, *i.e.*, $b_1 = b_1(i, j)$, $b_2 = b_2(i, j)$.

Proof of Proposition 8.1. Let us provide more details on the sequential stochastic sampling procedure. We sample the vertices at (i, j) in the order of growing $i + j$. When we sample a vertex at (i, j), we already know whether a path is entering into it from below, and whether a path is entering from the left. Hence, there are four cases:

- If no paths are entering from both directions, then the vertex at (i, j) must have Type (1).
- If paths are entering from both directions, then the vertex at (j, j) must have Type (2).
- If a path is only entering from the left, then we set the vertex to be of Type (3) with probability b_1 and of Type (5) with probability $1 - b_1$.
- If a path is only entering from below, then we set the vertex to be of Type (4) with probability b_2 and of Type (6) with probability $1 - b_2$.

After running the procedure for all (i, j) in the quadrant, be get a probability measure on the configurations of the six-vertex model in the quadrant $\mathbb{Z}_{>0} \times \mathbb{Z}_{>0}$. For any N, when we restrict the configuration

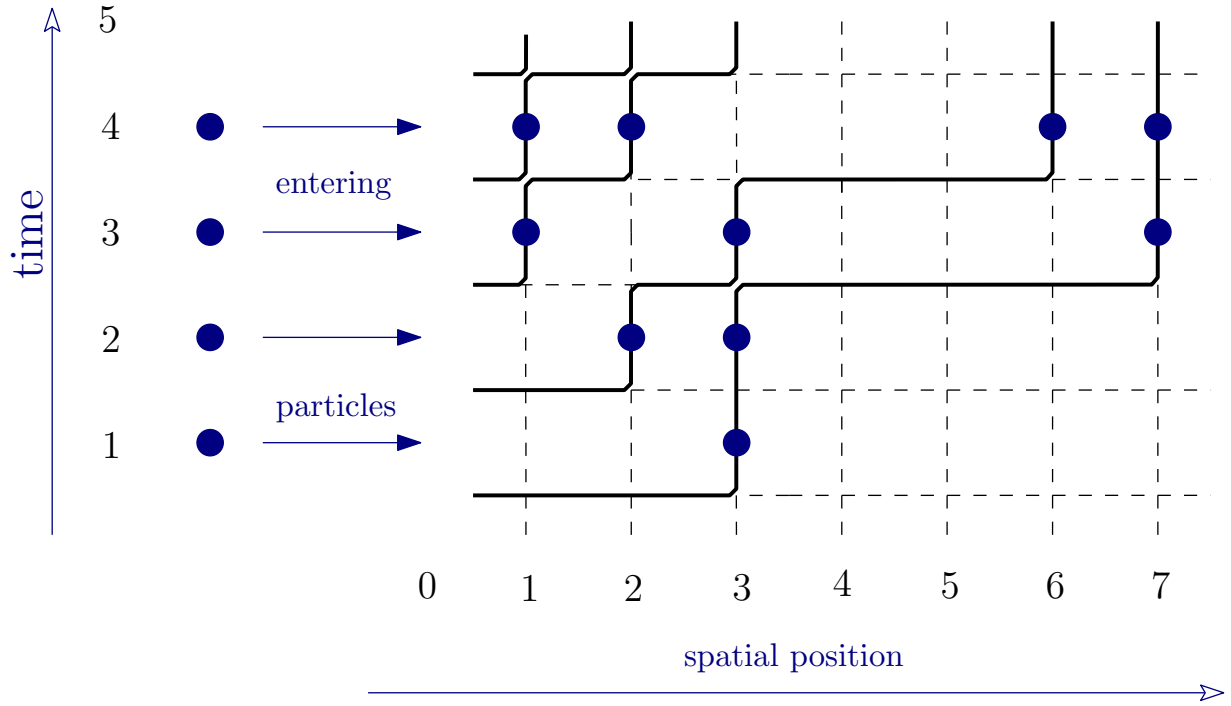


Figure 8.3: Stochastic six-vertex model as an interacting particle system.

to any bottom-left $\{1,\dots,N\}\times\{1,\dots,N\}$ square, we get a probability measure on the configurations in this square with probability of each configuration *equal* (rather than proportional) to the product of weights of the vertices in the square. The claims follow. □

The stochastic six-vertex model can be viewed in two dual ways. On one side, this is a model of 2d statistical mechanics, a relative of the square ice in finite domain and ASMs in Chapter 7, to domino tilings in Chapter 6, to collections of non-intersecting paths in Figures 3.4 and 6.2, to Schur processes in Section 3.4. On the other side, the configurations of the model are trajectories of an interacting particle system, as shown in Figure 8.3, in which we keep track of vertical segments of the paths, and interpret the vertical coordinate as time. Then the sampling rules of the stochastic six-vertex model can be restated as the following Markov evolution (for simplicity, we assume $b_1(i,j)\equiv b_1$ and $b_2(i,j)\equiv b_2$ are constant):

- At time $t=0,1,2,\dots$, the system has t particles, with new particles arriving from the left.
- The particle coordinates $x_t(t)<x_{t-1}(t)<\dots<x_2(t)<x_1(t)$ satisfy the interlacements:

$$x_i(t)\le x_i(t+1)\le x_{i-1}(t). \tag{8.1}$$

- The configuration $\big(x_i(t+1)\big)_{i=1}^{t+1}$ is constructed from left to right, *i.e.*, from $i=t+1$ to $i=1$.
- First, the new particle enters the system at position $x_{t+1}(t+1)\in\{1,2,\dots,x_t(t)\}$ distributed as a truncated geometric distribution:

$$\mathbb{P}\big(x_{t+1}(t+1)=k\big)=\begin{cases} b_1^{k-1}(1-b_1), & 1\le k<x_t(t),\\ b_1^{k}, & k=x_t(t).\end{cases}$$

- For $1 \le i \le t$, if $x_{i+1}(t+1) = x_i(t)$, then the ith particle must jump to the right. Otherwise, it decides whether to jump by flipping a coin. With probability b_2 it will not jump, and we set $x_i(t+1) = x_i(t)$. If the particle decided to jump, then the length of jump is a truncated geometric distribution on the interval $\{1, 2, \dots, x_{i-1}(t) - x_i(t)\}$:

$$\mathbb{P}\big(x_i(t+1) - x_i(t) = k \mid \text{ particle is jumping}\big) = \begin{cases} b_1^{k-1}(1-b_1), & 1 \le k < x_{i-1}(t) - x_i(t), \\ b_1^k, & k = x_{i-1}(t) - x_i(t). \end{cases}$$

  For the first particle with $i = 1$ there is no truncation and the jump length is unrestricted geometric.

Note that the trajectory of the ith particle, $x_i(i) \le x_i(i+1) \le x_i(i+2) \le \dots$, encodes the ith path from the right in the six-vertex configuration.

An alternative point of view on the resulting interacting particle system is delivered by looking at shifted locations $x_i(t) - t$. Because $(x_i(t+1) - (t+1)) - (x_i(t) - t) \in \{-1, 0, 1, 2, \dots\}$, each shifted particle either jumps to the left by 1, or jumps to the right by some distance. The interlacements (8.1) are then turned into blocking conditions. The nature of the dynamics is further simplified by considering the joint limit (see [Agg17] for a rigorous justification):

$$b_1 = \varepsilon \mathfrak{r}, \qquad b_2 = \varepsilon \mathfrak{l}, \qquad t = \varepsilon^{-1}\tau, \qquad y_i(\tau) = \lim_{\varepsilon \to 0} \big[x_i(\varepsilon^{-1}\tau) - \varepsilon^{-1}\tau\big].$$

Then $y_i(\tau)$, $\tau \ge 0$, $i = 1, 2, \dots$ is a continuous time Markov process on infinite particle configurations in $\mathbb{Z}$, known as the asymmetric simple exclusion process (ASEP) with step initial condition. The rules of this interacting particle system are:

- At time 0, $y_i(0) = 1 - i$, $i = 1, 2, \dots$.
- Each particle has two exponential clocks: a right clock and a left clock. The times when the clocks ring are independent Poisson processes of rates $\mathfrak{r}$ and $\mathfrak{l}$, respectively.
- When the right clock of y_i rings at time τ, the particle checks whether the position to the right is empty ($y_{i-1}(\tau-) > y_i(\tau-) + 1$). If so, then it jumps there by setting $y_i(\tau) = y_i(\tau-) + 1$. Otherwise, the particle is blocked and does nothing.
- When the left clock of y_i rings at time τ, the particle checks whether the position to the left is empty ($y_{i+1}(\tau-) < y_i(\tau-) - 1$). If so, then it jumps there by setting $y_i(\tau) = y_i(\tau-) - 1$. Otherwise, the particle is blocked and does nothing.

An equivalent point of view is to *swap* a particle with a particle or hole on its right, when the right clock rings, and with a particle or hole on its left when the left clock rings. In this way we do not need to explicitly spell out any blockages, because swapping positions of two adjacent particles is equivalent to doing nothing.

If we further identity the particle configuration at time t with a Young diagram λ in the same way as we did in Section 4.3:

$$\{y_i(\tau)\}_{i=1}^{\infty} = Y(\lambda) = \big\{\lambda_i - i + 1\big\}_{i=1}^{\infty} \subset \mathbb{Z},$$

then the boxes are added at internal corners at rate $\mathfrak{r}$ and removed from external corners at rate $\mathfrak{l}$, see Figure 8.4 for an illustration. In contrast to the last passage percolation (see Section 1.4 and Figure 1.4), both growth and decay of Young diagrams are now happening concurrently, which makes this interface evolution much more complicated.

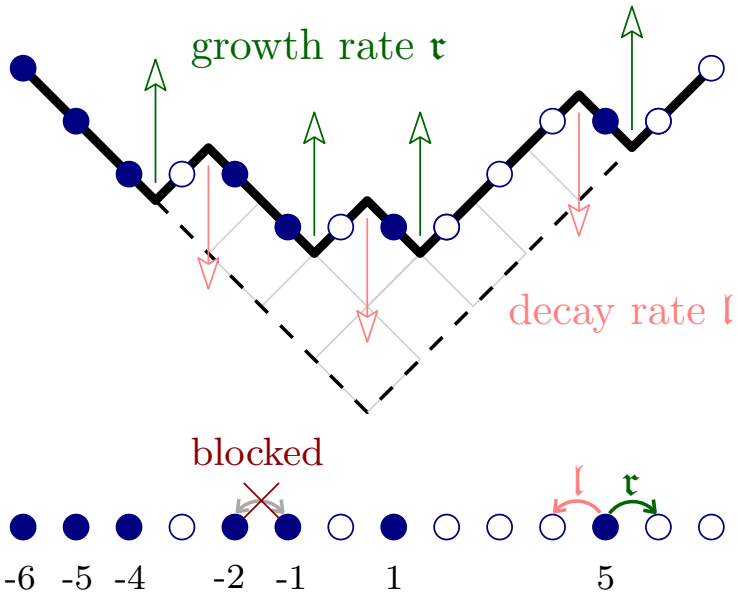


Figure 8.4: A possible finite time state of the asymmetric simple exclusion process with step initical condition.

8.2 A generalization of the Izergin-Korepin determinant

Our analysis of the stochastic six-vertex model is based on a generalization of the Izergin-Korepin determinant of Theorem 7.7. The setting is as in that theorem: the weights of the vertices depend on rapidities $x_1, x_2, \dots, y_1, y_2, \dots$ and quantization parameter q. For the vertex at (i, j) we use the spectral parameter $u = x_i y_j$ and the weight of Figure 8.1.

We also need a notion of the height function, which is very similar to Definition 6.16.

Definition 8.2. *Let σ be a configuration of the stochastic six-vertex model in the quadrant. For each $X, Y \in 1, 2, \dots,$ we define the height function $H[X, Y] = H[X, Y](\sigma)$ as the number of paths which leave the bottom-left $X \times Y$ rectangle in the horizontal direction* (i.e., *through its right border).*

For example, in Figure 8.2, we have $H[5, 5] = H[5, 4] = 2$, $H[5, 3] = 1$, $H[5, 2] = H[5, 1] = 0$.

Theorem 8.3. *Consider the stochastic six-vertex model in the quadrant (equivalently, fix N and consider the $N \times N$ square with free boundary conditions along the top and right boundaries) with paths entering from the left through every row. Suppose that the weights are as in Figure 8.1 with $u = x_i y_j$ for the vertex (i, j). Then for each $w \in \mathbb{C}$, we have*

$$\mathbb{E}\Big[(1-w)(1-wq)\cdots\big(1-wq^{H[N,N]-1}\big)\Big] = \frac{\prod_{i,j=1}^{N}(1-x_i y_j)}{\prod_{i<j}(x_i - x_j)(y_i - y_j)} \det\left[\frac{1-w-(q-w)x_i y_j}{(1-x_i y_j)(1-q x_i y_j)}\right]_{i,j=1}^{N}. \tag{8.2}$$

For $w = 1$, the right-hand side matches the Izergin-Korepin determinant (7.18). The left-hand side turns into $\mathbb{P}(H[N, N] = 0)$, which is precisely the partition function $Z_N(x_1, \dots, x_N; y_1, \dots, y_N; q)$. The generalization (8.2) is 30 years younger than the original (7.18). Our proof is from [ABW23, Proposition C.3], with other closely related identities obtained by other methods in [Bor18, BCG16].

Before proving Theorem 8.3, we connect the right-hand side of (8.2) to a Schur measure.

Proposition 8.4. *Let $\lambda = (\lambda_1, \dots, \lambda_N)$ be distributed according to the Schur measure*

$$\mathbb{P}(\lambda) = \prod_{i,j=1}^{N} (1 - x_i y_j) s_\lambda(x_1, \dots, x_N) s_\lambda(y_1, \dots, y_N).$$

Suppose that $0 < x_i y_j < 1$ for all i, j and $|q| < 1$. Then

$$\mathbb{E}\left[\prod_{i=1}^{N} \left(1 - w q^{\lambda_i + N - i}\right)\right] = \frac{\prod_{i,j=1}^{N}(1 - x_i y_j)}{\prod_{i<j}(x_i - x_j)(y_i - y_j)} \det\left[\frac{1 - w - (q-w) x_i y_j}{(1 - x_i y_j)(1 - q x_i y_j)}\right]_{i,j=1}^{N}. \tag{8.3}$$

Proof. Using the Cauchy-Binet formula of Proposition 2.10, we have

$$\begin{aligned}
\det\left[\frac{1 - w - (q-w) x_i y_j}{(1 - x_i y_j)(1 - t x_i y_j)}\right]_{i,j=1}^{N} &= \det\left[\frac{1}{1 - x_i y_j} - \frac{w}{1 - q x_i y_j}\right] \\
&= \det\left[\sum_{a=0}^{\infty} (1 - w q^a)(x_i y_j)^a\right] \\
&= \sum_{0 \le a_N < \dots < a_1} \left(\prod_{i=1}^{N} (1 - w q^{a_i})\right) \det\left[x_i^{a_j}\right]_{i,j=1}^{N} \det\left[y_i^{a_j}\right]_{i,j=1}^{N}.
\end{aligned}$$

Multiplying both sides by $\frac{\prod_{i,j}(1 - x_i y_j)}{\prod_{i<j}(x_i - x_j)(y_i - y_j)}$, identifying strictly decreasing sequences $a_1 > \dots > a_N \ge 0$ with partitions $\lambda_1 \ge \lambda_2 \dots \ge \lambda_N \ge 0$ via $a_i = \lambda_i + N - i$, and then observing that $\det[x_i^{a_j}]$ is the numerator in the definition of the Schur polynomial (2.14), we convert the right hand side of (8.3) into the left-hand side. □

Proof of Theorem 8.3. We denote $\boldsymbol{x} = (x_1, \dots, x_N), \boldsymbol{y} = (y_1, \dots, y_N)$ and follow the same strategy as in the proof of Theorem 7.7. We claim that the following four properties are satisfied by both sides of (8.2) denoted $R_N(\boldsymbol{x}; \boldsymbol{y};\, q, w)$:

(a) Symmetry in the variables $(x_1, \dots, x_N)$ and in the variables $(y_1, \dots, y_N)$.

(b) The function $R_N(\boldsymbol{x}; \boldsymbol{y};\, q, w) \cdot \prod_{i,j}(1 - q x_i y_j)$ is a polynomial in $x_1, \dots x_N$ and $y_1, \dots, y_N$, such that the degree of each variable is at most N.

(c) If $x_N = y_N^{-1}$, then

$$R_N(\boldsymbol{x}; \boldsymbol{y};\, q, w) = R_{N-1}(x_1, \dots, x_{N-1}; y_1, \dots, y_{N-1};\, q, w).$$

(d) If $x_i = 0$ for *all* i, then $R_N(0, \dots, 0; \boldsymbol{y};\, q, w) = (1 - w)(1 - wq) \cdots (1 - w q^{N-1})$.

The check that the right-hand side of (8.2) satisfies the properties (a), (b), and (c) is the same as in Theorem 7.7. The property (d) follows from (8.3): all $x_i = 0$ leads to the Schur measure being supported on the empty Young diagram with $\lambda_1 = \dots = \lambda_N = 0$, and the expectation becomes $(1 - w) \cdots (1 - w q^{N-1})$.

Let us check that the expectation in the left-hand side of (8.3) satisfies the four properties. For the property (a) we use the Yang-Baxter procedure, similar to the one we used in Figure 7.12, but in the reverse order. We first add cross at the very left position, between rows i and $i + 1$. Paths are entering from the left, and the cross is forced to have Type (2) vertex. Then we move the cross to the right. The Yang-Baxter equation of Theorem 7.6 and preservation of the height $H[N, N]$ under the transfomations

implies that the expectation is unchanged. Once the cross moved N steps to the right, we can remove it due to the stochasticity of the model: in the sequential sampling procedure the type of vertex of the cross would be sampled after all the vertices of the $N \times N$ square, and the type of the vertex of the cross does not affect the value of the random variable $H[N, N]$. The result of this procedure is the swap of variables y_i and y_{i+1} without changing the value of the expectation.

For the property (b) we note that multiplication of the weight of the vertex at (i, j) by $(1 - qx_iy_j)$ makes this weight a polynomial. For the property (c), setting $x_N = y_N^{-1}$ prohibits vertices of Type (3), by $b_1 = 0$, and Type (4), by $b_2 = 0$, in the top-right corner of the domain. Hence, any path which exited the bottom-left $(N - 1) \times (N - 1)$ square to the right, must also exit the $N \times N$ square to the right. Therefore, $H[N, N] = H[N - 1, N - 1]$, and the expectations are also the same. For the property (d) we observe that setting all $x_i = 0$ prohibits Type (5) vertices by $c_1 = 0$ and forces all vertices to be of Type (3), *i.e.*, the paths deterministically go right, and $H[N, N] = N$. This implies the value $(1 - w)(1 - wq) \cdots (1 - wq^{N-1})$ for the expectation.

Now we argue by induction that the four properties (a)-(d) imply the equality (8.3).

Base Case. In the base case $N = 1$, the model has two possible configurations (either Type (3) vertex of weight b_1 or Type (5) vertex of weight c_1) and we check the equality by direct calculation using the vertex weights and the definition of the observable. Both sides are equal to

$$\frac{1 - w - (q - w)x_1y_1}{1 - qx_1y_1} = 1 - w\frac{1 - x_1y_1}{1 - qx_1y_1}.$$

Induction Step. By the property (c) and symmetry, the value of $R_N(\boldsymbol{x}; \boldsymbol{y};\, q, w) \cdot \prod_{i,j}(1-qx_iy_j)$, viewed as a polynomial in x_N, is uniquely determined at N points $x_N = 1/y_i$. Therefore, if $Z_N(\boldsymbol{x}; \boldsymbol{y};\, q, w)$ is another rational function satisfying the same properties, then $Z_N - R_N$ vanishes at $\frac{1}{y_1}, \cdots, \frac{1}{y_N}$, so that

$$\prod_{i,j}(1 - qx_iy_j)\left(Z_N(\boldsymbol{x}; \boldsymbol{y};\, q, w) - R_N(\boldsymbol{x}; \boldsymbol{y};\, q, w)\right) = (\cdots)\prod_{i=1}^{N}\left(x_N - \frac{1}{y_i}\right),$$

where $(\cdots)$ is a polynomial independent of x_N, which we see by considering property (b) and the degree. By symmetry the same is true with x_N replaced by x_j for any $j = 1, \ldots, N - 1$. Therefore, we have

$$\prod_{i,j}(1 - qx_iy_j)\left(Z_N(\mathbf{x}; \mathbf{y};\, q, w) - R_N(\mathbf{x}; \mathbf{y};\, q, w)\right) = (\cdots)'\prod_{i,j=1}^{N}\left(x_j - \frac{1}{y_i}\right)$$

where $(\cdots)'$ must be independent of $(x_1, \ldots, x_N)$ by degree considerations. Setting $x_i = 0, 1 \le i \le N$, we see that this polynomial must be 0 by property (d). □

Remark 8.5. The properties (a), (b), and (c) for $\mathbb{E}\big[\big(1 - w\big)\big(1 - wq\big) \cdots \big(1 - wq^{H[N,N]-1}\big)\big]$ do not depend on the exact form of the observable and hold also for any expectation of the form $\mathbb{E}\big[f(H[N, N])\big]$. In contrast, property (d) relies on the form of the observable and uniquely determines the function $f(\cdot)$ under expectation: $f(L) = R_L(0, \ldots, 0; \boldsymbol{y};\, q, w) = (1 - w)(1 - wq) \cdots (1 - wq^{L-1})$.

8.3 Match with Schur measures and limit regimes

Combining Theorem 8.3 with Proposition 8.4, we arrive at an important match between the height function in the six-vertex model and *columns* in the Schur measure.

Corollary 8.6. *Consider the stochastic six-vertex model in the quadrant with all paths entering from the left. Suppose that the weights are as in Figure 8.1 with $u = x_i y_j$ for each vertex (i, j). Assume $|x_i y_j| < 1$ for all i, j, $|q| < 1$, and choose $M, N \in \mathbb{Z}_{>0}$, treated as horizontal and vertical coordinates, respectively. In addition, let λ be distributed according to the Schur measure*

$$\mathbb{P}(\lambda) = \prod_{i=1}^{M} \prod_{j=1}^{N} (1 - x_i y_j) s_\lambda(x_1, \dots, x_M) s_\lambda(y_1, \dots, y_N).$$

Then for each $w \in \mathbb{C} \setminus \{-q^i\}_{i \in \mathbb{Z}}$, we have

$$\mathbb{E}_{6v}\left[\prod_{i=1}^{\infty} \frac{1}{1 + wq^{H[M,N]-N+i}}\right] = \mathbb{E}_{\textit{Schur}}\left[\prod_{j=1}^{\infty} \frac{1}{1 + wq^{j-\lambda'_j}}\right]. \tag{8.4}$$

Proof. We start from $M = N$ case, where we combine (8.2) with (8.3) to obtain

$$\mathbb{E}_{6v}\Big[\big(1-w\big)\big(1-wq\big)\cdots\big(1-wq^{H[N,N]-1}\big)\Big] = \mathbb{E}_{\text{Schur}}\left[\prod_{i=1}^{N}\Big(1-wq^{\lambda_i+N-i}\Big)\right]. \tag{8.5}$$

We divide both sides by $(1-w)(1-qw)(1-q^2w)\cdots$ and recall from the particle-hole involution in (5.60), (5.84) and Figure 5.14 that

$$\{\lambda_i + N - i\}_{i=1}^{N} \bigsqcup \{-\lambda'_j + j + N - 1\}_{j=1}^{\infty} = \{0, 1, 2, \dots\}. \tag{8.6}$$

We get

$$\mathbb{E}_{6v}\left[\prod_{i=1}^{\infty} \frac{1}{1 - wq^{H[N,N]+i-1}}\right] = \mathbb{E}_{\text{Schur}}\left[\prod_{j=1}^{\infty} \frac{1}{1 - wq^{-\lambda'_j+j+N-1}}\right].$$

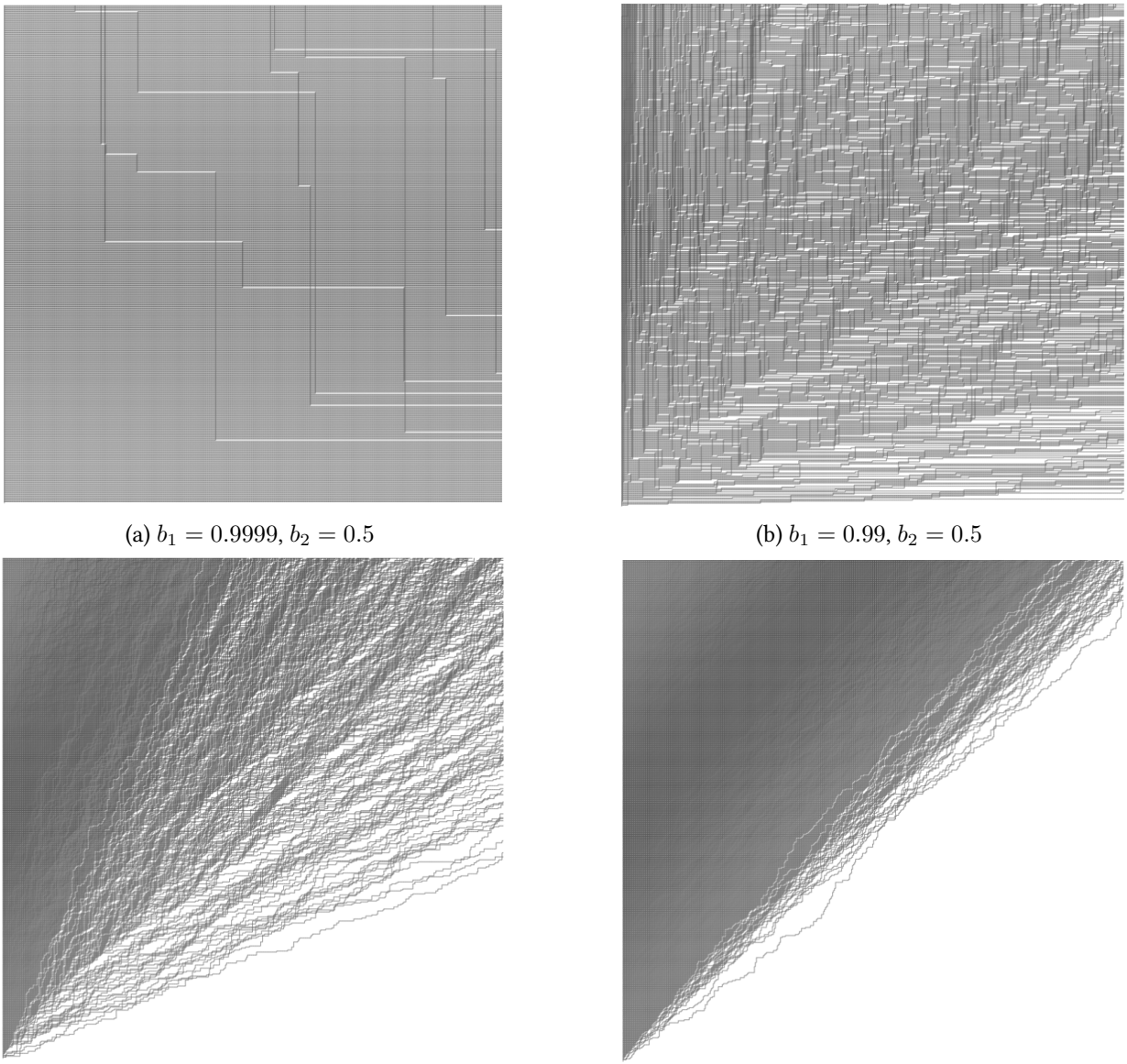
Finally, we replace $w \mapsto -wq^{1-N}$ to reach (8.4).

For the $M \neq N$ case, we have two subcases. First, the $M < N$ case can be obtained from $M = N$ by setting to 0 $N - M$ variables: $x_{M+1} = x_{M+2} = \cdots = x_N = 0$. Due to stability of the Schur polynomials in Lemma 2.7, in the right-hand side we get precisely $\mathbb{E}_{\text{Schur}}$ with M variables $x_1, \dots, x_M$. In the left-hand side, looking back at Figure 8.1 we see that setting $x_i = 0$ prohibits Type (5) vertex by $c_1 = 0$, and therefore forces all paths to go horizontally in the column i. Hence, $H[M, N] = H[N, N]$ and the left-hand of (8.4) gets converted to the desired form.

The case $M > N$ is obtained from $M = N$ by setting to 0 $M - N$ variables: $y_{N+1} = y_{N+2} = \cdots = y_M = 0$. Again, for the right-hand side of (8.4) we use stability of the Schur polynomials. In the left-hand side $y_i = 0$ forces all vertices in the ith row from the bottom to be Type (3), by $b_1 = 0$, *i.e.*, the ith path becomes completely horizontal. Hence, $H[M, M] = H[M, N] + (M - N)$ and the expression under $\mathbb{E}_{6v}$ transforms as desired. □

The match of expectations (8.4) allows us to use all the tools developed for the Schur measures (determinantal point process, contour integrals, steepest descent) in order to extract the asymptotic information about the height function of the stochastic six-vertex model. We set $x_1 = x_2 = \dots$, $y_1 = y_2 = \dots$, so that all $x_i y_j$ are equal to the same constant u, and the model is *homogenous*. A variety of different asymptotic regimes is possible:[1]

[1] Recall that we assumed $q < 1$ and, therefore, $b_1 > b_2$.



(a) $b_1 = 0.9999$, $b_2 = 0.5$

(b) $b_1 = 0.99$, $b_2 = 0.5$

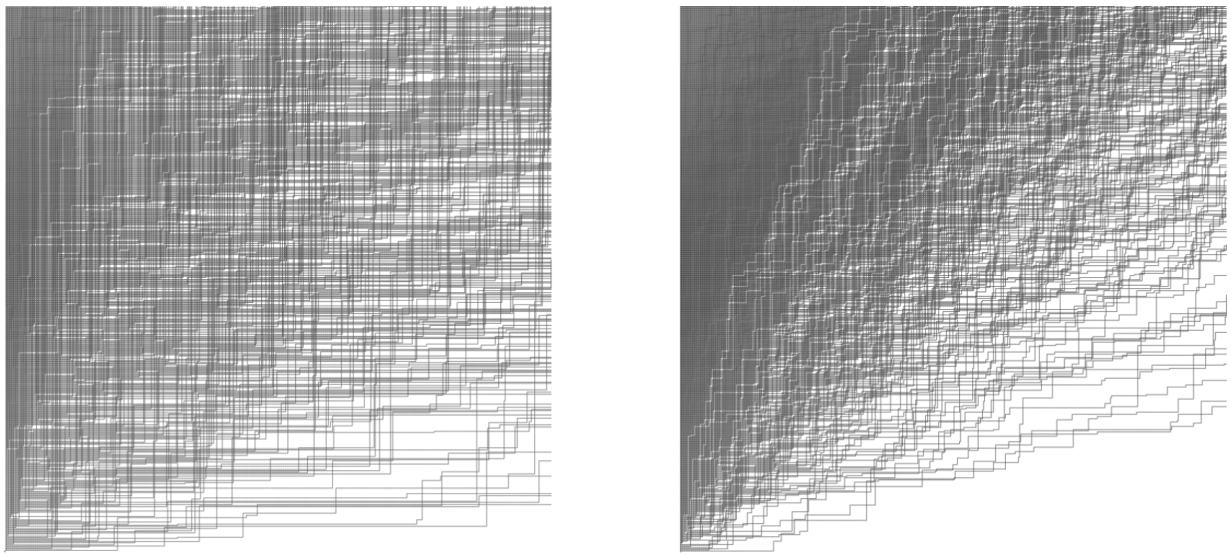
(c) $b_1 = 0.8$, $b_2 = 0.5$

(d) $b_1 = 0.52$, $b_2 = 0.5$

Figure 8.5: Simulations of 500×500 vertices in the stochastic six-vertex model with $b_2 = 0.5$.

1. Figure 8.5c: if both $0 < q < 1$ and $0 < u < 1$ are fixed (*i.e.*, $0 < b_1 < 1$, $0 < b_2 < 1$ are fixed), while $N, M \to \infty$ in such a way that N/M stays finite, then $\frac{1}{N} H[N, M]$ has a deterministic limit, with fluctuations given by the Tracy-Widom distribution, as stated in Theorem 1.7. The right-hand side of (8.4) is governed by the first column in the Schur measure, which itself has Tracy-Widom fluctuations, see Section 8.4 below and [BCG16].

2. Figure 8.5a: if $0 \leq q < 1$ is fixed, $u = \varepsilon^2$, and N and M are proportional to ε^{-1} as $\varepsilon \to 0$, then the stochastic six-vertex model turns into a q-deformation of the PNG growth process, see Problem 1 in Section 8.6 (at $q = 0$ we are back to $h(x, t)$ of the continuous PNG model of Section 3.5). The right-hand side of (8.4) turns into an expectation with respect to the Poissonized Plancherel measure, thus generalizing the $\ell = 1$ case of Theorem 3.11 at $q = 0$.



(a) $b_1 = 0.99, b_2 = 0.96$ (b) $b_1 = 0.95, b_2 = 0.9$

Figure 8.6: 500×500 vertices: $b_1, b_2 \to 1$ leading to Telegraph and KPZ regimes.



(a) $b_1 = 0.3, b_2 = 0.5$. (b) $b_1 = 0.15, b_2 = 0.1$

Figure 8.7: Stationary regime for $b_1 < b_2$ and convergence to ASEP as $b_1, b_2 \to 0$.

3. Figure 8.5d: if $q = \exp(-\sqrt{\varepsilon})$ and $u = \exp(-v\sqrt{\varepsilon})$ (*i.e.*, $b_2/b_1 \to 1$ and $b_1 \to b \in (0,1)$), then $\sqrt{\varepsilon}H[\varepsilon^{-2}t, \varepsilon^{-1}x + \varepsilon^{-2}t]$ after proper recentering converges as $\varepsilon \to 0$ to the (Hopf-Cole, with narrow wedge initial condition) solution $h(x,t)$ of the KPZ stochastic partial differential equation, see [CGST20]. In this limit, the left-hand side of (8.4) becomes the Laplace transform of $\exp(h(x,t))$, while the right-hand side becomes an expectation of a multiplicative functional (cf. Theorem 4.25) of the Airy point process. The latter arises as the scaling limit for the first columns in the Schur measure. The KPZ limit also arises if $0 < u < 1$ is fixed, as in Figure 8.6b, see Section 8.5.

4. Figure 8.6a: if $q \to 1$ and u stays strictly inside $(0,1)$, in such a way that $b_1 = \exp(-\varepsilon\beta_1)$, $b_2 = \exp(-\varepsilon\beta_2)$, then $\varepsilon H[\varepsilon^{-1}x, \varepsilon^{-1}y]$ has a deterministic $\varepsilon \to 0$ limit solving the Telegraph equation (which is a second order hyperbolic PDE), with Gaussian fluctuations given by a stochastic version of the same equation, see [BG19]. In this situation, rather than using (8.4) directly, it is convenient to consider the coefficients of w^k, $k = 1, 2, \ldots$, in (8.5). On the left-hand side they give moments of $q^{H[N,M]}$, while on the right-hand side their asymptotics is closely related to the limit shape and Gaussian fluctuations for the height function encoding the Young diagram distributed as a Schur measure, similarly as in Sections 6.4 and 6.5. In other words, rather than only the first columns, now the entire Young diagram contributes to the limit.

5. Figure 8.7b: if $0 < q < 1$ is fixed, while $u \to 1$ (*i.e.*, $b_1, b_2 \to 0$), then the stochastic six-vertex model turns into the ASEP, as at the end of Section 8.1 and in [Agg17]. The left-hand side of identity (8.4) keeps the same form, with $H[N, M]$ replaced by the height function of ASEP, counting the number of points to the right of a given point. The right-hand side becomes an expectation of the same type with respect to a determinantal point process on $\mathbb{Z}$, obtained as a limit of Schur measures.

In the rest of this chapter, we focus only on the first and third regimes, leading to the Tracy-Widom distribution and KPZ equation, respectively, and precise the asymptotic theorems for these cases. We discuss other limit transitions from the above list, and also introduce two more asymptotic regimes suggested by Figures 8.5b and 8.7a in the exercises.

8.4 Tracy-Widom limit for the height function

In this section we fix $1 > b_1 > b_2 > 0$ or, equivalently, $0 < q, u < 1$ and consider the homogeneous model with vertex weights of Figure 8.1. We analyze the asymptotics of the height function $H[N, N]$ along the diagonal in Figure 8.5c; same ideas can be used to compute the asymptotics of $H[M, N]$, leading to Theorem 1.7 stated earlier.

Theorem 8.7. *Consider the stochastic six-vertex model in the quadrant, with all paths entering from the left and weights of Figure 8.1 with $0 < q, u < 1$. Let $H[N, N]$ be the number of paths which leave the bottom-left $N \times N$ square to the right. Then*

$$\lim_{N\to\infty} N^{-1/3} \left(H[N,N] - N\frac{1-u^{1/2}}{1+u^{1/2}} \right) \stackrel{d}{=} -\mathfrak{a}_1 \cdot u^{1/6} \frac{(1-u^{1/2})^{1/3}}{1+u^{1/2}}, \tag{8.7}$$

where $\mathfrak{a}_1$ is the first point of the Airy point process (GUE Tracy–Widom distribution).

The idea of the proof is to show that the match of expectations (8.4) implies the same $N \to \infty$ asymptotic behavior for the random variables $H[N, N] - N$ and $-\lambda'_1$, where we emphasize the minus sign, which eventually leads to $-\mathfrak{a}_1$ in the right-hand side of (8.4). For the asymptotics of λ'_1, we choose $x_1 = \cdots = x_N = y_1 = \cdots = y_N = \sqrt{u}$ in the Schur measure and recall the result of Theorem 5.27 obtained by the steepest descent analysis, and in which we need to replace q by u:

Corollary 8.8. *For $N = 1, 2, \ldots$, let $\lambda \in \mathbb{Y}$ be distributed as the Schur measure*

$$\mathbb{P}(\lambda) = (1-u)^{N^2} \cdot s^2_\lambda \left(\left[u^{1/2} \right]^N \right).$$

Then the length of the first column of λ converges the Tracy-Widom distribution:

$$\lim_{N\to\infty} N^{-1/3} \left(\lambda'_1 - \frac{2u^{1/2}}{1+u^{1/2}} N \right) \stackrel{d}{=} \mathfrak{a}_1 \cdot u^{\frac{1}{6}} \frac{\left(1-u^{1/2}\right)^{\frac{1}{3}}}{1+u^{1/2}}. \tag{8.8}$$

Hence, if we take the asymptotic match for granted, we get

$$H[N,N] \approx N - \lambda_1' \approx N\left(1 - \frac{2u^{1/2}}{1+u^{1/2}}\right) - N^{1/3}\mathfrak{a}_1 \cdot u^{\frac{1}{6}}\frac{\left(1-u^{1/2}\right)^{\frac{1}{3}}}{1+u^{1/2}},$$

which is the desired (8.7).

Proof of Theorem 8.7. In view of (8.8), we only need to justify $H[N,N] - N \approx -\lambda_1'$. To that end, we choose $s \in \mathbb{R}$ and let

$$w = q^{\mathfrak{m}N - N^{1/3}s}, \qquad \mathfrak{m} = \frac{2u^{1/2}}{1+u^{1/2}}$$

in (8.4), leading to

$$\mathbb{E}_{6v}\left[\prod_{i=1}^{\infty}\frac{1}{1+q^{H[N,N]-N+\mathfrak{m}N-sN^{1/3}+i}}\right] = \mathbb{E}_{\text{Schur}}\left[\prod_{j=1}^{\infty}\frac{1}{1+q^{j-\lambda_j'+\mathfrak{m}N-sN^{1/3}}}\right]. \tag{8.9}$$

We claim that expressions under expectation in both sides of the last identity are smoothed versions of the indicator function. In other words, up to small error, (8.9) is

$$\mathbb{P}_{6v}\Big[H[N,N] - N + \mathfrak{m}N - sN^{1/3} \geq 0\Big] \approx \mathbb{P}_{\text{Schur}}\Big[-\lambda_1' + \mathfrak{m}N - sN^{1/3} \geq 0\Big].$$

In order to make this more precise, we choose a small $\varepsilon > 0$ and start from the right-hand side of (8.9). Notice that the expression under expectation is always between 0 and 1. If $-\lambda_1' + \mathfrak{m}N - sN^{1/3} > \varepsilon N^{1/3}$, then the expression tends to 1 as $N \to \infty$. If $-\lambda_1' + \mathfrak{m}N - sN^{1/3} < -\varepsilon N^{1/3}$, then the expression tends to 0 as $N \to \infty$. Hence,

$$\begin{aligned}\lim_{N\to\infty}\mathbb{P}_{\text{Schur}}\left(\frac{-\lambda_1'+\mathfrak{m}N}{N^{1/3}} > s+\varepsilon\right) &\leq \liminf_{N\to\infty}\mathbb{E}_{\text{Schur}}\left[\prod_{j=1}^{\infty}\frac{1}{1+q^{j-\lambda_j'+\mathfrak{m}N-sN^{1/3}}}\right]\\ &\leq \limsup_{N\to\infty}\mathbb{E}_{\text{Schur}}\left[\prod_{j=1}^{\infty}\frac{1}{1+q^{j-\lambda_j'+\mathfrak{m}N-sN^{1/3}}}\right] \leq \lim_{N\to\infty}\mathbb{P}_{\text{Schur}}\left(\frac{-\lambda_1'+\mathfrak{m}N}{N^{1/3}} > s-\varepsilon\right).\end{aligned}$$

By (8.8), both limits exist and continuously depend on $\varepsilon \geq 0$. Sending $\varepsilon \to 0$, we conclude

$$\lim_{N\to\infty}\mathbb{E}_{\text{Schur}}\left[\prod_{j=1}^{\infty}\frac{1}{1+q^{j-\lambda_j'+\mathfrak{m}N-sN^{1/3}}}\right] = \lim_{N\to\infty}\mathbb{P}_{\text{Schur}}\left(\frac{-\lambda_1'+\mathfrak{m}N}{N^{1/3}} > s\right). \tag{8.10}$$

For the left-hand side of (8.9) we notice that the expression under expectation is again between 0 and 1, tends to 1 if $H[N,N]-N+\mathfrak{m}N-sN^{1/3} > \varepsilon N^{1/3}$, and tends to 0 if $H[N,N]-N+\mathfrak{m}N-sN^{1/3} < \varepsilon N^{1/3}$. Therefore,

$$\begin{aligned}\lim_{N\to\infty}\mathbb{E}_{6v}\left[\prod_{i=1}^{\infty}\frac{1}{1+q^{H[N,N]-N+\mathfrak{m}N-(s+\varepsilon)N^{1/3}+i}}\right] &\leq \liminf_{N\to\infty}\mathbb{P}_{6v}\left(\frac{H[N,N]-N+\mathfrak{m}N}{N^{1/3}} > s\right)\\ \leq \limsup_{N\to\infty}\mathbb{P}_{6v}\left(\frac{H[N,N]-N+\mathfrak{m}N}{N^{1/3}} > s\right) &\leq \lim_{N\to\infty}\mathbb{E}_{6v}\left[\prod_{i=1}^{\infty}\frac{1}{1+q^{H[N,N]-N+\mathfrak{m}N-(s-\varepsilon)N^{1/3}+i}}\right].\end{aligned}$$

Transforming both limits using (8.9), (8.10) and sending $\varepsilon \to 0$, we conclude

$$\lim_{N\to\infty}\mathbb{P}_{6v}\left(\frac{H[N,N]-N+\mathfrak{m}N}{N^{1/3}} > s\right) = \lim_{N\to\infty}\mathbb{P}_{\text{Schur}}\left(\frac{-\lambda_1'+\mathfrak{m}N}{N^{1/3}} > s\right). \quad \square$$

8.5 Weak asymmetry and KPZ limit

In this section we consider a weak asymmetry regime in which b_1 and b_2 both tend to 1 in such a way that $q = b_2/b_1 \to 1$, while $u = \frac{1-b_1}{1-b_2}$ stays fixed inside $(0,1)$, as in Figure 8.6b. If we choose all the scales carefully, then we see a new interesting limit. We only produce the asymptotics on the diagonal, but the same method works equally well away from the diagonal.

Theorem 8.9. *Consider the stochastic six-vertex model in the quadrant, with all paths entering from the left and weights of Figure 8.1 with $0 < q, u < 1$. Suppose that $q \to 1$ and $N \to \infty$ in such a way that $q = \exp(-\varepsilon)$ and $\varepsilon^3 N \to \tau > 0$, while $0 < u < 1$ stays fixed. Then*

$$\lim_{\varepsilon \to 0,\, N \to \infty} \varepsilon \left(H[N,N] - N \frac{1-u^{1/2}}{1+u^{1/2}} + \frac{\ln(\varepsilon)}{\varepsilon} \right) \stackrel{d}{=} \mathfrak{H}, \tag{8.11}$$

where $\mathfrak{H}$ is a random variable such that the Laplace transform of its exponential is computed via the points of the Airy point process as

$$\mathbb{E}\Big[\exp\left(-v\exp\left(-\mathfrak{H}\right)\right)\Big] = \mathbb{E}_{\mathit{Airy}}\left[\prod_{i=1}^{\infty} \frac{1}{1+v\exp\left(\mathfrak{C}\mathfrak{a}_i\right)}\right], \qquad v \geq 0, \tag{8.12}$$

with

$$\mathfrak{C} = \tau^{1/3} u^{1/6} \frac{(1-u^{1/2})^{1/3}}{(1+u^{1/2})}.$$

The expectation in the right-hand side can be computed as a Fredholm determinant involving the Airy kernel by using Theorem 4.25. This can be used to identify $\mathfrak{H}$ with the distribution of the solution at position $x = 0$ and time $t = 2\mathfrak{C}^3$ (so that t depends on τ linearly) to the Kardar-Parisi-Zhang SPDE (1.4) with the narrow wedge initial condition, see [BG16] or [ACQ11, CLDR10, Dot10, SS10]. In more detail, $\mathfrak{Z} = \exp(-\mathfrak{H} - t/24)$ is a solution at time t and position 0, *i.e.*, $\mathfrak{Z} = \mathfrak{Z}(0,t)$, of the stochastic heat equation with δ–function initial condition and space-time white noise $\xi(x,t)$:

$$\frac{\partial}{\partial t}\mathfrak{Z} = \frac{1}{2}\frac{\partial^2}{\partial t^2}\mathfrak{Z} - \mathfrak{Z}\xi, \qquad \mathfrak{Z}(X,0) = \delta(X), \tag{8.13}$$

The stochastic heat equation is obtained from the KPZ equation (1.4) by a formal change of variables $\mathfrak{Z} = \exp(-h)$, which is known as Cole-Hopf transformation.

A more conceptual way to identification with the KPZ equation is to directly pass to the limit in the evolution equations for the stochastic six-vertex model and recognize the appearance of (1.4). This is being complicated by the delicate meaning of the KPZ equation: it is ill-posed as a classical SPDE and the usual approach is to instead consider a better behaved SPDE (8.13), see [BG97, ACQ11, CT17, CGST20] and [Qua11, Section 2.15] for related results.

Nevertheless, let us give a heuristic argument explaining why we should expect ASEP of Figure 8.4 to converge in a weak asymmetry limit towards the KPZ equation; since ASEP itself is a limit of the stochastic six-vertex model, this predicts a similar convergence for the latter. For ASEP with step initial condition, let $h(x,t)$ denote the height function at time t, which is a broken line of slopes ± 1 as in Figure 8.4. The ASEP evolution rules can be restated as follows: for $x \in \mathbb{Z} + \frac{1}{2}$, the height $h(t,x)$ increases by 2 at rate $\mathfrak{r}$ if $h(x,t) - h(x-1,t) = -1$ and $h(x+1,t) - h(x,t) = 1$; $h(t,x)$ decreases by 2 at rate $\mathfrak{l}$ if $h(x,t) - h(x-1,t) = 1$ and $h(x+1,t) - h(x,t) = -1$. Since the only possible slopes are ± 1, we further note that

$$\frac{h(x-1,t) - h(x,t) + 1}{2} = \begin{cases} 1, & \text{if } h(x,t) - h(x-1,t) = -1, \\ 0, & \text{otherwise.} \end{cases}$$

Using this and three other similar indicator identities, we rewrite the time evolution rule of ASEP as

$$\begin{aligned}\mathrm{d}h(x,t) = \mathfrak{r}\frac{(h(x-1,t)-h(x,t)+1)(h(x+1,t)-h(x,t)+1)}{2}\mathrm{d}t \\ - \mathfrak{l}\frac{(h(x,t)-h(x-1,t)+1)(h(x,t)-h(x+1,t)+1)}{2}\mathrm{d}t + \xi(x,t),\end{aligned}$$

where ξ is a Martingale (*i.e.*, of conditional mean 0) random term, which is what remains from random evolution after all deterministic drift terms are removed. Transforming the $\mathrm{d}t$ terms, we get

$$\begin{aligned}\mathrm{d}h(x,t) = \frac{\mathfrak{r}+\mathfrak{l}}{2}\big[h(x-1,t)-2h(x,t)+h(x+1,t)\big]\mathrm{d}t \\ + \frac{\mathfrak{l}-\mathfrak{r}}{2}\big[h(x,t)-h(x-1,t)\big]\big[h(x+1,t)-h(x,t)\big]\mathrm{d}t + \frac{\mathfrak{r}-\mathfrak{l}}{2}\mathrm{d}t + \xi(x,t). \quad (8.14)\end{aligned}$$

If all the rescalings are chosen appropriately, one can hope that then the first term in the right-hand side of (8.14) approximates the second derivative, the second term approximates the squared first derivative, the third term leads to a deterministic linear in time drift, and the noise in the fourth term becomes asymptotically Gaussian by an appropriate CLT. Hence, after subtracting the drift we see the appearance of the KPZ stochastic partial differential equation:

$$\frac{\partial h}{\partial t}(x,t) = \frac{1}{2}\frac{\partial^2 h}{\partial x^2}(x,t) - \frac{1}{2}\left(\frac{\partial h}{\partial x}(x,t)\right)^2 + \xi(x,t). \quad (8.15)$$

Proof of Theorem 8.9. We choose $u > 0$ and set

$$w = vq^{\mathfrak{m}N}, \qquad \mathfrak{m} = \frac{2u^{1/2}}{1+u^{1/2}}$$

in (8.4), leading to

$$\mathbb{E}_{6v}\left[\prod_{i=1}^{\infty}\frac{1}{1+vq^{H[N,N]-N+\mathfrak{m}N+i}}\right] = \mathbb{E}_{\text{Schur}}\left[\prod_{j=1}^{\infty}\frac{1}{1+vq^{j-\lambda'_j+\mathfrak{m}N}}\right]. \quad (8.16)$$

We are going to prove that two sides of this identity converge to the two sides of (8.12). We start from the right-hand side, in which we choose $x_1 = \cdots = x_N = y_1 = \cdots = y_N = \sqrt{u}$ in the Schur measure and use the result of Theorem 5.27:

$$\lim_{N\to\infty} N^{-1/3}\left(\lambda'_j - \mathfrak{m}N\right) \overset{d}{=} \tau^{-1/3}\mathfrak{Ca}_j, \qquad i = 1,2,\ldots. \quad (8.17)$$

Hence, jointly in distribution over finite collections of $j = 1,2,3,\ldots$, we have

$$\lim_{N\to\infty}\frac{1}{1+vq^{j-\lambda'_j+\mathfrak{m}N}} = \frac{1}{1+v\exp\left(\mathfrak{Ca}_j\right)}.$$

We would like to upgrade this to distributional convergence of the infinite products:

$$\lim_{N\to\infty}\prod_{j=1}^{\infty}\frac{1}{1+vq^{j-\lambda'_j+\mathfrak{m}N}} \overset{?}{=} \prod_{j=1}^{\infty}\frac{1}{1+v\exp\left(\mathfrak{Ca}_j\right)}, \quad \text{in distribution.} \quad (8.18)$$

Since individual factors have the desired limits, to prove (8.18) we need to produce a uniform tail bound. Note that the convergence of $\prod_j (1+x_j)$ is equivalent to convergence of $\sum_j x_j$ for positive x_j. Hence, we would like to show

$$\lim_{J\to\infty} \sum_{j=J}^{\infty} q^{j-\lambda'_j+\mathfrak{m}N} = \lim_{J\to\infty} \sum_{j=J}^{\infty} \exp\left(\mathfrak{C}\mathfrak{a}_j\right) = 0, \qquad \text{in probability, uniformly in } N. \tag{8.19}$$

Using Markov inequality, (8.19) follows from the fact that the following expectation is finite for each $\kappa > 0$:

$$\lim_{N\to\infty} \mathbb{E}_{\text{Schur}} \left[\sum_{j=1}^{\infty} q^{\kappa(j-\lambda'_j+\mathfrak{m}N)} \right] \stackrel{?}{=} \mathbb{E} \left[\sum_{j=1}^{\infty} \exp\left(\kappa \mathfrak{C}\mathfrak{a}_j\right) \right] < \infty. \tag{8.20}$$

The $\lim_{N\to\infty}$ limit in the left-hand side of (8.20) can be computed by using the contour integral expression that we developed in Theorem 6.13. The expectation in the right-hand admits an explicit formula (5.87). The details of checking (8.20) are left to the reader (this is one of the exercises at the end of this chapter).

Since the random variables in (8.18) are between 0 and 1, taking the expectations commutes with taking the limits, and we conclude:

$$\lim_{N\to\infty} \mathbb{E}_{\text{Schur}} \left[\prod_{j=1}^{\infty} \frac{1}{1+vq^{j-\lambda'_j+\mathfrak{m}N}} \right] = \mathbb{E}_{\text{Airy}} \left[\prod_{i=1}^{\infty} \frac{1}{1+v\exp\left(\mathfrak{C}\mathfrak{a}_i\right)} \right], \qquad u \geq 0. \tag{8.21}$$

Turning to the left-hand side of (8.16), we denote

$$\eta_N = \varepsilon \left(H[N,N] - N\frac{1-u^{1/2}}{1+u^{1/2}} + \frac{\ln(\varepsilon)}{\varepsilon} \right)$$

and notice the q–exponential approximating an exponential as $q = \exp(-\varepsilon) \to 1$:

$$\begin{aligned} \ln \left[\prod_{i=1}^{\infty} \frac{1}{1+vq^{H[N,N]-N+\mathfrak{m}N+i}} \right] &= \ln \left[\prod_{i=1}^{\infty} \frac{1}{1+\varepsilon v \exp(-\eta_N)\exp(-\varepsilon i)} \right] \\ &= -\sum_{i=1}^{\infty} \ln\left(1+\varepsilon v \exp(-\eta_N)\exp(-\varepsilon i)\right) \\ = -\sum_{i=1}^{\infty} \left(\varepsilon v \exp(-\eta_N)\exp(-\varepsilon i) + O\big(\varepsilon^2 v^2 \exp(-2\eta_N)\exp(-2\varepsilon i)\big)\right) &\to -v\exp(-\eta_N). \end{aligned} \tag{8.22}$$

Since the expression under expectation is between 0 and 1, we conclude

$$\mathbb{E}_{6v} \left[\prod_{i=1}^{\infty} \frac{1}{1+vq^{H[N,N]-N+\mathfrak{m}N+i}} \right] = \mathbb{E}_{6v} \left[\exp\big(-v\exp(-\eta_N)\big) \right] + o(1), \qquad \varepsilon \to 0, \qquad N \to \infty. \tag{8.23}$$

Combining (8.16) with (8.21), (8.23) and noting that convergence of Laplace transforms implies convergence in distribution (by the same argument as at the end of the proof of Theorem 7.13), we arrive at (8.11). □

8.6 Exercises

Problem 1. In the q–PNG the evolution rules are exactly the same as for the continuous PNG of Section 3.5, except that when two islands merge at point x, with probability q a new island is added at x. Explain how the second limit in Section 8.3 and Figure 8.5a lead to the limit from the stochastic six-vertex model to this object. Use Corollary 8.6 to show that the large-time limit of q–PNG is governed by the Tracy-Widom distribution. How do scaling constants change, relative to the $q = 0$ case in Theorem 5.19?

Problem 2. Figure 8.5b hints at the existence of another limit as $b_1 \to 0$, while b_2 is fixed, different from the q–PNG. Find such a limit, leading to a continuous time, discrete space interacting particle system.

Problem 3. Take the limit to ASEP, described in Section 8.1, in the identity of Corollary 8.6. Further applying steepest descent analysis to the correlation functions of the determinantal point process replacing the Schur measure, compute the large time limit of the height function $h(t, x)$ (which counts the number of particles in ASEP at time t to the right of a given point x). One should get a deterministic law of large numbers and Tracy-Widom fluctuations of size $t^{1/3}$. Compare with (5.85).

Problem 4. Make a computer simulation of ASEP to verify numerically your result in Problem 3.

Problem 5. Comparing the coefficients of w and w^2 in Theorem 8.3 *vs* Proposition 8.4, and using Theorem 6.13, obtain explicit formulas for the first two q–moments of the stochastic six-vertex height function $H[N, M]$. (One should be getting a contour integral for $\mathbb{E}q^H$ and a double contour integral for $\mathbb{E}q^{2H}$.

Problem 6. Setting $b_1 = \exp(-\varepsilon\beta_1)$, $b_2 = \exp(-\varepsilon\beta_2)$ and sending $\varepsilon \to 0$ in the result of Problem 5, show that $\varepsilon H[\varepsilon^{-1}x, \varepsilon^{-1}y]$ has a deterministic limit $\mathfrak{h}(x, y)$. Transforming the resulting contour integral, find a second order partial differential equation for $\mathfrak{h}$, which is especially simple in terms of $\exp(\mathfrak{h})$.

Problem 7. Analytically continuing of the result of Problem 5, extend the contour integral expressions for $\mathbb{E}q^H$ and $\mathbb{E}q^{2H}$ to the case $q > 1$. Using the particle system representation for the stochastic six-vertex model $x_1(t) > x_2(t) > \dots$, as in Section 8.1, conclude by taking the limit of the contour integral that for fixed $1 > b_2 > b_1 > 0$, the random variable $x_1(t) - t$ is tight as $t \to \infty$. This explains the configuration being frozen outside a small neighborhood of the diagonal in Figure 8.7a.

Problem 8. Using (8.12), show that the random variable $\mathfrak{H}$ after proper centering and rescaling converges to the Tracy-Widom distribution as $\tau \to \infty$. Thus, the solution of the KPZ equation has Tracy-Widom distributed large time fluctuations.

Problem 9. Using Theorem 6.13, write a contour integral expression for the expectation in the left-hand side of (8.20). Sending $n \to \infty$ and using (5.87), prove (8.20).

Literature. We used the following sources for composing problems and refer to them for more information, references, and connections: [TW09], [SS10], [ACQ11], [BG16], [BO17b], [BG19], and [ABW23].

Bibliography

[ABDF11] Gernot Akemann, Jinho Baik, and Philippe Di Francesco (eds.), *The Oxford handbook of random matrix theory*, Oxford University Press, 2011.

[ABW23] Amol Aggarwal, Alexei Borodin, and Michael Wheeler, *Deformed polynuclear growth in (1+1) dimensions*, International Mathematics Research Notices **2023** (2023), no. 7, 5728–5780, arXiv:2108.06018.

[ACJ23] Arvind Ayyer, Sunil Chhita, and Kurt Johansson, *GOE fluctuations for the maximum of the top path in alternating sign matrices*, Duke Mathematical Journal **172** (2023), no. 10, 1961–2014, arXiv:2109.02422.

[ACQ11] Gideon Amir, Ivan Corwin, and Jeremy Quastel, *Probability distribution of the free energy of the continuum directed random polymer in* $1 + 1$ *dimensions*, Communications on Pure and Applied Mathematics **64** (2011), no. 4, 466–537, arXiv:1003.0443.

[AD99] David Aldous and Persi Diaconis, *Longest Increasing Subsequences: From Patience Sorting to the Baik–Deift–Johansson Theorem*, Bulletin of the American Mathematical Society **36** (1999), no. 4, 413–432.

[ADCH$^+$26] Emile Averous, Hugo Duminil-Copin, Tiancheng He, Piet Lammers, and Ioan Manolescu, *Conformal invariance of the six-vertex model's height function*, Preprint, arXiv:2610.07454, 2026.

[Agg15] Amol Aggarwal, *Correlation functions of the Schur process through Macdonald difference operators*, Journal of Combinatorial Theory, Series A **131** (2015), 88–118, arXiv:1401.6979.

[Agg17] ———, *Convergence of the stochastic six-vertex model to the ASEP*, Mathematical Physics, Analysis and Geometry **20** (2017), no. 2, 3, arXiv:1607.08683.

[Agg20] ———, *Arctic boundaries of the ice model on three-bundle domains*, Inventiones mathematicae **220** (2020), no. 2, 611–671, arXiv:1812.03847.

[AGZ10] Greg W. Anderson, Alice Guionnet, and Ofer Zeitouni, *An introduction to random matrices*, Cambridge Studies in Advanced Mathematics, no. 118, Cambridge University Press, 2010.

[Ahn22] Andrew Ahn, *Airy point process via supersymmetric lifts*, Probability and Mathematical Physics **3** (2022), no. 4, 869–938, arXiv:2009.06839.

[Air38] George B. Airy, *On the intensity of light in the neighbourhood of a caustic*, Transactions of the Cambridge Philosophical Society **6** (1838), 379–402.

[Akh65] Naum I. Akhiezer, *The Classical Moment Problem and Some Related Questions in Analysis*, Oliver and Boyd, Edinburgh and London, 1965, Translated from the Russian by N. Kemmer.

[AKK99] Masoud Alimohammadi, Vahid Karimipour, and Mohammad Khorrami, *A two-parametric family of asymmetric exclusion processes and its exact solution*, Journal of Statistical Physics **97** (1999), no. 1–2, 373–394, arXiv:cond-mat/9805155.

[And86] Konstantin A. Andréief, *Note sur une relation entre les intégrales définies des produits des fonctions*, Mém. de la Société des Sciences physiques et naturelles de Bordeaux, 3e série **2** (1886), 1–14.

[ASLW+15] Gerardo Algara-Siller, Ossi Lehtinen, Fengchao Wang, Rahul R. Nair, Ute Kaiser, Heng-An Wu, Andre K. Geim, and Irina V. Grigorieva, *Square ice in graphene nanocapillaries*, Nature **519** (2015), no. 7544, 443–445, arXiv:1412.7498.

[Ass18] Theodoros Assiotis, *Random surface growth and Karlin–McGregor polynomials*, Electronic Journal of Probability **23** (2018), no. 106, 1–81, arXiv:1709.10444.

[Ass20] ———, *Determinantal structures in space-inhomogeneous dynamics on interlacing arrays*, Annales Henri Poincaré **21** (2020), no. 3, 909–940, arXiv:1910.09500.

[Avr39] Melvin Avrami, *Kinetics of Phase Change. I: General Theory*, The Journal of Chemical Physics **7** (1939), no. 12, 1103–1112.

[Avr40] ———, *Kinetics of Phase Change. II: Transformation-Time Relations for Random Distribution of Nuclei*, The Journal of Chemical Physics **8** (1940), no. 2, 212–224.

[Avr41] ———, *Granulation, Phase Change, and Microstructure: Kinetics of Phase Change. III*, The Journal of Chemical Physics **9** (1941), no. 2, 177–184.

[Bax72] Rodney J. Baxter, *Partition function of the eight-vertex lattice model*, Annals of Physics **70** (1972), no. 1, 193–228.

[Bax07] ———, *Exactly solved models in statistical mechanics*, Dover Publications, Mineola, NY, 2007, Reprint of the 1982 Academic Press edition.

[BB68] Robert M. Baer and Paul Brock, *Natural sorting over permutation spaces*, Mathematics of Computation **22** (1968), no. 102, 385–410.

[BBAP05] Jinho Baik, Gérard Ben Arous, and Sandrine Péché, *Phase transition of the largest eigenvalue for nonnull complex sample covariance matrices*, The Annals of Probability **33** (2005), no. 5, 1643–1697, arXiv:math/0403022.

[BBCS18] Jinho Baik, Guillaume Barraquand, Ivan Corwin, and Toufic Suidan, *Pfaffian Schur processes and last passage percolation in a half-quadrant*, The Annals of Probability **46** (2018), no. 6, 3015–3089, arXiv:1606.00525.

[BBD08] Jinho Baik, Robert Buckingham, and Jeffery DiFranco, *Asymptotics of Tracy–Widom distributions and the total integral of a Painlevé II function*, Communications in Mathematical Physics **280** (2008), no. 2, 463–497, arXiv:0704.3636.

[BBS+06] Eitan Bachmat, Daniel Berend, Luba Sapir, Steven Skiena, and Natan Stolyarov, *Analysis of aeroplane boarding via spacetime geometry and random matrix theory*, Journal of Physics A: Mathematical and General **39** (2006), no. 29, L453–L459, arXiv:physics/0512020.

[BC14] Alexei Borodin and Ivan Corwin, *Macdonald processes*, Probability Theory and Related Fields **158** (2014), no. 1–2, 225–400, arXiv:1111.4408.

[BCG16] Alexei Borodin, Ivan Corwin, and Vadim Gorin, *Stochastic six-vertex model*, Duke Mathematical Journal **165** (2016), no. 3, 563–624, arXiv:1407.6729.

[BCGS16] Alexei Borodin, Ivan Corwin, Vadim Gorin, and Shamil Shakirov, *Observables of Macdonald processes*, Transactions of the American Mathematical Society **368** (2016), no. 3, 1517–1558, arXiv:1306.0659.

[BD02] Alexei Borodin and Percy Deift, *Fredholm determinants, Jimbo-Miwa-Ueno τ-functions, and representation theory*, Communications on Pure and Applied Mathematics **55** (2002), no. 9, 1160–1230, arXiv:math-ph/0111007.

[BDJ99] Jinho Baik, Percy Deift, and Kurt Johansson, *On the distribution of the length of the longest increasing subsequence of random permutations*, Journal of the American Mathematical Society **12** (1999), no. 4, 1119–1178, arXiv:math/9810105.

[BF08] Alexei Borodin and Patrik L. Ferrari, *Large time asymptotics of growth models on space-like paths I: PushASEP*, Electronic Journal of Probability **13** (2008), 1380–1418, arXiv:0707.2813.

[BF09] ———, *Anisotropic KPZ growth in 2+1 dimensions: fluctuations and covariance structure*, Journal of Statistical Mechanics: Theory and Experiment **2009** (2009), no. 02, P02009, arXiv:0811.0682.

[BF14] ———, *Anisotropic growth of random surfaces in 2+1 dimensions*, Communications in Mathematical Physics **325** (2014), no. 2, 603–684, arXiv:0804.3035.

[BF18] ———, *Random tilings and Markov chains for interlacing particles*, Markov Processes and Related Fields **24** (2018), no. 3, 419–451, arXiv:1506.03910.

[BFLS14] Gerard T. Barkema, Patrik L. Ferrari, Joel L. Lebowitz, and Herbert Spohn, *Kardar-Parisi-Zhang universality class and the anchored Toom interface*, Physical Review E **90** (2014), no. 4, 042116, arXiv:1405.7837.

[BG97] Lorenzo Bertini and Giambattista Giacomin, *Stochastic Burgers and KPZ equations from particle systems*, Communications in Mathematical Physics **183** (1997), no. 3, 571–607.

[BG15] Alexey Bufetov and Vadim Gorin, *Stochastic monotonicity in Young graph and Thoma theorem*, International Mathematics Research Notices **2015** (2015), no. 23, 12920–12940, arXiv:1411.3307.

[BG16] Alexei Borodin and Vadim Gorin, *Moments match between the KPZ equation and the Airy point process*, SIGMA. Symmetry, Integrability and Geometry: Methods and Applications **12** (2016), 102, arXiv:1608.01557.

[BG18] Alexey Bufetov and Vadim Gorin, *Fluctuations of particle systems determined by Schur generating functions*, Advances in Mathematics **338** (2018), 702–781, arXiv:1604.01110.

[BG19] Alexei Borodin and Vadim Gorin, *A stochastic telegraph equation from the six-vertex model*, The Annals of Probability **47** (2019), no. 6, 4137–4194, arXiv:1803.09137.

[BGK25] Anna Bykhovskaya, Vadim Gorin, and Eszter Kiss, *Largevars: An R package for testing large VARs for the presence of cointegration*, Preprint, arXiv:2509.06295, 2025.

[BH86] Norman Bleistein and Richard A. Handelsman, *Asymptotic Expansions of Integrals*, Dover Publications, New York, 1986.

[Bil12] Patrick Billingsley, *Probability and Measure*, 4th / anniversary ed., John Wiley & Sons, Hoboken, NJ, 2012.

[BK18] Alexey Bufetov and Alisa Knizel, *Asymptotics of random domino tilings of rectangular Aztec diamonds*, Annales de l'Institut Henri Poincaré, Probabilités et Statistiques **54** (2018), no. 3, 1250–1290, arXiv:1604.01491.

[BN12] Gaëtan Borot and Céline Nadal, *Right tail asymptotic expansion of Tracy–Widom beta laws*, Random Matrices: Theory and Applications **1** (2012), no. 03, 1250006, arXiv:1111.2761.

[BNR24] Tomas Berggren, Matthew Nicoletti, and Marianna Russkikh, *Perfect t-embeddings of uniformly weighted Aztec diamonds and tower graphs*, International Mathematics Research Notices **2024** (2024), no. 7, 5963–6007, arXiv:2303.10045.

[BO99] Carl M. Bender and Steven A. Orszag, *Advanced Mathematical Methods for Scientists and Engineers I: Asymptotic Methods and Perturbation Theory*, Springer, New York, 1999.

[BO00a] Alexei Borodin and Andrei Okounkov, *A Fredholm determinant formula for Toeplitz determinants*, Integral Equations and Operator Theory **37** (2000), no. 4, 386–396, arXiv:math/9907165.

[BO00b] Alexei Borodin and Grigori Olshanski, *Distributions on partitions, point processes and the hypergeometric kernel*, Communications in Mathematical Physics **211** (2000), 335–358, arXiv:math/9904010.

[BO06] ———, *Markov processes on partitions*, Probability Theory and Related Fields **135** (2006), no. 1, 84–152, arXiv:math-ph/0409075.

[BO12] ———, *Markov processes on the path space of the Gelfand–Tsetlin graph and on its boundary*, Journal of Functional Analysis **263** (2012), no. 1, 248–303, arXiv:1009.2029.

[BO17a] ———, *Representations of the infinite symmetric group*, Cambridge Studies in Advanced Mathematics, vol. 160, Cambridge University Press, 2017.

[BO17b] ———, *The ASEP and determinantal point processes*, Communications in Mathematical Physics **353** (2017), no. 2, 853–903, arXiv:1608.01564.

[BO26] Alexey Bufetov and Evgeny Obukhov, *Limiting shape of alternating sign matrices*, Preprint, arXiv:2609.16994, 2026.

[BOO00] Alexei Borodin, Andrei Okounkov, and Grigori Olshanski, *Asymptotics of Plancherel measures for symmetric groups*, Journal of the American Mathematical Society **13** (2000), no. 3, 481–515, arXiv:math/9905032.

[Bor10a] Folkmar Bornemann, *On the numerical evaluation of distributions in random matrix theory: A review*, Markov Processes and Related Fields **16** (2010), no. 4, 803–866, arXiv:0904.1581.

[Bor10b] _____, *On the numerical evaluation of Fredholm determinants*, Mathematics of Computation **79** (2010), no. 270, 871–915, arXiv:0804.2543.

[Bor11a] Alexei Borodin, *Determinantal point processes*, The Oxford Handbook of Random Matrix Theory (Gernot Akemann, Jinho Baik, and Philippe Di Francesco, eds.), Oxford University Press, 2011, arXiv:0911.1153, pp. 231–249.

[Bor11b] _____, *Schur dynamics of the Schur processes*, Advances in Mathematics **228** (2011), no. 4, 2268–2291, arXiv:1001.3442.

[Bor18] _____, *Stochastic higher spin six vertex model and Macdonald measures*, Journal of Mathematical Physics **59** (2018), no. 2, 023301, arXiv:1608.01553.

[Böt01] Albrecht Böttcher, *One more proof of the Borodin-Okounkov formula for Toeplitz determinants*, Integral Equations and Operator Theory **41** (2001), no. 1, 123–125, arXiv:math/0012200.

[Böt02] _____, *On the determinant formulas by Borodin, Okounkov, Baik, Deift and Rains*, Toeplitz Matrices and Singular Integral Equations (Pobershau, 2001) (Albrecht Böttcher, Israel Gohberg, and Peter Junghanns, eds.), Operator Theory: Advances and Applications, vol. 135, Birkhäuser, Basel, 2002, arXiv:math/0101008, pp. 91–99.

[BP14] Alexei Borodin and Leonid Petrov, *Integrable probability: From representation theory to Macdonald processes*, Probability Surveys **11** (2014), 1–58, arXiv:1310.8007.

[BP16] _____, *Nearest neighbor Markov dynamics on Macdonald processes*, Advances in Mathematics **300** (2016), 71–155, arXiv:1305.5501.

[BR01] Jinho Baik and Eric M. Rains, *The asymptotics of monotone subsequences of involutions*, Duke Mathematical Journal **109** (2001), no. 2, 205–281, arXiv:math/9905084.

[BR05] Alexei Borodin and Eric M. Rains, *Eynard–Mehta theorem, Schur process, and their Pfaffian analogs*, Journal of Statistical Physics **121** (2005), no. 3–4, 291–317, arXiv:math-ph/0409059.

[BS95] Albert-László Barabási and Harry E. Stanley, *Fractal Concepts in Surface Growth*, Cambridge University Press, Cambridge, UK, 1995.

[BS99] Albrecht Böttcher and Bernd Silbermann, *Introduction to Large Truncated Toeplitz Matrices*, Universitext, Springer, New York, 1999.

[BS06] _____, *Analysis of Toeplitz Operators*, 2nd ed., Springer Monographs in Mathematics, Springer, Berlin, Heidelberg, 2006.

[Buf26] Alexey Bufetov, *Limit shape for domain-wall six-vertex model*, Preprint, arXiv:2609.20576, 2026.

[BW00] Estelle L. Basor and Harold Widom, *On a Toeplitz determinant identity of Borodin and Okounkov*, Integral Equations and Operator Theory **37** (2000), no. 4, 397–401, arXiv:math/9909010.

[BW22] Alexei Borodin and Michael Wheeler, *Coloured stochastic vertex models and their spectral theory*, Astérisque (2022), no. 437, ix+225, arXiv:1808.01866.

[BZJ66] Édouard Brézin and Jean Zinn-Justin, *Un problème à N corps soluble*, Comptes Rendus de l'Académie des Sciences Paris, Série A–B **263** (1966), 670–673.

[Car94] Élie Cartan, *Sur la structure des groupes de transformations finis et continus*, Ph.D. thesis, Faculté des Sciences de Paris, 1894.

[Cau15] Augustin-Louis Cauchy, *Mémoire sur les fonctions qui ne peuvent obtenir que deux valeurs égales et de signes contraires par suite des transpositions opérées entre les variables qu'elles renferment*, Journal de l'École Polytechnique **10** (1815), 29–112.

[CGST20] Ivan Corwin, Promit Ghosal, Hao Shen, and Li-Cheng Tsai, *Stochastic PDE limit of the six vertex model*, Communications in Mathematical Physics **375** (2020), no. 3, 1945–2038, arXiv:1803.08120.

[CJY15] Sunil Chhita, Kurt Johansson, and Benjamin Young, *Asymptotic domino statistics in the Aztec diamond*, The Annals of Applied Probability **25** (2015), no. 3, 1232–1278, arXiv:1212.5414.

[CKP01] Henry Cohn, Richard Kenyon, and James Propp, *A variational principle for domino tilings*, Journal of the American Mathematical Society **14** (2001), no. 2, 297–346, arXiv:math/0008220.

[CL95] Ovidiu Costin and Joel L. Lebowitz, *Gaussian fluctuation in random matrices*, Physical Review Letters **75** (1995), no. 1, 69–72.

[CLDR10] Pasquale Calabrese, Pierre Le Doussal, and Alberto Rosso, *Free-energy distribution of the directed polymer at high temperature*, EPL (Europhysics Letters) **90** (2010), no. 2, 20002, arXiv:1002.4560.

[Cop65] Edward T. Copson, *Asymptotic Expansions*, Cambridge University Press, Cambridge, 1965.

[CP10] Filippo Colomo and Andrei G. Pronko, *The arctic curve of the domain-wall six-vertex model*, Journal of Statistical Physics **138** (2010), no. 4–5, 662–700, arXiv:0907.1264.

[CP26] _____, *Frozen-corner enumeration of Alternating Sign Matrices*, The Electronic Journal of Combinatorics **33** (2026), no. 3, P3.32, arXiv:2509.14006.

[CR24] Dmitry Chelkak and Sanjay Ramassamy, *Fluctuations in the Aztec diamonds via a space-like maximal surface in Minkowski 3-space*, Confluentes Mathematici **16** (2024), 1–17, arXiv:2002.07540.

[CS16] Filippo Colomo and Andrea Sportiello, *Arctic curves of the six-vertex model on generic domains: the tangent method*, Journal of Statistical Physics **164** (2016), no. 6, 1488–1523, arXiv:1605.01388.

[CT17] Ivan Corwin and Li-Cheng Tsai, *KPZ equation limit of higher-spin exclusion processes*, The Annals of Probability **45** (2017), no. 3, 1771–1798, arXiv:1505.04158.

[Cue18] Cesar Cuenca, *Markov processes on the duals to infinite-dimensional classical Lie groups*, Annales de l'Institut Henri Poincaré, Probabilités et Statistiques **54** (2018), no. 3, 1359–1407, arXiv:1608.02281.

[DE02] Ioana Dumitriu and Alan Edelman, *Matrix models for beta ensembles*, Journal of Mathematical Physics **43** (2002), no. 11, 5830–5847, arXiv:math-ph/0206043.

[DE05] _____, *Eigenvalues of Hermite and Laguerre ensembles: large beta asymptotics*, Annales de l'Institut Henri Poincaré, Probabilités et Statistiques **41** (2005), no. 6, 1083–1099, arXiv:math-ph/0403029.

[DF90] Persi Diaconis and James Allen Fill, *Strong stationary times via a new form of duality*, The Annals of Probability **18** (1990), no. 4, 1483–1522.

[DF13] Philippe Di Francesco, *An inhomogeneous Lambda-determinant*, Electronic Journal of Combinatorics **20** (2013), no. 3, P19, arXiv:1209.6619.

[Dix77] Jacques Dixmier, *C*-algebras*, North-Holland Mathematical Library, vol. 15, North-Holland Publishing Co., Amsterdam & New York, 1977, Translated from the French *Les C*-algèbres et leurs représentations*.

[DLSS91] Bernard Derrida, Joel L. Lebowitz, Eugene R. Speer, and Herbert Spohn, *Dynamics of an anchored Toom interface*, Journal of Physics A: Mathematical and General **24** (1991), no. 20, 4805–4834.

[dM67] Abraham de Moivre, *The doctrine of chances: or, A method of calculating the probabilities of events in play. Reprint of the 3rd edition. London 1756*, New York, N.Y.: Chelsea Publishing Company. 368 p. (1967)., 1967.

[Dot10] Victor Dotsenko, *Bethe ansatz derivation of the Tracy-Widom distribution for one-dimensional directed polymers*, EPL (Europhysics Letters) **90** (2010), no. 2, 20003, arXiv:1003.4899.

[DV13] Laure Dumaz and Bálint Virág, *The right tail exponent of the Tracy-Widom β distribution*, Annales de l'Institut Henri Poincaré, Probabilités et Statistiques **49** (2013), no. 4, 915–933, arXiv:1102.4818.

[DVJ03] Daryl J. Daley and David Vere-Jones, *An Introduction to the Theory of Point Processes, Volume I: Elementary Theory and Methods*, 2 ed., Probability and Its Applications, Springer, New York, NY, USA, 2003.

[DVJ08] _____, *An Introduction to the Theory of Point Processes, Volume II: General Theory and Structure*, 2 ed., Probability and Its Applications, Springer, New York, NY, USA, 2008.

[DW08] Antonius B. Dieker and Jon Warren, *Determinantal transition kernels for some interacting particles on the line*, Annales de l'Institut Henri Poincaré, Probabilités et Statistiques **44** (2008), no. 6, 1162–1172, arXiv:0707.1843.

[Dys62a] Freeman J. Dyson, *Statistical Theory of the Energy Levels of Complex Systems. I*, Journal of Mathematical Physics **3** (1962), 140–156.

[Dys62b] _____, *Statistical Theory of the Energy Levels of Complex Systems. II*, Journal of Mathematical Physics **3** (1962), 157–165.

[Dys62c] ———, *Statistical Theory of the Energy Levels of Complex Systems. III*, Journal of Mathematical Physics **3** (1962), 166–175.

[Edr53] Albert Edrei, *Proof of a conjecture of Schoenberg on the generating function of a totally positive sequence*, Canadian Journal of Mathematics **5** (1953), 86–94.

[EKLP92] Noam Elkies, Greg Kuperberg, Michael Larsen, and James Propp, *Alternating-sign matrices and domino tilings I and II*, Journal of Algebraic Combinatorics **1** (1992), 111–132; 219–234, arXiv:math/9201305.

[EPS14] Alan Edelman, Per-Olof Persson, and Brian D. Sutton, *Low-temperature random matrix theory at the soft edge*, Journal of Mathematical Physics **55** (2014), no. 6, 063302.

[ES07] Alan Edelman and Brian D. Sutton, *From random matrices to stochastic operators*, Journal of Statistical Physics **127** (2007), no. 6, 1121–1165, arXiv:math-ph/0607038.

[Fer04] Patrik L. Ferrari, *Polynuclear growth on a flat substrate and edge scaling of GOE eigenvalues*, Communications in Mathematical Physics **252** (2004), no. 1–3, 77–109, arXiv:math-ph/0402053.

[Fom88] Sergey V. Fomin, *Generalized Robinson–Schensted–Knuth Correspondence*, Journal of Soviet Mathematics **41** (1988), no. 2, 979–991, Translation of Russian original in: Zap. Nauchn. Sem. Leningrad. Otdel. Mat. Inst. Steklov. (LOMI) 155 (1986).

[Fom95] ———, *Schensted algorithms for dual graded graphs*, Journal of Algebraic Combinatorics **4** (1995), no. 1, 5–45.

[Fom99] ———, *Knuth equivalence, jeu de taquin, and the Littlewood–Richardson rule*, Enumerative Combinatorics, Volume 2 (by Richard P. Stanley), Cambridge Studies in Advanced Mathematics, vol. 62, Cambridge University Press, Cambridge, 1999, Appendix 1 to Chapter 7, pp. 413–439.

[For10] Peter J. Forrester, *Log-gases and random matrices*, Princeton University Press, 2010.

[Fra74] Frederick C. Frank, *Nucleation-controlled growth on a one-dimensional growth of finite length*, Journal of Crystal Growth **22** (1974), no. 3, 233–236.

[FS03] Patrik L. Ferrari and Herbert Spohn, *Step fluctuations for a faceted crystal*, Journal of Statistical Physics **113** (2003), no. 1–2, 1–46, arXiv:cond-mat/0212456.

[FS06] ———, *Domino tilings and the six-vertex model at its free-fermion point*, Journal of Physics A: Mathematical and General **39** (2006), no. 33, 10297–10306, arXiv:cond-mat/0605406.

[FS11] ———, *Random growth models*, The Oxford Handbook of Random Matrix Theory (Gernot Akemann, Jinho Baik, and Philippe Di Francesco, eds.), Oxford University Press, Oxford, 2011, arXiv:1003.0881, pp. 782–801.

[FSA24] Gabriel Frieden and Florian Schreier-Aigner, *$qtRSK^*$: A probabilistic dual RSK correspondence for Macdonald polynomials*, Preprint, arXiv:2403.16243, 2024.

[Ful97] William Fulton, *Young tableaux*, London Mathematical Society, Student texts, vol. 35, Cambridge University Press, 1997.

[FZJ08] Tiago Fonseca and Paul Zinn-Justin, *On the Doubly Refined Enumeration of Alternating Sign Matrices and Totally Symmetric Self-Complementary Plane Partitions*, The Electronic Journal of Combinatorics **15** (2008), no. 1, R81, arXiv:0803.1595.

[GC79] Jeffrey S. Geronimo and Kenneth M. Case, *Scattering theory and polynomials orthogonal on the unit circle*, Journal of Mathematical Physics **20** (1979), no. 2, 299–310.

[Ges90] Ira M. Gessel, *Symmetric functions and P-recursiveness*, Journal of Combinatorial Theory, Series A **53** (1990), no. 2, 257–285.

[GK24] Vadim Gorin and Victor Kleptsyn, *Universal objects of the infinite beta random matrix theory*, Journal of the European Mathematical Society **26** (2024), no. 9, 3429–3496, arXiv:2009.02006.

[GL25] Vadim Gorin and Karl Liechty, *Boundary statistics for the six-vertex model with DWBC*, Communications on Pure and Applied Mathematics **78** (2025), no. 10, 1847–1948, arXiv:2310.12735.

[GN25] Vadim Gorin and Matthew Nicoletti, *Six-vertex model and random matrix distributions*, Bulletin of the American Mathematical Society **62** (2025), no. 2, 175–234, arXiv:2309.12495.

[Gol84] Nigel Goldenfeld, *Kinetics of a model for nucleation-controlled polymer crystal growth*, Journal of Physics A: Mathematical and General **17** (1984), no. 14, 2807–2821.

[Gor21] Vadim Gorin, *Lectures on random lozenge tilings*, Cambridge Studies in Advanced Mathematics, vol. 193, Cambridge University Press, 2021.

[GP15] Vadim Gorin and Greta Panova, *Asymptotics of symmetric polynomials with applications to statistical mechanics and representation theory*, The Annals of Probability **43** (2015), no. 6, 3052–3132, arXiv:1301.0634.

[GP17] Massimiliano Gubinelli and Nicolas Perkowski, *KPZ reloaded*, Communications in Mathematical Physics **349** (2017), no. 1, 165–269, arXiv:1508.03877.

[GRAS96] César Gómez, Martí Ruiz-Altaba, and Germán Sierra, *Quantum groups in two-dimensional physics*, Cambridge Monographs on Mathematical Physics, Cambridge University Press, Cambridge, 1996.

[Gre74] Curtis Greene, *An extension of Schensted's theorem*, Advances in Mathematics **14** (1974), no. 2, 254–265.

[GRSZ25] Pablo Groisman, Alejandro F. Ramírez, Santiago Saglietti, and Sebastián Zaninovich, *GUE Fluctuations Near the Axis in One-Sided Ballistic Deposition*, Preprint, arXiv:2504.15837, 2025.

[GS92] Leh-Hun Gwa and Herbert Spohn, *Six-vertex model, roughened surfaces, and an asymmetric spin Hamiltonian*, Physical Review Letters **68** (1992), no. 6, 725–728.

[GS15] Vadim Gorin and Mykhaylo Shkolnikov, *Limits of multilevel TASEP and similar processes*, Annales de l'Institut Henri Poincaré, Probabilités et Statistiques **51** (2015), no. 1, 18–27, arXiv:1206.3817.

[GS18] _____, *Stochastic Airy semigroup through tridiagonal matrices*, The Annals of Probability **46** (2018), no. 4, 2287–2344, arXiv:1601.06800.

[GXZ24] Vadim Gorin, Jiaming Xu, and Lingfu Zhang, *Airy$_\beta$ line ensemble and its Laplace transform*, Preprint, arXiv:2411.10829, 2024.

[Hai13] Martin Hairer, *Solving the KPZ equation*, Annals of Mathematics **178** (2013), no. 2, 559–664, arXiv:1109.6811.

[Ham72] John M. Hammersley, *A Few Seedlings of Research*, Proceedings of the Sixth Berkeley Symposium on Mathematical Statistics and Probability, vol. 1, University of California Press, 1972, pp. 345–394.

[HKPV06] J. Ben Hough, Manjunath Krishnapur, Yuval Peres, and Bálint Virág, *Determinantal Processes and Independence*, Probability Surveys **3** (2006), 206–229, arXiv:math/0503110.

[HKPV09] _____, *Zeros of Gaussian analytic functions and determinantal point processes*, University Lecture Series, vol. 51, American Mathematical Society, Providence, RI, 2009.

[HM80] Stuart P. Hastings and John B. McLeod, *A boundary value problem associated with the second Painlevé transcendent and the Korteweg–de Vries equation*, Archive for Rational Mechanics and Analysis **73** (1980), no. 1, 31–51.

[IO02] Vladimir Ivanov and Grigori Olshanski, *Kerov's central limit theorem for the Plancherel measure on Young diagrams*, Symmetric functions 2001: surveys of developments and perspectives (Sergey Fomin, ed.), NATO Science Series II: Mathematics, Physics and Chemistry, vol. 74, Kluwer Academic Publishers, Dordrecht, 2002, arXiv:math/0304010, pp. 93–151.

[Iss18] Leon Isserlis, *On a formula for the product-moment coefficient of any order of a normal frequency distribution in any number of variables*, Biometrika **12** (1918), no. 1/2, 134–139.

[Ize87] Anatoli G. Izergin, *Partition function of the six-vertex model in a finite volume*, Soviet Physics Doklady **32** (1987), 878.

[JB25] Camille Jorge and Denis Bartolo, *Active-hydraulic flows solve the six-vertex model (and vice versa)*, Physical Review Letters **134** (2025), 188302, arXiv:2410.13377.

[Jim94] Michio Jimbo, *Introduction to the Yang-Baxter equation*, Braid group, knot theory and statistical mechanics, II, Adv. Ser. Math. Phys., vol. 17, World Sci. Publ., River Edge, NJ, 1994, pp. 153–176. MR 1338602

[JM39] William A. Johnson and Robert F. Mehl, *Reaction Kinetics in Processes of Nucleation and Growth*, Transactions of the American Institute of Mining and Metallurgical Engineers **135** (1939), 416–442.

[JN06] Kurt Johansson and Eric Nordenstam, *Eigenvalues of GUE minors*, Electronic Journal of Probability **11** (2006), no. 50, 1342–1371, arXiv:math/0606760.

[Joh00] Kurt Johansson, *Shape fluctuations and random matrices*, Communications in Mathematical Physics **209** (2000), 437–476, arXiv:math/9903134.

[Joh01a] _____, *Discrete orthogonal polynomial ensembles and the Plancherel measure*, Annals of Mathematics **153** (2001), no. 1, 259–296, arXiv:math/9906120.

[Joh01b] _____, *Random growth and random matrices*, European Congress of Mathematics, Vol. I (Barcelona, 2000) (Basel), Progress in Mathematics, vol. 201, Birkhäuser, 2001, pp. 445–456.

[Joh02] ———, *Non-intersecting paths, random tilings and random matrices*, Probability Theory and Related Fields **123** (2002), no. 2, 225–280, arXiv:math/0011250.

[Joh03] ———, *Discrete polynuclear growth and determinantal processes*, Communications in Mathematical Physics **242** (2003), no. 1–2, 277–329, arXiv:math/0206208.

[Joh05] ———, *The arctic circle boundary and the Airy process*, The Annals of Probability **33** (2005), no. 1, 1–30, arXiv:math/0306216.

[Joh06] ———, *Random matrices and determinantal processes*, Mathematical Statistical Physics (Les Houches Session LXXXIII, 2005), Les Houches, vol. 83, Elsevier, 2006, arXiv:math-ph/0510038, pp. 1–56.

[JPS26] William Jockusch, James Propp, and Peter Shor, *Random domino tilings and the arctic circle theorem*, Annales de l'Institut Henri Poincaré D, Combinatorics, Physics and their Interactions (2026), Preprint 1998, arXiv:math/9801068.

[JS16] In-Jee Jeong and Sasha Sodin, *A limit theorem for stochastically decaying partitions at the edge*, Random Matrices: Theory and Applications **5** (2016), no. 04, 1650016, arXiv:1604.01104.

[Juc66] Algimantas Jucys, *On the Young operators of the symmetric group*, Lietuvos Fizikos Rinkinys **6** (1966), 163–180.

[Kac90] Victor G. Kac, *Infinite-Dimensional Lie Algebras*, 3rd ed., Cambridge University Press, Cambridge, 1990.

[Ken00] Richard Kenyon, *Conformal invariance of domino tiling*, The Annals of Probability **28** (2000), no. 2, 759–795, arXiv:math-ph/9910002.

[Ken09] ———, *Lectures on dimers*, Statistical Mechanics, IAS/Park City Mathematics Series, vol. 16, American Mathematical Society, 2009, Lecture notes from the Park City Mathematics Institute, 2007. arXiv:0910.3129, pp. 191–230.

[Ker93] Sergei V. Kerov, *Gaussian limit for the Plancherel measure of the symmetric group*, Comptes Rendus de l'Académie des Sciences, Série I, Mathématique **316** (1993), 303–308.

[Ker98] ———, *A differential model for the growth of Young diagrams*, American Mathematical Society Translations, Series 2 **188** (1998), 111–130.

[Ker03] ———, *Asymptotic Representation Theory of the Symmetric Group and Its Applications in Analysis*, Translations of Mathematical Monographs, vol. 219, American Mathematical Society, Providence, RI, 2003.

[Kin93] John F. C. Kingman, *Poisson Processes*, Oxford Studies in Probability, no. 3, Clarendon Press, Oxford, 1993.

[Knu70] Donald Knuth, *Permutations, matrices and generalized Young tableaux*, Pacific Journal of Mathematics **34** (1970), 709–727.

[Kol37] Andrei N. Kolmogorov, *On the Statistical Theory of the Crystallization of Metals*, Izvestiya Akademii Nauk SSSR, Seriya Matematicheskaya **1** (1937), no. 3, 355–359 (Russian).

[KOO98] Sergei V. Kerov, Andrei Okounkov, and Grigori Olshanski, *The boundary of the Young graph with Jack edge multiplicities*, International Mathematics Research Notices **1998** (1998), no. 4, 173–199, arXiv:q-alg/9703037.

[Kor82] Vladimir E. Korepin, *Calculation of norms of Bethe wave functions*, Communications in Mathematical Physics **86** (1982), no. 3, 391 – 418.

[KP16] Richard Kenyon and Robin Pemantle, *Double-dimers, the Ising model and the hexahedron recurrence*, Journal of Combinatorial Theory, Series A **137** (2016), 27–63, arXiv:1308.2998.

[KPZ86] Mehran Kardar, Giorgio Parisi, and Yi-Cheng Zhang, *Dynamic scaling of growing interfaces*, Physical Review Letters **56** (1986), 889–892.

[KT12] Alex Kulesza and Ben Taskar, *Determinantal point processes for machine learning*, Foundations and Trends® in Machine Learning **5** (2012), no. 2–3, 123–286, arXiv:1207.6083.

[Kup96] Greg Kuperberg, *Another Proof of the Alternating-Sign Matrix Conjecture*, International Mathematics Research Notices **1996** (1996), no. 3, 139–150, arXiv:math/9712207.

[Kup02] ———, *Symmetry classes of alternating-sign matrices under one roof*, Annals of Mathematics **156** (2002), no. 3, 835–866, arXiv:math/0008184.

[Lam15] Jules Lamers, *Introduction to quantum integrability*, Proceedings of 10th Modave Summer School in Mathematical Physics — PoS(Modave2014), vol. 232, Sissa Medialab, 2015, arXiv:1501.06805.

[Lap74] Pierre-Simon Laplace, *Mémoire sur la probabilité des causes par les événemens*, Mémoires de mathématique et de physique présentés à l'Académie royale des sciences, par divers savans, et lûs dans ses assemblées **6** (1774), 621–656, Reprinted in Oeuvres complètes de Laplace, Vol. 8, pp. 27–65.

[Lap20] ———, *Théorie analytique des probabilités*, 3rd ed., Mme Ve Courcier, Paris, 1820, Translations and analysis available at `https://www.probabilityandfinance.com/pulskamp/Laplace/`.

[Lap86] ———, *Memoir on the probability of the causes of events*, Statistical Science **1** (1986), no. 3, 364–378, English translation by Stephen M. Stigler of the original memoir published in 1774.

[Lax02] Peter D. Lax, *Functional Analysis*, Wiley-Interscience, New York, 2002.

[Len73] Andrew Lenard, *Correlation Functions and the Uniqueness of the State in Classical Statistical Mechanics*, Communications in Mathematical Physics **30** (1973), no. 1, 35–44.

[Li26] Yinjie Li, *The Colomo-Pronko conjecture for frozen-corner alternating sign matrices*, Preprint, arXiv:2609.14351, 2026.

[Lia26] Yuchen Liao, *The Airy line ensemble at the edge of uniform alternating sign matrices*, Preprint, arXiv:2609.20603, 2026.

[Lie67a] Elliott H. Lieb, *Residual Entropy of Square Ice*, Physical Review **162** (1967), no. 1, 162–172.

[Lie67b] ———, *Solution of the Dimer Problem by the Transfer Matrix Method*, Journal of Mathematical Physics **8** (1967), no. 12, 2339–2341.

[Lig85] Thomas M. Liggett, *Interacting Particle Systems*, Grundlehren der mathematischen Wissenschaften, vol. 276, Springer-Verlag, New York, 1985, Reprinted in Classics in Mathematics, Springer, 2005.

[Lig99] ———, *Stochastic Interacting Systems: Contact, Voter and Exclusion Processes*, Grundlehren der mathematischen Wissenschaften, vol. 324, Springer-Verlag, Berlin, 1999.

[Lin22] Jarl W. Lindeberg, *Eine neue Herleitung des Exponentialgesetzes in der Wahrscheinlichkeitsrechnung*, Mathematische Zeitschrift **15** (1922), 211–225.

[LS77] Benjamin F. Logan and Lawrence A. Shepp, *A variational problem for random Young tableaux*, Advances in Mathematics **26** (1977), no. 2, 206–222.

[LW72] Elliott H. Lieb and Fa-Yueh Wu, *Two Dimensional Ferroelectric Models*, Phase Transitions and Critical Phenomena (Cyril Domb and Melville S. Green, eds.), vol. 1, Academic Press, 1972, pp. 331–490.

[Lya01] Aleksandr M. Lyapunov, *Nouvelle forme du théorème sur la limite de probabilité*, Mémoires de l'Académie Impériale des Sciences de St.-Pétersbourg, Classe physico-mathématique **12** (1901), no. 5, 1–24.

[Lyo03] Russell Lyons, *Determinantal probability measures*, Publications Mathématiques de l'IHÉS **98** (2003), 167–212, arXiv:math/0204325.

[Mac75] Odile Macchi, *The coincidence approach to stochastic point processes*, Advances in Applied Probability **7** (1975), 83–122.

[Mac95] Ian G. Macdonald, *Symmetric Functions and Hall Polynomials*, 2nd ed., Oxford Mathematical Monographs, Oxford University Press, 1995.

[Mal73] Colin L. Mallows, *Patience Sorting*, Bulletin of the Institute of Mathematics and Its Applications **9** (1973), 216–224.

[McG64] James B. McGuire, *Study of exactly soluble one-dimensional N-body problems*, Journal of Mathematical Physics **5** (1964), no. 5, 622–636.

[Meh04] Madan L. Mehta, *Random Matrices*, 3rd ed., Pure and Applied Mathematics, vol. 142, Elsevier/Academic Press, Amsterdam, 2004.

[MGP68] Carolyn T. MacDonald, Julian H. Gibbs, and Allen C. Pipkin, *Kinetics of biopolymerization on nucleic acid templates*, Biopolymers **6** (1968), no. 1, 1–25.

[MRR83] William H. Mills, David P. Robbins, and Howard Rumsey, Jr., *Alternating sign matrices and descending plane partitions*, Journal of Combinatorial Theory, Series A **34** (1983), no. 3, 340–359, Received March 15, 1982.

[MRR86] ———, *Self-complementary totally symmetric plane partitions*, Journal of Combinatorial Theory, Series A **42** (1986), 277–292.

[MS17] James A. Mingo and Roland Speicher, *Free Probability and Random Matrices*, Fields Institute Monographs, vol. 35, Springer New York, 2017.

[Nor10] Eric Nordenstam, *On the Shuffling Algorithm for Domino Tilings*, Electronic Journal of Probability **15** (2010), 75–95, arXiv:0802.2592.

[Oka98] Soichi Okada, *Applications of minor summation formulas to rectangular-shaped representations of classical groups*, Journal of Algebra **205** (1998), no. 2, 337–367.

[Oka06] ———, *Enumeration of symmetry classes of alternating sign matrices and characters of classical groups*, Journal of Algebraic Combinatorics **23** (2006), no. 1, 43–69, arXiv:math/0408234.

[Oko99] Andrei Okounkov, *On representations of the infinite symmetric group*, Journal of Mathematical Sciences **96** (1999), 3550–3589, Originally appeared in Russian. arXiv:math/9803037.

[Oko00] ———, *Random matrices and random permutations*, International Mathematics Research Notices **2000** (2000), no. 20, 1043–1095, arXiv:math/9903176.

[Oko01a] ———, *Infinite wedge and random partitions*, Selecta Mathematica **7** (2001), 57–81, arXiv:math/9907127.

[Oko01b] ———, *SL(2) and z-measures*, Random Matrix Models and Their Applications (Pavel M. Bleher and Alexander R. Its, eds.), Mathematical Sciences Research Institute Publications, vol. 40, Cambridge University Press, Cambridge, 2001, arXiv:math/0002135, pp. 407–420.

[Oko02] ———, *Generating functions for intersection numbers on moduli spaces of curves*, International Mathematics Research Notices **2002** (2002), no. 18, 933–957, arXiv:math/0101201.

[OLBC10] Frank W. J. Olver, Daniel W. Lozier, Ronald F. Boisvert, and Charles W. Clark (eds.), *NIST Handbook of Mathematical Functions*, Cambridge University Press, New York, 2010.

[Olv97] Frank W. J. Olver, *Asymptotics and Special Functions*, A K Peters, Wellesley, MA, 1997, Reprint of the 1974 Academic Press edition.

[Ons44] Lars Onsager, *Crystal statistics. I. A two-dimensional model with an order-disorder transition*, Physical Review **65** (1944), no. 3–4, 117–149.

[OR03] Andrei Okounkov and Nikolai Reshetikhin, *Correlation function of Schur process with application to local geometry of a random 3-dimensional Young diagram*, Journal of the American Mathematical Society **16** (2003), no. 3, 581–603, arXiv:math/0107056.

[OR06] ———, *The Birth of a Random Matrix*, Moscow Mathematical Journal **6** (2006), no. 3, 553–566.

[Pau35] Linus Pauling, *The Structure and Entropy of Ice and of Other Crystals with Some Randomness of Atomic Arrangement*, Journal of the American Chemical Society **57** (1935), no. 12, 2680–2684.

[Pla10] Michel Plancherel, *Contribution à l'étude de la représentation d'une fonction arbitraire par des intégrales définies*, Rendiconti del Circolo Matematico di Palermo **30** (1910), no. 1, 289–335.

[Pra94] Viktor Prasolov, *Problems and Theorems in Linear Algebra*, Translations of Mathematical Monographs, vol. 134, American Mathematical Society, Providence, RI, 1994, Translated from the Russian manuscript by D. A. Leĭtes.

[Pro03] James Propp, *Generalized domino-shuffling*, Theoretical Computer Science **303** (2003), no. 2–3, 267–301, arXiv:math/0111034.

[PS00] Michael Prähofer and Herbert Spohn, *Universal distributions for growth processes in 1+1 dimensions and random matrices*, Physical Review Letters **84** (2000), no. 21, 4882–4885, arXiv:cond-mat/9912264.

[PS02] ———, *Scale invariance of the PNG droplet and the Airy process*, Journal of Statistical Physics **108** (2002), no. 5–6, 1071–1106, arXiv:math/0105240.

[Qua11] Jeremy Quastel, *Introduction to KPZ*, Current Developments in Mathematics **2011** (2011), 125–194.

[Rap25] Gabriel Raposo, *Global fluctuations for standard Young tableaux*, Preprint, arXiv:2507.18601, 2025.

[Res10] Nikolai Reshetikhin, *Lectures on the integrability of the 6-vertex model*, Exact Methods in Low-dimensional Statistical Physics and Quantum Computing, Oxford Univ. Press, 2010, arXiv:1010.5031, pp. 197–266.

[Rob38] Gilbert de B. Robinson, *On the representations of the symmetric group*, American Journal of Mathematics **60** (1938), no. 3, 745–760.

[Rom15] Dan Romik, *The surprising mathematics of longest increasing subsequences*, Institute of Mathematical Statistics Textbooks, no. 4, Cambridge University Press, 2015.

[RR86] David P. Robbins and Howard Rumsey, Jr., *Determinants and alternating sign matrices*, Advances in Mathematics **62** (1986), no. 2, 169–184.

[RRV11] José Ramírez, Brian Rider, and Bálint Virág, *Beta ensembles, stochastic Airy spectrum, and a diffusion*, Journal of the American Mathematical Society **24** (2011), no. 4, 919–944, arXiv:math/0607331.

[Sag01] Bruce E. Sagan, *The Symmetric Group: Representations, Combinatorial Algorithms, and Symmetric Functions*, 2nd ed., Graduate Texts in Mathematics, vol. 203, Springer, New York, 2001.

[Sch01] Issai Schur, *Über eine Klasse von Matrizen, die sich einer gegebenen Matrix zuordnen lassen*, Ph.D. thesis, Universität Berlin, 1901.

[Sch61] Craige E. Schensted, *Longest increasing and decreasing subsequences*, Canadian Journal of Mathematics **13** (1961), 179–191.

[Sch97] Gunter M. Schütz, *Exact solution of the master equation for the asymmetric exclusion process*, Journal of Statistical Physics **88** (1997), no. 1–2, 427–445, arXiv:cond-mat/9701019.

[SD71] Isaac C. Sanchez and Edmund A. DiMarzio, *Dilute solution theory of polymer crystal growth: a kinetic theory of chain folding*, The Journal of Chemical Physics **55** (1971), no. 2, 893–908.

[Ser77] Jean-Pierre Serre, *Linear representations of finite groups*, Springer, 1977.

[She07] Scott Sheffield, *Gaussian free fields for mathematicians*, Probability Theory and Related Fields **139** (2007), no. 3–4, 521–541, arXiv:math/0312099.

[SI04] Tomohiro Sasamoto and Takashi Imamura, *Fluctuations of the one-dimensional polynuclear growth model in half-space*, Journal of Statistical Physics **115** (2004), no. 3–4, 749–803, arXiv:cond-mat/0307011.

[Sim05a] Barry Simon, *Orthogonal Polynomials on the Unit Circle, Part 1: Classical Theory*, AMS Colloquium Publications, vol. 54, American Mathematical Society, Providence, RI, 2005.

[Sim05b] _____, *Trace Ideals and Their Applications*, 2nd ed., Mathematical Surveys and Monographs, vol. 120, American Mathematical Society, Providence, RI, 2005.

[Sim11] _____, *Szegő's Theorem and Its Descendants: Spectral Theory for L^2 Perturbations of Orthogonal Polynomials*, M.B. Porter Lectures, Princeton University Press, Princeton, NJ, 2011.

[Sos00a] Alexander B. Soshnikov, *Determinantal random point fields*, Russian Mathematical Surveys **55** (2000), no. 5, 923–975, arXiv:math/0002099.

[Sos00b] _____, *Gaussian fluctuation for the number of particles in Airy, Bessel, sine, and other determinantal random point fields*, Journal of Statistical Physics **100** (2000), no. 3–4, 491–522, arXiv:math-ph/9907012.

[Spi70] Frank Spitzer, *Interaction of Markov processes*, Advances in Mathematics **5** (1970), no. 2, 246–290.

[SS10] Tomohiro Sasamoto and Herbert Spohn, *One-Dimensional Kardar-Parisi-Zhang Equation: An Exact Solution and its Universality*, Physical Review Letters **104** (2010), no. 23, 230602, arXiv:1002.1883.

[Sta99] Richard P. Stanley, *Enumerative Combinatorics, Volume 2*, Cambridge Studies in Advanced Mathematics, vol. 62, Cambridge University Press, Cambridge, UK, 1999.

[Sto50] George G. Stokes, *On the numerical calculation of a class of definite integrals and infinite series*, Transactions of the Cambridge Philosophical Society **9** (1850), 166–187.

[Str06] Yuri G. Stroganov, *Izergin-Korepin determinant at a third root of unity*, Theoretical and Mathematical Physics **146** (2006), no. 1, 53–62, arXiv:math-ph/0204042.

[Sze52] Gábor Szegő, *On certain Hermitian forms associated with the Fourier series of a positive function*, Communications du Séminaire Mathématique de l'Université de Lund [Medd. Lunds Univ. Mat. Sem.] **Tome Supplémentaire** (1952), 228–238.

[Tho64] Elmar Thoma, *Die unzerlegbaren, positiv-definiten Klassenfunktionen der abzählbar unendlichen, symmetrischen Gruppe*, Mathematische Zeitschrift **85** (1964), no. 1, 40–61.

[Thu90] William P. Thurston, *Conway's tiling groups*, The American Mathematical Monthly **97** (1990), no. 8, 757–773.

[Ton18] Fabio Toninelli, *(2+1)-dimensional interface dynamics: mixing time, hydrodynamic limit and anisotropic KPZ growth*, Proceedings of the International Congress of Mathematicians (ICM 2018), vol. III, World Scientific, 2018, arXiv:1711.05571, pp. 2733–2758.

[Tro84] Hale F. Trotter, *Eigenvalue distributions of large Hermitian matrices; Wigner's semi-circle law and a theorem of Kac, Murdock, and Szegö*, Advances in Mathematics **54** (1984), no. 1, 67–82.

[TW94] Craig A. Tracy and Harold Widom, *Level-spacing distributions and the Airy kernel*, Communications in Mathematical Physics **159** (1994), 151–174, arXiv:hep-th/9211141.

[TW96] _____, *On orthogonal and symplectic matrix ensembles*, Communications in Mathematical Physics **177** (1996), 727–754, arXiv:solv-int/9509007.

[TW01] _____, *On the distributions of the lengths of the longest monotone subsequences in random words*, Probability Theory and Related Fields **119** (2001), no. 3, 350–380, arXiv:math/9904042.

[TW09] _____, *Asymptotics in ASEP with step initial condition*, Communications in Mathematical Physics **290** (2009), no. 1, 129–154, arXiv:0807.1713.

[Ula61] Stanislaw M. Ulam, *Monte Carlo Calculations in Problems of Mathematical Physics*, Modern Mathematics for the Engineer: Second Series (Edwin F. Beckenbach, ed.), McGraw–Hill, 1961, pp. 261–281.

[Uly24] Vladimir V. Ulyanov, *From classical to modern nonlinear central limit theorems*, Mathematics **12** (2024), no. 14, 2276, arXiv:2405.19828.

[Vie77] Gérard Viennot, *Une forme géométrique de la correspondance de Robinson–Schensted*, Combinatoire et représentation du groupe symétrique (Berlin, Heidelberg), Lecture Notes in Mathematics, vol. 579, Springer, 1977, pp. 29–58.

[VK77] Anatoly M. Vershik and Sergei V. Kerov, *Asymptotic behavior of the Plancherel measure of the symmetric group and the limit form of Young tableaux*, Doklady Akademii Nauk SSSR **233** (1977), no. 6, 1024–1027, English translation: Soviet Mathematics Doklady.

[VK81] _____, *Characters and factor representations of the infinite symmetric group*, Doklady Akademii Nauk SSSR **257** (1981), 1037–1040, English translation in Soviet Mathematics Doklady.

[Vol63] Marjorie J. Vold, *Computer simulation of floc formation in a colloidal suspension*, Journal of Colloid Science **18** (1963), 684–695.

[War07] Jon Warren, *Dyson's Brownian motions, intertwining and interlacing*, Electronic Journal of Probability **12** (2007), no. 19, 573–590, arXiv:math/0509720.

[Wey26] Hermann Weyl, *Theorie der Darstellung kontinuierlicher halb-einfacher Gruppen durch lineare Transformationen. I, II, III*, Mathematische Zeitschrift **23, 24** (1925–1926), 271–309 (vol. 23); 328–376, 377–395 (vol. 24).

[Wey39] _____, *The Classical Groups: Their Invariants and Representations*, Princeton University Press, Princeton, NJ, 1939.

[Wic50] Gian-Carlo Wick, *The evaluation of the collision matrix*, Physical Review **80** (1950), no. 2, 268–272.

[WP21] Wendelin Werner and Ellen Powell, *Lecture Notes on the Gaussian Free Field*, Cours Spécialisés, vol. 28, Société Mathématique de France, Paris, 2021, arXiv:2004.04720.

[Yan67] C.-N. Yang, *Some exact results for the many-body problem in one dimension with repulsive delta-function interaction*, Physical Review Letters **19** (1967), no. 23, 1312–1315.

[Zei96] Doron Zeilberger, *Proof of the Alternating Sign Matrix Conjecture*, The Electronic Journal of Combinatorics **3** (1996), no. 2, R13, arXiv:math/9407211.

[ZJ08] Paul Zinn-Justin, *Six-Vertex, Loop and Tiling models: Integrability and Combinatorics*, Habilitation à diriger des recherches (HDR) thesis, 2008, arXiv:0901.0665.

[ZYW+15] Wu Zhou, Kuibo Yin, Canhui Wang, Yuyang Zhang, Tao Xu, Albina Borisevich, Litao Sun, Juan Carlos Idrobo, Matthew F. Chisholm, Sokrates T. Pantelides, Robert F. Klie, and Andrew R. Lupini, *The observation of square ice in graphene questioned*, Nature **528** (2015), no. 7583, E1–E2.